Aston University

Some pages of this thesis may have been removed for copyright restrictions.

If you have discovered material in AURA which is unlawful e.g. breaches copyright, (either yours or that of a third party) or any other law, including but not limited to those relating to patent, trademark, confidentiality, data protection, obscenity, defamation, libel, then please read our Takedown Policy and contact the service immediately

THE STRENGTH OF COLUMN-TO-FOUNDATION JOINTS IN REINFORCED CONCRETE

BY

MAHMUT TURAN

A THESIS SUBMITTED FOR THE DEGREE

OF

DOCTOR OF PHILOSOPHY

DEPARTMENT OF CIVIL ENGINEERING

THE UNIVERSITY OF ASTON IN BIRMINGHAM

MARCH 1983

TO MY

MOTHER AND FATHER

THE STRENGTH OF COLUMN-TO-FOUNDATION JOINTS IN REINFORCED CONCRETE

BY

MAHMUT TURAN

A THESIS SUBMITTED FOR THE DEGREE OF

DOCTOR OF PHILOSOPHY 1983

SUMMARY

This thesis is concerned with the experimental and theoretical investigation into the compression bond of column longitudinal reinforcement in the transference of axial load from a reinforced concrete column to a base.

Experimental work includes twelve tests with square twisted bars and twenty four tests with ribbed bars. The effects of bar size, anchorage length in the base, plan area of the base, provision of base tensile reinforcement, links around the column bars in the base, plan area of column and concrete compressive strength were investigated in the tests. The tests indicated that the strength of the compression anchorage of deformed reinforcing steel in the concrete was primarily dependent on the concrete strength and the resistance to bursting, which may be available within the anchorage. It was shown in the tests without concreted columns that due to a large containment over the bars in the foundation, failure occurred due to the breakdown of bond followed by the slip of the column bars along the anchorage length.

The experimental work showed that the bar size, the stress in the bar, the anchorage length, provision of the transverse steel and the concrete compressive strength significantly affect the bond stress at failure. The ultimate bond stress decreases as the anchorage length is increased, while the ultimate bond stress increases with increasing each of the remainder parameters. Tests with concreted columns also indicated that a section of the column contributed to the bond length in the foundation by acting as an extra anchorage length.

The theoretical work is based on the Mindlin equation[3], an analytical method used in conjunction with finite difference calculus. The theory is used to plot the distribution of bond stress in the elastic and the elastic-plastic stage of behaviour. The theory is also used to plot the load-vertical displacement relationship of the column bars in the anchorage length, and also to determine the theoretical failure load of foundation. The theoretical solutions are in good agreement with the experimental results and the distribution of bond stress is shown to be significantly influenced by the bar stiffness factor K.

A comparison of the experimental results with the current codes shows that the bond stresses currently used are low and in particular, CP110[56] specifies very conservative design bond stresses.

FOUNDATION CONCRETE DEFORMED BAR SLIP BOND STRESS

ACKNOWLEDGEMENTS

The author wishes to express his sincere gratitude to his supervisor, the late A.W. Astill, Lecturer, BSc(Eng), CEng, FIStructE, for his help, guidance and wise counsel throughout this investigation, and to his present supervisor L.H. Martin, Reader, BSc, PhD, CEng, MICE, for his interest, encouragement and advice during the writing-up stages of this research project.

The author is deeply grateful to Dr J. Graham, who was a postgraduate research student within the Civil Engineering Department during the time of experimental programme, for his help in preparing and testing several of the specimens. Thanks are due to Mr S.M. Wagstaff, a technician within the department, for his assistance with the preparation of some specimens, to Mr I.A.Sparkes, Advisor to Overseas Students, and to Dr T. Celik for their help. Thanks are also due to Mrs H. Wilcox for typing the manuscript neatly and efficiently.

Finally, the author is deeply indebted to his parents and brothers for their encouragement, patience and financial support.

M E M O R A N D U M

No part of this thesis has been submitted in support of an application for another degree or qualification at any university or institution.

A paper which includes some of the work described in this thesis has been published as follows.

ASTILL A.W. and TURAN M., Compression Anchorage Stresses in Bases, Bond in Concrete - Proceedings of the International Conference on Bond in Concrete held in Paisley, Scotland - Applied Science Publishers, London 1982.

C O N T E N T S

LIST OF TABLES

LIST OF FIGURES

CHAPTER 7

APPENDIX A

N O T A T I O N

A	length of foundation
a	radius of a reinforcing bar
A_b	unloaded area of base
$A_c = a_1 x a_2$	plan area of column
a_{c1}, a_{c2}	lateral dimensions of core in a column
A_{cc}	net concrete area in a column
A_{core}	core area in a column
a_{core}	core length in a square column
A_p	periphery of a reinforcing bar
A_s	cross sectional area of a reinforcing bar
A_{sb}	area of base tension reinforcement
A_{sc}	area of column longitudinal reinforcement
A_{st}	bar end area
A_{sv}	area of column core confining reinforcement
α	ratio of actual concrete stress in a column to characteristic concrete cube strength
α_{av}	mean value of α
B	width of foundation
β	ratio of steel stress in compression to yield stress in tension
β_{av}	mean value of β
[C]	compound matrix (in chapter 5)
[CP]	matrix of coefficients for bar action
[CS]	overall vertical displacement influence factors matrix for concrete
D	ratio of unloaded area to loaded area
d	effective depth of tension reinforcement in foundation

d_b	distance between bottom link and end of column bars in foundation
[DB],[DC],[DF]	submatrices of the vertical displacement influence factors matrix for concrete
[DEF]	column matrix for vertical displacements of concrete along bar elements and under bar tip in elastic stage
$[DEF]^{\lambda}$,$[DEF]^{\lambda_1}$	column matrices for vertical displacements under load factors λ and λ_1, respectively
$(DEF)_i$	vertical displacement of concrete at load factor λ^i
d_s	spacing of links over column longitudinal reinforcement in foundation
d_t	distance between top link and top face of foundation
$[\Delta c]$	vertical displacement matrix of concrete
Δc_b	vertical displacement of concrete under bar tip due to bond stress on bar elements and normal stress on bar tip
Δc_{bb}	vertical displacement of concrete under bar tip due to normal stress on bar tip
Δc_{bj}	vertical displacement of concrete under bar tip due to bond stress on bar element j
Δc_i	vertical displacement of concrete at point i due to bond stress on bar elements and normal stress on bar tip
Δc_{ib}	vertical displacement of concrete at point i due to normal stress on bar tip
Δc_{ij}	vertical displacement of concrete at point i due to bond stress on bar element j

Δf_s	change of steel stress over a length Δl_a
Δ_h	experimentally measured horizontal displacement of column cage
Δl_a	length of bar on which bond stress is computed
$[\Delta_s]$	vertical displacement matrix of bar elements
$\Delta_{si}, \Delta_{sn}, \Delta_{sb}$	displacements at mid points of bar elements i, n and bar tip, respectively
Δ_{sv}	theoretically predicted vertical displacement of column cage
Δ_v	experimentally measured vertical displacment of column cage
Δ_{vb}	experimentally measured vertical deflection of foundation
Δ_{vc}	experimentally measured vertical deflection of column
Δ_{vt}	experimentally measured total shortening of specimen
δ	length of cylindrical bar element
E_c	Young's modulus of concrete
E_s	Young's modulus of steel
$\varepsilon, \varepsilon_s$	strains in steel
$\varepsilon_{v1}, \varepsilon_{v2}, \varepsilon_{v3}$	vertical strains measured on concrete cylinders
$\varepsilon_{vav.}$	average vertical strain of concrete
$\varepsilon_{l1}, \varepsilon_{l2}, \varepsilon_{l3}$	horizontal strains measured on concrete cylinders
$\varepsilon_{lav.}$	average horizontal strain of concrete
f_{bs}	average bond stress
$f_{bsav.}$	experimentally determined average bond stress at failure

f_{bsu}	ultimate average bond stress obtained from regression analysis of test results
ACI f_{bs}	design bond stress according to American code ACI318-77
CP110 f_{bs}	design bond stress according to British code CP110
f_c	actual concrete strength in column
f_{cu}	characteristic concrete cube strength
f_{cy}	concrete cylinder compressive strength
f_s	compressive stress in column longitudinal reinforcement
f_t	tensile strength of concrete
f_u	ultimate stress of steel in tension
f_y	yield stress of steel in tension
G_c	shear modulus of concrete
γ	ratio of unequal intervals
H	overall height of test specimen
h	overall depth of foundation
i,j,k	integers
[I]	identity matrix
K	bar stiffness factor
K_p	pile stiffness factor
l_a	anchorage length of column bars in foundation
l_{amin}	minimum anchorage length used in tests
l_b	distance between bottom strain gauge and end of column bar in foundation
l_c	unconfined length of column bars above foundation
l_o	overall length of column cage

$l_{s1}, l_{s2}, l_{s3}, l_{s4}$	spacing of strain gauges in anchorage length
l_t	distance between very top and top strain gauges on column cage
l_v	length of column cage above top face of base
λ	overall load factor
$\lambda_1, \lambda_2, \lambda^i, \lambda_1^k$	load factors
$\Delta\lambda$	increment in the load factor
M	grid indication number for numerical integration
n,N	number of cylindrical bar elements
P	axial load on column bar
p	axial working load
P_c	cracking load in test specimen
P_{test}	experimental ultimate load
P_u	ultimate load obtained from regression analysis of test results
P_{ult}	theoretical ultimate load
R	correlation coefficient
$\bar{r}, r, r_{mean}$	radial distance (in chapter 5)
R_A	ratio of bar cross-sectional area to the area bounded by circumference of bar
R_1, R_2	geometrical variables (in chapter 5)
ρ_b	tension reinforcement percentage in foundation
ρ_c	longitudinal reinforcement percentage in column
ρ_{sv}	column core confining reinforcement percentage in foundation
[ST]	column matrix for bond stresses on bar elements and normal stress on bar tip in elastic stage

$[ST]^{\lambda}, [ST]^{\lambda_1}$	column matrices for stresses on column bar under load factors λ and λ_1, respectively
$S_v, \overline{V}_i, \overline{V}_2, \overline{V}_3, .. \overline{V}_6$	spacing of links in column
σ	normal stress in column bar in axial compression
T	constant depending on concrete characteristics
t	constant
θ	angle
τ	uniformly distributed shear stress or bond stress on bar surface
τ_b	uniformly distributed normal stress on bar tip
τ_j, τ_n	bond stresses on bar elements j and n, respectively
$[\tau]$	column matrix representing bond stress distribution on bar shaft and normal stress on bar tip
τ_u	ultimate bond stress on bar elements
τ_{bu}	ultimate bearing resistance of concrete under bar tip
$[\tau_u]$	ultimate stress column matrix for bar elements and bar tip
ν_c	Poisson's ratio of concrete
X,Y,Z,x,y,z	cartesian coordinates
[Y]	column matrix of constants (chapter 5)
W/C	water cement ratio
$\overline{z}, z, z_1, c$	geometrical variables (in chapter 5)
ϕ	bar size or nominal bar diameter
ϕmax	maximum bar size used in tests
ϕ_t	diameter of bar tip

ω_b	influence factor for vertical displacement at any point in a semi-infinite elastic solid due to a vertical point load in the interior of the solid
ω_{ij}	influence factor for vertical displacement at point i due to a uniform bond stress on element j
ω_{ib}	influence factor for vertical displacement at point i due to uniform normal stress on bar tip
ω_{bj}	influence factor for vertical displacement of the centre of bar tip due to bond stress on element j
ω_{bb}	influence factor for vertical displacement of bar tip due to normal stress on the bar tip

Note: Some notations not included in the above list, will be specifically defined when they are first introduced.

CHAPTER 1

INTRODUCTION AND HISTORICAL REVIEW

1.1 Introduction

Foundations are structural members that transmit superstructure loads to the soil. In transferring the loads to the ground the foundation should be capable of supporting the loads from the structure. In foundation design, it is therefore vital to ensure that two principal criteria are satisfied. The first criterion is that there should be sufficient strength and stiffness without risk of failure due to bond, shear or bending within the foundation itself. The second criterion is that there should be a reasonable factor of safety for the soil in relation to the settlement capacity of the soil. Most common foundation types may be described as independent, square, circular or rectangular, strip footing for carrying a wall, combined foundation for carrying more than one column and a raft foundation carrying a whole structure. Each type may be built on piles if necessary.

The research carried out on reinforced concrete foundations is mostly concentrated on shear and flexural strength and to a lesser extent on bond stress between the tension reinforcement and base concrete. However, in the transference of load from columns to foundations the compression bond of column longitudinal reinforcement within the foundation has been almost totally ignored. Numerous attempts have been made to present theoretically acceptable formulae which are also in satisfactory agreement with the experimental data for the developments in the structural design of foundations. Yet wide differences

exist in the methods of designing due to the differences in the assumptions made with reference to the structural action of the foundation.

Bond between steel and concrete has been subjected to extensive investigation since the beginning of this century due to the fact that it plays an important role in the performance of reinforced concrete as a structural material. In fact, the reliability and consistency of the reinforced concrete is primarily dependent on this fundamental phenomenon. Despite extensive research there is no generally accepted bond theory suitable for all range of parameters and stress conditions. This is not surprising because the bond phenomenon has a very complex nature. One notable example of this complexity of the bond is the unknown degree of interdependence of the governing component variables and as a result the general solution to predict the bond resistance for many different stress situations is not obtainable.

The bond performance of a reinforcing bar in tension is different from that in compression. When the bar is subjected to tension, the tendency for the bar diameter to decrease weakens the bond strength. Conversely, in compression the bar diameter tends to increase and hence exerts extra frictional forces at the interface between steel and concrete resulting in higher bond stresses. The end bearing of a bar in compression also affects the bond strength. With the introduction and growing demand of deformed bars in practice, a great deal of research has been carried out on their bond performance. The large majority of works have been devoted to bond in tension and compression bond of deformed bars has been given little attention.

The work on compression has concentrated on lapped joints in reinforced concrete columns. Radial forces i.e. bursting forces, in addition to the shear stresses, were observed with the use of deformed bars and have been subject to extensive investigation. A large number of experiments have made it clear that bond failure of deformed bars takes place by extensive splitting of the concrete cover due to inefficient containment. Typical examples are the tensile lapped joints in beams and compression lapped joints in columns. In contrast, the failure could occur by shearing off the concrete, i.e. slip of bar, provided that sufficient containment over the bar is present.

It is known that the transfer of load from a reinforced concrete column to a base is affected partly by compression stress in concrete and steel and, the compression in the steel is transferred to the foundation by bond. While there is information on the behaviour of deformed bars under varying stress conditions, there is very little information available concerning the compression bond of column longitudinal reinforcement in foundations. This lack of data on compression bond in the foundations is reflected in design codes of practice. CP110[56] for example makes no reference to the compression bond in the foundation and does not distinguish between design compression bond stresses having different locations. In practice, very excessive bond lengths are used for column longitudinal reinforcement in foundations due to the low design bond stresses specified by the code.

Recognition of the importance of load transfer in foundation design and the need for quantitative estimates of the magnitude and distri-

bution of bond stress along the anchorage length of a reinforcing bar in the foundation makes it necessary to undertake a research on the subject. In this study the compression bond of column longitudinal reinforcement in the transference of axial load from a column to a foundation is considered. Deformed bars are used, where failure due to shearing off the concrete, i.e. slip of the bars in the anchorage lengths, is the principal criterion.

1.2 Historical Review

The review of published works related to the present investigation, directly or indirectly, are given under the heading of the following sub-sections.

1.2.1 Reinforced Concrete Bases and Columns

The first comprehensive investigation on reinforced concrete foundations was carried out by Talbot[1]. A total of 114 rectangular wall footings and 83 square column footings were tested using plain round and deformed bars. Particular attention was given to the structural action of foundations with reference to tension, diagonal tension and bond between the bending steel and base concrete. Both wall and column footings were supported by a bed of car springs, to simulate the conditions of uniform upward pressure, while they were loaded to failure through a 12x12x12 in. stem or stub. It was reported that both types of foundation produced three different failures, namely tension failure, diagonal tension failure and bond failure between the tension reinforcement and base concrete. Sixteen of the wall footings and twenty eight of the column footings failed

in bond, while the rest in both series failed either in tension or diagonal tension. Talbot's investigation formed the basis of reinforced concrete foundation design practice in countries throughout the world for many years.

Marshall[4] conducted tests on square isolated reinforced concrete column bases to study the effect of the bed and the bending reinforcement on the strength of the base. The model specimens 8 in. square and $1\frac{1}{8}$ and $1\frac{5}{8}$ in. thick, made from cement-sand mortar, were loaded to failure at the centre through a 2 in. square steel block. The foundations were supported by one of three different beds, namely, rubber sheets, dry sand and moist clay. It was reported that these tests failed in direct or diagonal tension. The tests showed that the pressure under the base became more uniform as the flexibility of the base was reduced. Other tests concerning the effect of the reinforcement on the foundation strength, were carried out on concrete bases, 2 feet square and 4 in. thick, using a 4 in. square stanchion. These specimens were reinforced with mild steel and supported by a compacted sand bed during loading. The test results indicated that the relationship between the load and the area of reinforcement was a family of straight lines, the slope of which increased as the bar diameters decreased from $\frac{1}{2}$ in. to 3/16 in.

In 1948, an extensive experimental study on reinforced concrete foundations was reported by Richart[6]. His investigation covered 24 wall and 132 column footings, tested to failure through a concrete stub while supported by a bed of car springs to simulate soil pressure. The principal object of the series of tests reported, was to investigate the failure strength of the bases by bond, diagonal tension

and tension in the steel. It was reported that all of the wall footings initially failed in tension due to the yield stress development in the reinforcement. It was also observed that the bond stress was not crucial in these tests, however, it attained a value of 25% of the concrete cylinder compressive strength with considerable slip at critical load in two bases.

Tests on column footings resulted in bond, diagonal tension and tension failures, a majority of them failing in diagonal tension alone. It was stated that most of the bases which failed initially due to tension or excessive bond slip, collapsed finally by diagonal tension failure. Richart concluded that the bars with new improved types of deformations developed maximum bond streses of 19 to 29% of the concrete cylinder compressive strength. Bars with hooks indicated no clear advantage over straight bars as far as the maximum bond stress development and the slip were concerned. Richart also came to the conclusion that the maximum shearing stresses calculated on the critical section, i.e. at a distance (d) from the faces of the column, varied considerably with the effective depth of the base (d), being larger for the thinner bases. The use of a critical section at less than the distance (d) outside the column face was reported to be worth considering from an interpretation of the test results. Richart presented his work as a research report with no recommendation concerning improved design methods.

Hognestad[11] presented his work on the analysis and re-evaluation of the shearing strength of reinforced concrete bases, which were reported by Richart[6]. The objective of the investigation was to produce a mathematical expression to calculate the ultimate shearing

strength of column footings. Hognestad concluded that the shearing stress should be computed at the face of the column. On this basis he also proposed an empirical equation for the ultimate shearing stress.

Whitney[21] proposed a method for the ultimate shear strength which was based on a re-evaluation of previously published experimental results by Richart[6] and Elstner and Hognestad[13]. He computed the shearing stress on a critical section at a distance (d/2) from the face of the column.

King[7] conducted tests on small scale specimens to examine the effect of the core size, concrete quality and steel quality on the strength of short reinforced concrete columns. He observed that for a column of fixed cross-section and length, core size, cover area, concrete strength, main and binder steel strength and binder pitch had a considerable effect on the ultimate strength. King also concluded that an increase in the core area for the same concrete and longitudinal steel with close pitch binders led to increase in the column strength and, there was material advantage in using high quality steel as main reinforcement in columns.

An experimental study on concentrically loaded columns having high strength deformed longitudinal reinforcement with and without splices, was presented by Pfister and Mattock[28]. The investigation consisted of 9 circular columns with spiral reinforcement and 7 columns with links, tested to failure. In the experiments major emphasis was placed on an examination of lapped splices, however, butt joints were also incorporated in columns of each type. The main parameter studied

was the effect of splice length on the stress development in the reinforcement away from the splice. Pfister and Mattock observed that force in a compression lapped joint was transferred by bond on the surface of the longitudinal reinforcement and end bearing of this steel on the conrete. They also came to the conclusion that in compression, butt joints in longitudinal reinforcements were capable of producing the same stress at ultimate resistance of a column as would a continuous bar without any joint.

Sargin, Ghosh and Handa[49] reported their work on the effect of lateral reinforcement upon the strength and deformation characteristics of concrete. Tests were undertaken by varying size, spacing and grade of lateral reinforcement, strain gradient, concrete strength and thickness of cover with a view to establishing formulas for calculating the strength of laterally reinforced concrete. In the analysis of the experimental results, they treated laterally reinforced specimens as composite members comprising a confined core and unconfined cover. Sargin, Ghosh and Handa observed that spacing of lateral reinforcement was a most important parameter since the effect of transverse reinforcement decreased rapidly by increasing the spacing. They concluded that lateral reinforcement improved the strength and ductility of confined concrete but it had a detrimental effect upon the cover. They also concluded that the overall strength of a laterally reinforced member might be less than that of an identical plain member, depending upon the relative areas of core, cover and arrangement of reinforcement.

Later, an experimental investigation concerning the contribution of cover to the ultimate strength of reinforced concrete compression

members, was published by Ghosh, Sargin and Handa[50]. They found that the cover in a laterally reinforced concrete compression member was less effective than the core in resisting loads, and this effectiveness increased as the cover thickness was increased. The test results also confirmed the earlier conclusion reached in the previous work[49] that the overall strength of a concrete compression member with transverse reinforcement could be less than that of an identical plain concrete member because of the low load carrying capacity over the cover.

Somerville[51] studied structural joints in precast concrete columns and beams. He employed conventional two part addition formula to compute the theoretical ultimate load for axially loaded short columns, in which he assessed the actual concrete strength (f_c) in the column as 67% of the cube compressive strength (f_{cu}) and the effective steel stress (f_s) in the longitudinal reinforcement as 75% of its tensile yield stress (f_y). He observed from the experimental results that the size of the bars used for the longitudinal reinforcement had a significant effect on the joint strength. On this basis he concluded that a proportion of the force in the longitudinal bars was transferred to the concrete by end bearing.

Somerville and Taylor[55] published the results of 5 tests on joggled splices in columns. The specimens were tested to failure in axial compression. They computed the theoretical ultimate load for each specimen from strain compatibility considerations. On the basis of the tests it was also suggested that some of the load in the longitudinal reinforcement was transferred to the concrete by end bearing.

Arthur and Cairns[62] presented their work on compression lapped joints in reinforced concrete columns, with a view to comparing the commonly used rules in design practice with the results of their work. It was reported that an investigation carried out on the subject, details of which have been given elsewhere[60], led to the development of a theory considering the combined action of bond and end bearing for lapped joints with ribbed bars confined by round mild steel links. It was also stated that 51 tests were conducted on reinforced concrete columns to examine the effect of several parameters upon the strength of compression lapped joints.

As a result of the investigation, Arthur and Cairns concluded that in a compression lapped joint the force was transferred between the bars partly by bond stresses on the surface of the bars and partly by end bearing of the bars on the concrete. It was found that both effects exerted bursting forces on the surrounding concrete, and therefore the ultimate joint strength in bond and end bearing was dependent upon the resistance available against the bursting forces. The rib properties of the reinforcing steel was found to have an effect on the ultimate bond strength. It was stated that quantity and position of the transverse reinforcement within the lapped joint influenced the ultimate joint strength, and the absence of links close to the ends of the lap joint led to a decrease of the ultimate strength. Provided that sufficient links were available at the ends of laps and they have yielded, Arthur and Cairns proposed an equation to predict the compression stress in the column longitudinal reinforcement within $\pm$20% accuracy at the failure of the joint. In addition, employing the limit state philosophy of CP110[56], an expression for the design lap length was given. Both equations were reported

to be confirmed by tests for mild steel links and hot-rolled straight deformed longitudinal reinforcement only.

Arthur and Cairns also compared the computed results with the specifications for compression lapped joints in several codes of practice including the British code CP110[56]. They stated that the bond length requirements in CP110 were inadequate. On this basis, they concluded that if the bond stresses in CP110 were to be employed, extra links had to be provided at the ends of laps to control the bursting forces.

Later, Cairns and Arthur[71] published another paper reporting the results of the experimental investigation carried out on 51 reinforced concrete columns, in which the longitudinal reinforcement was lapped. Tests were undertaken in order to study the contribution of the end bearing, effect of lap length, concrete strength, amount and position of the transverse reinforcement, as well as the deformation properties of the reinforcing bars. Details of experiments were presented elsewhere[60]. It was reported that difficulties were encountered in relating the ultimate strength of lapped joints in the tests to the results of standard concrete cube strength. A method was evolved therefore to utilise the concrete stress-strain curve in the column to compute the ultimate strength of the concrete in the joint zone. Finally from the conventional ultimate strength equation of an axially loaded column the ultimate stress in the main compression steel in the splice was obtained.

It was observed in the tests that failure of lapped joints always took place by extensive splitting of the concrete cover along the

line of lapped bars with wedges of concrete adhering to ribs, following the yield of links placed at the ends of the lap. Cairns and Arthur concluded that the strength of a compression lapped joint could be divided into two components, one related to the resistance to withstand the bursting forces exerted by bond and end bearing, and the other related to concrete strength. They found that the position of links within the splice had a significant effect on strength and proposed that links always be provided at the ends of the splice. It was also found that increases in bar surface roughness and in lap length both resulted in increases in the joint strength in the ranges examined. However, it was observed that increasing the strength of transverse reinforcement was not effective beyond a certain limit, and an increase in the concrete strength led to improved joint strength for only shorter lap lengths.

A theoretical analysis related to the ultimate strength of compression lapped joints with ribbed deformed bars was carried out by Cairns[74], as part of the investigation given elsewhere[60]. Based on Coulomb-Mohr failure criterion and the equilibrium of stress acting on a model of concrete failure wedge below rib, a theory was developed for the bond failure of reinforcement due to splitting of the concrete cover. Considering that the bond action of a ribbed bar exerted a radial bursting force on the concrete cover, the ultimate strength of a lapped joint was computed by equating the bursting force produced by bond to the ultimate confining force available on the lapped bars in a member. The related equations were derived to obtain the relationship between the compression stress in a lapped bar and the resultant bursting force. The contribution of the end bearing of lapped bars to the ultimate strength was also included in the analysis.

Cairns concluded that the lap length was mainly affected by the concrete strength, ultimate confining force on the bar and the deformation characteristics of the bar. The contribution of the end bearing to the joint strength was found to depend on the concrete strength in the member. Cairns also concluded that for cases where reinforcing steel was heavily confined, the mode of bond failure changed and therefore the proposed method of analysis was no longer applicable.

An experimental study concerning the compression bond of column longitudinal reinforcement in bases was presented by Astill and Al-Sajir[76]. Three series of tests comprising 17 specimens were carried out with a view to determining some of the factors influencing the strength of column to base joint. In three series of tests, the effects of the variation of base thickness with fixed amount of tensile steel, quantity of tension reinforcement percentage with constant base thickness, and the lateral dimensions of the plain base with fixed thickness were considered, respectively. Each test specimen included a square base with a 200 mm square short column with 4-20 mm square twisted bars continued straight to the underside of the base to allow free slip of bars. Each specimen was tested to failure in axial compression while supported by a bed plate with 200 mm square hole under the column resting on a rigid steel platen. In the tests strain measurement in the column bars was made using strain gauges attached to the bars at a distance of 90 mm above the top of the base. Full particular details of experiments have been given elsewhere[59].

It was reported that all tests produced bond failure between steel

and concrete in the base except two tests in the first series, one with 100 mm base thickness which failed in punching shear and the other with 400 mm base thickness which failed entirely in axial compression in column without any loss of bond between steel and concrete in the base. It was found that total load carrying capacity of the column to base joint increased linearly with base thickness. It was also observed that part of the column length was acting as an extra anchorage length in addition to the embedment length in the base. The tests showed that increasing the percentage of base tension steel for a constant base thickness resulted in an increase in the joint strength. Likewise an increase in the ratio of unloaded area to loaded area also led to increased joint capacity.

The average bond stress was computed from the measured strain in the reinforcement employing two different bond lengths, one equal to the base thickness and the other equal to the sum of the base thickness and column core dimension and plotted against the related variable. The bond stresses for each series of tests were also compared with the design bond stresses in CP110[56] and ACI318-77[61]. Astill and Al-Sajir observed that the available bursting control in bases was much greater than that proposed by Arthur and Cairns[62] for compression lapped joints and, consequently the bond stresses at failure were higher than those given by CP110. On the basis of the test results, Astill and Al-Sajir concluded that the anchorage bond strength of column longitudinal reinforcement was improved as the percentage of base tension reinforcement and the ratio of the base unloaded area to loaded area was increased and, both variables rendered increased control of bursting effects. It was also concluded that the design bond stresses given in CP110 were too low, while

ACI318-77 values were in better agreement with the test results. They recommended that a specific requirement should be introduced into CP110 for the bond stress in bases because using general clauses of CP110 results in excessive anchorage lengths. They also stated that the change in joint strength could not be determined without further research.

Seferovic[84] published a paper dealing with the column-foundation joints in prefabricated reinforced concrete structures erected by the anchorage technique. The object of the study was to establish an anchoring length and an adequate cement-base compound to replace the costly expoxy compound. Tests were made in tension on 20x20xn cm model specimens (where n=10, 20, 30, ..., 100) using deformed bars of 16, 19, 22 and 25 mm as steel anchors. Two cases were considered in the tests, namely, anchor directly in the concrete and anchor in a protective pipe injected with a cement-base compound with the addition of expandite. The limit state was taken as the stress casued 0.01 mm end slip of the anchor. It was found that the column to foundation anchoring lengths could be much smaller than those applied in construction practice.

Tanigawa et al.[85] carried out an experimental and analytical study concerning the hysteretic bond-slip characteristics between concrete and reinforcement at the end-hinges of reinforced concrete columns with particular reference to the spacing of reinforcement and volume fraction of steel fibres in concrete matrix. In the experimental part 4 reinforced concrete column and 4 steel fibre reinforced concrete column specimens were tested in axial load plus bending. The analytical study considering the bond-slip relationships was based on

orthogonal partitioning method. From the comparison of the results it was concluded that the slip between concrete and reinforcement was decreased as the ratio of shear reinforcement was increased in the column, and the slippage in a steel fibre reinforced concrete column was smaller than that in a reinforced concrete column. It was also reported that the proposed method was effective in an analysis of the inelastic behaviour of reinforced and steel fibre reinforced concrete columns.

1.2.2 Pull-out Specimens and Reinforced Concrete Beams

This section is concerned with the studies on bond in tension, which were carried out on pull-out specimens and beams. A great deal of research has been done in this field and there is a mass of publication in the extensive literature. Due to the volume of the published work, a comprehensive review of it is beyond the scope of this thesis, so that reference is made only to some major and recent papers with particular interest to those dealing with deformed bars.

An extensive experimental study on bond comprising the pull-out and beam tests was carried out by Abrams[2]. A total of 1500 pull-out tests and 110 beam tests were conducted to investigate the nature and the value of the bond resistance of reinforcing bars for a wide range of parameters and conditions. In both forms of the test attention was given to obtaining the slip of the bar through concrete, which was particularly important in interpreting the results. Abrams divided bond resistance into two principal elements designated as adhesive resistance and sliding resistance. The term adhesive resistance was used to designate the bond resistance that developed

before the movement of bar with respect to the adjacent concrete begins. Sliding resistance was applied to the resistance developed as a result of the movement of the bar when the adhesive resistance is overcome.

In determining the comparative merits of deformed bars the bond stress developed at an end slip of 0.001 in. (0.025 mm) furnished the principal basis of comparison for different types of deformed bars. The tests showed that projections of a deformed bar did not materially assist in resisting a force tending to withdraw the bar, until a slip had occurred approximately corresponding to the maximum sliding resistance of plain bars, i.e. a slip of about 0.01 in. (0.254 mm). The bond stresses corresponding to an end slip of 0.1 in. (2.54 mm) were the highest stress reported for deformed bars.

Abrams reported that most of the beams failed in bond while a few failed by a combination of bond and diagonal tension, or by tension in the steel. In the tests, the mean bond resistance for deformed bars was found to be not materially different from that of plain bars until a slip of about 0.01 in. (0.254 mm) was developed, though with a continuation of slip the projections came into action and with much larger slip, high bond stresses were developed. Abrams concluded that by comparison for similar amounts of slip the pull-out tests and beam tests gave nearly identical bond stresses.

Mylrea[5] published his work on bond and anchorage, in which he summarized the earlier tests and concepts of bond action deduced from them. It was reported that for bars in full length there was a definite relation between bar length and diameter, beyond which no

unit bond stresses needed to be computed, hence the concept of a minimum length in beams was emphasized. Bar extensions and hooks were calculated according to their efficiency as anchors under high bond stress.

Wilkins[8] performed pull-out tests to investigate the bond stress distribution in tubes embedded in concrete cylinders. Plain, fine knurl, heavy knurl and Hi-bond tubes were used in the tests. He employed strain gauges attached in straight lengths of steel tubing to evaluate the load distribution along the anchorage length. The variation of bond stress was then studied from the data given by the load distribution curves. The values were presented for average and maximum bond stress for various embedment lengths and types of tube surface. The character of surface texture was found to be the most important factor in bond. Wilkins came to the conclusion that the bond might be caused by adhesion, friction and mechanical wedging. He also concluded that the average maximum bond stress was dependent on the embedded length but beyond a definite length of bar, which develops resistance to withdrawal from concrete, added length of embedment would provide little extra resistance.

Mains[9] studied the distribution of both tensile and bond stresses along the plain and deformed reinforcing bars in pull-out specimens and beams, using strain gauges attached in a milled groove channel inside the sliced bar. He reported that all deformed bars in pull-out tests failed by fracture without bond failures despite the average bond stresses of 800 psi (5.6 N/mm^2) or more. It was also observed that in beams, measured local maximum bond stress consistently exceeded computed average bond stress by a factor of about two for

all loads after cracking as reported [2] and inferred [5] before. Beams with deformed bars were also reported to fail by fracture of bar or by bar yielding at computed bond stresses varying from 335 to 890 psi (2.4 to 6.3 N/mm^2), while local maximum bond stresses as high as 1800 psi (12.7 N/mm^2) and more were measured. On the basis of all tests Mains concluded that measured local maximum bond stresses could be twice the computed average values or more.

Further experimental[14,15,18] and theoretical[16,17,19] studies concerning the bond strength of various types of reinforcing steel subjected to tension were carried out on pull-out and beam specimens. The theories put forward by several investigators on the bond phenomenon and crack formation in tension zone of a beam subjected to a bending moment, were outlined in reference[20] and, their merits were discussed with particular reference to the distribution and maximum value of bond stress on which the opinions differed considerably.

An experimental study concerning the bond performance of deformed bars in reinforced concrete beams was carried out by Ferguson and Thompson[26]. The chief object of the investigation was to establish the development length required for high strength reinforcing bars in bond in a negative moment region of beams. A series of tests covering 76 beams were conducted. Ferguson and Thompson concluded that the ultimate bond stress varied with square root of concrete cylinder compressive strength. It was observed that the developed bond stress decreased with increasing the development length. The width of beam and clear cover over the bar were found to have a significant effect on the ultimate bond strength, the latter being also particularly

important for the resistance to splitting. Ferguson and Thompson also found that effective development for multiple cutoff would require more length than for continuous bars, and provision of stirrups materially improved the bond resistance.

A theoretical study associated with an experimental work concerning the bond resistance of deformed bars in tension was published in a C.U.R. report[29]. In the experimental part, tests were undertaken to investigate the effect of concrete cover, concrete quality and embedment length with varying diameter and type of deformed bars on 214 specimens. The tests corresponded to a portion of a beam subjected to a shear force constant over the whole length and to a linearly distributed bending moment. It was reported that all tests terminated in the formation of cracks in the concrete starting from the bars and there was no visible slip of the bars. It was found that the concrete cover, concrete quality and embedment length had a significant effect on the ultimate bond stress. An approximate linear relationship was also established between the bond stress and these variables, respectively.

In the theoretical part of the investigation, an equation was derived by computing the bursting force introduced by one rib of a deformed bar to the resistance to splitting of the cover concrete. The derived equation consisted of two parts, one indicating the component of bond stress due to the shear stress over the plain steel surface between the ribs and the other referring to the component of bond stress due to bearing of the ribs. The proposed equation was found to be in a reasonably good agreement with the experimental results. On the other hand, the results also showed that most of the bond resistance

of the ribbed bars was due to the shear stress developed over the plain surface between the ribs rather than the bearing on the ribs, so that little of the load was carried by the ribs.

Ferguson and Breen[31] reported their work on tensile lapped splices in beams with a principal view of determining the required development length for each bar. Tests were made on 35 beams reinforced with high strength large bars in constant moment region, some beams being furnished with stirrups over the splices. It was observed that failure occurred by splitting of the concrete over the splice length. Provision of links did not prevent, but retarded, the splitting and increased the splice length in the order of 20 to 50%, depending on its percentage, and resulted in less violent failure. It was concluded that the bond stress varied with the square root of the concrete cylinder compressive strength (f_{cy}). Contrary to expectation, the tests showed conclusively that the average bond stress on larger bar splices was greater for a given splice length than that developed by smaller ones, within the range of bars used.

The nature of bond failure for deformed bars was discussed in an ACI report compiled by Ferguson et al[32]. The influence of splitting was emphasized and the factors influencing splitting were related. The bond performance and the absolute value of bond resistance were reviewed with reference to splices and other special members. It was reported that a pull-out specimen with deformed bars most often failed by splitting due to the wedging action of the lugs against the concrete or by shearing on the cylindrical surface which the lugs tend to strip out. In contrast, for small bars or top cast bars, or bars with large concrete cover the lugs sheared the concrete and pulled

out without splitting the concrete. It was stated that splitting was not the same thing as bond failure by traditional concept, but it was considered as a normal part of bond resistance since the splitting was the first evidence of bond distress. The clear cover over a deformed bar was found to be significant in connection with splitting resistance.

Ferguson et al. deduced that the ultimate bond strength decreased with increasing the embedment length. It was also reported that the bond capacity of compression bars would normally be greater than the usable bond capacity of tension bars because compression bars could provide additional resistance developed by end bearing. Attention was drawn to the fact that the bond was an extremely variable type of stress, so that it is necessary to investigate many different stress situations.

A detailed investigation concerning the bond stress for various surface configurations of reinforcing bars was carried out by Rehm[35]. Pull-out tests were conducted on bars embedded in concrete cubes in such a fashion that only very short length was in contact with concrete. The experiments were generally confined to ribbed bars prepared by machining. From the tests, the curves representing the relationship between local bond stress and the associated local displacement (i.e. slip) were obtained on very short embedded length of bars and labelled as 'fundamental relationships'. It was reported that the pressure under a rib could be as high as 12 times the concrete cube strength (f_{cu}) and even higher values (up to 16 times the f_{cu}) were observed for large values of slip. He stated that there were two types of the fundamental relationships characterized

by two failure modes. The first type was related to the case (mode one) where shear resistance of concrete was overcome and ribs sheared the concrete. The second form was related to the case (mode two) where the splitting of the concrete specimen occurred due to the bursting action of the bar.

Rehm reported that when the ratio of clear rib spacing to rib height was less than 7, failure occurred by the shearing of concrete along the tops of the ribs. If this ratio was greater than 10, a wedge shaped portion of the concrete tooth under the rib failed in the direction of principal shear stress over a length corresponding to 5 to 7 times the rib height, the subsequent behaviour depending on whether the concrete split. It was stated that failure started as the shear stresses on the fracture surface reached 0.4 to 0.6 times the concrete cube strength. It was found that in case of insufficient concrete cover, the bond could be prematurely destroyed by spalling of concrete due to transverse stresses before the maximum shear resistance was approached. In case of sufficient lateral restraint the concrete teeth between the ribs could be completely sheared off even with widely spaced ribs. The maximum shear resistance was reported to be as high as the magnitude of cube strength and, it was independent of the height and spacing of the ribs as long as the rib height was more than 0.5 mm and rib spacing was more than 2 mm.

Rehm concluded that the bond strength varied with concrete compressive strength. He also proposed an analytical method, on the basis of experimental results, to estimate the magnitude and distribution of bond stress in bars with large embedment lengths (e.g. in beams).

Roberts[36] described the bond phenomenon with reference to plain round, square twisted and ribbed bars from the observations made on a large number of tests. The main differences between the types of reinforcement were reported to be the failure mechanism and enhanced bond strength. Two mechanisms of bond failure for deformed bars were emphasized, namely, type one where concrete allows shearing of the bar provided that unity of concrete is sustained, type two where concrete surrounding the bar permits bursting of the cover. Attention was also drawn to the fact that in type one failure of deformed bars the relevant measurement of bond performance should be based on the amount of slip that could be tolerated in an anchorage in the design practice. Roberts also pointed out the importance of different tests simulating actual conditions to establish the bond performance of deformed bars.

Based on a survey of 67 references suggestions on bond related to several subjects, failure modes, joint details and bar deformations were given in an ACI report[45]. Further work on the bond characteristics of deformed bars and crack formation in the concrete due to presence of them was reported by Lutz[46] and Goto[48].

Roberts and Ho[58] studied tensile lapped joints in beams. Tests were carried out on a simulated block of a beam including the lapped joint. It was observed that in the tests with ribbed bars bond failure occurred by extensive splitting of the concrete cover and the residual bond strength after failure was 25 percent of the ultimate. Square twisted bars followed a similar pattern with less splitting but in this case the residual bond resistance was 75 percent of the ultimate. It was reported that concrete cover had a signifcant effect

on the bond resistance of tensile lapped joints, such that increasing the cover from 1 to 3 times of bar size led to 30% increase in the ultimate strength for ribbed bars, while doubling cover ratio for square twisted bars caused an increase of 50%. Provision of links was found to improve the bond strength as well as controlling the bursting effect. Roberts and Ho suggested that a tensile lapped joint could be considered as two anchorages back to back rather than overlapping side by side, such that each anchorage was half the length of the lapped joint and produced approximately half the total stress developed by the lapped joint.

Losberg and Olsson[65] suggested that the anchorage bond capacity of deformed bars was limited to one of two failure modes, namely, slip failure and splitting failure. It was emphasized that in a beam the bond failure occurred as the splitting of the concrete cover proceeded throughout the anchorage zone along the bar due to bursting forces exerted by the lugs, which yielded much smaller anchorage capacity than bond slip failure. To varify both types of failure, tests were carried out with particular reference to the geometrical configuration properties of reinforcement. The pull-out test with short anchorage lengths resulted in pure shear-slip failure and, on this basis, it was regarded as inadequate to simulate the bond strength in beams since no splitting occurred in the surrounding concrete.

To investigate the bond stress-slip relationship Mirza and Houde[66] conducted experiments on 62 standard tension specimens with a single deformed bar of varying size subjected to an axial force at both ends. The bond stress at the steel-concrete interface was reported to reach maximum value at slip of 0.0012 in. (0.0305 mm). Before the

peak value was reached, the relationship between the bond stress and the local slip was given by an equation derived from experimental data. Mirza and Houde reported that the inspection of the sliced specimens indicated no evidence of polished surfaces due to sliding or any powdery areas on account of crushing. On this basis they concluded that the slip between steel and concrete was due to the bending of the comb-like structures of the first layers surrounding the bar. This could be unlikely in the case of compression members provided that the bond failure takes place as the bar shears the concrete.

Kemp and Wilhelm[67] studied the longitudinal bond splitting of large deformed bars on specimens simulating an end portion of a beam subjected to bending. The phenomenon of splitting due to the internal radial forces produced by the lugs was examined with reference to various parameters. To establish a method for predicting the bond splitting and using this as a basis for developing design criteria at both the initiation of cracking and at ultimate bond load, 36 cantilever test specimens were employed. The statistically evaluated experimental data yielded an expression for the average bond stress at first visible bond crack in terms of concrete cylinder strength (f_{cy}), concrete cover, bar diameter, area and yield stress of stirrups with a correlation coefficient of R = 0.849. Similarly an analysis of generalized regression equations against the ultimate load data produced a new equation in terms of the same parameters for the ultimate average bond stress with a better correlation coefficient of R = 0.926. It was concluded that the proposed empirical equations could predict the limit states of cracking and ultimate load strength in beams with multiple reinforcing bars in a single layer.

Jimenez, White and Gergely[68] analysed other investigators experiments statistically with the aid of an assumed model of behaviour and obtained an equation to estimate the tensile stress in a bar at the time of splitting failure in beams. The proposed expression was found to predict 30% conservative results for specimens having a concrete cover less than or equal to bar diameter.

Further experimental work was then carried out on a splitting bond failure of large deformed bars[69] and the effect of the geometrical properties of deformed bars on bond[70,75], and on bond behaviour of ribbed bars under repeated loads[72].

Tepfers[73] reported a theoretical investigation concerning the splitting failure of concrete cover due to the radial component of bond forces exerted into the surrounding concrete from an anchored deformed bar. To determine the cracking resistance of the concrete cover the analysis was based on a concrete ring model such that radial components of the bond forces were balanced against the rings of the tensile stress in the concrete. It was considered that the ribs could split the cover when the surrounding concrete resistance was exceeded, and that this is most likely the case in an ordinary beam. In the analysis, the bond action based on the formation of the cover cracks, was handled for three different cases, namely uncracked elastic stage, plastic stage and partly cracked elastic stage for the concrete. From the comparison of experimental results Tepfers concluded that concrete cover cracks along the deformed bars in the bond region could be determined by employing the mean of the values obtained for the plastic and partly cracked elastic stages.

Later, Tepfers[83] presented another analytical investigation to predict the strength of tensile deformed bar laps with confining reinforcement. It was stated that lap confining reinforcement could not prevent but only delay the cracks. Based on the comparison of experimental and theoretical results, he concluded that the bond failure load could be determined from theoretical ultimate pattern analysis including the contributions of the splitting resistance from concrete and confining steel.

Further theoretical and experimental studies concerning the bond performance of reinforcing bars in tension members have been published by several investigators[78,80,81,86]. Somayaji and Shah[80] proposed an analytical method to predict the cracking response and the tension-stiffening effect in a reinforced concrete member subjected to uniaxial tension. Then, uniaxial tests were performed on reinforced mortar specimens to verify the method, which was reported to compare well with the experimental data. The theoretical local bond stress-slip relationship appeared to be nonlinear and was not unique at every section of the tension member. Reynolds[81] tested 39 beams with tor bars and proposed a theoretical lower bound to bond strength. He concluded that laps and single bar anchorages showed similar performance and same length could be used for both. Reynolds recommended a change in the CP110[56] bond requirements for deformed bars, on basis that bond stresses were too high when the cover was small and too low when the cover was large. He also proposed a design equation which considered the effect of cover and transverse steel.

Diederichs and Scneider[79] examined the bond resistance of various types of reinforcement at high temperatures. Pull-out tests with

short embedment lengths were conducted in the temperature range 20 to 800°C. The bond stress-slip curves for each type of bar were obtained at elevated temperatures. At room temperature, i.e. at 20°C for ribbed tor steel, the average bond stress increased with increasing the slip and reached to almost 30 N/mm^2 at a slip of 1.8 mm. The prestressing deformed bars behaved in a similar manner and the maximum average bond stress attained at 2.9 mm slip was 18 N/mm^2. Rusted plain round bars demonstrated different bond performance and the bond stress reached 5.5 N/mm^2 as a maximum at 0.3 mm slip then reduced gradually to nearly 4 N/mm^2 at a slip of 1.8 mm. From the force-slip relationships at variable temperatures it was concluded that failure could occur in the bond region at relatively low temperatures.

Further work on bond in tension covering recent papers dealing with wide range of parameters and various load conditions are available in reference(82).

1.2.3 Bearing Strength of Concrete

The bearing strength of concrete has been studied by various investigators. One of the pioneering works in this field was reported by Meyerhof(10) on the bearing capacity of concrete and rock. Based on the Coulomb-Mohr's theory of rupture, he proposed a method to determine the ultimate bearing strength of footings on blocks of various sizes and compared the method with the results of previously published model tests. With a veiw to obtaining further information for large blocks and in order to check the proposed analysis, Meyerhof also carried out a series of tests on a circular model footing on

plain and reinforced concrete blocks of various sizes. The proposed method indicated that the bearing capacity increased in direct proportion to the ratio of block thickness to footing width. It was also concluded that when the splitting of the material was prevented, the ultimate load increased with the size of the block and approached the limiting value for a footing on a semi-infinite solid.

Shelson[22] studied experimentally the maximum bearing pressure that could be sustained by concrete footings loaded through steel base plates. The test results of the concrete blocks bedded on massive steel bases showed that for a given ratio of footing area to loaded area, the ultimate bearing pressure increased as the depth to width ratio decreased. He proposed an empirical formula that until recently formed the basis in American design practice in this subject. Shelson concluded that bearing capacity increased with increasing the ratio of the footing area to loading area until this ratio reaches 30, then the bearing pressure approaches a limiting value.

Further work on bearing capacity of concrete blocks was reported by Au and Baird[23]. Using two concrete mixes with different maximum aggregate size in the specimens, they carried out tests on 60 square concrete blocks with the ratio of the block area to contact area ranging from 2 to 16. It was found that the bearing capacity of the concrete increased with an increase in the ratio of block area to loaded area. Au an Baird also proposed a theoretical approach based on the hypothesis of the formation of an inverted pyramid beneath the loaded area, which yielded an equation for an approximate evaluation of the bearing capacity.

Ersoy and Hawkins[24] in their discussion of the work published by Au and Baird[23] suggested that the bearing capacity of the concrete reaches a limiting value as the ratio of the block area to the contact area increased indefinitely. It was pointed out that the formation of the inverted pyramid would be prevented when the ratio of the block thickness to the side dimension of the loading plate was small, so that failure in such cases would occur by crushing of concrete beneath the loading plate. However, it was concluded that the depth of the loaded block had no effect on the bearing capacity of the concrete, so long as the block was deep enough to ensure that the formation of the inverted pyramid was not restricted.

An extensive experimental and analytical investigation on the bearing strength of the concrete was carried out by Hawkins[34]. He conducted tests on some 100 concentrically loaded and 130 eccentrically loaded concrete blocks, in which the principal variables were concrete strength, size of test specimen and size and shape of the loading plate. He demonstrated that Shelson's[22] approach was conservative when estimating the bearing strength in the range of the lower values of the ratio of concrete area to base plate area, i.e. ratio of unloaded to loaded area. Hawkins derived an approximate theoretical analysis based on a failure criterion suggested by Cowan[12], to predict the ultimate bearing strength of concrete over a broad range of thicknesses and ratio of concrete area to base plate area (i.e. ratio of unloaded to loaded area). An equation proposed on the basis of the theoretical approach was reported to estimate the concrete bearing strength satisfactorily for the ratios of unloaded to loaded area less than 40. Hawkins' equation is reproduced in chapter 5 and employed in a simplified form to predict the ultimate end

bearing resistance of the concrete under column bars.

1.2.4 Current Codes

In this section British[56] and American[61] codes are reveiwed with particular reference to the bond stress in reinforced concrete column bases. The traditional concept of bond stress is shear stress, defined as the change in force in a bar divided by the product of the bar perimeter and the anchorage length of the bar over which the change in force occurs. It has been conventional practice for deformed bars to express the bond stress as the stress per unit area of the nominal bar surface, which is equivalent to that of plain round bar of identical diameter by ignoring the extra surface produced by the lugs and ribs.

The British code of practice CP110:Part 1:1972[56] defines two types of bond stress, namely, local bond and anchorage bond. Local or flexural bond stress is caused by the change of force in reinforcing bars due to the variation in moment along a structural member. Anchorage bond stresses develop as the force in a straight bar is transferred by bond to the surrounding concrete. In bar connections the force in a bar is transferred by bond to the adjacent concrete and thus by bond to the other bar in a lapped joint.

In the British code, the design ultimate bond stresses are given in table 22 with respect to the concrete grade, i.e. cube strength of concrete for plain and deformed bars in tension and in compression, and the values of bond stress are higher for compression bars than tension bars. The code allows 30% increase in the values of design

ultimate bond stresses given in table 22 for type 2 deformed bars, e.g. ribbed bars.

According to CP110, the length of a lap in compression reinforcement is required to be at least equal to the anchorage length needed to develop the appropriate anchorage bond stress taken from table 22 in the smaller of the two bars lapped, and in no case should it be less than 20 times the bar size plus 150 mm (i.e. $20\phi + 150$ mm).

CP110 considers three strength conditions for the design of independent column bases, namely resistance to bending, shear and bond and anchorage. The code describes the critical section for local bond and specifies the local bond stress to be checked in tension reinforcement for bending, against the values given in table 21. On the other hand, despite the fact that the ultimate design bond stresses for compression bars are given, the code makes no mention of anchorage bond stress in the clauses specifically relating to the design of column bases.

In America, where only deformed bars are now used, the American code of practice ACI318-77(61) considers not only the resistance to bending and shear but also the development length of the compression reinforcement in the design of the column bases. As a matter of fact, specific emphasis is placed on the need for the footing depth to be sufficient to ensure a safe bond stress for the column starter bars in the transference of the compression load.

The code states that all forces applied at the base of column shall be transferred to top of the supporting footing by bearing (i.e.

compression) on the concrete and by reinforcement of the column. The code specifies that where the transfer of force is accomplished by reinforcement, the development or the anchorage length (l_a) of a deformed bar required in compression is $l_a = 0.02\ f_y\ \phi / \sqrt{f_{cy}}$ in. ($l_a = 0.24\ f_y \phi / \sqrt{f_{cy}}$ mm) but not less than $l_a = 0.0003\ f_y\ \phi$ in. ($l_a = 0.044\ f_y\ \phi$ mm) or $l_a = 8$ in. ($l_a = 203.2$ mm). Where f_{cy} is the 6x12 in. concrete cylinder compressive strength in psi, f_y is the specified yield strength of steel or the stress corresponding to a strain of 0.35% for f_y>60000 psi unless it is determined by a test on full size bar, and ϕ is the nominal diameter of bar in in. The expressions for l_a in brackets are the corresponding SI metric equivalents, in which f_{cy} and f_y in N/mm^2 and ϕ in mm. According to the code hooks are not considered effective in adding to the compressive resistance of reinforcement.

1.2.5 Theoretical Studies Indirectly Related to Present Work

In 1936, Mindlin[3] published his theoretical work on a solution of the three dimensional elasticity equations for homogeneous isotropic solid for the case of a concentrated force acting in the interior of a semi-infinite solid. The Mindlin solution[3] for a force at a point in the interior of a semi-infinite mass, has found many practical applications in the study of the load transfer and settlement behaviour of piles and in certain problems of soil mechanics.

One of the first applications of the Mindlin equation[3] to load transfer in end-bearing steel H-piles was reported by D'Appolonia and Romualdi[27]. They proposed a method for computing interaction forces in the transference of load from an end-bearing pile without tip

movement to the surrounding soil. The pile was divided into n equal segments of length, and it was assumed that interaction shear stress between the pile and soil was constant over the segment length and resultant force was taken to act at the mid-point of the segment. The vertical displacement of the soil at any location due to a unit force at another location was referred to the pile centre line, considering that the pile was narrow compared with its length, and the vertical displacement coefficients of the soil were obtained from the Mindlin equation(3). The criterion from which they computed interaction forces was that there be no relative movement between the pile and the surrounding soil, which produced a set of n simultaneous equations for the interaction forces. The solution of these equations yielded the interaction forces in terms of the applied load.

Thurman and D'Appolonia(30) extended the previous method of analysis(27) to compute the movement of friction and end-bearing piles under any load, embedded in uniform or staratified elastic soils. Friction i.e. interaction forces on the pile-soil interface were assumed to be replaced by a series of point forces on pile elements. Slip without change in the friction forces was considered beyond the element failure, defined by a Coulomb failure stress on the pile-soil interface. A compatible force-displacement realtionship was maintained between non-failed elements and the soil in the analysis. Thurman and D'Appolonia defined the ultimate pile load as the load which caused the friction forces on all pile elements reaching slipping condition and the pile tip force reaching a punching condition. They concluded that the proposed method could be used for a wide range of pile-soil problems.

Following the rapid development in digital computers over the past two decades, the focus of interest was concentrated on more sophisticated methods based on elastic theory for the analysis of piles with regard to different aspects of the load displacement behaviour for a wide range of parameters. Using the Mindlin equations[3], a theoretical investigation concerning the settlement behaviour of a single axially loaded incompressible pile in an ideal elastic soil mass was published by Poulos and Davis[37]. They assumed that the pile consisted of n equal cylindrical elements each acted upon by a uniform shear stress and a circular base subjected to a uniform vertical stress. It was also assumed that the sides of the pile were perfectly rough while the pile base was perfectly smooth, on which no shear stress would develop. It was stated that consideration of compatibility of both vertical and radial displacements yielded a solution for the distribution of shear stress and the settlement of the pile which was almost identical with the solution obtained by considering compatibility of vertical displacement alone. Thus only the compatibility of vertical displacement was taken into consideration in the analysis.

The vertical displacement influence factors at the mid-height of the periphery of each element due to all the other elements comprising the pile, were computed from the integration of the Mindlin equations[3] for the displacement due to a point load in a semi-infinite elastic mass. To obtain the solutions for the distribution of shear stress on the pile shaft and the normal stress on the base and the displacement of the pile, the displacement of the soil adjacent to the pile was equated to the displacement of the pile itself. Then, an (n + 1) order of matrix for the vertical displacement of the soil

adjacent to all pile elements was established. For the pile itself, the displacement of all points was considered uniform. Then putting this displacement equal to unity, final equation was obtained by equating the displacement of the pile and the soil adjacent to pile, the solution of which produced the distribution of shear stress and the normal stress for the condition of unit displacement. Using the equilibrium condition between the applied load on the pile and the stresses on the pile, the vertical displacement for unit applied load was then obtained.

It was shown that the distribution of shear stress was varied with length to diameter ratio of the pile. For slender piles the shear stress increased gradually from a minimum near the top of the pile to a maximum near the base of the pile. As the length to diameter ratio decreased, the shape of the shear stress distribution changed, and for values less than 5 the shear stress concentrated near the pile ends with a minimum value near the centre.

The effect of the length to diameter ratio of the pile, Poisson's ratio of the soil and the depth of the soil layer on the behaviour of the pile were studied and influence factors for the settlement of the pile in a semi-inifinite mass and in a finite layer were given, which were relevant to the case of piles in soft clay. The effect of an enlarged base on the behaviour of a single pile was found to be of major significance only for relatively short piles. The elastic analysis was extended to include the effect of local shear failure between the pile and cohesive soil, similar to that previously proposed[30], and the load-settlement behaviour up to failure was given for a typical case of a floating pile in a saturated clay loaded

under undrained conditions.

Following the previous investigations dealing with the behaviour of single incompressible piles[37] and incompressible pile groups[38], Mattes and Poulos[39] reported their work on the settlement of a single floating compressible pile. They used linear elastic theory to examine the behaviour of a compressible pile in an ideal elastic soil mass. The principal object of the work was to study the effect of compressibility on load transfer and settlement of the pile with particular interest given to the difference between a compressible and incomressible pile. Emphasis was also placed on the piles with an enlarged base. In their analysis, Mattes and Poulos also divided the bar into n equal cylindrical elements, each element being subjected to uniformly distributed shear stress on its surface and the circular pile base having a uniform vertical stress. Only the vertical displacement compatibility was taken into consideration for the reason reported before[37], and these displacements were similarly calculated at the midpoint on the surface of each element and at the centre of the base. Then the vertical displacement of the soil due to the shear stress on the pile shaft was obtained from the Mindlin equation[3], as proposed by Poulos and Davis[37] in relation to the analysis of an incompressible pile.

Considering vertical displacement compatibility between the pile and the soil adjacent pile, equilibrium and compatibility equations were written for all pile elements. After the necessary manipulations, the resulting equation for the vertical displacement of the soil along the pile was obtained. In determining the displacement of the pile itself, only axial compression of the pile was assumed. Simi-

larly, using equilibrium and compatibility conditions the governing equations for all pile elements were obtained. In these equations the terms indicating the vertical displacement of all pile elements were expressed in finite difference form. After the necessary manipulations, an equation in terms of the stresses on all pile elements, applied load and the vertical displacement of all pile elements were obtained. Considering that elastic conditions prevail in the pile and the surrounding soil, the displacement of the soil was equated to the displacement of the pile and the final equation was obtained, the solution of which yielded unknown stresses acting on the pile surface. The displacement distribution along the pile was computed from the related equation. The majority of the solutions were given for purely elastic behaviour. However, some solutions were also given for piles in which local yield along the sides, but not of the base, was considered in a similar manner to that described by others.(27,30,37)

Poulos and Davis found that the distribution of shear stress along the pile varied with the pile stiffness factor $K_p = (E_{pile}/E_{soil})R_A$, which is the measure of pile compressibility. It was shown that for $K_p = 5000$ the distribution of shear stress along the pile was almost uniform, with a maximum value occuring near the tip. Conversely, for $K_p = 50$ the shape of the shear stress distribution altered, with very high shear stresses occuring near the top of the pile and small values near the tip. Hence, as the pile became more compressible the proportion of the load transferred to the base rapidly decreased.

Mattes and Poulos showed that for a very compressible pile ($K_p = 10$) the layer depth had very little effect on the settlement of the

pile. Thus for such piles, they came to the conclusion that the effect of layer depth on settlement might be ignored and the influence factors for a pile in a semi-infinite mass could be used for all layer depths.

It was found that the load-settlement relationship for a pile loaded to failure in a saturated clay under undrained conditions, was influenced considerably by the compressibility of the pile, and as the K_p decreased, local yield occurred at smaller loads with the load-settlement curve becoming nonlinear over a larger range. It was also found that the reduction in settlement due to an enlarged pile base was virtually independent of K_p.

Further theoretical work based on Mindlin equations[3] was reported by Poulos[40] on the behaviour of a single axially loaded end-bearing pile, Poulos and Mattes[52,53] on the settlement and load distribution analysis of pile groups and, Butterfield and Banerjee[54] on the elastic analysis of compressible piles and pile groups with floating caps spaced in an arbitrary manner.

Rieve[44] integrated the Mindlin vector function[3] and obtained a new function suitable for the analysis of a uniform continuous load acting at the boundary of an elastic, isotropic half-space. Using this new function he proposed a method for the analysis of the pull-out test, which was based on the theory of elasticity. The solution of bond problem for a bar in tension was obtained by expressing the equilibrium equations for points spaced at an interval along the embedment length of the bar and solving the shear stresses at these points. Bond stresses were found to vary with the elastic modulus

and Poisson's ratio of both steel and concrete. It was shown that Poisson's ratio was not of primary importance and a non-dimensionalized stress distribution was obtained, depending only on the elastic modulus of concrete.

A method based on Rieve's functions [44] for semi-inifite solid, was proposed by Ivering[77] for the elastic analysis of the bond stress of a thick-walled tube embedded at the surface of an elastic, semi-infinite medium, with a view to designing a compression-tube rock anchorage. He considered three dimensional compatibility between the tube and the anchorage medium and obtained an equilibrium equation for an embedded tube segment, from which bond stresses acting on the tube could be calculated. The general solution obtained was related to the vector function for a uniform linear load acting perpendicularly to the surface of an elastic half-space. It was reported that the solution was in agreement with the equations derived independently for the cases of one dimensional (linear) compatibility[44]. The equilibrium equation obtained for a tube segment embedded at the surface of an elastic half-space was then transformed to a form suitable to solve the bond stresses for a tube anchorage embedded at some distance from the surface.

The computed bond stress curve for a compression-tube anchor embedded in an elastic half-space was compared with the bond stress curve obtained experimentally from a test on two concrete blocks with reinforcing stirrups, in which strains on a steel tube surface was recorded with strain gauges. There was considerable discrepancy between the two curves, however, on both curves bond stresses along the anchorage length decreased to a negligible magnitude at approxi-

mately the same distance from the point of load application.

1.3 Conclusions

It is evident from the review of the published work that the bond performance of deformed bars in tension has been the subject of extensive investigations, providing a vast volume of numerical data and information. In contrast, the study of bond in compression has received very little attention. In this field, recently undertaken studies have concentrated on compression lapped joints in reinforced concrete columns, which eventually produce a splitting type of bond failure similar to tensile lapped joints, despite the several significant differences between the two. The literature review has also shown that a considerable number of tests exist for shear, bending and bond strength of tensile reinforcement in a foundation. However, there is a lack of information and shortage of experimental results on the performance and the value of bond strength of deformed bars in the base. The problem of the magnitude and distribution of bond stress in the anchorage length of the column longitudinal bars in the foundation has not been closely studied. In fact, to date, no work on this particular topic has been carried out except a pilot study[76] with square twisted bars.

It is therefore concluded that there is a need to undertake a more fundamental investigation of bond in foundations, and this investigation should consist of both square twisted and ribbed bars.

CHAPTER 2

EXPERIMENTAL PROCEDURE

2.1 Introduction

This chapter deals with the experimental procedure employed throughout the research project. The tests were carried out on independent square foundations with high strength deformed bars.

The experimental work consists of 36 full scale foundations, subdivided into two main parts. Part one contains twelve test specimens performed with square twisted bars. In the second part twenty four tests are conducted with high strength ribbed bars. Test specimens are denoted 'Si-j' in part one and 'SRi-j' in part two, respectively. Test structures, instrumentation, testing rigs and test procedure are described in this chapter and all relevant materials are referred to.

2.2 Description of Test Specimens

The test specimens were designed to suit the facilities provided in the laboratories of the Civil Engineering Department. In general, each test structure consisted of a column cage, forming a square cross section with four deformed bars welded to a 20 mm thick steel plate on the top and, either a plain or reinforced concrete foundation. However for 4 of those in part two the column cage was also concreted to form a short reinforced concrete column. General views of the specimens are shown in figures (2.1) and (2.2), respectively. According to the type of reinforcement and the variables investigated

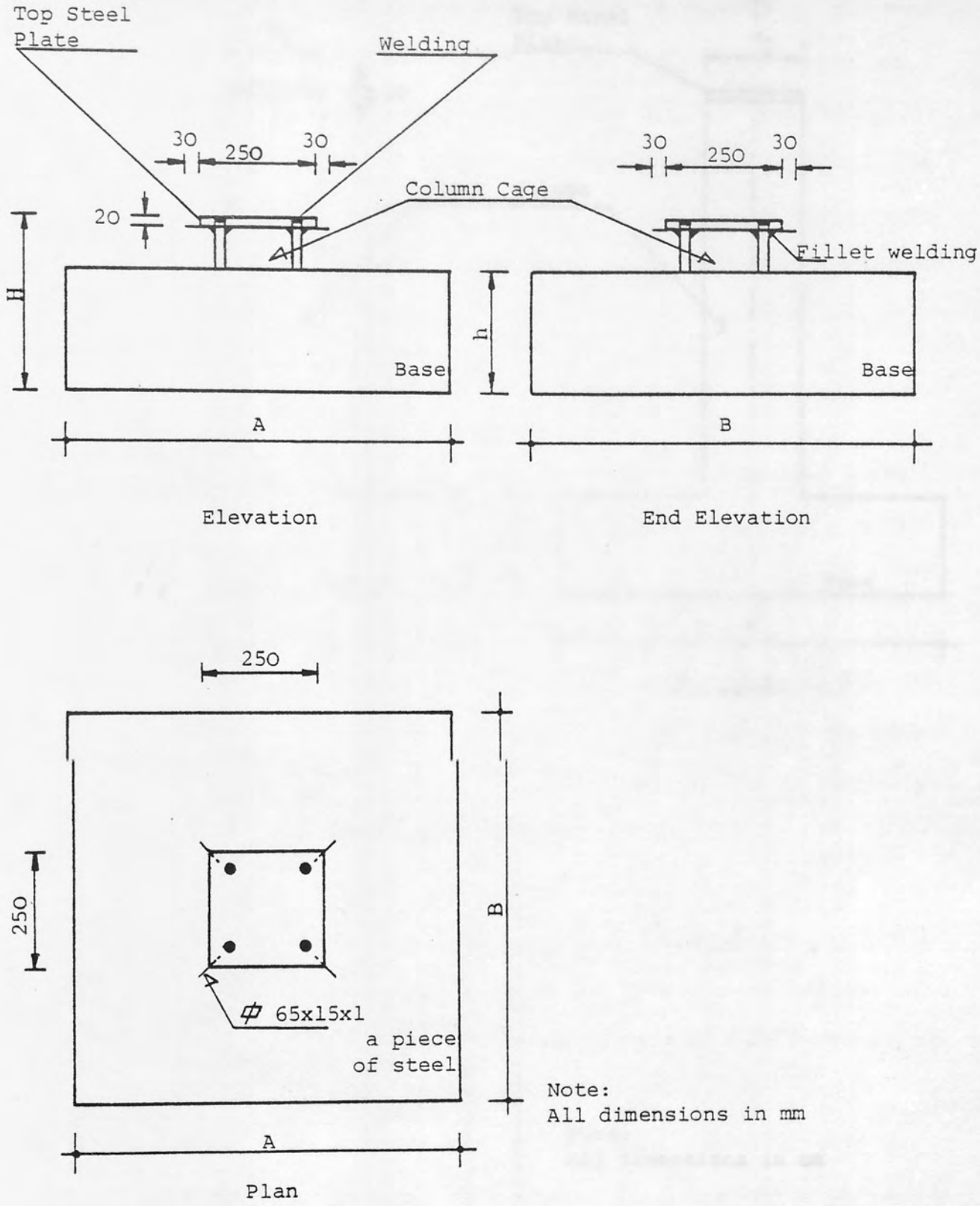

FIGURE 2.1: GENERAL VIEWS OF TEST SPECIMENS IN PART ONE AND FOR THOSE WITHOUT A SHORT COLUMN IN PART TWO RESPECTIVELY

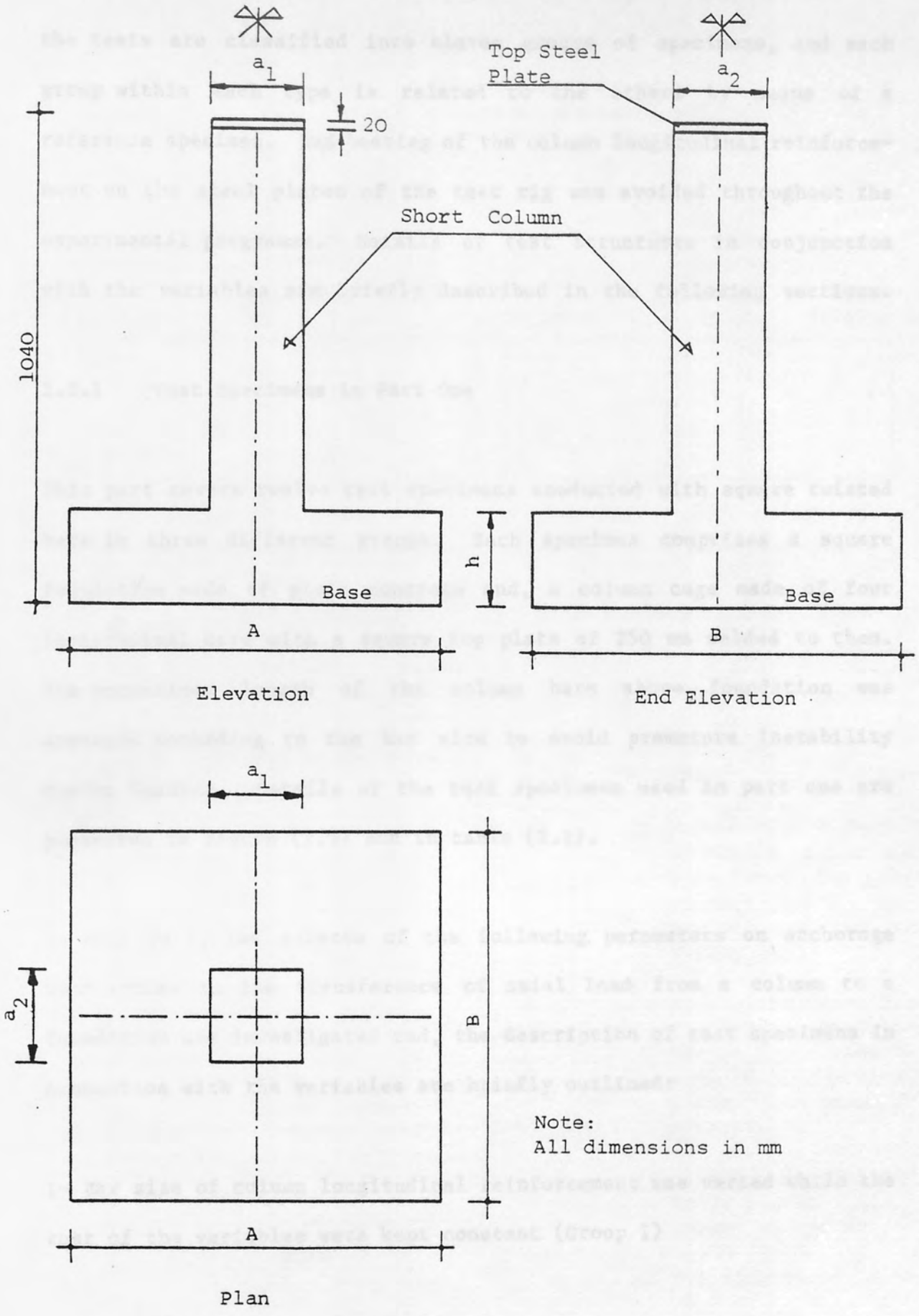

FIGURE 2.2: GENERAL VIEWS OF TEST SPECIMENS WITH A SHORT COLUMN IN PART TWO

the tests are classified into eleven groups of specimens, and each group within each type is related to the others by means of a reference specimen. End bearing of the column longitudinal reinforcement on the steel platen of the test rig was avoided throughout the experimental programme. Details of test structures in conjunction with the variables are briefly described in the following sections.

2.2.1 Test Specimens in Part One

This part covers twelve test specimens conducted with square twisted bars in three different groups. Each specimen comprises a square foundation made of plain concrete and, a column cage made of four longitudinal bars with a square top plate of 250 mm welded to them. The unconfined length of the column bars above foundation was arranged according to the bar size to avoid premature instability during loading. Details of the test specimens used in part one are presented in figure (2.3) and in table (2.1).

In this part, the effects of the following parameters on anchorage bond stress in the transference of axial load from a columm to a foundation are investigated and, the description of test specimens in connection with the variables are briefly outlined:

1- Bar size of column longitudinal reinforcement was varied while the rest of the variables were kept constant (Group 1)

In this group the high strength square twisted bars of 16 mm, 20 mm, and 25 mm were used in four tests, two of the test being performed with the 25 mm bars. Having a size of 800 mm square, the overall

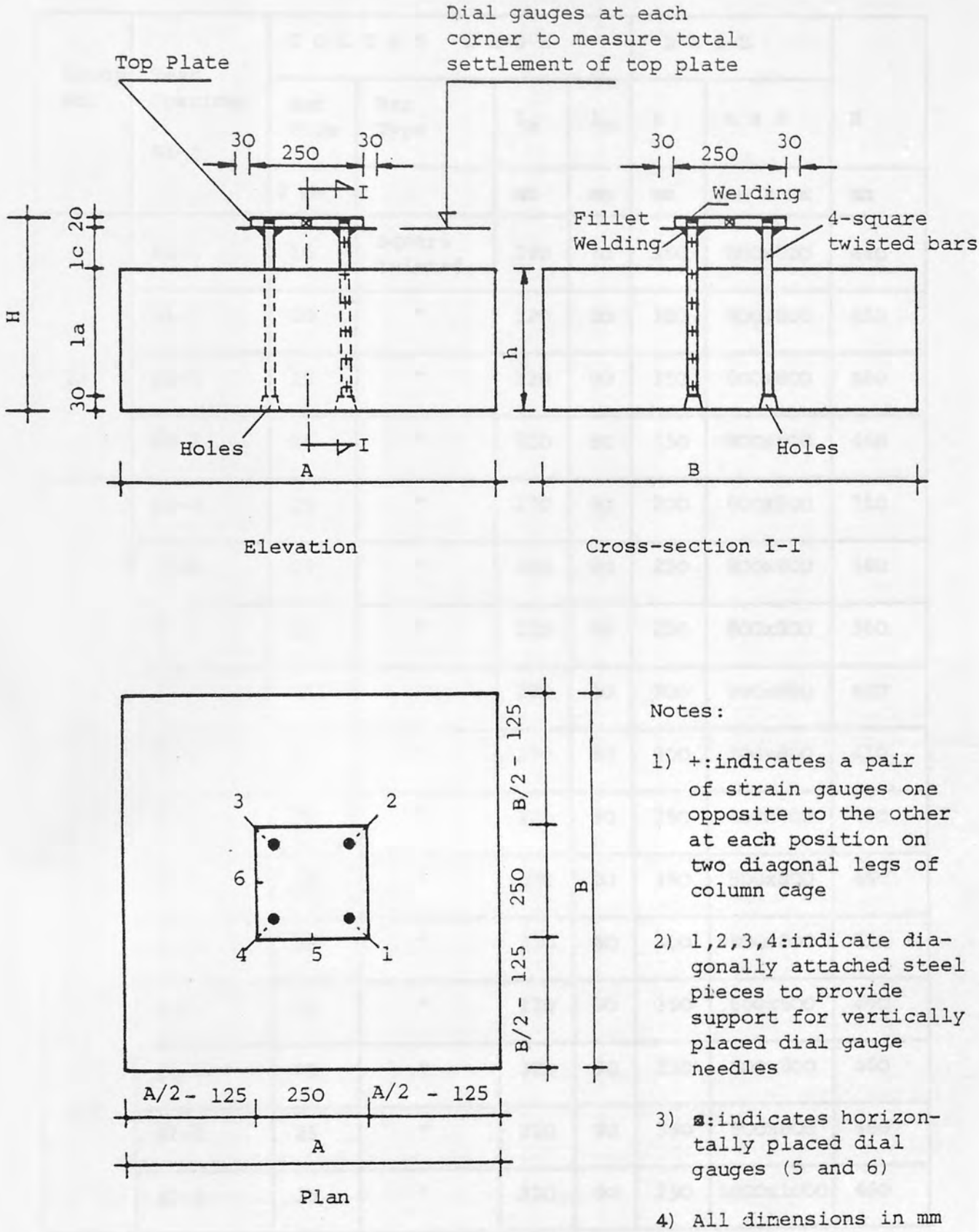

Notes:

1) +:indicates a pair of strain gauges one opposite to the other at each position on two diagonal legs of column cage

2) 1,2,3,4:indicate diagonally attached steel pieces to provide support for vertically placed dial gauge needles

3) ⊠:indicates horizontally placed dial gauges (5 and 6)

4) All dimensions in mm

FIGURE 2.3: DETAILS OF TEST SPECIMENS WITH SQUARE TWISTED BARS IN PART ONE

Group No:	Test Specimen Si-j	COLUMN CAGE				BASE		H
		Bar Size	Bar Type	l_a	l_c	h	A x B	
		ϕ mm		mm	mm	mm	mm x mm	mm
I	S1-1	16	Square twisted	320	70	350	800x800	440
	S1-2	20	"	320	80	350	800x800	450
	S1-3	25	"	320	90	350	800x800	460
	$\overline{S}$1-3	25	"	320	90	350	800x800	460
II	S2-4	25	"	170	90	200	800x800	310
	S2-1	25	"	220	90	250	800x800	360
	$\overline{S}$2-1	25	"	220	90	250	800x800	360
	S2-2	25	"	270	90	300	800x800	410
	$\overline{S}$2-2	25	"	270	90	300	800x800	410
	S1-3	25	"	320	90	350	800x800	460
	$\overline{S}$1-3	25	"	320	90	350	800x800	460
	S2-3	25	"	370	90	400	800x800	510
III	S3-1	25	"	320	90	350	600x600	460
	S1-3	25	"	320	90	350	800x800	460
	$\overline{S}$1-3	25	"	320	90	350	800x800	460
	S3-2	25	"	320	90	350	1000x1000	460

TABLE 2.1: SPECIFICATIONS OF TEST SPECIMENS IN PART ONE

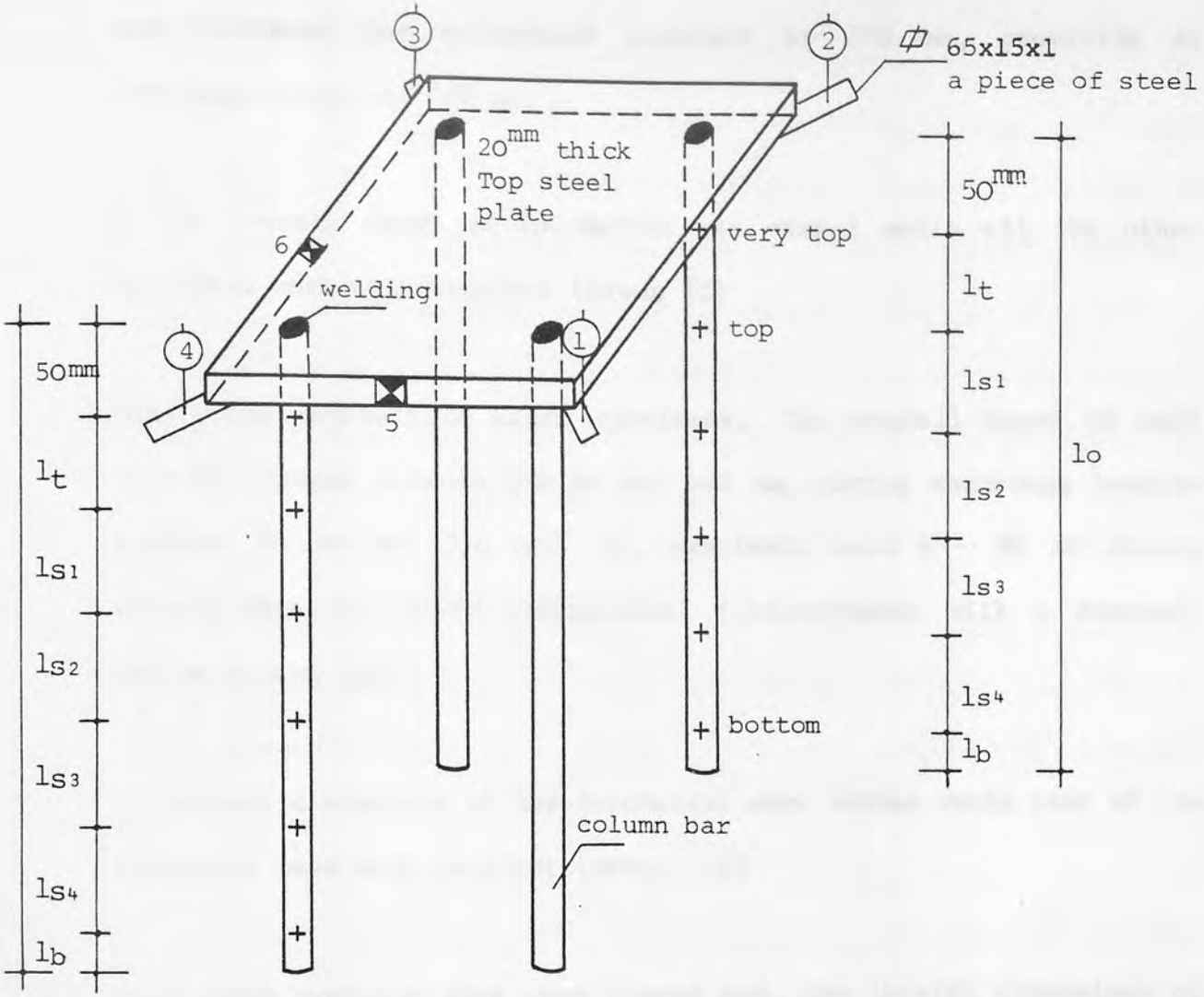

Si-j	l_t	l_{s1}	l_{s2}	l_{s3}	l_{s4}	l_b	l_o	NOTES
	mm	mm	mm	mm	mm	mm	mm	
S1-1	51	71	71	71	71	25	410	+: indicates a pair of strain gauges at each position on two diagonal legs ▣: indicates horizontally placed dial gauges (5 and 6) 1,2,3and4: indicate vertically placed dial gauges at each corner of top plate
S1-2	61	71	71	71	71	25	420	
S1-3	71	71	71	71	71	25	430	
$\overline{S}$1-3	71	71	71	71	71	25	430	
S2-4	75	65	65	-	-	25	280	
S2-1	70	65	65	65	-	15	330	
$\overline{S}$2-1	70	65	65	65	-	15	330	
S2-2	70	60	60	60	60	20	380	
$\overline{S}$2-2	70	60	60	60	60	20	380	
S2-3	80	80	80	80	80	30	480	
S3-1	71	71	71	71	71	25	430	
S3-2	71	71	71	71	71	25	430	

FIGURE 2.4: POSITION OF STRAIN AND DIAL GAUGES ON COLUMN CAGE FOR SPECIMENS CONDUCTED WITH SQUARE TWISTED BARS IN PART ONE

base thickness was maintained constant at 350 mm, providing an anchorage length of 320 mm.

2- The overall depth of foundation was varied while all the other variables were kept constant (Group II)

This group consists of eight specimens. The overall depth of base slab is changed between 200 mm and 400 mm, giving anchorage lengths between 170 mm and 370 mm. All specimens have 4 - 25 mm square twisted bars as column longitudinal reinforcement with a constant 800 mm square base.

3- Lateral dimensions of the foundation were varied while rest of the variables were kept constant (Group III)

This group contains four test pieces and, the lateral dimensions of the foundation are varied from 600 x 600 mm to 1000 x 1000 mm. Each specimen has 4 - 25 mm square twisted bars as column longitudinal reinforcement with a constant overall base thickness of 350 mm, providing an anchorage length of 320 mm.

In each specimen a pair of strain gauges were attached at a number of positions on two diagonal legs of column cage as shown in figure (2.4). They are described under the heading of instrumentation in section 2.7.

2.2.2 Test Specimens in Part Two

This part consists of twenty four test specimens with high strength

ribbed bars. They are divided into eight groups according to the variables investigated. In six of the eight groups each test structure contains a square foundation and a column cage similar to those in part one. In these groups designated IV to IX the unconfined length of column bars was arranged according to the bar size used in the specimen to avoid premature instability during loading. Details of test specimens in groups IV to IX are given in figures (2.5) and (2.6), and in tables (2.2) and (2.3).

In the other groups designated X to XI each test specimen consists of a short reinforced concrete column and a reinforced concrete foundation. Details of test specimens in these groups are given in figure (2.8).

In this part the effect of the following parameters on anchorage bond stress in foundations are investigated and, the test structures in connection with the variables are briefly described:

1- Bar size of column longitudinal reinforcement is varied while all the other variables are kept constant (Group IV)

This group consists of three specimens. In the specimens the ribbed bars of 16 mm, 20 mm, and 25 mm are used, respectively. Having a size of 800 mm square, the overall base thickness is maintained constant at 200 mm, providing an anchorage length of 170 mm. The base is made of plain concrete.

2- The overall depth of foundation is varied while the rest of the variables are kept constant (Group V)

This group covers three specimens. The overall depth of base is changed between 200 mm and 350 mm, giving anchorage lengths between 170 mm and 320 mm. All specimens have 4 - 25 mm ribbed bars as column longitudinal reinforcement with a constant 800 mm square base made of plain concrete.

3- Lateral dimensions of the foundation are varied while all the other variables are kept constant (Group VI)

The lateral dimensions of the foundation are varied from 600 x 600 mm to 800 x 800 mm in two tests. The specimens made of plain concrete, have the same type and amount of reinforcement as group V but, the overall base thickness is maintained constant at 350 mm, giving an anchorage length of 320 mm.

4- Percentage of tension reinforcement in foundation (ρ_b) is varied while the rest of the variables are kept constant (Group VII)

Each specimen has 4 - 25 mm ribbed bars as column longitudinal reinforcement with a constant 800 mm square base and, required number of 12 mm ribbed bars in each direction as tension reinforcement. This group is further divided into two sub-groups, namely VIIa and VIIb. In group VIIa the overall base thickness is kept constant at 350 mm and, the percentage of tension reinforcement (ρ_b) is varied from zero to 0.642 in four specimens. On the other hand in group VIIb, the overall base thickness is maintained constant at 200 mm while the percentage of tension reinforcement (ρ_b) is varied from zero to 1.253 in four specimens. Cover to the tension reinforcement

is 30 mm in both.

5- Amount of links provided on column cage in the embedment length is varied while other variables are maintained constant (Group VIII)

The links used in the specimens are made of 8 mm ribbed deformed bars. This group is also divided into two sub-groups, namely VIIIa and VIIIb. In group VIIIa, the number of links is varied from zero to five in the embedment length of column cage in three specimens. No tension reinforcement is provided in the base but the rest of the specifications are the same as the specimens in group VIIa. In group VIIIb the number of links in the embedment length is changed between zero and three in three specimens. Base tension reinforcement is provided in the specimen with one link while the others have a base of plain concrete. The rest of the specifications are the same as group VIIb

6- Characteristic strength of concrete (f_{cu}) in foundation is varied while the rest of the variables are kept constant (Group IX)

This group covers five specimens with bases made of plain concrete. Specimens tested in this group consists of 4 - 25 mm ribbed bars as column longitudinal reinforcement and the rest of the specifications are the same with group IV. The concrete compressive strength (f_{cu}) is varied from 21.90 N/mm^2 to 36.30 N/mm^2 in the specimens.

7- Bar size in short reinforced concrete column is varied while all the other variables are maintained constant (Group X)

In this group the dimensions of foundation are the same as group IV but 5/12 mm ribbed bars are provided in each direction in the base. The column size is kept constant at 250 mm square, while 4 - 25 mm and 4 - 20 mm ribbed bars are used as column longitudinal reinforcement in two specimens, respectively.

The column bars are welded to a 250 mm square steel plate on the top and continued straight through the base 30 mm above the bottom. Normally spaced links made of 8 mm ribbed bars are included in the column shaft, however near the top the pitch is reduced to prevent local failure of the column. Cover to both the column main reinforcement and base tension reinforcement is 30 mm.

8- Size of the short reinforced concrete column is varied while the rest of the variables are kept constant (Group XI)

This group covers three test structures. In all the specimens column cross-section is maintained square and contains 4 - 25 mm ribbed bars. Size of the column is varied from 160 x 160 mm to 250 x 250 mm. Rest of the specifications in column and foundation are the same as the specimens in group X.

In all groups, each test specimen is fitted with electrical resistance strain gauges. They are placed on two diagonal legs of column cage in any case and, at the legs of links and on the central bars in each direction in the base when these are present. They are described under the heading of instrumentation in section 2.7.

In both parts, the possibility of end bearing of column longitudinal

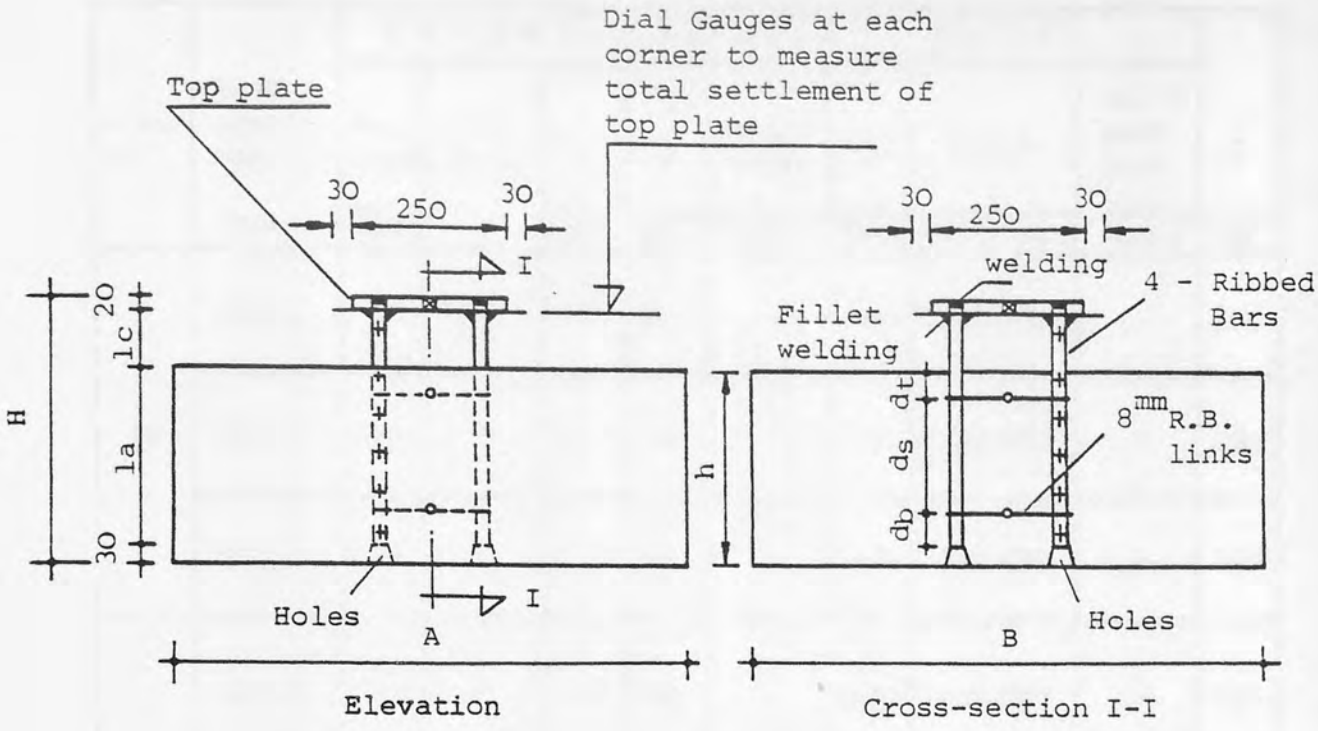

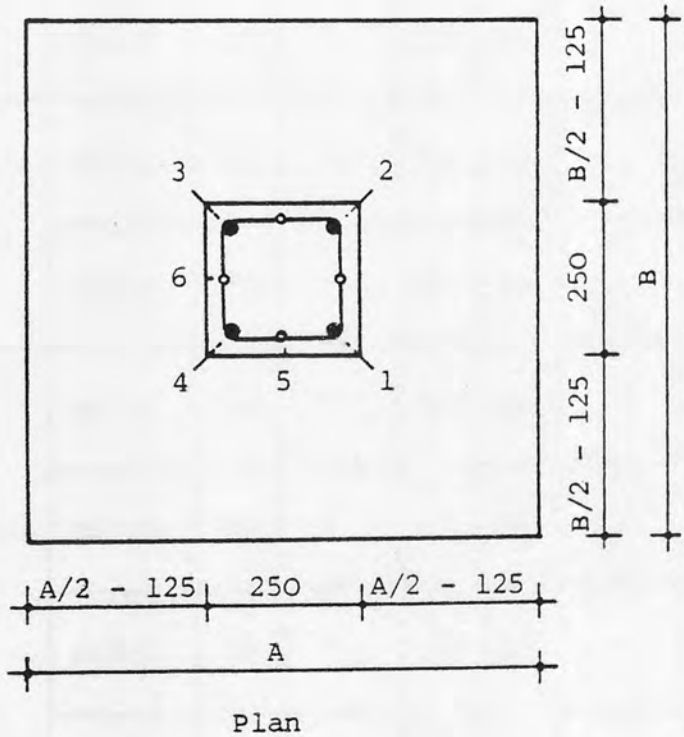

Notes:

1) +:indicates a pair of strain gauges one opposite to the other at each position on two diagonal legs of column cage

2) o:indicates the position of strain gauges at each leg on the upper face of each link

3) 1,2,3,4:indicate diagonally attached steel pieces to provide support for vertically placed dial gauge needles

4) ▣:indicates horizontally placed dial gauges (5 and 6)

5) All dimensions in mm

FIGURE 2.5: DETIALS OF TEST SPECIMENS CONDUCTED WITH RIBBED BARS WITHOUT TENSION REINFORCEMENT IN BASE WITH OR WITHOUT LINKS ON COLUMN CAGE IN PART TWO

Group No:	Test specimen SRi-j	COLUMN CAGE					BASE			H
		Bar Size	Bar Type	l_a	l_c	No. of Links	h	A x B	No. of bars each way	
		ϕmm		mm	mm	No./ϕ	mm	mm x mm	No./ϕ	mm
IV	SR1-1	16	Ribbed Bar	170	60	-	200	800x800	-	280
	SR1-2	20	"	170	70	-	200	800x800	-	290
	SR2-1	25	"	170	90	-	200	800x800	-	310
V	SR2-1	25	"	170	90	-	200	800x800	-	310
	SR2-2	25	"	220	90	-	250	800x800	-	360
	SR1-3	25	"	320	90	-	350	800x800	-	460
VI	SR3-1	25	"	320	90	-	350	600x600	-	460
	SR1-3	25	"	320	90	-	350	800x800	-	460
VIIa	SR1-3	25	"	320	90	-	350	800x800	-	460
	SR4-1	25	"	320	90	-	350	800x800	3/12	460
	SR4-2	25	"	320	90	-	350	800x800	5/12	460
	SR4-3	25	"	320	90	-	350	800x800	7/12	460
VIIIa	SR1-3	25	"	320	90	-	350	800x800	-	460
	SR5-1	25	"	320	90	2/8	350	800x800	-	460

TABLE 2.2: SPECIFICATIONS OF TEST SPECIMENS WITHOUT SHORT COLUMN IN PART TWO

Group No:	Test specimen	COLUMN CAGE					BASE			H
		Bar Size	Bar Type	l_a	l_c	No.of Links	h	A x B	No.of bars each way	
	SRi-j	ϕmm		mm	mm	No./ϕ	mm	mm x mm	No./ϕ	mm
VIIIa	SR5-2	25	Ribbed Bar	320	90	5/8	350	800x800	-	460
VIIb	SR2-1	25	"	170	90	-	200	800x800	-	310
	SR6-2	25	"	170	90	-	200	800x800	3/12	310
	SR6-3	25	"	170	90	-	200	800x800	5/12	310
	SR6-4	25	"	170	90	-	200	800x800	7/12	310
VIIIb	SR2-1	25	"	170	90	-	200	800x800	-	310
	SR7-1	25	"	170	90	3/8	200	800x800	-	310
	SR7-2	25	"	170	90	1/8	200	800x800	5/12	310
IX	SR2-1	25	"	170	90	-	200	800x800	-	310
	SR8-1	25	"	170	90	-	200	800x800	-	310
	SR8-2	25	"	170	90	-	200	800x800	-	310
	SR8-3	25	"	170	90	-	200	800x800	-	310
	SR8-4	25	"	170	90	-	200	800x800	-	310

TABLE 2.2: (continued)

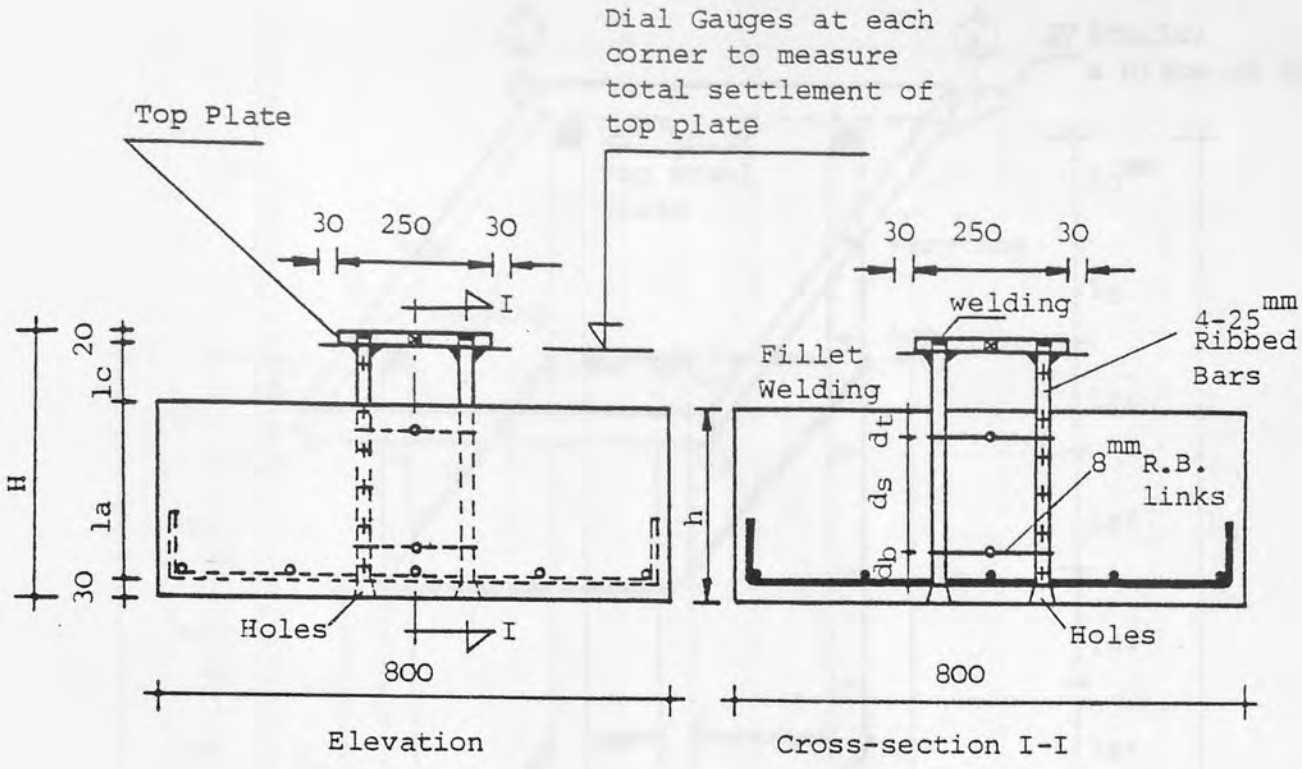

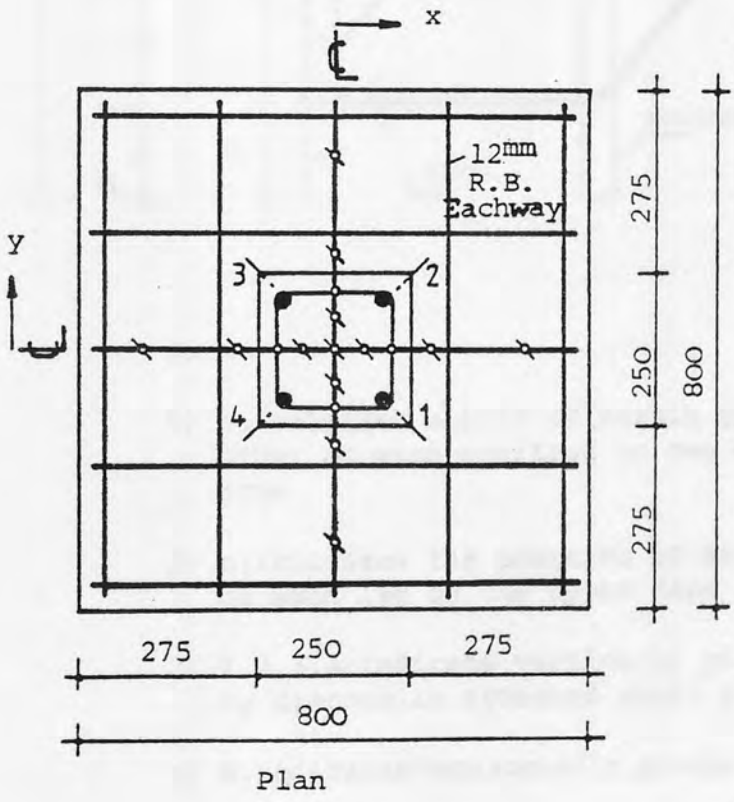

Notes:

1) +:indicates a pair of strain gauges one opposite to the other at each position on two diagonal legs of column cage

2) o:indicates the postion of strain gauges at each leg on the upper face of each link

3) ○:indicates the position of strain gauges on the lower face of base tension reinforcement

4) 1,2,3,4:indicate diagonally attached steel pieces to provide support for vertically placed dial gauge needles

5) ⊠:indicates horizontally placed dial gauges

6) All dimensions in mm.

FIGURE 2.6: DETAILS OF TEST SPECIMENS WITH RIBBED BARS CONSISTING OF TENSION REINFORCEMENT IN BASE WITH OR WITHOUT LINKS ON COLUMN CAGE IN PART TWO

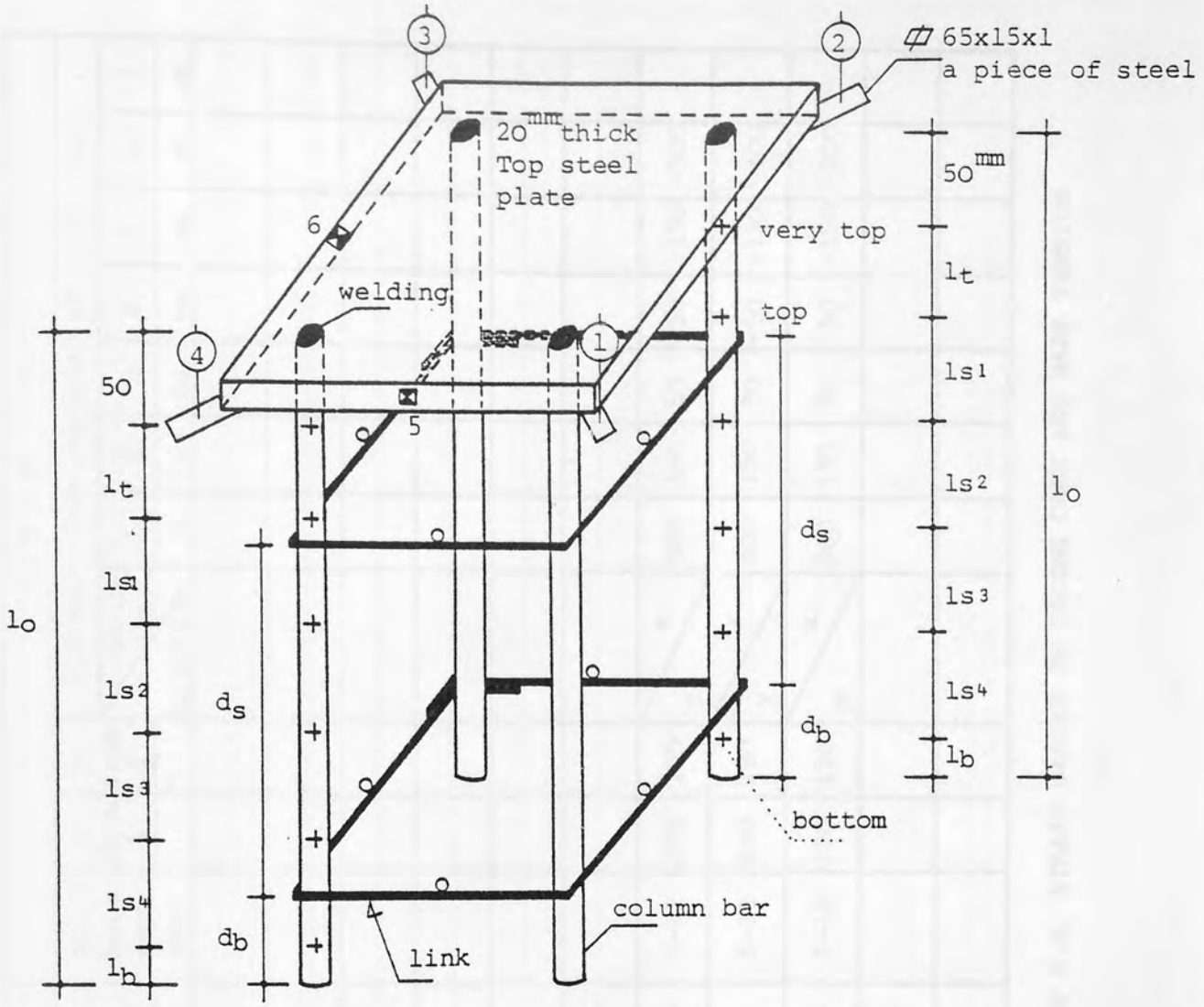

Notes:

1) +:indicates a pair of strain gauges one opposite to the other at each position on two diagonal legs of column cage

2) o:indicates the position of strain gauges at the centre of each leg on the upper face of each link

3) 1,2,3,4:indicate vertically placed dial gauges supported by diagonally attached steel pieces

4) ▪:indicates horizontally placed dial gauges (5 and 6)

FIGURE 2.7: DETAILS OF COLUMN CAGE FOR SPECIMENS WITH RIBBED BARS IN PART TWO

Test Specimen	COLUMN CAGE											BASE									
	l_t	ls_1	ls_2	ls_3	ls_4	l_b	l_o	No.of Links	d_t	d_s	d_b	No.of bars each way	x from ℄	y from ℄	DISTANCE FROM CENTROID OF BASE (mm)							
															Gauge No. / Direction	1	2	3	4	5	6	7
SRi-j	mm	mm	mm	mm	mm	mm	mm	No./ϕ	mm	mm	mm					mm	mm	mm	mm	mm	mm	mm
SR1-1	50	65	65	-	-	25	250															
SR1-2	60	65	65	-	-	25	260															
SR1-3	71	71	71	71	71	25	430															
SR2-1	75	65	65	-	-	25	280															
SR2-2	70	65	65	65	-	15	330															
SR3-1	71	71	71	71	71	25	430															
SR4-1	71	71	71	71	71	25	430	-	-	-	-	3-12	220	220	x / y	300	150	50	-50	-150	-300	-
SR4-2	71	71	71	71	71	25	430	-	-	-	-	5-12	180	180	x / y	300	150	50	-50	-150	-300	-
SR4-3	71	71	71	71	71	25	430	-	-	-	-	7-12	120	120	x / y	300	150	50	-50	-150	-300	-
SR5-1	71	71	71	71	71	25	430	2/8	45	230	45											
SR5-2	71	71	71	71	71	25	430	5/8	25	71	11											

TABLE 2.3: SPACING OF LINKS ON COLUMN CAGE AND POSITION OF E.R. STRAIN GAUGES ON COLUMN CAGE AND BASE TENSION REINFORCEMENT

Test Specimen	COLUMN CAGE											BASE									
	l_t	ls_1	ls_2	ls_3	ls_4	l_b	l_o	No. of Links	d_t	d_s	d_b	No. of bars each way	x from ℄	y from ℄	DISTANCE FROM CENTROID OF BASE (mm)							
															Gauge No.	1	2	3	4	5	6	7
SRi-j	mm	mm	mm	mm	mm	mm	mm	No./ϕ	mm	mm	mm		mm	mm	Direction	mm	mm	mm	mm	mm	mm	mm
SR6-2	75	65	65	-	-	25	280	-	-	-	-	3-12	220	220	x / y	300	150	50	0	-50	-150	-300
SR6-3	75	65	65	-	-	25	280	-	-	-	-	5-12	180	180	x / y	300	150	50	0	-50	-150	-300
SR6-4	75	65	65	-	-	25	280	-	-	-	-	7-12	120	120	x / y	300	150	50	0	-50	-150	-300
SR7-1	75	65	65	-	-	25	280	3/8	30	65	10											
SR7-2	75	65	65	-	-	25	280	1/8	30	--	-	5-12	180	180	x / y	300	150	50	0	-50	-	-
SR8-1	75	65	65	-	-	25	280															
SR8-2	75	65	65	-	-	25	280															
SR8-3	75	65	65	-	-	25	280															
SR8-4	75	65	65	-	-	25	280															

TABLE 2.3: (continued)

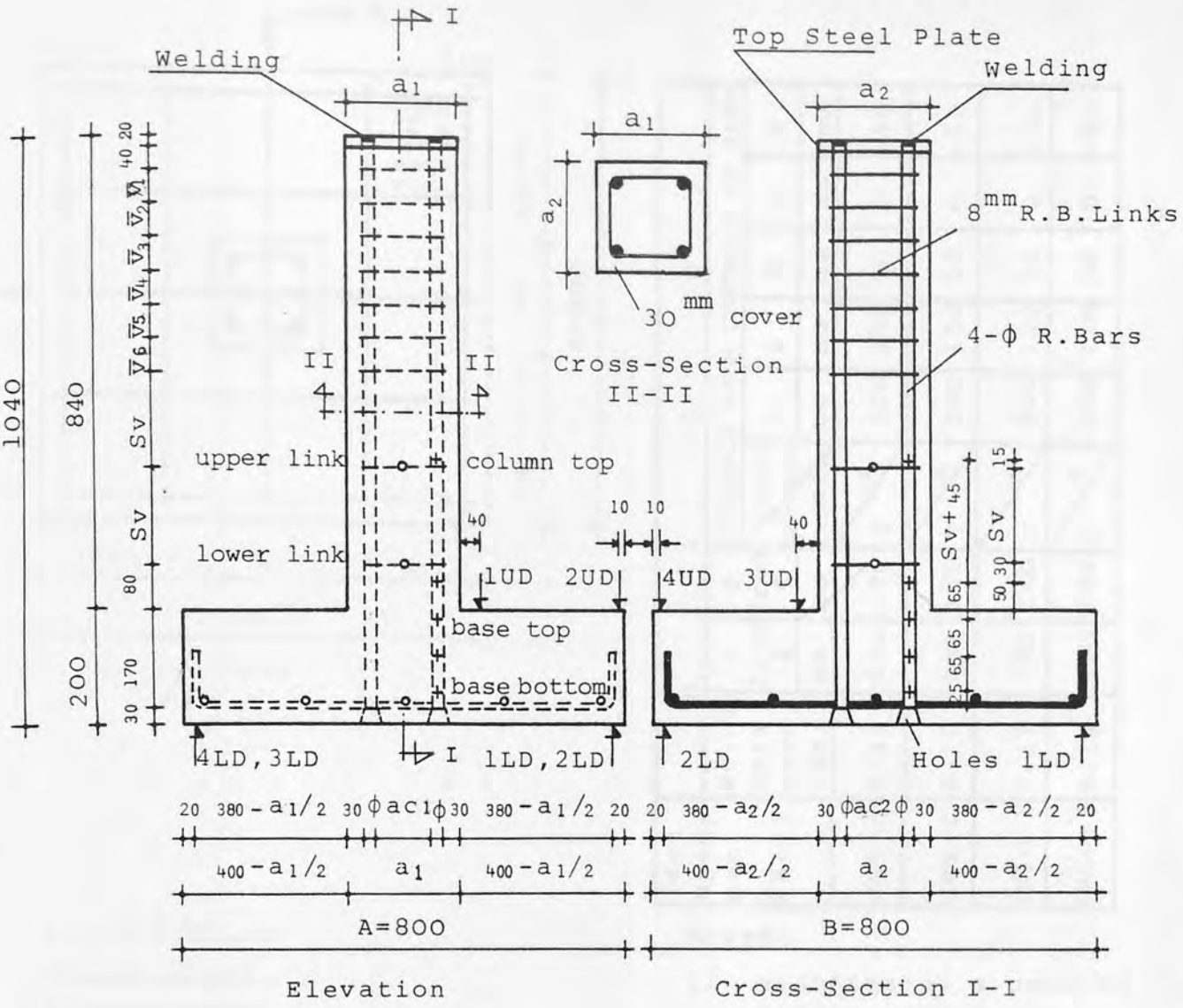

Group No:	Test Specimen SRi-j	Column Size $a_1 \times a_2$ mm×mm	Longitudinal Reinforcement ϕ mm	Type	C.Core ac_1 mm	ac_2 mm	Spacing of Links in Column Sv mm	$\bar{V}_1$ mm	$\bar{V}_2$ mm	$\bar{V}_3$ mm	$\bar{V}_4$ mm	$\bar{V}_5$ mm	$\bar{V}_6$ mm
X	SR9-1	250x250	25	Ribbed	140	140	230	60	60	60	60	-	-
	SR9-2	250x250	20	Ribbed	150	150	230	60	60	60	60	-	-
XI	SR9-1	250x250	25	Ribbed	140	140	230	60	60	60	60	-	-
	SR10-1	200x200	25	Ribbed	90	90	200	60	60	60	60	-	-
	SR10-2	160x160	25	Ribbed	50	50	160	60	60	60	60	60	80

FIGURE 2.8: DETAILS OF TEST SPECIMENS WITH A SHORT COLUMN IN PART TWO

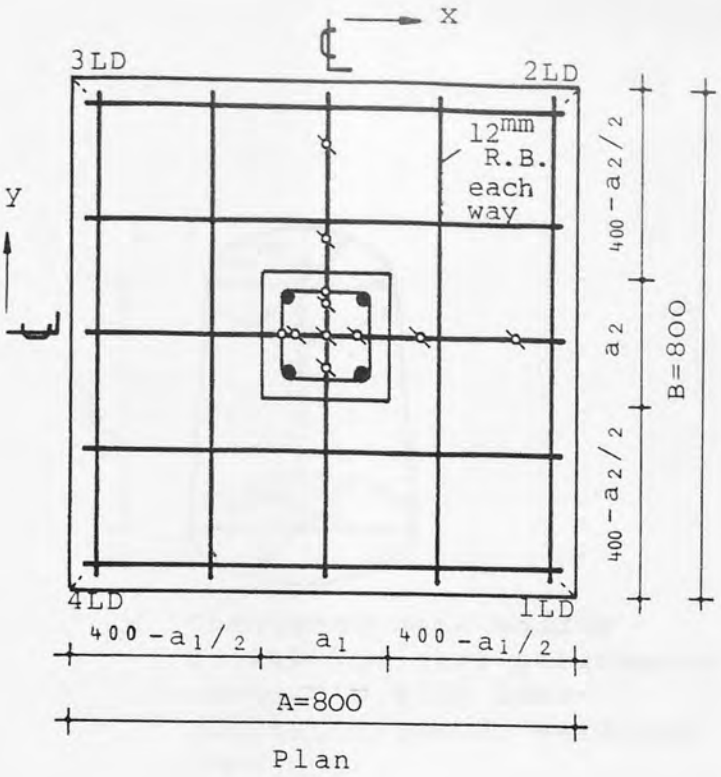

Test Specimen SRi-j	B: No. of bars each way	B: x from ℄ mm	B: y from ℄ mm	A: Gauge Direction	S E: DISTANCE FROM CENTROID OF BASE 1 mm	2 mm	3 mm	4 mm	5 mm
SR9-1	5-12	180	180	x	300	150	50	0	-50
				y	300	150	50	0	-50
SR9-2	5-12	180	180	x	300	150	50	0	-50
				y	300	150	50	0	-50
SR10-1	5-12	180	180	x	300	150	50	0	-50
				y	300	150	50	0	-50
SR10-2	5-12	180	180	x	300	150	50	0	-50
				y	300	150	50	0	-50

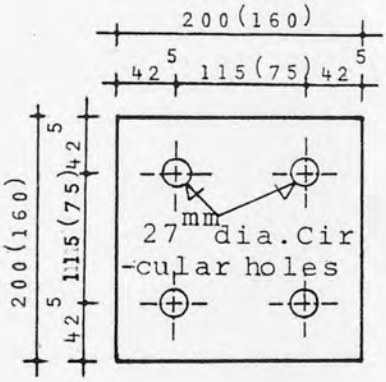

Fig a) Top steel plate details for SR10-1 & SR10-2
-values in brackets for SR10-2
-See Fig.(2.10)for SR9-1 & SR9-2

Notes:

1) +:indicates a pair of strain gauges one opposite to the other at each position on two diagonal legs of column cage
2) o:indicates position of strain gauges at two legs on the upper face of two links as shown
3) ϒ:indicates the position of strain gauges on the lower face of base tension reinforcement
4) 1LD,2LD,3LD,4LD:indicate vertically placed lower dial gauges
5) 1UD,2UD,3UD,4UD:indicate vertically placed upper dial gauges
6) See Fig.2.6 for wooden block details
7) All dimensions in mm.

FIGURE 2.8: (continued)

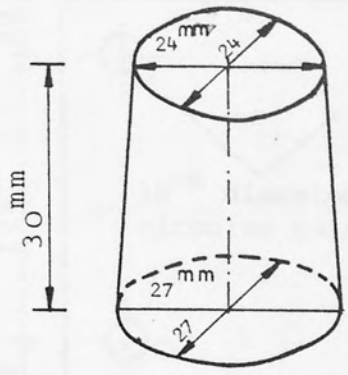

a) Truncated cone wooden blocks for test structures conducted with 16mm nominal diameter deformed bars

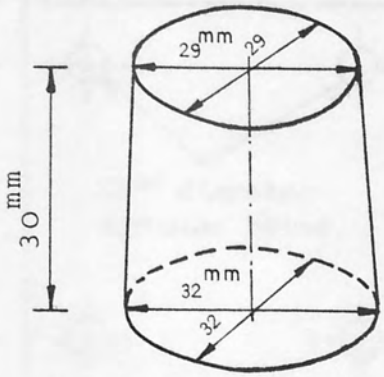

b) Truncated cone wooden blocks for test structures conducted with 20mm nominal diameter deformed bars

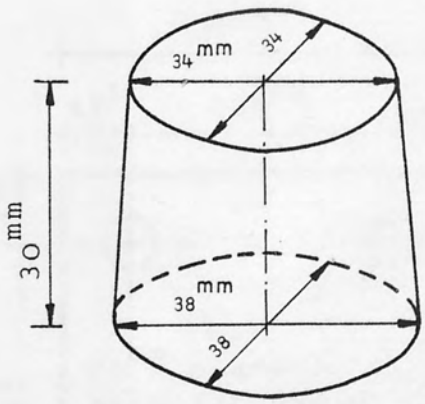

c) Truncated cone wooden blocks for test structures conducted with 25 mm nominal diameter deformed bars

FIGURE 2.9: WOODEN BLOCK DETAILS IN PARTS ONE AND TWO

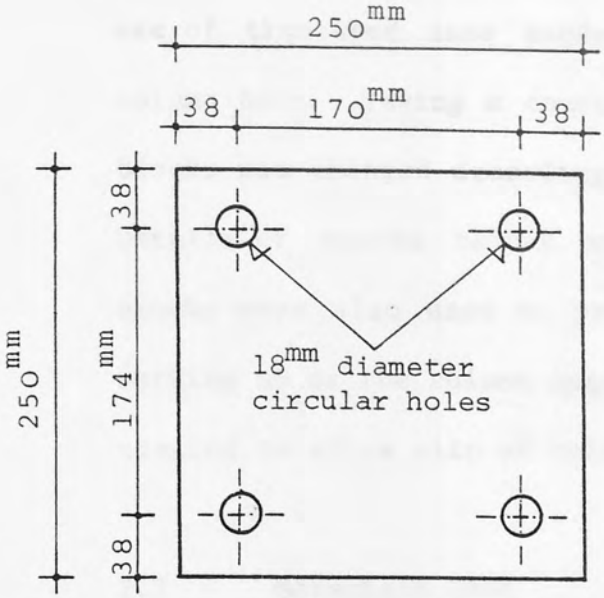

a) 20 mm thick top steel plate for test structures conducted with 16 mm nominal diameter deformed bars

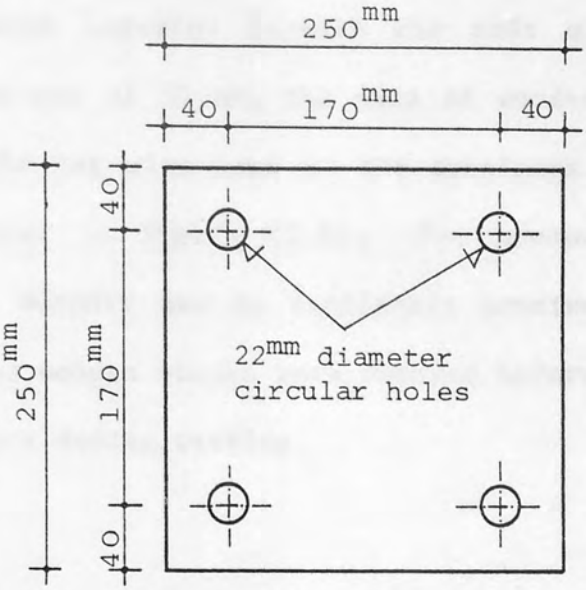

b) 20 mm thick top steel plate for test structures conducted with 20 mm nominal diameter deformed bars

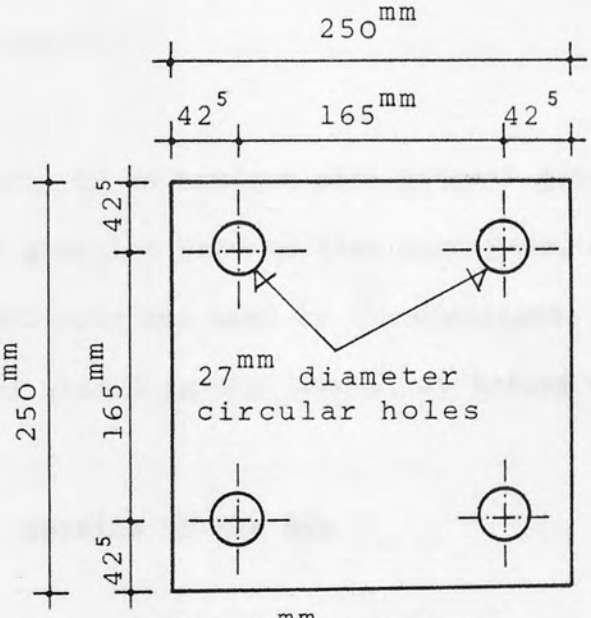

c) 20 mm thick top steel plate for test structures conducted with 25 mm nominal diameter deformed bars

FIGURE 2.10: TOP STEEL PLATE DETAILS IN PARTS ONE AND TWO

bars was eliminated in each test structure. It was achieved by the use of truncated cone wooden blocks inserted beneath the ends of column bars. Having a constant height of 30 mm, the size of wooden blocks was changed according to the bar size used in the specimens. Details of wooden blocks are shown in figure (2.9). The wooden blocks were also used to provide support and to facilitate precise setting up of the column cage. The wooden blocks were removed before testing to allow slip of column bars during testing.

2.3 Materials Used

2.3.1 Concrete Materials

Cement: Ordinary Portland Cement (O.P.C) was used in all specimens throughout the experimental work. It was purchased in bags from a local supplier.

Aggregate: 20 mm maximum size natural gravel as coarse aggregate and zone III granular sand as fine aggregate, supplied from local pits in Birmingham area was used in the specimens. Gravel and sand were oven-dried and stored in the laboratory before mixing.

2.3.1.1 Details of the Mix

A number of trial tests were carried out on standard cubes by varying the mix proportions and water/cement ratios. Each trial set included four specimens. The cube moulds were filled and compacted in layers with an internal vibrator. Specimens were cured in water at controlled temperature and tested in compression at the age of seven days.

Considering the workability and concrete characteristic strength, proportions of the mix and water/cement ratio (W/C) were chosen that would be satisfactory both in the fresh and in the hardened state. The dry-weight of cement, sand and gravel were 1:2:3.6 with a water/cement ratio of 0.54 throughout the experimental scheme except for those specimens tested in group IX. The following dry-weight mix proportions and water/cement ratios were used in the same order as above in group IX;

1:2:3.6, W/C = 0.58; 1:2.4:3.6, W/C = 0.60

1:2.6:4, W/C = 0.63; 1:2:3, W/C = 0.50

2.3.2 Steel

Two types of high strength deformed reinforcing bars were used in the experimental programme. In part one test specimens were manufactured with Type 1 cold worked high yield square twisted bars to BS.4461: 1978[63]. 16 mm, 20 mm and 25 mm nominal diameter bars were used as column longitudinal reinforcement. Manufacturing of square twisted bars ceased nearly a year after commencing the experimental investigation. It was therefore decided to change to Unisteel, Type 2 hot rolled high yield ribbed deformed bars to BS.4449:1978[64], since they are extensively used in practice because of their high bond strength.

Specimens tested in part two were manufactured with ribbed deformed bars. In columns 16 mm, 20 mm and 25 mm diameter bars as main reinforcement, 8 mm diameter bars as secondary reinforcement and in bases 12 mm diameter bars as tension reinforcement were used. Each size of bar was delivered in standard lengths and then saw cut to required

size for all specimens. All reinforcing bars were used as purchased, their condition varying from clean to lightly rusted. However imperfections like bends, dents, distortions and cut ends were removed by cold sawing.

For the fabrication of the top steel plate, 20 mm thick and 250 mm wide flat strip plates of mild steel grade 43 A to BS.4360:1972[57] were used. They were cut to size needed after removing the flame cut ends and other imperfections by cold sawing. The column heads fitted in test rig No. 2 were also fabricated from this steel.

2.4 Construction of Column Cage and Base Reinforcement Mesh

2.4.1 Column Cage

To transmit the applied load equally to all column bars a 20 mm thick mild steel square plate was welded to the top. Details of top steel plates are given in figure (2.10).

Four steel bars were used to form the column cage in all cases. They were square cut to the required length from a single bar to a precision of $\mp$ 0.5 mm by cold sawing. Two 450 mm long bars as control specimens were also saw cut from the same bar at random during the cutting of the column bars. The top steel plate was saw cut slightly larger than the required size from original flat strip plate. Then the sides of the plate were machined to the exact square size. After that, the position of four holes were marked out on top face and the plate was set into a drilling machine. Then four circular holes were drilled to required diameter according to design. Another auxiliary

steel plate used during welding to hold the bars in position at bottom was also prepared in a similar way. After the preparation of plates four bars were inserted into the holes on top as well as at bottom. A cruciform wooden frame was placed between the two plates to hold the top plate in position. Then by using the spirit level four bars were arranged and checked to be vertical and the top plate to be horizontal. Approximately 10 mm gap was left between the top of bars and upper face of top plate and this gap was filled with weld, provided that the top plate and column bars held their proper position. The bars were also welded to the lower face of the plate all around. Because of the firm attachment to the top plate, all bars were equally loaded and relative movement was eliminated. Details of the column cage made from square twisted bars are given in figure (2.4).

The column cage in specimens tested in group VIII included links in the embedment length. After preparing the required number of them, the links were placed in their correct position on the column bars and tied in place with wire. Details of the column cage in specimens with ribbed bars, but without the short reinforced concrete column, are given in figure (2.7) and table (2.3).

Specimens in groups X and XI included a short reinforced concrete column. To facilitate the casting of the vertical column, the top steel plate was not welded to column bars in advance. The required number of links were prepared and their position on column bars were marked out. Then the links were placed to their position on the bars and tied together with wire into a stiff cage which could be set directly into the metal form. A column cage for the short column is shown in figure (2.11). Spacing of links was measured from centre to centre in

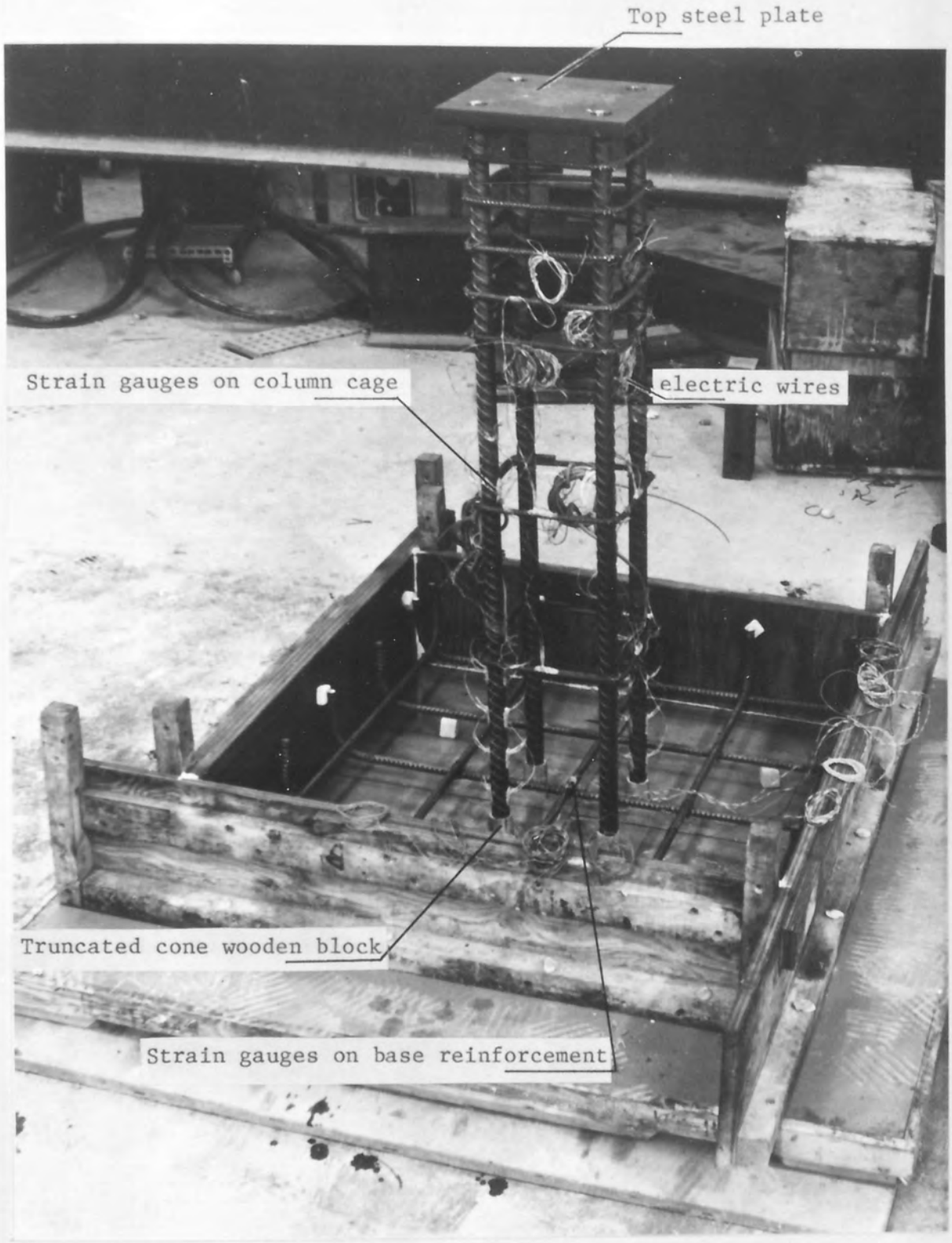

FIGURE 2.11: VIEW OF A COLUMN CAGE AND A BASE REINFORCEMENT MESH

the bars and, bending dimensions were in accordance with BS.4466: 1969[42].

The top plate is bedded on to the concrete shortly before testing so that it is in direct contact with the concrete. Thus and concrete shrinkage is allowed for and the load is transferred direct to the concrete of the column. The top plate is welded to the bars after bedding down on the concrete.

2.4.2 Base Reinforcement Mesh

A number of bars were cut to the size needed by cold sawing. Then each bar was bent at both ends for anchorage, according to BS.4466:1969[42]. After marking out the bars were aligned in each direction and tied together with wire into a stiff grillage. Spacing of mesh was measured from centre to centre in the bars as shown in figure (2.6). A base reinforcement mesh already set up in the mould is shown in figure (2.11).

2.5 Control Specimens

In order to determine the physical properties of materials used in each main specimen tests were carried out on concrete and steel specimens throughout the experimental programme.

2.5.1 Concrete Specimens

For each main test structure the following control specimens were prepared.

- Four 150 mm cubes to determine the concrete characteristic strength (f_{cu})
- Three 150 x 300 mm cylinders for the splitting test for the tensile strength of concrete (f_t)
- Three 150 x 300 mm capped cylinders to determine Young's modulus of concrete (E_c) and Poisson's ratio (ν_c).

2.5.2 Steel Specimens

The following 450 mm long control specimens for tensile tests were prepared.

- Two for column longitudinal reinforcement obtained from the same bar as used in main test by cold sawing
- Two for links taken by cold sawing from the same bar as used in main test
- Three for base tension reinforcement obtained from the same bar as used in main specimen by cold sawing.

The following physical properties were obtained from the tensile tests conducted on steel specimens.

- The ultimate load and resulting ultimate tensile stress (f_u)
- Yield stress or 0.2% proof stress (f_y)
- Young's modulus of steel (E_s)

One set of stress-strain relationship diagrams for each size and type of steel are given in Appendix A.

2.6 Manufacturing of Specimens

2.6.1 Mould

The casting moulds for foundation and column were fabricated from 20 mm plywood. The base of the foundation mould was also lined with formica on the upper face to give an accurate and smooth finish, it was also braced with wooden strip planks in each direction on the lower face to prevent deformation during the casting process. Three different moulds were used to manufacture the specimens at the time of the test scheme. The first one was used for the specimens with square twisted bars. The second mould was used for the specimens with ribbed bars except for specimens in groups X and XI. Lastly the third mould was used to generate the specimens in groups X and XI.

2.6.2 Assembly

The foundation mould sides and base were assembled and checked for squareness, then the four truncated cone wooden blocks were fixed to the base as shown in figures (2.9) and (2.11). All joints in the mould were sealed to prevent leakage of cement mortar and water, and then the mould was oiled. After that, to brace the sides during casting a cruciform frame was mounted on top of the mould and adjusted to form a 250 mm square hollow section for centralizing the base. It also served to hold the column cage in position before and during casting.

For the fabrication of the specimens with a short reinforced concrete column, a cruciform frame was mounted on top of the foundation mould

and adjusted as before. Finally the column mould was checked for verticality on each face and finally braced in position.

For the concrete control specimens the steel moulds (four cubes and six cylinders) were cleaned, assembled, oiled and placed alongside the casting mould.

2.6.3 Adjustment of Reinforcement

After preparing the mould the column cage was secured in place. It rested on top of the truncated cone wooden blocks which were already fixed on the base. The column cage was held in position by inserting 30 mm wooden cube spacers in two directions between column bars and cruciform wooden frame. Then the top steel plate was checked to be horizontal using a spirit-level, so were the four longitudinal bars to be vertical.

In case of the specimens reinforced in base, the tension reinforcement mesh was first placed in the mould with precast cement mortar spacers under the bars to give the correct concrete cover. Then the column cage was set up in a similar way as before.

Specimens in groups X and XI included a short column as well. In that case, base tension reinforcement was first placed in the mould in a similar way as mentioned above, then the column mould was mounted and adjusted. Finally the column cage was secured in place. It also rested on the truncated cone wooden blocks. The electric wires connected to strain gauges on the column cage were taken out through the

holes made on the column mould, then the holes were sealed to prevent the escape of water and cement mortar. To hold the column cage in position and to maintain the correct concrete cover over the column longitudinal reinforcement during the casting operation 30 mm wooden spacer cubes were inserted in two directions between the column bars and the inside faces at intervals from bottom to top in the column mould. Again the column bars were checked to be vertical using a spirit level. The wooden spacers were eventually withdrawn as casting progressed.

In all cases after setting the reinforcement cages the strain gauges were finally checked to be functioning properly to ensure that they were undamaged. Then all electric wires were rolled and, either placed on the top steel plate or temporarily fixed to the mould to prevent any damage occuring during concreting.

2.6.4 Casting and Curing

Materials, sufficient to manufacture one main test specimen and accompanying concrete control specimens were calculated by weight, according to the mix proportions and water/cement ratio. Considering the limited capacity of the mixer used, the materials were then divided into the required batches. Then quantities of gravel, sand, cement and water for each batch were determined and weighed to an accuracy of 50 gr.

The cast was made of two batches in all cases with the exceptions of specimens labelled S2-3 and S3-2 in part one and those which included

a short reinforced concrete column in part two. For the production of these specimens the cast was made of three batches. Each batch was mixed for four minutes and then discharged. This period of mixing proved to be satisfactory to avoid segregation.

The specimen was cast in layers and compacted by vibration. After filling the first layer in the mould it was vibrated with a poker vibrator internally until air bubbles on the surface disappeared. The same procedure was repeated for each layers. The concrete control specimens were also cast and vibrated internally in layers as the casting progressed. Once all the concrete was placed in the foundation mould four steel hooks were installed in the concrete to facilitate the lifting of the specimen during set up for testing. Then the concrete was struck off with a trowel and the cruciform wooden frame holding the column cage in position was removed, finally the top surface was trowelled smooth and level with the top of the mould. The control specimens were also struck off and finished level with a trowel except for the three cylinders to be capped later.

For the specimens with a short column the cast was made in two stages. First the foundation and 60 mm of the column were cast in the morning in exactly the same way as described above, but the cruciform wooden frame was not removed since it was holding the column mould in position. Two cubes and four cylinders were taken as concrete control specimens from the first cast. Then in the second stage the rest of the column was cast with two cubes and two cylinders as control specimens in the afternoon. The column concrete was mixed in the same way above and placed in the mould in layers. Each layer was compacted internally with a poker vibrator. The top of the column was levelled

with top of the mould leaving 10 mm space between top of the column longitudinal bars and concrete to be filled by fitting the top steel plate before the test. The low workability of concrete made it possible to proceed to the second cast in the column on the same day without causing the concrete to flow over the base during compaction.

After the cast was completed the specimens were left overnight in the moulds in the laboratory without any special protection. The following morning three cylinders were capped with cement mortar and rest of the control specimen moulds were split. Then the wooden mould was stripped and the cubes and cylinders were placed alongside the main specimen. They were manually soaked and covered with wet hessian. To prevent rapid drying the specimens were further covered with a polythene sheet. In the evening, the already capped cylinders were stripped and after soaking them seperately they were placed alongside the main specimen under the wet hessian.

All specimens were soaked daily in the morning under the wet hessian and kept covered with a polythene sheet for the following four days. Finally, when six days old the wet hessian and polythene sheet were removed and all specimens were prepared for test on the seventh day.

2.7 Instrumentation

This section describes the instrumentation for deflection and strain measurement for all test specimens throughout the experimental scheme. Mechanical dial gauges were used to measure deflection, while electric resistance strain gauges were employed for strain measurement. These measurements were recorded in tabular form for each load increment up

to failure. The type of mechanical dial gauges and their placement, and the type of strain gauges, their location and fixing procedure are described in general terms in the following subsections, pointing out any special operation for a particular specimen or group of specimens.

2.7.1 Mechanical Dial Gauges

For each main test structure six Mercer dial gauges of 0.001" per division were used in all cases except those specimens with a short reinforced concrete column in groups X and XI. Four dial gauges of 2" range were placed vertically at each corner of top steel plate. The other two with 1" travel range were positioned horizontally in the middle plane at the centres of two neighbouring sides of the top steel plate. Vertically placed dial gauge needles rested on flat strip steel pieces, diagonally attached at each corner of top steel plate under the lower face. The positions of the dial gauges are shown in figures (2.3) and (2.4) for specimens with square twisted bars in part one and in figures (2.5), (2.6) and (2.7) for those with ribbed deformed bars without a short column in part two. For vertical deflections the dial gauges were mounted on stands resting on top of the concrete surface far enough from the column bars so that they were virtually unaffected by any deflection of the foundation. Vertically placed dial gauges served to measure the total vertical displacement of the top steel plate and hence to observe any slip of the column bars which might occur at any stage of loading up to failure. On the other hand, horizontally placed dial gauges were used to measure the horizontal displacement of column loading plate in two directions, i.e. to monitor the lateral stability of the bare

column bars during loading. It became apparent that both sets of dial gauges would indicate the failure of column cage once the ultimate load carrying capacity of column bars was reached.

In the case of specimens with a short reinforced concrete column, eight dial gauges were employed for deflection measurement. All of them were situated vertically and according to their location and functions, four of them were named lower gauges, while other four were named upper gauges. The position of lower and upper dial gauges are shown in figure (2.8).

Four Mercer dial gauges of 0.001" per division and of 2" range were used as lower gauges to measure total vertical deflection of specimens, i.e. overall shortening of specimen during loading sequence up to failure. They were situated on the lower face of the underlying solid base steel platen at the corners and supported by their stands which rested on the base of test rig.

On the other hand, four Oldak dial gauges of 0.002 mm per division and of 5 mm range with magnetic backs were employed as upper gauges. They were supported by a light weight frame which rested on the ground close to test rig. These dial gauges were placed on the centre lines of the foundation in one quadrant as shown in figure (2.8). Two of the upper gauges were situated near the neighbouring two faces of column, while the other two were placed close to edges of the corresponding neighbouring two sides of the foundation. These gauges measured the vertical deflections of the foundation and column, respectively, during loading up to failure.

2.7.2 Electrical Resistance Strain Gauges

In the present investigation one of the main tasks was to trace the full strain history in specimens by measuring the strains in several locations during the loading sequence; then, using the available data to determine the corresponding internal stresses which could develop in the specimens. First of all the anchorage bond stress distribution in the embedment length was of primary importance which could be derived from changes in strain hence of stress along the bar. The strain gauges often indicated the first slip of column bars because they were damaged when slip occurred. For the reasons outlined above, the strain gauges were extensively used throughout the experimental investigation to produce accurate data about the magnitude, distribution and directions of strains in specimens.

2.7.2.1 Steel Strains

Steel strains were measured by using Tokyo Sokki Kenkyujo PL-5-11 gauges with a 5 mm gauge length and 120 $\pm$ 0.3 ohm resistance.

Test specimens with square twisted bars were furnished with strain gauges on two diagonally opposed legs of the column cage. They were attached in pairs one opposite to the other at each position in alignment with the longitudinal axis of the bars. Positions and spacing of strain guages for specimens in this part are shown in figures (2.3) and (2.4).

Test specimens with ribbed deformed bars included strain gauges on main and secondary reinforcement in the column cage and on base

tension reinforcement in the foundation. In all cases these gauges were placed on two diagonally opposed legs of the column cage in pairs as before. Specimens including links on column cage in the anchorage length were also furnished with strain gauges in each link. Being in alignment with the horizontal axis of each leg of the link, these gauges were attached at the centre of each leg on its upper face. Position of strain gauges in specimens without base tension reinforcement are shown in figures (2.5) and (2.7).

In the case of specimens with base tension reinforcement, two central bars in alignment with the centre lines of foundation in two directions were also fitted with strain gauges. These gauges were positioned in line with the longitudinal axis of the bars on their lower face with the exception of a central gauge located at the centre of the bar in the second layer which was located on the upper face. Positions of strain gauges in specimens including base tension reinforcement are shown in figures (2.6) and (2.7). In all the above mentioned cases referencing and spacing of the strain gauges are given in table (2.3).

Test specimens manufactured with a short reinforced concrete column were also fitted with strain gauges in main and base tension reinforcement in the same way as described above. But this time, in the column only two bottom links included strain gauges and they were placed on two neighbouring legs in each link in the same way as before. Position and spacing of strain gauges in specimens with a short column are shown in figure (2.8).

Steps taken for the attachment of strain gauges on steel are described

as follows:

After the preparation of steel bars the positions of strain gauges were marked out. In order to ensure a strong bond between the gauge and surface the marked areas on which the gauges to be attached were abraded by using two grades of abrasive paper until to get a smooth surface in a gross sense. Then to do a thorough cleaning job the already abraded surfaces were degreased with Genklene and finally neutralized with ammonia solution. In order to orient the strain gauges in the desired position guide lines were marked on the prepared surfaces without interfering with the exact gauge location. The gauges were then handled individually with a piece of transparent tape and precisely adjusted and glued to the steel by using M-Bond 200 adhesive, a Micro-Measurements product. A gentle thumb pressure was maintained over the gauge for a minute to ensure that all sections of the gauge were in intimate contact with the surface, then the tape was peeled back later on. The electric wires were then soldered to the leads of strain gauges. Extreme care was taken during lead-wire installations in order to avoid the probability of damaging the strain gauges and to assure precision and stability in the electrical output. After the gauges have been soldered the gauge resistance was checked, if a value significantly different from the manufacturer's specifications was found the gauge was removed and replaced with a new one. The final check was made on the gauges by the following process. The strain gauge was connected to a strain indicator and it was balanced by bringing the pointer to the zero point. After that the gauge was lightly pressed with the eraser end of a lead pencil. If the pointer returned to zero or nearly so, the strain gauge was regarded to be functioning satisfactorily. If the pointer failed to

return at all or became unsteady, then the gauge was regarded as either imperfectly bonded or accidentally damaged, and it was replaced. As a final step the strain gauges were waterproofed. It was achieved by covering the strain gauges and solder joints with a thin layer of M-Coat D, a fast drying prime coating and M-Coat G paste. This paste was made by mixing two parts curing agent with one part resin and applied to the solder joints and the strain gauges in one layer.

Dummy gauges were also prepared from each size and type of steels. For each dummy gauge a piece of steel bar was cut, strain gauged, soldered and waterproofed in a same way as mentioned above. Then it was embedded in a 100 mm concrete cube.

2.7.2.2 Concrete Strains

The concrete strains were measured by using Tokyo Sokki Kenkyujo PL-60-11 gauges with a 60 mm guage length and 120 $\pm$ 0.3 ohm resistance.A day before the test,the already cast and cured capped cylinders were fitted with strain gauges. Each specimen included four diametrically opposed gauges mounted at the mid-height in pairs, one vertically and the other circumferencially in alignment with the longitudinal and the horizontal axis.

The positions of strain gauges were marked, sanded with abrasive paper and cleaned. The gauge resistances were checked to be satisfactory. Then a thin film of bonding cement was applied and the gauges were wiped into place with a light, progressive pressure. When the bonding cement had dried the electric wires were soldered to the gauge leads with care, checked to be functioning properly and made ready

for test. A dummy gauge for concrete was also prepared on a 100 mm concrete cube in a similar way. The bonding cement was an Araldite Strain Gauge Cement used in conjunction with a HY 951 hardener. This compound was found to be satisfactory.

These strain gauges measured vertical and horizontal strains developed in the concrete cylinders up to failure load to obtain stress-strain relationship of concrete and, then to determine the Young's modulus (E_c) and Poisson's ratio (ν_c).

2.8 Test Rigs

Two test rigs were used to carry out the tests on specimens in parts one and two, respectively. Test specimens fabricated with square twisted bars were tested in test rig No.1, while the others fabricated with ribbed deformed bars in part two were tested in test rig No.2.

2.8.1 Test Rig No.1

A new test rig was designed in accordance with the recommendations of BS.449, Part 2:1969[41], to suit a maximum loading capacity of 1000 kN safely without excessive deflection. The two basic elements of the test rig were the structural steel frame fitted with a 1000 kN capacity hydraulic jack and the solid base steel platen. The frame consisted of horizontally and vertically placed structural steel members - channels, universal beams and columns - to form a closed system. All the joints were connected by using a sufficient number of M20 and M24 hexagonal black bolts to BS.4190:1967[33]. To eliminate effect of bending moment on the specimens, an underlying solid base

steel platen made out of mild steel was designed. The thickness of the platen was determined to limit the deflection at the maximum loading capacity. It was placed over the lower universal beams in the rig to support the specimen during loading. Detail of the test rig No.1 is shown in figure (2.12). The hydraulic jack was mounted in the mid-span of the top beam in a vertical direction symmetrical with respect to the frame in both horizontal directions, hence movement of the frame due to subsequent loading was prevented. As is readily seen from the figure that the top beam was adjustable to provide the required gap between the hydraulic jack and the base steel platen to fit the specimens. The load was applied to the specimen through the top steel plate which was stiffened with two packing plates of the same size. The hydraulic jack was driven by a Losenhausenwerk automatic testing machine which had been previously calibrated to grade A standard. The testing machine indicated the applied load due to the applied pressure in the jack by means of a built-in gauge to an accuracy of 0.05 ton.

2.8.2 Test Rig No.2

When the experimental programme commenced this rig was not available. After carrying out a number of tests with square twisted bars the reinforcement was changed to ribbed deformed bars for the reasons mentioned earlier in section 2.3.2 therefore a higher capacity test rig was required and this rig became available by fitting a 5000 kN capacity hydraulic jack. The specimens fabricated with ribbed bars, were tested in this rig. The loading capacity of the rig was 10000 kN. A view of test rig No.2 is shown in figure (2.13). To set up the specimens without a short column in the test

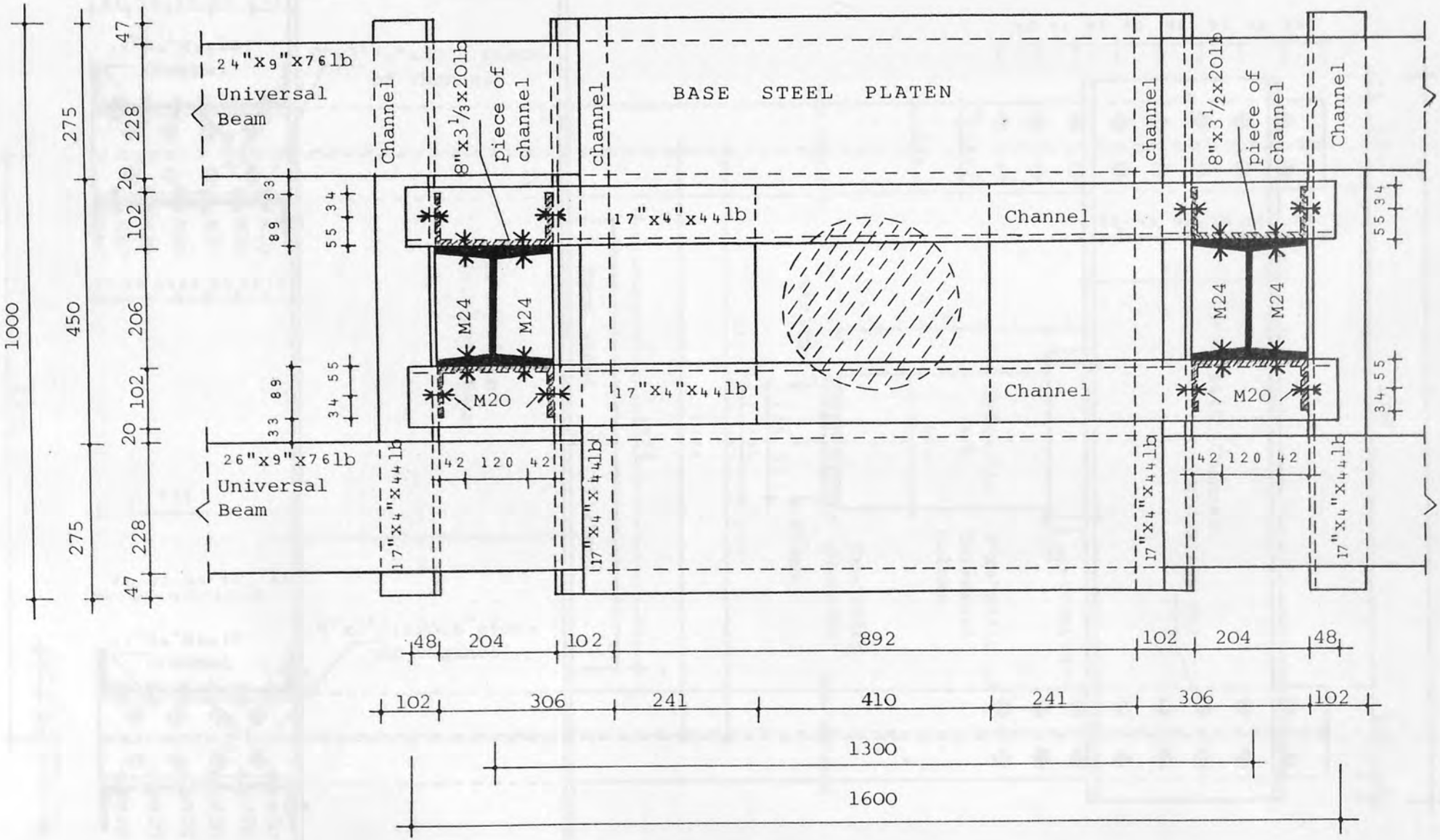

FIGURE 2.12: TEST RIG No.1, PLAN (All dimensions in mm)

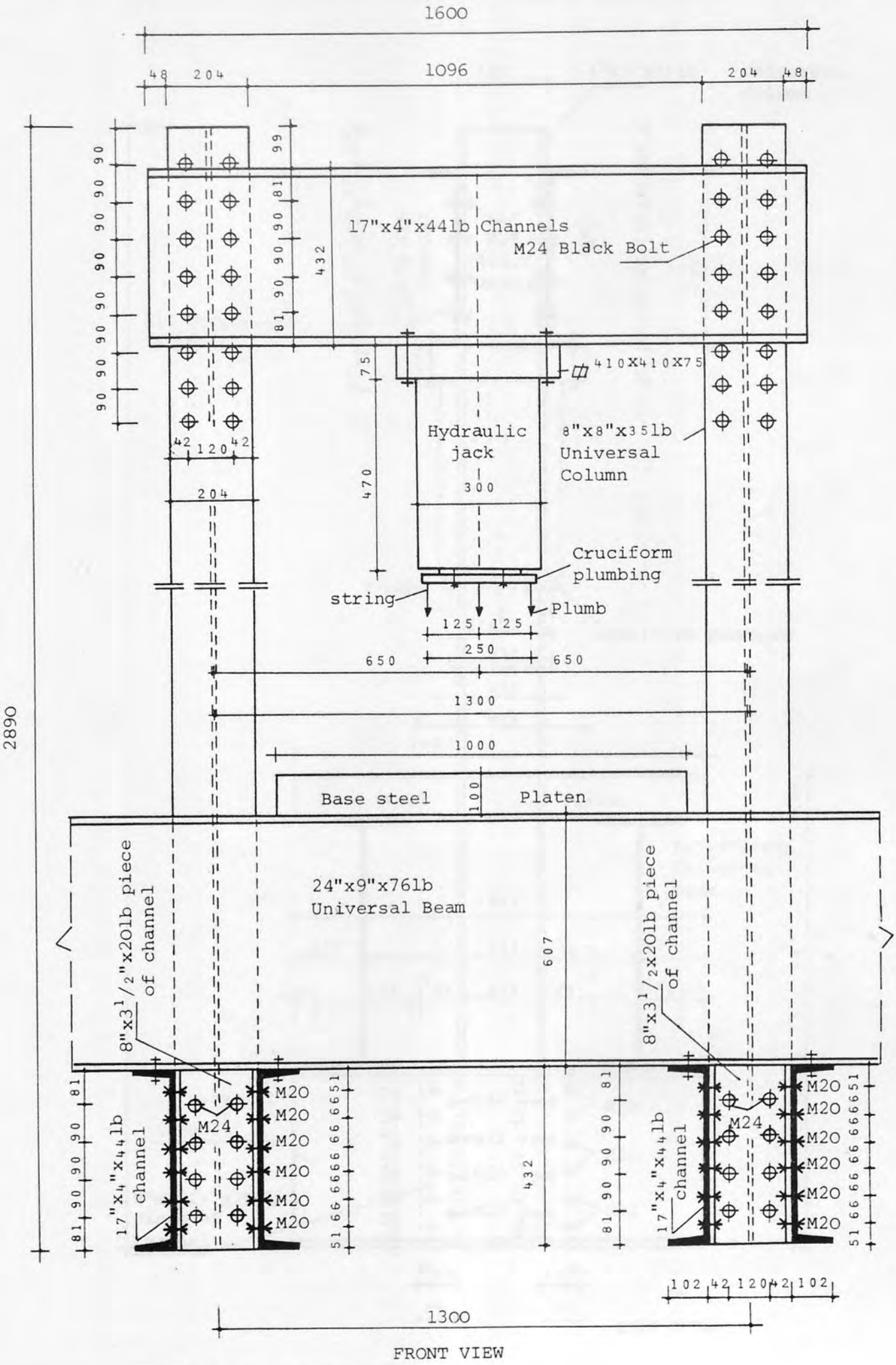

FIGURE 2.12: (continued)

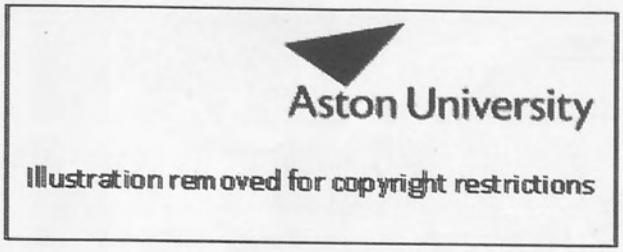
Aston University
Illustration removed for copyright restrictions

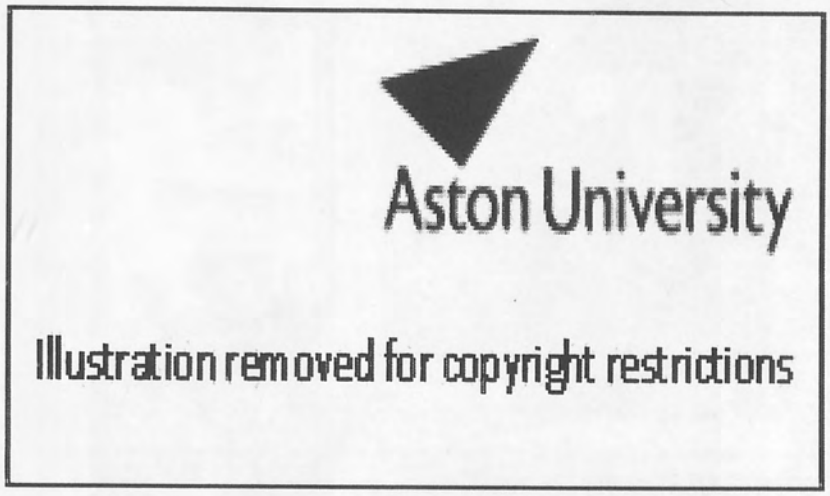
Aston University
Illustration removed for copyright restrictions

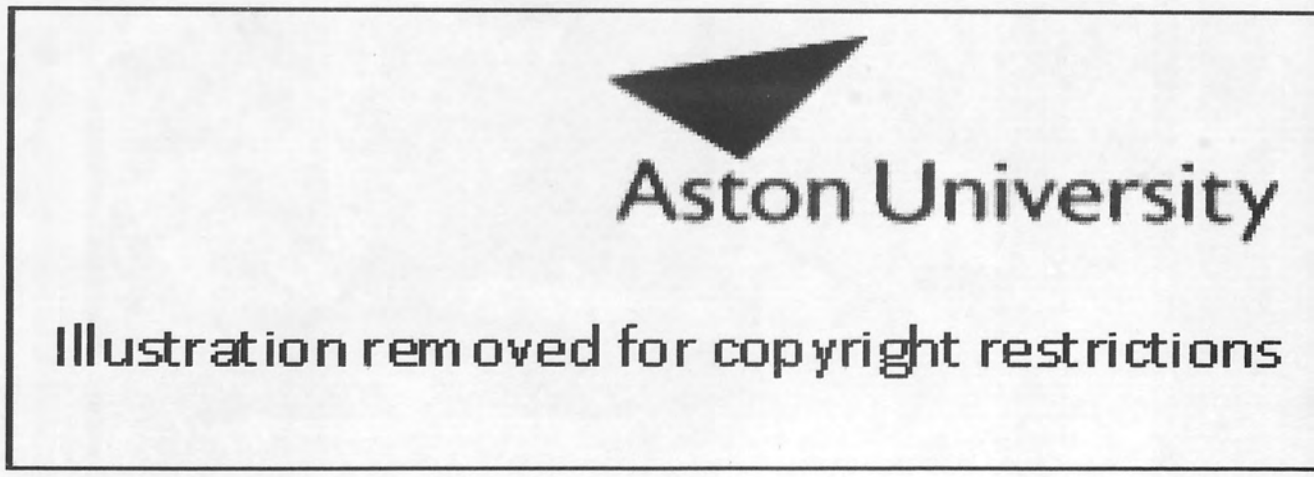
Aston University
Illustration removed for copyright restrictions

rig, the gap between the top beam and the base bed plate was filled by fitting the required size of column heads as seen in figure (2.13). Two column heads, made out of grade 43A mild steel flat strip plates were designed and constructed by welding to transmit the applied load safely without excessive deflection. These heads had the same cross sectional area at the bottom ends as the top steel plate of specimens. According to the need each one was mounted in the mid-span of the top beam in vertical direction symmetrical with respect to the loading frame in both horizontal directions. This time the load was applied to the specimen by a 5000 kN capacity hydraulic jack through a solid steel platen resting on it and the base bed plate, while the top steel plate stiffened as before was in contact with the column head. The jack was part of the same grade A Losenhausenwerk system as used before. To carry out the tests on the specimens with a short column, the same rig was used, however the column head was removed and, the column was in direct contact with the top beam of the rig.

2.9 Test Set Up

Test specimens were set up in the test rigs when six days old. In the following the steps taken to set up each specimen is described in general terms referring to the both test rigs.

The specimen was lifted up and the truncated cone wooden blocks inserted beneath the column longitudinal bars, were removed to ensure that free slip of the bars could occur during loading. The depth of the each hole under the bars were measured from the bottom face of foundation, using a depth micrometer, and recorded. Then the centre and the mid points of four edges of the top steel plate were precisely

marked out on the upper face.

A cruciform steel device named as "cruciform plumbing" was prepared to adjust the specimens in position with respect to the hydraulic jack and to the column head in test rigs No.1 and No.2, respectively. The cruciform plumbing was fitted with five plumb lines; one passing through its centre and, the others symmetrical with respect to its centre passing through four arms in alignment with the central horizontal axes. The distance between two plumb lines on oppposite arms was equal to the square top steel plate size in the both directions. Details of the cruciform plumbing are shown on test rig No.1 in figure (2.12).

To set up the specimen in test rig No.1, the cruciform plumbing was mounted to the hydraulic jack in such a fashion that the central plumb line and the vertical central axis of the jack coincided with each other. A thin layer of plaster of paris was placed over the base steel platen to bed the specimen and ensure complete contact between the specimen and the base platen. To prevent the plaster of paris filling the holes under the column bars a piece of polythene sheet was placed over the central part. Then, the specimen was lifted into the rig and placed over the underlying base steel platen. It was mounted in position, using five vertical plumb lines in such a way that the already marked centre and the mid points of four edges of the top steel plate coincided exactly with the respective plumb lines. The top steel plate was then checked to be horizontal in both directions, using a spirit level. Extreme care was exercised during this operation to ensure that the load would be axially applied to the specimen.

Four pieces of steel were diagonally attached at the corners of the lower face of the top steel plate to provide support to vertically placed dial gauge needles. To stiffen the top steel plate, two packing plates were placed on it, using a thin layer of plaster of paris between them and the specimen was very lightly loaded until the plaster squeezed out. The load was maintained until the plaster was set, then it was released.

The steps taken to set up the specimens without a short column in test rig No.2 was exactly the same with the exceptions of that the cruciform plumbing was mounted to the column head and the specimen was placed over the underlying bed steel plate which rested on the solid steel platen.

Before setting up the specimen fabricated with a short reinforced concrete column, the top steel plate was welded to the column longitudinal bars. A thin layer of plaster of paris was placed over the top of the column and the steel plate was mounted and levelled to be horizontal in both directions. When the plaster was set the gap between the top of the bars and the upper face of the plate was filled by welding to ensure that the bars will take their proper share of load without slip. The top of the welds were ground level with the upper face of the plate.

To set up the specimen the column area was marked out on the lower face of the solid top beam in the rig with respect to its central horizontal axes. To ensure the complete contact between the specimen and the underlying bed plate, a thin layer of plaster of paris was placed over the plate. Then the specimen was lifted into the rig

and placed over the bed plate and adjusted in position in such a way that the edge of the column faces coincided with the edges of the marked column area over the lower face of the top beam. All faces of the column were checked to be vertical, using a spirit level. Extreme care was taken to ensure that the column was mounted in exact position with respect to the top beam while all column faces were vertical, hence the load would be axially applied to the specimen. A complete contact between the column and the top beam was ensured, by using a thin layer of plaster of paris between them.

Finally to complete the process the dial gauges were placed in their locations and, the strain gauge wires were connected to the terminals of a strain indicator and the specimen was made ready for the test.

2.10 Test Procedure

2.10.1 Main Test Specimens

Specimens were tested when seven days old. The general approach to the test was to obtain strain and deflection readings and, to observe the slip and crack formation at applied load increments until failure took place. To carry out the tests on main specimens a Losenhausen-werk testing machine was employed throughout the experimental programme. The testing machine furnished with load maintainer, measured the applied load by means of a built-in pendulum gauge.

When the test programme commenced a compulog data logger for automatic strain reading was not available in the testing laboratory. Strain readings were taken manually. The strain indicator used was

type 105B a Peekel strain gauge instrument.In the early stages of the test programme the data logger became available. Some tests were carried out by using it, since it reduced the testing period to half the time.

However the data logger did not behave correctly and very often broke down in the middle of the test spoiling the strain readings. After a few trials it was replaced by the Peekel strain indicator used before, and the tests with erratic strain readings were repeated. Tests with erratic strain readings were labelled $\overline{S1}$-3, $\overline{S2}$-1 and $\overline{S2}$-2 as shown in table (2.1). These tests were accepted because of the reasons given below.Firstly,the rest of the data for them was available at the conclusion of tests. Secondly in comparison with the repeated tests, respectively, their testing periods were about half the time, while ultimate loads in comparison with each other were almost identical. Thus, it was concluded that the loading sequence had no effect on the load carrying capacity of the specimens.

Prior to starting the test, final checks were made on dial and strain gauges, then the testing machine was switched on and the control panel was set up. After taking the initial readings of dial and strain gauges the load was applied to the specimen in increments. A lapse of time was allowed between the application of each load increment and the recording of the readings to ensure that all the gauge movements due to this load had ceased. The lapse of time was gradually increased as the ultimate load was approached, while the magnitude of each subsequent load increment was reduced. The increments of load were varied from 20 kN to 100 kN according to the type and the properties of specimens.

At each load increment the readings were recorded in a tabular form, the specimen was carefully examined. Slip of the column bars was recorded, crack formations and their propogation in the foundation or column were marked and, the whole process was continued until failure took place.

Vertical dial gauges labelled 1, 2, 3 and 4, measured the vertical displacement of the top steel plate and indicated the slip of the column bars. The horizontal dial gauges labelled 5 and 6, checked the lateral stability of the top steel plate by measuring horizontal displacement, up to failure load. In the case of specimens with a short column, lower dial gauges labelled 1LD, 2LD, 3LD and 4LD, measured the overall shortening of the specimen, while upper dial gauges labelled 1UD, 2UD, 3UD and 4UD, measured vertical deflections of the foundation and the column, respectively, up to failure load. Strain gauges in the reinforcement measured the strain developed in their respective locations up to failure and indicated the yield of steel.

At the conclusion of the test the specimen was unloaded and all dial gauges and electric wires were removed. Then, the crack patterns on the top face and four sides were sketched and the specimen recovered from the test rig. The depth of the hole under each column bar was measured, using a depth micrometer and, crack patterns on the bottom face were sketched. Finally, all sides and faces of the specimen were photographed.

2.10.2 Control Specimens

The concrete control specimens were tested on the same day as the main test, using a 3000 kN capacity Dennison compression machine. Crushing load of four cubes for determining concrete compressive strength (f_{cu}) and splitting load of three uncapped cylinders for determining the tensile strength of concrete (f_t) were recorded. Three capped cylinders were also tested in compression to determine the Young's modulus (E_c) and Poisson's ratio (ν_c) of concrete. Vertical and horizontal strains were recorded at each loading step up to failure of the cylinder, using the Peekel strain indicator. All the tests were carried out in accordance to the recommendations in BS.1881: 1970[47] except (E_c) and (ν_c) tests.

To determine the physical properties of reinforcement steel control specimens were tested in tension, using a 500 kN capacity Dennison universal testing machine incorporated with Baldwin recorder which produced a load-extension graph.

Each complete sequence of preparation, manufacturing and testing for an individual specimen took approximately ten man-days of laboratory work.

CHAPTER 3

EXPERIMENTAL RESULTS

3.1 Introduction

This chapter is concerned with the results of the test specimens described in chapter 2 in sections 2.2.1 and 2.2.2, respectively. As described in the previous chapter, the tests were classified into eleven groups according to the variables investigated. In this chapter the observed failure modes in connection with the variables are reported in general terms referring to a group of tests or a particular specimen. The strain and deflection data obtained from the tests are studied. Deflection is plotted against load up to failure in the column and foundation. The failure load of the specimen and slip of the column longitudinal reinforcement along the anchorage length in foundation is given. Load versus strain development in the column and foundation steel and the resulting bond stress distribution in the embedment length of the foundation as well as in the column are presented and discussed.

The physical properties of the concrete and reinforcing steel employed in the main tests in parts one and two are also given in this chapter.

3.2 Test Results

The test results are classified into those recorded from the main specimens and those for the control specimens. Both the results of the main tests and control specimens are described in the following subsections.

3.2.1 Control Specimens

A number of tests were carried out on control specimens to determine the physical properties of concrete and reinforcing steel employed in the main tests. These tests produced values for the characteristic concrete cube strength (f_{cu}), tensile strength (f_t), cylinder compressive strength (f_{cy}), Young's modulus (E_c), Poisson's ratio (ν_c), the ratio of cylinder strength to cube strength (f_{cy}/f_{cu}), and, yield stress of steel (f_y), ultimate stress (f_u) and Young's modulus (E_s). The test results of the concrete and steel specimens in parts one and two are presented in tables (3.1) and (3.2), respectively. In both tables, each result for concrete represents the average from three or four tests, while each result for steel represents the average from two or three tests, carried out at the time of testing the corresponding control specimen to failure as described in sections (2.5.1) and (2.5.2), respectively, in chapter 2. The mean and the standard deviation of each physical property for both concrete and steel are also given in tables (3.1) and (3.2).

From table (3.1) the mean concrete cube strength in part one is 35.82 N/mm^2 with a standard deviation of 4.27%. In part two, excluding group IX, the mean concrete cube strength is 31.58 N/mm^2 with a standard deviation of 6.68% as shown in table (3.2). In group IX tests, the concrete cube strength was deliberately varied, and therefore, the test results in this group were excluded in determining the mean and standard deviation for each physical property of concrete given in table (3.2). The mean ratio of cylinder strength to cube strength (f_{cy}/f_{cu}) for all group of tests in parts one and two is 0.832 with a standard deviation of 5.10%.

Test Specimen No:	CONCRETE						STEEL (SQUARE TWISTED BAR)				
	cube compressive strength f_{cu} N/mm^2	tensile strength f_t N/mm^2	cylinder compressive strength f_{cy} N/mm^2	Young's modulus E_c kN/mm^2	Poisson's ratio ν_c	$\frac{f_{cy}}{f_{cu}}$	Bar Size ϕ mm	Yield stress f_y N/mm^2	Ultimate stress f_u N/mm^2	Young's modulus E_s kN/mm^2	Remarks
S1-1	35.84	2.52	31.40	29.87	0.145	0.876	16	495.00	595.65	206.50	M.R.
S1-2	34.55	2.56	27.77	28.98	0.134	0.804	20	470.54	577.71	208.78	M.R.
S1-3	35.85	2.68	28.48	27.21	0.143	0.794	25	451.63	550.41	211.00	M.R.
$\bar{S}$1-3	37.49	2.54	29.39	32.68	0.132	0.784	25	439.92	547.35	207.80	M.R.
S2-1	37.29	2.92	29.43	31.34	0.139	0.789	25	454.68	557.03	209.49	M.R.
$\bar{S}$2-1	35.58	2.40	26.37	29.95	0.141	0.741	25	444.00	548.88	210.13	M.R.
S2-2	37.20	2.68	28.53	28.73	0.155	0.767	25	450.61	552.44	210.03	M.R.
$\bar{S}$2-2	37.12	2.50	32.59	32.34	0.119	0.878	25	448.06	547.35	211.30	M.R.
S2-3	33.04	2.74	28.75	28.84	0.140	0.870	25	457.23	554.99	213.36	M.R.
S2-4	37.42	2.44	29.94	30.05	0.130	0.800	25	450.61	547.35	210.13	M.R.
S3-1	34.19	2.51	29.81	28.03	0.153	0.872	25	461.30	552.44	192.43	M.R.
S3-2	34.22	2.57	27.95	30.62	0.138	0.817	25	451.12	551.43	211.19	M.R.
MEAN	35.82	2.59	29.20	29.89	0.139	0.816		450.92	550.97	208.69	
STANDARD % DEVIATION	4.27	5.41	5.65	5.55	7.05	5.74	25mm only	1.36	0.61	2.82	
							M.R: Column bars as main reinforcement				

TABLE 3.1: PHYSICAL PROPERTIES OF THE CONCRETE AND REINFORCING STEEL IN PART ONE

Test Specimen No:	CONCRETE						STEEL (RIBBED BAR)				
	cube compressive strength f_{cu} N/mm^2	tensile strength f_t N/mm^2	cylinder compressive strength f_{cy} N/mm^2	Young's modulus E_c kN/mm^2	Poisson's ratio ν_c	$\frac{f_{cy}}{f_{cu}}$	Bar Size ϕ mm	Yield stress f_y N/mm^2	Ultimate stress f_u N/mm^2	Young's modulus E_s kN/mm^2	Remarks
SR1-1	31.76	2.23	27.28	26.42	0.144	0.859	16	482.58	612.44	210.08	M.R.
SR1-2	32.31	2.46	27.74	25.62	0.152	0.858	20	437.90	638.54	201.04	M.R.
SR1-3	31.13	2.07	27.46	25.56	0.156	0.882	25	416.50	669.04	196.07	M.R.
SR2-1	32.96	3.03	27.00	27.14	0.151	0.819	25	547.86	766.80	210.00	M.R.
SR2-2	34.71	2.66	28.52	27.60	0.143	0.822	25	551.93	767.82	206.00	M.R.
SR3-1	34.47	2.73	26.44	26.71	0.144	0.767	25	507.13	712.83	208.00	M.R.
SR4-1	30.60	2.48	22.10	22.14	0.159	0.722	25	413.44	664.97	203.67	M.R.
							12	495.14	603.89	202.88	T.R.
SR4-2	31.22	2.26	27.11	23.79	0.145	0.868	25	414.46	664.46	185.15	M.R.
							12	500.00	628.20	207.00	T.R.
SR4-3	29.29	2.23	26.34	23.86	0.159	0.899	25	407.33	656.82	203.11	M.R.
							12	503.09	623.34	205.03	T.R.
SR5-1	29.40	2.12	26.05	24.84	0.158	0.886	25	403.26	654.79	188.04	M.R.
							8	474.49	712.23	195.63	S.R.
SR5-2	32.80	2.16	27.84	25.76	0.142	0.848	25	406.30	660.89	206.95	M.R.
							8	489.41	712.23	195.29	S.R.

TABLE 3.2: PHYSICAL PROPERTIES OF THE CONCRETE AND REINFORCING STEEL IN PART TWO

Test Specimen No:	CONCRETE						STEEL (RIBBED BAR)				
	cube compressive strength f_{cu} N/mm^2	tensile strength f_t N/mm^2	cylinder compressive strength f_{cy} N/mm^2	Young's modulus E_c kN/mm^2	Poisson's ratio ν_c	$\frac{f_{cy}}{f_{cu}}$	Bar Size ϕ mm	Yield stress f_y N/mm^2	Ultimate stress f_u N/mm^2	Young's modulus E_s kN/mm^2	Remarks
SR6-2	34.70	2.54	28.92	27.20	0.147	0.833	25	412.42	664.97	203.89	M.R.
							12	495.14	617.60	207.59	T.R.
SR6-3	31.67	2.16	25.73	25.64	0.142	0.812	25	414.64	648.67	203.90	M.R.
							12	515.03	636.16	210.00	T.R.
SR6-4	32.02	2.50	27.80	25.88	0.143	0.868	25	414.46	645.62	174.97	M.R.
							12	506.04	620.10	208.30	T.R.
SR7-1	32.56	2.64	28.59	27.48	0.143	0.878	25	402.24	680.24	200.27	M.R.
							8	480.45	708.25	201.37	S.R.
SR7-2	32.67	2.52	27.91	26.51	0.142	0.854	25	407.33	678.72	201.12	M.R.
							8	475.48	713.72	203.86	S.R.
							12	496.02	613.92	214.41	T.R.
SR8-1	25.56	2.23	20.59	23.84	0.160	0.806	25	413.44	679.23	216.41	M.R.
SR8-2	21.90	2.07	18.40	21.91	0.143	0.840	25	416.50	683.30	217.00	M.R.
SR8-3	27.82	2.26	23.41	26.24	0.146	0.841	25	434.8	677.19	216.80	M.R.
SR8-4	36.30	3.13	29.93	30.36	0.154	0.824	25	424.64	662.93	208.63	M.R.

TABLE 3.2: (continued)

Test Specimen No:	CONCRETE						STEEL (RIBBED BAR)				
	cube compressive strength f_{cu} N/mm^2	tensile strength f_t N/mm^2	cylinder compressive strength f_{cy} N/mm^2	Young's modulus E_c kN/mm^2	Poisson's ratio ν_c	f_{cy} / f_{cu}	Bar Size ϕ mm	Yield stress f_y N/mm^2	Ultimate stress f_u N/mm^2	Young's modulus E_s kN/mm^2	Remarks
SR9-1	27.00	2.30	22.92	26.41	0.159	0.849	25	418.53	680.25	214.33	M.R.
							8	509.80	716.20	203.68	S.R.
							12	503.32	631.74	215.54	T.R.
SR9-2	29.22	2.39	25.26	27.98	0.157	0.864	20	425.16	651.27	200.56	M.R.
							8	485.43	701.78	202.08	S.R.
							12	518.13	633.95	215.74	T.R.
SR10-1	28.27	2.26	23.65	27.15	0.160	0.837	25	416.50	681.77	209.21	M.R.
							8	487.42	720.18	206.05	S.R.
							12	496.46	618.92	209.94	T.R.
SR10-2	32.91	2.47	27.39	27.03	0.146	0.832	25	413.44	678.72	205.93	M.R.
							8	482.14	714.22	209.56	S.R.
							12	508.40	633.07	216.48	T.R.
MEAN	31.58	2.41	26.60	26.04	0.150	0.840	25	431.29	680.00	203.78	M.R.
							12	503.34	623.72	210.26	T.R.
							8	485.58	712.35	202.19	S.R.
STANDARD DEVIATION %	6.68	9.96	7.03	5.65	4.67	4.64	25	10.41	4.78	5.20	M.R.
							12	1.58	1.60	2.22	T.R.
							8	2.29	0.77	2.41	S.R.

M.R.: Column bars as main reinforcement, S.R.: Links as secondary reinforcement,
T.R.: Tension reinforcement in base

TABLE 3.2: (continued)

To determine Young's modulus and Poisson's ratio of concrete the strain data was obtained from capped cylinder tests. Young's modulus was determined from the stress-strain relationship of the concrete. The slope of the vertical strain curve was calculated at various stress levels up to failure and then the mean value was found and expressed as Young's modulus of the concrete. Poisson's ratio was also calculated at the various stress levels and the mean value was taken as Poisson's ratio of the concrete. One set of typical strain data and the resulting values of Young's modulus and Poisson's ratio of concrete at various stress levels are given in the tabular form in Appendix A.

From the inspection of tables (3.1) and (3.2) it can be seen that the physical properties of square twisted bars were more consistent than that of ribbed bars.

In the comparison of the test results with existing code of practices and theoretial predictions, the actual physical properties of materials determined from control specimens for both concrete and steel are employed.

3.2.2 Main Test Specimens

The ultimate loads of the specimens in parts one and two except for those in groups X and XI are given in table (3.3). The first visible cracking load, the total vertical displacement of the column cage, i.e. the overall slip of the column longitudinal bars along the anchorage length in the foundation after failure, and the observed manner of failure are also shown in this table. The ultimate loads

related to each variable for each test group are also shown in a series of graphs in figures (3.1a to k).

Figure (3.1a) relates the ratio of ultimate load to concrete compressive strength (P_{test}/f_{cu}) and ($P_{test}/\sqrt{f_{cu}}$) to the bar size (ϕ) in group I. It can be seen from the figure that the ultimate load increases linearly with increasing the bar size within the range of bars used. A linear regression analysis yields the following expressions along with the correlation coefficient (R).

$(P_u/f_{cu}) = 1.479\ (\phi) - 12.546,\ R = 0.999$ (3.1a)

$(P_u/\sqrt{f_{cu}}) = 9.105\ (\phi) - 80.146,\ R = 0.9995$ (3.1b)

It is evident from these equations that the results are marginally better related to the ratio ($P_{test}/\sqrt{f_{cu}}$) than the ratio (P_{test}/f_{cu}).

In group II the ultimate load divided by square root of concrete compressive strength is plotted against the anchorage length ratio (l_{amin}/l_a) and ($1000/l_a$). The relationships for both are illustrated in figure (3.1b). From the figure the ultimate load decreases linearly with increasing values of both ratios and a regression analysis yields the following results.

$(P_u/\sqrt{f_{cu}}) = -115.223\ (l_{amin}/l_a) + 206.998,\ R = -0.996$ (3.2a)

$(P_u/\sqrt{f_{cu}}) = -19.608\ (1000/l_a) + 207.072,\ R = -0.995$ (3.2b)

Where

P_u = the ultimate load (kN)

l_a = the anchorage length (mm)

l_{amin} = the minimum anchorage length used in the tests (mm)

f_{cu} = the concrete compressive strength (N/mm^2)

Figures (3.1c) and (3.1d) illustrate the relationship between the ultimate load (P_{test}) and the ratio of ($P_{test}/\sqrt{f_{cu}}$) against the base

area (AxB), and the ratio of the base unloaded area to column core area (A_b/A_{core}), respectively for group III. As could be seen from the figures an increase in base size or the ratio, (A_b/A_{core}) leads to increase in the ultimate load.

As stated in chapter 2 tests designated as groups IV to XI in part two were carried out with ribbed bars.

When the bar size is varied, as for group IV, the relationships between ($P_{test}/\sqrt{f_{cu}}$) and the bar size (ϕ) and bar size ratio (ϕ_{max}/ϕ) are shown in figure (3.1e). From the figure the ratio of ($P_{test}/\sqrt{f_{cu}}$) is related to the bar size ratio by a straight line given by the following expression.

$$(P_u/\sqrt{f_{cu}}) = -82.875\ (\phi_{max}/\phi) + 195.824,\ R = -0.992 \qquad (3.3)$$

Where ϕ_{max} is the maximum nominal bar size used in the tests.

Figure (3.1f) represents the results of group V and shows that the ultimate load is related to the anchorage length (l_a) and the ratio of (l_{amin}/l_a). From the figure the ultimate load increases linearly with the anchorage length and, this relationship can be expressed by the following equation obtained from a regression analysis.

$$(P_u/\sqrt{f_{cu}}) = 0.954\ (l_a) - 57.621,\ R = 0.993 \qquad (3.4)$$

Two test results from group VI relating ($P_{test}/\sqrt{f_{cu}}$) and base area (AxB) are also shown in figure (3.1f). Although two results are not conclusive it can be seen from the figure that there is an increase in the ultimate load as the base size increases.

Figures (3.1g) and (3.1h) relate the ratio of ultimate load to

square root of concrete compressive strength ($P_{test}/\sqrt{f_{cu}}$) to the base tension reinforcement percentage (ρ_b) in group VIIa and VIIb, respectively. From both figures, it can be seen that the ultimate load increases by increasing the base tension reinforcement.

The effect of the column core confining reinforcement (ρ_{sv}) on the ultimate load in bond is shown in figures (3.1i) and 3.1j) for groups VIIIa and VIIIb, respectively. It can be seen from the figures that the ultimate load increases with increasing the confining reinforcement except for test SR5-2. This test specimen failed in the column cage by the buckling of the exposed column bars above the base before they developed the full bond strength due to the confinement provided by the links. It should be noted that test SR7-2 also included base tension reinforcement. It was taken into account in calculating column core confining reinforcement percentage since the base tension reinforcement introduced confinement to the bottom portion of the column bars.

The variation of the ultimate load with respect to the concrete compressive strength (f_{cu}) and ($\sqrt{f_{cu}}$) is shown in figure (3.1k). From the figure, the ultimate load varies linearly with the concrete compressive strength and $\sqrt{f_{cu}}$. The respective expressions obtained from a regression analysis are as follows.

$$P_u = 12.957\ (f_{cu}) + 203.947,\ R = 0.993 \qquad (3.5)$$

$$P_u = 139.288\ \sqrt{f_{cu}} - 167.414,\ R = 0.994 \qquad (3.6)$$

The ultimate loads of the specimens with a short column for groups X and XI are given in table (3.4). The cracking load, the measured slip of column longitudinal bars in the foundation and, the manner of failure are indicated in the table. It can be observed from table

Test Specimen No:	Cracking Load P_c	Ultimate Load P_{test}	Average slip of column bars	Manner of Failure
	kN	kN	mm	
S1-1	-	397.5	7.77	Type 1a
S1-2	-	590.0	9.75	Type 1a
S1-3	-	890.0	18.39	Type 1a
$\overline{S}$1-3	-	900.0	21.41	Type 1a
S2-1	720.0	720.0	28.61	Type 1b
$\overline{S}$2-1	710.0	710.0	27.73	Type 1b
S2-2	800.0	800.0	25.88	Type 1b
$\overline{S}$2-2	805.0	805.0	24.59	Type 1b
S2-3	-	885.0	9.98	Type 1a
S2-4	565.0	565.0	26.71	Type 1b
S3-1	870.0	870.0	17.28	Type 1b
S3-2	-	920.0	18.62	Type 1a
SR1-1	-	365.0	30.00	Type 1a
SR1-2	543.75	543.75	26.50	Type 1b
SR1-3	1400.0	1400.0	13.57	Type 1c
SR2-1	637.5	637.5	25.82	Type 1b
SR2-2	840.0	840.0	27.35	Type 1b
SR3-1	1075.0	1125.0	6.08	Type 1c

TABLE 3.3: FAILURE LOADS OF SPECIMENS IN PARTS ONE & TWO EXCEPT FOR GROUPS X & X1

Test Specimen No:	Cracking Load P_c	Ultimate Load P_{test}	Average slip of column bars	Manner of Failure
	kN	kN	mm	
SR4-1	1400.0	1400.0	15.79	Type 1c
SR4-2	-	1450.0	8.77	Type 1c
SR4-3	-	1575.0	4.68	Type 1c
SR5-1	1525.0	1525.0	3.89	Type 1c
SR5-2	-	1500.0	0.32	Type 1c*
SR6-2	650.0	650.0	30.00	Type 1b
SR6-3	-	680.0	30.00	Type 1a
SR6-4	-	756.25	30.00	Type 1a
SR7-1	725.0	725.0	11.34	Type 1b
SR7-2	837.5	837.5	30.00	Type 1b
SR8-1	-	525.0	30.00	Type 1a
SR8-2	-	487.5	30.00	Type 1a
SR8-3	-	575.0	30.00	Type 1a
SR8-4	667.5	667.5	24.87	Type 1b

Notes:

1) 30 mm slip indicates the full slip length provided beneath the column longitudinal bars by means of the wooden blocks

2) * indicates failure of column cage

TABLE 3.3: (continued)

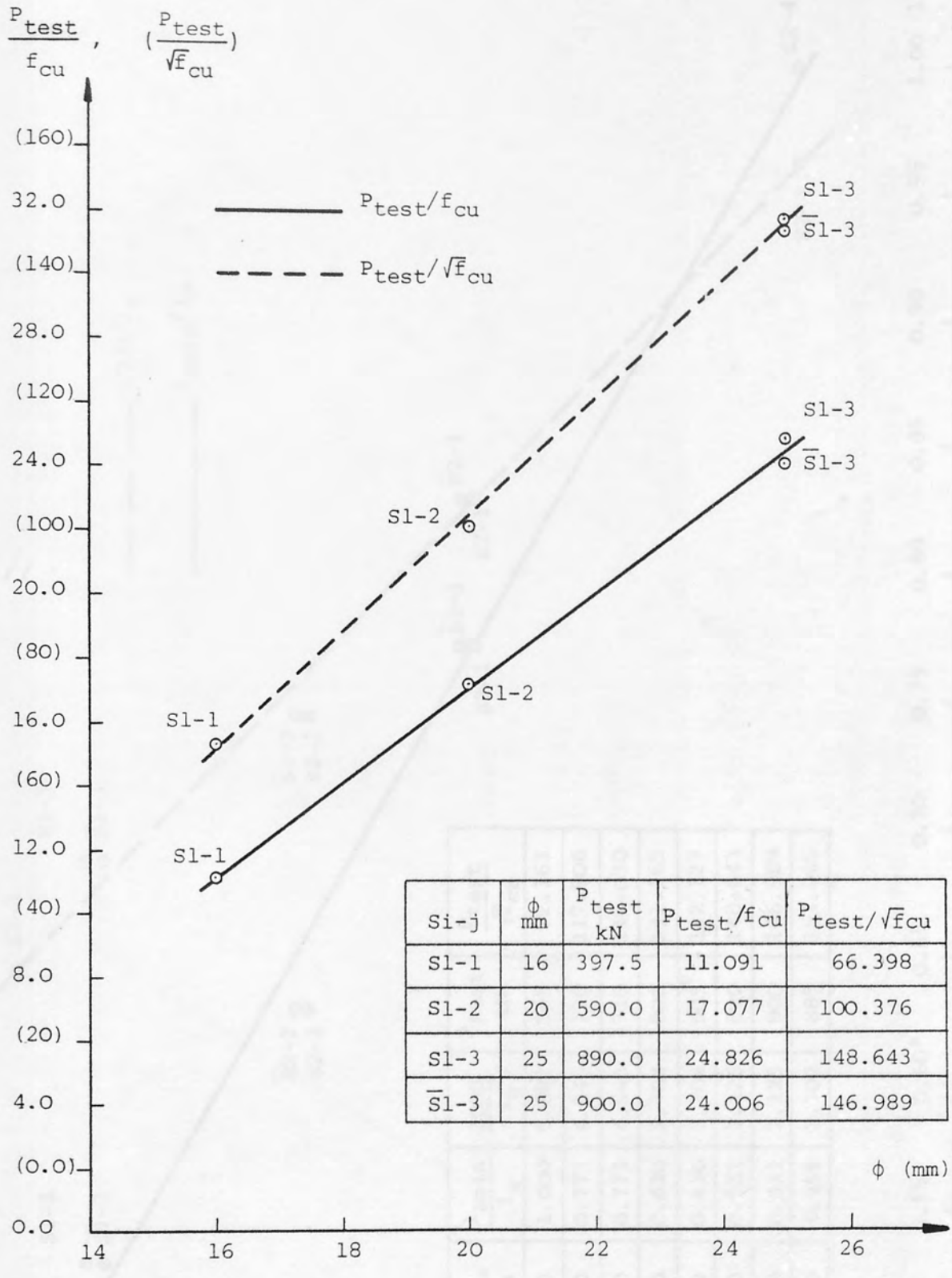

Si-j	ϕ mm	P_{test} kN	P_{test}/f_{cu}	$P_{test}/\sqrt{f_{cu}}$
S1-1	16	397.5	11.091	66.398
S1-2	20	590.0	17.077	100.376
S1-3	25	890.0	24.826	148.643
$\overline{S1}$-3	25	900.0	24.006	146.989

FIGURE 3.1a: BAR SIZE VERSUS RATIO OF (P_{test}/f_{cu}) & $(P_{test}/\sqrt{f_{cu}})$ IN BOND IN GROUP I

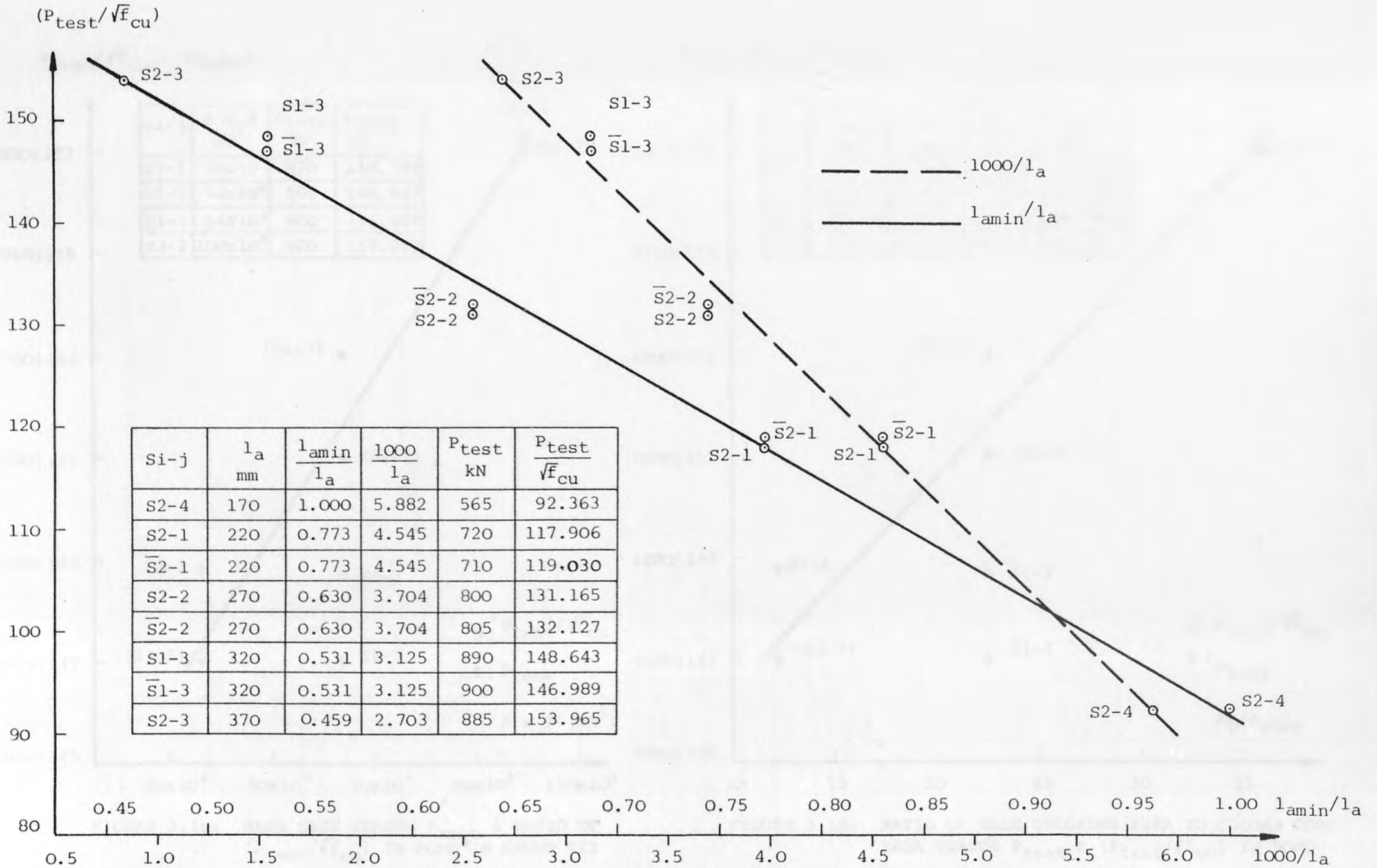

Si-j	l_a mm	$\frac{l_{amin}}{l_a}$	$\frac{1000}{l_a}$	P_{test} kN	$\frac{P_{test}}{\sqrt{f}_{cu}}$
S2-4	170	1.000	5.882	565	92.363
S2-1	220	0.773	4.545	720	117.906
$\bar{S}$2-1	220	0.773	4.545	710	119.030
S2-2	270	0.630	3.704	800	131.165
$\bar{S}$2-2	270	0.630	3.704	805	132.127
S1-3	320	0.531	3.125	890	148.643
$\bar{S}$1-3	320	0.531	3.125	900	146.989
S2-3	370	0.459	2.703	885	153.965

FIGURE 3.1b: RATIO OF (l_{amin}/l_a) & $(1000/l_a)$ VERSUS $(P_{test}/\sqrt{f}_{cu})$ IN BOND IN GROUP II

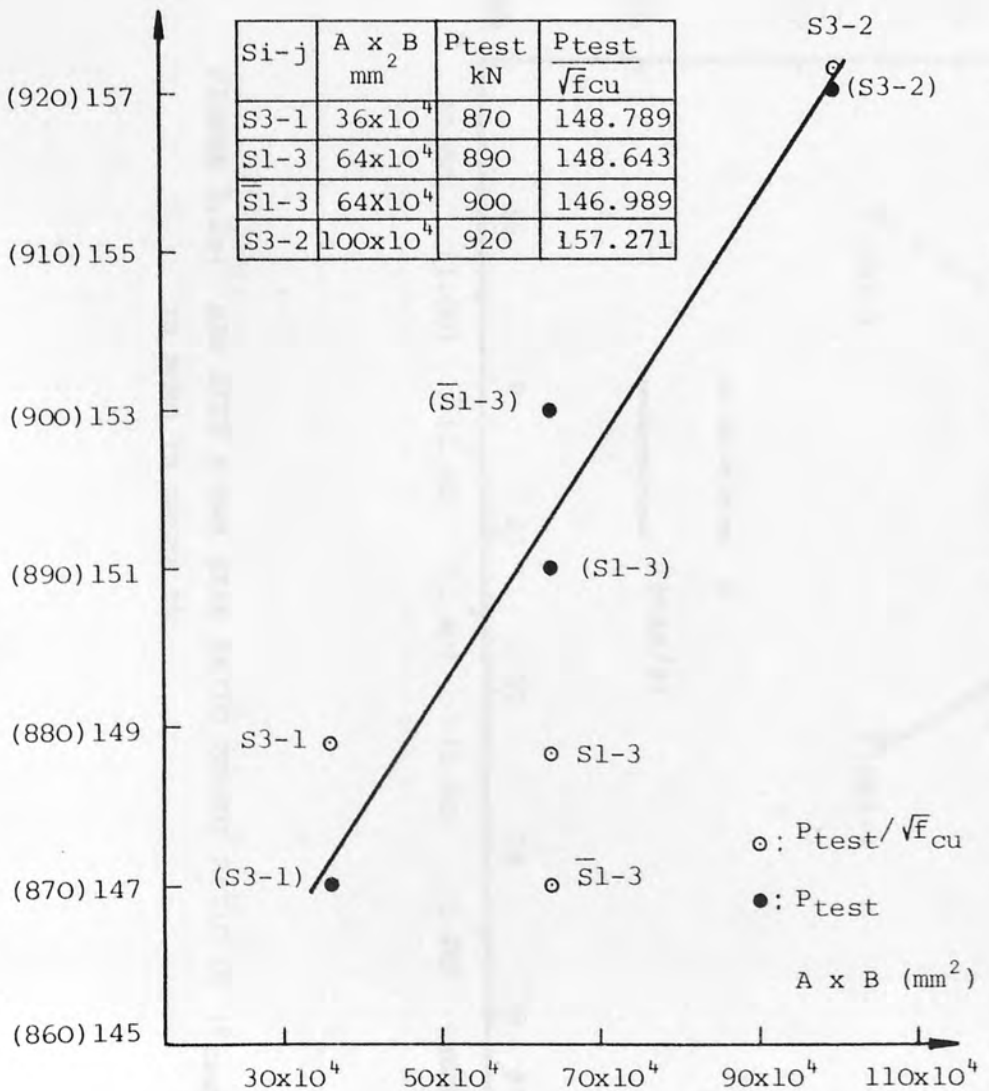

Si-j	A x B mm^2	Ptest kN	$\frac{P_{test}}{\sqrt{f}_{cu}}$
S3-1	$36x10^4$	870	148.789
S1-3	$64x10^4$	890	148.643
$\bar{S}$1-3	$64x10^4$	900	146.989
S3-2	$100x10^4$	920	157.271

FIGURE 3.1c: BASE SIZE VERSUS P_{test} & RATIO OF ($P_{test}/\sqrt{f}_{cu}$) IN BOND IN GROUP III

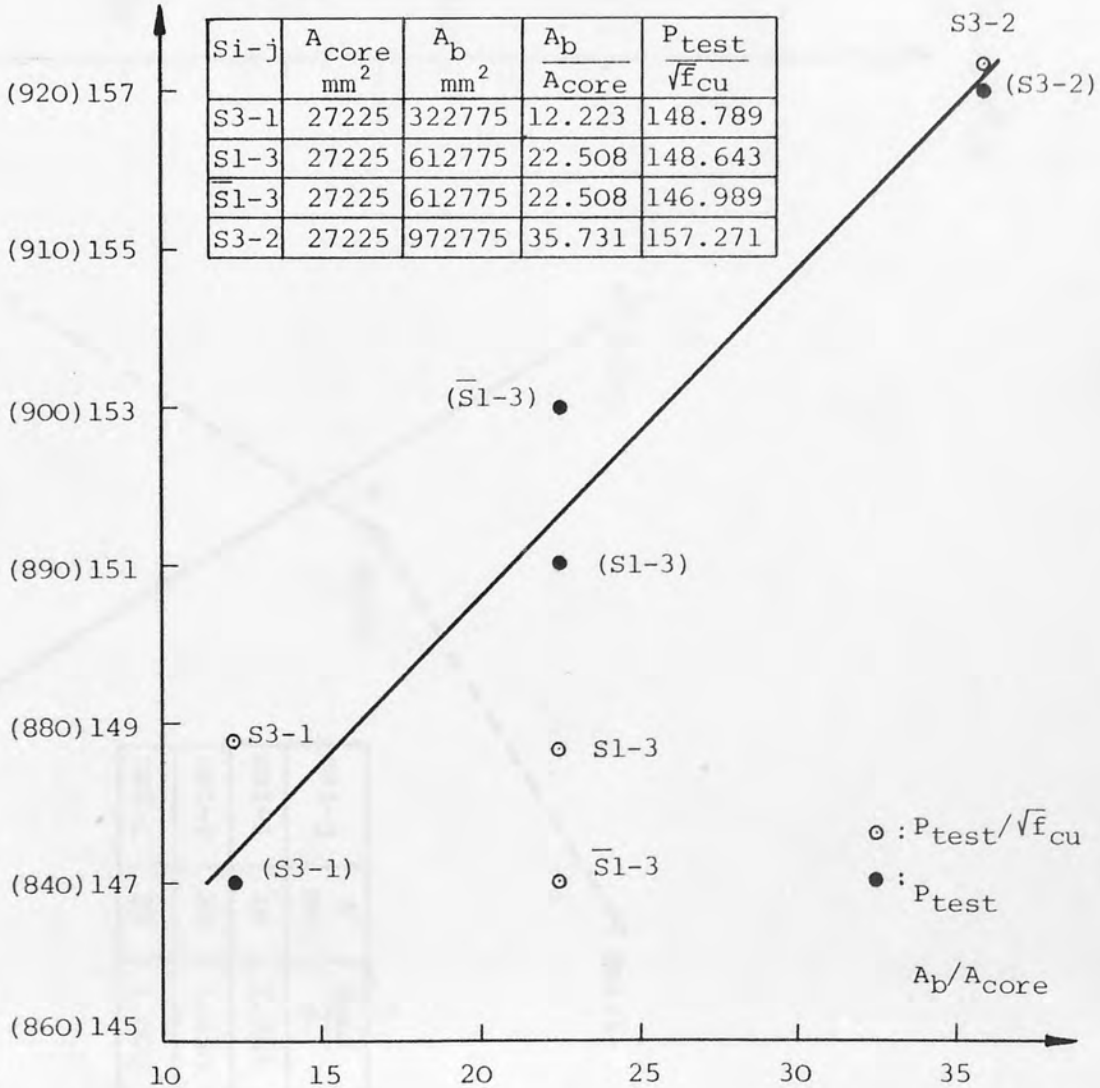

Si-j	A_{core} mm^2	A_b mm^2	$\frac{A_b}{A_{core}}$	$\frac{P_{test}}{\sqrt{f}_{cu}}$
S3-1	27225	322775	12.223	148.789
S1-3	27225	612775	22.508	148.643
$\bar{S}$1-3	27225	612775	22.508	146.989
S3-2	27225	972775	35.731	157.271

FIGURE 3.1d: RATIO OF BASE UNLOADED AREA TO COLUMN CORE AREA VERSUS P_{test} & ($P_{test}/\sqrt{f}_{cu}$) IN BOND IN GROUP III

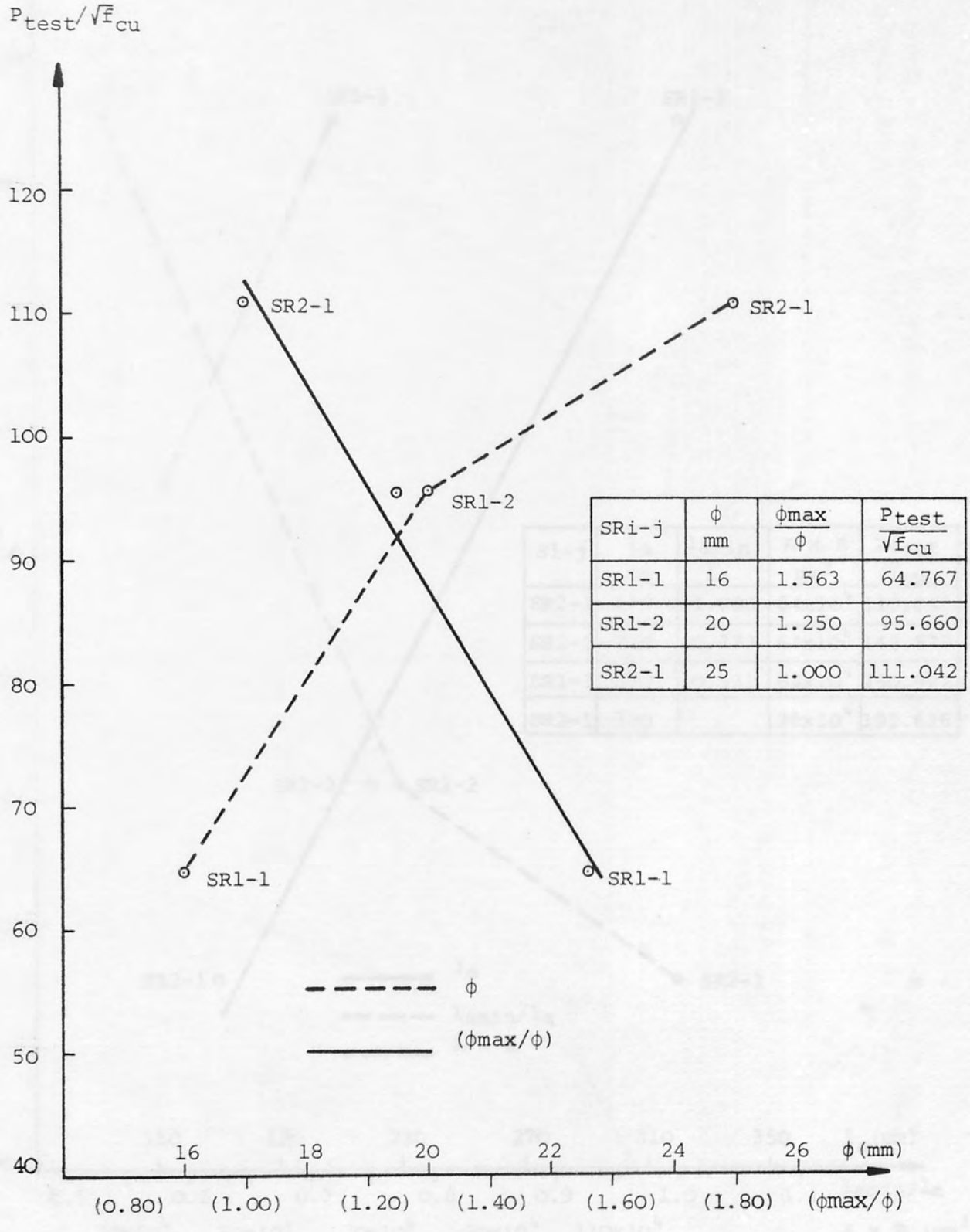

SRi-j	ϕ mm	ϕmax / ϕ	$P_{test}/\sqrt{f_{cu}}$
SR1-1	16	1.563	64.767
SR1-2	20	1.250	95.660
SR2-1	25	1.000	111.042

FIGURE 3.1e: BAR SIZE & BAR SIZE RATIO VERSUS RATIO OF ($P_{test}/\sqrt{f_{cu}}$) IN BOND IN GROUP IV

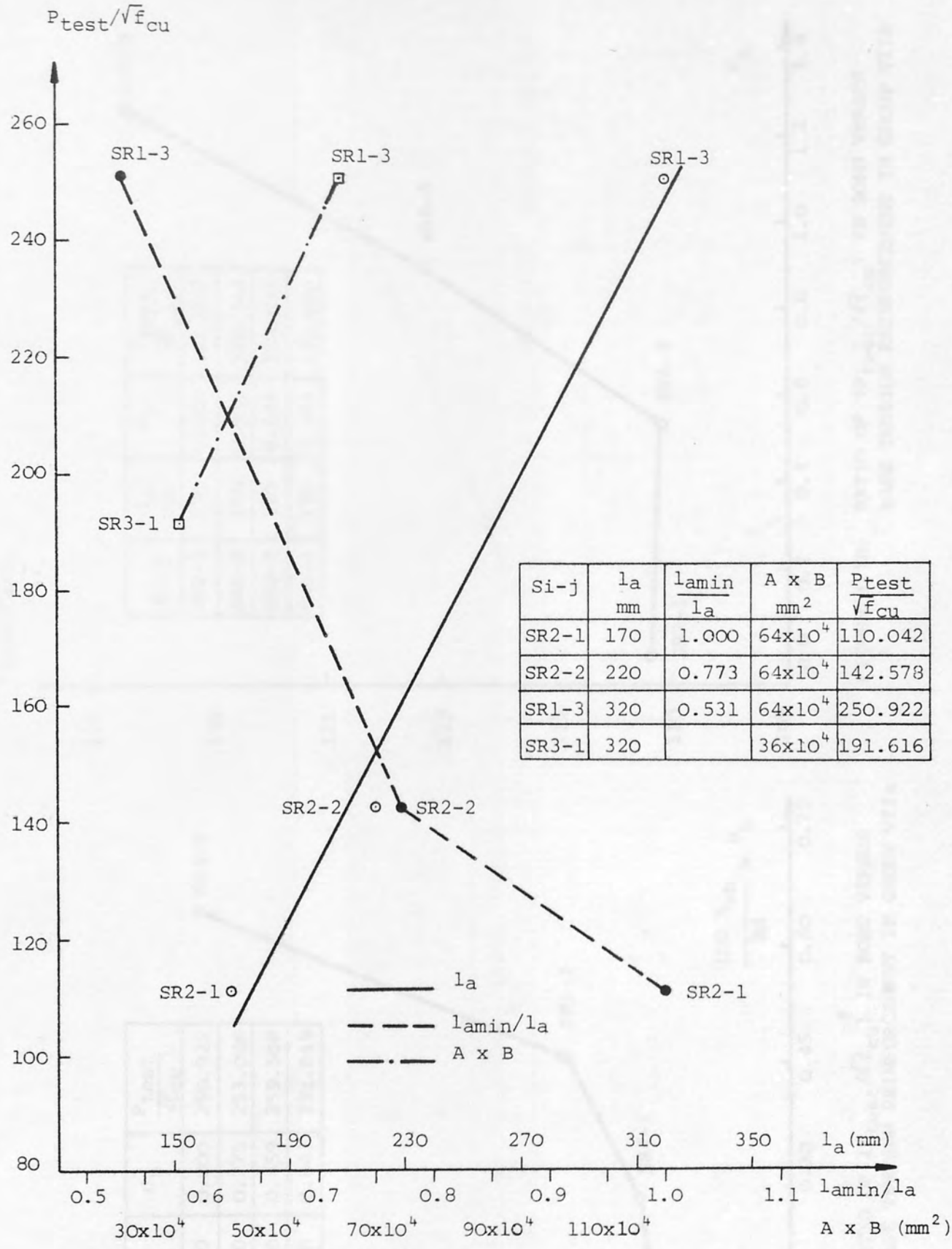

Si-j	l_a mm	$\frac{l_{amin}}{l_a}$	A x B mm^2	$\frac{P_{test}}{\sqrt{f_{cu}}}$
SR2-1	170	1.000	$64x10^4$	110.042
SR2-2	220	0.773	$64x10^4$	142.578
SR1-3	320	0.531	$64x10^4$	250.922
SR3-1	320		$36x10^4$	191.616

FIGURE 3.1f: RATIO OF ($P_{test}/\sqrt{f_{cu}}$) IN BOND VERSUS ANCHORAGE LENGTH & ANCHORAGE LENGTH RATIO AND BASE SIZE IN GROUPS V & VI RESPECTIVELY

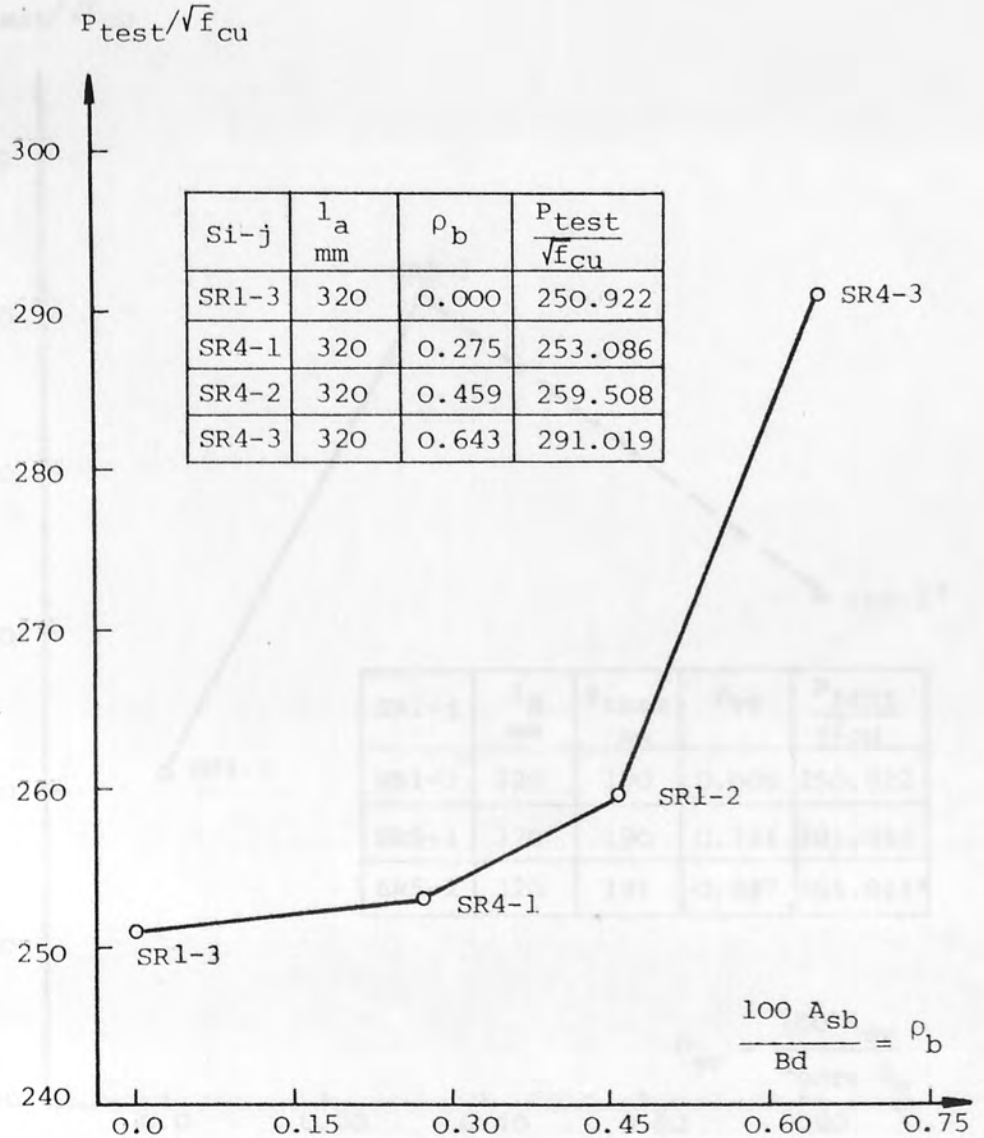

Si-j	l_a mm	ρ_b	$\frac{P_{test}}{\sqrt{f_{cu}}}$
SR1-3	320	0.000	250.922
SR4-1	320	0.275	253.086
SR4-2	320	0.459	259.508
SR4-3	320	0.643	291.019

FIGURE 3.1g: RATIO OF ($P_{test}/\sqrt{f_{cu}}$) IN BOND VERSUS BASE TENISON REINFORCEMENT IN GROUP VIIa

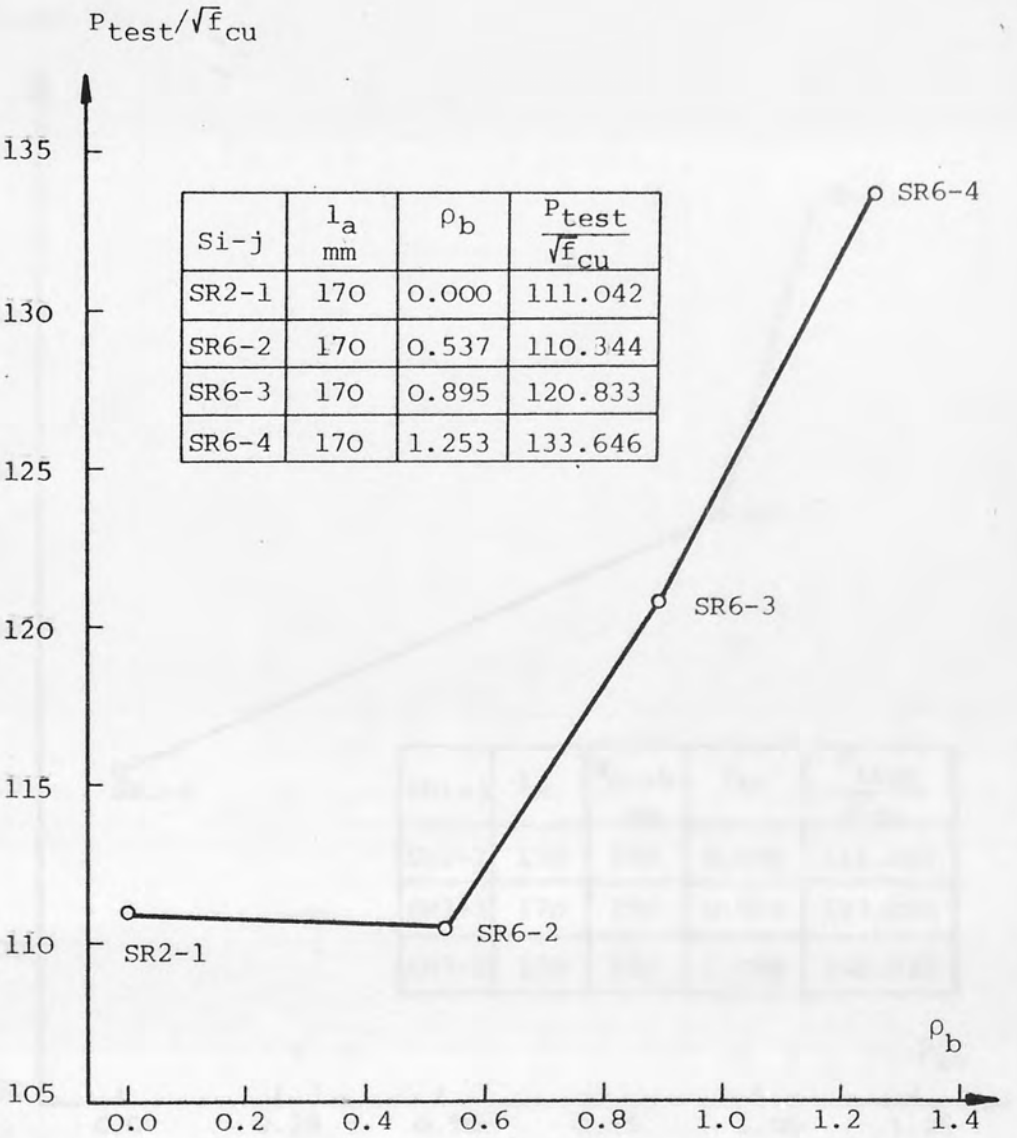

Si-j	l_a mm	ρ_b	$\frac{P_{test}}{\sqrt{f_{cu}}}$
SR2-1	170	0.000	111.042
SR6-2	170	0.537	110.344
SR6-3	170	0.895	120.833
SR6-4	170	1.253	133.646

FIGURE 3.1h: RATIO OF ($P_{test}/\sqrt{f_{cu}}$) IN BOND VERSUS BASE TENSION REINFORCEMENT IN GROUP VIIb

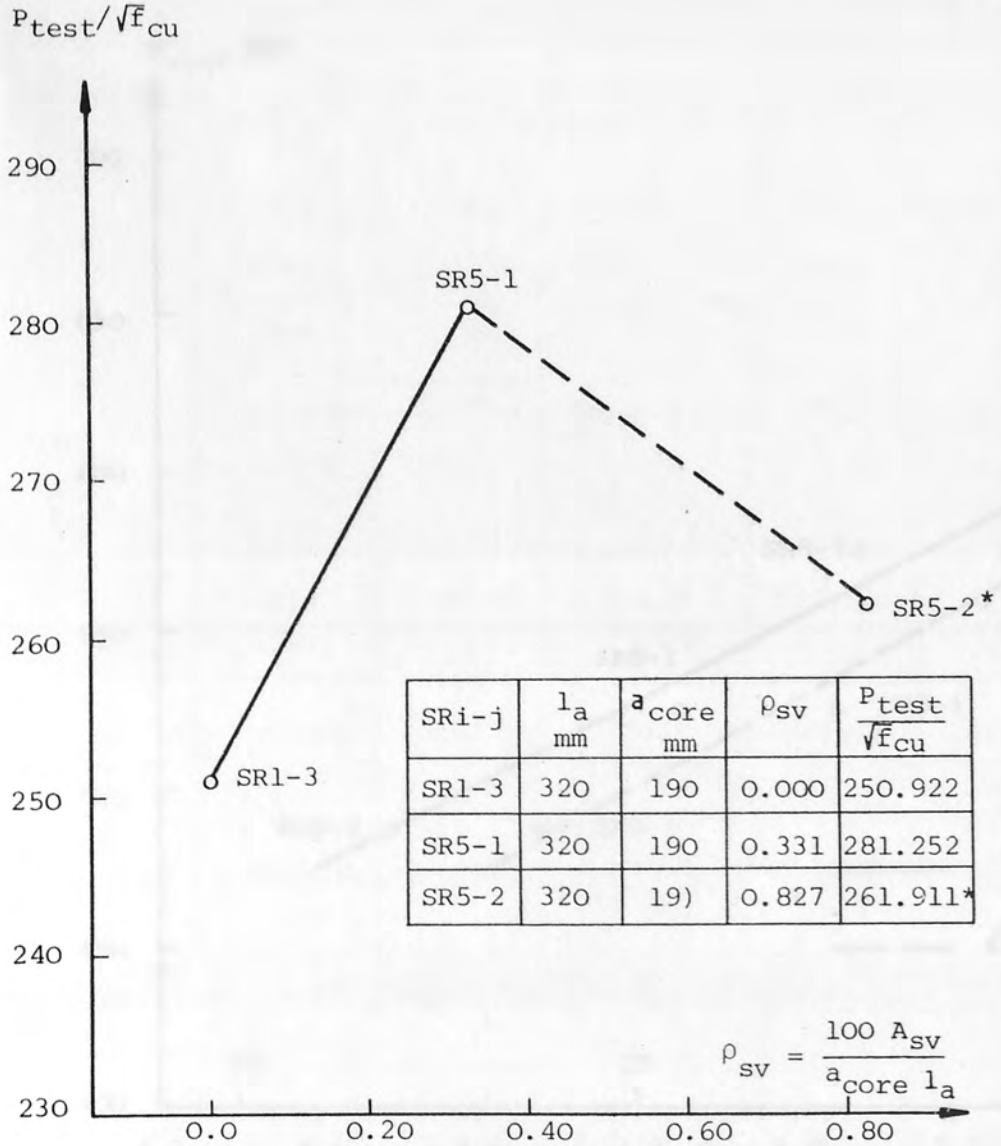

SRi-j	l_a mm	a_{core} mm	ρ_{sv}	$\frac{P_{test}}{\sqrt{f_{cu}}}$
SR1-3	320	190	0.000	250.922
SR5-1	320	190	0.331	281.252
SR5-2	320	19)	0.827	261.911*

FIGURE 3.1i: RATIO OF ($P_{test}/\sqrt{f_{cu}}$) IN BOND VERSUS COLUMN CORE CONFINING REINFORCEMENT IN GROUP VIIIa

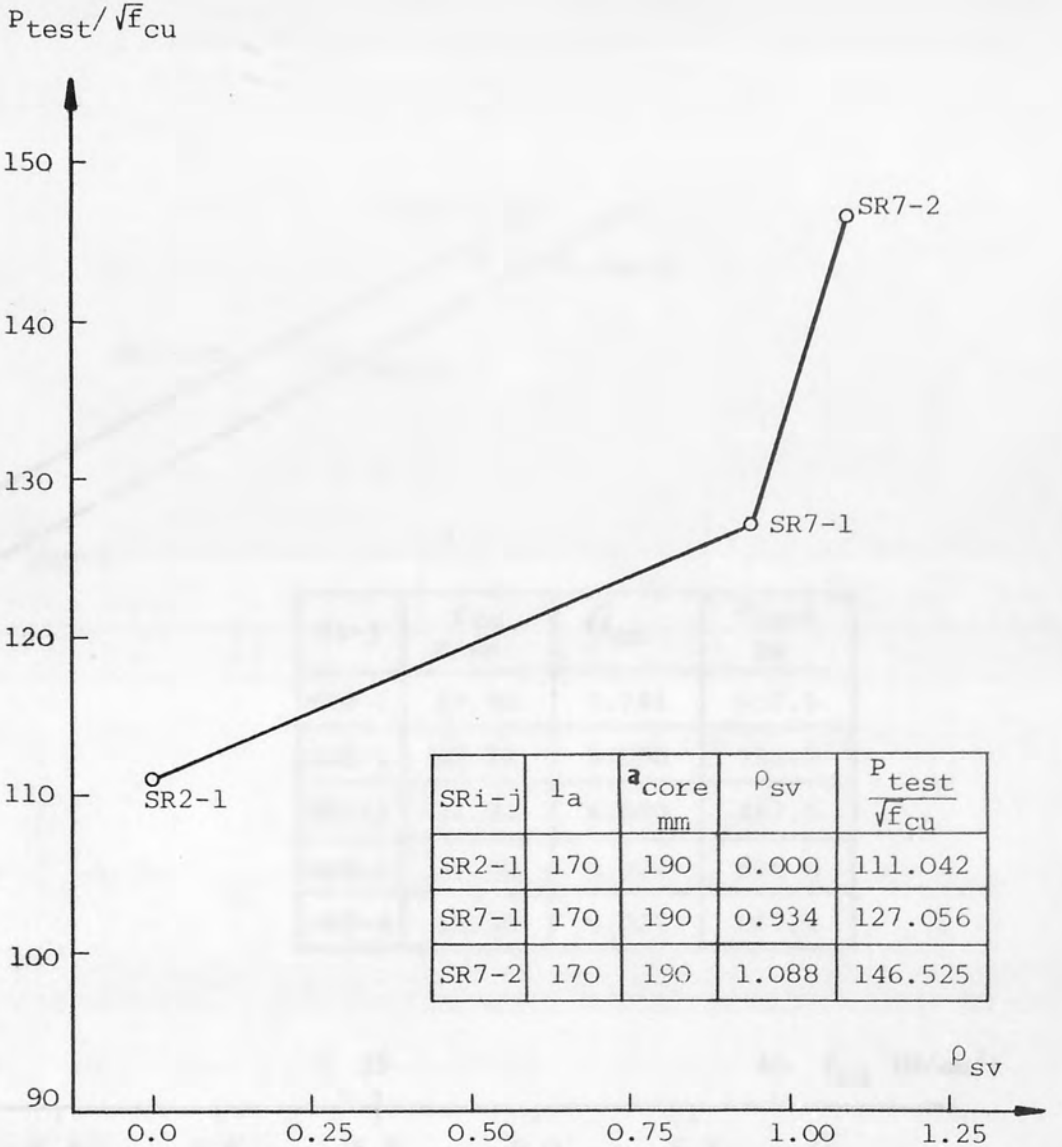

SRi-j	l_a	a_{core} mm	ρ_{sv}	$\frac{P_{test}}{\sqrt{f_{cu}}}$
SR2-1	170	190	0.000	111.042
SR7-1	170	190	0.934	127.056
SR7-2	170	190	1.088	146.525

FIGURE 3.1j: RATIO OF ($P_{test}/\sqrt{f_{cu}}$) IN BOND VERSUS COLUMN CORE CONFINING REINFORCEMENT IN GROUP VIIIb

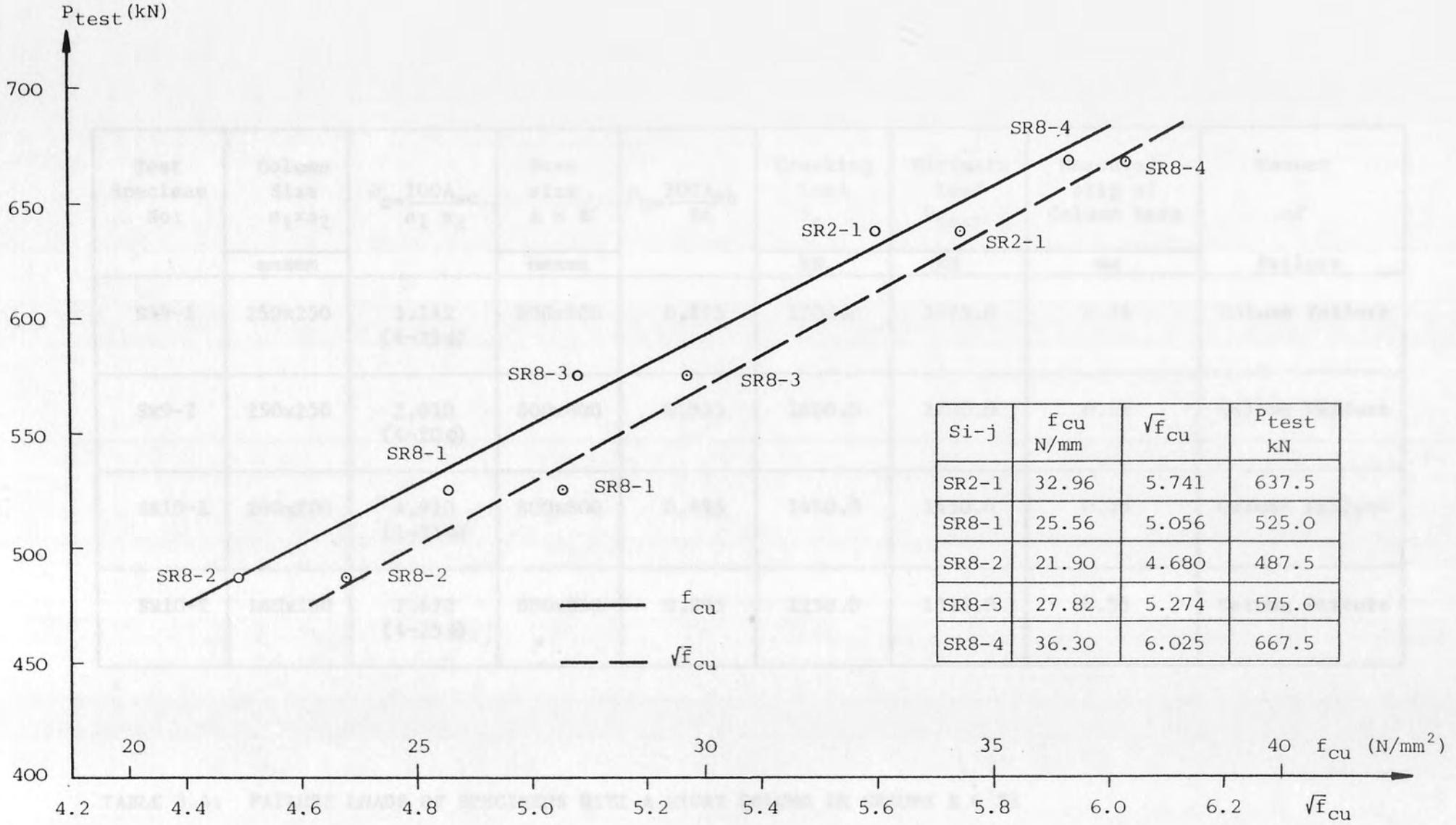

Si-j	f_{cu} N/mm	$\sqrt{f}_{cu}$	P_{test} kN
SR2-1	32.96	5.741	637.5
SR8-1	25.56	5.056	525.0
SR8-2	21.90	4.680	487.5
SR8-3	27.82	5.274	575.0
SR8-4	36.30	6.025	667.5

FIGURE 3.1k: CONCRETE CHARACTERISTIC STRENGTH (f_{cu}) & $\sqrt{f}_{cu}$ VERSUS ULTIMATE LOAD IN BOND IN GROUP IX

Test Specimen No:	Column Size $a_1 x a_2$ mmxmm	$\rho_c = \frac{100 A_{sc}}{a_1 a_2}$	Base size A x B mmxmm	$\rho_c = \frac{100 A_{sb}}{Bd}$	Cracking Load P_c kN	Ultimate Load P_{test} kN	Measured slip of Column bars mm	Manner of Failure
SR9-1	250x250	3.142 (4-25 ϕ)	800x800	0.895	1700.0	1775.0	0.14	Column Failure
SR9-2	250x250	2.010 (4-20 ϕ)	800x800	0.895	1600.0	1700.0	0.12	Column Failure
SR10-1	200x200	4.910 (4-25 ϕ)	800x800	0.895	1450.0	1450.0	0.25	Column Failure
SR10-2	160x160	7.672 (4-25 ϕ)	800x800	0.895	1250.0	1325.0	0.55	Column Failure

TABLE 3.4: FAILURE LOADS OF SPECIMENS WITH A SHORT COLUMN IN GROUPS X & XI

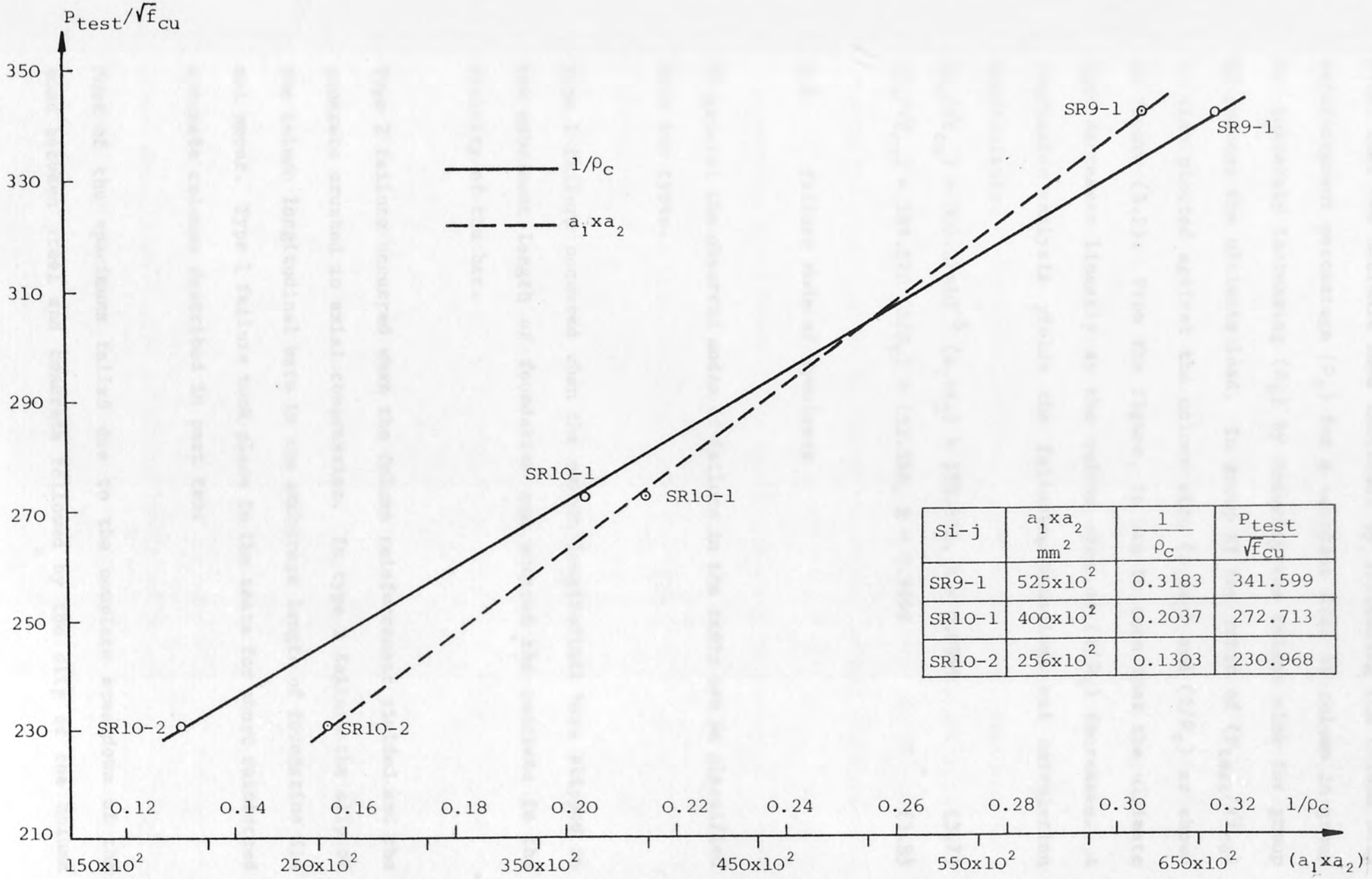

Si-j	$a_1 x a_2$ / mm^2	$\frac{1}{\rho_c}$	$\frac{P_{test}}{\sqrt{f_{cu}}}$
SR9-1	$525x10^2$	0.3183	341.599
SR10-1	$400x10^2$	0.2037	272.713
SR10-2	$256x10^2$	0.1303	230.968

FIGURE 3.2: COLUMN SIZE & $(1/\rho c)$ VERSUS $(P_{test}/\sqrt{f_{cu}})$ IN GROUP XI

(3.4) that the ultimate load increases by increasing the column main reinforcement percentage (ρ_c) for a constant size of column in group X. Conversly increasing (ρ_c) by reducing the column size for group XI reduces the ultimate load. In group XI the ratio of ($P_{test}/\sqrt{f_{cu}}$) is also plotted against the column size ($a_1 x a_2$) and ($1/\rho_c$) as shown in figure (3.2). From the figure, it can be seen that the ultimate load decreases linearly as the column size or ($1/\rho_c$) decreases. A regression analysis yields the following equations and correlation coefficients.

$$(P_u/\sqrt{f_{cu}}) = 300.37 \times 10^{-5} (a_1 x a_2) + 153.502, \quad R = 0.9999 \qquad (3.7)$$

$$(P_u/\sqrt{f_{cu}}) = 589.570 (1/\rho_c) + 153.568, \quad R = 0.9999 \qquad (3.8)$$

3.3 Failure Mode of Specimens

In general the observed modes of failure in the tests can be classified into two types.

Type 1 failure occurred when the column longitudinal bars slipped in the embedment length of foundation and sheared the concrete in the vicinity of the bar.

Type 2 failure occurred when the column reinforcement yielded and the concrete crushed in axial compression. In type 2 failure the slip of the column longitudinal bars in the anchorage length of foundation did not occur. Type 2 failure took place in the tests for short reinforced concrete columns described in part two.

Most of the specimens failed due to the complete breakdown of the bond between steel and concrete followed by the slip of the column

longitudinal bars along the anchorage length in the foundation. In some cases the concrete cracked or split in the foundation at the ultimate load, but the governing failure factor was slip of the column bars, because the slip had occurred at the previous load stages. When the ultimate load was reached prior to any crack formation or split in concrete, the slip became very rapid by shearing the concrete on a surface along the periphery of the square twisted bars or along the tops of the ribs of the ribbed bars. At the very end the concrete cracked or split in the foundation. In some tests the specimens were loaded beyond the yield stress of the column longitudinal reinforcement, but slip occurred prior to any crack formation in the concrete. Finally the column cage distorted in the exposed length of column bars.

The previous brief descriptions of the test may be explained in more detail as follows. Type 1 failure is further divided into three sub-failures, namely type 1a, type 1b and type 1c.

Type 1a failure manner is described as the slip of the column longitudinal bars in the embedment length of the foundation without cracks in the concrete.

Type 1b failure manner is specified as the slip of the column longitudinal bars along the anchorage length in the foundation with cracks in the concrete.

Finally type 1c failure is described as the slip of the column longitudinal bars in the embedment length of foundation and failure of column longitudinal reinforcement with or without cracks in the concrete.

The observed failure types in the tests are given in figures (3.3) to (3.6). Figure (3.3) shows type 1a failure of the specimens. Type 1b failure is illustrated in figure (3.4) and type 1c failure is shown in figure (3.5). Finally type 2 failure of the specimens is shown in figure (3.6). In the following sections the observed failure modes and the behaviour of the specimens in parts one and two are described in general terms with reference to the above mentioned failure types.

3.3.1 Failure of Specimens in Part One

Failure of the specimens with square twisted bars is presented in this section. In these tests the governing failure mode was type 1 and included type 1a and type 1b depending on the specimen. The loading sequence together with recorded measurements for each individual test piece are given in Appendix B, and crack patterns are shown in Appendix C. The general description of the behaviour, and where present the crack pattern for each individual test structure, are reported referring to the test groups as described in chapter 2.

Group 1 contained specimens S1-1, S1-2, S1-3 and $\overline{S1}$-3, tested with 16 mm, 20 mm and 25 mm square twisted bars, respectively. In these specimens failure took place by the slip of the column longitudinal bars along the anchorage length in the foundation. No visible crack took place in the base concrete during the loading sequence including the failure load, so type 1a failure occurred in the specimens. Generally the performance of the specimens in this group was similar. As the loading progressed the slip of the column bars in the embedment length continued at different rates until failure and finally the major slip occurred at the ultimate load. However the first effective

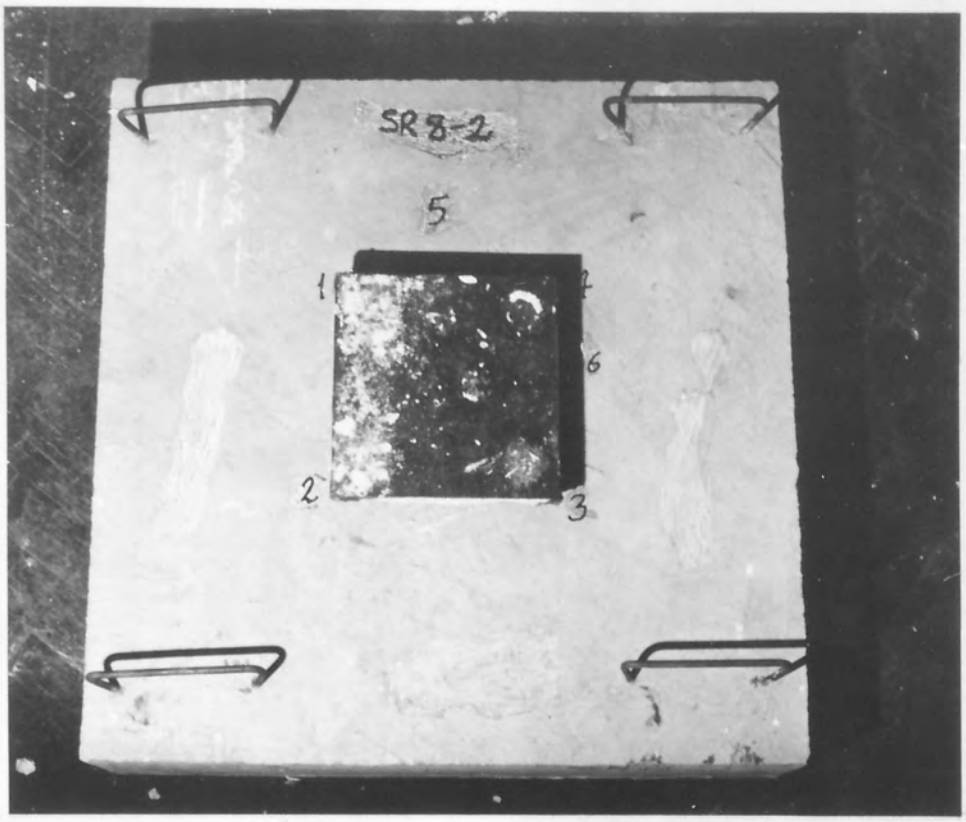

Top View

Bottom View

FIGURE 3.3: TYPE 1a FAILURE

Top View

Bottom View

FIGURE 3.4: TYPE 1b FAILURE

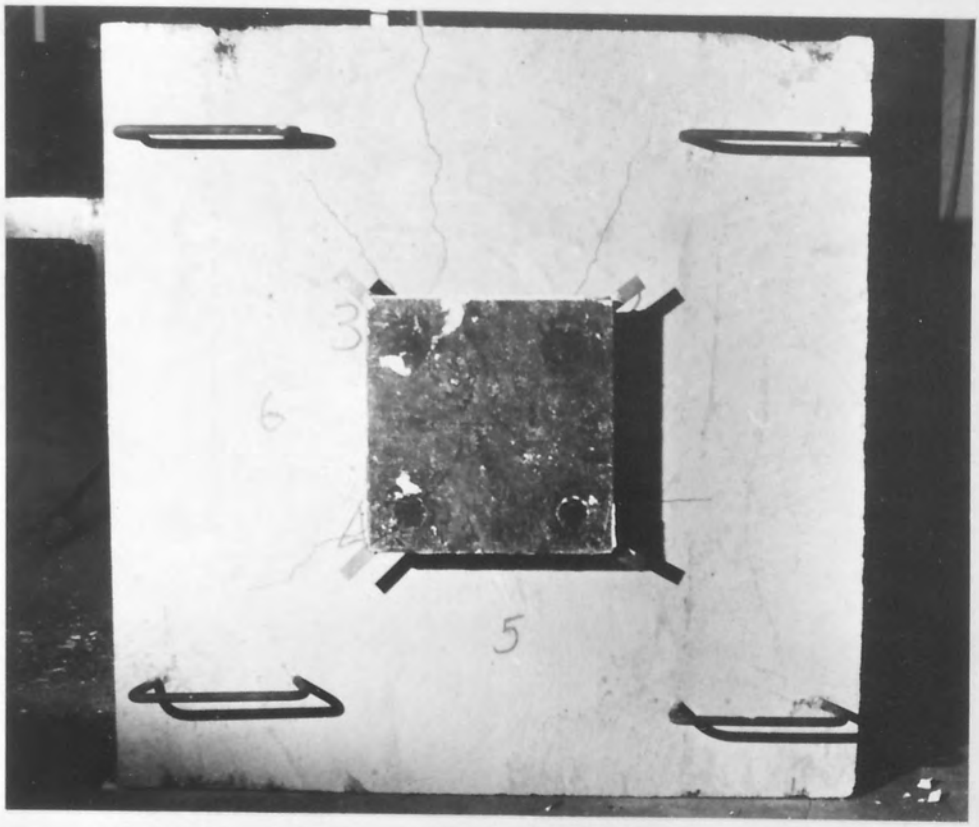

Top View

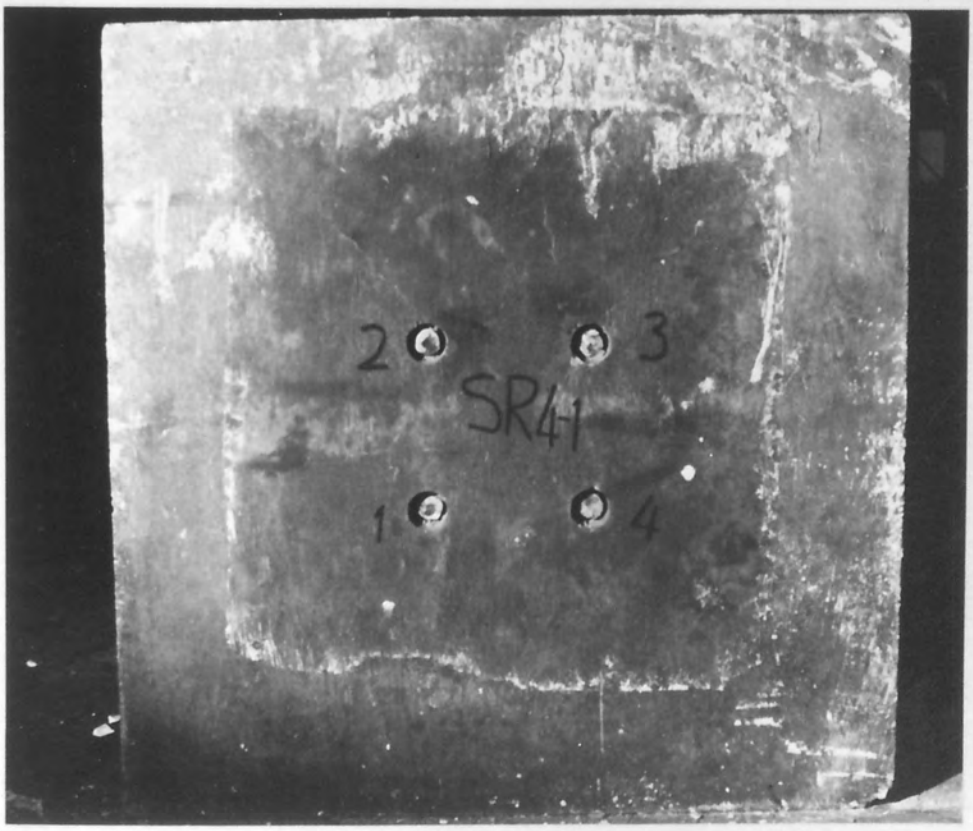

Bottom View

FIGURE 3.5: TYPE 1c FAILURE

FIGURE 3.6: TYPE 2 FAILURE

slip took place at different loads in the specimens.

The first effective slip is defined as the slip in mm which damaged the strain gauges placed on the column longitudinal bars in the embedment length of the foundation. In most cases this amount of slip was approximately 1 mm and subsequently no further strain recording was possible.

The governing types of failure in the tests in group II were type la and type 1b. As the base thickness was increased type 1b failure changed to type la. In foundations labelled S2-4, $\overline{S2}$-1, S2-1, S2-2 and $\overline{S2}$-2 type 1b failure took place, while the rest in this group failed in type la. The performance of the specimens failed in type la was similar to those in group I. After the first slip, the vertical displacement of the column cage, i.e. slip of the column bars along the anchorage length continued progressively until failure, then at the ultimate load the column bars slipped down to the bottom of the base without cracking the concrete.

Specimens of type 1b showed the same behaviour as those described as type la except that the base concrete also cracked and split at ultimate load. The crack pattern of the concrete on the top and bottom faces of the foundation was of similar form. The cracks initiated from the column bars and propagated through the foundation and extended on the top and bottom faces. Those on the top and bottom faces joined each other and extended into the side faces, were splitting cracks. They enlarged towards the sides of the base. Other cracks which initiated at the column bars were smaller and eventually became invisible. In foundations S2-4, S2-1 and $\overline{S2}$-1 sudden failure

took place by rapid slip of the column bars accompanied by cracking and splitting in the base concrete. In contrast when the ultimate load was reached in foundations S2-2 and $\overline{S2}$-2, the slip of the column bars became rapid and, after slip the concrete cracked and split in the base.

Specimens tested in group III failed as type 1a with the exception of test piece S3-1 which failed as type 1b. The performance of the specimens in this group was similar to those tested in group I and, at ultimate load the column longitudinal bars sheared the surrounding concrete. In foundation S3-1 however a crack initiated from one of the column bars at the bottom, extended in the base, travelled upward in the side face and joined the same bar on the top. No further cracks developed in the base.

3.3.2 Failure of Specimens in Part Two

Specimens tested in this part failed as type 1 and and type 2, respectively. For the tests performed with a short reinforced concrete column in groups X and XI type 2 failure took place, while all the other specimens in the rest of groups failed as type 1. As the specifications of the foundations were varied the type 1 failure emerged in one of the subfailure manners, namely, type 1a, 1b and 1c. In the following paragraphs the observed failure manner of specimens is reported with reference to the test groups. Loading sequence and recorded measurements for each individual test structure are presented in Appendix B. Crack patterns of the specimens are given in Appendix C.

In group IV foundation SR1-1 failed as type 1a while the others failed

as type 1b. Generally the performance of the specimens was similar until failure. After first slip as loading progressed the slip of the column longitudinal bars continued. At the ultimate load due to complete breakdown of the bond between steel and concrete the column bars sheared the surrounding concrete at gradually increasing speed and reached to the bottom without any crack in the base in test SR1-1. In contrast in specimens SR1-2 and SR2-1, following the slip of the column bars by shearing the adjacent concrete along the anchorage length, the base concrete also cracked and split. The failure pattern on the top and bottom faces of each base was almost in the same geometrical form (see Appendix C for reference). The cracks generated from the column bars on top and bottom faces and proceeded through the concrete. Some cracks also propagated in the side faces and joined each other, while the others became finer and disappeared in the concrete as they extended from the column bars.

Specimens tested in group V failed as type 1b, except SR1-3, for which type 1c failure took place. As the base thickness was increased in group V tests type 1b failure changed to type 1c. Specimens which failed as type 1b behaved in the same manner as those which failed as type 1b in group IV. In test SR1-3 after the first slip the bare column bars reached yield strength but the column cage maintained its stability and hence it was possible to continue subsequent loading steps. Eventually at the ultimate load following a large slip, the column cage lost its stability due to distortion in the exposed column bars, and at the same time the base concrete cracked on top and bottom faces and split in one of the side faces.

The governing failure type in group VI tests was also type 1c. In

specimen SR3-1 which had smallest base size, prior to ultimate load very fine crack generated in one of the side faces at the bottom and travelled upwards at the two subsequent load increments. At the ultimate the column bars slipped and the base cracked on the top, bottom, and side faces, meanwhile the existing crack enlarged and propagated on the top face as the base split in this side face. It is noted that as the base size is reduced the concrete surrounding the column bars decreases and the bursting forces are larger.

Specimens tested in group VIIa failed as type 1c. In this group the specimens were loaded beyond the yield stress of the longitudinal steel. As the loading progressed the exposed column bars reached yield stress but the column cage remained stable which made it possible to increase the loading. The first slip for specimen SR4-1 followed the yield of steel in the column cage. At the later stages of loading the slip of the column bars continued at low rates until failure. At the ultimate the column bars sheared the concrete followed by distortion of the exposed column bars. The cracks initiated from the column bars progressed on the top face and disappeared before reaching the side faces. At the bottom face cracks generated from two column bars only and propagated in the same way, but one of them extended to the side face, travelled upwards and progressed on the top face. Specimens SR4-2 and SR4-3 showed similar performance but no crack occurred in the base concrete.

In group VIIb types 1a and 1b failure occurred in the specimens. As the base tension reinforcement percentage was increased type 1b failure changed to type 1a. Specimens SR6-3 and SR6-4 failed as type 1a while the others failed as type 1b. When the ultimate load

was reached in test piece SR6-2, due to complete breakdown of bond, the column bars slipped down to the bottom of the base as the ribs progressively crushed the surrounding concrete along the anchorage length. At the same time the cracks generated from the column bars and propagated on the top and bottom as well as in the two side faces (see crack pattern in Appendix C for reference). Both foundations SR6-3 and SR6-4 behaved in the same manner and, as the full bond strength was attained at the final stage of loading the column bars slowly sheared the surrounding concrete and slipped to the bottom with an increasing slip rate. No cracks occurred in the concrete in both specimens.

The observed failure manner of specimens in groups VIIIa and VIIIb was type 1c and type 1b, respectively. Test specimens in group VIIIa showed similar performance to that of specimens in group VIIa. The relative movement between steel and concrete i.e. slip of the column bars, however, was significantly restricted by the links provided in the embedment length of foundation. At the ultimate load failure of the column cage in specimen SR5-1 was accompanied by the slip of the column bars and cracking of concrete in the base, while in specimen SR5-2 neither effective slip nor cracking occurred. Due to the confinement provided by the links, test piece SR5-2 failed in the column cage by buckling of exposed column bars.

In foundations tested in group VIIIb, at the ultimate load the column longitudinal bars slipped as the ribs sheared the surrounding concrete and then the cracks occurred in the base concrete similar to that of specimens in group VIIb. However, in specimen SR7-1, full slip of the column bars was restricted by the confinement of the links provided

along the anchorage length, while in specimen SR7-2 full slip was attained as the column bars slipped to the bottom of the base.

Specimens tested in group IX behaved in the same manner as those in group IV. As the characteristic compressive strength of the concrete was increased type 1a failure changed to type 1b. In foundations SR8-1, SR8-2 and SR8-3 at the ultimate load due to complete breakdown of bond the column bars sheared the concrete and slipped to the bottom of the base without cracking the base, i.e. type 1a failure. The performance of the rest of the specimens that failed as type 1b was similar and, at failure the slip of the column bars was followed by cracking and splitting in the base. The failure pattern of the concrete was approximately the same geometrical form as those in group IV.

The observed failure mode in the specimens tested in groups X and XI was type 2. Group X included specimens SR9-1 and SR9-2 and both failed in compression in the column which produced yielding of the steel and crushing of concrete. As can be seen from table (3.4) in these tests at failure the slip of the column bars was negligible and there was little or no loss of bond between the base slab and the column longitudinal reinforcement.

In test SR9-1 vertical cracks were first observed on faces 1, 2 and 4 of the column under an axial load of 1700 kN as the main column reinforcement yielded. At a load of 1750 kN face 3 also cracked and the existing cracks progressively became worse as they dispersed and travelled upwards. At the ultimate load all faces of the column cracked extensively and the upper link located in the failure zone

yielded. The cracks were concentrated generally on faces 1 and 2 with some spalling, and to a lesser extent on faces 3 and 4 of the column. Part of the column length above the base to column interface was still clear of cracks.

In test SR9-2 as the main reinforcement reached yielding vertical cracks appeared on faces 2 and 3 of the column at a load of 1600 kN. Under an axial load of 1650 kN the other faces also cracked and the existing cracks extended. At the final stage of loading failure occurred by extensive cracking on all faces of the column accompanied by spalling at the side corners. Part of the column above the base slab was again clear.

Group XI covered specimens SR9-1, SR10-1 and SR10-2, and in these tests as the main reinforcement yielded the columns failed in compression. In specimen SR10-1 the column longitudinal bars yielded at a load of 1350 kN but no cracks were observed on the faces of the column until failure. At the ultimate load on all faces of the column vertical cracks appeared at a distance above the column to the base interface. These cracks gradually expanded and finally the cover to the reinforcement completely spalled off, and at that time the upper link located in the failure zone also yielded. Close examination of the failure zone showed that the column longitudinal bars buckled between the links. Failure of the column concrete was again at a distance of the column to base joint.

The performance of test piece SR10-2 at failure was typical. Under an axial load of 1200 kN the longitudinal reinforcement yielded in the column. At a load of 1250 kN vertical cracks started on faces 2

and 3 of the column at the column to base joint, and at the following load stage other faces also cracked at the same location. These cracks propagated on the respective faces and at the ultimate load the failure took place by spalling of concrete on all faces, accompanied by some loss of bond between the steel and concrete in the base. After failure, from the inspection of the holes beneath the column bars, it was observed that there was a relative movement between the column reinforcement and the base and hence partial bond failure had occurred in the base. It was also noted that the strains developed in the lower link (see figure (2.8) for reference) were always higher than the upper link during the loading sequence.

From the preceding descriptions of failure of the specimens it is assumed that part of the column length contributes to the anchorage bond length in a foundation.

3.4 Strain and Deflection Recordings

This section is concerned with strain and deflection measurements in the tests carried out in parts one and two. Due to the volume of recorded data it is impossible to refer to the strain and deflection recordings of each specimen and representative tests are therefore selected from each part. In the following two sections the strain versus load and deflection versus load relationships are examined and discussed with reference to selected test specimens.

3.4.1 Strain Recordings

Electrical resistance strain gauges were used to obtain the magnitude,

distribution and direction of strains in the column's main and secondary reinforcement and the base tension reinforcement for the tests as described in chapter 2. In the tests belonging to groups I to IX inclusive, the strain measurements in the column bars were recorded until the first slip and in the rest of reinforcement it was possible to record the values until failure occurred. When the first slip occurred in these tests the strain gauges placed on the embedded portion of the column bars in the base were damaged so that no more readings were available. The strain readings in the reinforcing steel were recorded until failure in the remainder of the groups of tests which included a short reinforced concrete column. To produce accurate data for the determination of the bond stress distribution along the anchorage length in foundation as well as in the column the strain gauges were always used in pairs at each position on the column longitudinal reinforcement. This method eliminated the erratic and misleading strains that may be produced by aggregate jamming around the gauge or improper functioning of the gauge due to any accidental damage during casting etc. The strain measurements for each individual test are tabulated in Appendix B. Strain readings which exceeded the value of the 'yield strain' are indicated with an asterisk.

The strain development in the column bars along the anchorage length of the foundation at various loading stages until first slip are given in figure (3.7a to g). Referencing and spacing of the strain gauges on column bars in the tests conducted with square twisted and ribbed bars are given in chapter 2 figures (2.4), (2.7) and table (2.3), respectively. In figure (3.7a to g) the strain at each gauge location represents the average of four strain readings on two

diagonal legs of the column cage at that particular location.

Figure (3.7a) shows strain development with respect to the applied load in test S1-3. From the figure it can be seen that at small loads the strain developed at the top rapidly decreases along the anchorage length and consequently part of the column bars at bottom are free of strain. At later stages of loading, with a maximum value at the top and a minimum value at bottom, the bars are strained over the full anchorage length. The strain distribution curves descend smoothly from the top with loading until close to first slip as shown in figure (3.7a). The slope of strain curves is minimum at the top and increases towards the bottom along the anchorage length, and indicates that rate of change of the internal forces along the anchorage length is maximum at the top with a minimum at bottom.

Figures (3.7b) and (3.7c) indicate the strain distribution in tests S2-1 and S2-4. The loading increments were identical in both tests and, the anchorage length provided for the column bars was 170 mm in test S2-4 and 220 mm in test S2-1. At the first load increment the column bars in test S2-4 develop strain over the full embedment length though it is very small at the bottom, but portions of the column bars at the bottom are not strained in test S2-1. At succeeding load stages, having the maximum value at the top the column bars are strained all over the anchorage length in both tests. At each load increment the magnitude of the strain significantly reduces towards the bottom of the bar. Both figures show a similar strain distribution, but in test S2-1 the strain curves are smoother and almost linear between the top and bottom gauge locations in the anchorage length as shown in figure (3.7b).

In the remainder of the tests with square twisted bars the strain distribution in the anchorage length followed the same trend as already described in the preceding paragraphs. The strain distribution curves reveal that square twisted bars develop the maximum bond stress at the top portion of the anchorage length and a minimum bond stress at the bottom until first slip takes place.

Figures (3.7d) and (3.7e) indicate the strain distribution in the column bars along the anchorage length of the foundation plotted against the applied load for tests SR2-1 and SR2-2. The loading sequence was identical for both tests. At small increments of load part of the column bars in the anchorage length develops no strain at the bottom, this is more pronounced in test SR2-1. As the loading continues the column bars are strained over the full bond length with a maximum at the top and minimum at the bottom. The maximum strain developed at the top of the bars reduces rapidly along the anchorage length towards the bottom. This effect is less for test SR2-2 and implies a more regular bond stress distribution over the anchorage length. From figures (3.7d) and (3.7e) the strain curves descend smoothly between the top and bottom gauge locations over the column bars with a maximum at the top portion of the embedment length and minimum at the bottom until the first slip occurs.

Strain development in the embedment length of column bars with respect to load in test SR4-3 is shown in figure (3.7f). Test specimen SR4-3 was reinforced in the base and loaded beyond the yield stress of the column longitudinal reinforcement. From the figure the trend of strain development in the anchorage length is the same as previous tests. The strain distribution curves in figure (3.7f) show that bond

stresses are a maximum at the top, decrease rapidly downwards and are a minimum at the bottom of the anchorage length. The strain development in base tension reinforcement for test SR4-3 is also given in table (3.5). In the table each value represents the average of two readings obtained at the respective locations symmetrical with respect to the centre of the base. The negative sign indicates tension. From table (3.5) the strains are higher in the first layer, decreases rapidly towards the sides of the base in both layers and near the edge a compression strain develops in the bars. This indicates that part of the base, beyond the central column area, is not affected by the applied load.

In test SR7-1 the column bars were confined by closely spaced links in the anchoarge length. The slip of the column bars was small and it was possible to obtain the strain development along the anchorage length near to the failure load as shown in figure (3.7g). From the figure the strain distribution between the top and bottom gauge locations is approximately linear up to one-third of the ultimate load. Then the strain curves become increasingly nonlinear with load increments and reveal very high bond stress at the top with a minimum at the bottom part of the anchorage length. The strain measurement in the links is also given in table (3.6), each value represents the average of four recordings at the legs of each link, and the negative sign indicates tension. From the table, from zero to nearly two-thirds of the ultimate load the top and middle links have compression strain. The strain increases with load at low rates in the top link while it is very small and almost constant in the middle one. Subsequently the positive strain decreases in the top link up to failure load, being still positive, while in the middle link the

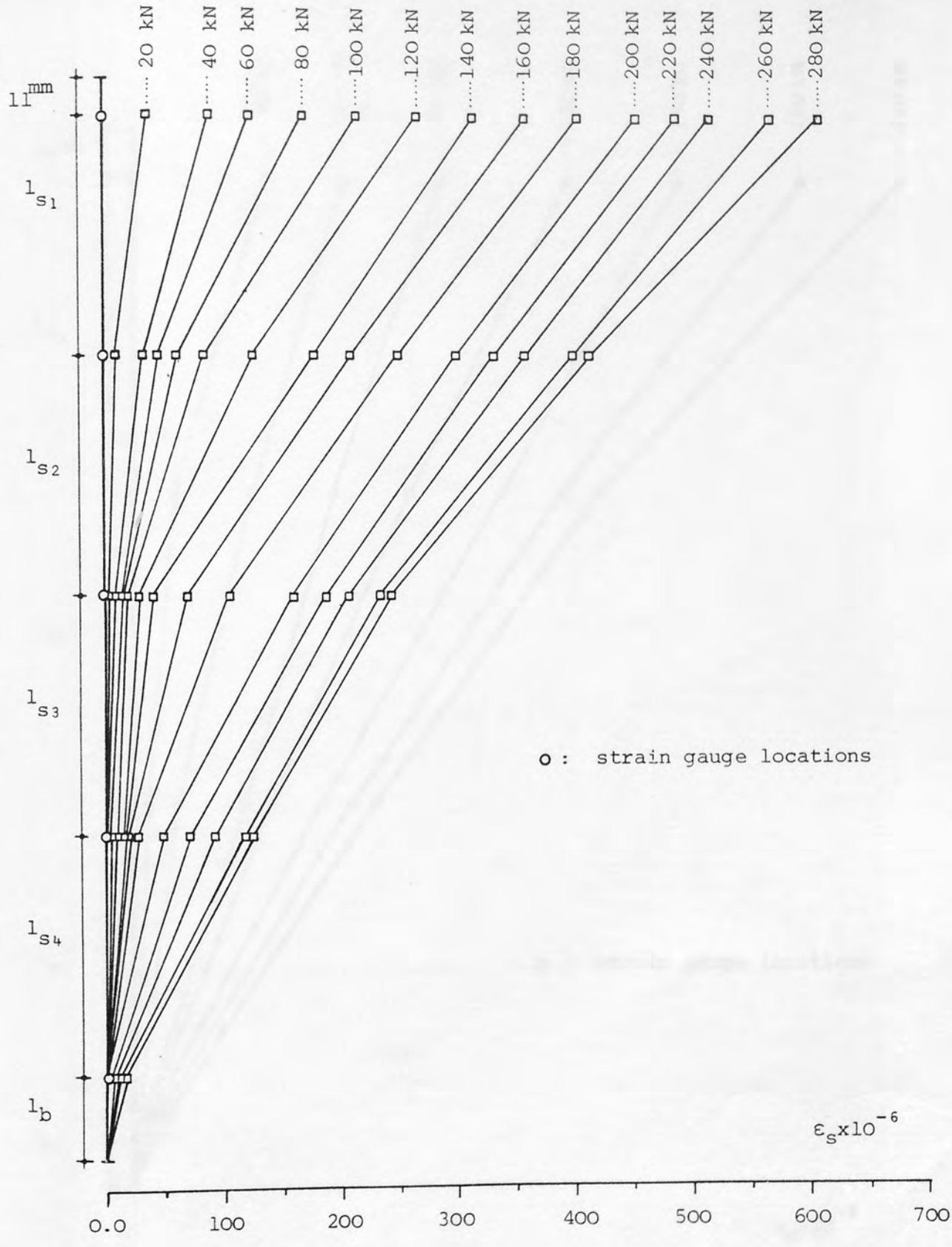

FIGURE 3.7a: LOAD VERSUS STRAIN DEVELOPMENT IN THE COLUMN BARS ALONG THE ANCHORAGE LENGTH IN TEST S1-3

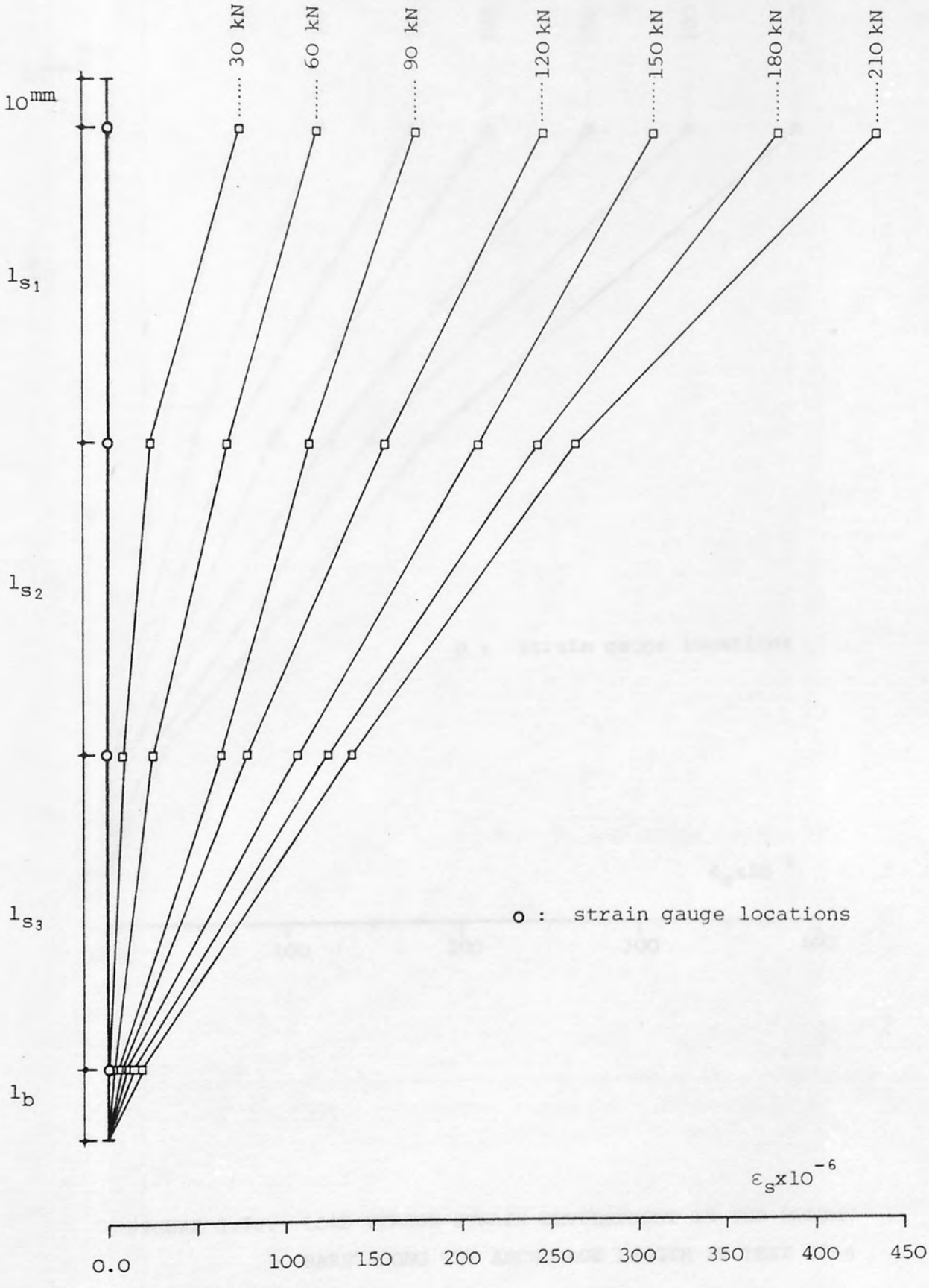

FIGURE 3.7b: LOAD VERSUS STRAIN DEVELOPMENT IN THE COLUMN BARS ALONG THE ANCHORAGE LENGTH IN TEST S2-1

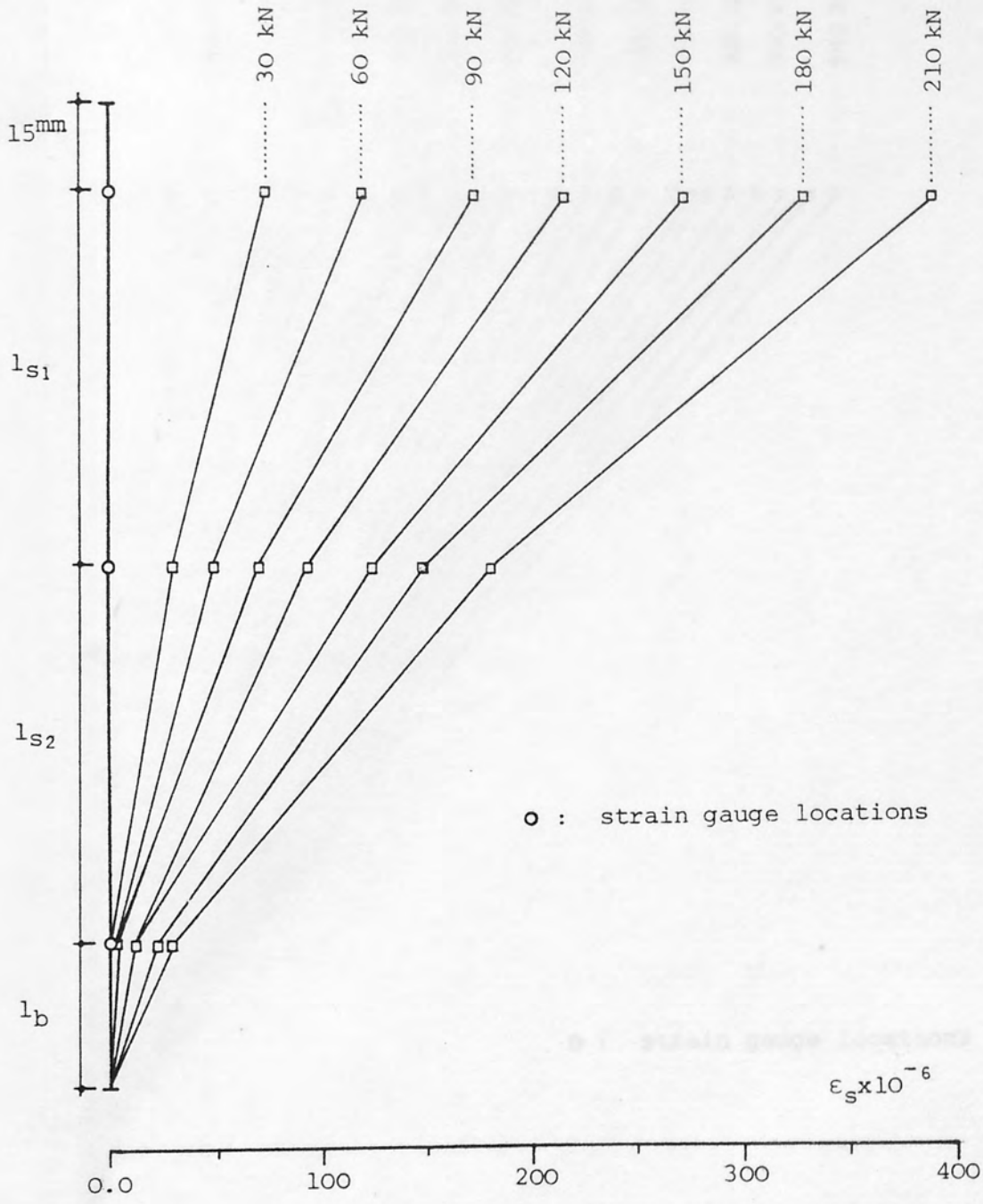

FIGURE 3.7c: LOAD VERSUS STRAIN DEVELOPMENT IN THE COLUMN BARS ALONG THE ANCHORAGE LENGTH IN TEST S2-4

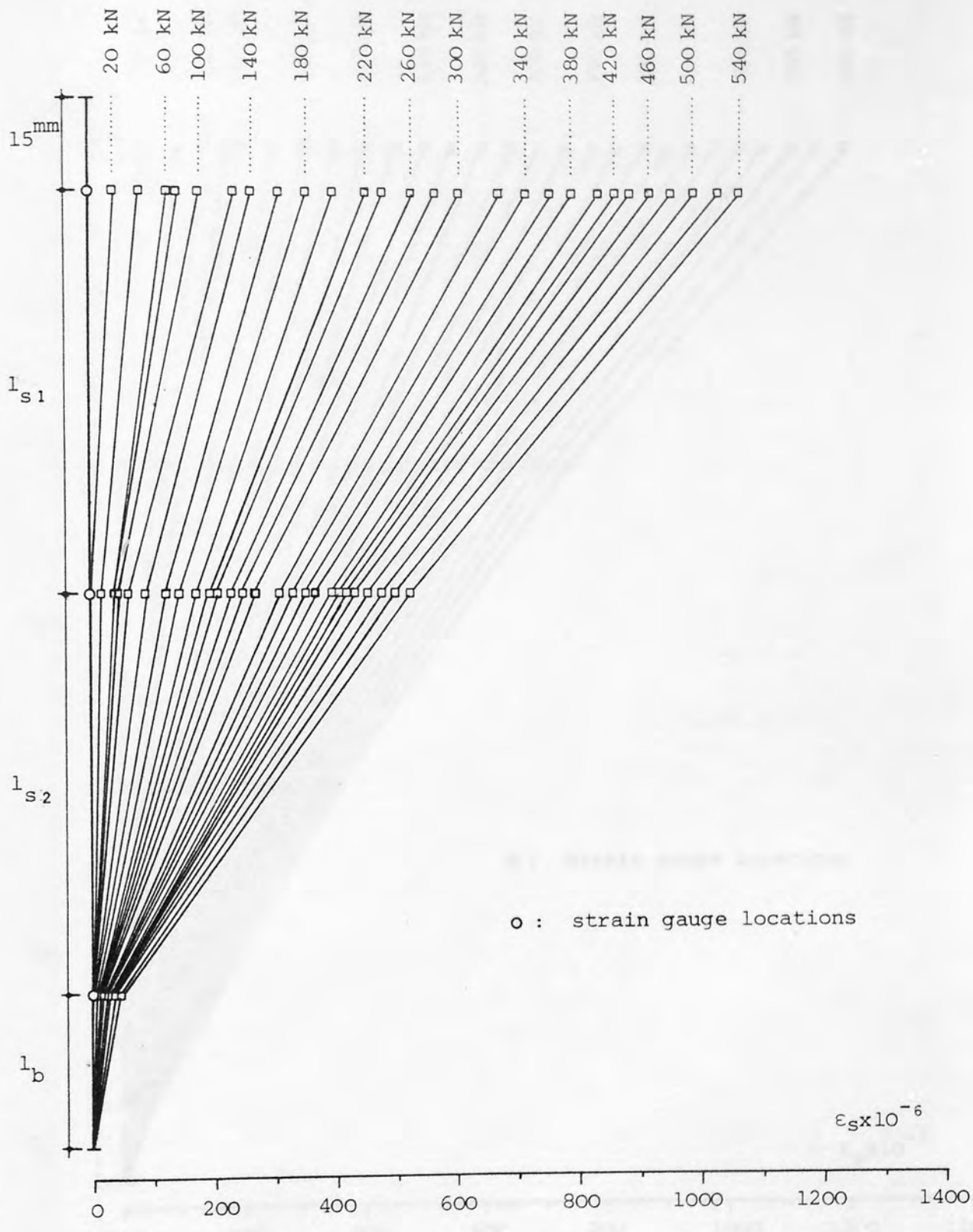

FIGURE 3.7d: LOAD VERSUS STRAIN DEVELOPMENT IN THE COLUMN BARS ALONG THE ANCHORAGE LENGTH IN TEST SR2-1

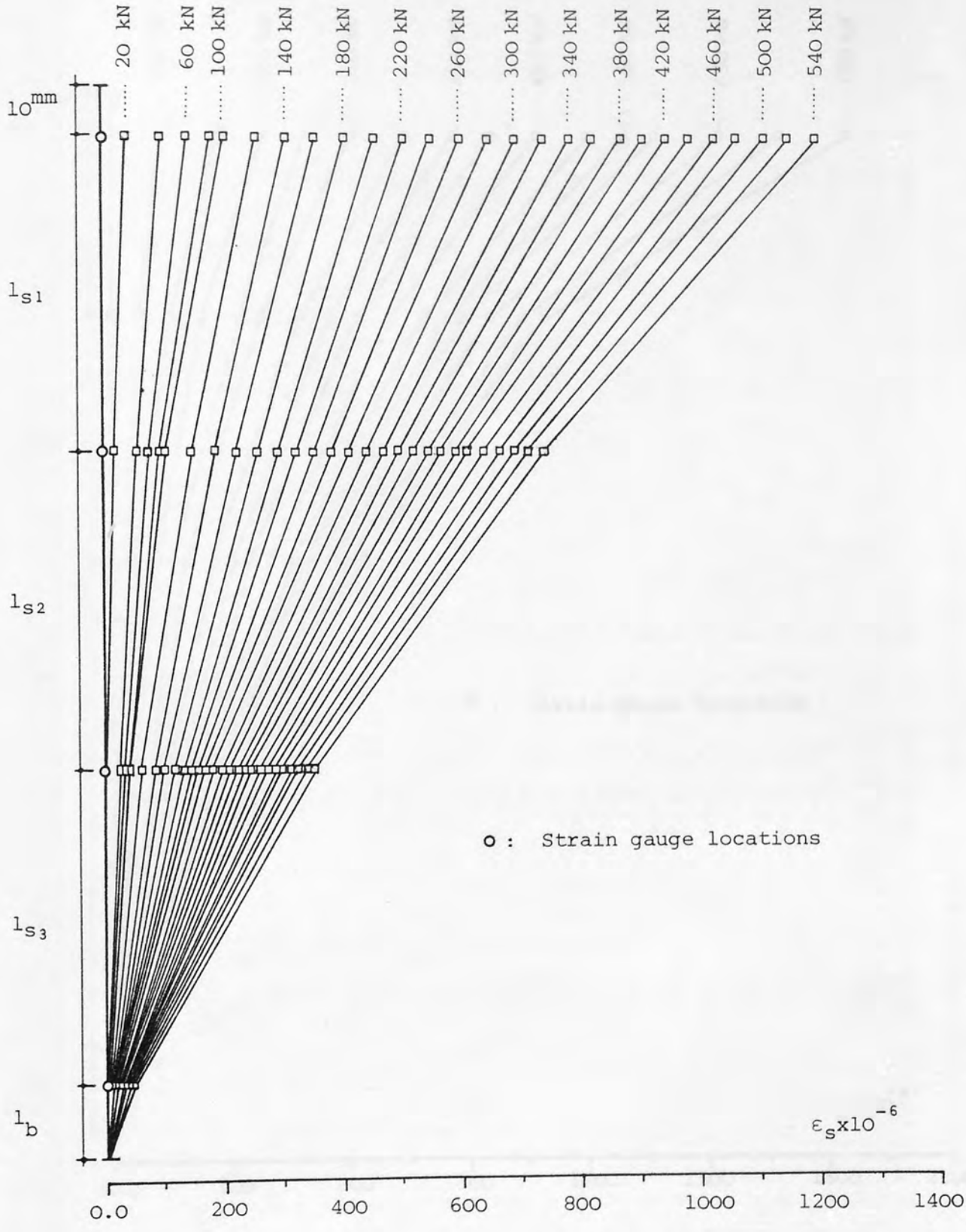

FIGURE 3.7e: LOAD VERSUS STRAIN DEVELOPMENT IN THE COLUMN BARS ALONG THE ANCHORAGE LENGTH IN TEST SR2-2

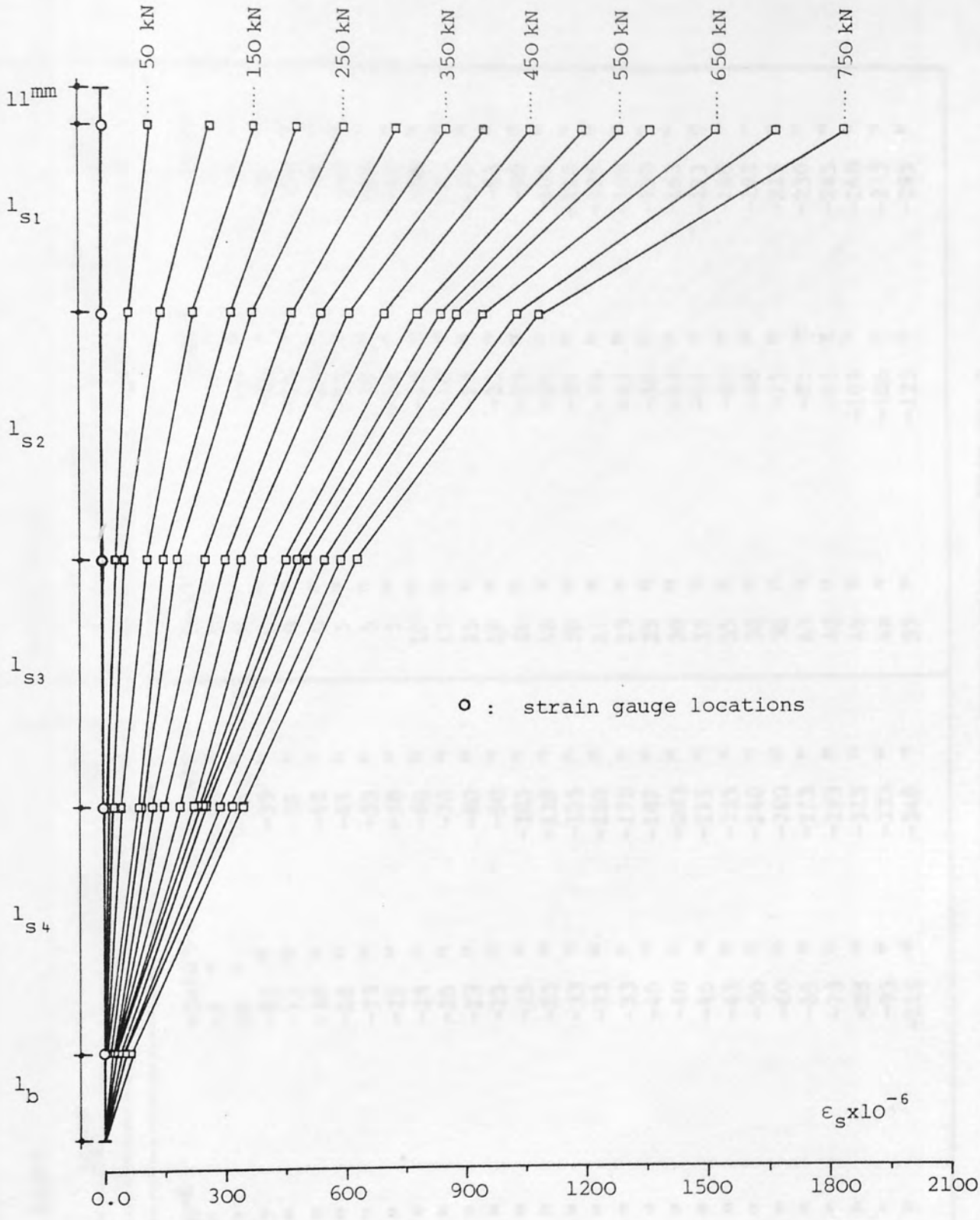

FIGURE 3.7f: LOAD VERSUS STRAIN DEVELOPMENT IN THE COLUMN BARS ALONG THE ANCHORAGE LENGTH IN TEST SR4-3

Load kN	First Layer ℄ 150mm 100mm 50mm			Second Layer ℄ 150mm 100mm 50mm		
50	$3x10^{-6}$	$-3x10^{-6}$	$-13x10^{-6}$	$0x10^{-6}$	$-5x10^{-6}$	$-8x10^{-6}$
100	3 "	-5 "	-20 "	0 "	-5 "	-15 "
150	3 "	-8 "	-23 "	0 "	-5 "	-20 "
200	3 "	-13 "	-33 "	0 "	-10 "	-28 "
250	3 "	-13 "	-38 "	0 "	-13 "	-30 "
300	3 "	-18 "	-43 "	0 "	-15 "	-38 "
350	8 "	-18 "	-45 "	5 "	-13 "	-40 "
400	8 "	-23 "	-53 "	5 "	-18 "	-45 "
450	13 "	-25 "	-58 "	5 "	-18 "	-50 "
500	15 "	-25 "	-60 "	10 "	-18 "	-58 "
550	20 "	-25 "	-70 "	15 "	-18 "	-63 "
600	18 "	-23 "	-80 "	15 "	-23 "	-70 "
650	23 "	-23 "	-90 "	18 "	-23 "	-83 "
700	23 "	-25 "	-105 "	18 "	-25 "	-90 "
750	25 "	-25 "	-110 "	18 "	-30 "	-105 "
800	25 "	-33 "	-125 "	20 "	-35 "	-115 "
850	30 "	-33 "	-150 "	23 "	-35 "	-125 "
900	30 "	-33 "	-170 "	23 "	-43 "	-140 "
950	30 "	-40 "	-187 "	25 "	-50 "	-150 "
1000	35 "	-40 "	-203 "	30 "	-53 "	-163 "
1050	40 "	-45 "	-215 "	35 "	-55 "	-173 "
1100	40 "	-45 "	-225 "	35 "	-60 "	-188 "
1150	40 "	-50 "	-240 "	38 "	-68 "	-198 "
1200	40 "	-60 "	-260 "	38 "	-75 "	-215 "
1250	45 "	-65 "	-273 "	40 "	-85 "	-230 "
1300	50 "	-73 "	-293 "	40 "	-95 "	-245 "
1350	50 "	-88 "	-313 "	40 "	-103 "	-260 "
1400	55 "	-95 "	-333 "	48 "	-108 "	-273 "
1450	58 "	-115 "	-348 "	55 "	-123 "	-295 "

TABLE 3.5: STRAIN DEVELOPMENT IN THE BASE TENSION REINFORCEMENT IN TEST SR4-3

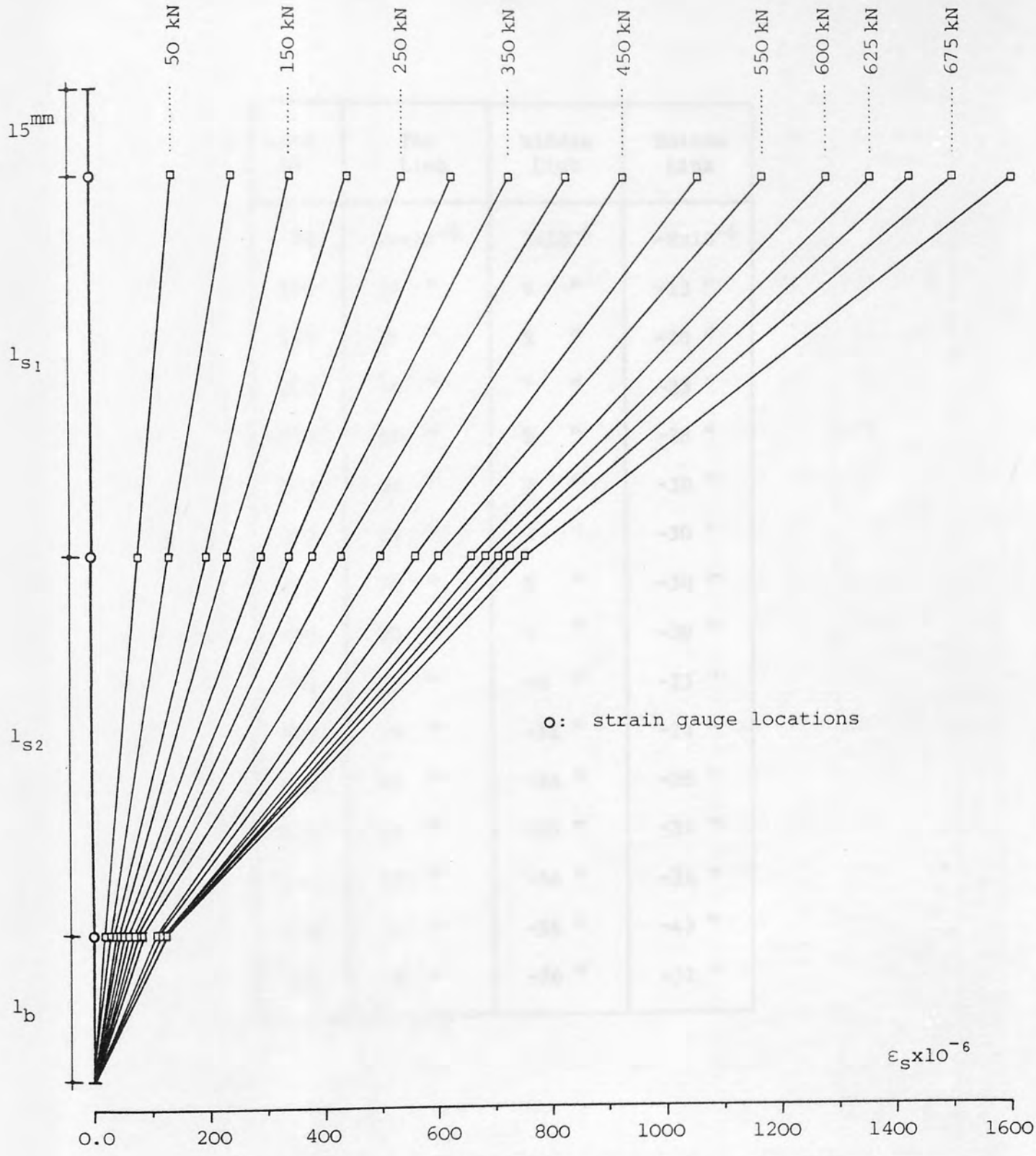

FIGURE 3.7g: LOAD VERSUS STRAIN DEVELOPMENT IN THE COLUMN BARS ALONG THE ANCHORAGE LENGTH IN TEST SR7-1

Load kN	Top Link	Middle Link	Bottom Link
50	14×10^{-6}	3×10^{-6}	-8×10^{-6}
100	26 "	5 "	-13 "
150	36 "	5 "	-20 "
200	48 "	7 "	-25 "
250	59 "	8 "	-28 "
300	66 "	7 "	-30 "
350	73 "	9 "	-30 "
400	78 "	8 "	-30 "
450	80 "	4 "	-30 "
500	82 "	-4 "	-25 "
550	79 "	-11 "	-24 "
600	67 "	-24 "	-28 "
625	53 "	-35 "	-34 "
650	47 "	-54 "	-34 "
675	30 "	-56 "	-43 "
700	9 "	-76 "	-51 "

TABLE 3.6: STRAIN DEVELOPMENT IN THE LINKS PLACED OVER THE ANCHORAGE LENGTH OF COLUMN BARS IN TEST SR7-1

Load kN	Column top	Column bottom	Base top		Base bottom	Column upper link	Column lower link
	1	2	3	4	5	6	7
100	58×10^{-6}	51×10^{-6}	34×10^{-6}	16×10^{-6}	1×10^{-6}	-33×10^{-6}	-21×10^{-6}
200	113 "	101 "	70 "	38 "	2 "	-56 "	-41 "
300	171 "	155 "	109 "	57 "	3 "	-79 "	-59 "
400	229 "	204 "	146 "	69 "	4 "	-105 "	-88 "
500	296 "	258 "	181 "	76 "	3 "	-130 "	-94 "
600	368 "	312 "	217 "	84 "	3 "	-161 "	-118 "
700	452 "	373 "	353 "	93 "	3 "	-193 "	-139 "
800	536 "	431 "	286 "	102 "	4 "	-230 "	-162 "
900	647 "	495 "	305 "	109 "	6 "	-277 "	-194 "
1000	748 "	558 "	349 "	120 "	8 "	-332 "	-222 "
1100	867 "	626 "	379 "	129 "	8 "	-405 "	-256 "
1200	1044 "	710 "	408 "	140 "	9 "	-511 "	-298 "
1300	1210 "	794 "	438 "	154 "	12 "	-622 "	-337 "
1400	1428 "	907 "	474 "	171 "	13 "	-781 "	-386 "
1500	1662 "	1032 "	526 "	195 "	18 "	-1000 "	-436 "
1550	1884 "	1125 "	562 "	209 "	18 "	-1181 "	-474 "
1600	2275*"	1233 "	628 "	241 "	24 "	-1492 "	-510 "
1650	2894*"	1284 "	663 "	254 "	25 "	-2100 "	-524 "

TABLE 3.7: STRAIN DEVELOPMENT IN THE MAIN AND SECONDARY REINFORCEMENT OF COLUMN CAGE IN TEST SR9-2

Load kN	Column top	Column bottom	Base top		Base bottom	Column upper link	Column lower link
	1	2	3	4	5	6	7
100	$103x10^{-6}$	$91x10^{-6}$	$71x10^{-6}$	$26x10^{-6}$	$0x10^{-6}$	$-14x10^{-6}$	$-17x10^{-6}$
200	197 "	176 "	129 "	52 "	0 "	-41 "	-55 "
300	302 "	273 "	199 "	88 "	4 "	-75 "	-85 "
400	405 "	364 "	259 "	104 "	6 "	-109 "	-123 "
500	517 "	460 "	315 "	119 "	7 "	-150 "	-165 "
600	636 "	560 "	373 "	139 "	12 "	-197 "	-212 "
700	774 "	668 "	430 "	165 "	16 "	-249 "	-264 "
800	929 "	784 "	488 "	197 "	24 "	-309 "	-325 "
900	1127 "	911 "	548 "	232 "	33 "	-389 "	-413 "
950	1229 "	983 "	583 "	253 "	39 "	-435 "	-467 "
1000	1366 "	1063 "	622 "	277 "	47 "	-492 "	-536 "
1050	1470 "	1123 "	652 "	292 "	50 "	-549 "	-604 "
1100	1640 "	1187 "	676 "	305 "	56 "	-602 "	-715 "
1150	1837 "	1250 "	692 "	309 "	52 "	-732 "	-900 "
1200	2046*"	1341 "	722 "	326 "	57 "	-838 "	-1097 "
1250	2301*"	1437 "	752 "	344 "	60 "	-955 "	-1273 "
1300	3060*"	1555 "	797 "	353 "	51 "	-1386 "	-1802 "

TABLE 3.8: STRAIN DEVELOPMENT IN THE MAIN AND SECONDARY REINFORCEMENT OF COLUMN CAGE IN TEST SR10-2

strain changes sign and increases at low rates until failure. The bottom link is strained in tension with loading although the rate of strain is also very small. In general from these observations the strain development in the links is seen to be very small and the bursting forces produced by the bond action of the column bars are low due to the containment of the base concrete.

Tests in groups X and XI were conducted on a short reinforced concrete column. Strain readings were taken until failure in the main and secondary reinforcement of the column cage and in the base tension reinforcement, see figure (2.8) for reference. The recorded measurements of strain and deflection for each individual test is given in Appendix B.

Tables (3.7) and (3.8) show the strain development in the main longitudinal bars in the column and foundation and in the links placed in the lower part of the column for tests SR9-2 and SR10-2, respectively. The tables show that the strains reduce with an increasing rate from column towards the bottom of the base such that the bond stress increases from the top to the bottom in the column while it reduces from the top to the bottom in the base. From table (3.8) it can be seen that the lower link in the column, which is situated near the column to base interface, develops higher strain than the upper one. This implies that the column bars produce higher bursting forces in the bottom part of the column due to the development of higher bond stresses in this zone above the base.

3.4.2 Deflection Readings

Deflection readings were taken in all groups of tests and are tabulated

in Appendix B. Vertical and horizontal displacements were taken of the column cage for the specimens in groups I to IX inclusive, and vertical deflections were taken for the specimens with a short reinforced concrete column in groups X and XI. In the tests with square twisted bars early slip of the column bars was always present. Vertical displacement of the column cage, i.e. slip of the column bars until failure is given in figure (3.8a to h) while horizontal displacement of the column cage in both directions is illustrated in figure (3.9a to c). The values given for the vertical displacement of the column cage are the average of four vertically placed dial gauge readings (see figures (2.4) and (2.7) for reference) and also include the vertical deflection of the column cage itself, i.e. contraction of the column bars, which is highly pronounced in the tests loaded beyond the yield stress of the column longitudinal reinforcement.

Typical load-deflection curves for test S1-3 are shown in figures (3.8a) and (3.9a). Figure (3.8a) illustrates the vertical displacement of column cage until failure. At low loads there is no relative movement between the column bars and the surrounding concrete along the anchorage length. As the load increases the slip begins and continues although it is very small. Later the slip suddenly increases at about one-fourth of the ultimate load and the curve ascends smoothly to nearly two-thirds of the ultimate load. It becomes gradually flatter after additional increments of load and near to failure the slope of the curve suddenly drops and continues nonlinearly indicating larger amounts of slips. Finally at the ultimate load the major slip takes place. The total average slip of the column bars after failure is 18.39 mm in the test.

Figure (3.9a) shows the horizontal displacement of the column cage. From the figure the column cage has no horizontal movement up to a quarter of the ultimate load when the slip rate of the column bars is low. Later as the slip rate gradually increases with loading the top steel plate tends to rotate due to the unscrewing action of the column bars. This effect is followed by the two horizontally placed dial gauges in the neighbouring two sides of the top plate which indicate the corresponding horizontal displacements in the x and y directions with respect to the original postion of the top steel plate as shown in the figure. From figure (3.9a) the horizontal displacement of the column cage is very small hence the stability of the bare column bars is maintained.

Figures (3.8b) and (3.8c) illustrate the vertical displacement of column cage with load for tests S2-1 and S2-4, respectively. Both tests were idential except the embedment length provided to the column bars in foundation. It can be seen from both figures that the vertical displacement curves ascend nonlinearly until failure which indicate a gradually increasing slip rate with loading. However, at comparable loads the slip rate of column bars decreases as the anchorage length is increased for test S2-1. The maximum average slip attained at ultimate load is 28.61 mm in test S2-1 and 26.71 mm in test S2-4. The horizontal displacement of column cage for test S2-4 is alo plotted in figure (3.9b). From the figure the stability of the exposed column bars is sustained during the loading sequence.

Figures (3.8d) and (3.8e) show the vertical displacement of column bars with respect to applied load for tests SR2-1 and SR2-2, respectively. From both figures the slip is small to approximately

half the ultimate load for each test and, both slip curves ascend non-linearly through the loading sequence, being more pronounced in test SR2-2. Close to failure the slope of the curve reduces rapidly in test SR2-1 and becomes almost horizontal. This indicates a large slip of approximately three times that already attained as shown in figure (3.8d). In test SR2-2 a similar effect takes place but to a lesser extent as shown in figure (3.8e). The measured average slip of the column bars over the anchorage length at ultimate is 25.82 mm in test SR2-1 and 27.35 mm in test SR2-2. Monitoring of the lateral stability of the column cage for test SR2-1 is also given in figure (3.9c). From the figure the bare column bars maintain their stability during the test.

Tests SR2-1 and SR2-2 were identical to the tests S2-4 and S2-1, respectively, except for the type of reinforcement. At comparable loads the slip rate is significantly higher in tests S2-4 and S2-1 than in tests SR2-1 and SR2-2.

Load versus vertical displacement of the column cage for test SR4-3 is shown in figure (3.8f). The column cage was loaded beyond the yield stress of the longitudinal reinforcement. From the figure the load-vertical displacement curve ascends nonlinearly and indicates low rates of slip until yield of the exposed column bars. After yielding of the column reinforcement the curve becomes flatter because of the contraction of the column bars combined with some slip at each load increment. At the ultimate load the column cage loses its stability and major slip occurs. The average slip of the column bars at failure is 4.68 mm.

Figure (3.8g) illustrates the vertical displacement of column cage against load for test SR7-1 in which the column bars were confined along the anchorage length by closely spaced links. As a result the slip rate of the column bars was significantly restrained near to the ultimate load. From the figure the curve rises approximately linearly to one-third of the failure load accompanied by a small rate of slip. Then the curve gradually becomes nonlinear with loading and as ultimate load is reached the major slip takes place. The average slip of the column bars at ultimate load is 11.34 mm.

The vertical displacement of the column cage with respect to applied load for test SR7-2 is shown in figures (3.8h). From the figure the displacement curve ascends nonlinearly through successive loading stages. Close to failure the slope of the curve suddenly reduces and the curve becomes almost flat which indicates a large slip approximately equal to three quarters of that already attained. At ultimate load the column bars slip 30 mm.

Tests in groups X and XI included a short reinforced concrete column. Vertical deflection of the column and, at a distance of 40 mm from the column face vertical deflection of the base were also measured by means of the upper dial guages. Lower dial gauges measured total shortening of the specimen (see figure (2.8) in chapter 2). Beyond the column area the base showed no vertical deflection so that the vertical deflection of the column was idential to the total shortening of the specimen. Table (3.9) shows the vertical deflection with respect to the applied load until failure in test SR9-2. In the table each value for the total shortening of the specimen is the average of four lower dial gauge readings, while others are the average

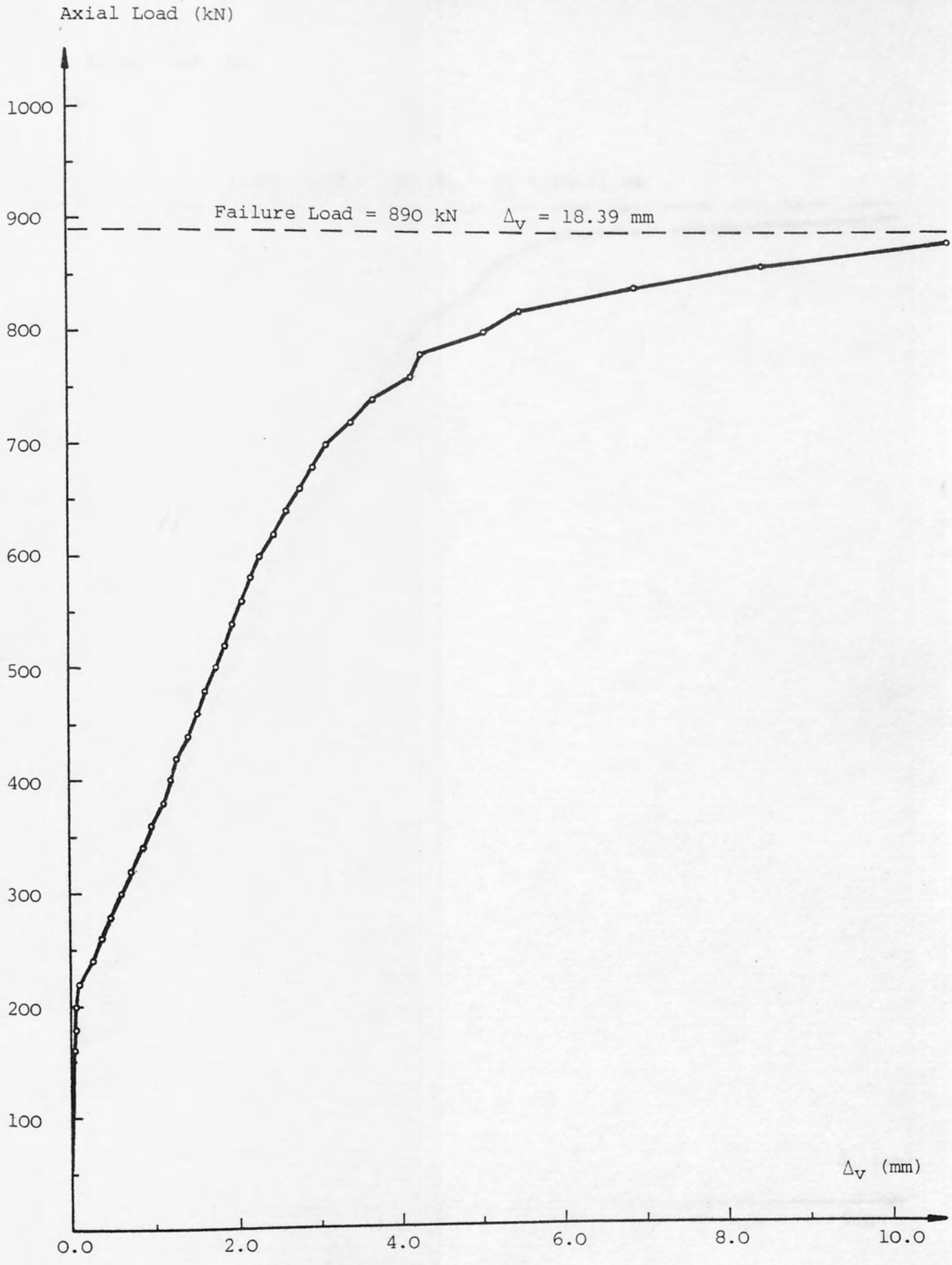

FIGURE 3.8a: LOAD VERSUS VERTICAL DISPLACEMENT OF COLUMN CAGE IN TEST S1-3

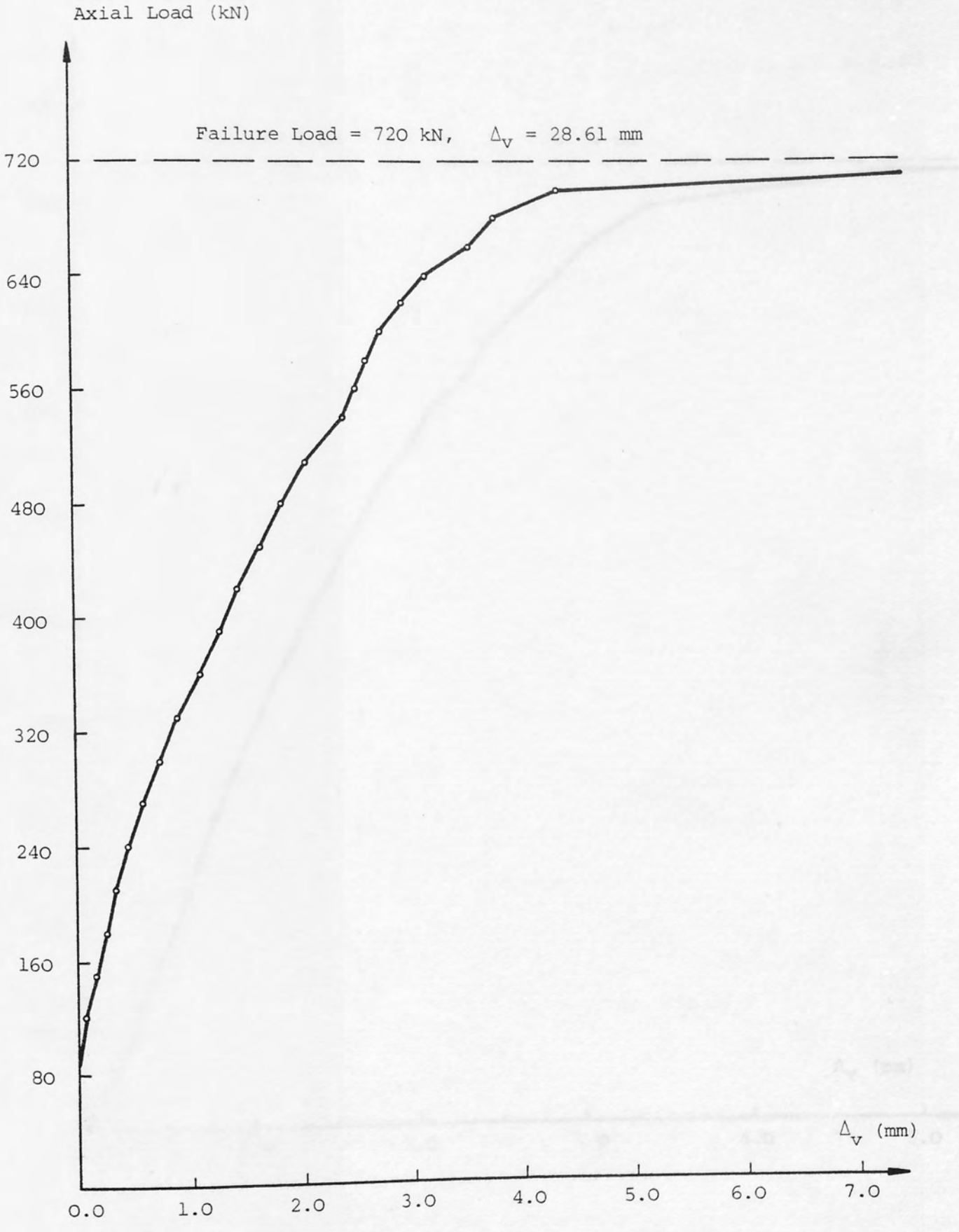

FIGURE 3.8b: LOAD VERSUS VERTICAL DISPLACEMENT OF COLUMN CAGE IN TEST S2-1

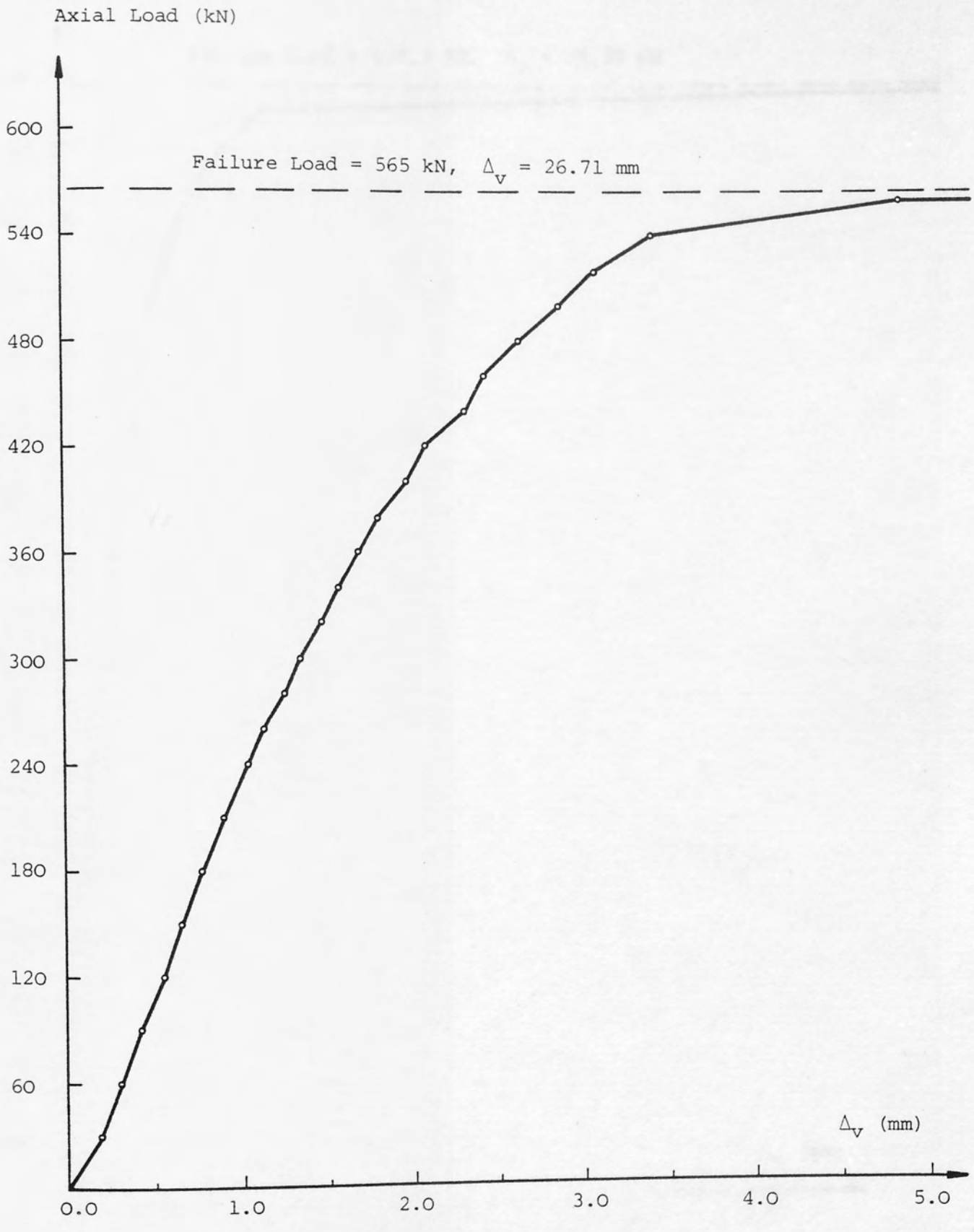

FIGURE 3.8c: LOAD VERSUS VERTICAL DISPLACEMENT OF COLUMN CAGE IN TEST S2-4

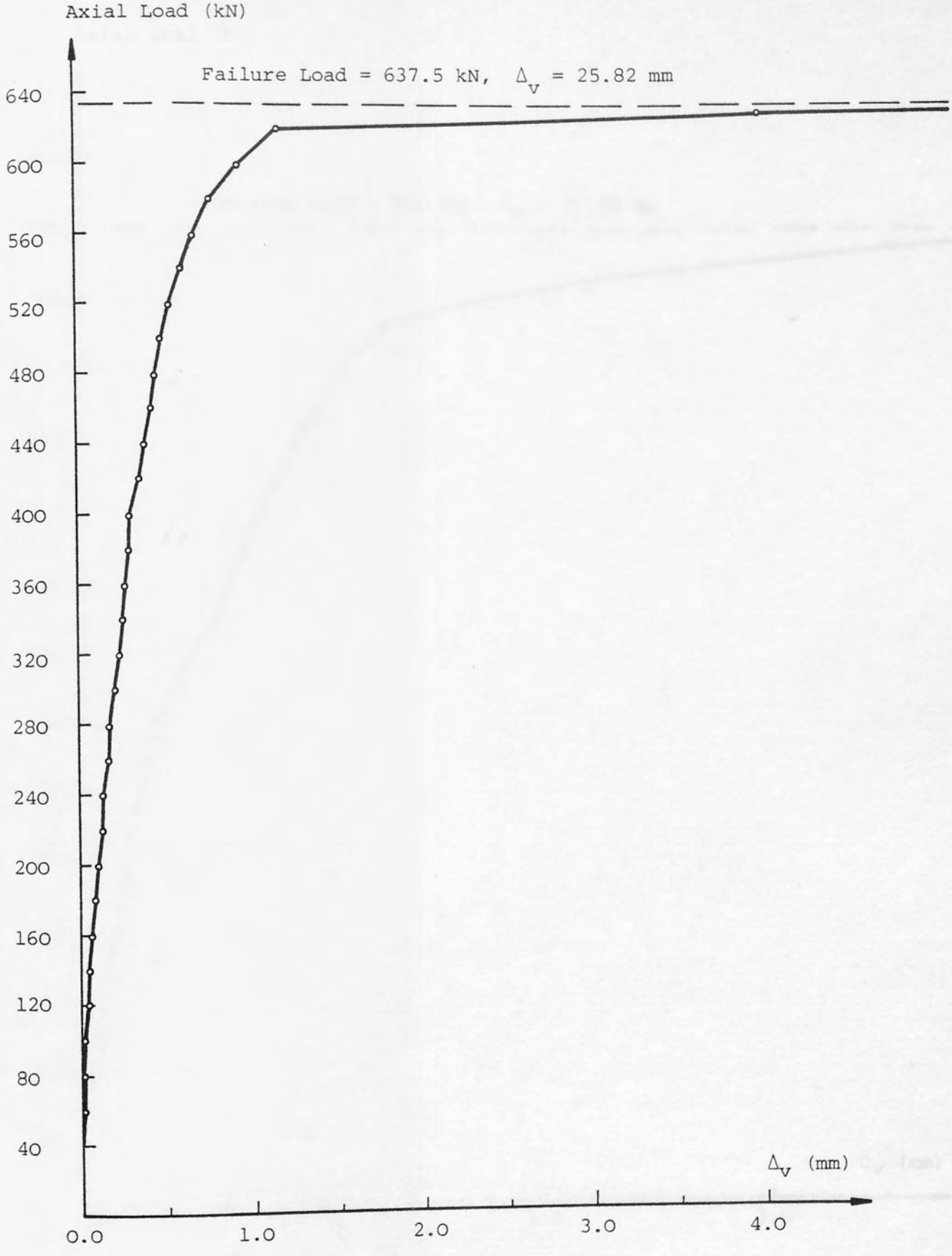

FIGURE 3.8d: LOAD VERSUS VERTICAL DISPLACEMENT OF COLUMN CAGE IN TEST SR2-1

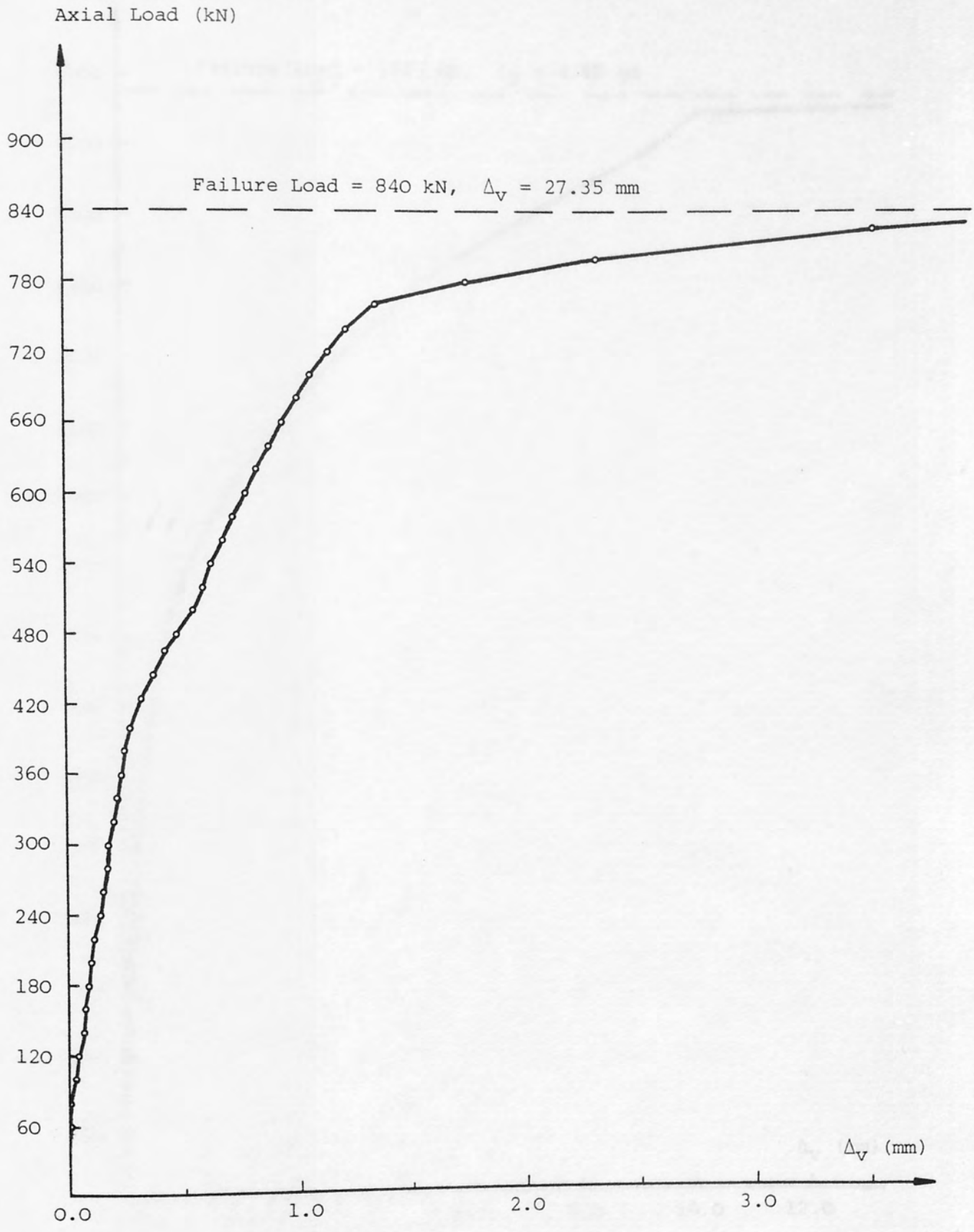

FIGURE 3.8e: LOAD VERSUS VERTICAL DISPLACEMENT OF COLUMN CAGE IN TEST SR2-2

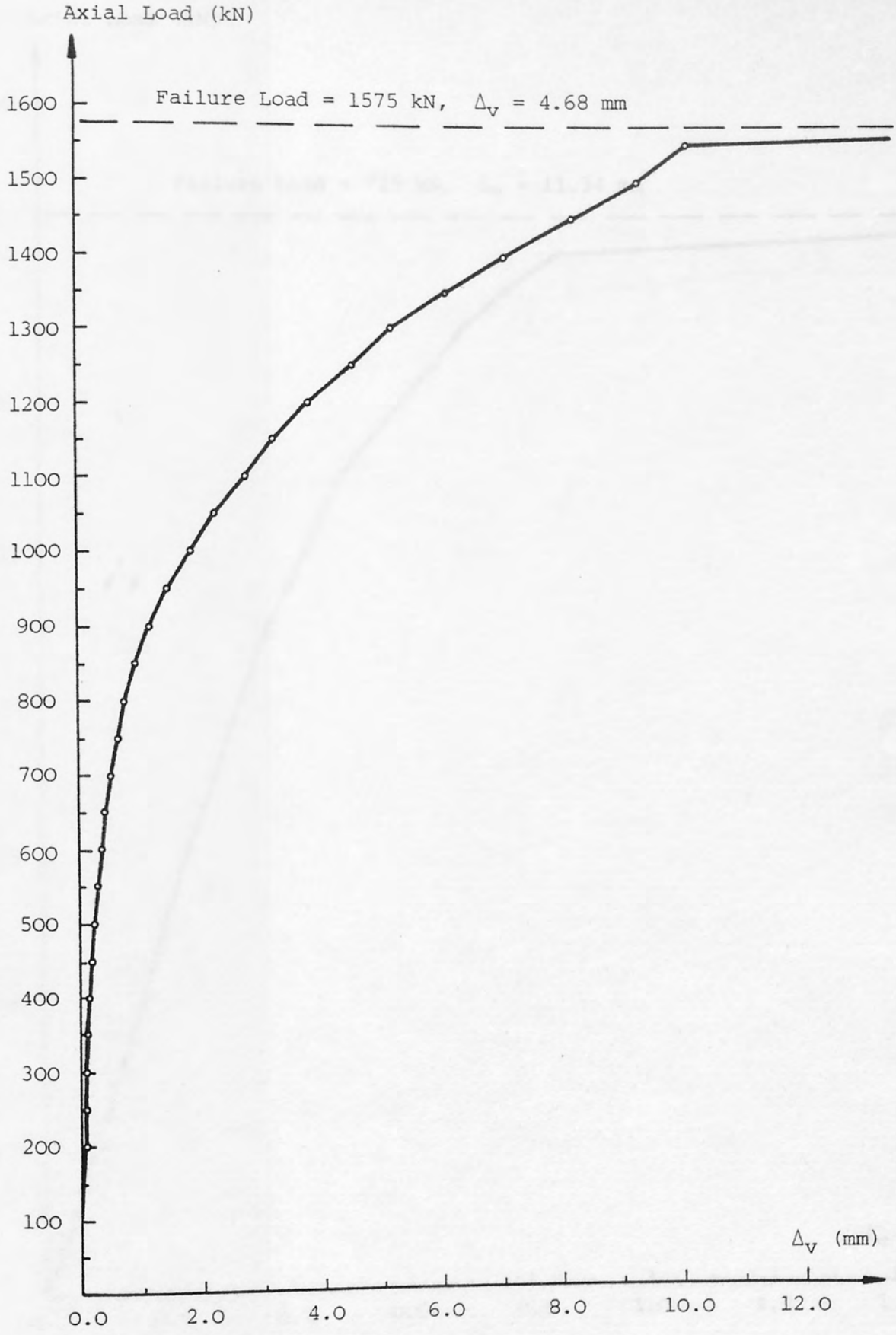

FIGURE 3.8f: LOAD VERSUS VERTICAL DISPLACEMENT OF COLUMN CAGE IN TEST SR4-3

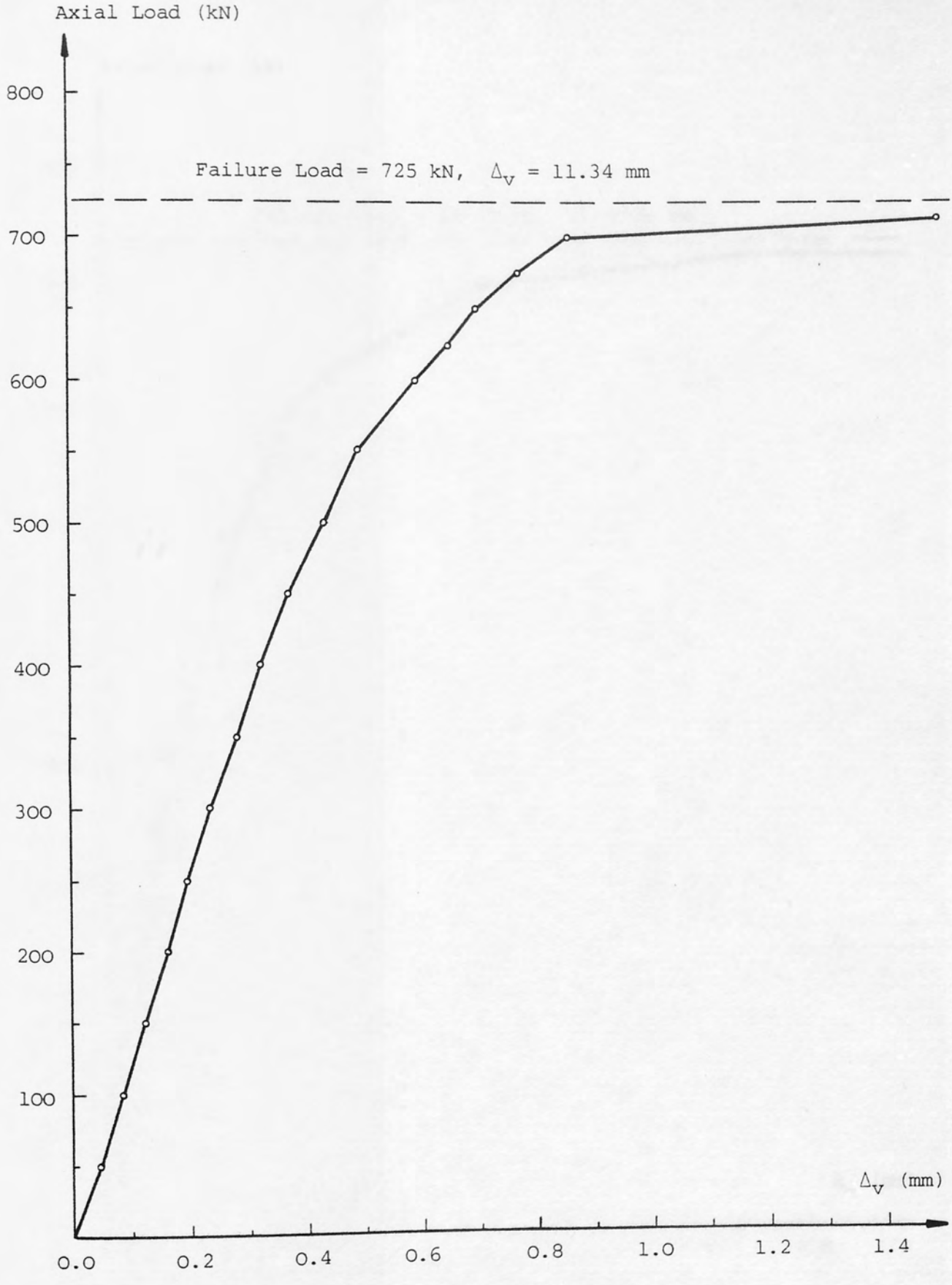

FIGURE 3.8g: LOAD VERSUS VERTICAL DISPLACEMENT OF COLUMN CAGE IN TEST SR7-1

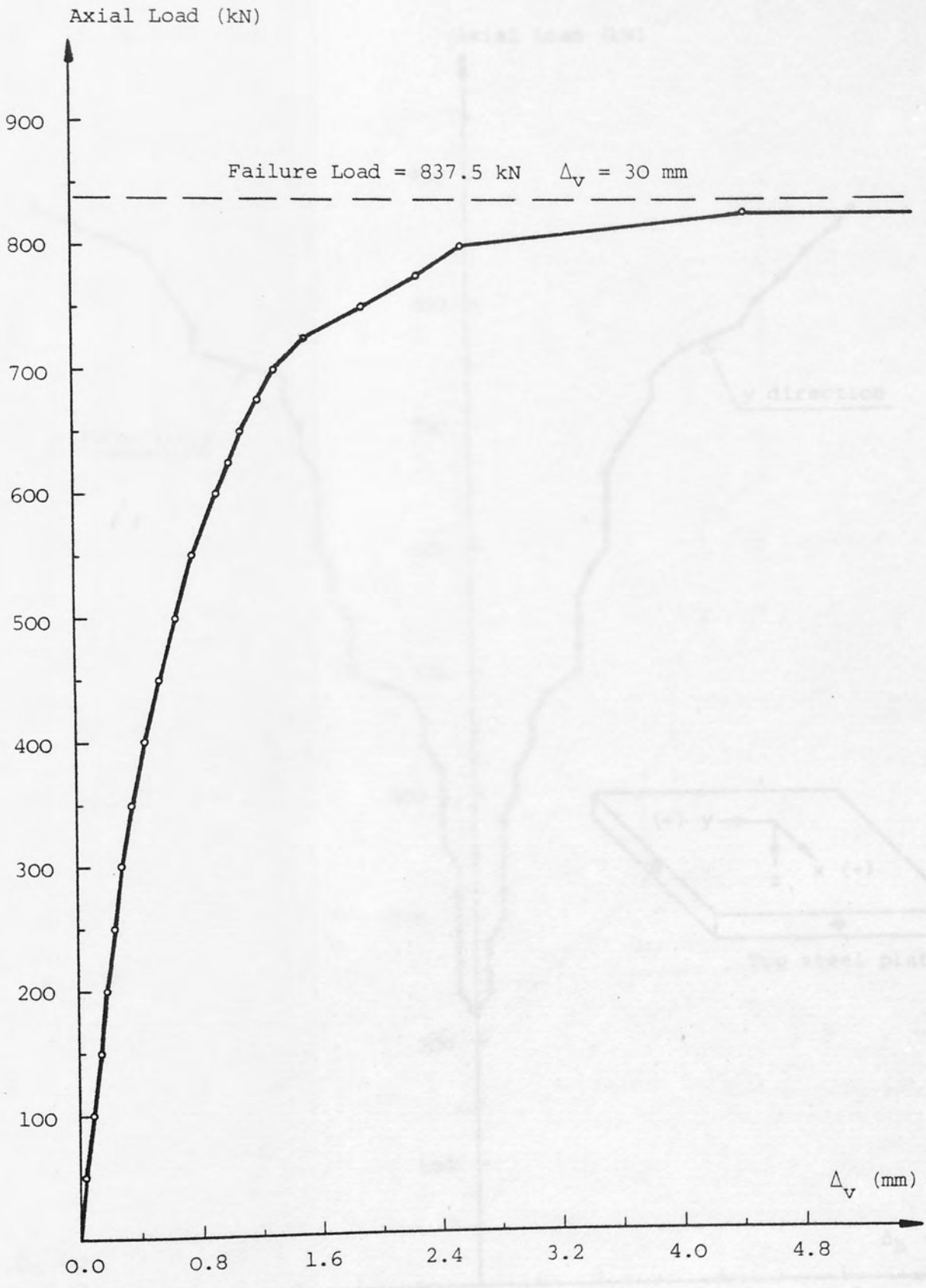

FIGURE 3.8h: LOAD VERSUS VERTICAL DISPLACEMENT OF COLUMN CAGE IN TEST SR7-2

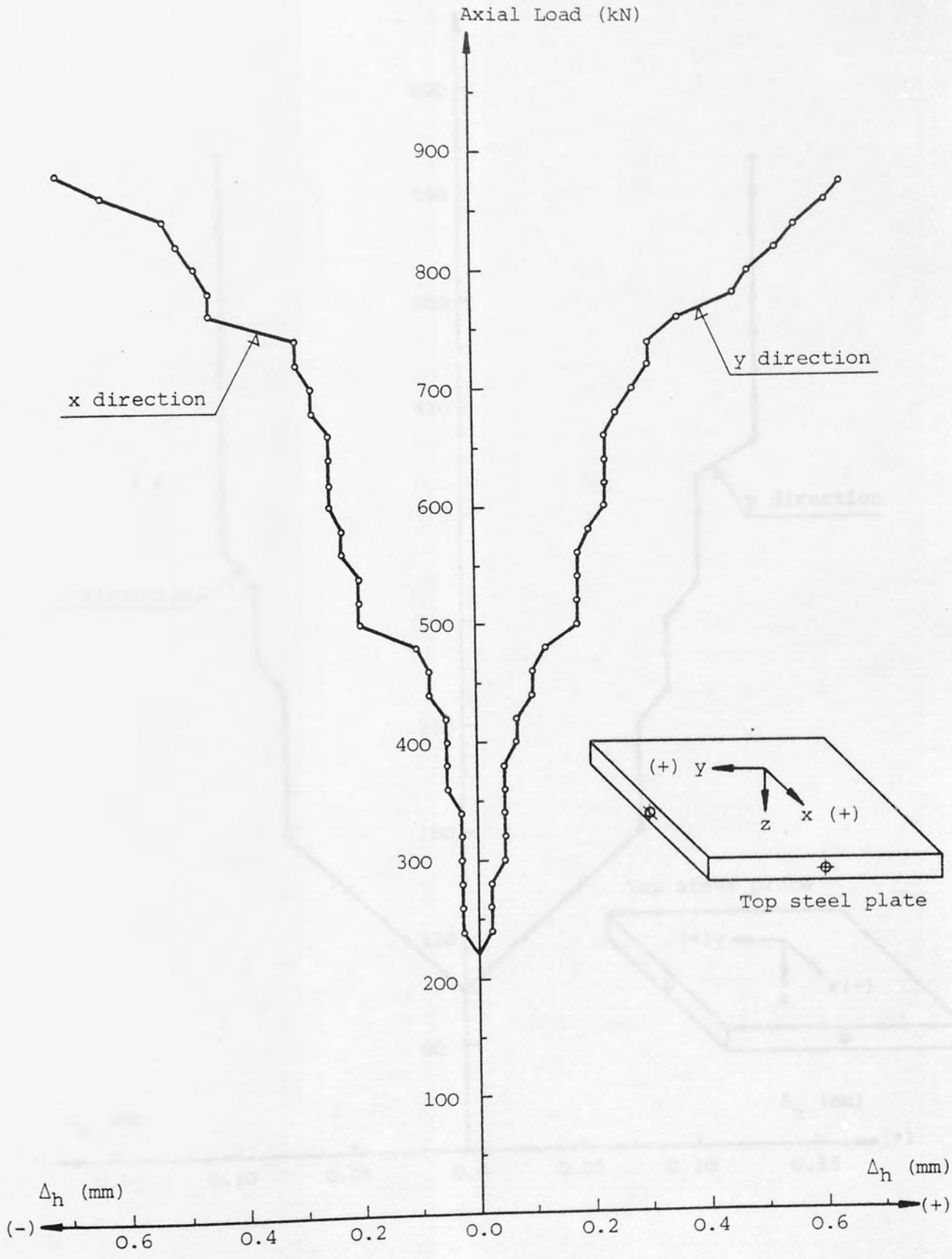

FIGURE 3.9a: LOAD VERSUS HORIZONTAL DISPLACEMENT OF COLUMN CAGE IN TEST S1-3

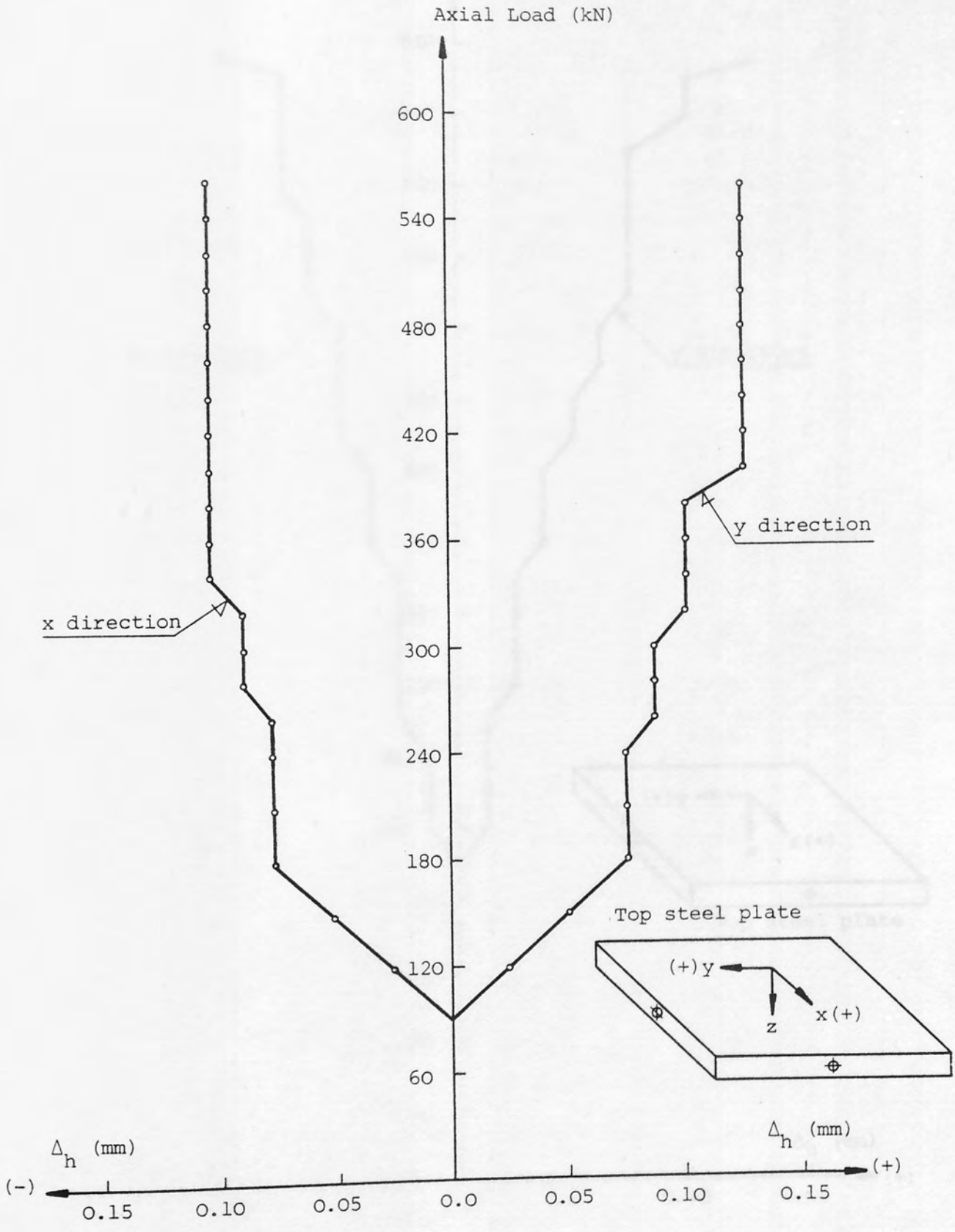

FIGURE 3.9b: LOAD VERSUS HORIZONTAL DISPLACEMENT OF COLUMN CAGE IN TEST S2-4

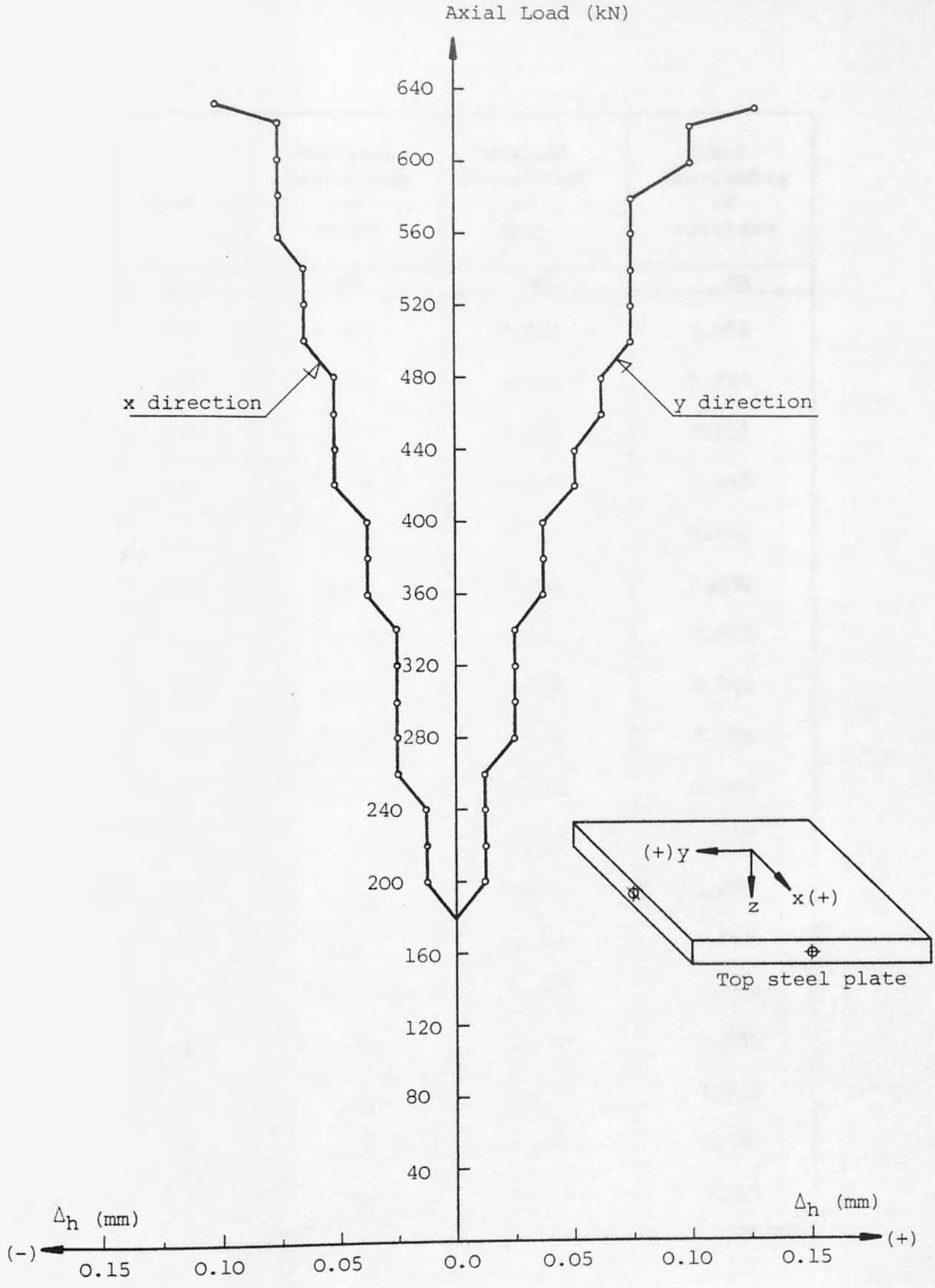

FIGURE 3.9c: LOAD VERSUS HORIZONTAL DISPLACEMENT OF COLUMN CAGE IN TEST SR2-1

Load	Vertical deflection of column	Vertical deflection of base	Total Shortening of specimen
kN	mm	mm	mm
100	0.101	0.022	0.098
200	0.203	0.025	0.203
300	0.317	0.032	0.311
400	0.438	0.059	0.440
500	0.540	0.059	0.542
600	0.647	0.068	0.652
700	0.775	0.084	0.770
800	0.901	0.088	0.901
900	1.042	0.093	1.046
1000	1.143	0.102	1.143
1100	1.348	0.123	1.342
1200	1.600	0.132	1.592
1300	1.803	0.139	1.795
1400	2.051	0.141	2.053
1500	2.296	0.149	2.301
1550	2.413	0.150	2.413
1600	2.692	0.156	2.696
1650	3.088	0.178	3.099

TABLE 3.9: LOAD VERSUS VERTICAL DEFLECTION IN TEST SR9-2

of the two corresponding upper dial gauge readings.

3.5 Bond Stress Distribution in the Anchorage Length of the Foundation

In this section the distribution of the anchorage bond stress with axial compression load is examined over the embedded part of the column longitudinal bars in foundation. In all of the tests the strain readings were taken at several locations along the anchorage length of column bars (see figures (2.4), (2.7) and table (2.3) for reference) until first slip took place. This provides an opportunity to determine the variation in stress along the bar and thereby to compute the bond stress at intervals between the gauges. Due to large number of recorded data it is impossible to refer to the anchorage bond stress distribution in each individual specimen, representative tests are therefore selected. However, if required, the anchorage bond stress variation with load can be determined for each test from the strain recording tabulated in Appendix B.

To obtain the bond stress distribution along the anchorage length the following procedure was adopted. The strain modified by bond in the bar between two gauge positions was measured and, using the basic Hooke's Law the corresponding steel stress was calculated. For the modulus of elasticity of steel the actual values determined from the tensile test results were employed. The average bond stress over the considered length of bar was computed from

$$f_{bs} = \frac{\Delta f_s A_s}{\pi \phi \Delta l_a} \qquad (3.9)$$

Where

f_{bs} = the average bond stress

Δf_s = the change of steel stress over the length Δl_a

A_s = the cross sectional area of the bar

ϕ = the nominal bar size

Δl_a = the length of the bar on which the bond stress is computed. The bond stress variation with load over the anchorage length of column bars in the foundation until the first slip is given in figure (3.10a to h).

Figure (3.10a) illustrates the bond stress distribution over the anchorage length of column longitudinal reinforcement in test S1-3. From the figure the maximum bond stress is at the top near the column to base interface at each load step until first slip takes place. The bond stress developed at the top reduces nonlinearly towards the bottom in the anchorage length. At loads where the relative movement between the steel and concrete is zero or very small, the column bars develop no bond stress at the bottom part of the anchorage length as shown in figure (3.10a). As the relative movement, i.e. slip begins the bond stress distribution changes in the embedment length and a distinct rise in the maximum bond stress occurs. The reducing bond stress curves also indicate a minimum bond stress at the bottom part of anchorage length. It can be seen from figure (3.10a) that the column bars develop very high bond stress at the top of the embedded length which is greater than the average anchorage bond stress at failure.

Load versus bond stress distribution for tests S2-1 and S2-4 is shown in figures (3.10b) and (3.10c), respectively. From both figures the bond stress is a maximum at the top and a minimum at the bottom region of the anchorage length. The bond stress curves are nonlinear in

both cases and show considerable similarity of shapes in test S2-4, while they are less consistent in test S2-1. Both figures indicate very high bond stresses near the column to base interface.

Load versus bond stress distribution along the anchorage length of the foundation for tests SR2-1 and SR2-2 is shown in figures (3.10d) and (3.10e), respectively. In both tests the bottom part of the column bars is not stressed in bond at small loads. The variation of bond stress over the embedded length of column bars is nonlinear. At each load stage the bond stress developed at the top part decreases and becomes a minimum at the bottom part of the anchorage length. It can be seen from figures (3.10d) and (3.10e) that the bond stress curves within each test are consistent and similar through the loading stages. The bond stress at the top of the anchorage length shows a distinct increase as the loading continues, so that the column bars produce very high bond stresses near the column to base interface. The bond stress curves excluding the top portion, rise more steeply in test SR2-2 than those in test SR2-1 which displays a more even distribution of bond stress over the column bars. Finally from figures (3.10d) and (3.10e) it is obvious that the bond stress developed by the ribbed bars at the column to base joint is greater than the average bond stress at failure.

Figure (3.10f) illustrates the variation of bond stress over the anchorage length of column bars against load in test SR4-3. From the figure the bond stress curves descend nonlinearly towards the bottom and show similarity of shapes. The maximum and minimum bond stresses are at the top and bottom parts of the anchorage length, respectively. Through the loading sequence there is a clear rise in

the bond stress at the top portion of the embedment length. This bond stress exceeds the average bond stress at failure until first slip takes place.

Load versus bond stress distribution along the anchorage length for tests SR7-1 and SR7-2 are illustrated in figures (3.10g) and (3.10h) respectively. Due to the restricted slip introduced by the links it was possible to trace the bond stress distribution close to failure in test SR7-1. From figure (3.10g) the bond stress distribution is approximately linear at small loads. Through the loading sequence the bond stress curves descend nonlinearly from top to bottom of the anchorage length maintaining a similarity of shape until close to failure. Near the column to base interface the column bars gradually produce excessive bond stresses which are approximately twice the average bond stress at failure.

From figure (3.10h) at the early stages of loading, the bond stress over the anchorage length of column bars decreases almost linearly towards the bottom. At higher loads the bond stress curves become nonlinear with a bond stress at the top part of the anchorage length which is greater than the average bond stress at failure. From figures (3.10g) and (3.10h) at comparable loads, the bond stress at the top and bottom locations is smaller in test SR7-2 than SR7-1 which shows a more even distribution of bond stress along the anchorage length.

In the rest of tests with ribbed bars the bond stress distribution along the anchorage length followed the same trend as already described in the preceding paragraphs.

3.6 Bond Stress Distribution in Column and Foundation

The variation of bond stress over the longitudinal bars in the column and foundation with respect to the load is shown in figures (3.11a) and (3.11b) for tests SR9-2 and SR10-2, respectively. From both figures the bond stress increases towards the bottom in the column, while it decreases towards the bottom in the foundation. Up to nearly two-thirds of the ultimate load the bond stresses are higher in the base than in the column. Then the column to base joint becomes more critical as the column bars produce higher bond stresses in the column than in the base until failure. This produces large bursting forces from the bond action of the bars. When the bursting forces exceed the resistance of the column, failure will take place in the column to base joint zone, provided that no compression failure occurs in the column. This is demonstrated in test SR10-2. In this test when the bond stress reached its maximum in the column, the first cracks started from the column to base interface and extended upwards in the column and finally resulted in crushing of the concrete. It is concluded that part of the column length is critical in bond, and may be considered as an additional anchorage length to the embedment length in the base.

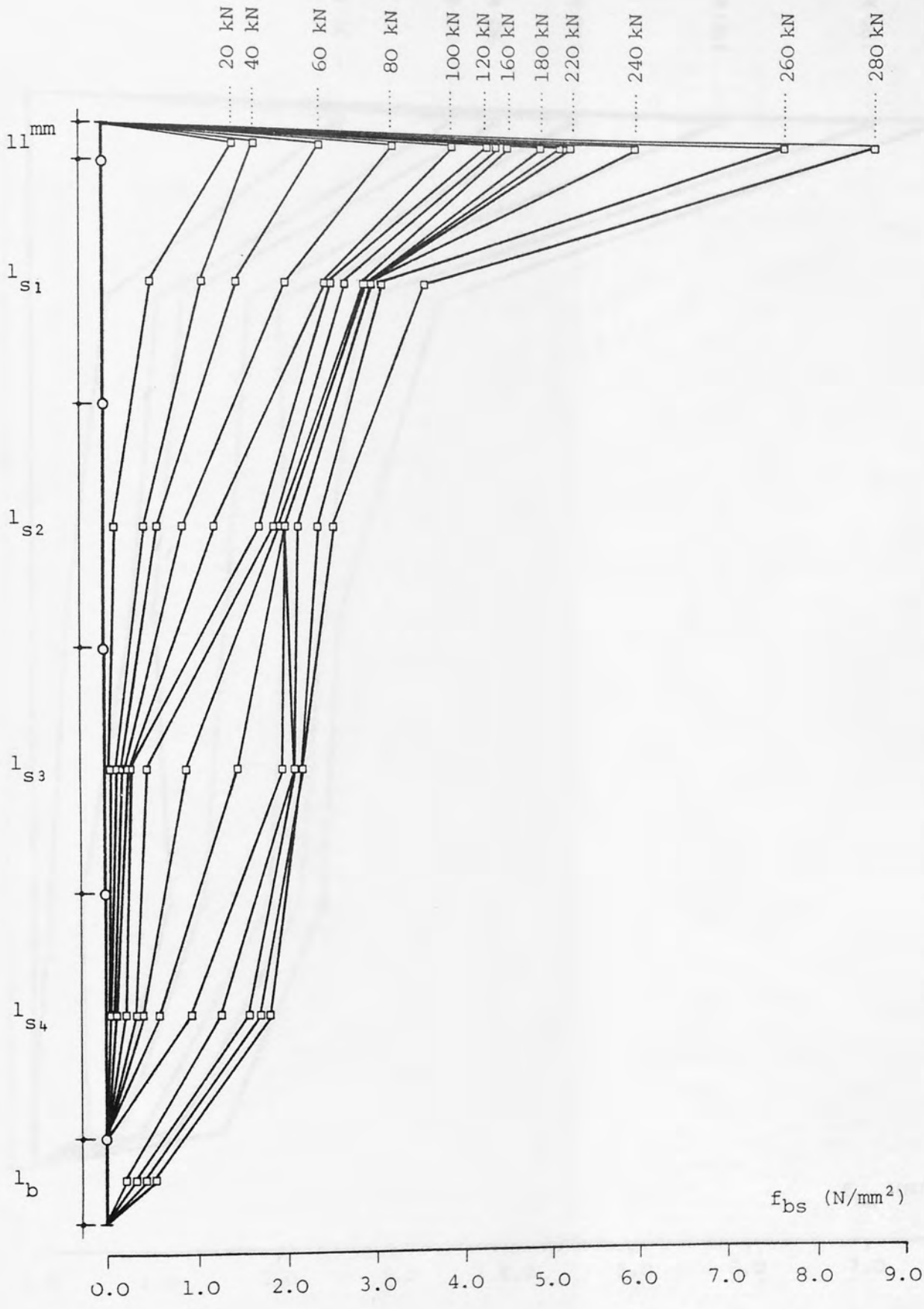

FIGURE 3.10a: LOAD VERSUS BOND STRESS DISTRIBUTION IN THE ANCHORAGE LENGTH OF COLUMN REINFORCEMENT IN TEST S1-3

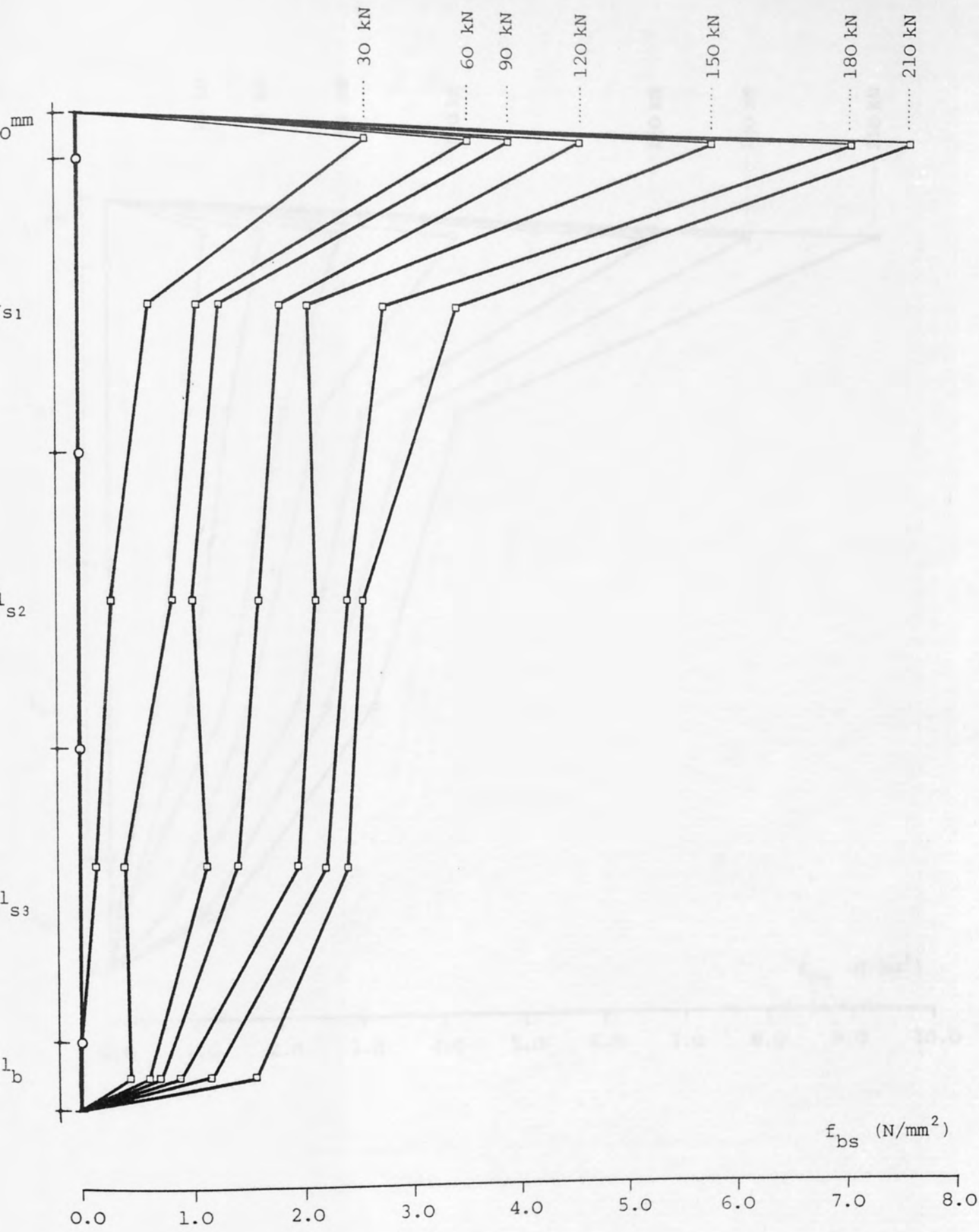

FIGURE 3.10b: LOAD VERSUS BOND STRESS DISTRIBUTION IN THE ANCHORAGE LENGTH OF COLUMN REINFORCEMENT IN TEST S2-1

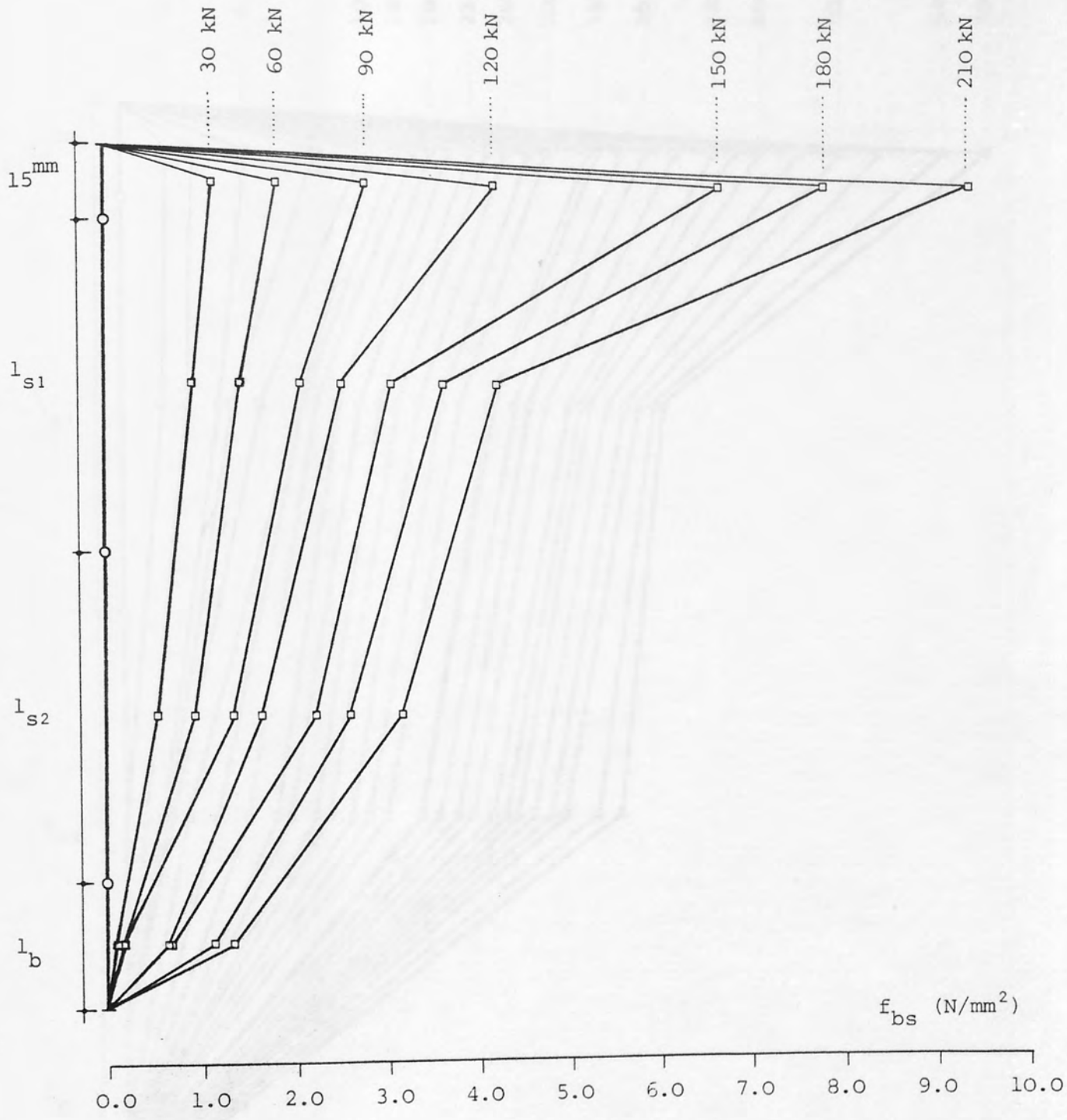

FIGURE 3.10c: LOAD VERSUS BOND STRESS DISTRIBUTION IN THE ANCHORAGE LENGTH OF COLUMN REINFORCEMENT IN TEST S2-4

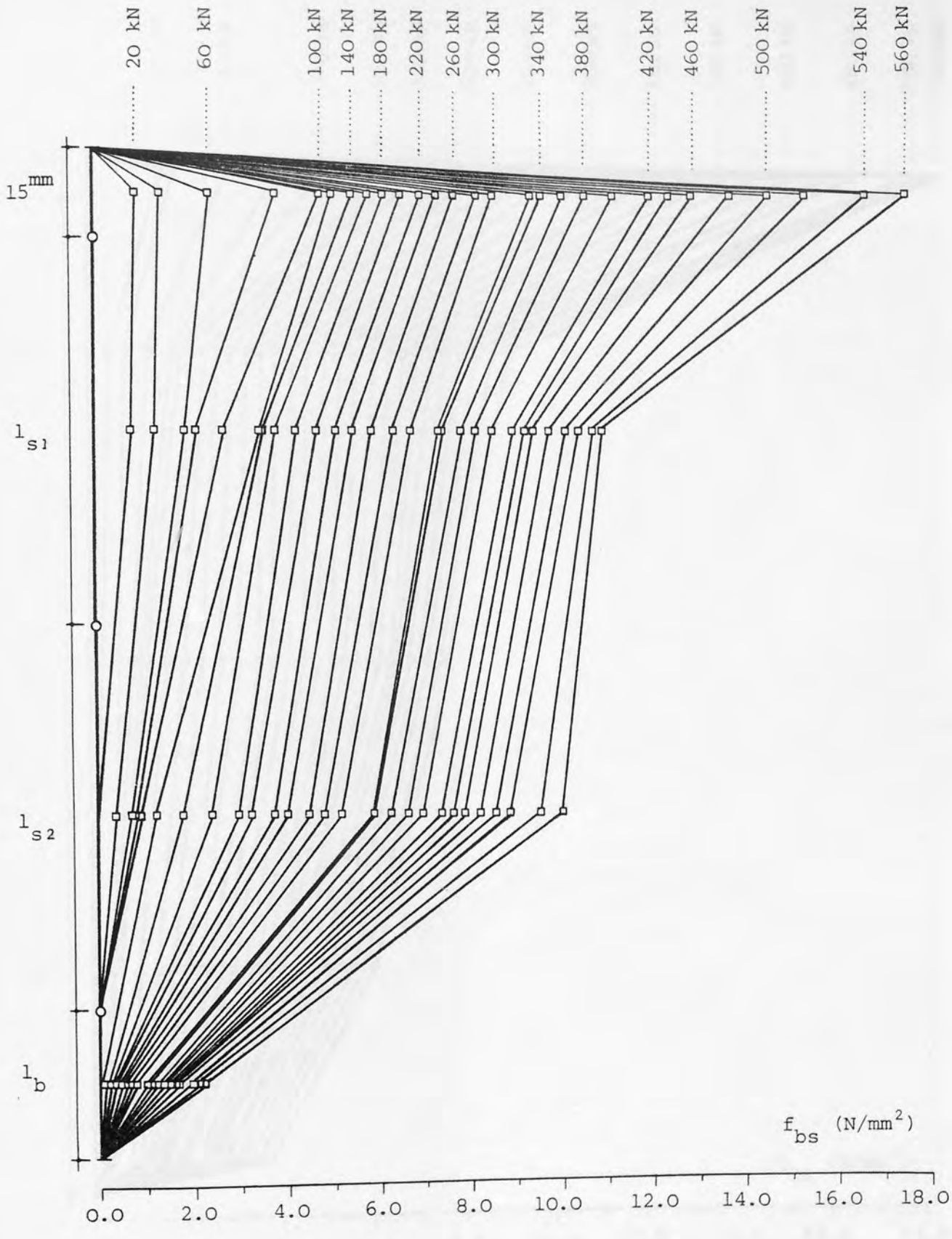

FIGURE 3.10d: LOAD VERSUS BOND STRESS DISTRIBUTION IN THE ANCHORAGE LENGTH OF COLUMN REINFORCEMENT IN TEST SR2-1

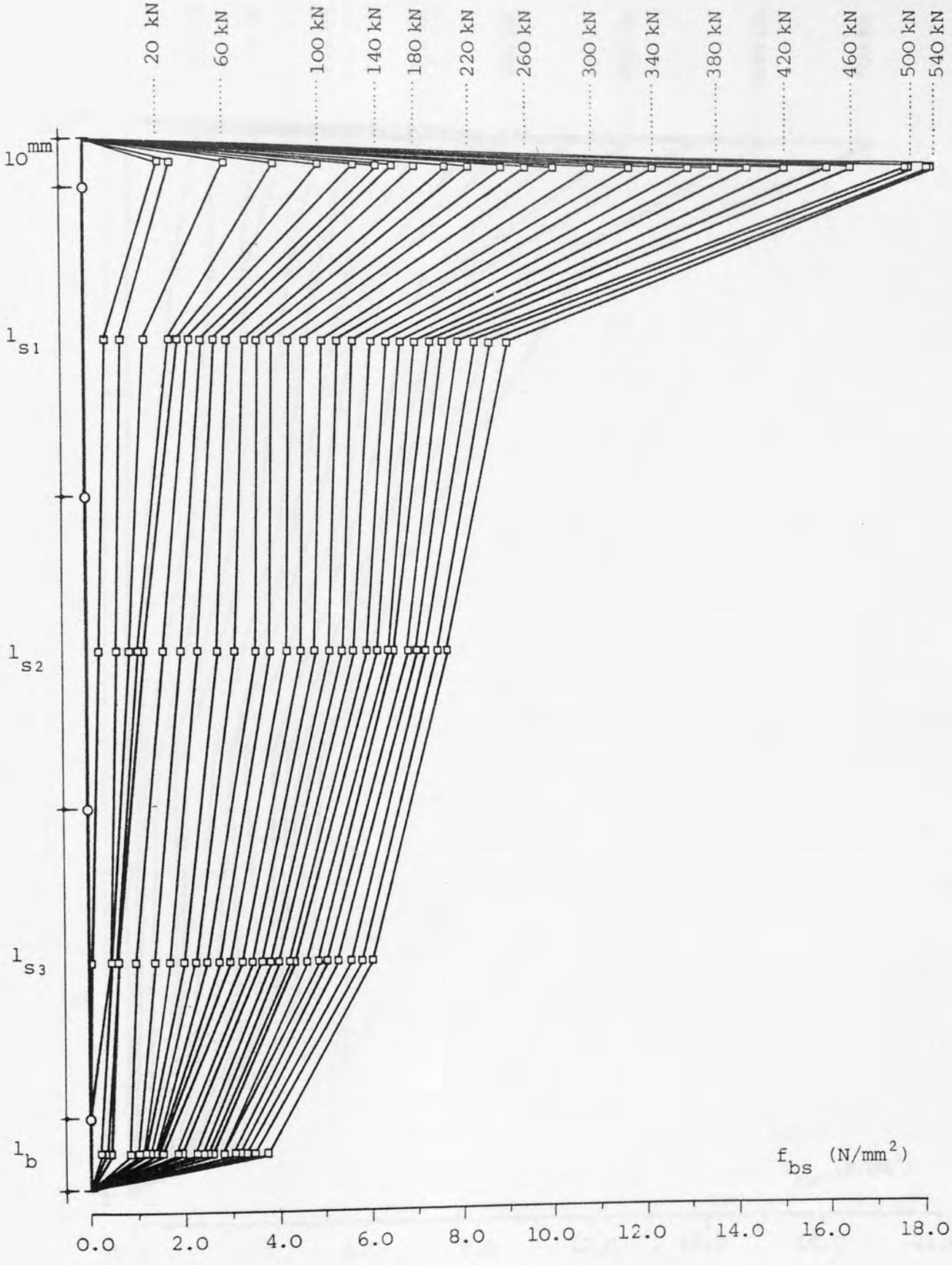

FIGURE 3.10e: LOAD VERSUS BOND STRESS DISTRIBUTION IN THE ANCHORAGE LENGTH OF COLUMN REINFORCEMENT IN TEST SR2-2

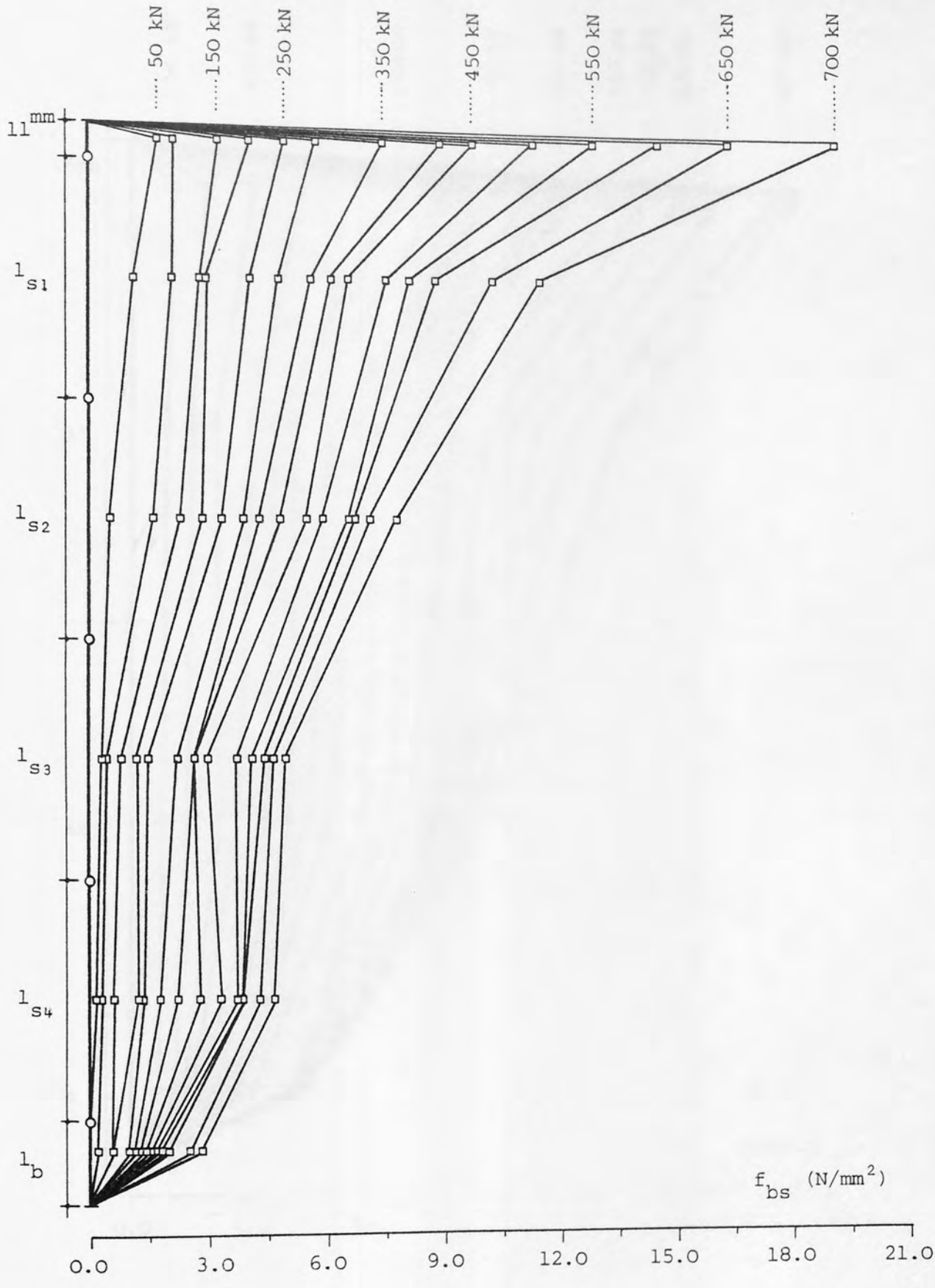

FIGURE 3.10f: LOAD VERSUS BOND STRESS DISTRIBUTION IN THE ANCHORAGE LENGTH OF COLUMN REINFORCEMENT IN TEST SR4-3

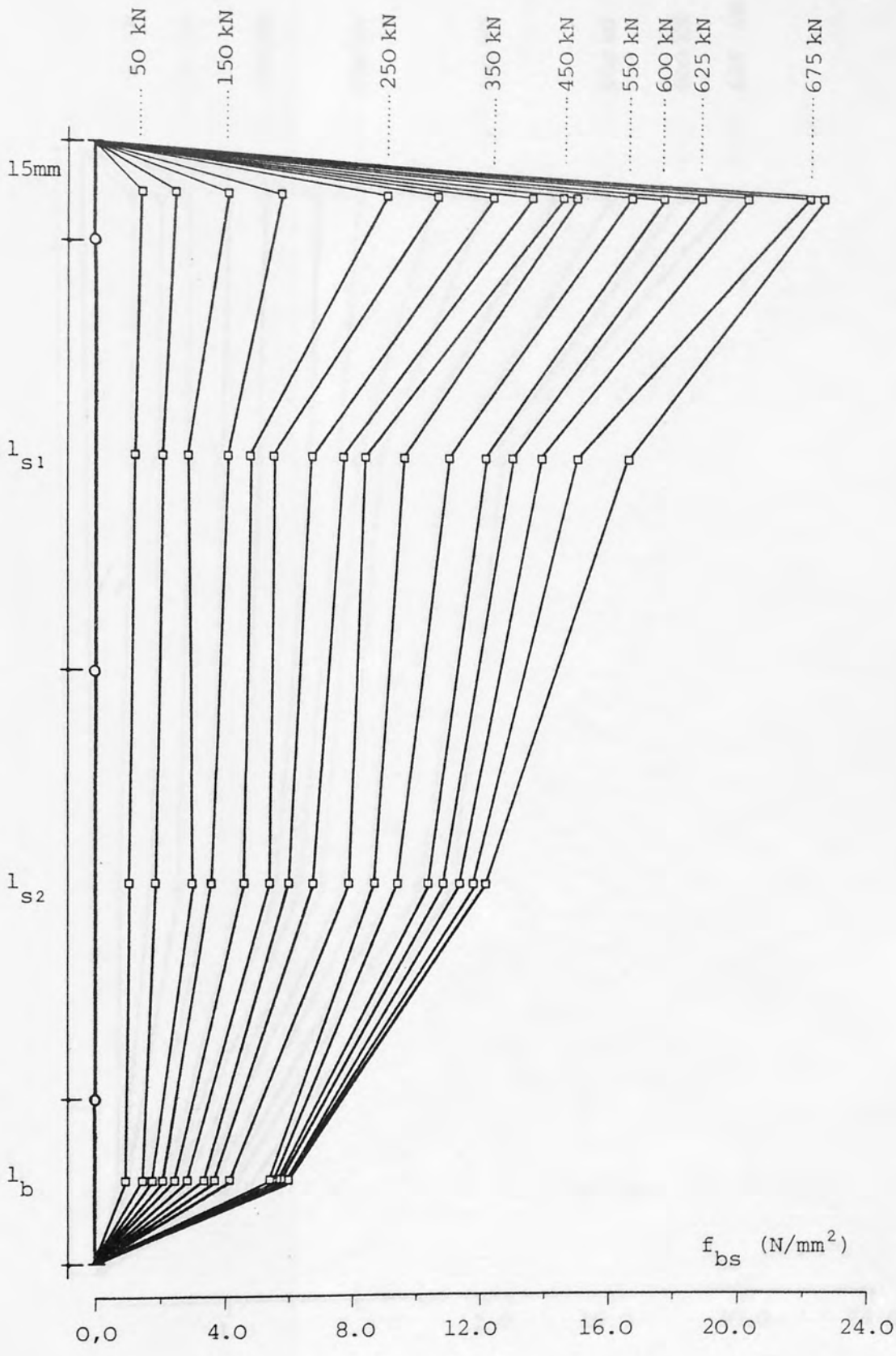

FIGURE 3.10g: LOAD VERSUS BOND STRESS DISTRIBUTION IN THE ANCHORAGE LENGTH OF COLUMN REINFORCEMENT IN TEST SR7-1

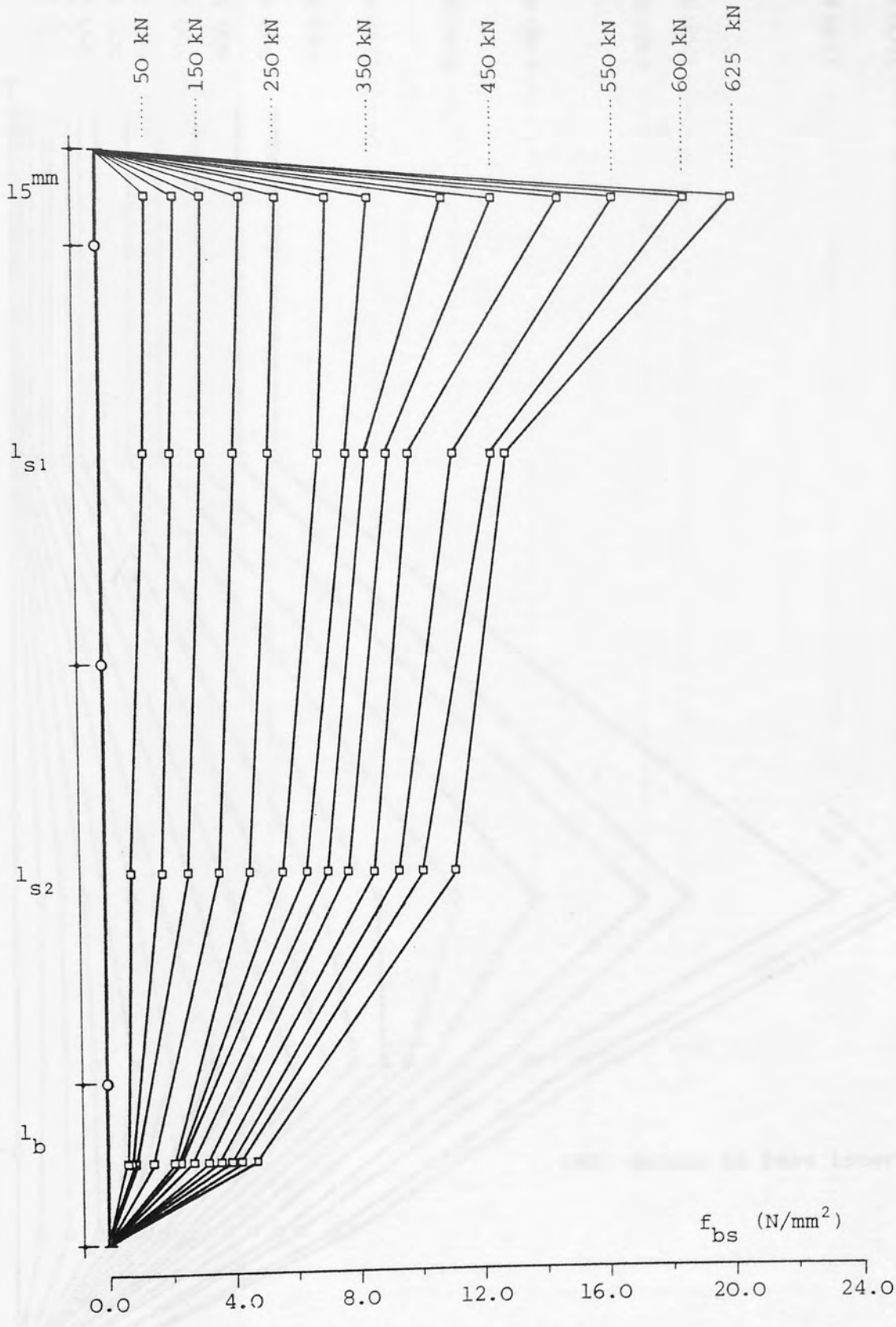

FIGURE 3.10h: LOAD VERSUS BOND STRESS DISTRIBUTION IN THE ANCHORAGE LENGTH OF COLUMN REINFORCEMENT IN TEST SR7-2

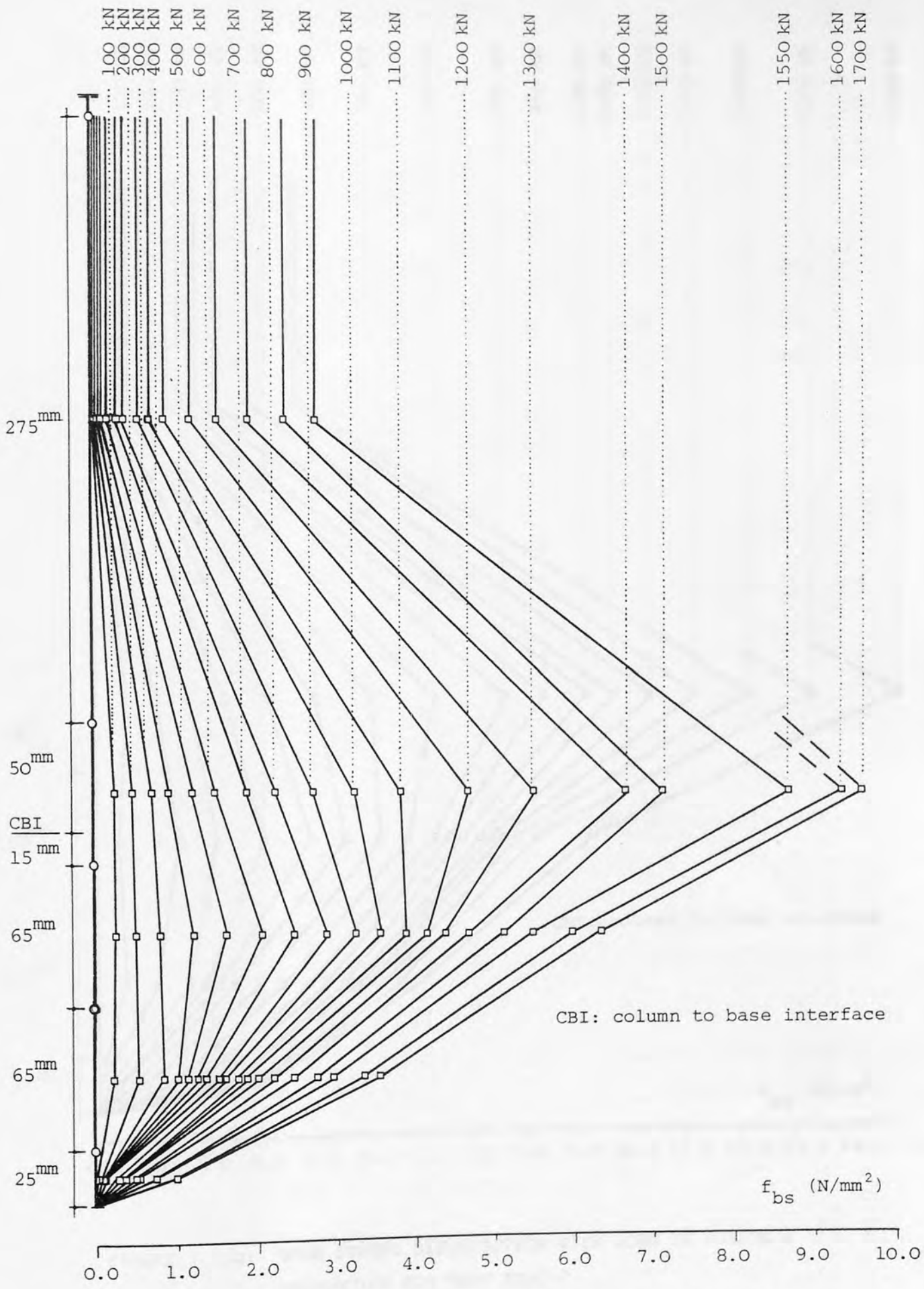

FIGURE 3.11a: BOND STRESS DISTRIBUTION WITH LOAD IN COLUMN & FOUNDATION FOR TEST SR9-2

CHAPTER 4

DISCUSSION OF EXPERIMENTAL RESULTS

4.1 General Considerations

This chapter refers to the discussion of experimental results obtained at the conclusion of the test specimens. To investigate the compression bond of column longitudinal reinforcement in the transference of axial load from a column to a base, eleven groups of tests covering nine variables were undertaken. The first general information obtained from an examination of the test results is that there is a distinct variation in the failure load with the corresponding variable. The behaviour of the test piece is also influenced by the variable investigated.

In general there are two principal modes of bond failure of deformed bars. In a type one, failure takes place as the bar shears the concrete and slips down. This type of failure occurs in a structural member where sufficient containment is present over the reinforcing bar so that the bursting forces produced by the bond action of the bar will not overcome the splitting resistance of the member prior to shearing forces. On the other hand, in a type two, the bursting forces govern the failure by splitting the surrounding concrete cover over the reinforcement. This type of failure most likely takes place in the reinforced concrete columns and beams.

In all groups of tests with square twisted bars and except groups X and XI in the other groups of tests with ribbed bars the load was

applied directly to the bars. The transfer of the load from the bars to the concrete could only be sustained by bond. The governing failure mode in these tests was type one as previously described in chapter 3. It is obvious that in an independent square foundation there is a large amount of concrete containment surrounding the embedded length of column longitudinal steel. On the other hand, the provision of the base tension reinforcement, which is generally the case in normal design practice stiffens the foundation concrete and introduces an extra confining element to resist the bursting forces. It is therefore quite understandable that the shearing forces exerted by the bond action of a deformed bar will be the principal cause of bond failure in the foundation. In fact the adjacent concrete in the vicinity of a deformed bar will reach its ultimate bearing capacity due to the shearing force components of bond and let the bar slip down before the bursting force components of bond come into force by overcoming the counteracting resistance of large concrete containment. This type of bond phenomenon was observed in the foundation tests, during the present experimentation. In cases where the failure of specimens due to the slip of bars was associated with the cracking of concrete at final collapse may be considered as a secondary effect for the reasons given below. Firstly, being progressive with loading, the amount of slip which has occurred before any crack formation in the concrete was sufficient to regard the specimen already failed. The column bars were non-effective at this stage due to the non-stop slip and resulting continuous loss of bond. Secondly, the local shearing of concrete along a cylindrical surface enveloping the bars was clearly observed for both types of steel. In fact inspection of cracked specimens after failure indicated powdery polished hole surfaces throughout the anchorage length of the bars.

Some of the variables studied had a considerable influence on the anchorage bond in the foundation. The bar size for instance for both square twisted and ribbed bars significantly affects the ultimate bond strength. The bond stress increases linearly with increasing the bar size for square twisted bars, but ribbed bars do not plot in the same linear fashion. The embedment length provided to the column bars in the base has an effect on the anchorage bond stress for both types of steel. Being linear, increases in the anchorage length lead to decrease in the ultimate bond stress for square twisted bars. On the other hand, increasing the plan area of the foundation increases the bond stress for both types of reinforcement.

Base tension reinforcement increases anchorage bond strength and prevents cracking of the concrete. The provision of links over the embedded part of column longitudinal reinforcement in the base significantly increases the bond stress at failure. Links also provide very strong confinement to the column bars so that the slip rate is significantly reduced close to failure. In particular the provision of links together with base tension reinforcement leads to a very significant increase in the ultimate bond resistance.

The concrete compressive strength has an apparent effect on the anchorage bond strength. The bond stress increases as the concrete compressive strength is increased.

Tests with a short reinforced concrete column indicate that part of the column length acting as an extra anchorage length is the critical zone in the compression bond since the maximum bond stresses develop in this part rather than the base.

In all groups of tests the end bearing of the column bars which could contribute to the ultimate bond strength, was eliminated. On the other hand the effect of bending was not taken into consideration in the tests because the specimens were supported on an underlying solid steel platen of the testing rigs.

The effects of the variables considered upon the anchorage bond resistance for both square twisted and ribbed deformed bars are discussed in detail in the following sections.

4.2 Square Twisted Bars

Tests in part one examined the anchorage bond strength of the square twisted reinforcement in the foundation. The performance of the specimens was similar and due to the configuration of square twisted bar early slip of the column bars in the anchorage length was always present. Close to the ultimate load the slip was large in most of the tests and much greater than would be permissible in reinforced concrete construction.

A computation of the values of the average bond stress at failure ($f_{bsav.}$) for the foundations tested in this part was made from the data of table (3.3) and results are given in table (4.1). Three groups of tests were undertaken to determine the effect of the bar size, the anchorage length and the plan size of the foundation. They are discussed in the following subsections.

Group No:	Si-j	ϕ	A_p	A_s	l_a	A x B	$f_{bsav.}$	$\frac{f_{bsav.}}{\sqrt{f_{cu}}}$
		mm	mm	mm^2	mm	mmxmm	N/mm^2	
I	S1-1	16	50.27	201	320	800x800	6.178	1.032
	S1-2	20	62.83	314	320	800x800	7.336	1.248
	S1-3	25	78.54	491	320	800x800	8.853	1.479
	$\overline{S}$1-3	25	78.54	491	320	800x800	8.952	1.462
II	S2-4	25	78.54	491	170	800x800	10.579	1.729
	S2-1	25	78.54	491	220	800x800	10.417	1.706
	$\overline{S}$2-1	25	78.54	491	220	800x800	10.273	1.722
	S2-2	25	78.54	491	270	800x800	9.431	1.546
	$\overline{S}$2-2	25	78.54	491	270	800x800	9.490	1.558
	S1-3	25	78.54	491	320	800x800	8.853	1.479
	$\overline{S}$1-3	25	78.54	491	320	800x800	8.952	1.462
	S2-3	25	78.54	491	370	800x800	7.614	1.325
III	S3-1	25	78.54	491	320	600x600	8.654	1.480
	S1-3	25	78.54	491	320	800x800	8.853	1.479
	$\overline{S}$1-3	25	78.54	491	320	800x800	8.952	1.462
	S3-2	25	78.54	491	320	1000x1000	9.151	1.564

TABLE 4.1: SUMMARY OF SPECIFICATIONS AND AVERAGE BOND STRESS AT FAILURE FOR TESTS WITH SQUARE TWISTED BARS IN PART ONE

4.2.1 Effect of Bar Size

Group I tests investigated the effect of bar size (which denotes nominal bar diameter, unless otherwise stated) upon the anchorage bond resistance. Expressed as part the square root of the concrete compressive strength, the average bond stress at failure is represented in a series of graphs shown in figures (4.1a) and (4.1b).

In figure (4.1a) the ratio of bond stress to square root of the concrete compressive strength ($f_{bsav.}/\sqrt{f_{cu}}$) is plotted against the bar size (ϕ) and the bar size ratio (ϕ_{max}/ϕ), respectively. From the figure both methods of plotting the results give a straight line which shows that the bond stress increases linearly with increasing the bar size or decreasing the bar size ratio. A regression analysis of the results is

$$(f_{bsu}/\sqrt{f_{cu}}) = 0.0482\ (\phi) + 0.270, \quad R = 0.998 \qquad (4.1a)$$

$$(f_{bsu}/\sqrt{f_{cu}}) = -0.789\ (\phi_{max}/\phi) + 2.254, \quad R = -0.998 \qquad (4.1b)$$

To trace the bond stress variation with respect to the geometrical properties of the reinforcement the ratio ($f_{bsav.}/\sqrt{f_{cu}}$) is also plotted against the bar periphery (A_p), bar cross sectional area (A_s) and the ratio of (A_s/A_p). The results shown in figure (4.1b) indicate that the bond stress also increases linearly with the increase of these geometrical properties. The corresponding relationships obtained from a linear regression analysis are given below.

$$(f_{bsu}/\sqrt{f_{cu}}) = 0.0153\ (A_p) + 0.270, \quad R = 0.998 \qquad (4.2a)$$

$$(f_{bsu}/\sqrt{f_{cu}}) = 0.00147\ (A_s) + 0.756, \quad R = 0.994 \qquad (4.2b)$$

$$(f_{bsu}/\sqrt{f_{cu}}) = 0.1927\ (A_s/A_p) + 0.270, \quad R = 0.998 \qquad (4.2c)$$

From the preceding expressions it is concluded that the bond stress

varies linearly with the geometrical properties of the square twisted bars considered. An increase in bar size results in a proportional increase in the anchorage bond stress.

4.2.2 Effect of Embedment Length in Foundation

The variation of bond stress with respect to the embedment length in the foundation was investigated in group II. The anchorage length of the column longitudinal reinforcement was changed between 170 mm and 370 mm in eight tests.

Group II test results are shown in figure (4.2a) as $(f_{bsav.}/\sqrt{f_{cu}})$ plotted against the anchorage length (l_a). It can be seen from the figure that increasing the anchorage length of the column bars produces low bond stresses. The variation of the ultimate bond stress with respect to the anchorage length may be represented with a straight line given by the following expression obtained from a regression analysis.

$$(f_{bsu}/\sqrt{f_{cu}}) = -0.00216\ (l_a) + 2.149, \quad R = -0.978 \qquad (4.3)$$

In figure (4.2b) $(f_{bsav.}/\sqrt{f_{cu}})$ is plotted against the ratios of anchorage length to bar size (l_a/ϕ), anchorage length to bar periphery (l_a/A_p) and anchorage length to bar cross sectional area (l_a/A_s), respectively. From the figure the bond stress at failure decreases linearly with increasing values of these ratios. A regression analysis yields the following expressions.

$$(f_{bsu}/\sqrt{f_{cu}}) = -0.054\ (l_a/\phi) + 2.149, \quad R = -0.978 \qquad (4.4a)$$

$$(f_{bsu}/\sqrt{f_{cu}}) = -0.170\ (l_a/A_p) + 2.149, \quad R = -0.978 \qquad (4.4b)$$

$$(f_{bsu}/\sqrt{f_{cu}}) = -1.058\ (l_a/A_s) + 2.148, \quad R = -0.978 \qquad (4.4c)$$

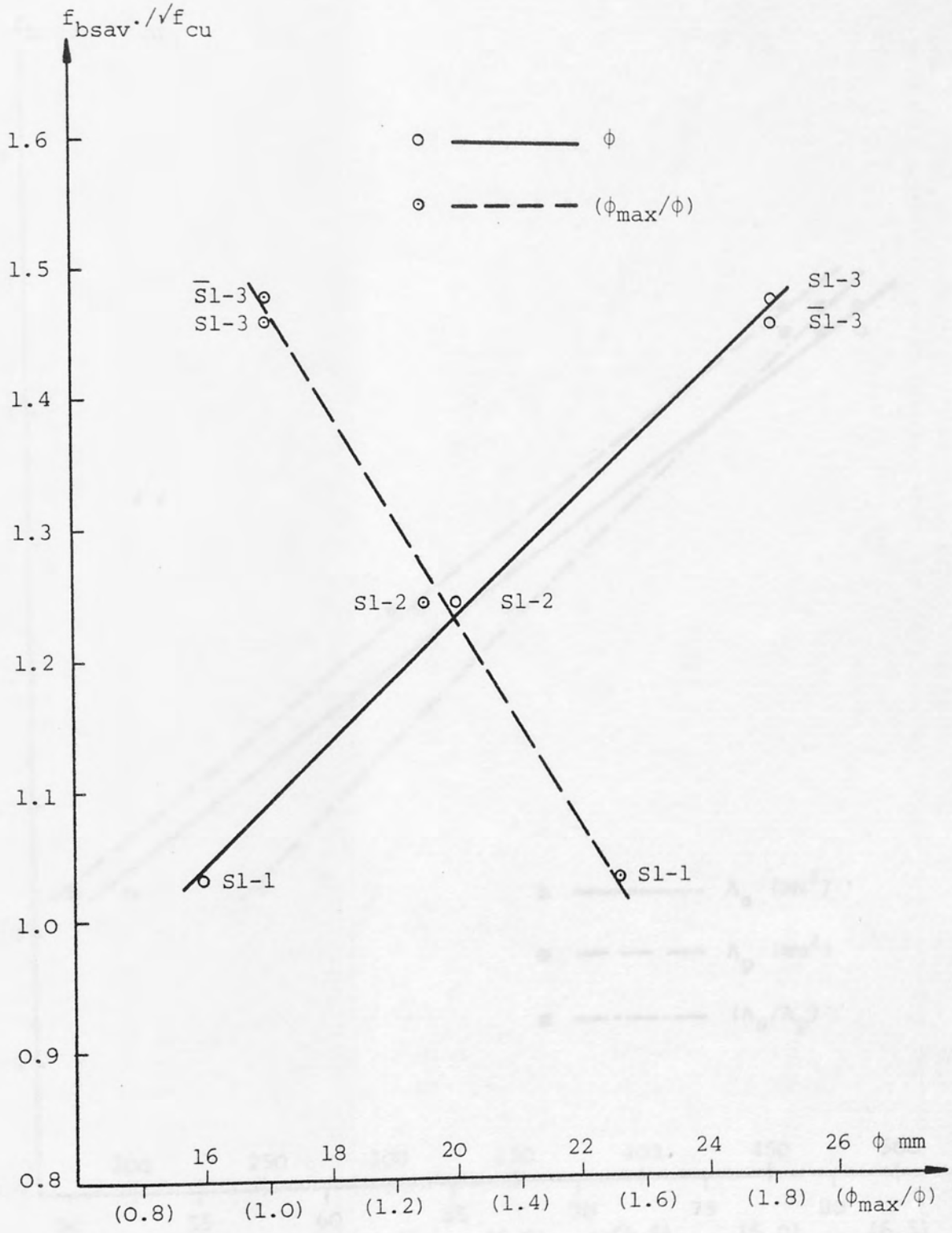

FIGURE 4.1a: BAR SIZE & BAR SIZE RATIO VERSUS RATIO OF BOND STRESS TO SQUARE ROOT OF CONCRETE COMPRESSIVE STRENGTH IN GROUP I

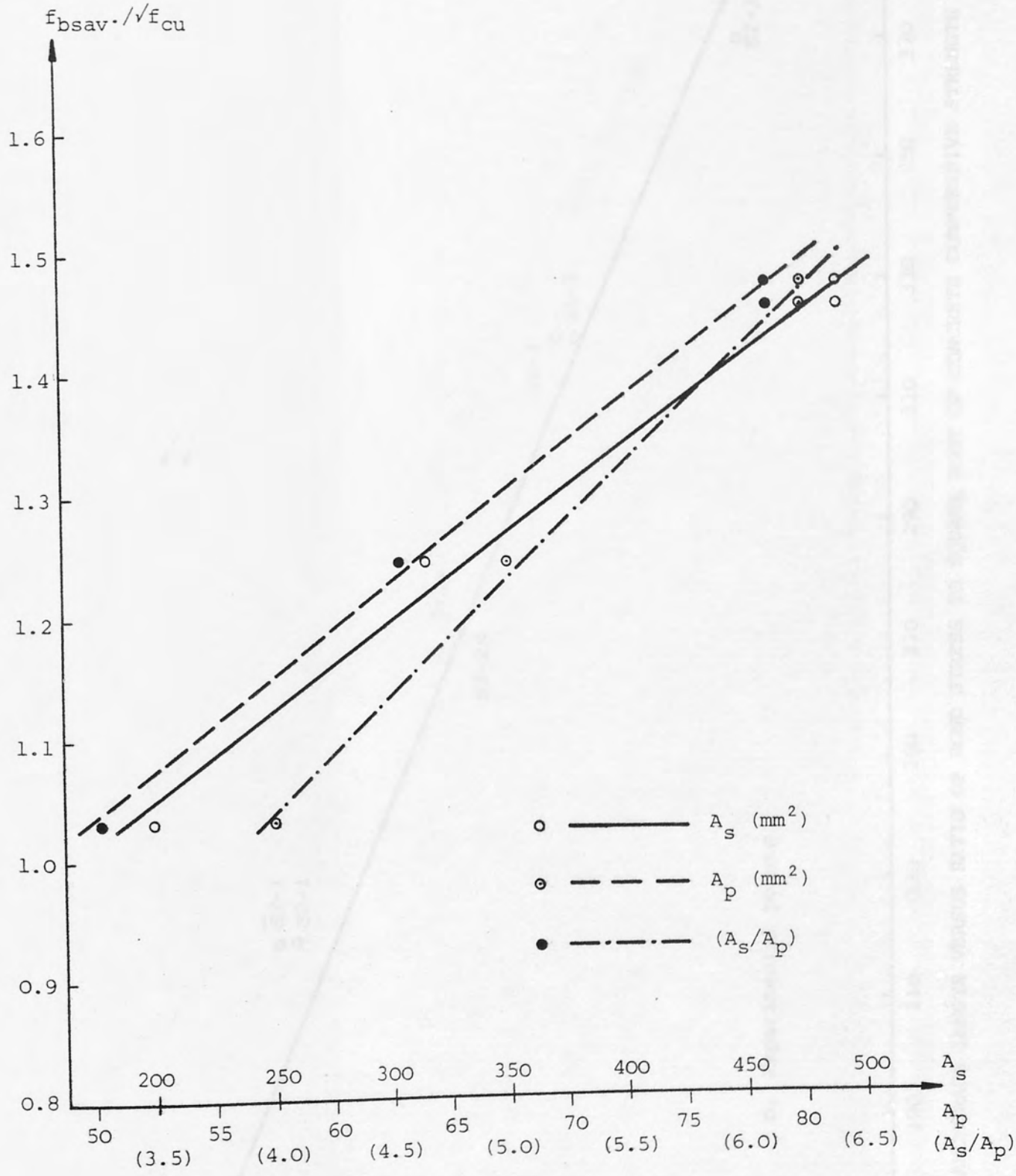

FIGURE 4.1b: BAR PERIPHERY & BAR CROSS-SECTIONAL AREA AND RATIO OF (A_s/A_p) VERSUS RATIO OF BOND STRESS TO SQUARE ROOT OF CONCRETE COMPRESSIVE STRNGTH IN GROUP I

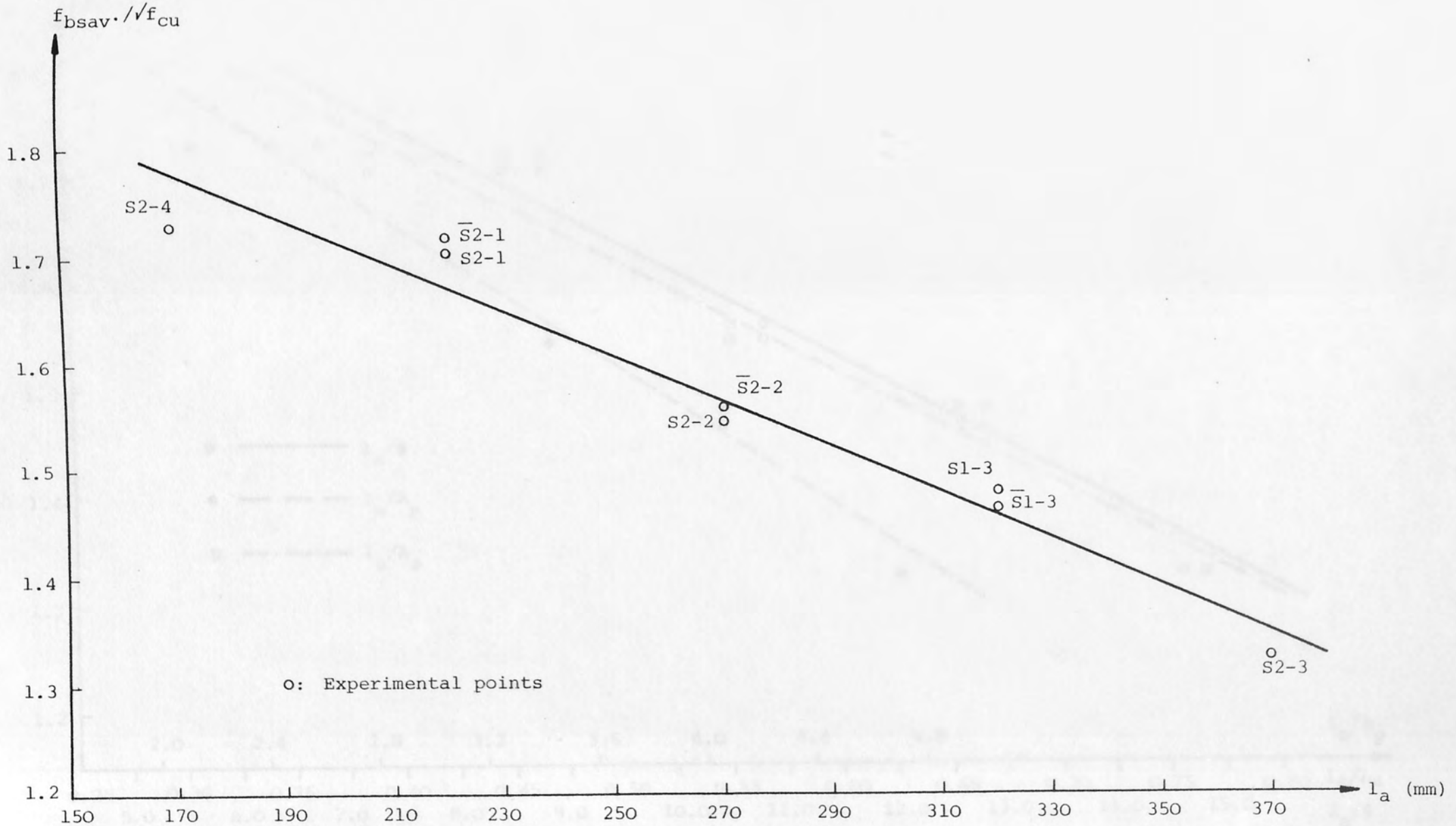

FIGURE 4.2a: ANCHORAGE LENGTH VERSUS RATIO OF BOND STRESS TO SQUARE ROOT OF CONCRETE COMPRESSIVE STRENGTH IN GROUP II

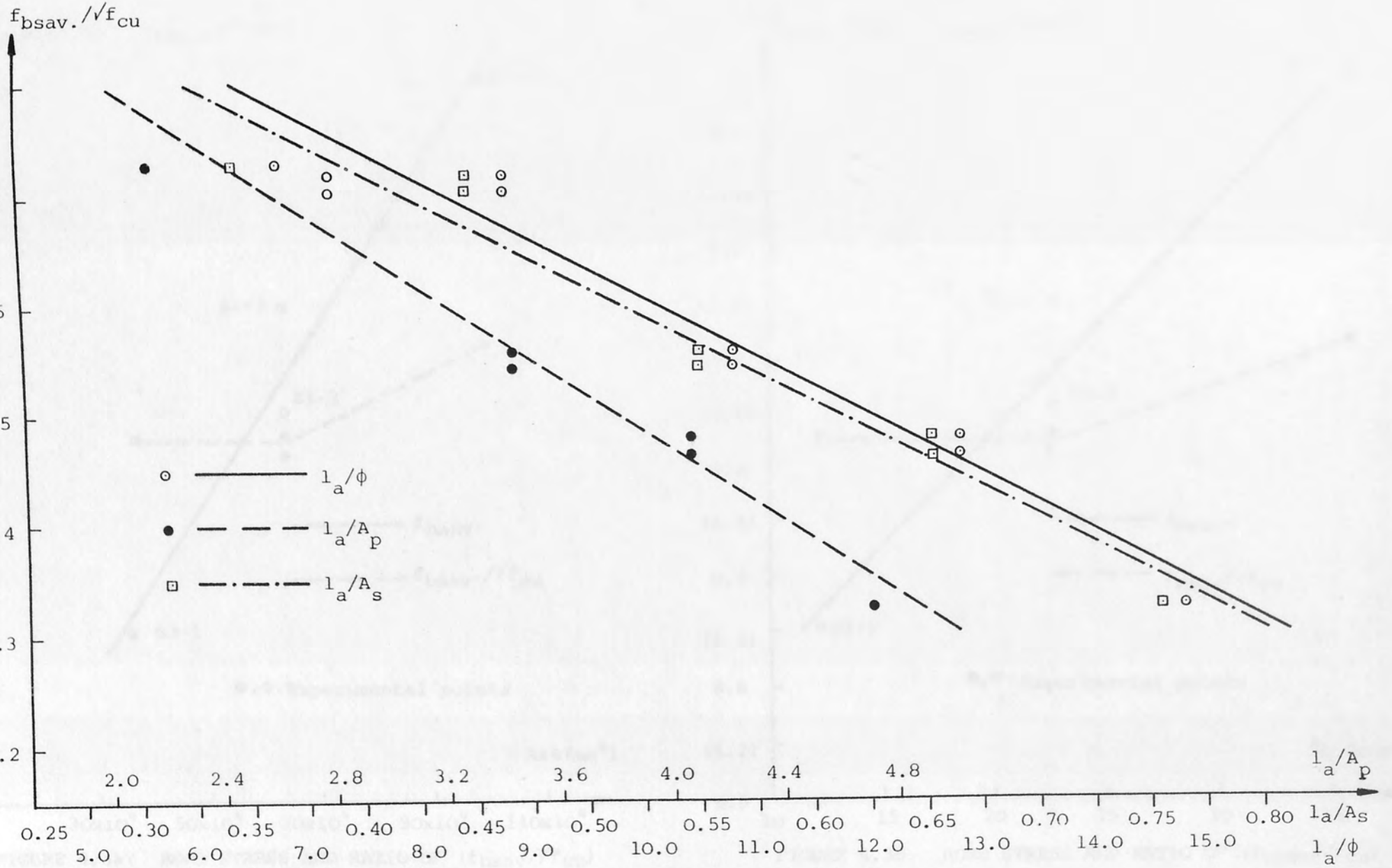

FIGURE 4.2b: ($f_{bsav.}/\sqrt{f_{cu}}$) VERSUS RATIO OF (l_a/ϕ), (l_a/A_p) & (l_a/A_s) IN GROUP II

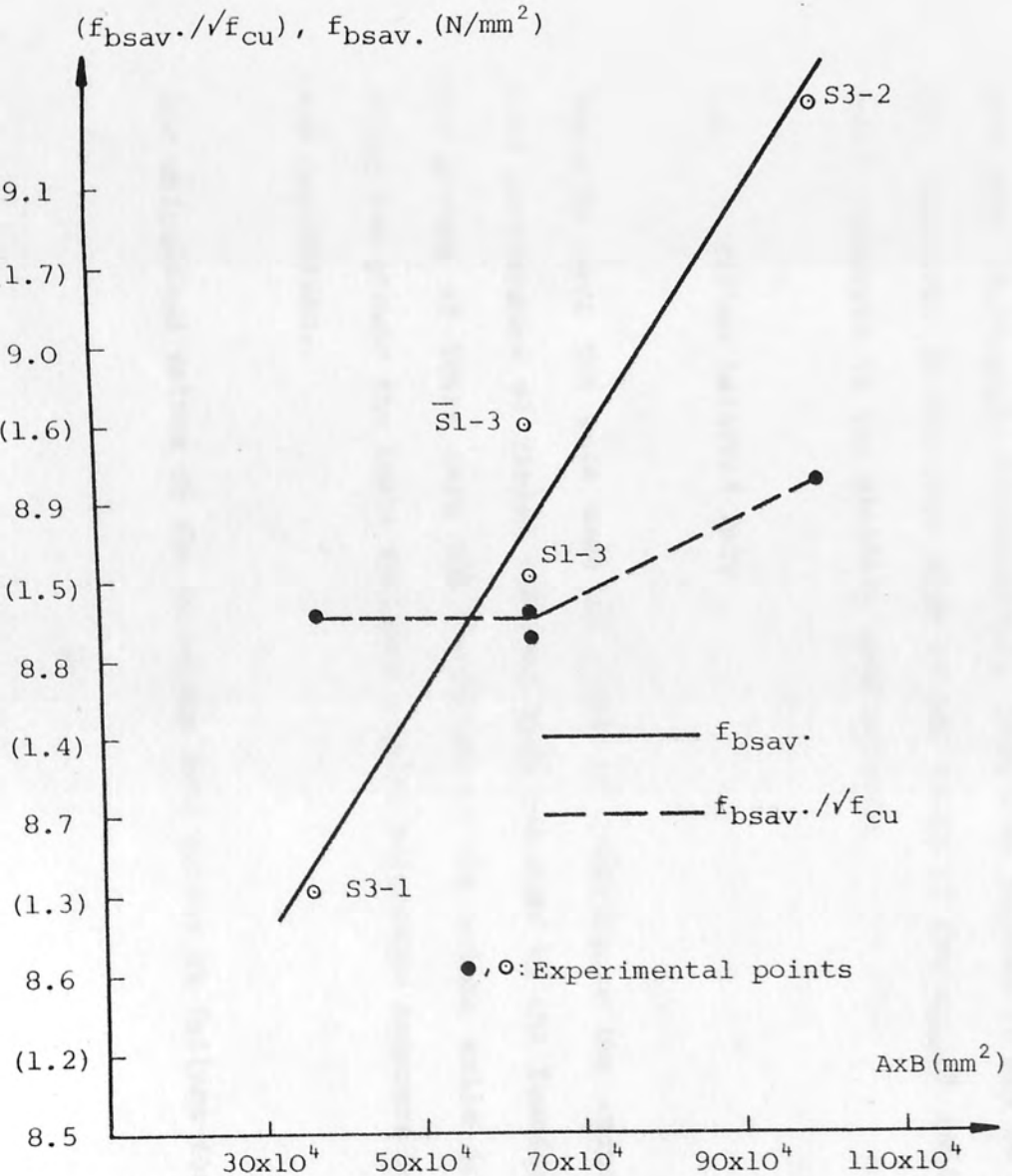

FIGURE 4.3a: BOND STRESS AND RATIO OF $(f_{bsav}/\sqrt{f_{cu}})$ VERSUS BASE SIZE IN GROUP III

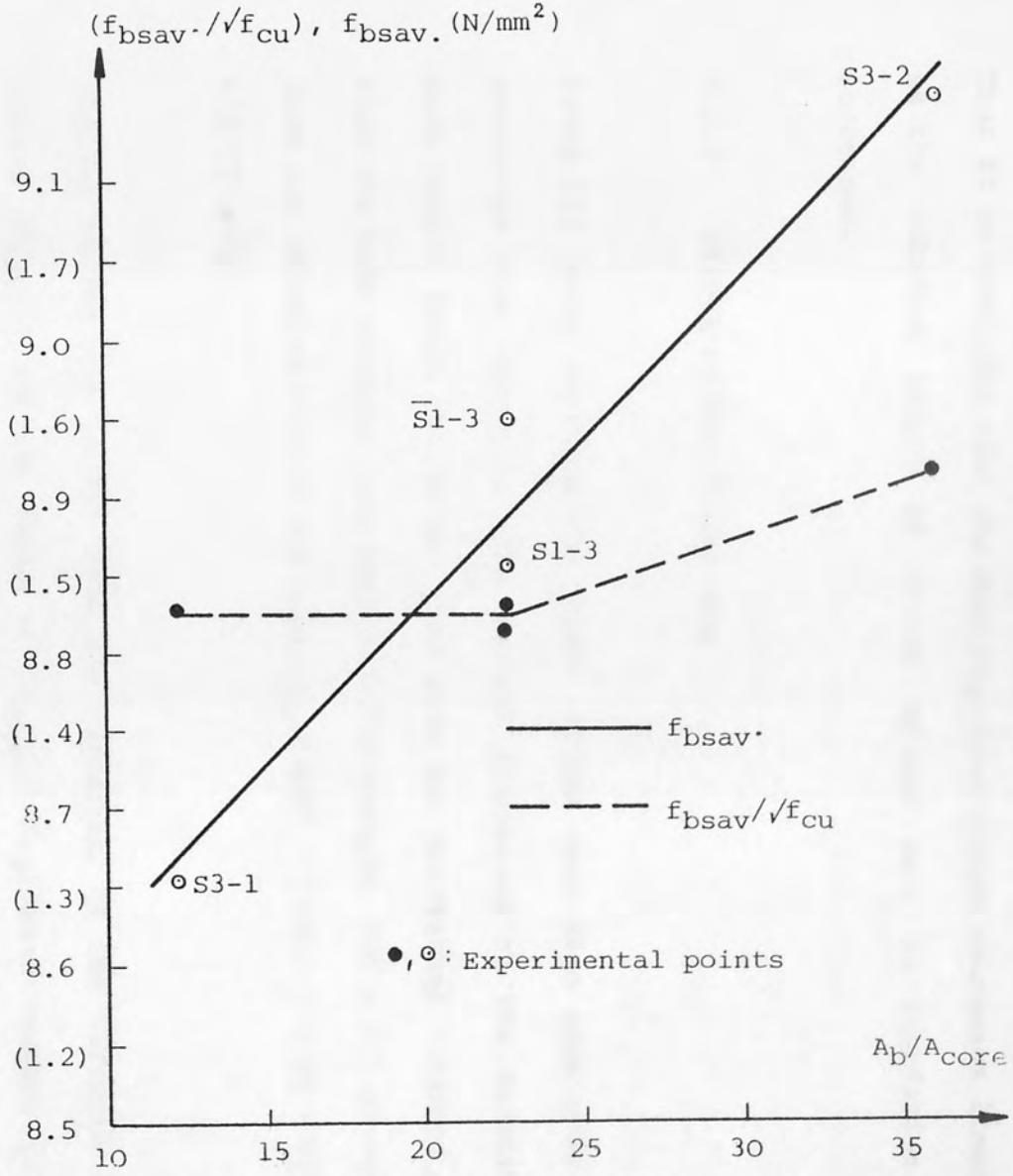

FIGURE 4.3b: BOND STRESS AND RATIO OF $(f_{bsav}/\sqrt{f_{cu}})$ VERSUS RATIO OF UNLOADED BASE AREA TO COLUMN CORE AREA IN GROUP III

Thus it is concluded that the anchorage bond stress decreases linearly as the embedded length of square twisted bars in foundation is increased.

4.2.3 Effect of Foundation Size

Group III tests examined the effect of the base plan size upon the anchorage bond strength. The lateral dimensions of the foundation were varied while the column core area was maintained constant, so that the base unloaded area varied. (For example, for a 800 mm square base the unloaded area of the base, $A_b = 800^2 - (250 - 2 \times 30 - 25)^2 = 612775\ mm^2$).

Figures (4.3a) and (4.3b) show the variation of the ultimate bond stress ($f_{bsav.}$) and the ratio of ($f_{bsav.}/\sqrt{f_{cu}}$) with respect to the base plan area (A x B) and the ratio of base unloaded area to column core area (A_b/A_{core}), respectively. From both figures it may be seen that increases in the base size or the ratio of (A_b/A_{core}) leads to small increases in the ultimate bond stress.

4.3 Ribbed Deformed Bars

Tests in part two were made in order to investigate the anchorage bond performance of ribbed deformed bars embedded in the foundation. Six groups of tests were not concreted in the column while in the other two groups the tests included a short reinforced concrete column and foundation.

The calculated values of the anchorage bond stress at failure for the

foundations without a short column in part two was made from the data of table (3.3) and, the results are given in table (4.2). In this table the ultimate bond stress ($f_{bsav.}$) is also presented as a portion of the square root of the concrete compressive strength. In these tests the effect of the following parameters on the anchorage bond stress were examined. Bar size, embedment length provided to the column longitudinal reinforcement in the foundation, plan area of foundation, base tension reinforcement, provision of the links in the anchorage length and the concrete compressive strength. They are discussed in the following subsections.

4.3.1 Effect of Bar Size

To examine the effect of bar size group IV tests were made using 16 mm, 20 mm and 25 mm bars with an anchorage length of 170 mm. The ultimate bond stress divided by the square root of the concrete compressive strength ($f_{bsav.}/\sqrt{f_{cu}}$) is plotted against the bar size (ϕ) and the bar size ratio (ϕ_{max}/ϕ) in figure (4.4a) and, bar periphery (A_p), bar cross-sectional area (A_s) and the ratio of (A_s/A_p) in figure (4.4b), respectively. It can be seen from both figures that the bond stress varies nonlinearly with respect to the geometrical properties of the ribbed bars. The ultimate bond stress for test SR1-2 with 20 mm bars is higher than that for test SR2-1 with 25 mm bars, which does not agree with the results obtained for the tests using square twisted bars. Test SR1-1 with 16 mm bars produced lower bond stress at failure than that for the other tests as would be expected. The low bond performance of 16 mm bars may be attributed to the geometrical properties of the bar. Because of the small rib height and spacing it seems probable that the bar is acting like a plain round bar.

Group	SRi-j	ϕ	A_p	A_s	l_a	ρ_b	ρ_{sv}	$f_{bsav.}$	$\frac{f_{bsav.}}{\sqrt{f_{cu}}}$
		mm	mm	mm^2	mm			N/mm^2	
IV	SR1-1	16	50.27	201	170	-	-	10.679	1.895
	SR1-2	20	62.83	314	170	-	-	12.727	2.239
	SR2-1	25	78.54	491	170	-	-	11.927	2.079
V	SR2-1	25	78.54	491	170	-	-	11.937	2.079
	SR2-2	25	78.54	491	220	-	-	12.154	2.063
	SR1-3	25	78.54	491	320	-	-	13.926	2.496
VI	SR3-1	25	78.54	491	320	-	-	11.191	1.906
	SR1-3	25	78.54	491	320	-	-	13.926	2.496
VIIa	SR1-3	25	78.54	491	320	0.00	-	13.926	2.496
	SR4-1	25	78.54	491	320	0.275	-	13.926	2.517
	SR4-2	25	78.54	491	320	0.459	-	14.423	2.581
	SR4-3	25	78.54	491	320	0.643	-	15.667	2.895
VIIIa	SR1-3	25	78.54	491	320	-	0.00	13.926	2.496
	SR5-1	25	78.54	491	320	-	0.331	15.169	2.798
	SR5-2	25	78.54	491	320	-	0.827	14.911	2.605

TABLE 4.2: SUMMARY OF SPECIFICATIONS AND AVERAGE BOND STRESS AT FAILURE FOR TESTS WITH RIBBED BARS WITHOUT SHORT COLUMN IN PART TWO

Group	SRi-j	ϕ	A_p	A_s	l_a	ρ_b	ρ_{sv}	$f_{bsav.}$	$\frac{f_{bsav.}}{\sqrt{f_{cu}}}$
		mm	mm	mm^2	mm			N/mm^2	
VIIb	SR2-1	25	78.54	491	170	0.00	-	11.937	2.079
	SR6-2	25	78.54	491	170	0.537	-	12.171	2.066
	SR6-3	25	78.54	491	170	0.895	-	12.732	2.262
	SR6-4	25	78.54	491	170	1.253	-	14.160	2.502
VIIIb	SR2-1	25	78.54	491	170	0.00	0.00	11.937	2.079
	SR7-1	25	78.54	491	170	0.00	0.934	13.575	2.379
	SR7-2	25	78.54	491	170	0.895	0.311	15.681	2.743
IX	SR2-1	25	78.54	491	170	-	-	11.937	2.079
	SR8-1	25	78.54	491	170	-	-	9.830	1.944
	SR8-2	25	78.54	491	170	-	-	9.128	1.951
	SR8-3	25	78.54	491	170	-	-	10.766	2.041
	SR8-4	25	78.54	491	170	-	-	12.498	2.074

TABLE 4.2: (continued)

In these tests the concrete compressive strength was approximately constant varying less than two percent, so that the effect of the concrete strength on the ultimate bond stress can be regarded as negligible. A closer examination of the test results indicates that at bond failure the column bars in tests SR1-1 and SR1-2 are stressed to 94 percent and 99 percent of their yield stresses, respectively, while in test SR2-1 they are stressed to only 59 percent of their yield stress. However, it should be noted that the yield stress of the column bars in SR2-1 was considerably higher than that in SR1-1 and SR1-2, see table (3.2) for reference.

In figures (4.4a) and (4.4b) the ratio of ultimate bond stress to square root of the steel compressive stress at failure ($f_{bsav.}/\sqrt{f_s}$) is also plotted against the same geometrical properties of the bars used before. From figure (4.4a) the ratio of ($f_{bsav.}/\sqrt{f_s}$) increases as the bar size is increased or the bar size ratio is reduced. On the other hand an increase in the bar cross-sectional area, bar periphery or the ratio (A_s/A_p) also leads to increase in the ($f_{bsav.}/\sqrt{f_s}$) ratio as seen in figure (4.4b). It is evident from both figures that the bond stress is also dependent on the compressive stress in the bar and the potential bond strength capacity increases with increasing bar size. Due to the axial compression load the exposed column bars above the base concrete are subjected to contraction. When the compression stress approaches yield in the bar, the increase in the bar diameter exerts additional frictional forces over surface of the bar, and consequently there is an increase in the bond stress. Hence it may be concluded that the bond stress is higher for the bar stressed at or above the yield than that for the bar stressed below yield in compression.

4.3.2 Effect of Embedment Length in Foundation

Group V tests investigated the variation of bond stress with respect to the embedment length of column bars. The anchorage length was varied from 170 mm to 320 mm in the tests. In figure (4.5a) the ratio of ultimate bond stress to square root of concrete cube strength ($f_{bsav.}/\sqrt{f_{cu}}$) is plotted against the anchorage length (l_a) and anchorage length ratio (l_{amin}/l_a). The results are further plotted against the ratios of anchorage length to bar size (l_a/ϕ), anchorage length to bar periphery (l_a/A_p) and anchorage length to bar cross-sectional area (l_a/A_s) respectively, as shown in figure (4.5b). It can be seen from both figures that the bond stress at failure increases nonlinearly with increasing anchorage length which does not agree with the results obtained for square twisted bars.

On further examination of the test results it can be observed that the yield stresses of the column bars in tests SR2-1 and SR2-2 are very high - see table (3.2) for reference - and at bond failure the bars are stressed below their yield stress, 59 percent for bars in SR2-1 and 77 percent for bars in SR2-2. From figures (4.5a) and (4.5b) the bond stress decreases as the anchorage length is increased for these two tests which follows the same trend obtained for the results of square twisted bars. In contrast in test SR1-3 at bond failure, the compressive stress in the bars is not only higher than the tensile yield stress but also higher than the ultimate tensile stress. The bond stress obtained for test SR1-3 is higher than that for tests SR2-1 and SR2-2. This can be explained by the tendency for the bar diameter to increase at yield, which produces a large increase in the bond stress as discussed for group IV tests in

section 4.3.1.

4.3.3 Effect of Foundation Size

Two tests were carried out which varied the plan area of the base in group VI. The ultimate bond stress ($f_{bsav.}$) and the ratio of ($f_{bsav.}/\sqrt{f_{cu}}$) for both tests are given in table (4.2). Although two tests are not conclusive it can be seen from the table that increasing the plan area of the base leads to a large increase in the ultimate bond stress. It is also noted that the column bars at bond failure were stressed significantly above the yield stress in both tests.

4.3.4 Contribution of Base Tension Reinforcement

Tests in groups VIIa and VIIb examined the effect of the base tension reinforcement on the anchorage bond stress in foundation. In group VIIa tests the embedment length of column bars was maintained at 320 mm and the base tension reinforcement percentage ($\rho_b=100\ A_{sb}/Bd$) was varied from zero to 0.643. In these tests the column cage was loaded beyond the yield stress of the column longitudinal reinforcement which led to an increase in the anchorage bond stress as discussed in the preceding sections.

In figure (4.6a) the ratio of the ultimate bond stress to square root of concrete compressive strength ($f_{bsav.}/\sqrt{f_{cu}}$) is plotted against the base tension reinforcement for group VIIa tests. It can be seen from the figure that the anchorage bond stress significantly increases as the quantity of base tension reinforcement is increased. The

curve ascends almost linear indicating approximately proportional increases in the ultimate bond stress until more than 0.46% steel is used and thereafter there is a greater increase in the bond stress as shown in figure (4.6a).

In group VIIb tests the anchorage length of column bars in the base was kept constant at 170 mm and the tension reinforcement percentage (ρ_b) was varied from zero to 1.253. These tests investigated the effect of bending tensile reinforcement at higher percentages while the column bars were stressed at less than their yield strength at bond failure. Group VIIb test results are shown in figure (4.6b) as the ratio of ultimate bond stress to square root of concrete compressive strength ($f_{bsav.}/\sqrt{f_{cu}}$) plotted against the base tension reinforcement percentage (ρ_b). It can be seen from the figure that provision of the bending tensile reinforcement in the foundation allows significant increases in the bond stress although it appears to be no increase in the bond stress until more than 0.54% steel is used as indicated by the curve. Thereafter the curve suddenly rises and continues almost as a straight line showing approximately proportional increases in the ultimate bond stress as seen in figure (4.6b).

4.3.5. Contribution of Links Placed in the Anchorage Length

Tests in groups VIIIa and VIIIb examined the contribution of the transverse reinforcement to the anchorage bond stress in foundation. In group VIIIa the embedment length of the column bars was maintained constant at 320 mm and the number of links placed over the reinforcement varied between zero and five. These tests were loaded

beyond the yield stress of the column bars, hence the ultimate bond stresses are increased owing to compressive stress in the bars being higher than the ultimate tensile strength as discussed before. The provision of the links in the anchorage length not only increases the bond stress but also confines the column bars and restrains the slip near failure.

Figure (4.7a) shows a plot of the ratio of ultimate bond stress to the square root of the concrete compressive strength ($f_{bsav.}/\sqrt{f_{cu}}$) against the column core confining reinforcement percentage ($\rho_{sv}=100A_{sv}/a_{core}xl_a$). For example, for test SR5-1 with two 8 mm links ρ_{sv} = $(100x4x0.25x\pi x8^2)/(190x320)$ = 0.331. From the figure the bond stress increases with increasing number of links except for test SR5-2. However, it must be stated that the bond stress indicated for test SR5-2 in figure (4.7a) does not represent the ultimate bond stress but shows the bond stress developed at the compression failure of the column cage. Due to the heavy confinement of the column bars by closely spaced links no bond failure occurred in test SR5-2. Provision of two links in SR5-1 leads to 12.1% increase in bond stress against SR1-3 in which no link was included. Even in SR5-2 the bond stress at column failure is 4.4% higher than the ultimate bond stress in SR1-3.

In group VIIIb tests the anchorage length of column bars was kept constant at 170 mm and the number of links was changed between zero and three. Test SR7-2 with one link also included base tension reinforcement and, it was taken into account in calculating the column core confining reinforcement percentage.

The ratio of the ultimate bond stress to square root of concrete compressive strength ($f_{bsav.}/\sqrt{f_{cu}}$) is plotted against the column core confining reinforcement percentage (ρ_{sv}) for group VIIIb tests as shown in figure (4.7b). It can be seen from the figure that increases in the core confining steel allow significant increases in the ultimate bond stress. For example, provision of three links in test SR7-1 leads to 14.4% increase in the bond stress comparing with test SR2-1 which included no links. On the other hand, the addition of the links in the presence of base tension reinforcement causes more significant increases in the bond stress. Test SR7-2 was identical to test SR6-3 except that one link was included on the column cage on the top. Consequently the ultimate bond stress for test SR7-2 was 21.2% higher than that for SR6-3.

4.3.6 Effect of Concrete Compressive Strength

In group IX tests the effect of the concrete compressive strength on the anchorage bond stress was examined. In the tests the anchorage length of column bars was maintained constant at 170 mm and the concrete compressive strength was varied from 21.90 N/mm^2 to 36.30 N/mm^2 to cover the practical range of reinforced concrete construction.

Figure (4.8a) shows the variation of the ultimate bond stress ($f_{bsav.}$) with respect to the concrete compressive strength (f_{cu}). It can be seen from the figure that the bond stress varies linearly as the concrete compressive strength is increased. A linear regression analysis produces the following expression.

$$f_{bsu} = 0.243\ (f_{cu}) + 3.819, \quad R = 0.993 \qquad (4.5)$$

In figure (4.8b) the bond stress at failure is plotted against the square root of concrete compressive strength ($\sqrt{f_{cu}}$). From the figure increases in the $\sqrt{f_{cu}}$ lead to proportional increases in the ultimate bond stress and this relationship can be expressed by the following expression obtained from a regression analysis

$$f_{bsu} = 2.608\ (\sqrt{f_{cu}}) - 3.135\ ,\quad R = 0.994 \qquad (4.6)$$

From the comparison of equations (4.5) and (4.6) it can be observed that the ultimate bond stresses are marginally better related to the ($\sqrt{f_{cu}}$) than (f_{cu}).

4.3.7 Bond Stress in Column and Foundation

Tests in groups X and XI included a short reinforced concrete column and foundation. The average bond stresses developed in the column and foundation up to failure together with the summary of specifications for groups X and XI tests are given in table (4.3). The bond stesses were computed from the measured strain in the bars. It should be made clear that in the table the bond stress given for the column is the average bond stress developed between the column bottom and the base top strain gauge locations, see figure (2.8) for reference.

Tests in group X failed in compression in the column at a distance from column to base interface, and hence there was no loss of bond between the steel and concrete in the base. It can be seen from table (4.3) that the bond stress is higher in the column than in the base, so that the most critical section is the column to base joint zone in the column. The bond stress in the column and base decreases as the bar size is decreased for these tests.

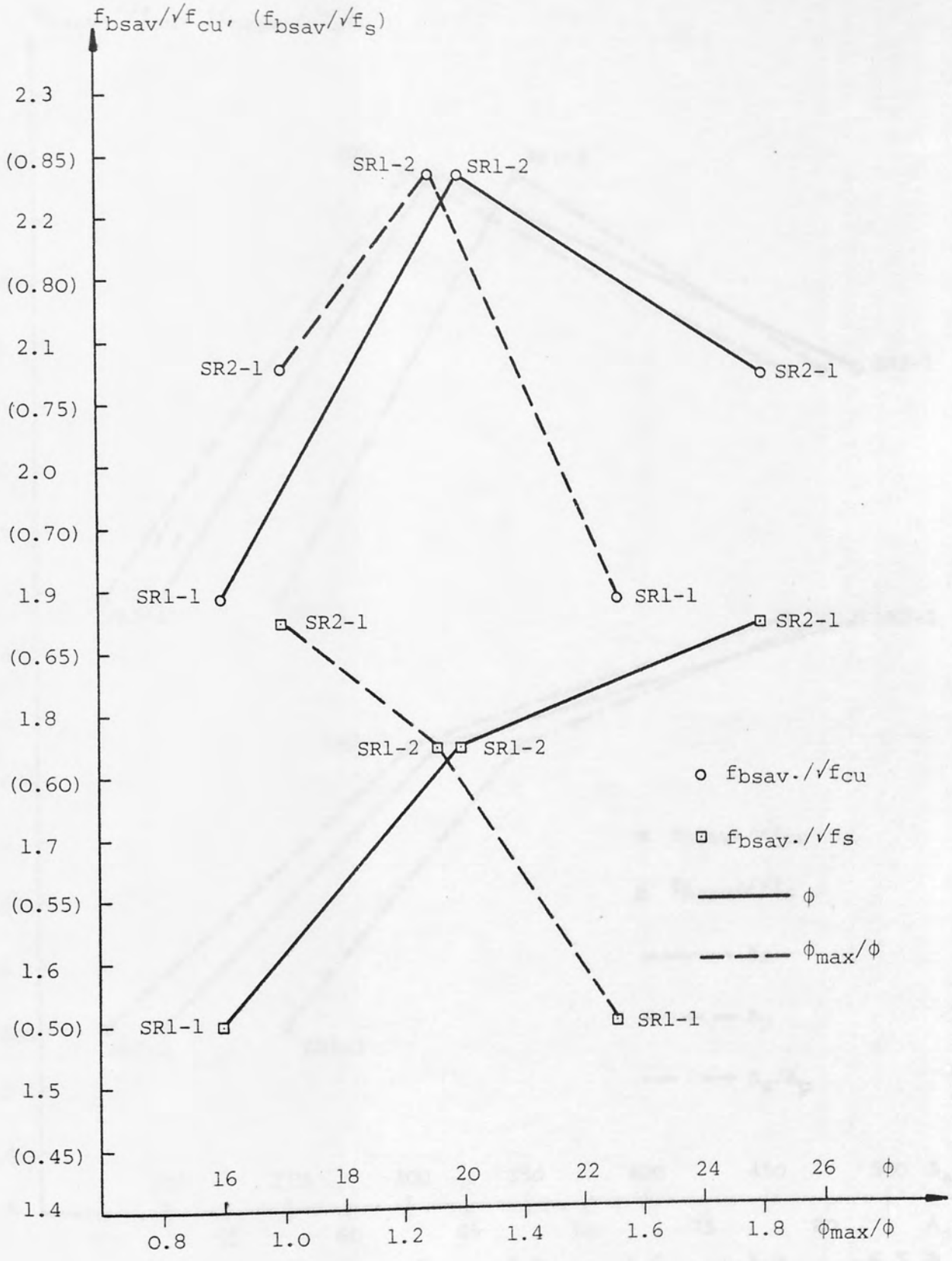

FIGURE 4.4a: BAR SIZE & BAR SIZE RATIO VERSUS RATIO OF BOND STRESS TO SQUARE ROOT OF CONCRETE COMPRESSIVE STRENGTH AND RATIO OF BOND STRESS TO SQUARE ROOT OF STEEL STRESS AT FAILURE IN GROUP IV

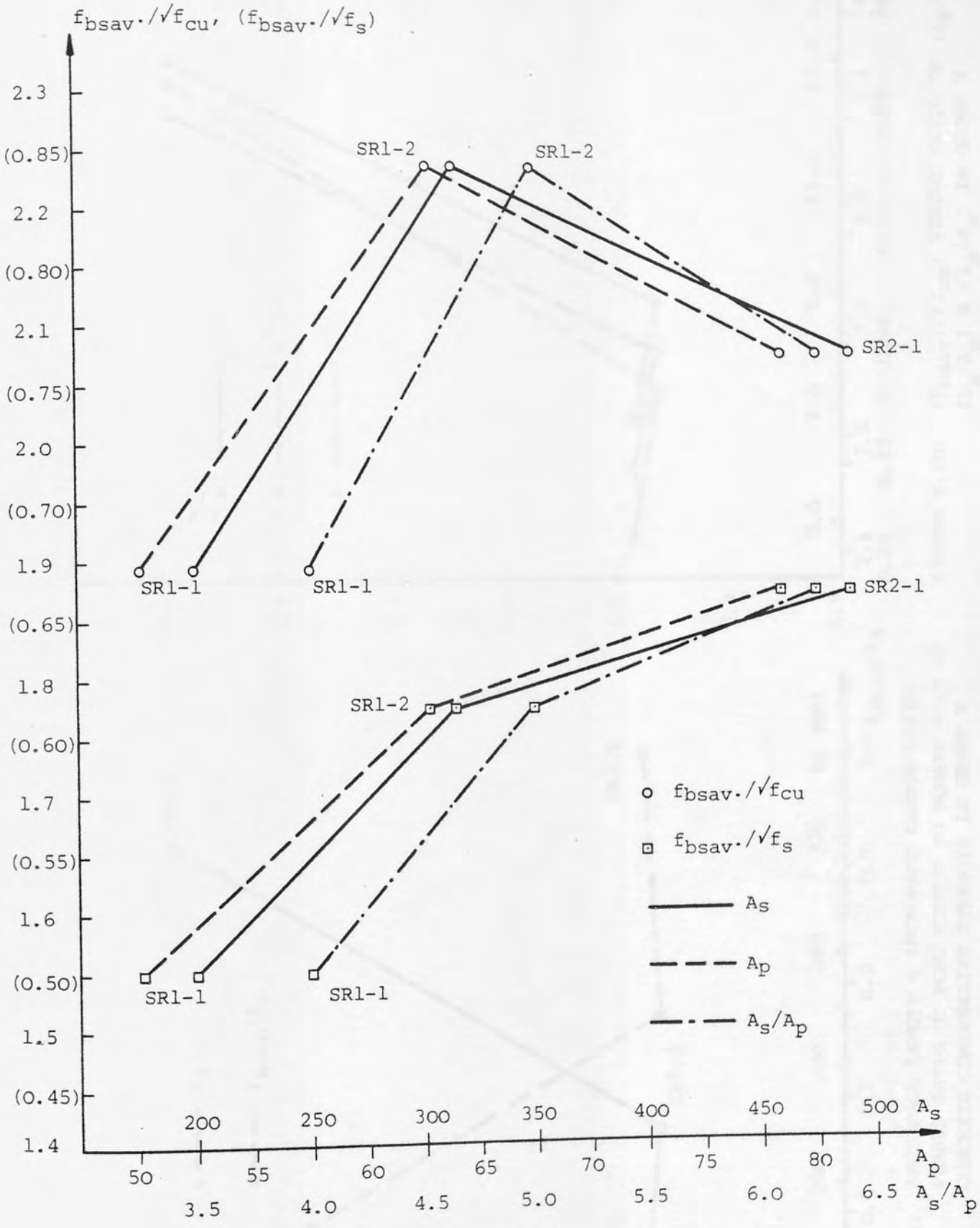

FIGURE 4.4b: BAR PERIPHERY, BAR CROSS-SECTIONAL AREA & RATIO OF (A_s/A_p) VERSUS RATIO OF BOND STRESS TO SQUARE ROOT OF CONCRETE COMPRESSIVE STRENGTH AND RATIO OF BOND STRESS TO SQUARE ROOT OF STEEL STRESS AT FAILURE IN GROUP IV

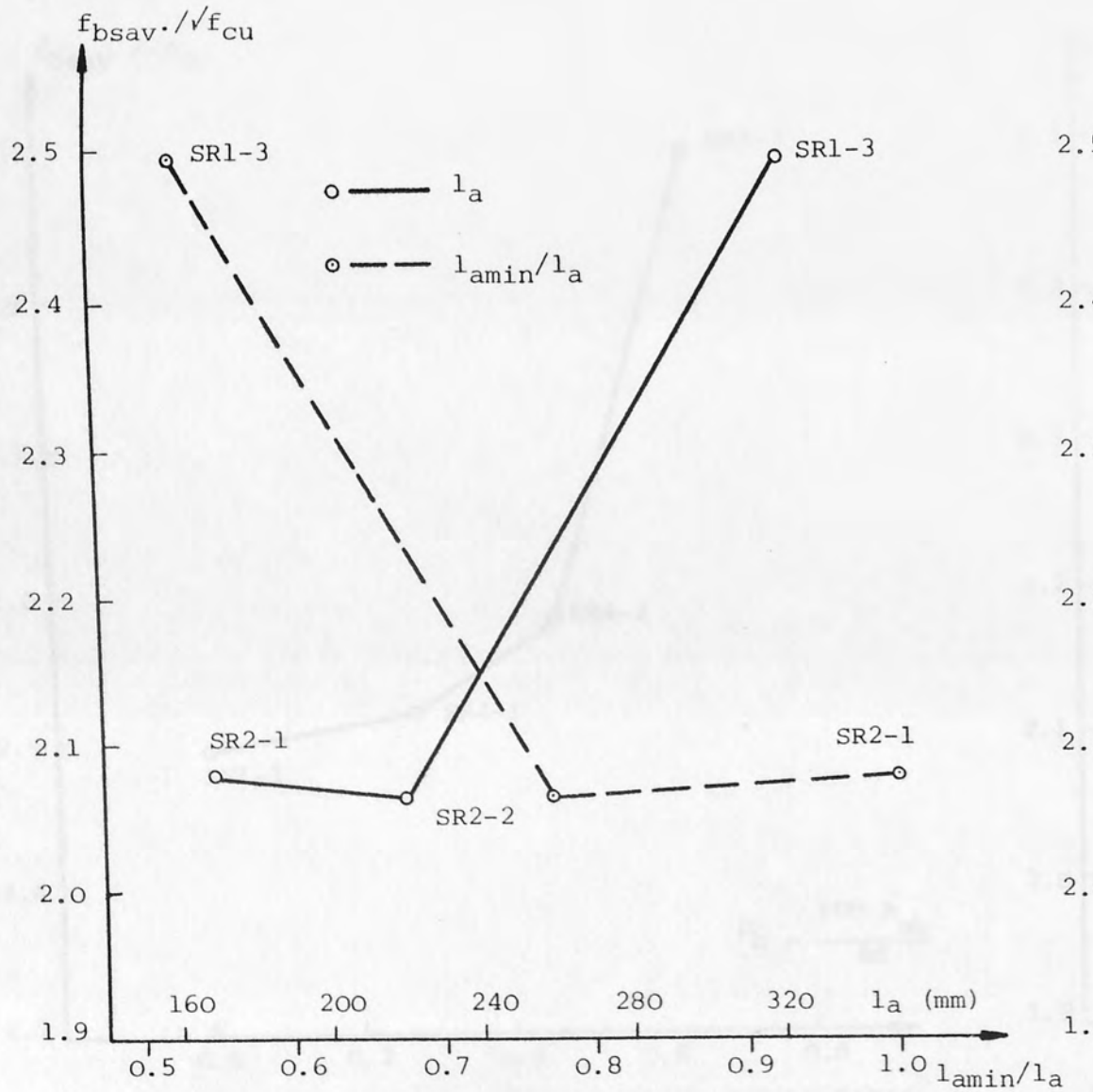

FIGURE 4.5a: ANCHORAGE LENGTH & ANCHORAGE LENGTH RATIO VERSUS RATIO OF BOND STRESS TO SQUARE ROOT OF CONCRETE COMPRESSIVE STRENGTH IN GROUP V

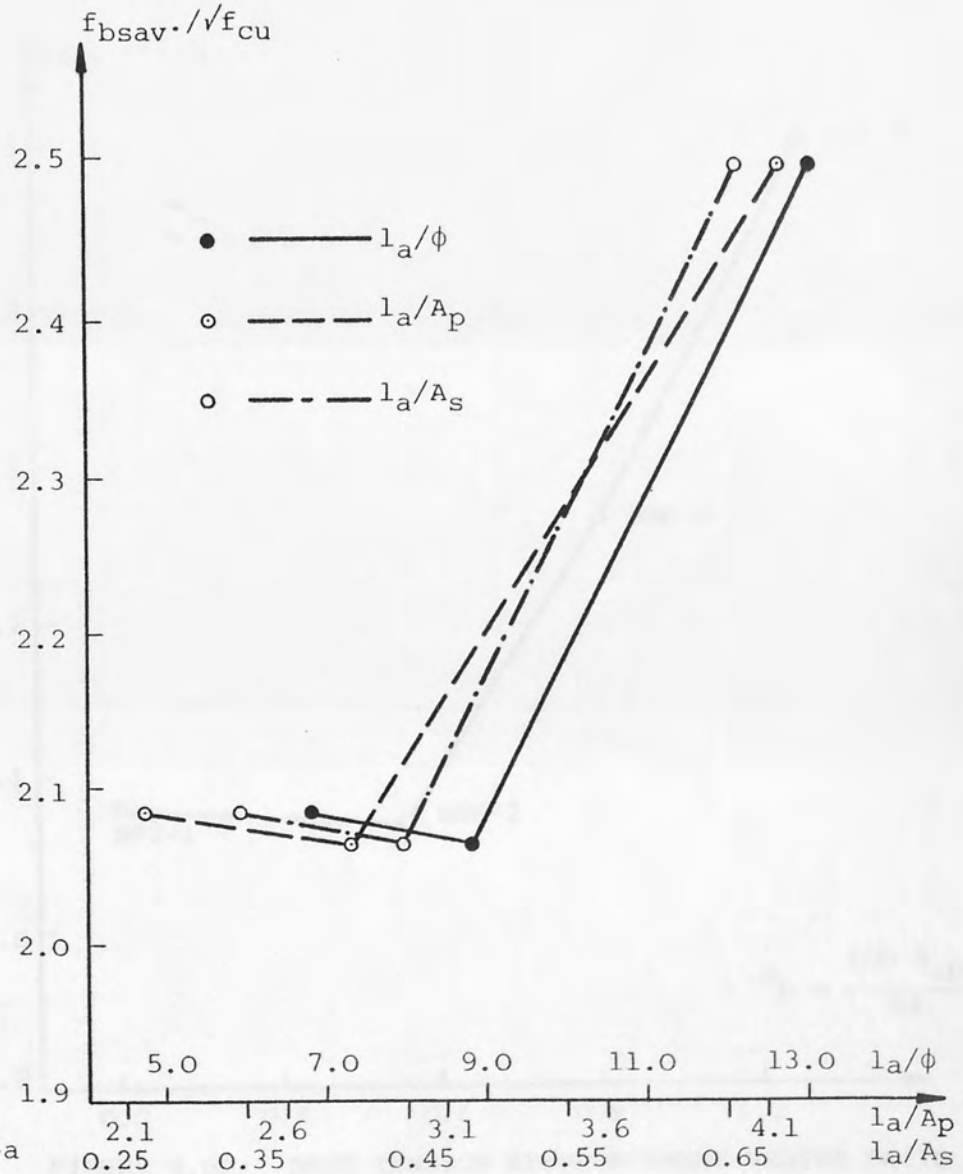

FIGURE 4.5b: $(f_{bsav}./\sqrt{f_{cu}})$ VERSUS RATIO OF (l_a/ϕ), (l_a/A_p) & (l_a/A_s) IN GROUP V

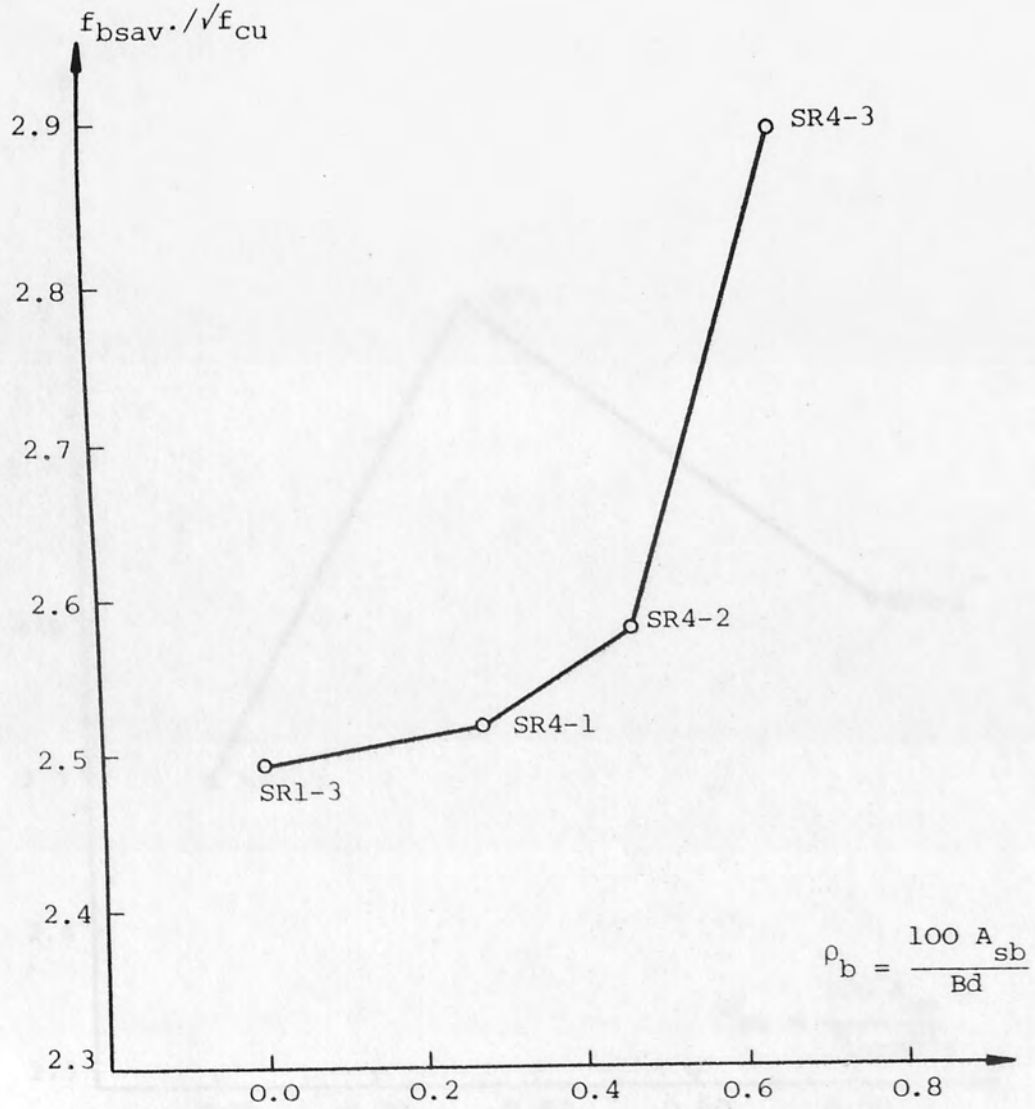

FIGURE 4.6a: BASE TENSION REINFORCEMENT VERSUS RATIO OF ($f_{bsav.}/\sqrt{f_{cu}}$) IN GROUP VIIa

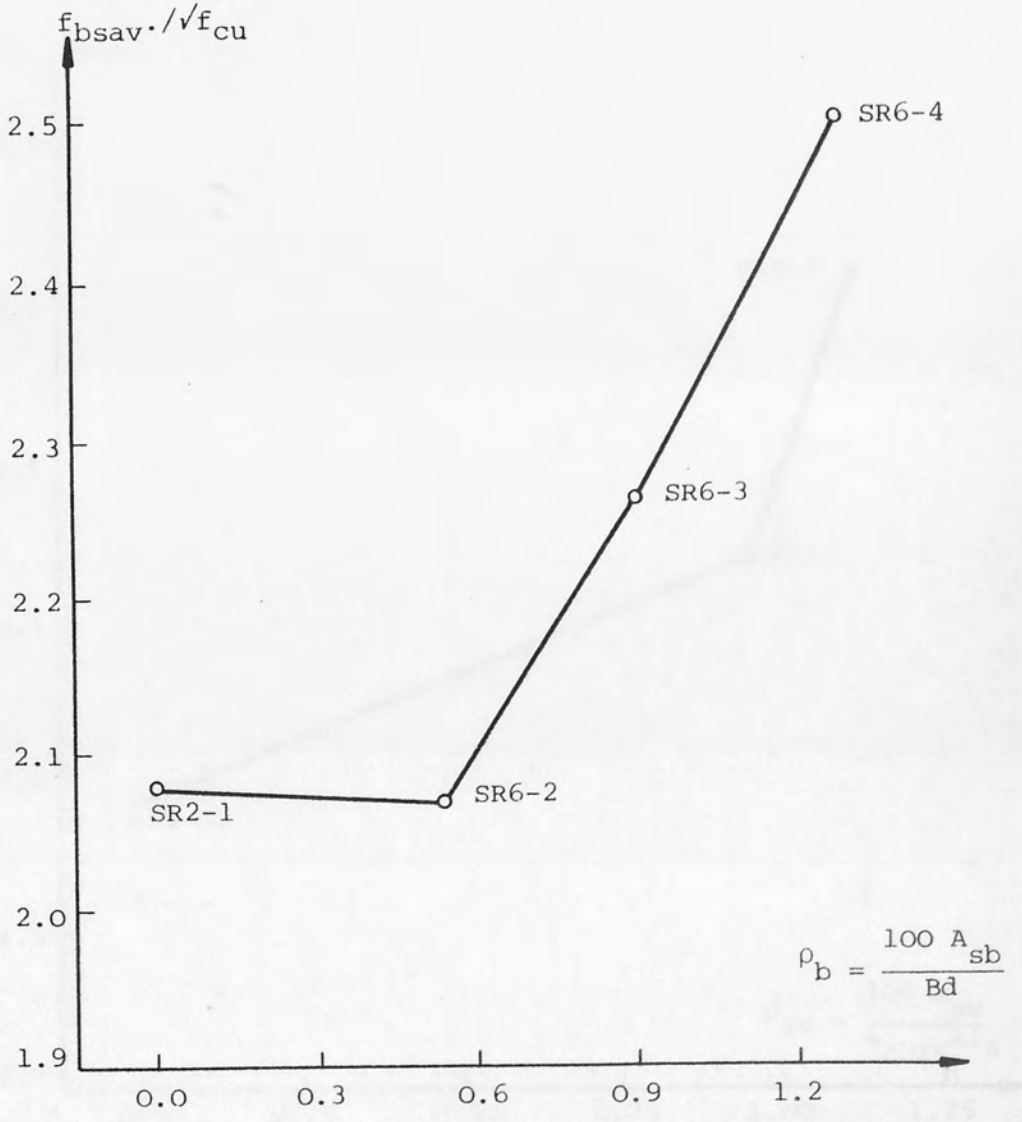

FIGURE 4.6b: BASE TENSION REINFORCEMENT VERSUS RATIO OF ($f_{bsav.}/\sqrt{f_{cu}}$) IN GROUP VIIb

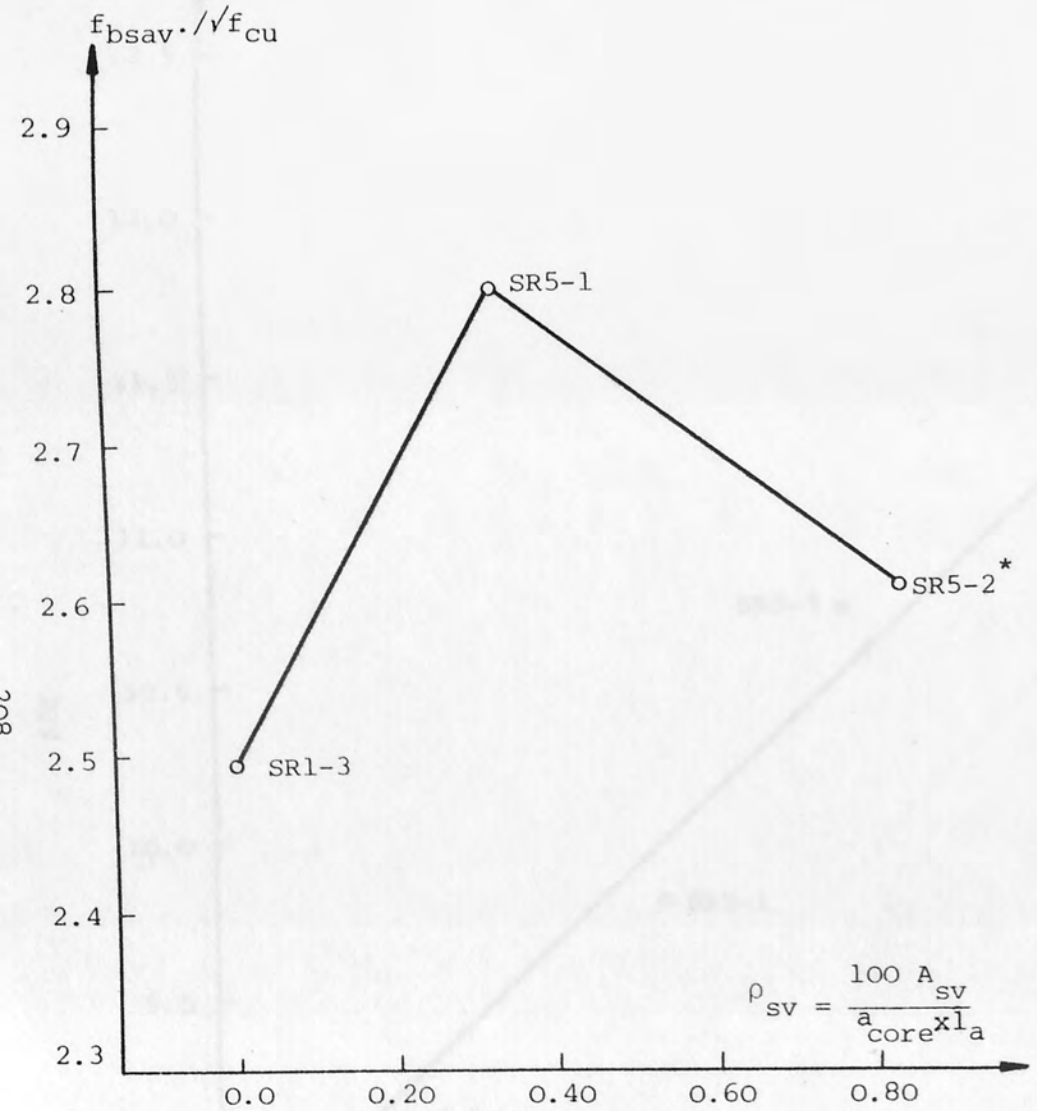

FIGURE 4.7a: COLUMN CORE CONFINING REINFORCEMENT VERSUS RATIO OF ($f_{bsav.}/\sqrt{f_{cu}}$) IN GROUP VIIIa

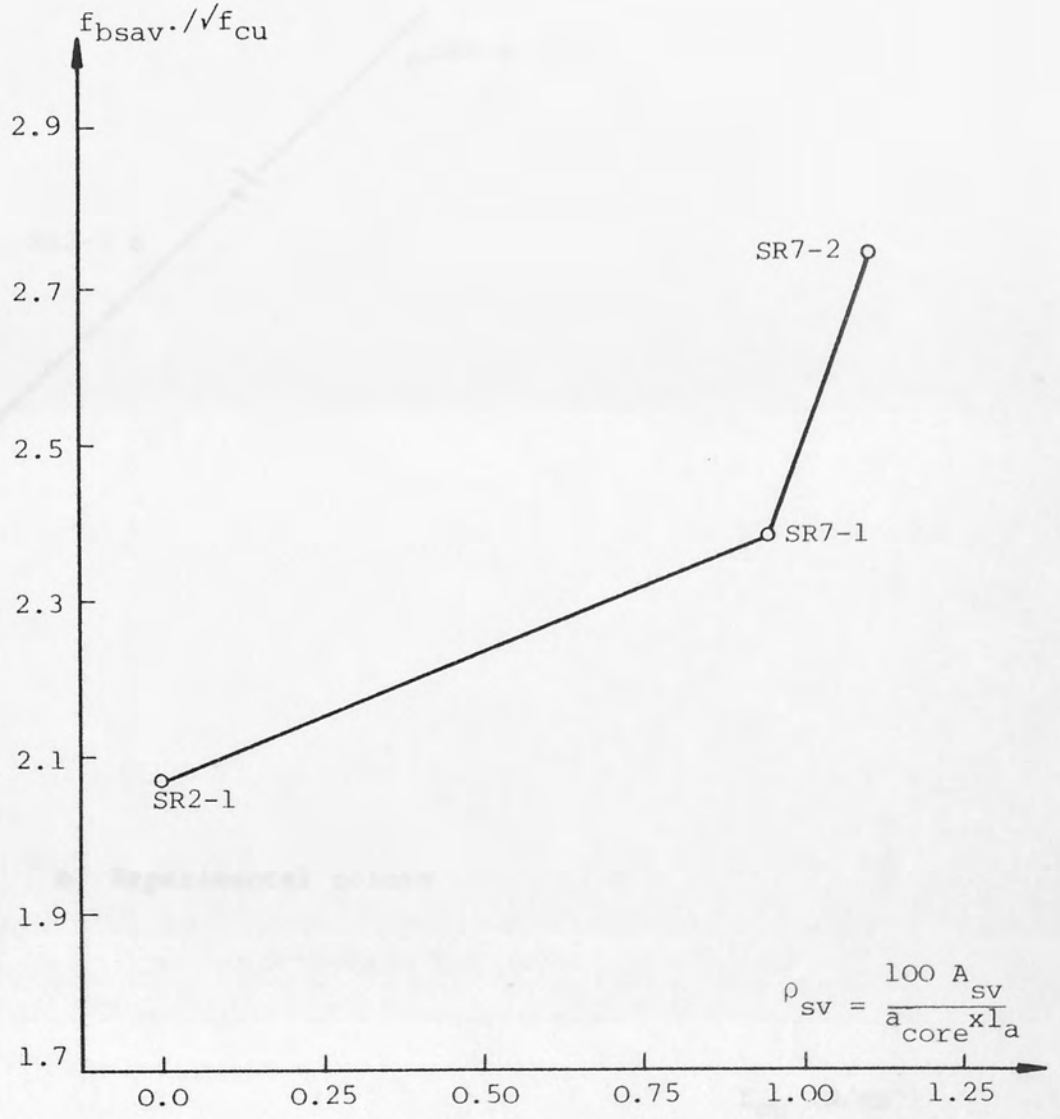

FIGURE 4.7b: COLUMN CORE CONFINING REINFORCEMENT VERSUS RATIO OF ($f_{bsav.}/\sqrt{f_{cu}}$) IN GROUP VIIIb

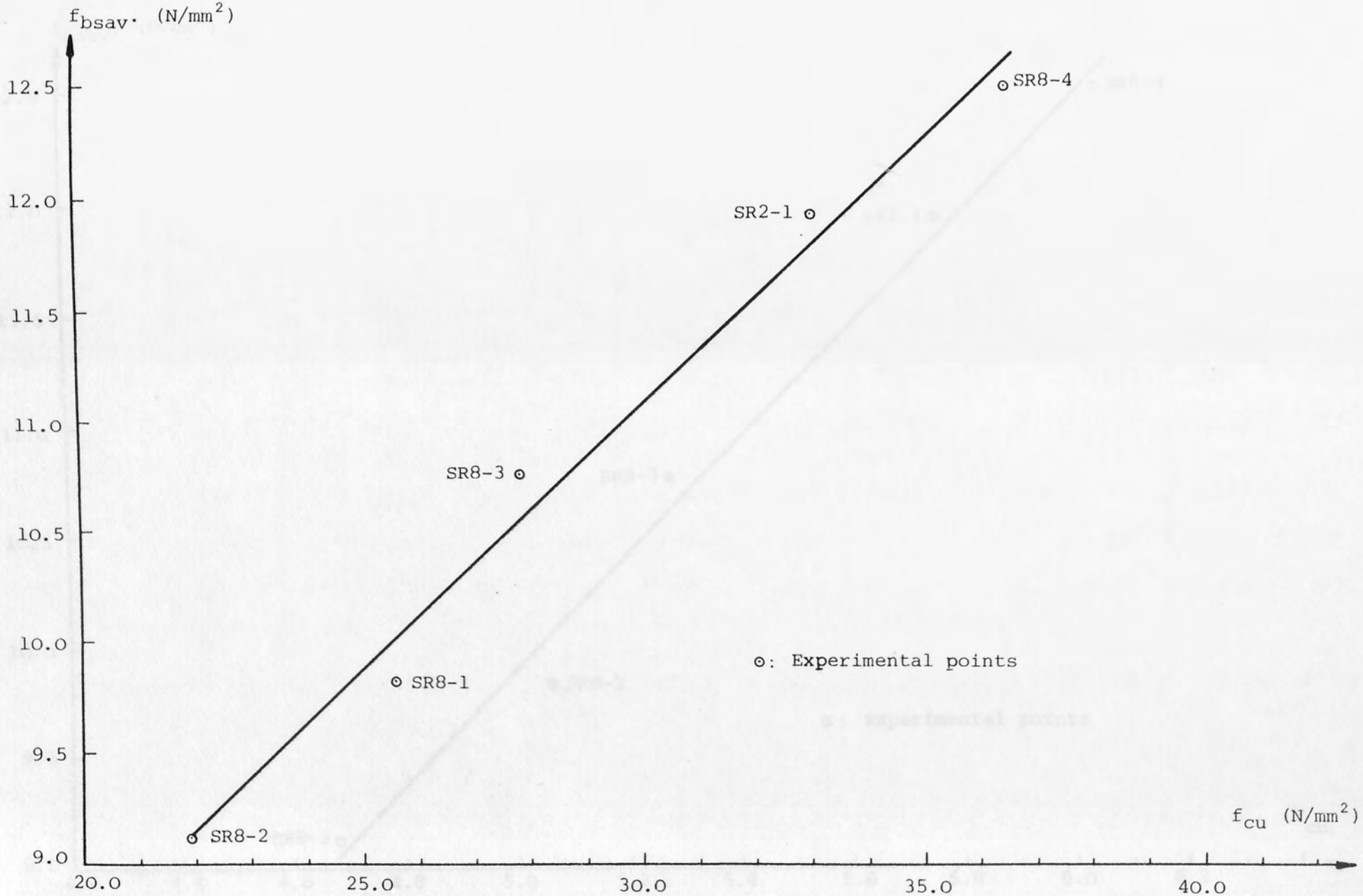

FIGURE 4.8a: CONCRETE COMPRESSIVE STRENGTH VERSUS BOND STRESS AT FAILURE IN GROUP IX

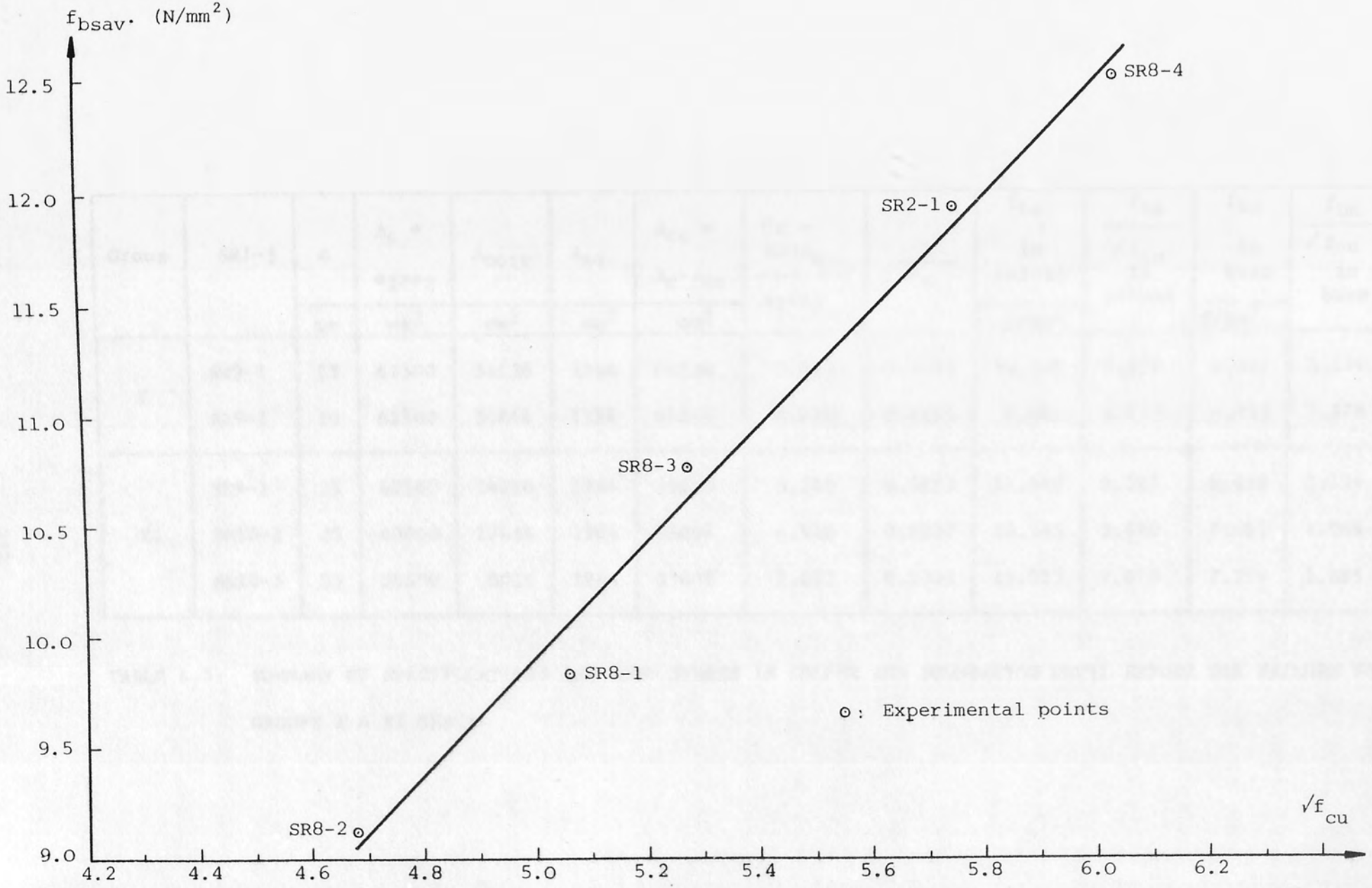

FIGURE 4.8b: $\sqrt{f_{cu}}$ VERSUS BOND STRESS AT FAILURE IN GROUP IX

Tests in group XI also failed in the column but the column longitudinal bars also produced some slip in the base in test SR10-2 which had the smallest size of column. In this test in contrast to the others the column failure started from the column to base interface rather than at a distance as reported in chapter 3. From the inspection of table (4.3) it is observed that the bond stresses in the column and foundation increase with decreasing plan area of the column, for group XI tests, and thus the column to base joint becomes more critical as the size of the column is reduced. It appears probable that when the ultimate bond resistance is attained, the failure takes place in the column to base interfacing zone. This is demonstrated by test SR10-2 which failed in the joint zone. From the foregoing observations it is concluded that part of the column length acting as an extra anchorage length, in addition to the embedment length in foundation, is the most critical zone in bond. When the bursting forces produced by the bond action of the bars exceed the counteracting resistance due to inefficient concrete containment in the column the extra anchorage length fails first.

In group XI tests the bond stress developed in the joint zone of the column varies linearly with both the geometrical properties of column and the column main reinforcement. To show that the ratio of bond stress to square root of concrete compressive strength ($f_{bs}/\sqrt{f_{cu}}$) is related to the column plan area (A_c), column core area (A_{core}), reciprocal of the column longitudinal reinforcement percentage ($1/\rho_c$) and the ratio of column core area to the area of the column longitudinal reinforcement (A_{core}/A_{sc}), respectively, a regression analysis produces the following expressions

$$(f_{bs}/\sqrt{f_{cu}}) = -10.795\text{x}10^{-6}\ (A_c) + 2.913, \quad R = -0.992 \qquad (4.7a)$$

$$(f_{bs}/\sqrt{f_{cu}}) = -15.251\text{x}10^{-6}\ (A_{core}) + 2.756,\ R = -0.995 \qquad (4.7b)$$

$$(f_{bs}/\sqrt{f_{cu}}) = -2.119\ (1/\rho_c) + 2.913,\ \ R = -0.992 \qquad (4.7c)$$

$$(f_{bs}/\sqrt{f_{cu}}) = -2.995\text{x}10^{-2}\ (A_{core}/A_{sc}) + 2.756,\ R = -0.992 \qquad (4.7d)$$

From the above expressions the bond stress developed in the joint zone of the column increases proportionally with decreasing (A_c), (A_{core}), $(1/\rho_c)$ and (A_{core}/A_{sc}).

4.4 Ultimate Strength of Short Columns

As reported earlier, in the tests in groups X and XI the columns failed in axial compression owing to yielding of the reinforcement and crushing of concrete, except for test SR10-2 in which a small slip of the column bars also occurred in the base. These tests provide an opportunity to assess the theoretical failure load in a short axially loaded column.

The steel stress developed before yielding was calculated from the measured strains in the bars. The ratio of steel stress in compression to yield stress in tension $(\beta = f_s/f_y)$ was evaluated from tests SR9-1, SR9-2 and SR10-1. The numerical value of (β) was 0.847, 0.888 and 0.880 for tests, respectively, with an average of $(\beta_{av}) = 0.871$. The actual concrete stress (f_c) in the columns at failure was found to be 17.822 N/mm^2, 20.012 N/mm^2 and 19.185 N/mm^2. These values were determined indirectly from the respective steel stress in compression for tests SR9-1, SR9-2 and SR10-1, respectively. The resulting ratio of actual concrete stress to concrete cube strength $(\alpha = f_c/f_{cu})$ was 0.660, 0.685 and 0.679 with an average of $(\alpha_{av}) = 0.675$.

The theoretical ultimate strength (P_{ult}) in an axially loaded short column is given by the following conventional equation

$$P_{ult} = \alpha f_{cu} A_{cc} + \beta f_y A_{sc} \qquad (4.8)$$

Substituting for (α) and (β) in equation (4.8) gives

$$P_{ult} = 0.68 f_{cu} A_{cc} + 0.87 f_y A_{sc} \qquad (4.9)$$

Where

f_{cu} = the measured concrete cube strength in compression

A_{cc} = the net area of column concrete

f_y = the measured yield stress of the reinforcement in tension

A_{sc} = the area of the column main reinforcement

It will be seen later that equation (4.9) compares well with the other investigators experimental results.

CHAPTER 5

THEORETICAL INVESTIGATION

5.1 General Remarks

This chapter is concerned with the theoretical approach associated with the bond resistance of deformed reinforcing bars subjected to axial compression in a foundation. As reported in chapter 2, two types of reinforcement were employed in the experimental programme, namely, square twisted bars and ribbed bars. In the most of the tests the column bars were embedded in a base, without being concreted in the column, so that load transference between the concrete and reinforcing bars could only be by bond. These tests produced a type 1 bond failure where the column bars sheared the surrounding concrete in the foundation. The deformed bars may be treated as plain round bars in the embedment length of the foundation with an improved bond capacity due to surface configurations. In this chapter, type 1 failure of the deformed bars due to shear stresses between bar and concrete is considered.

It is evident from the experimental investigation that the bond stress distribution is not uniform along the anchorage length of the foundation. It has been observed that the bond stress is always a maximum near the top of the embedment length with a minimum at the bottom and, between these limits it varies nonlinearly until first slip takes place. In soil mechanics Mattes and Poulos[39] found that the shear stress distribution varied with the pile stiffness factor $K_p = (E_{pile}/E_{soil})\ R_A$. For $K_p = 5000$ the distribution of

shear stress along the pile was found almost uniform with a maximum value occurring near the tip. On the other hand, for a much smaller value of K_p = 50, the shear stress distribution was different with very high shear stresses occurring near the top of the pile and small values near the tip.

For a very compressible pile (K_p = 10) Mattes and Poulos[39] found that the finite layer depth had very little influence on the settlement of the pile. Thus for such piles, they concluded that the influence of layer depth on settlement might be ignored and the influence factors for a pile in a semi-infinite medium could be used for all layer depths.

In the present investigation the reinforcing bar stiffness factor $K = E_s/E_c$ varies between 6.36 and 9.90, i.e. the bar is compressible in relation to the surrounding concrete in the foundation. The bond stress distribution obtained along the anchorage length of the bars is very similar to those obtained theoretically by Mattes and Poulos[39] for the piles having small stiffness factor, i.e. compressible piles. Hence there is an analogy between the reinforcing bar and concrete and the compressible pile and soil. The Mindlin equation[3] can therefore be used to carry out a theoretical analysis for the compression bars embedded in a foundation similar to that proposed by Mattes and Poulos for compressible piles.

5.2 Introduction to the Theoretical Approach

The conventional concept of bond stress is shear stress acting parallel to the bar on the interface between the bar and concrete. It is

customary for deformed bars to define the bond stress as the stress per unit area of the nominal bar surface and ignore the extra surface created by the lugs and ribs. The bond phenomenon between two different surfaces has formed the basis of analytical models of many composite materials employed in engineering practice, such as reinforced concrete and friction piles. The solution of the vector function defining the effect of a single force acting at a point in the interior of a semi-infinite elastic solid by Mindlin[3] has led to the elastic analysis of many engineering problems associated with friction, bond[27,30,37,38,39,40,43,44,52,53,54,77].

The theoretical analysis of the anchorage bond of deformed bars in the foundation is carried out using the Mindlin equation in conjunction with finite difference calculus. The theoretical work is divided into two parts, namely, elastic analysis and elastic-plastic analysis.

5.3 Elastic Analysis

5.3.1 Assumptions

In this analysis the following assumptions are made for the establishment of the theoretical model:

1- A cylindrical surface is assumed for both square twisted and ribbed bars with a nominal diameter of circular cross-section such that the bar configurations act as exaggerated roughness.

2- The column longitudinal reinforcement is considered compressible in relation to the surrounding concrete with a constant elastic modulus (E_s).

3- The anchorage length of the bar is divided into n equal cylindrical elements. It is assumed that each bar element is subjected to a uniform vertical shear stress acting on the surface of the element (i.e. uniform bond stress).

4- The bar tip i.e. the end of the bar is assumed to be a smooth, rigid circular disc of the same diameter as the bar shaft, across which a vertical stress is uniformly distributed.

5- The embedding concrete medium is considered to be an ideal elastic material with constant elastic parameters of Young's modulus (E_c) and Poisson's ratio (ν_c).

The solution to the problem involves the computation of the displacement factors.

5.3.2 Computation of Displacement Factors

The vertical displacement influence factors for the bar elements may be obtained from a solution for displacements due to a point load in a semi-infinite elastic solid given by Mindlin[3]. From the Mindlin equation the vertical displacement influence factor, at any point in a semi-infinite elastic, isotropic solid, due to a downward force in the interior of the solid is

$$\omega_b = \frac{1}{16\,\pi\,G_c\,(1-\nu_c)}\left[\frac{3-4\,\nu_c}{R_1}+\frac{8\,(1-\nu_c)^2-(3-4\,\nu_c)}{R_2}+\frac{(\bar{z}-c)^2}{R_1^3}\right.$$

$$\left.+\frac{(3-4\,\nu_c)\,(\bar{z}+c)^2-2c\bar{z}}{R_2^3}+\frac{6c\bar{z}\,(\bar{z}+c)^2}{R_2^5}\right] \qquad (5.1)$$

In this equation (ν_c) is the Poisson's ratio and (G_c) is the shear modulus of the concrete. (R_1), (R_2), ($\bar{z}$) and (c) are geometric

relationships as shown in figure (5.1) and, (R_1) and (R_2) are given by

$$R_1 = [\bar{r}^2 + (\bar{z} - c)^2]^{\frac{1}{2}}$$
$$R_2 = [\bar{r}^2 + (\bar{z} + c)^2]^{\frac{1}{2}} \qquad (5.1.1)$$

The geometry for a cylindrical bar element is given in figure (5.2). As readily seen from the figure

$$\bar{z} = (i - 1/2)\delta$$
$$z = (\bar{z} + c) = (i - 1/2)\delta + c \qquad (5.2)$$
$$z_1 = (\bar{z} - c) = (i - 1/2)\delta - c$$

Substituting $z = (\bar{z} + c)$, $z_1 = (\bar{z} - c)$, $\bar{z} = (z - c)$ and $G_c = E_c/2(1+\nu_c)$ in equation (5.1) and rearranging produces

$$\omega_b = \frac{(1 + \nu_c)}{8\pi(1 - \nu_c)E_c}\left[\frac{z_1^2}{R_1^3} + \frac{3 - 4\nu_c}{R_1} + \frac{5 - 12\nu_c + 8\nu_c^2}{R_2}\right.$$
$$\left. + \frac{(3 - 4\nu_c)z^2 - 2cz + 2c^2}{R_2^3} + \frac{6cz^2(z - c)}{R_2^5}\right] \qquad (5.3)$$

where

$$R_1 = (4a^2\cos^2\theta + z_1^2)^{\frac{1}{2}}$$
$$R_2 = (4a^2\cos^2\theta + z^2)^{\frac{1}{2}} \qquad (5.3.1)$$

Defining

$$V = (1 + \nu_c)/[8\pi(1 - \nu_c)E_c];\ V_1 = z_1^2/R_1^3$$
$$V_2 = (3 - 4\nu_c)/R_1;\ V_3 = (5 - 12\nu_c + 8\nu_c^2)/R_2 \qquad (5.3.2)$$
$$V_4 = [(3 - 4\nu_c)z^2 - 2cz + 2c^2]/R_2^3;\ V_5 = [(6cz^2(z - c)]/R_2^5$$

it follows that

$$\omega_b = V(V_1 + V_2 + V_3 + V_4 + V_5) \qquad (5.3.3)$$

Referring to figure (5.2), consider a point i at the mid-height of the ith element on the periphery of the bar having radius a. As proposed by Poulos and Davis[37], for the point i the influence factor for vertical displacement due to a uniform bond stress on the jth element is given by

$$\omega_{ij} = 4a \int_{(j-1)\delta}^{j\delta} \int_{o}^{\pi/2} \omega_b d\theta dc \qquad (5.4.1)$$

where (ω_b) is as defined in equation (5.3.3). Hence

$$\omega_{ij} = 4a \int_{(j-1)\delta}^{j\delta} \int_{o}^{\pi/2} [V(V_1 + V_2 + V_3 + V_4 + V_5)] d\theta dc \qquad (5.4.2)$$

The geometric representation for the end of the bar (i.e. bar tip) is indicated in figure (5.3). Similarly for the point i on the bar periphery the influence factor for vertical displacement due to uniform stress on the bar end is

$$\omega_{ib} = \int_{o}^{2\pi} \int_{o}^{a} \omega_b r dr d\theta \qquad (5.5.1)$$

where (ω_b) is given by equation (5.3.3) in which (c), (R_1) and (R_2) are defined as follows

$$c = n\delta$$

$$R_1 = (z_1^2 + a^2 + r^2 - 2racos\theta)^{\frac{1}{2}} \qquad (5.5.2)$$

$$R_2 = (z^2 + a^2 + r^2 - 2racos\theta)^{\frac{1}{2}}$$

The substitution of (5.3.3) with the use of (5.5.2) in equation (5.5.1) gives

$$\omega_{ib} = \int_{o}^{2\pi} \int_{o}^{a} [V(V_1 + V_2 + V_3 + V_4 + V_5)] r dr d\theta \qquad (5.5.3)$$

On the other hand, if the influence factor for the displacement of the centre of the bar end due to the bond stress on element j is taken into account, it will be

$$\omega_{bj} = 2\pi a \int_{(j-1)\delta}^{j\delta} \omega_b dc \qquad (5.6.1)$$

in which (ω_b) is as defined in equation (5.3.3). This time for use in (5.3.3) (i), (R_1) and (R_2) are given by

$$\begin{aligned} i &= n + 1/2 \\ R_1 &= (z_1^2 + a^2)^{\frac{1}{2}} \\ R_2 &= (z^2 + a^2)^{\frac{1}{2}} \end{aligned} \qquad (5.6.2)$$

Substituting (5.3.3) with the use of (5.6.2) in equation (5.6.1) results

$$\omega_{bj} = 2\pi a \int_{(j-1)\delta}^{j\delta} [V(V_1 + V_2 + V_3 + V_4 + V_5)]dc \qquad (5.6.3)$$

Finally if the vertical displacement of the bar tip (i.e. the end of the bar) due to the bar tip itself is considered, an approximate correction for the effect of the rigidity of the bar tip is essential. This is made by multiplying the displacement of the centre of the uniformly loaded circular bar base with a factor of $\pi/4$ as proposed by Poulos and Davis[37]. This factor is the ratio of the surface displacement of a rigid circle on the surface of a semi-infinite mass to the displacement of the centre of a corresponding uniformly loaded circle which approximately represents the case of a circle founded below the surface of a semi-infinite mass. With this assumption the influence factor for vertical displacement of the bar tip due to the

load on the tip is

$$\omega_{bb} = \frac{\pi}{4} 2\pi \int_0^a \omega_b r dr \qquad (5.7.1)$$

Where (ω_b) is given by equation (5.3.3) in which (i), (c), (R_1) and (R_2) are defined as

$$\begin{aligned} i &= n + 1/2 \\ c &= n\delta \\ R_1 &= r \\ R_2 &= (4c^2 + r^2)^{\frac{1}{2}} \end{aligned} \qquad (5.7.2)$$

Therefore

$$\omega_{bb} = \frac{\pi^2}{2} \int_0^a [V(V_1 + V_2 + V_3 + V_4 + V_5)] r dr \qquad (5.7.3)$$

The integrals in equations (5.4.2) and (5.5.3) do not lend themselves to easy analytical evaluations, and therefore, these integrals are carried out numerically. Although analytical integration is possible for the integrals in equations (5.6.3) and (5.7.3), for convenience they are also evaluated numerically. To carry out the numerical integration the grid meshwork for the cylindrical bar elements and the circular bar tip is shown in figure (5.4). From the figure each bar element is divided into (M x M) grids on its half surface for the numerical integration with respect to c while the interval ($0 - \pi/2$) is divided into M grids to carry out numerical integration with respect to θ. The bar tip also divided into (M x M) grids radially and circumferentially as indicated in the figure (i.e. intervals

(0 - a)and (0 - 2π) are divided into M grids, respectively). Then the related integrals are carried out.

The integration of equation (5.4.2) for n bar elements produces vertical displacement influence factors of all n elements of the bar due to a bond stress on each element, which may be written in a matrix form as

$$[DB] = \begin{bmatrix} \omega_{11} & \omega_{12} & \omega_{13} & \cdots\cdots\cdots\cdots & \omega_{1n} \\ \omega_{21} & \omega_{22} & \omega_{23} & \cdots\cdots\cdots\cdots & \omega_{2n} \\ \omega_{31} & \omega_{32} & \omega_{33} & \cdots\cdots\cdots\cdots & \omega_{3n} \\ \cdots\cdots & \cdots\cdots & \cdots\cdots & \cdots\cdots & \cdots\cdots \\ \cdots\cdots & \cdots\cdots & \cdots\cdots & \cdots\cdots & \cdots\cdots \\ \omega_{n1} & \omega_{n2} & \omega_{n3} & \cdots\cdots\cdots\cdots & \omega_{nn} \end{bmatrix} \qquad (5.8.1)$$

Likewise, the integration of equation (5.5.3) produces vertical displacement influence factors for n bar elements due to a normal stress on the bar tip, which may be given by the following column matrix

$$[DC] = \begin{bmatrix} \omega_{1b} \\ \omega_{2b} \\ \cdot\cdot \\ \cdot\cdot \\ \omega_{nb} \end{bmatrix} \qquad (5.8.2)$$

Similarly, the integration of equation (5.6.3) yields the displacement influence factors for the bar tip due to a bond stress on n elements of the bar, which may be expressed by the following row matrix

$$[DF] = [\omega_{b1} \quad \omega_{b2} \quad \omega_{b3} \cdots\cdots\cdots \omega_{bn}] \qquad (5.8.3)$$

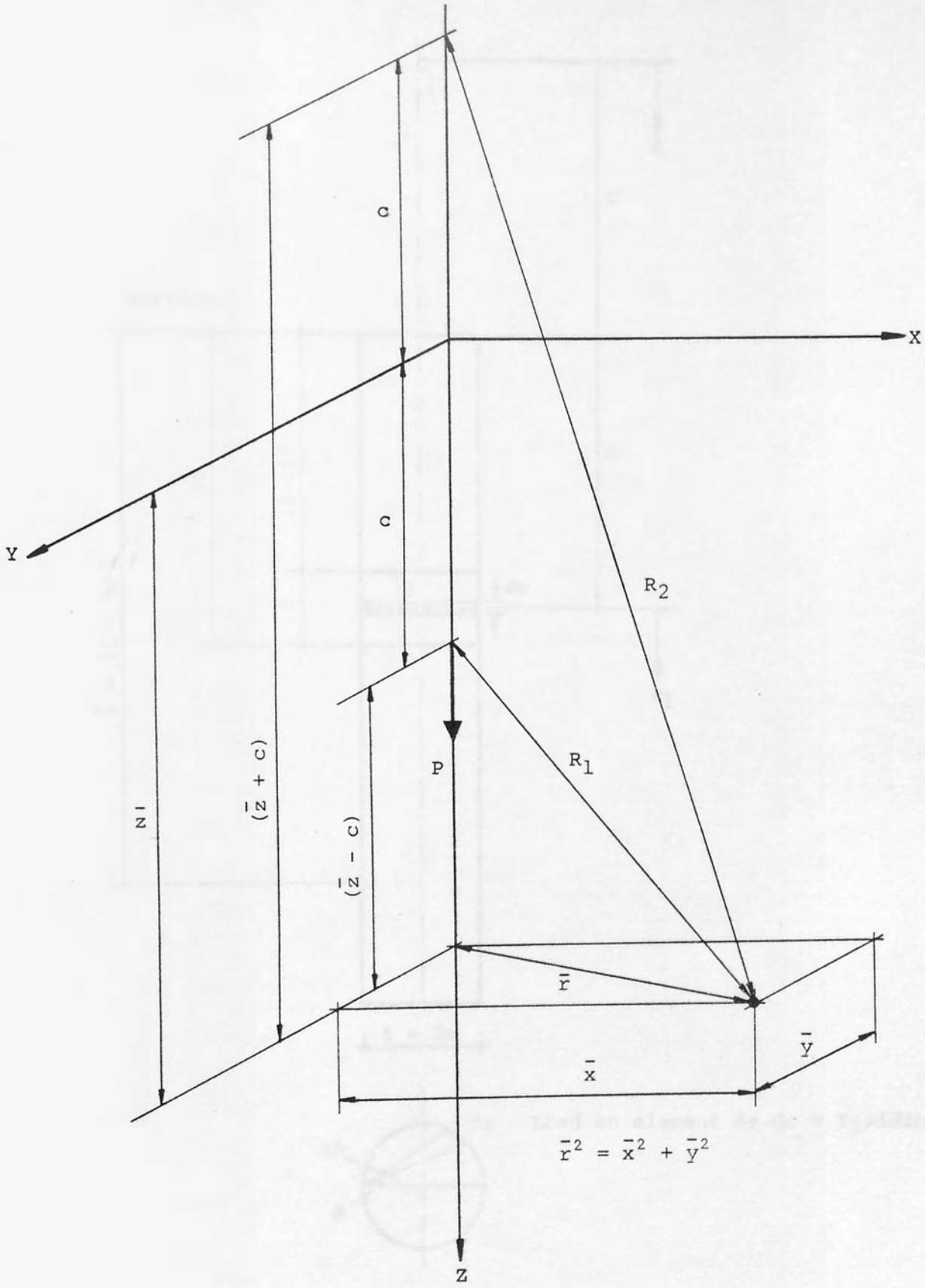

FIGURE 5.1: GEOMETRIC REPRESENTATION FOR MINDLIN PROBLEM

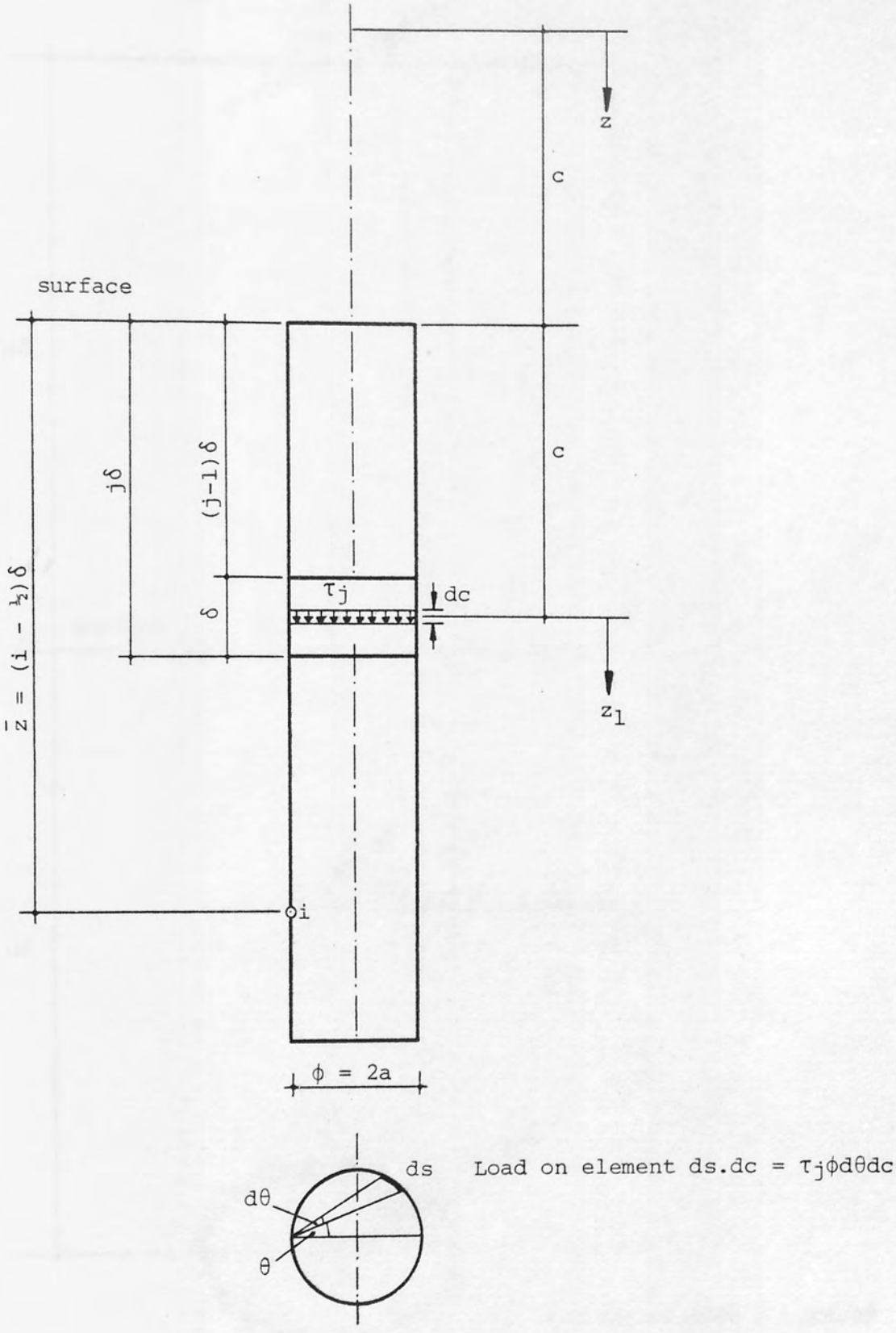

FIGURE 5.2: GEOMETRIC REPRESENTATION FOR A CYLINDRICAL BAR ELEMENT

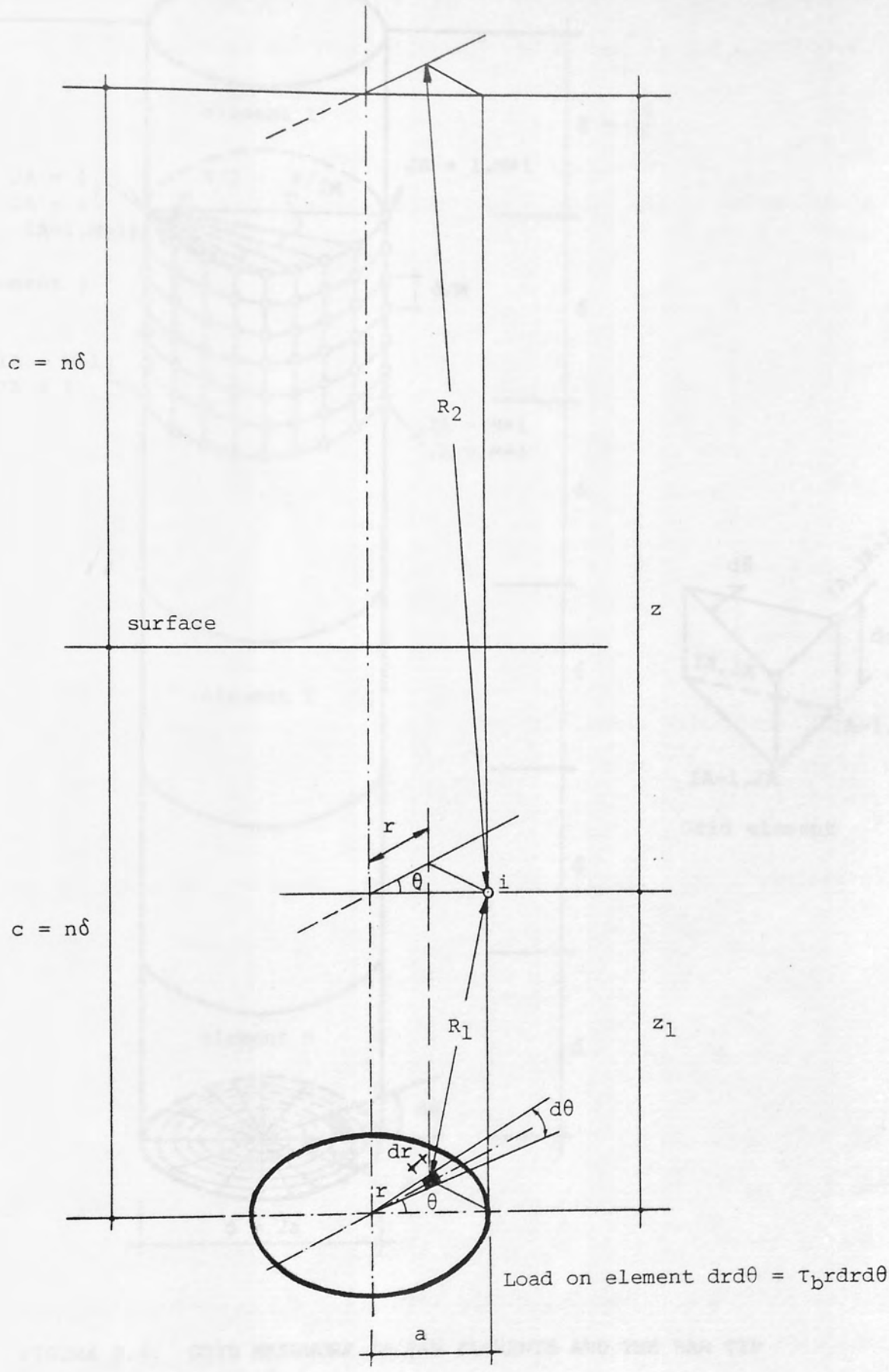

FIGURE 5.3: GEOMETRIC REPRESENTATION FOR THE END OF THE BAR

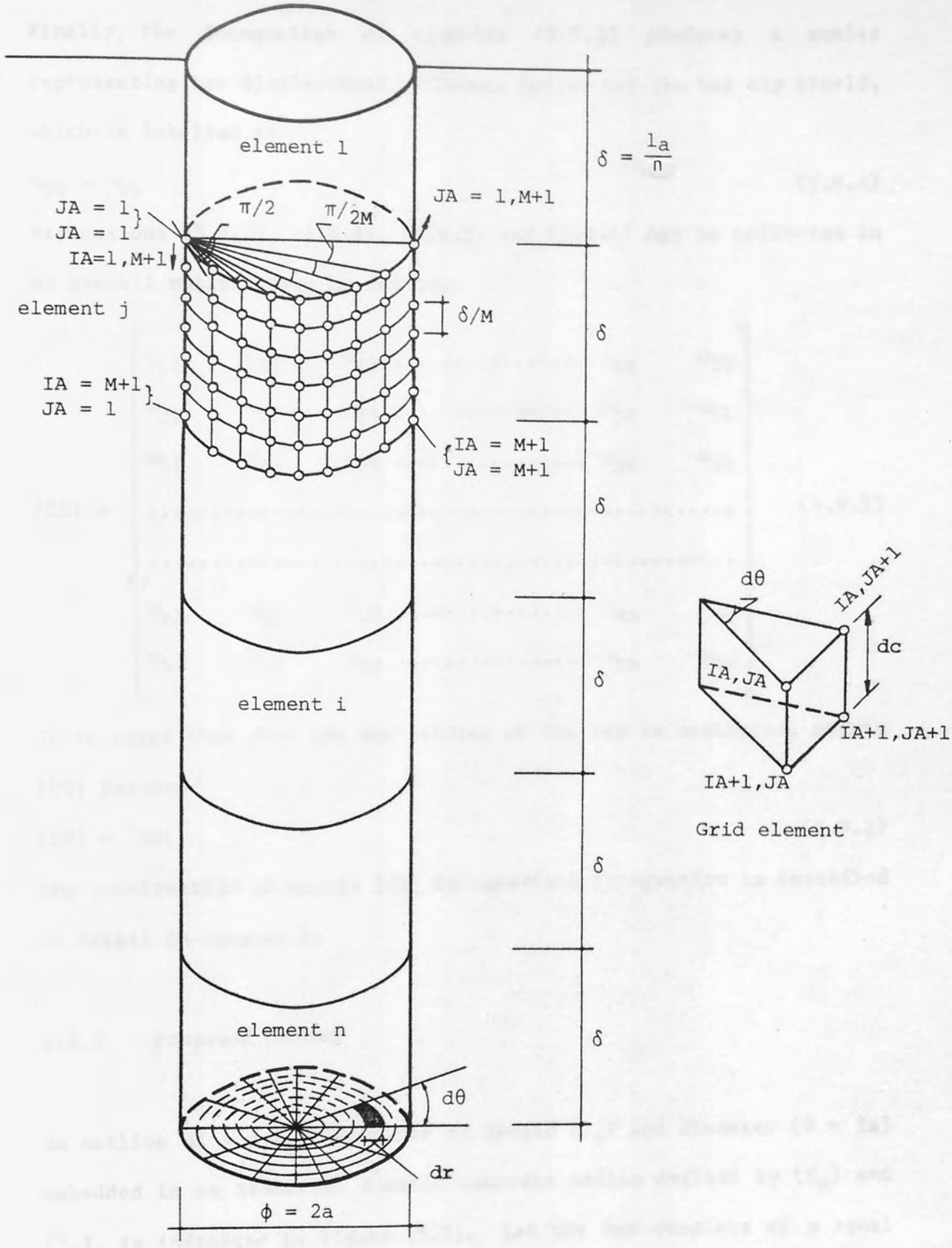

FIGURE 5.4: GRID MESHWORK OF BAR ELEMENTS AND THE BAR TIP

Finally, the integration of equation (5.7.3) produces a scalar representing the displacement influence factor for the bar tip itself, which is labelled as

$$\omega_{bb} = \omega_{bb} \qquad (5.8.4)$$

Expressions (5.8.1), (5.8.2), (5.8.3) and (5.8.4) may be collected in an overall matrix given as follows:

$$[CS] = \begin{bmatrix} \omega_{11} & \omega_{12} & \omega_{13} \cdots\cdots\cdots\cdots\cdots & \omega_{1n} & \omega_{1b} \\ \omega_{21} & \omega_{22} & \omega_{23} \cdots\cdots\cdots\cdots\cdots & \omega_{2n} & \omega_{2b} \\ \omega_{31} & \omega_{32} & \omega_{33} \cdots\cdots\cdots\cdots\cdots & \omega_{3n} & \omega_{3b} \\ \cdots\cdots & \cdots\cdots & \cdots\cdots\cdots\cdots\cdots & \cdots\cdots & \cdots\cdots \\ \cdots\cdots & \cdots\cdots & \cdots\cdots\cdots\cdots\cdots & \cdots\cdots & \cdots\cdots \\ \omega_{n1} & \omega_{n2} & \omega_{n3} \cdots\cdots\cdots\cdots\cdots & \omega_{nn} & \omega_{nb} \\ \omega_{b1} & \omega_{b2} & \omega_{b3} \cdots\cdots\cdots\cdots\cdots & \omega_{bn} & \omega_{bb} \end{bmatrix} \qquad (5.9.1)$$

It is noted that when the end bearing of the bar is neglected, matrix [CS] becomes

$$[CS] = [DB] \qquad (5.9.2)$$

The construction of matrix [CS] by numerical integration is described in detail in chapter 6.

5.3.3 Proposed Method

An outline of a cylindrical bar of length (l_a) and diameter ($\phi = 2a$) embedded in an isotropic elastic concrete medium defined by (E_c) and (ν_c), is indicated in figure (5.5). Let the bar consists of n equal elements, each being subjected to a uniformly distributed shear stress (i.e. bond stress) on its perphery, and the bar tip being acted upon by a uniform normal stress as shown in the figure. Since the elastic conditions prevail in the surrounding concrete, at any point along

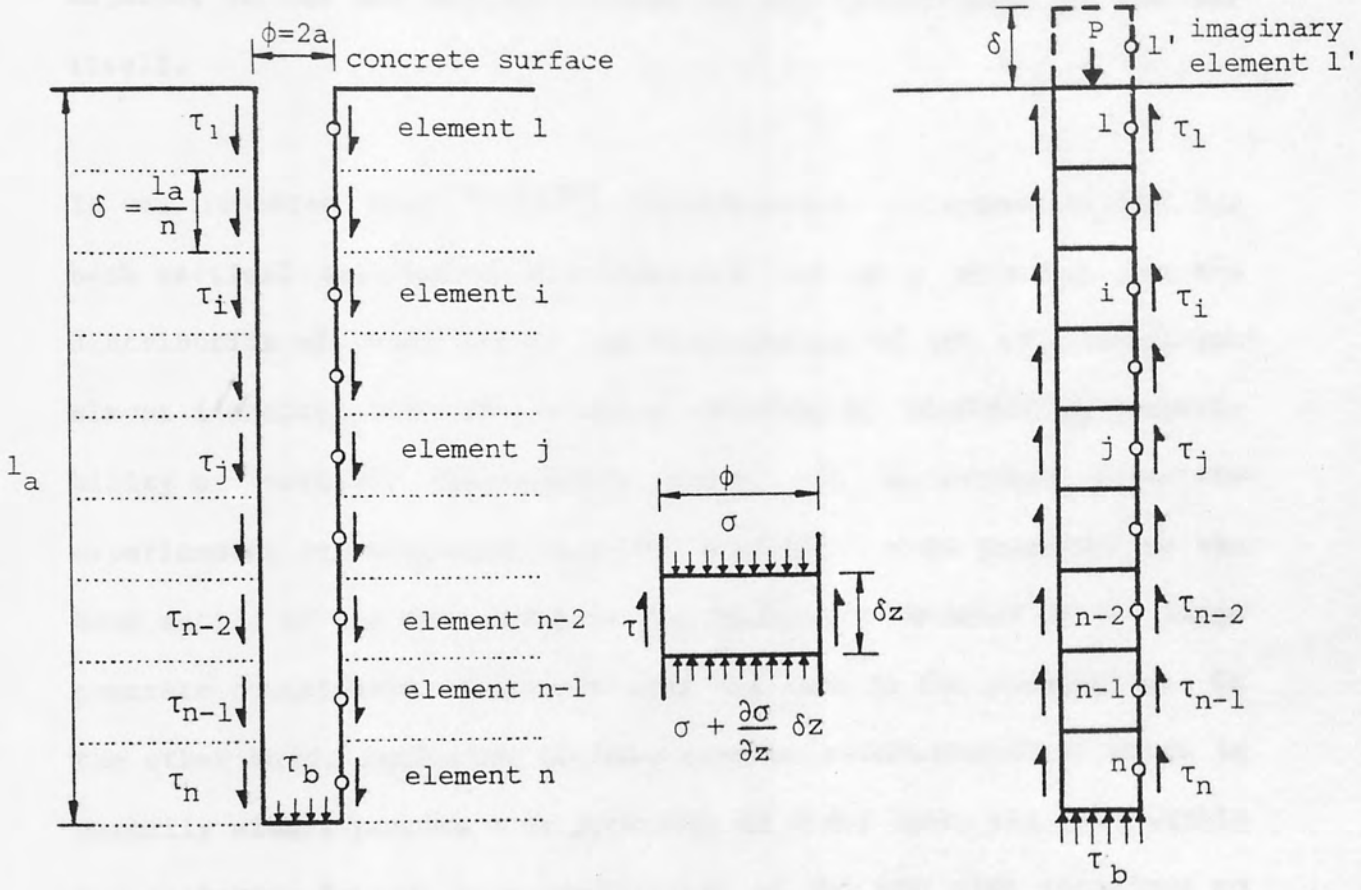

a) Interaction stresses on the bar-concrete interface

b) Stresses in a small cylindrical element of the bar

c) Stresses acting on the bar

FIGURE 5.5: STRESSES IN THE BAR AND SURROUNDING CONCRETE MEDIUM

the bar periphery the displacements of the concrete must be compatible to those of the bar itself. Thus to obtain a solution for the unknown stresses on the bar-to-concrete interface (i.e. bond stresses on the periphery of each bar element and the normal stress on the bar tip) and the corresponding displacements, the displacement of the concrete adjacent to the bar may be equated to the displacement of the bar itself.

It was reported that[30,37,39] consideration of compatibility for both vertical and radial displacements led to a solution for the distribution of shear stress and displacement of the pile which was almost identical with the solution obtained by considering compatibility of vertical displacement alone. It is evident from the experimental investigation that the bursting forces produced by the bond action of the deformed bars are ineffective because of the large concrete containment available over the bars in the foundation. On the other hand, inclusion of base tension reinforcement - which is normally always present - or provision of links round the bars within the anchorage length or a combination of the two also introduce an extra confining element to the bars against the bursting effect. Thus the bursting forces are virtually negligible in the foundation and hence the radial displacement of the concrete is very small. As a matter of fact, using the test specifications the computed radial displacements from Mindlin equation[3] are less than one-percent of the vertical displacements in the vicinity of the bars along the anchorage length. Therefore, the radial displacement of the concrete is neglected in the analysis and, only the compatibility of the vertical displacement is taken into account. The vertical displacements are computed at the mid-point of the periphery of each bar

element as indicated in figure (5.5).

The vertical displacement of the concrete due to the bond stress along the anchorage length of the bar is obtained by double integration of Mindlin equation for vertical displacement on the surface of each bar element as described in the preceding section. Referring to figure (5.5a) let the vertical displacement of the concrete adjacent to the bar at the mid-point of any element i, due to a bond stress τ_j on element j, be Δc_{ij}. Taking downward displacement as positive Δc_{ij} may be given by

$$\Delta c_{ij} = (\phi/E_c)\ \omega_{ij}\ \tau_j \qquad (5.10)$$

where ϕ is the bar diameter, E_c is the Young's modulus of concrete and, ω_{ij} is the vertical displacement influence factor for i due to the bond stress τ_j on element j which is as defined in equation (5.4.2).

Similarly, the displacement at i due to a normal stress τ_b on the bar tip is

$$\Delta c_{ib} = (\phi/E_c)\ \omega_{ib}\ \tau_b \qquad (5.11)$$

where ω_{ib} is the influence factor for the displacement at i due to the normal stress τ_b on the bar tip which is given by equation (5.5.3).

Thus, the vertical displacement at i due to all n bar elements and to the bar tip may be expressed as

$$\Delta c_i = \frac{\phi}{E_c} \left(\sum_{j=1}^{n} \omega_{ij}\ \tau_j + \omega_{ib}\ \tau_b \right) \qquad (5.12)$$

On the other hand, when the vertical displacement of the concrete under the bar tip, due to the bond stress τ_j on element j is considered, it

will be

$$\Delta c_{bj} = (\phi/E_c)\ \omega_{bj}\ \tau_j \qquad (5.13)$$

where ω_{bj} is the vertical displacement influence factor at the centre of the bar tip due to the bond stress τ_j on element j which is given by equation (5.6.3).

Finally, the vertical displacement of the concrete under the bar tip due to the normal stress τ_b on the bar tip may be expressed as

$$\Delta c_{bb} = (\phi/E_c)\ \omega_{bb}\ \tau_b \qquad (5.14)$$

where ω_{bb} is the vertical displacement influence factor for the bar tip due to the normal stress τ_b on the bar tip itself, which is defined in equation (5.7.3).

Hence, the vertical displacement of the concrete under the bar tip due to all n bar elements and to the bar tip itself is

$$\Delta c_b = \frac{\phi}{E_c} \left(\sum_{j=1}^{n} \omega_{bj}\ \tau_j + \omega_{bb}\ \tau_b \right) \qquad (5.15)$$

Equations (5.12) and (5.15) may be formulated in the following matrix form which comprises the vertical displacement of the concrete adjoining to all n bar elements and the bar tip as

$$[\Delta c] = \frac{\phi}{E_c} [CS][\tau] \qquad (5.16)$$

where [CS] is the (n + 1) square matrix of concrete displacement influence factors given by equation (5.9.1) and $[\tau]$ is the (n + 1) column matrix defined as

$$[\tau] = \begin{bmatrix} \tau_1 \\ \tau_2 \\ \cdot\cdot \\ \cdot\cdot \\ \tau_n \\ \tau_b \end{bmatrix} \qquad (5.17)$$

In equation (5.16) the sizes of the matrices [CS] and [τ] vary according to the end condition of the bar. When the end bearing of the bar is neglected, all elements of the sub-matrices [DC], [DF] and ω_{bb} given by equations (5.8.2), (5.8.3) and (5.8.4), respectively, are equal to zero. Therefore, matrix [CS] in equation (5.16) becomes identical to matrix [DB] defined in equation (5.8.1). On the other hand, the column matrix [τ] in equation (5.16) is

$$[\tau] = \begin{bmatrix} \tau_1 \\ \tau_2 \\ \cdot\cdot \\ \cdot\cdot \\ \tau_n \end{bmatrix} \qquad (5.18)$$

In order to determine the displacement of the bar itself, the bar is assumed to be subjected to pure axial compression only. Consider a small cylindrical bar element on which the stresses act as shown in figure (5.5b). From the vertical equilibrium of the bar element, resolving forces leads to the following expression

$$\frac{\partial \sigma}{\partial z} A_S = -\tau \pi \phi$$

or

$$\frac{\partial \sigma}{\partial z} = -\frac{\tau \pi \phi}{A_S} \qquad (5.19)$$

where σ is the normal stress in the bar and τ is the bond stress acting on the bar surface.

Defining R_A as

$$R_A = \frac{A_S}{(\pi \phi^2/4)} = \frac{4A_S}{\pi \phi^2} \qquad (5.20.1)$$

then it follows that

$$A_S = (R_A \pi \phi^2)/4 \qquad (5.20.2)$$

Substituting for A_S in equation (5.19) and simplifying we have

$$\frac{\partial \sigma}{\partial z} = -\frac{4\tau}{R_A \phi} \qquad (5.21)$$

where R_A is the ratio of the bar cross-sectional area to the area bounded by the circumference of the bar. Both square twisted and ribbed bars are solid and the cross-sectional area for both is equal to the area bounded by the circumference of the bar, therefore, $R_A = 1$. It is beyond the scope of this analysis, however, to allow for the more general case, i.e. where the bar cross-sectional area is different from that of the area bounded by the outer circumference of the bar, the ratio R_A is inserted into subsequent equations. So that, if required, a bar having any shape of cross-section may similarly be analysed, provided that its outer surface is cylindrical.

Referring to figure (5.5b) consideration of the axial strain of the bar element gives

$$\frac{\partial \Delta_s}{\partial z} = \frac{-\sigma}{E_s} \qquad (5.22)$$

where Δ_s is the displacement of the bar and E_s is Young's modulus of the bar.

Differentiating equation (5.22) with respect to z and substituting for $\frac{\partial \sigma}{\partial z}$ from equation (5.21) leads to the following equation for the displacement of the bar

$$\frac{\partial^2 \Delta_s}{\partial z^2} = \frac{4\tau}{R_A \phi E_s} \qquad (5.23)$$

Equation (5.23) may be represented in terms of the finite difference expressions, the details of which are given elsewhere[25]. Employing central differences - which use the points located symmetrically with respect to the point under consideration - for a cylindrical element i within the interval $n - 1 \geq i \geq 2$, equation (5.23) may be expressed in the following finite difference form to give the bond stress as

$$\tau_i = \frac{\phi}{4\delta^2} E_s R_A (\Delta_{si-1} - 2\Delta_{si} + \Delta_{si+1}) \quad (5.24)$$

where Δ_{si-1}, Δ_{si} and Δ_{si+1} are the displacements of the mid-points of the elements i-1, i and i+1 respectively, and δ is the length of an element i.e., $\delta = l_a/n$.

Referring to figure (5.5c), at the top of the bar consider an imaginery element of length δ having a mid-point displacement Δ'_{s1}, above the first real element as proposed by Mattes and Poulos[39]. At the top of the bar, the normal stress in the bar is

$$\sigma = P/A_s \quad (5.25)$$

where P is the total axial load on the bar. Hence, referring to equation (5.22) the displacement of the imaginery element (Δ'_{s1}) may be related to the displacement of the uppermost real element (Δ_{s1}) as follows

$$\frac{\Delta_{s1} - \Delta'_{s1}}{\delta} = -\frac{\sigma}{E_s} \quad (5.26.1)$$

or

$$\Delta'_{s1} = \Delta_{s1} + \frac{\sigma\delta}{E_s} \quad (5.26.2)$$

Substituting (5.25) in equation (5.26.2) results

$$\Delta'_{s1} = \Delta_{s1} + \frac{P\delta}{A_s E_s} \quad (5.26.3)$$

On the other hand, for the first real element equation (5.24) is in the following form

$$\tau_1 = \frac{\phi}{4\delta^2} E_s R_A (\Delta'_{s1} - 2\Delta_{s1} + \Delta_{s2}) \quad (5.27)$$

Substituting value of Δ'_{s1} from equation (5.26.3) in equation (5.27) and simplifying leads to the following expression for bond stress τ_1 on the first element as

$$\tau_1 = \frac{\phi}{4\delta^2} E_s R_A (-\Delta_{s1} + \Delta_{s2}) + \frac{P}{\pi\phi^2} \cdot \frac{n}{(l_a/\phi)} \quad (5.28)$$

In order to obtain the finite difference expression for the bottom cylindrical element of the bar (n), the bond stress τ_n may be related to the displacements of the mid-point of elements (n-2), (n-1), (n) and the bar tip, using equation (5.23) and finite differences for points with unequal spacing. For the element (n), an equation with an error of order (δ^2) to be consistent with the finite difference computation may be written as

$$\left(\frac{\partial^2 \Delta_s}{\partial z^2}\right)_n = \frac{1}{\gamma(\gamma+1)(\gamma+2)\delta^2}\left[\gamma(\gamma^2-1)\Delta_{sn-2} - 2(\gamma^3-4\gamma)\ \Delta_{sn-1} + (\gamma^3-7\gamma-6)\ \Delta_{sn} + 6\Delta_{sb}\right] \quad (5.29.1)$$

where Δ_{sn-2}, Δ_{sn-1}, Δ_{sn} and Δ_{sb} are the displacements of the mid-points of elements (n-2), (n-1), (n) and the bar tip, respectively, and γ is the ratio of unequal intervals, i.e. $\gamma = \frac{\delta}{2\delta} = \frac{1}{2}$

Inserting value of γ and simplifying gives

$$\left(\frac{\partial^2 \Delta_s}{\partial z^2}\right)_n = \frac{1}{\delta^2}\left(-0.2\ \Delta_{sn-2} + 2\Delta_{sn-1} - 5\Delta_{sn} + 3.2\Delta_{sb}\right) \quad (5.29.2)$$

Substituting (5.29.2) in equation (5.23) and rearranging, we have the required expression for the bond stress (τ_n) as follows.

$$\tau_n = \frac{\phi}{\delta^2} E_s R_A\left(-0.2\ \Delta_{sn-2} + 2\Delta_{sn-1} - 5\Delta_{sn} + 3.2\Delta_{sb}\right) \quad (5.30)$$

Finally, to obtain the expression for the bar tip, i.e. (n+1)th element, equation (5.22) may be applied to the bar tip, employing a finite difference expression for an unequal spacing of pivotal points, and with an error of order δ^2, namely[39]

$$-\frac{\tau_b}{E_s} = \frac{1.33\ \Delta_{sn-1} - 12\Delta_{sn} + 10.67\ \Delta_{sb}}{4\delta} \quad (5.31)$$

leads to

$$\tau_b = \frac{\phi}{4\delta^2} E_s R_A\left[\frac{(l_a/\phi)}{nR_A}\right](-1.33\ \Delta_{sn-1} + 12\Delta_{sn} - 10.67\Delta_{sb}) \quad (5.32)$$

Equations (5.24), (5.28), (5.30) and (5.32) may be given in a matrix form as

$$[\tau] = \frac{\phi}{4\delta^2} E_s R_A [CP][\Delta_s] + [Y] \qquad (5.33)$$

where [CP] is the (n + 1) square matrix of coefficients for bar action and is defined by

$$[CP] = \begin{bmatrix} -1 & 1 & 0 & 0.....0 & 0 & 0 & 0 \\ 1 & -2 & 1 & 0.....0 & 0 & 0 & 0 \\ 0 & 1 & -2 & 1.....0 & 0 & 0 & 0 \\ \cdots & \cdots & \cdots & \cdots & \cdots & \cdots & \cdots \\ \cdots & \cdots & \cdots & \cdots & \cdots & \cdots & \cdots \\ 0 & 0 & 0 & 0.....-0.2 & 2 & -5 & 3.2 \\ 0 & 0 & 0 & 0 \quad 0 & -1.33t & 12t & -10.67t \end{bmatrix} \qquad (5.34)$$

in which

$$t = (l_a/\phi)\, n\, R_A \qquad (5.35)$$

$[\Delta_s]$ is the (n + 1) column matrix given as

$$[\Delta_s] = \begin{bmatrix} \Delta_{s1} \\ \Delta_{s2} \\ \Delta_{s3} \\ .. \\ .. \\ \Delta_{sn} \\ \Delta_{sb} \end{bmatrix} \qquad (5.36)$$

and [Y] is the (n + 1) columm matrix defined by

$$[Y] = \begin{bmatrix} \frac{P}{\pi\phi^2} & \frac{n}{(l_a/\phi)} \\ o \\ .. \\ .. \\ o \\ o \end{bmatrix} \qquad (5.37)$$

In equation (5.33), when the end bearing of the bar is neglected, the order of matrices [CP], $[\Delta_s]$ and [Y] is (n x n), (n x 1) and (n x 1)

respectively.

Since the conditions within the concrete remain elastic, the displacements of the concrete and the bar must be compatible. Hence

$$[\Delta_s] = [\Delta c] \tag{5.38}$$

From equations (5.16) and (5.33)

$$[\tau] = \frac{\phi}{4\delta^2} E_s R_A \frac{\phi}{E_c} [CP] [CS] [\tau] + [Y] \tag{5.39}$$

then

$$[I] [\tau] - \frac{\phi^2}{4\delta^2} \frac{E_s}{E_c} R_A [CP] [CS] [\tau] = [Y]$$

Hence

$$[\tau] = ([I] - \frac{\phi^2}{4\delta^2} \frac{E_s}{E_c} R_A [CP] [CS])^{-1} [Y] \tag{5.40}$$

where [I] is the identity matrix.

Defining

$$K = (E_s/E_c) R_A \tag{5.41}$$

$$\delta = (l_a/n) \tag{5.42}$$

$$[C] = [I] - \frac{n^2}{4(l_a/\phi)^2} K [CP] [CS] \tag{5.43}$$

it follows that

$$[\tau] = [C]^{-1} [Y] \tag{5.44}$$

Solution of equation (5.44) produces the unknown stresses i.e. bond stress on the bar surface along the anchorage length of foundation and the normal stress acting on the bar tip, or in the case of no end bearing, bond stresses on the bar periphery only. Then, the distribution of displacement along the bar can be computed from equation (5.16).

The elastic analysis is extended to carry out elastic-plastic analysis by considering the local bond failure between the reinforcing bar and

surrounding concrete medium. This is studied in the next section.

5.4 Elastic-Plastic Analysis

The development of the elastic-plastic analysis is based on the following further assumptions.

1- A uniform and constant ultimate bond strength is considered for each cylindrical element of the bar along the anchorage length, and a uniform ultimate end bearing resistance for the bar tip when the end bearing is present.

2- When the bond stress developed on the surface of any element of the bar reaches to the ultimate bond strength, local yield will occur in the related surrounding concrete layer.

3- As the local bond failure takes place in the concrete layer due to the ultimate bond strength, the displacement compatibility does not exist between the bar element and the concrete layer, while the rest of the concrete layers remain elastic.

Consider a bar with n cylindrical elements embedded in a concrete medium and subjected to axial load as shown in figure (5.6a). Let the corresponding bond stresses on the bar elements be τ_1, τ_2,....., τ_n and the normal stress on the bar tip be τ_b if end bearing is considered, as indicated in figure (5.6b). As the externally applied load increases the stresses and displacements increase proportionally until the bond stress somewhere on a bar element reaches ultimate bond strength in the related concrete layer. From then this layer is not compatible with the bar element concerned. The displacements and bond stresses elsewhere in the bar now increase at a faster rate because any increase in the applied load will cause redistribution of

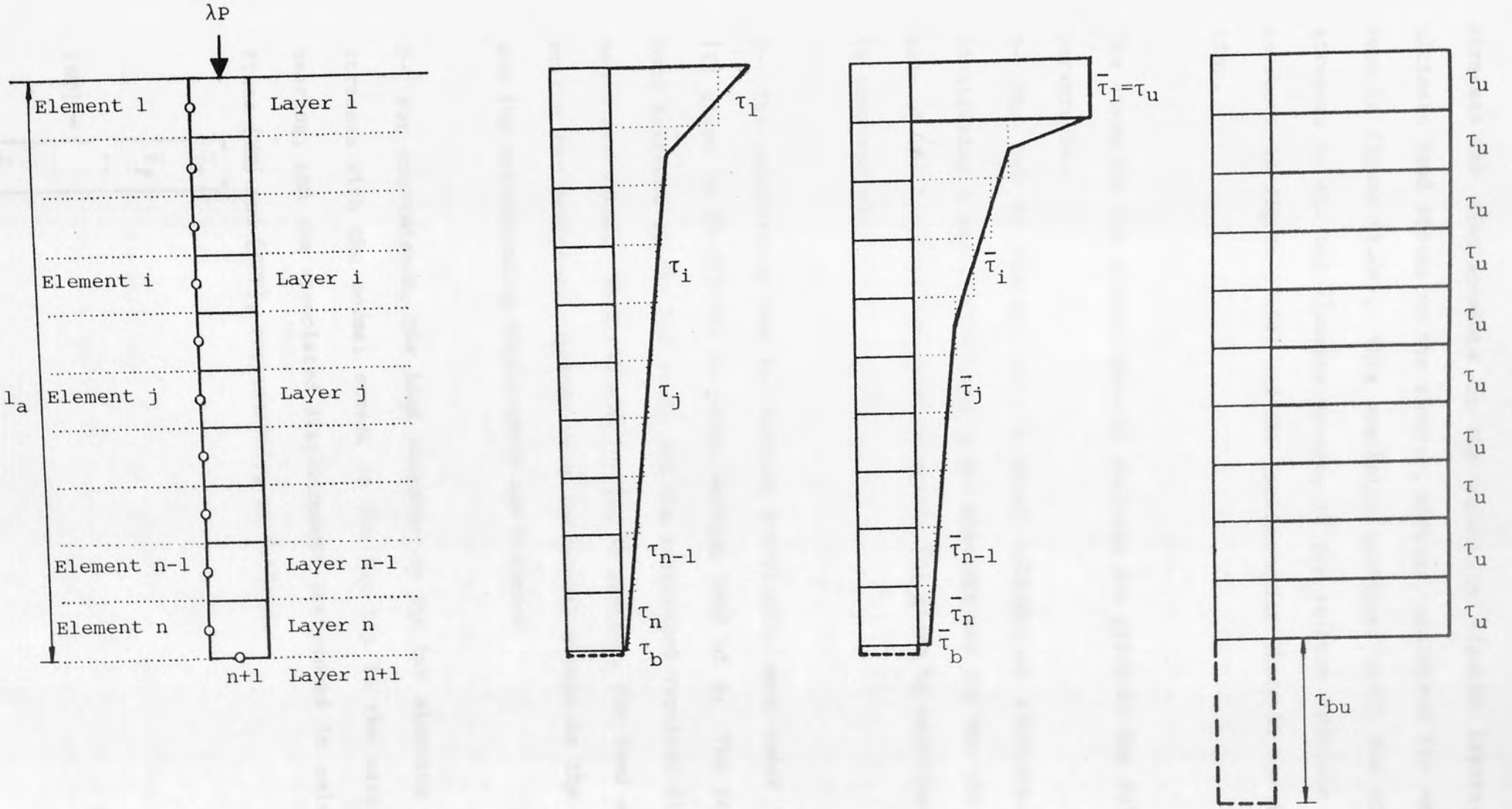

a) Bar in concrete medium and loading

b) Stresses at elastic case

c) Stresses at elastic-plastic case

d) Stresses at ultimate

FIGURE 5.6: GEOMETRIC REPRESENTATION FOR ELASTIC-PLASTIC ANALYSIS

stresses and displacements in the remaining elastic layers. The ultimate bond stress on the element, however, preserves its value as seen in figure (5.6c). This condition continues until the ultimate stresses on all bar elements develop in the related concrete layers as shown in figure (5.6d) and the failure takes place in the foundation.

The steps for the elastic-plastic analysis are given in the following paragraphs.

1- The bar is divided into n equal cylindrical elements. Then considering n bar elements, or n bar elements and the bar tip in the case of end bearing, the compound matrix [C] given by equation (5.43) is constructed.

2- The reinforcing bar is analysed elastically once under [C] and [Y] given by (5.37) for an axial working load of p. The resulting bond stresses on the bar shaft and the associated vertical displacements are found. When the end bearing is present, the bond stresses on the bar periphery together with the normal stress on the bar tip and the corresponding displacement are computed.

3- For convenience, the bond stresses on the bar elements or bond stresses with the normal stress on the bar tip in the case of end bearing, and the associated displacements are stored in column matrices [ST] and [DEF], respectively, as follows.

$$[ST] = \begin{bmatrix} \bar{\tau}_1 \\ \bar{\tau}_2 \\ .. \\ .. \\ \bar{\tau}_n \\ \bar{\tau}_b \end{bmatrix} \qquad (5.45)$$

in which $\bar{\tau}_1$, $\bar{\tau}_2$,....., $\bar{\tau}_n$, $\bar{\tau}_b$ are the bond stresses developed on the bar elements 1, 2,....., n, respectively, and $\bar{\tau}_b$ is the normal stress on the bar tip due to the applied load. When the end bearing of the bar is neglected $\bar{\tau}_b$ is equal to zero.

$$[DEF] = \begin{bmatrix} \bar{\Delta}_{c1} \\ \bar{\Delta}_{c2} \\ .. \\ .. \\ \bar{\Delta}_{cn} \\ \bar{\Delta}_{cb} \end{bmatrix} \qquad (5.46)$$

in which $\bar{\Delta}_{c1}$, $\bar{\Delta}_{c2}$, ..., $\bar{\Delta}_{cn}$ and $\bar{\Delta}_{cb}$ are the displacements along the bar elements and under the bar tip in the respective concrete layers as well as the displacements of the bar elements and the bar tip, since the compatibility holds between the bar and the concrete. In the case of no end bearing $\bar{\Delta}_{cb}$ in [DEF] is disregarded.

4- Every possible local yield location within the concrete layers due to the ultimate bond stress on the related bar element is taken into consideration in turn, and the load factor λ_1^k at which local yield occurs in concrete layer k is computed from the following equation.

$$\lambda_1^k = \frac{\tau_u^k}{\bar{\tau}_k} \qquad (5.47)$$

where τ_u^k is the ultimate bond strength of the bar element in layer k and $\bar{\tau}_k$ is the bond stress on the bar element in layer k due to the applied working load.

The lowest of these predicted load factors is chosen. This is now the load factor λ_1 at which the first yield occurs in layer k*. The

current stresses on the bar elements and displacements are obtained by scalar multiplying the column matrices [ST] and [DEF] by λ_1.

Since the layer k* has yielded, the free slip of the bar occurs in this layer because the bar and the concrete for this element are not compatible. To proceed further, the bond stresses and displacements of the bar with yielding at layer k* under the applied load is necessary. Because any increase in the applied load will lead to a redistribution of stress on the bar elements in the remaining elastic layers. The displacement compatibility between the bar and the concrete in the elastic layers must therefore be considered. Then the resulting compatibility equations are solved to obtain the distribution of stress and displacement along the bar until the yield of next concrete layer takes place due to the ultimate bond stress development on the related bar element. A fresh solution of compound matrix [C] is then required and matrix [CP] must now be constructed for the remaining bar elements in the elastic concrete layers. This is done in a similar way as previously described, by taking the uppermost bar element within the remaining elastic layer as the first element. Reconstruction of matrix [CP] is continued in this way at the yield of each concrete layer, until all concrete layers have yielded and failure takes place.

5- For a further increase $\Delta\lambda = \lambda - \lambda_1$, in the load factor the current stresses and displacements are calculated as

$$[ST]^{\lambda} = [ST]^{\lambda_1} + \Delta\lambda[\tau] \tag{5.48}$$

$$[DEF]^{\lambda} = [DEF]^{\lambda_1} + \Delta\lambda[\Delta c] \tag{5.49}$$

where $[ST]^{\lambda}$ represents the bond stresses or bond stresses and the normal stress under the load parameter λ, while $[ST]^{\lambda_1}$ relates

the same stresses under load factor λ_1. Similarly $[DEF]^{\lambda}$ and $[DEF]^{\lambda_1}$ represent the vertical displacements under the load factors λ and λ_1, respectively. Again each yield location in the concrete layers is considered in turn. The load factor at which a local yield occurs in that layer is calculated by equating the current bond stress to the ultimate bond strength of the layer. Thus

$$\lambda_2 = \lambda_1 + \frac{\tau_{u(i)} - ST(i)}{\bar{\tau}(i)} \qquad (5.50)$$

The smallest of these load factors is selected as the load factor which causes the next yield in one of the concrete layers.

The bar stiffness factor K is very small, i.e. the bar is compressible in relation to the surrounding concrete medium and therefore high bond stresses develop at the top on the surface of the first bar element, as shown in figure (5.6b). Consequently the yield starts at the top of the bar in the first concrete layer and continues progressively downward in the remaining elastic layers towards the bottom as the applied load is increased.

6- The current stresses on the bar elements and the associated vertical displacements are calculated from equations (5.48) and (5.49) by substituting $\Delta\lambda = \lambda_2 - \lambda_1$ and $\lambda = \lambda_2$. If all concrete layers have yielded due to the ultimate bond stress development on the periphery of the bar elements and the ultimate bearing resistance of the concrete under the bar tip has been attained when end bearing is present, the process is stopped. Otherwise, λ_2 is taken as λ_1 and the steps 4 and 5 are repeated until failure takes place.

5.4.1 Assessment of the Ultimate Bond Strength and Bearing Resistance

The ultimate bond stress on the surface of each cylindrical element along the bar shaft for square twisted bars is predicted from equations (4.1a) and (4.3), which considers the variation of the bond strength due to the bar size and the anchorage length, respectively. The increases in bond strength with base size was not significant, therefore, equation (4.1a) is used for the prediction of the ultimate bond stress.

To assess the ultimate bond strength of the ribbed bars the following procedure is employed.

Equation (3.3) is used to obtain the variation of the bond stress due to the bar size, while the variation of the bond strength according to the anchorage length is obtained from equation (3.4). To consider the variation of the ultimate bond strength with the concrete characteristic cube strength equation (4.6) is used. To allow the contribution of the base tension reinforcement on the ultimate bond stress, the following expressions obtained from a regression analysis of the test results are used.

$$(f_{bsu}/\sqrt{f_{cu}}) = 0.609\ (\rho_b) + 1.732,\ R = 0.998 \qquad (5.51)$$

$$(f_{bsu}/\sqrt{f_{cu}}) = 1.027\ (\rho_b) + 2.193,\ R = 0.934 \qquad (5.52)$$

Equation (5.51) is used to predict the ultimate bond stress for the tests loaded below the yield stress of the column longitudinal steel, while equation (5.52) is employed for the tests loaded beyond the yield stress of the column reinforcement. To consider the contribution of the links alone or links together with the base bending

steel, 13% and 21% increases are assumed in the ultimate bond strength, respectively, due to the provision of such reinforcement, as indicated by the tests.

Hawkins[34] proposed the following equation for the determination of the bearing strength of the concrete loaded through rigid plates

$$\tau_{bu}/f_{cu} = 1 + [(T/\sqrt{f_{cu}})(\sqrt{D} - 1)] \qquad (5.53)$$

in which τ_{bu} is the ultimate bearing resistance, f_{cu} is the concrete cube strength, T is the constant depending on the concrete characteristics and, D is the ratio of the unloaded area to the loaded area.

As reported in the preceding chapters, the end bearing of the column bars was eliminated in the tests. However, to consider the end bearing in the theoretical analysis the ultimate bearing resistance may be estimated from equation (5.53). Ignoring the second term in brackets on the right hand side in equation (5.53) for simplicity the ultimate bearing resistance of the concrete under the bar is assumed to be equal to the concrete crushing strength, that is

$$\tau_{bu} = f_{cu} \qquad (5.54)$$

CHAPTER 6

COMPUTER PROGRAMMING

6.1 Introduction

This chapter refers to a computer program which makes use of the theoretical analyses presented in the previous chapter for the compression bond of deformed reinforcing bars embedded in a foundation. The program was written in extended Fortran and run on the I.C.L. 1904 computer at the University. It was developed to be capable of carrying out the following types of analysis.

1- Elastic analysis without end bearing

2- Elastic analysis with end bearing

3- Elastic-plastic analysis without end bearing

4- Elastic-plastic analysis with end bearing.

The program consists of a master segment and two subroutines. Their functions will be described in the following sections and illustrated in the flow diagrams.

6.2 Description of the Program

The flow diagram of the master segment is illustrated in figure (6.1). The input data is divided into two parts. The first part is the data concerning the geometrical and the physical properties of both reinforcing bar and concrete. The second is the data which is relevant to the programming procedure, i.e. selection of the type of analysis. The first input card contains the anchorage length of the bar, the

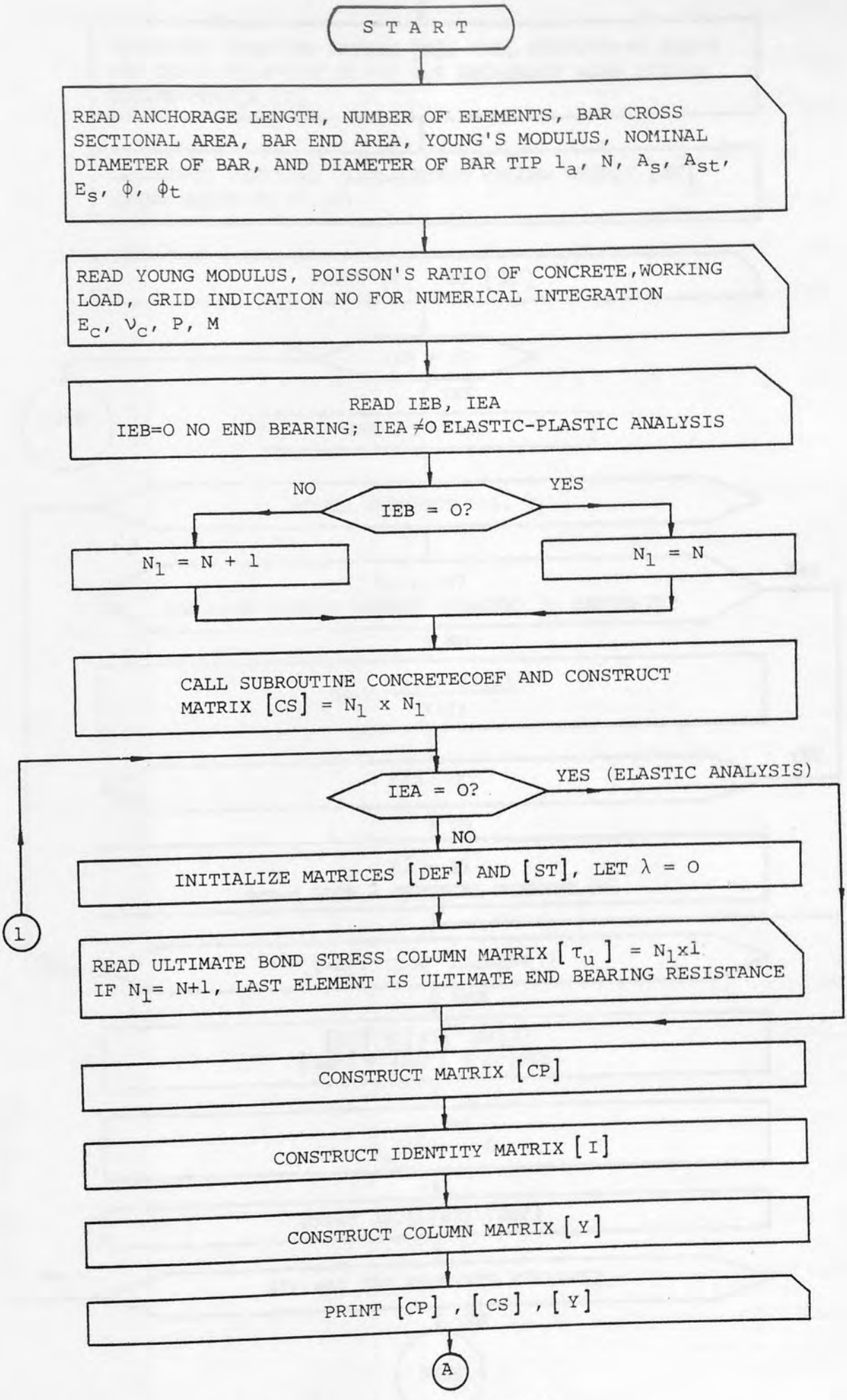

FIGURE 6.1: FLOW DIAGRAM FOR MASTER SEGMENT

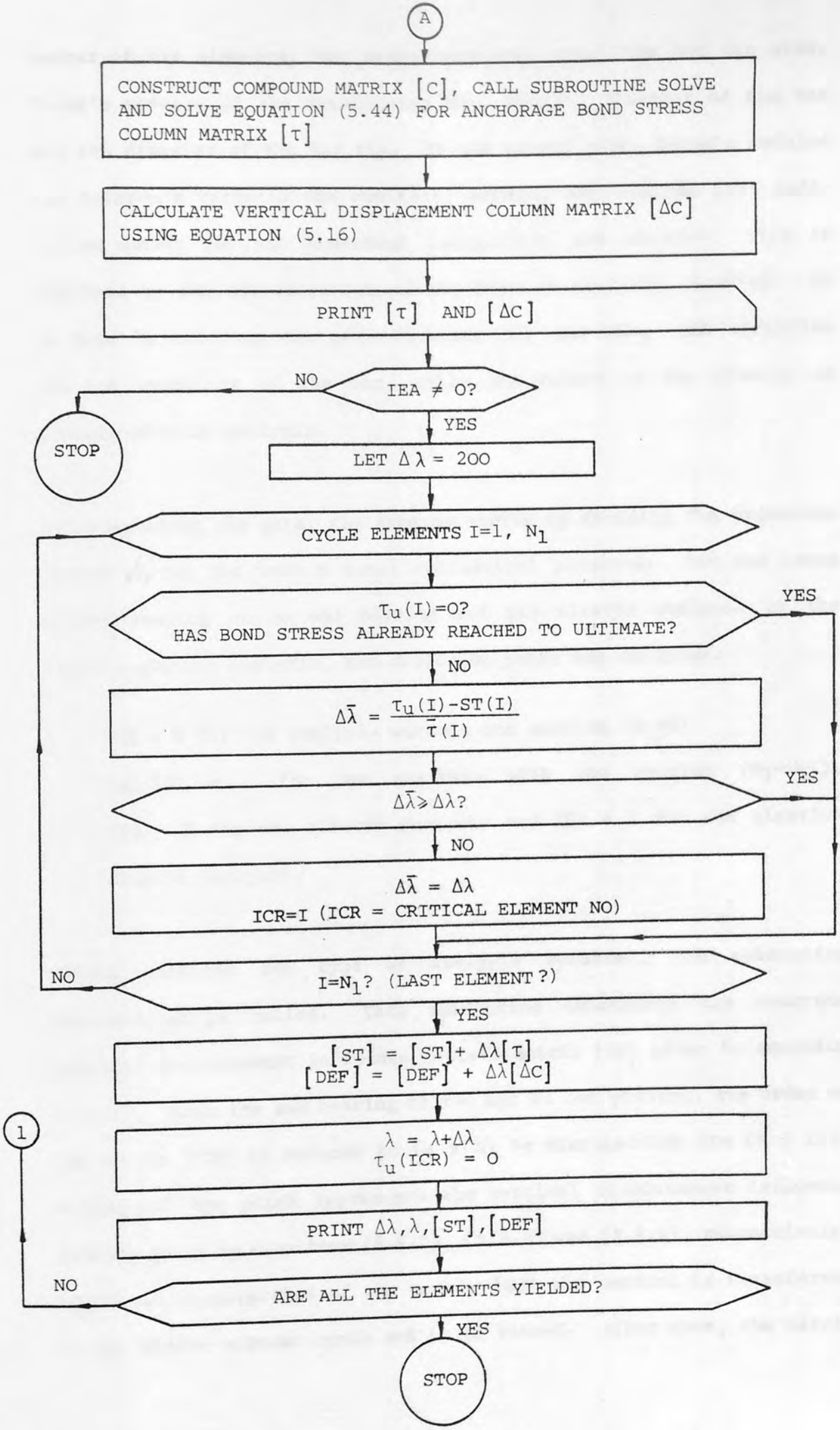

FIGURE 6.1: (continued)

number of bar elements, bar cross-sectional area, the bar tip area, Young's modulus of the reinforcing bar, nominal diameter of the bar and the diameter of the bar tip. In the second card, Young's modulus and Poisson's ratio of the concrete, working load and the grid indication number for the numerical integration are entered. This is followed by the specification of the type of analysis required. It is done by entering the path counters IEB and IEA. IEB specifies the end condition of the bar, while IEA refers to the elastic or elastic-plastic analysis.

After entering the data, the program starts by dividing the anchorage length of the bar into n equal cylindrical elements. For the cases of end bearing or no end bearing and the elastic analysis or the elastic-plastic analysis, the following paths are followed.

i - IEB = 0 for the analysis without end bearing (N_1=N)
and IEB = 1 for the analysis with end bearing (N_1=N+1).

ii - IEA = 0 for the elastic analysis and IEA = 1 for the elastic-plastic analysis.

Having specified the type of analysis required, the subroutine Concretecoef is called. This subroutine constructs the concrete vertical displacement influence factors matrix [CS] given by equation (5.9.1). When the end bearing of the bar is not present, the order of the matrix [CS] is reduced to (n x n) by disregarding its (n + 1)th column and row which represents the vertical displacement influence factors given by equations (5.8.2), (5.8.3) and (5.8.4), respectively. After the construction of the matrix [CS] the control is transferred to the master segment again and it is stored. After that, the matrix

[CP] given by equation (5.34) is constructed and stored. Then the program proceeds to construct the identity matrix [I] and the column matrix [Y] given by equation (5.37) and the both are stored. The matrices [CS], [CP] and [Y] are printed out if required.

Having accomplished the above process the compound matrix [C] defined by equation (5.43) is constructed. It is done by performing the matrix operations in equation (5.43). After this process, the subroutine Solve is entered to solve the equation (5.44) by carrying out the inverse transformation. The solution of the equation (5.44) produces the column matrix [τ] which designates the anchorage bond stress distribution on the bar shaft in the embedment length of the foundation. The control is then returned back to the master segment again and the associated vertical displacement column matrix [Δc] given by equation (5.16) is computed.

After the completion of the preceding computations, the following operations can be carried out as required by the user.

1 - For the elastic analysis without end bearing, IEB = 0 and IEA = 0, the process is already completed. The bond stress distribution along the anchorage length of the bar in the foundation and the associated vertical displacements are printed out and, the program is ended.

2 - For IEB = 1 and IEA = 0, the elastic analysis with end bearing is required. The compound matrix [C] is established in the order of (n + 1) x (n + 1) by constructing the matrices [CS], [CP] and [I] in the order of (n + 1) x (n + 1), respectively, and carrying out the matrix operations in equation (5.43). Then the process described for

case 1 is repeated. The anchorage bond stress distribution on the bar shaft with the normal stress on the bar tip and the associated displacements are printed out and, the program is terminated.

3 - IEB = 0 and IEA = 1 refer to the elastic-plastic analysis without end bearing. In this case, the reinforcing bar is analysed elastically once under an axial working load of p in the manner given for case 1. Then the elastic-plastic analysis is carried out within the corresponding block of the master segment, which will be described below.

4 - When the elastic-plastic analysis with end bearing is required, the path counters are IEB = 1 and IEA = 1. First, the elastic analysis is carried out under an axial working load of p in the manner described for case 2. After that, the elastic-plastic analysis is performed within the corresponding block of the master segment.

Steps taken for the elastic-plastic analysis procedure are described in the following paragraphs.

Before the execution of the elastic-plastic analysis the column matrices [ST] and [DEF] given by equation (5.45) and (5.46) are initialized and the overall load factor λ is set to zero. Then the ultimate bond stress column matrix $[\tau_u]$ predicted from the equations given in section (5.4.1) of chapter 5 is entered. When the end bearing of the bar is present, the last element of $[\tau_u]$ is the ultimate end bearing resistance given by equation (5.54). Following the elastic analysis of the bar with or without end bearing under an axial working load p, the resulting bond stresses on the bar elements

or the bond stresses with the normal stress on the bar tip and the associated displacements are stored in matrices [ST] and [DEF], respectively.

The elastic-plastic analysis is commenced by cycling the possible local yield location within the concrete layers. The lowest load factor at which the first local yield occurs in a concrete layer due to the ultimate bond stress development on the related bar element is computed from equation (5.47). The concrete layer at which the local yield takes place is disregarded. The predicted load factor $\lambda_1 = \Delta\bar{\lambda}$ is compared with the given load factor $\Delta\lambda$ which has been set to a large number. If $\Delta\bar{\lambda}<\Delta\lambda$, the current bond stresses or the bond stresses with the normal stress on the bar tip when end bearing is present, and the associated displacements are obtained by scalar multiplying the matrices [ST] and [DEF] by the predicted load factor $\Delta\bar{\lambda}$, respectively. The respective results are stored in [ST] and [DEF] again. Then $\Delta\bar{\lambda}$, λ, [ST] and [DEF] are printed out. In contrast, if $\Delta\bar{\lambda}\geq\Delta\lambda$, the current stresses and the displacements are determined by scalar multiplying the matrices [ST] and [DEF] by the given load factor $\Delta\lambda$, respectively. However, since the elastic-plastic analysis is continued until the ultimate load, the $\Delta\lambda$ is set to a very large number (see flow diagram in figure (6.1) for reference) therefore, the condition $\Delta\bar{\lambda}\geq\Delta\lambda$ can never be reached. Thus, the program continues to carry out the elastic-plastic analysis by employing the predicted load factor at each local yield within the concrete layers until failure takes place.

After obtaining the first local yield in a concrete layer the search is continued by cycling the remaining elastic layers for the next

local yield. Each yield location in the concrete layers is considered in turn. The load parameter at which a local yield occurs in that layer is calculated from equation (5.50). The concrete layer which produces the smallest of these predicted load factors is selected as the critical layer and singled out. The current stresses on the bar elements and the associated vertical displacements are calculated from equations (5.48) and (5.49), respectively. The resulting stresses and the displacements are again stored in [ST] and [DEF], respectively. Then $\Delta\bar{\lambda}$, λ, [ST] and [DEF] are printed out.

The whole process is continued until all concrete layers have yielded due to the ultimate bond stress development on the bar elements and the ultimate end bearing strength of the concrete under the bar tip has been reached when the end bearing is present. Then the program is terminated.

6.3 Subroutine Concretecoef

Subroutine Concretecoef establishes the overall vertical displacement influence factors matrix [CS] given by equation (5.9.1). This is done by the numerical integration of the equations (5.4.2), (5.5.3), (5.6.3) and (5.7.3), which yields the corresponding submatrices [DB], [DC], [DF] and the scalar ω_{bb} defined by the equations (5.8.1), (5.8.2), (5.8.3) and (5.8.4), respectively. To evaluate the integrals involved each cylindrical bar element is divided into (M x M) grids on its half surface for the integration with respect to c and the angular interval (0 - $\pi/2$) is divided into M grids for the integration with respect to θ (see figure (5.4) in chapter 5 for reference).

The related integrals for the bar tip are carried out by dividing the intervals (0 - a) and (0 - 2π) into M grids for the integrations with respect to r and θ, respectively.

The flow diagram of subroutine Concretecoef is given in figure (6.2). As seen from the figure it consists of six nested loops. The two outer loops take each cylindrical bar element and the bar tip in turn. In the two inner-upper loops the grid meshwork on the surface of the bar elements and the bar tip is scanned. The two inner-lower loops cycle the grid meshwork. The execution of subroutine Concrete-coef is initiated by dividing the all elements into grids of dimension (M x M). After cycling the all elements, the values of the initial geometrical parameters c, z, z_1 and $\overline{R}$ are calculated. Then the grids of all elements are scanned. The geometrical variables R_1 and R_2 given by equations (5.3.1), (5.5.2), (5.6.2) and (5.7.2) in relation to the location of the element are calculated accordingly. After that ω_b of equation (5.3.3) is calculated for the present values and stored as CP(IA, JA).

The execution of the program continues by cycling the grids for all elements. Then matrix [CS] is initialized and the C_{mean} is computed as

C_{mean} = CP(IA,JA) + CP(IA,JA + 1) + CP(IA + 1,JA) + CP(IA + 1,JA + 1)

Following this operation the equation (5.4.2) which defines the vertical displacement influence factor for a point i due to a bond stress on element j is computed as

CS(I, J) = CS(I, J) + C_{mean}. a. dθ. dc

where dθ = π/2M and dc = δ/M. Similarly, equation (5.5.3) is computed

as

$CS(I, J) = CS(I, J) + C_{mean} \cdot r_{mean} \cdot d\theta \cdot dr$

which represents the vertical displacement influence factor for the point i on the bar shaft due to a normal stress on the bar tip and, where $r_{mean} = (i - \frac{1}{2})\, r/M$, $dr = a/M$ and $d\theta = 2\pi/M$. The above procedure is repeated for all grids on the cylindrical bar elements and the bar tip which yields the submatrices [DB] and [DC] of the overall matrix [CS].

C_{mean} for the end of the bar is calculated as

$C_{mean} = CP(IA,1) + CP(IA + 1,1)$

Then equation (5.6.3) given for the vertical displacement influence factor of the bar tip due to a bond stress on the element j is computed as

$CS(I, J) = CS(I, J) + C_{mean} \cdot \pi \cdot a \cdot dc$

Finally, the displacement influence factor related to the bar tip defined by equation (5.7.3) is calculated as

$CS(I, J) = CS(I, J) + C_{mean} \cdot r_{mean} \cdot dr \cdot \pi^2/4$

After the above operations are finished, as a result the submatrix [DF] and the scalar ω_{bb}, i.e. the last element of the overall matrix [CS], is obtained.

The process described to evaluate the integrals and construct the overall matrix [CS] is arranged in such a way that whole operations are carried out within the specified storage of [CP] and [CS] in a compact scheme to save the amount of computer storage. After the construction of matrix [CS] the control is transferred back to the master segment again.

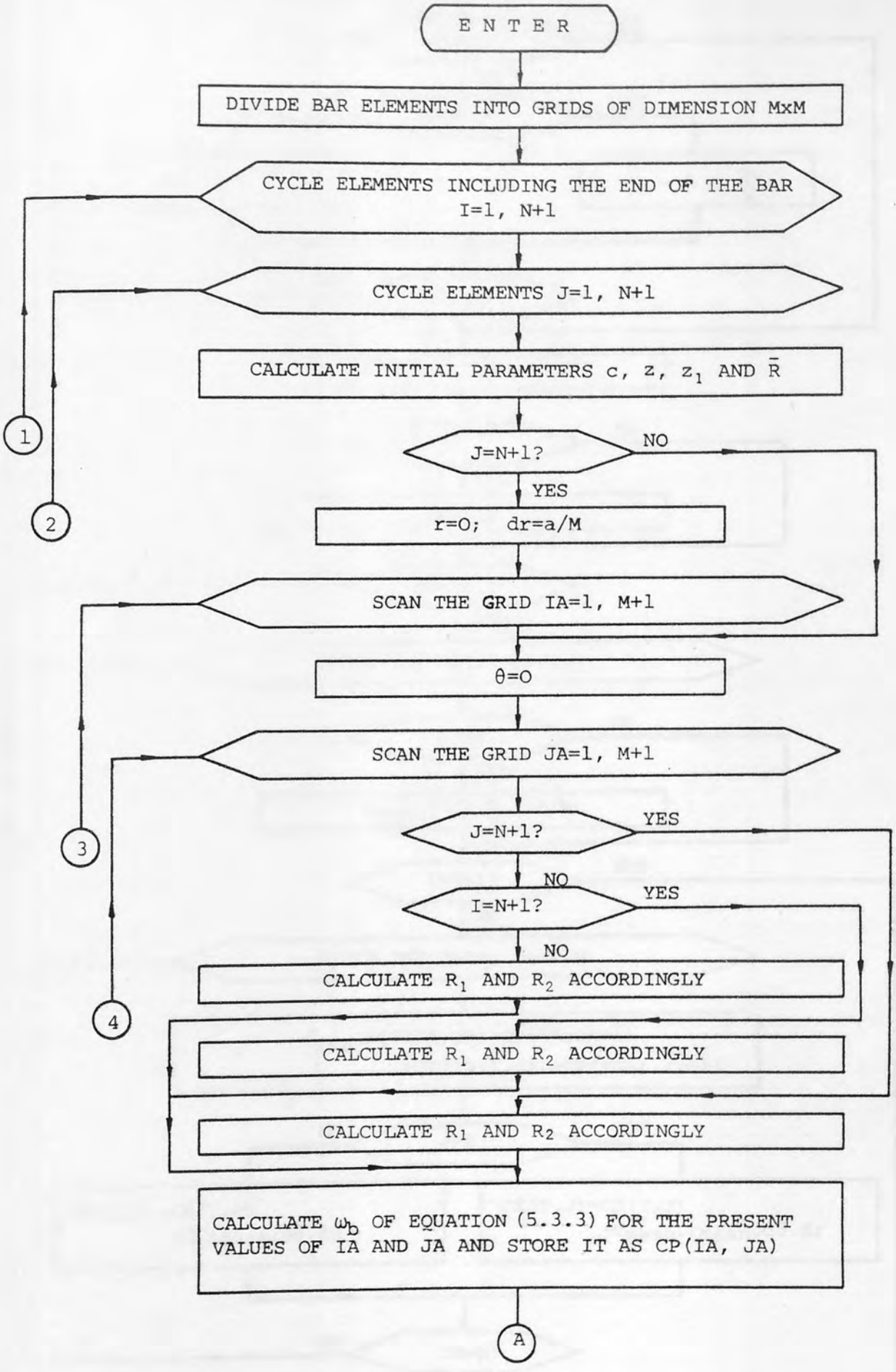

FIGURE 6.2: FLOW DIAGRAM OF THE SUBROUTINE CONCRETECOEF

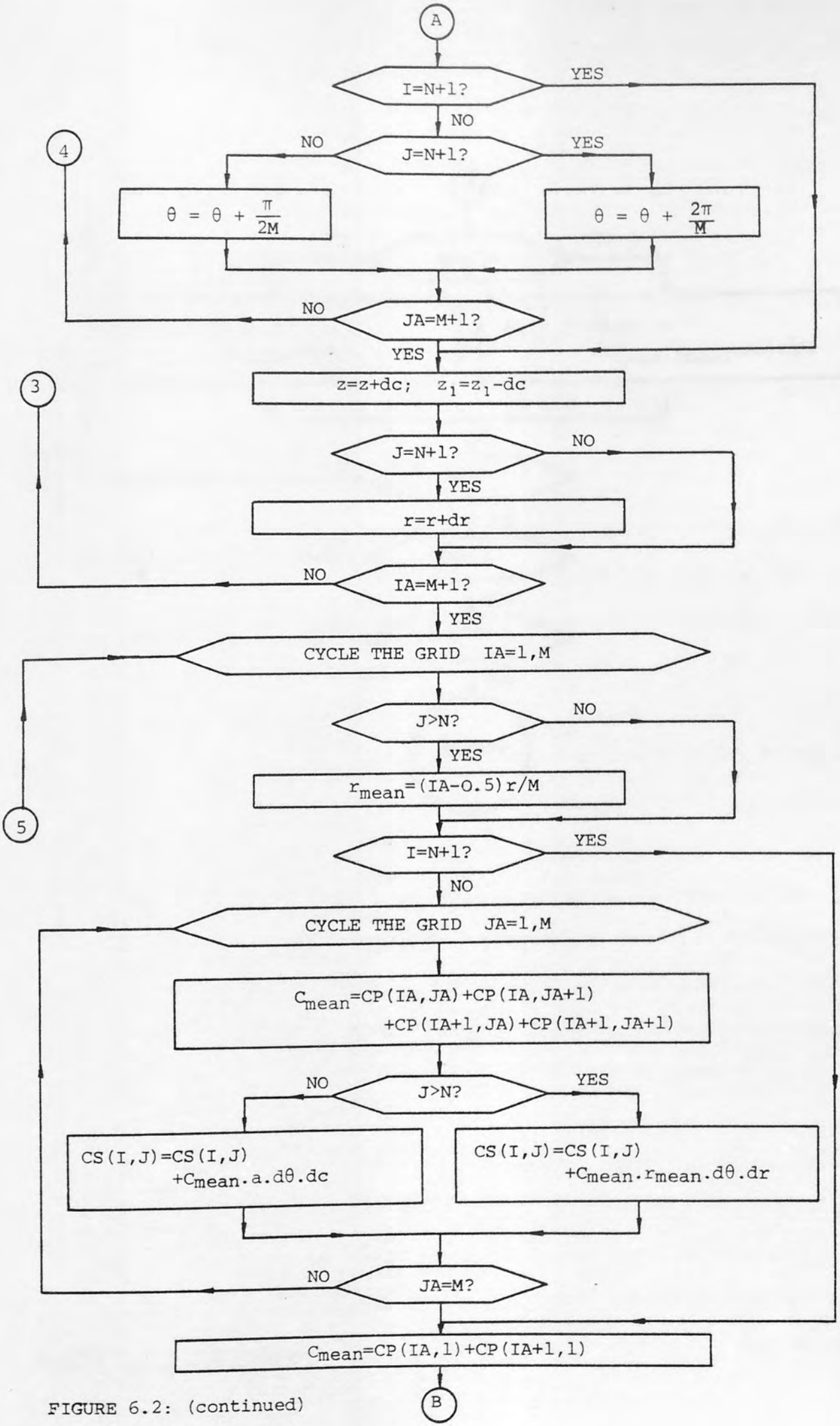

FIGURE 6.2: (continued)

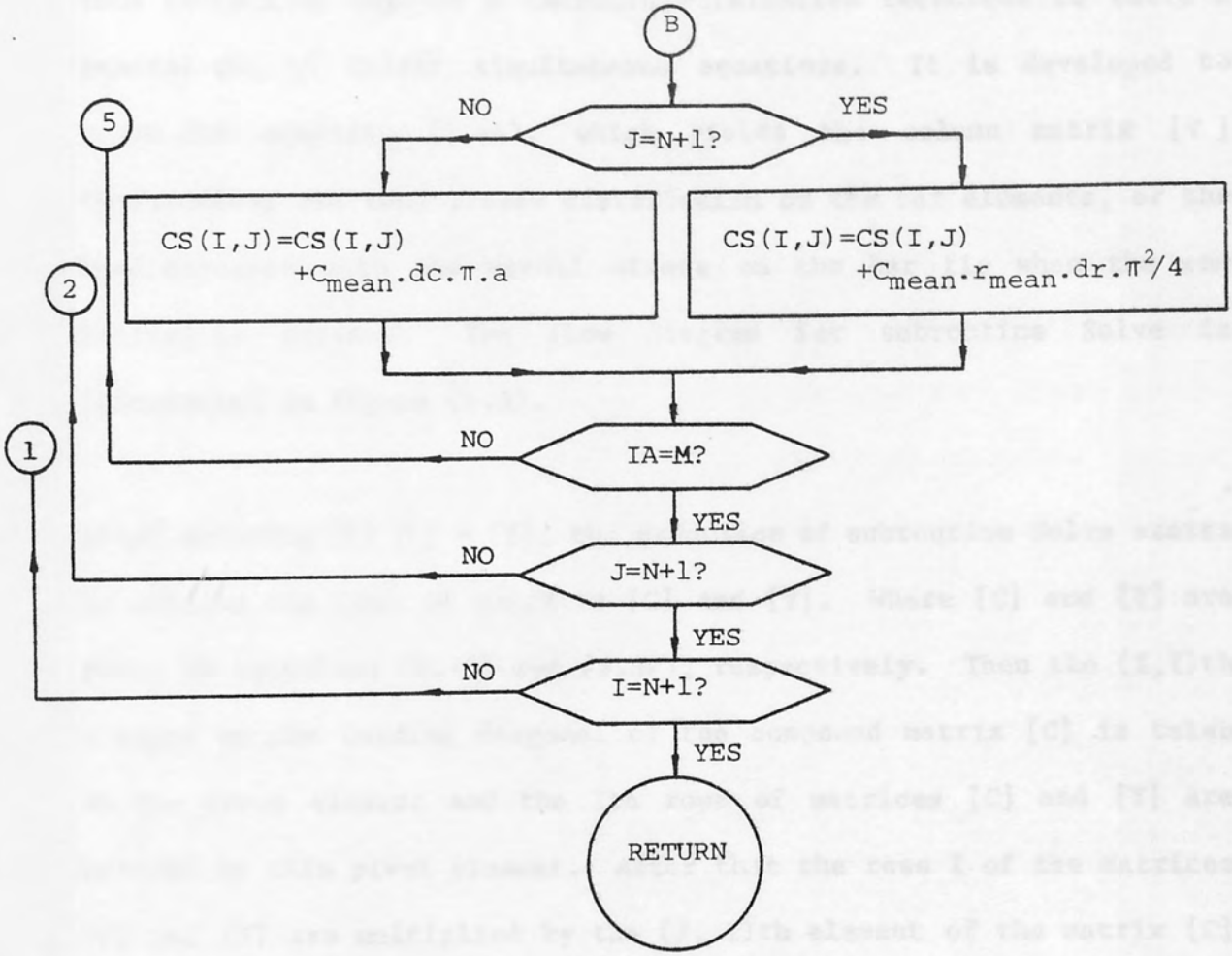

FIGURE 6.2: (continued)

6.4. Subroutine Solve

This subroutine employs a Gaussian elimination technique to solve a general set of linear simultaneous equations. It is developed to solve the equation (5.44), which yields the column matrix $[\tau]$ representing the bond stress distribution on the bar elements, or the bond stresses with the normal stress on the bar tip when the end bearing is present. The flow diagram for subroutine Solve is illustrated in figure (6.3).

After entering $[C]\ [\tau] = [Y]$, the execution of subroutine Solve starts by cycling the rows of matrices [C] and [Y]. Where [C] and [Y] are given by equations (5.43) and (5.37), respectively. Then the (I,I)th element on the leading diagonal of the compound matrix [C] is taken as the pivot element and the Ith rows of matrices [C] and [Y] are divided by this pivot element. After that the rows I of the matrices [C] and [Y] are multiplied by the (J, I)th element of the matrix [C] and subtracted from the Jth rows of matrices [C] and [Y]. This procedure is repeated by taking the each leading diagonal element of the matrix [C] as pivot element and carrying out the above operations. Thus the elimination process is completed. At this stage, all elements on the leading diagonal of matrix [C] are set to unity and all the others below the leading diagonal are reduced to zero.

Once the elimination is completed, the back substitution is initiated by cycling the new rows of the matrices [C] and [Y], respectively. Subsequently, the rows of the matrix [Y] are taken in turn and the (K, J)th row of the compound matrix [C] is multiplied by the Jth row of the matrix [Y], and then subtracted from the Kth row of the matrix

[Y]. The same procedure is repeated for all remaining rows of the [Y]. All the operations for the elimination and the back substitution are carried out within the matrices [C] and [Y] in a compact scheme and therefore no additional storage is required.

After the whole process is completed the compound matrix [C] is transformed to a unit matrix, i.e. all the elements on the leading diagonal are reduced to unity and all the others are reduced to zero. Thus the final values of the original elements of the column matrix [Y] are the required values of the unknown bond stresses and the normal stress on the bar tip defined by [τ]. The control is then returned back to the master segment.

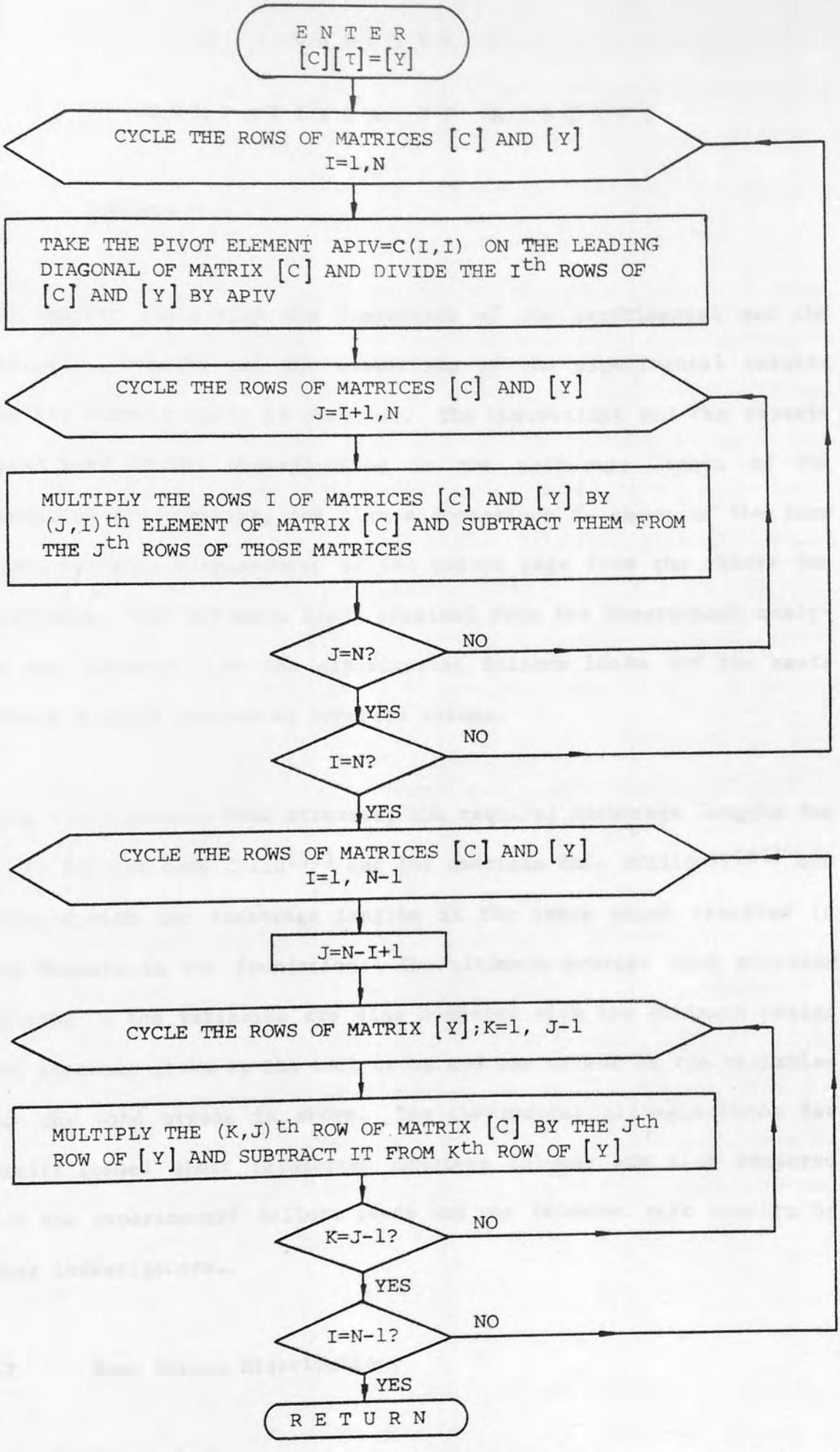

FIGURE 6.3: FLOW DIAGRAM OF THE SUBROUTINE SOLVE

CHAPTER 7

COMPARISON OF RESULTS

7.1 Introduction

This chapter deals with the comparison of the experimental and the theoretical results and the comparison of the experimental results with the current codes of practice. The theoretical and the experimental bond stress distributions in the anchorage length of the foundation are compared, and also a comparison is shown of the load versus vertical displacement of the column cage from the theory and experiment. The ultimate loads obtained from the theoretical analysis are compared with the experimental failure loads for the tests without a short reinforced concrete column.

Using the allowable bond stresses, the required anchorage lengths due to the British code CP110[56] and the American code ACI318-77[61] are compared with the anchorage lengths in the tests which resulted in bond failure in the foundation. The ultimate average bond stresses relating to the variables are also compared with the ultimate design bond stresses given by the both codes and the effect of the variables upon the bond stress is shown. The theoretical ultimate loads for axially loaded short reinforced concrete columns are also compared with the experimental failure loads and the relevant test results by other investigators.

7.2 Bond Stress Distributions

This section is concerned with the comparison of the experimental and

the theoretical bond stress distributions along the anchorage length of the column bars in the foundation. The theoretical bond stress distribution over the embedded length of column longitudinal reinforcement in the base was obtained from the solution of equation (5.44). In obtaining the solutions for the distribution of the anchorage bond stress, the column bar was divided into n = 5 equal cylindrical elements, since this number has been found to give results of sufficient accuracy in the analyses and to save considerable amount of computing time. To carry out the numerical integration of the equations involved, each bar element was divided into MxM = 49x49 grid elements. It should be made clear that the grid indication number M must be taken as an uneven number (e.g. M = 25, 49, 67, etc.) for the numerical integration of the equations to avoid stress singularities in the solutions. It is also noted that M = 49 was found to be satisfactory to produce sufficient accuracy in the numerical integrations, and was therefore used consistently throughout the theoretical analyses.

Using the computer program given in chapter 6, two types of analysis, namely elastic and elastic-plastic analyses, were carried out for the prediction of the bond stress distribution with load. To simulate the conditions in the tests and for direct comparison, the end bearing of the column bars was not considered in both types of analysis. The theoretical and experimental load-anchorage bond stress distribution curves are compared in a series of graphs given in figures (7.1a to e).

Figure (7.1a) shows a series of typical theoretical and experimental load-bond stress distribution curves along the anchorage length of

column bars in test S1-3. The bar stiffness factor, which is the measure of the compressibility of the bar, is very small, i.e. K = 7.75 in the test. The theoretical analysis therefore shows that the bond stress is a maximum on the first bar element at the top and minimum on the last element at the bottom region of the anchorage length. This is the general trend observed experimentally in all tests. From the figure in the elastic stage, both theoretical and experimental curves descend nonlinearly towards the bottom in the anchorage length. Up to a load of 120 kN the experimental records show slightly higher bond stress at the top than the theoretical values, with no bond stress recorded at the bottom part of the base. The theoretical curve indicates a bond stress on the last bar element in the base but it is very small. Beyond this stage, the theoretical values are higher than the experimental ones at the top, while experimental values are higher than theoretical ones in the middle part of the anchorage length as shown in the figure. However, the experimental curve does not record any bond stress at the bottom region of the base.

As a further step, the bond stress distribution at a load of 280 kN is shown in figure (7.1a). This is the load, beyond which no more experimental data was available due to the first effective slip. The theoretical analysis also shows that at that load the bond stress has reached to the ultimate value over the first bar element. Hence, no displacement compatibility exists between the steel and concrete in the first layer, resulting in slip of the bar in this layer. From the figure, the theoretical curve indicates greater bond stress in the upper part and smaller bond stress in the lower part of the anchorage length than that recorded by the experimental curve, except the experimental peak value at the top part of the base. The resulting

differences between these areas at the upper and lower parts of the anchorage length approximately balance. If the ratio of the theoretical bond stress to the experimental bond stress is considered on the bar elements, the mean value of this ratio is 0.951.

A series of theoretical and experimental load-anchorage bond stress distribution curves for test S1
the figure both curves indicate
are at the top and bottom parts
In the elastic stage, the theo
slightly higher than the experi
of the anchorage length, while
stress is slightly higher than
part of the anchorage length
load, the discrepancy between t
of the anchorage length gradually increases.

At a load of 360 kN, where the theoretical bond stress has reached the ultimate value on two bar elements (i.e. elastic-plastic case), the theoretical curve indicates greater values in the upper part and smaller values in the lower part of the anchorage length than that recorded by the experimental curve. The mean value of the ratio of the theoretical bond stress to the experimental bond stress for all bar elements is 0.975. At a load of 490 kN both curves indicate closer agreement and, the mean value of the ratio of the theoretical bond stress to the experimental bond stress is 0.992. Finally at a load of 560 kN, beyond which no more experimental data was available due to the first effective slip in the anchorage length, both curves are in close agreement. At the lower part of the anchorage length

both curves agree approximately, while the experimental curve indicates a peak at the top. It can also be seen from figure (7.1b) that on both curves bond stresses reduce to a very small magnitude at approximately the same location at the bottom part of the anchorage length. This effect was also observed by Ivering[77] in the elastic analysis of the tube anchorage in rock.

Load versus theoretical and experimental bond stress distributions along the anchorage length for test SR2-2 are shown in figure (7.1c). From the figure, the theoretical and experimental curves indicate that the bond stress is a maximum at the top and minimum at the bottom region of the anchorage length. In the elastic stage there is close agreement with the theoretical curve, the experimental curve records slightly higher bond stresses at the top and slightly smaller bond stresses at the bottom part of the base up to a load of 160 kN. After this load the theoretical values are greater at the upper part, while experimental values increase at a higher rate at the lower part of the anchorage length.

The theoretical and experimental bond stress curves are illustrated in figure (7.1c) for the loads of 360 kN, 465 kN and 540 kN, respectively, the latter being the load beyond which no experimental data was available due to the first slip. At these load stages, except that of the highest experimental bond stresses at the top part of the base, the theoretical values are greater at the upper part and smaller at the lower part of the anchorage length than those experimentally recorded. The mean ratio of the theoretical bond stress to the experimental bond stress is 0.977, 0.985 and 0.988 at loads of 360 kN, 465 kN and 540 kN, respectively.

Figure (7.1d) shows the theoretical and experimental load-bond stress distribution curves in test SR7-1, which included closely spaced links over the column bars in the base. From the figure both curves indicate that the maximum and minimum bond stresses are at the top and bottom parts of the anchorage length, respectively. In the elastic stage, both curves descend nonlinearly towards the bottom of the base and show similarity of shapes.However, the theoretical curve indicates higher values at the top and smaller values at the bottom part of the anchorage length than those recorded by the experimental curve.

In the elastic-plastic stage, the theoretical and experimental curves are shown at loads of 400 kN, 550 kN and 700 kN, respectively, the latter being the load stage beyond which the experimental data was not obtainable due to the first slip. The mean of the ratio of the theoretical bond stress to the experimental bond stress indicated by the curves shown in figure (7.1d) is 0.992, 0.975 and 1.022 at loads 400 kN, 550 kN and 700 kN, respectively.

Figure (7.1e) shows a series of theoretical and experimental load-bond stress distribution curves in test SR7-2, in which transverse reinforcement was introduced. From the figure, both curves indicate that the maximum bond stress is at the top near the column to base interface at each load step until first slip occurs. Both curves also show that the maximum bond stress at the top decreases downwards and becomes minimum at the bottom part of the anchorage length. In the elastic stage, the experimental curve records smaller values at the upper part and higher values at the lower part of the base than those indicated by the theoretical curve. In the elastic-plastic

stage the theoretical and experimental bond stress curves are also shown in figure (7.1e) at loads of 500 kN and 625 kN, the latter being the load beyond which first slip occurred. The mean value of the ratio of the theoretical bond stress to the experimental bond stress for the above loads is 0.973 and 0.978, respectively.

In the remainder of the tests the theoretical bond stress distribution along the anchorage length followed the same trend as already described in the preceding paragraphs. From the above observations it is concluded that the proposed theory predicts the bond stress distribution with reasonable accuracy by comparison with the experimental results. Bar stiffness factor K has a significant influence on the distribution of bond stress and, as K decreases the magnitude of the bond stress at the top part of the anchorage length increases.

It should be noted that by considering the end bearing of the bar, a separate series of computations were carried out. These solutions showed that the distribution of bond stress along the anchorage length is little different from that of distribution without end bearing. This may be attributed to the small bar stiffness factor K, i.e. the bar is compressible, so that only small stresses develop at the bottom part of the bar including the normal stress on the bar tip. As a result a small proportion of the load is transferred by the end of the bar. This effect was also observed by Mattes and Poulos[39] for compressible piles. However, to clarify that further experimental work with end bearing and further theoretical analysis are needed.

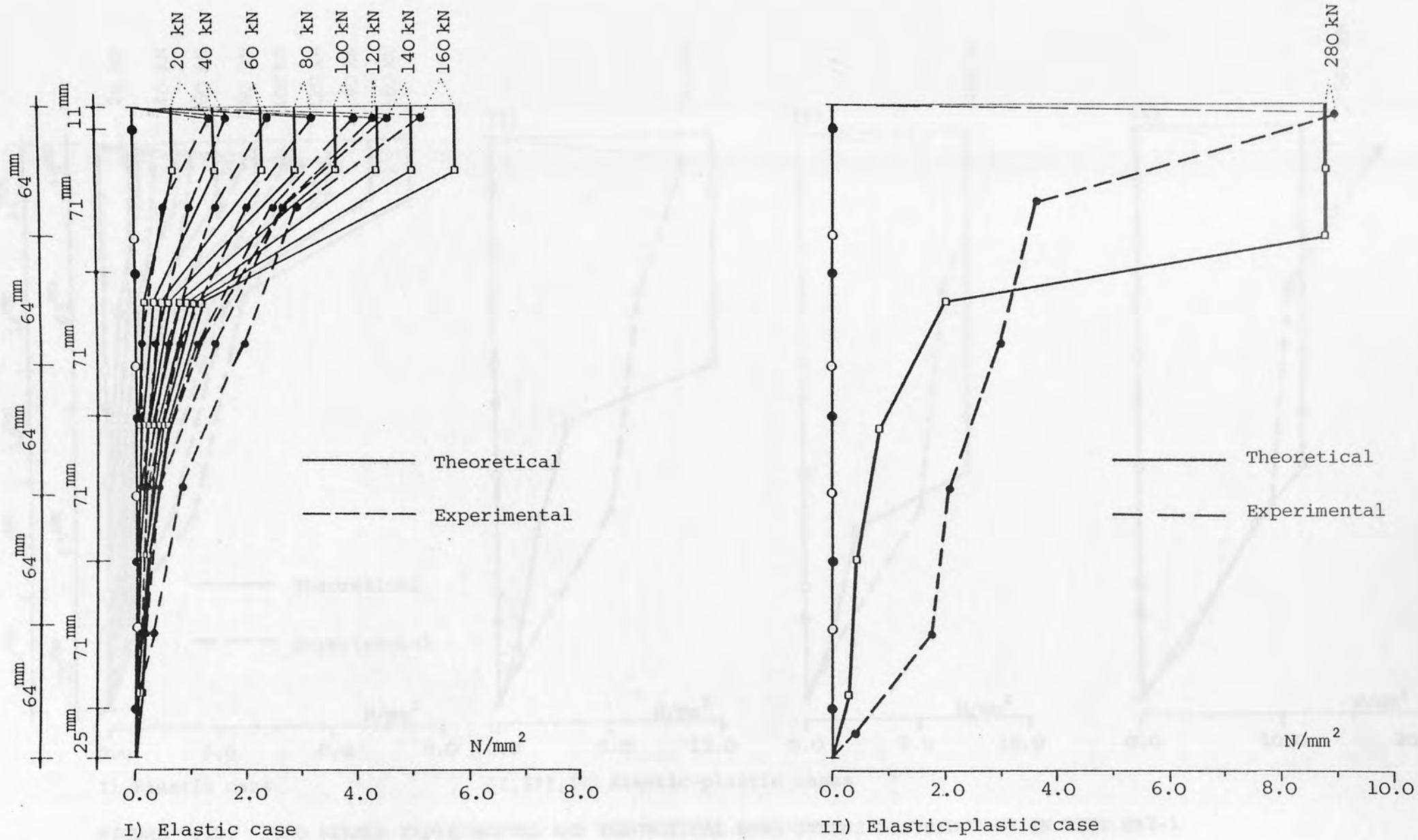

FIGURE 7.1a: LOAD VERSUS EXPERIMENTAL AND THEORETICAL BOND STRESS DISTRIBUTION IN TEST S1-3

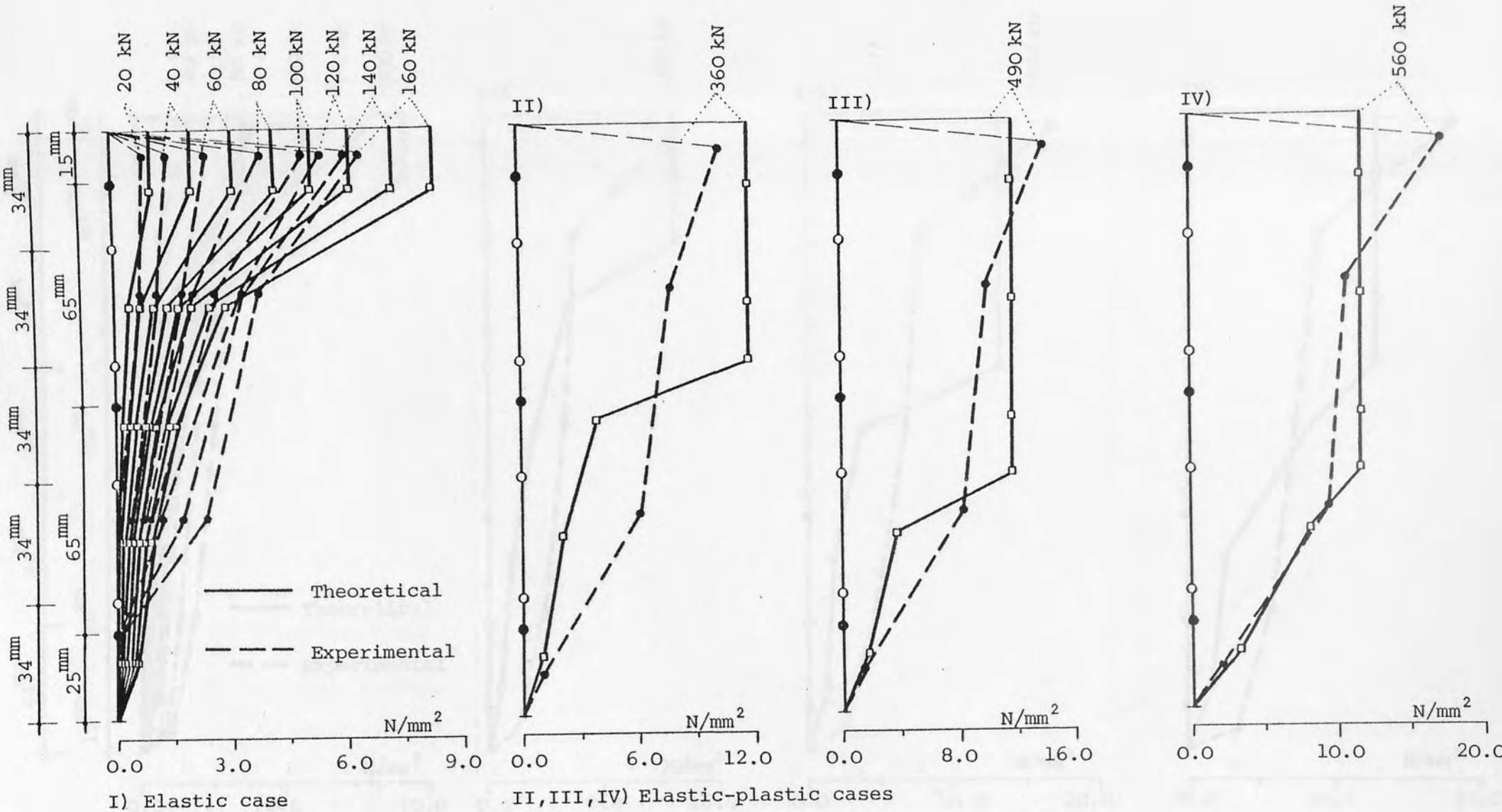

FIGURE 7.1b: LOAD VERSUS EXPERIMENTAL AND THEORETICAL BOND STRESS DISTRIBUTION IN TEST SR2-1

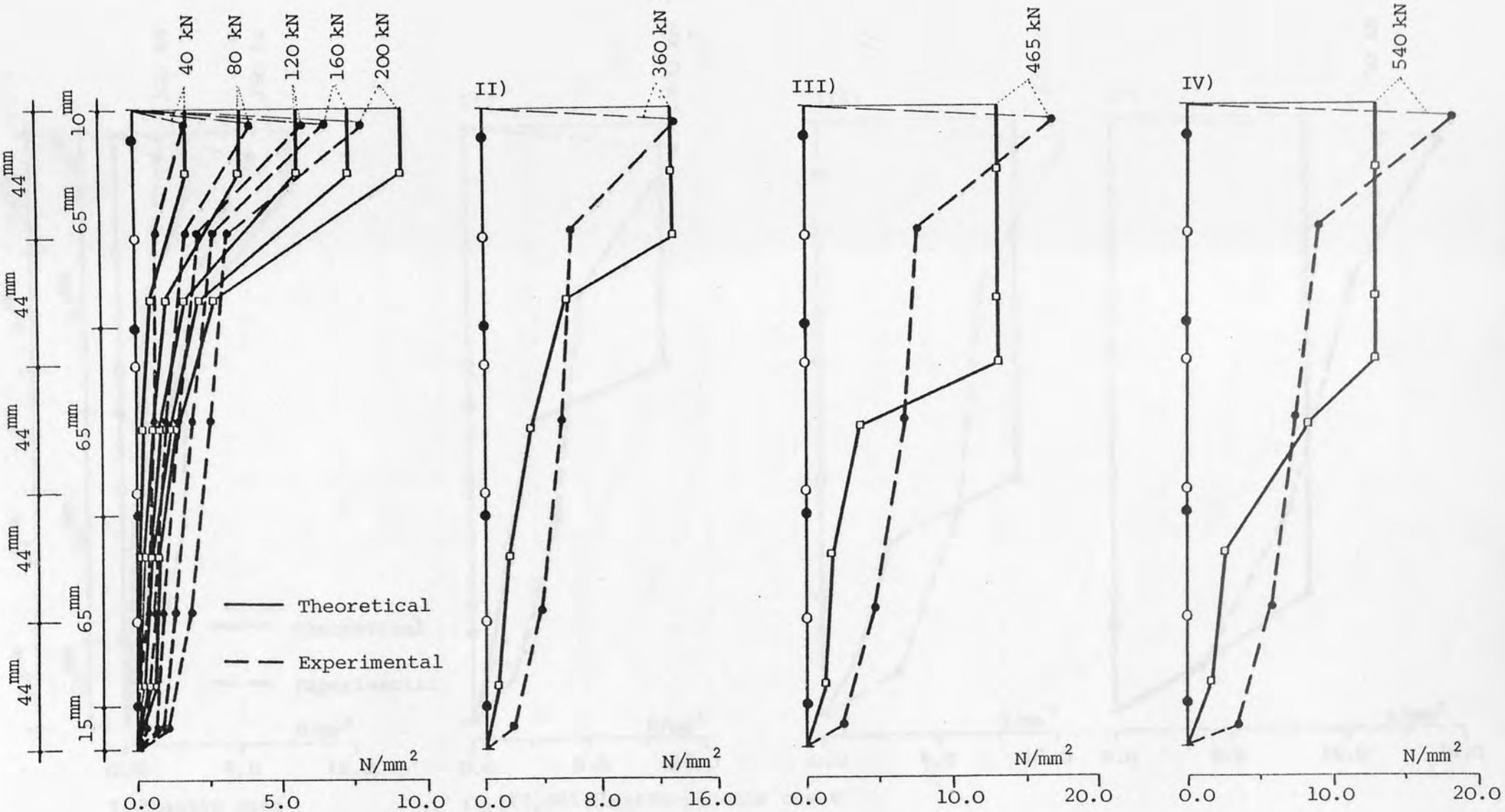

FIGURE 7.1c: LOAD VERSUS EXPERIMENTAL AND THEORETICAL BOND STRESS DISTRIBUTION IN TEST SR2-2

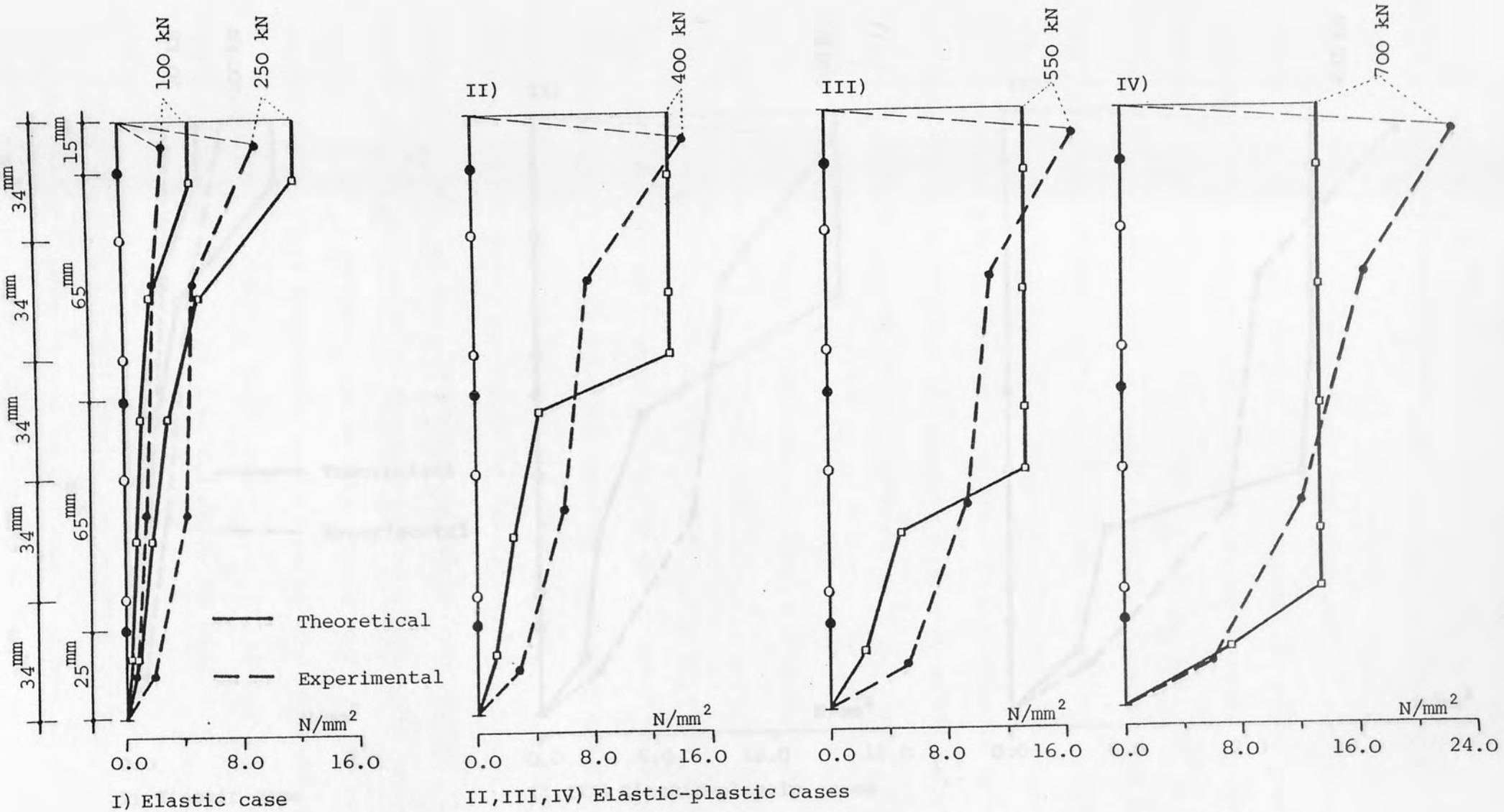

FIGURE 7.1d: LOAD VERSUS EXPERIMENTAL AND THEORETICAL BOND STRESS DISTRIBUTION IN TEST SR7-1

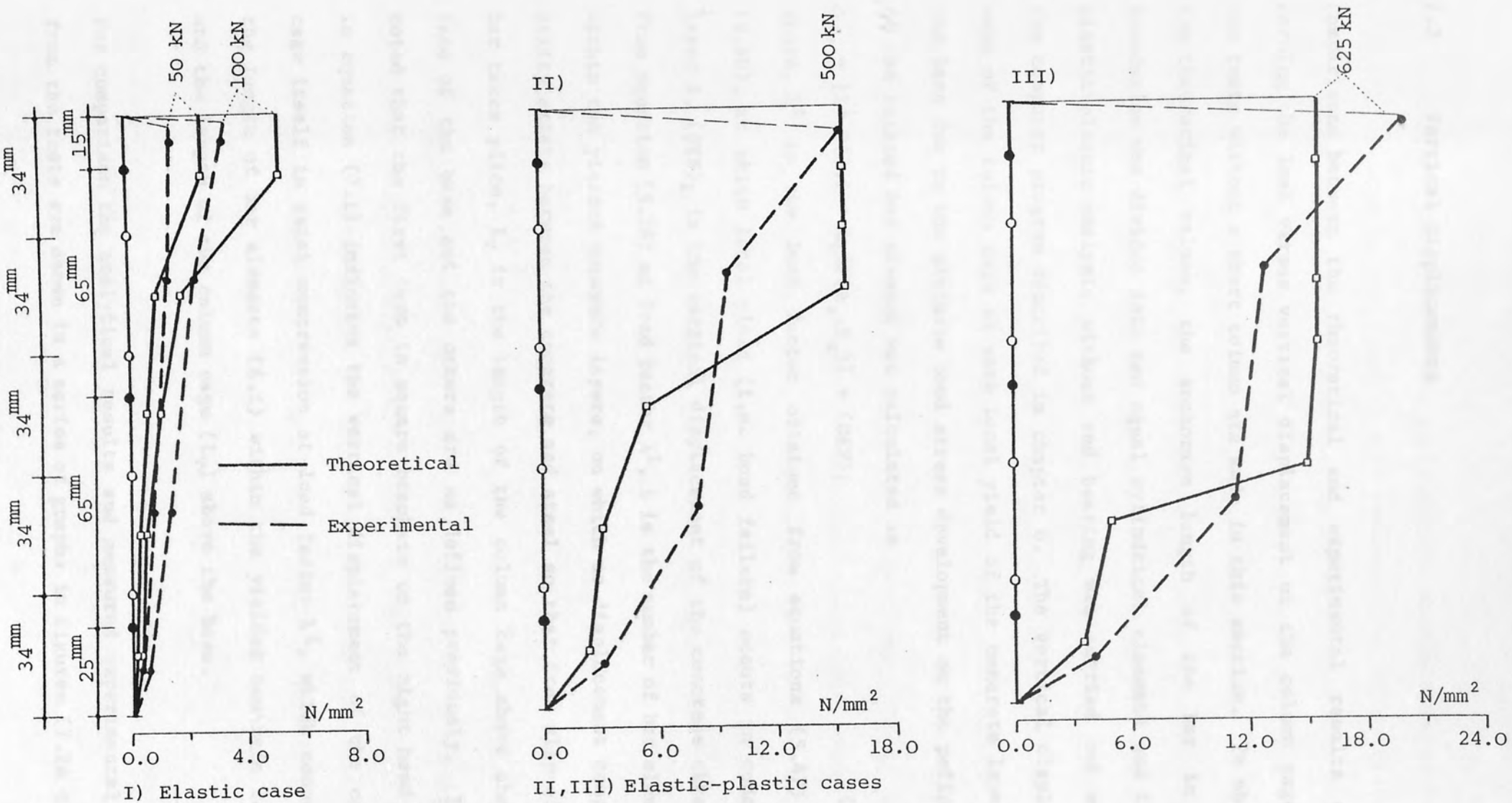

FIGURE 7.1e: LOAD VERSUS EXPERIMENTAL AND THEORETICAL BOND STRESS DISTRIBUTION IN TEST SR7-2

7.3 Vertical Displacements

Comparisons between the theoretical and experimental results concerning the load versus vertical displacement of the column cage in the tests without a short column are made in this section. To obtain the theoretical values, the anchorage length of the bar in the foundation was divided into ten equal cylindrical elements and then, elastic-plastic analysis without end bearing was carried out using the computer program described in chapter 6. The vertical displacement of the column cage at each local yield of the concrete layer in the base due to the ultimate bond stress development on the periphery of the related bar element was calculated as

$$\Delta_{sv} = [\lambda^i . P(\delta . i + l_v)/(A_s . E_s)] + (DEF)_i \qquad (7.1)$$

Where, λ^i is the load factor obtained from equations (5.47) and (5.50), at which local yield (i.e. bond failure) occurs in concrete layer i, $(DEF)_i$ is the vertical displacement of the concrete obtained from equation (5.16) at load factor λ^i, i is the number of bar elements within the yielded concrete layers, on which no displacement compatibility exists between the concrete and steel so that free slip of the bar takes place, l_v is the length of the column cage above the top face of the base and the others are as defined previously. It is noted that the first term in square brackets on the right hand side in equation (7.1) indicates the vertical displacement of the column cage itself in axial compression at load factor λ^i, which comprises the length of bar elements ($\delta . i$) within the yielded concrete layers and the length of the column cage (l_v) above the base.

For comparison the analytical results and measured experimental data from the tests are shown in a series of graphs in figures (7.2a to e.)

The experimental and theoretical load-vertical displacement curves for the column cage in test specimen S1-3 are shown in figure (7.2a). Test S1-3 used 25 mm square twisted bars as column longitudinal reinforcement in the foundation. It can be seen from the figure that the experimental curve is slightly steeper than the theoretical one and, both curves almost match each other with the loading up to approximately one-third of the experimental failure load. At this stage of the applied load, it was experimentally observed that first effective slip of the column bars took place along the anchorage length of the foundation as described in chapter 3. On the other hand, the theoretical analysis shows that first two upper-most concrete layers in the foundation have produced local yield due to the ultimate bond stress development on the related bar elements as seen from the theoretical curve in the figure. Consequently slip of the column bars takes place in these layers while the vertical displacement compatibility between the steel and the concrete holds for the rest of the elastic layers.

As already discussed in the previous section, since the bar stiffness factor K is very small, i.e. the bar is compressible in relation to the surrounding concrete, high bond stresses develop on the bar element within the uppermost concrete layer of the base. The first local yield therefore starts in this concrete layer and continues progressively downward with loading in the remainder of elastic layers towards the bottom.

After the one-third of the failure load, the experimental curve is less steep with larger displacements than the theoretical curve. Through successive loading stages until failure the curves progres-

sively diverge as the experimental curve indicates excessive vertical displacements, at an increasing rate, with loading, as seen from figure (7.2a). The large slip recording by the experimental curve can be attributed to the poor slip characteristics of the square twisted bars. According to the theoretical analysis, the slip of the column bars can only take place within the yielded concrete layers due to the loss of displacement compatibility between the steel and concrete in these layers. On the other hand, because of the poor slip characteristics of the square twisted bar the early slip of column longitudinal reinforcement occurs within the whole anchorage length and continues with increasing rate until the ultimate load. The theoretical analysis shows that at the failure load the vertical displacement compatibility between the steel and concrete is entirely lost due to the ultimate bond stress development on the bar shaft. Hence full slip of the bars occurs in the anchorage length of the foundation. The experimental curve also indicates that major slip takes place at the ultimate load.

In the rest of the tests with square twisted bars the load-vertical displacement curves followed the same trend as already described in the preceding paragraphs. From the above observations it is deduced that the theoretical analysis yields conservative vertical displacement values for square twisted bars between the first effective slip and the failure loads.

In contrast, it is shown below that the agreement between theoretically predicted and experimentally measured values for ribbed bars is satisfactory in regard to the vertical displacements.

Figure (7.2b) indicates the theoretical and experimental vertical displacements plotted against the applied load for test SR2-1, which used 25 mm ribbed bars in plain concrete base. It can be seen from the figure that the load-vertical displacement curves do not show any significant change and almost match each other near to the ultimate load. Up to two-thirds of the experimental failure load, the experimental curve is slightly steeper than the theoretical one. Beyond this stage the theoretical curve becomes steeper as the experimental curve diverges close to the failure. However, the value of the vertical displacement indicated by the experimental curve is insignificantly different in numerical terms than the theoretical values. Finally, the experimental curve records a very large amount of slip indicating the failure of the test. At the ultimate load, the theoretical curve also shows that as the displacement compatibility is lost between the steel and concrete, due to the ultimate bond stress development all over the bar elements, full slip occurs in the anchorage length of the foundation.

A comparison of the theoretical and experimental load-vertical displacement diagrams for test SR2-2, which varied the anchorage length of the column reinforcement in the base, is made in figure (7.2c). From the figure, both curves ascend through the loading sequence and, the theoretical curve indicates slightly over estimated values compared with the experimental one up to approximately 60% of the experimental failure load. Beyond this stage, the experimental curve becomes gradually flatter with loading, but the displacements are relatively small close to the failure. Eventually, the curve shows that major slip takes place at the ultimate load. The theoretical curve also shows that as the failure load is approached full

slip occurs in the foundation.

The theoretical and experimental load-vertical displacement curves for the column cage in test SR7-1 is shown in figure (7.2d). In test SR7-1 the column bars were confined along the anchorage length by the links. It can be seen from the figure that both curves almost match each other, the experimental curve being slightly steeper than the theoretical one, up to approximately two-thirds of the failure load. Then, the experimental curve gradually diverges close to the failure. The experimental curve also shows that major slip occurs at the ultimate load. When the theoretical failure load is approached, full slip of the column bars in the anchorage length is attained as shown in the figure.

Figure (7.2e) shows the theoretical and the experimental vertical displacement of the column bars with respect to the applied load for test SR7-2, which included tension reinforcement in the base and one link around the column bars in the anchorage length. From the figure, both curves agree without any significant change, from zero to nearly half the ultimate load. Then, the theoretical curve becomes steeper as the experimental curve gradually diverges with loading. However, the difference between the theoretical and experimental values is not significant near to the failure load. Finally, both curves indicate that full slip of the bars occurs in the anchorage length of the foundation at the ultimate load shown in the figure.

From the comparison of the theoretical and experimental results it is concluded that the proposed theoretical method predicts with a reasonable degree of accuracy the vertical displacement of ribbed bars.

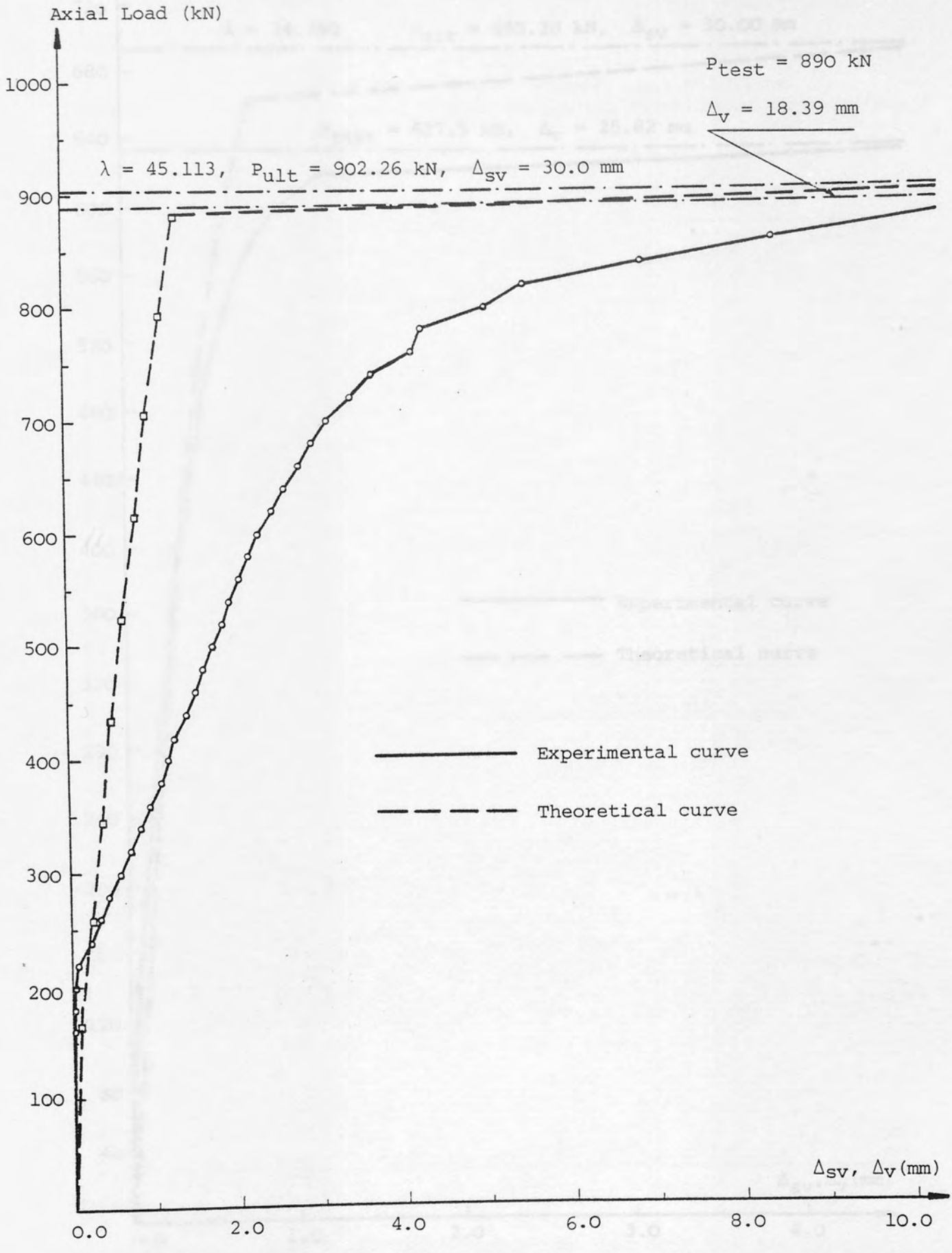

FIGURE 7.2a: THEORETICAL AND EXPERIMENTAL LOAD-VERTICAL DISPLACEMENT CURVES FOR THE COLUMN CAGE IN TEST S1-3

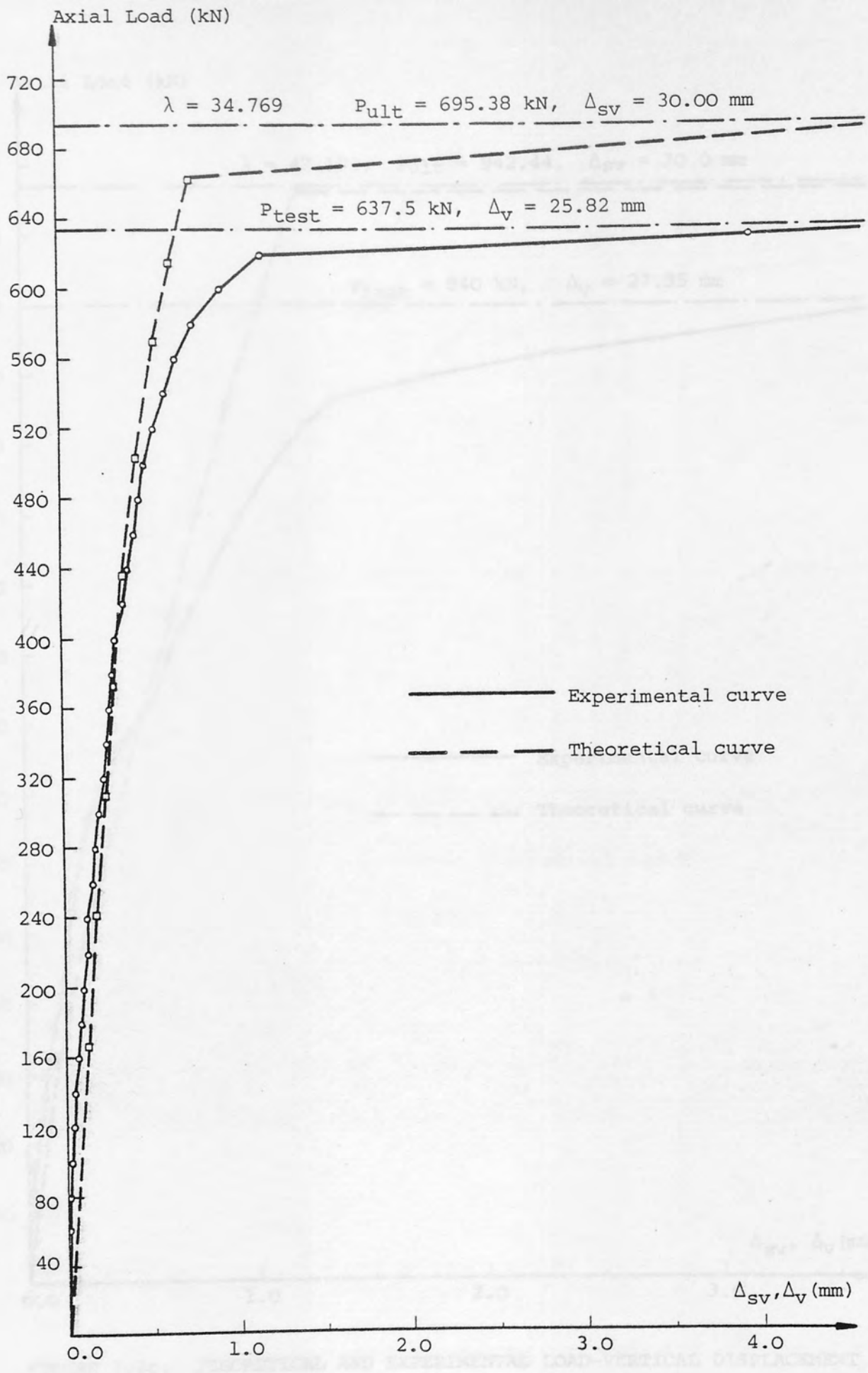

FIGURE 7.2b: THEORETICAL AND EXPERIMENTAL LOAD-VERTICAL DISPLACEMENT CURVES FOR THE COLUMN CAGE IN TEST SR2-1

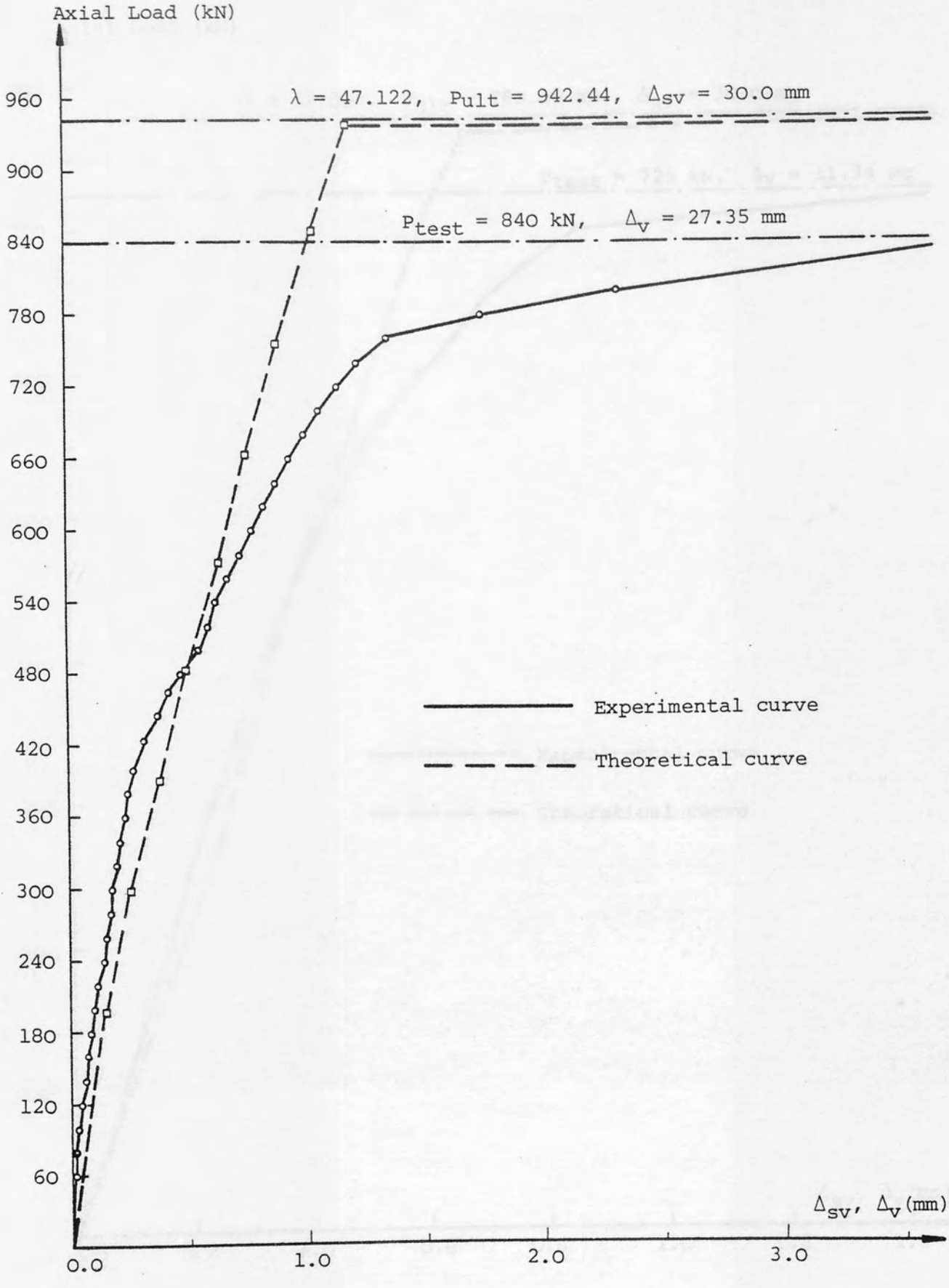

FIGURE 7.2c: THEORETICAL AND EXPERIMENTAL LOAD-VERTICAL DISPLACEMENT CURVES FOR THE COLUMN CAGE IN TEST SR2-2

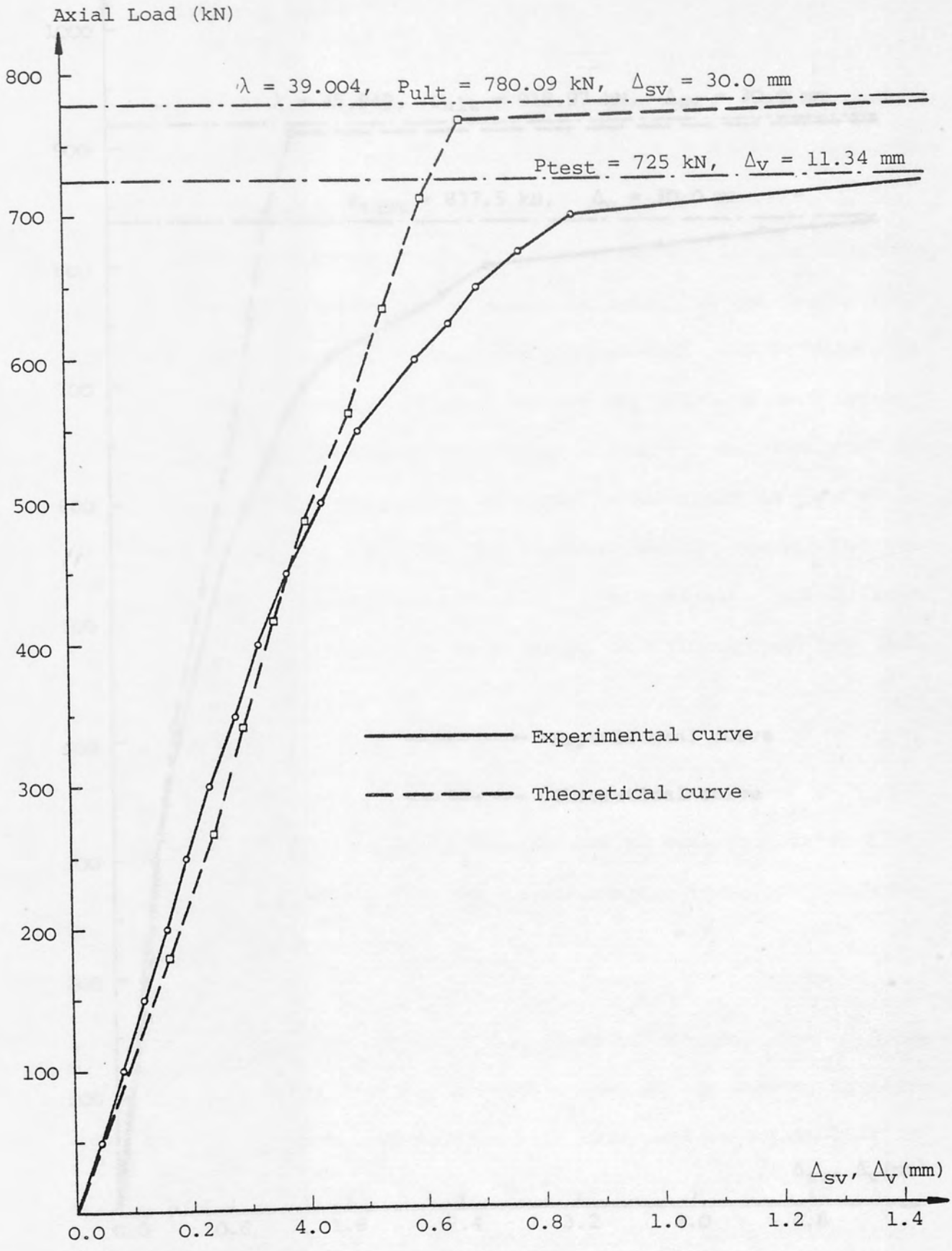

FIGURE 7.2d: THEORETICAL AND EXPERIMENTAL LOAD-VERTICAL DISPLACEMENT CURVES FOR THE COLUMN CAGE IN TEST SR7-1

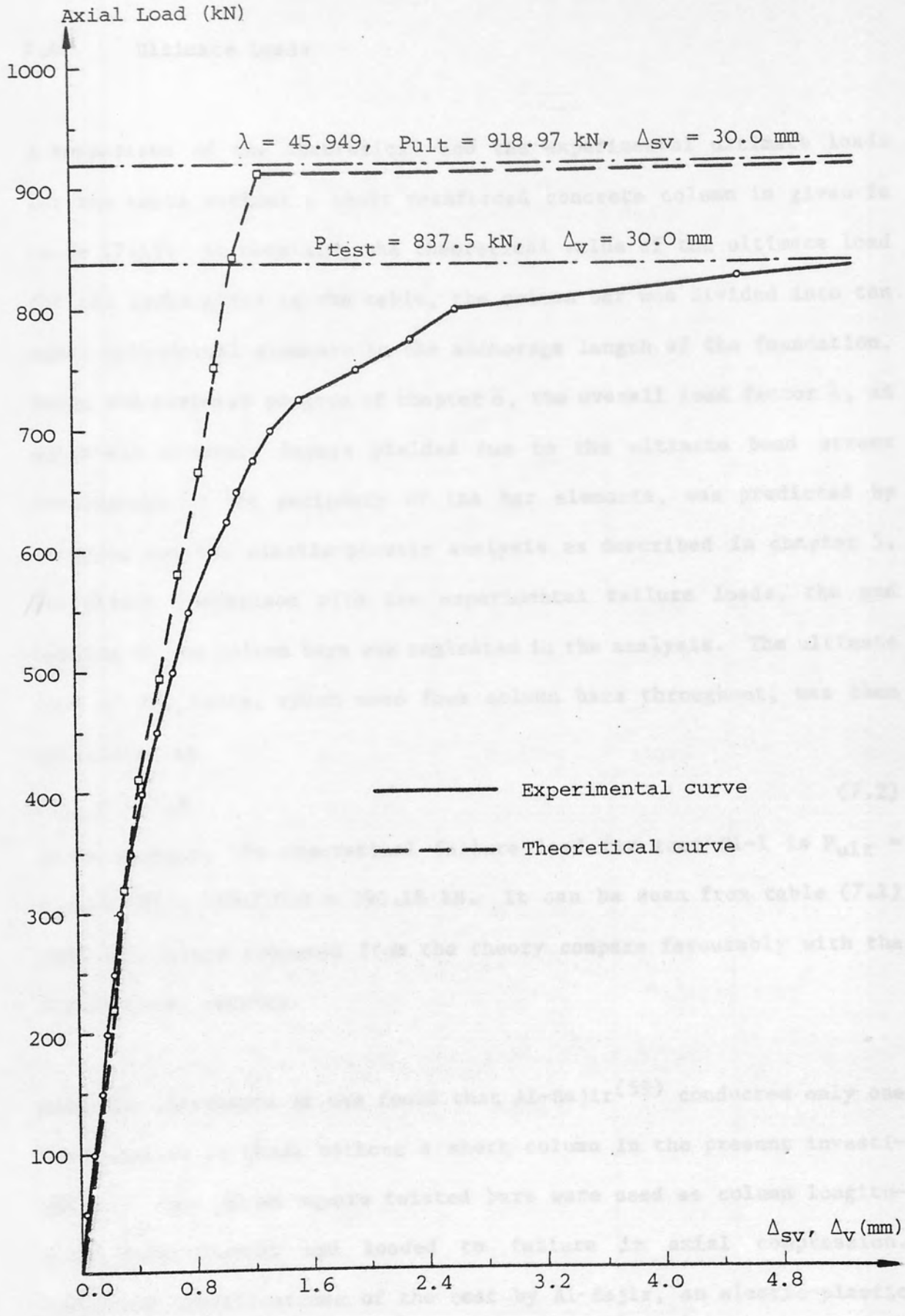

FIGURE 7.2e: THEORETICAL AND EXPERIMENTAL LOAD-VERTICAL DISPLACEMENT CURVES FOR THE COLUMN CAGE IN TEST SR7-2

7.4 Ultimate Loads

A comparison of the theoretical and the experimental ultimate loads for the tests without a short reinforced concrete column is given in table (7.1). In obtaining the theoretical value of the ultimate load for the tests given in the table, the column bar was divided into ten equal cylindrical elements in the anchorage length of the foundation. Using the computer program of chapter 6, the overall load factor λ, at which all concrete layers yielded due to the ultimate bond stress development on the periphery of the bar elements, was predicted by carrying out the elastic-plastic analysis as described in chapter 5. For direct comparison with the experimental failure loads, the end bearing of the column bars was neglected in the analysis. The ultimate load of the tests, which used four column bars throughout, was then calculated as

$$P_{ult} = 4.\lambda.p \qquad (7.2)$$

As an example, the theoretical failure load for test S1-1 is P_{ult} = 4 x 19.809 x 5000/1000 = 396.18 kN. It can be seen from table (7.1) that the values computed from the theory compare favourably with the experimental results.

From the literature it was found that Al-Sajir[59] conducted only one test similar to those without a short column in the present investigation. Four 20 mm square twisted bars were used as column longitudinal reinforcement and loaded to failure in axial compression. Using the specifications of the test by Al-Sajir, an elastic-plastic analysis by the proposed theory yields the theoretical ultimate load approximately equal to the experimentally obtained value as seen in table (7.2).

Test Specimen No.	Experimental Ultimate Load P_{test}	Theoretical Ultimate Load P_{ult}	$\frac{P_{test}}{P_{ult}}$
	kN	kN	
S1-1	397.50	396.18	1.003
S1-2	590.00	581.02	1.015
S1-3	890.00	902.26	0.986
$\overline{S1}$-3	900.00	911.06	0.988
S2-1	720.00	700.45	1.028
$\overline{S2}$-1	710.00	688.53	1.031
S2-2	800.00	830.20	0.964
$\overline{S2}$-2	805.00	819.96	0.982
S2-3	885.00	905.28	0.978
S2-4	565.00	586.94	0.963
S3-1	870.00	876.28	0.993
S3-2	920.00	869.52	1.058
SR1-1	365.00	378.50	0.964
SR1-2	543.75	527.02	1.032
SR1-3	1400.00	1407.10	0.995
SR2-1	637.50	695.38	0.917
SR2-2	840.00	942.44	0.891
SR3-1	1125.00	1144.41	0.983
SR4-1	1400.00	1428.68	0.980
SR4-2	1450.00	1530.71	0.947
SR4-3	1575.00	1595.94	0.987

TABLE 7.1: COMPARISON OF EXPERIMENTAL AND THEORETICAL FAILURE LOADS

Test Specimen No.	Experimental Ultimate Load P_{test}	Theoretical Ultimate Load P_{ult}	$\frac{P_{test}}{P_{ult}}$
	kN	kN	
SR5-1	1525.00	1567.68	0.973
SR5-2	1500.00*	1656.78	0.905
SR6-2	650.00	708.68	0.917
SR6-3	680.00	755.86	0.900
SR6-4	756.25	820.02	0.922
SR7-1	725.00	780.09	0.929
SR7-2	837.50	918.97	0.911
SR8-1	525.00	616.68	0.851
SR8-2	487.50	573.18	0.881
SR8-3	575.00	631.38	0.911
SR8-4	667.50	719.58	0.928
Mean			0.961
Coefficient of variation %			5.28

*: indicates no bond failure in the base

TABLE 7.1: [continued]

Test No.	Bar Size ϕ	Anchorage Length l_a	Young's Modulus E_s	Young's Modulus E_c	Poisson's Ratio ν_c	Experimental Ultimate Load P_{test}	Theoretical Ultimate Load P_{ult}	$\frac{P_{test}}{P_{ult}}$
	mm	mm	kN/mm^2	kN/mm^2		kN	kN	
Pilot Specimen	20	300	207.00	24.20	0.135	525.00	528.00	0.994

TABLE 7.2: COMPARISON OF EXPERIMENTAL RESULTS BY AL-SAJIR(59)

By considering the end bearing of the column longitudinal reinforcement in the foundation, further theoretical solutions were carried out for a number of tests. These results indicated, as an average, only a 7% increase at the ultimate load by comparison to the theoretical failure load without end bearing. However, in the analysis the ultimate end bearing resistance was taken as the concrete compressive strength as described in chapter 5. This is a crude estimate on the conservative side. However, due to the absence of experimental data, it was uncertain whether the concrete cover under the bar in the foundation could allow the failure cone to develop, which results in much higher end bearing resistance than currently used in these computations. Therefore, further tests with end bearing and on the basis of the test results, further theoretical work with the assessment of more realistic ultimate end bearing resistance, are required.

7.5 Comparison with Current Codes

In this section the experimental results are compared with British code CP110[56] and American code ACI318-77[61]. In both codes the design ultimate bond stresses vary with the square root of the concrete compressive strength and, CP110 uses standard cubes while ACI318-77 employs standard cylinders, as the main control test to determine the concrete characteristic strength.

In CP110, the ultimate anchorage bond stresses with respect to the concrete grade for Type 1 (square twisted) and Type 2 (ribbed) deformed bars are given in table 22 and, the code allows 30% increase in the bond stress for Type 2 reinforcing steel. Considering 30% increase in the values of bond stress for Type 2 bars, the bond stresses given

for both types of reinforcement in CP110 may be expressed as follows.

CP110 $f_{bs} = 0.60\ (\sqrt{f_{cu}} - 1)$, for Type 1 (square twisted) bar (7.3)

CP110 $f_{bs} = 0.78\ (\sqrt{f_{cu}} - 1)$, for Type 2 (ribbed) bar (7.4)

To determine the bond stresses due to the American code ACI318-77 the following procedure was employed. The SI formula given for the anchorage or the development length of a bar in ACI318-77 is

$$l_a = (0.24\ f_y \phi)/\sqrt{f_{cy}} \quad (7.5)$$

On the other hand, the ultimate design load (P_u) for a single bar in bond is

$P_u = f_{bs}\ \pi\ \phi\ l_a$, then $l_a = P_u/(f_{bs}\ \pi\ \phi\ )$

Hence, substituting for l_a in equation (7.5) and rearranging gives

$f_{bs} = P_u\sqrt{f_{cy}}/[0.24\ f_y(\pi\phi^2/4)4]$

Then, taking $P_u = (\pi\phi^2/4)f_y$ for a single bar and $f_{cy} = 0.83\ f_{cu}$, which was obtained for all groups of tests as the mean, it follows that

$$\text{ACI } f_{bs} = 0.949\sqrt{f_{cu}} \quad (7.6)$$

A comparison of experimental results with British code CP110 and American code ACI318-77 is shown in table (7.3). In the table, the values of bond stress according to CP110 for square twisted and ribbed bars were calculated from equations (7.3) and (7.4), respectively, while the bond stresses according to ACI318-77 were calculated from the equation (7.6) for both types of reinforcement. Using the design ultimate bond stresses, the required anchorage lengths due to CP110 and ACI318-77 to produce the same ultimate load in the tests are also given in the table. From an examination of the table (7.3) it is observed that allowable bond stresses in both codes are significantly

below the ultimate bond stresses obtained from the tests and, the value of bond stress specified by CP110 is consistently lower than that given by ACI318-77. Consequently, excessive anchorage lengths are needed according to the British code. The American code, to a lesser extent, also leads to large anchorage lengths and this effect is particularly noticeable for ribbed bars. It is noted that the bond stresses given for the tests in groups X and XI are not the ultimate but the average bond stresses developed in the base close to the failure of the column. The bond stress indicated for test SR5-2 is also the average bond stress at the failure of the column cage. Excluding these tests, the mean value of the ratio of CP110 required l_a to the test l_a and ACI318-77 l_a to the test l_a is 3.34 and 2.08 with the coefficient of variation 16.08% and 24.02%, respectively.

To show the effect of variables on the bond strength, the ultimate anchorage bond stresses are also compared with the allowable bond stresses given by CP110 and ACI318-77 in figures (7.3) to (7.7).

The test results related to the bar size for test groups I and IV are compared with CP110 and ACI318-77 in figure (7.3). The mean concrete compressive strength for all tests in both groups is f_{cu} = 34.4 N/mm^2 and the average yield stress of column reinforcement, excluding test SR2-1, is f_y = 459 N/mm^2. The yield stress of column bars in test SR2-1 was significantly higher than the average yield stress (see table (3.2) for reference), and therefore, was not taken into account because its inclusion would more than double the standard deviation obtained when averaging the yield stresses for the other six tests. The bond stress required to achieve average yield stress in column reinforcement is plotted against bar size using the mean concrete

Group	Test No.	Present work (1)		CP110 (2)		ACI318-77 (3)		$\frac{l_a(2)}{l_a(1)}$	$\frac{l_a(3)}{l_a(1)}$
		$f_{bsav.}$	l_a	f_{bs}	req'd. l_a	f_{bs}	req'd. l_a		
		N/mm^2	mm	N/mm^2	mm	N/mm^2	mm		
I	S1-1	6.178	320	2.992	661	5.681	348	2.07	1.09
	S1-2	7.336	320	2.928	802	2.578	421	2.51	1.32
	$\overline{S}$1-3	8.853	320	2.993	946	5.682	499	2.96	1.56
	S1-3	8.952	320	3.075	932	5.811	493	2.91	1.54
II	S2-4	10.579	170	3.071	586	5.805	310	3.45	1.82
	S2-1	10.417	220	3.065	748	5.795	396	3.40	1.80
	$\overline{S}$2-1	10.273	220	2.979	759	5.661	399	3.45	1.81
	S2-2	9.431	270	3.060	832	5.788	440	3.08	1.63
	$\overline{S}$2-2	9.49	270	3.056	838	5.782	443	3.10	1.64
	S1-3	8.853	320	2.993	946	5.682	499	2.96	1.56
	$\overline{S}$1-3	8.952	320	3.075	932	5.811	493	2.91	1.54
	S2-3	7.614	370	2.852	988	5.455	517	2.67	1.40
III	S3-1	8.654	320	2.910	952	5.549	499	2.98	1.56
	S1-3	8.853	320	2.993	946	5.682	499	2.96	1.56
	$\overline{S}$1-3	8.952	320	3.075	932	5.811	493	2.91	1.54
	S3-2	9.151	320	2.911	1006	5.551	528	3.14	1.65
IV	SR1-1	10.679	170	3.616	502	5.348	340	2.95	2.00
	SR1-2	12.727	170	3.654	592	5.394	401	3.48	2.36
	SR2-1	11.937	170	3.698	549	5.448	373	3.23	2.19

TABLE 7.3: COMPARISON OF THE EXPERIMENTAL RESULTS WITH BRITISH CODE CP110 & AMERICAN CODE ACI318-77

Group	Test No.	Present work (1)		CP110 (2)		ACI318-77 (3)		$\frac{l_a(2)}{l_a(1)}$	$\frac{l_a(3)}{l_a(1)}$
		$f_{bsav.}$	l_a	f_{bs}	req'd. l_a	f_{bs}	req'd. l_a		
		N/mm^2	mm	N/mm^2	mm	N/mm^2	mm		
V	SR2-1	11.937	170	3.698	549	5.448	373	3.23	2.19
	SR2-2	12.154	220	3.815	701	5.591	478	3.19	2.17
	SR1-3	13.926	320	3.572	1248	5.295	842	3.90	2.63
VI	SR3-1	11.191	320	3.799	943	5.572	643	2.95	2.01
	SR1-3	13.926	320	3.572	1248	5.295	842	3.90	2.63
VIIa	SR1-3	13.926	320	3.572	1248	5.295	842	3.90	2.63
	SR4-1	13.926	320	3.535	1261	5.250	849	3.94	2.65
	SR4-2	14.423	320	3.578	1290	5.303	870	4.03	2.72
	SR4-3	15.667	320	3.441	1457	5.136	976	4.55	3.05
VIIb	SR2-1	11.937	170	3.698	549	5.448	373	3.23	2.19
	SR6-2	12.171	170	3.815	543	5.590	370	3.19	2.18
	SR6-3	12.732	170	3.610	600	5.341	405	3.53	2.38
	SR6-4	14.160	170	3.634	663	5.370	448	3.90	2.64
VIIIa	SR1-3	13.926	320	3.572	1248	5.295	842	3.90	2.63
	SR5-1	15.169	320	3.449	1408	5.146	943	4.40	2.95
	SR5-2	14.911*	320	3.687	1295	5.435	879	4.05	2.75
VIIIb	SR2-1	11.937	170	3.698	549	5.448	373	3.23	2.19
	SR7-1	13.576	170	3.671	629	5.415	426	3.70	2.51
	SR7-2	15.681	170	3.678	725	5.424	492	4.26	2.89
IX	SR2-1	11.937	170	3.698	549	5.448	373	3.23	2.19
	SR8-1	9.830	170	3.163	528	4.798	348	3.11	2.05
	SR8-2	9.128	170	2.870	541	4.441	350	3.18	2.06
	SR8-3	10.766	170	3.334	549	5.005	366	3.23	2.15
	SR8-4	12.498	170	3.906	544	5.702	373	3.20	2.19

TABLE 7.3: [continued]

Group	Test No.	Present work (1)		CP110 (2)		ACI318-77 (3)		$\frac{l_a(2)}{l_a(1)}$	$\frac{l_a(3)}{l_a(1)}$
		$f_{bsav.}$	l_a	f_{bs}	req'd. l_a	f_{bs}	req'd. l_a		
		N/mm^2	mm	N/mm^2	mm	N/mm^2	mm		
X	SR9-1	6.099≠	170	3.273	317	4.931	210	1.86	1.24
	SR9-2	4.753≠	170	3.436	235	5.130	158	1.38	0.93
XI	SR9-1	6.099≠	170	3.273	317	4.931	210	1.86	1.24
	SR10-1	7.265≠	170	3.367	367	5.046	245	2.16	1.44
	SR10-2	7.359≠	170	3.695	339	5.444	230	1.99	1.35
Mean								3.34	2.08
Coefficient of variation %								16.08	24.02

Notes:
*: No bond failure in the base.
≠: Values in the base close to column failure, and no bond failure in the base.

TABLE 7.3: [continued]

compressive strength for two anchorage lengths, namely, 170 mm for ribbed bars and 320 mm for square twisted bars as shown in figure (7.3). For comparison the values from CP110 and ACI318-77 are also shown on the same graph. It can be seen from figure (7.3) that both codes do not consider the effect of bar size on the bond strength. However, it is evident from the figure that the bond strength increases with increasing the bar size, this relationship being linear for square twisted bars but not ribbed bars, as discussed in detail before, in chapter 4. This effect, i.e. an increase in the bond strength with the increase of bar size, was also observed by Ferguson and Breen[31] in tensile lapped splices in beams. It can also be observed from the figure that CP110 gives design bond stresses significantly below the ultimate bond stresses found in the tests. ACI318-77 also gives significantly low design stresses for ribbed bars, while this effect is less pronounced for square twisted bars.

A comparison of the test results with CP110 and ACI318-77 is shown in figure (7.4) for the tests related to the anchorage length in groups II and V. The mean concrete compressive strength for all tests involved is f_{cu} = 35.44 N/mm^2 and the average yield stress of column reinforcement, excluding the bars in tests SR2-1 and SR2-2, is f_y = 446 N/mm^2. The values of the yield stress for the reinforcement in tests SR2-1 and SR2-2 were very high (see table (3.2) for reference) so that if they were included the standard deviation would be increased form 2.6% to 8.9%. The bond stress required to produce the yield stress of 446 N/mm^2 and 425 N/mm^2 for a given anchorage length is calculated and then, the values of $f_{bs}/\sqrt{f_{cu}}$ are obtained by using the mean concrete strength and plotted against the anchorage length as shown in figure (7.4). Using the mean concrete strength, the values

of $f_{bs}/\sqrt{f_{cu}}$ given by CP110 and ACI318-77 are also indicated in the figure. It is readily seen from the figure that both codes do not consider the effect of the anchorage length upon the bond strength. However, the ultimate bond stress varies with the anchorage length of the column bars in the base. This relationship is nonlinear for ribbed bars but linear for square twisted bars and, the bond stress decreases with increasing the anchorage length as discussed before in chapter 4. A number of investigators[8,26,29,32] have also observed that the ultimate bond stress decreases as the embedment length of the bars is increased. It can also be seen from figure (7.4) that the allowable design bond stresses specified by CP110 and ACI318-77 are significantly lower than the values indicated by the tests.

The tests results varying the ratio of unloaded base area to column core area A_b/A_{core} in groups III and VI are compared with CP110 and ACI318-77 in figure (7.5). A number of researchers[22,23,34] showed that the bearing strength of concrete increases with increasing the ratio of unloaded area to loaded area. Astill and Al-Sajir[76] also observed that increasing the ratio of unloaded base area to column area improved the bond strength. From the figure (7.5), an increase in the ratio A_b/A_{core} allows a small increase in the ultimate bond stress for square twisted bars loaded up to the yield stress. On the other hand, for the two tests with ribbed bars loaded beyond the yield stress an increase in the ratio A_b/A_{core} leads to very significant increase in the bond stress as discussed in chapter 4. The mean compressive strength of the concrete and the average yield stress of column reinforcement for all tests involved is f_{cu} = 34.56 N/mm^2, and f_y = 454.6 N/mm^2, respectively. The bond stress required to achieve yield in the column bars is calculated for the anchorage

length of 320 mm and, using the mean concrete strength the yield stress line is plotted in figure (7.5). CP110 and ACI318-77 values are also plotted using the mean concrete strength. It can be seen from the figure that the design bond stresses given by CP110 are significantly below the bond stresses found in the tests. Contrary to the finding by Astill and Al-Sajir[76] the bond stresses indicated by the tests are not smaller but significantly greater than the values given by ACI318-77.

The test results showing the effect of transverse reinforcement upon the anchorage bond strength are compared with CP110 and ACI318-77 in figure (7.6) for groups VIIa, VIIb, VIIIa and VIIIb. As discussed in chapter 4, the provision of the transverse reinforcement - base tension reinforcement, links around the compression bars within the base thickness or the presence of both - produces a significant increase in the ultimate bond stress. However, both codes do not make any allowance in the design bond stress for the inclusion of such reinforcement in the base. The mean concrete compressive strength for all the tests shown is f_{cu} = 31.75 N/mm^2 and the average yield stress of column reinforcement, excluding the bars in test SR2-1, is f_y = 410 N/mm^2. The bond stress required to produce yield in the column bars is calculated for a given anchorage length. Then using the mean concrete strength, the values of $f_{bs}/\sqrt{f_{cu}}$ are found and the yield stress lines are plotted for two different anchorage lengths of 170 mm and 320 mm as shown in figure (7.6). It can be seen from the figure that the design bond stresses given by CP110 and ACI318-77 are significantly lower than the bond stresses indicated by these test results using ribbed bars with a bond length of either 170 mm or 320 mm.

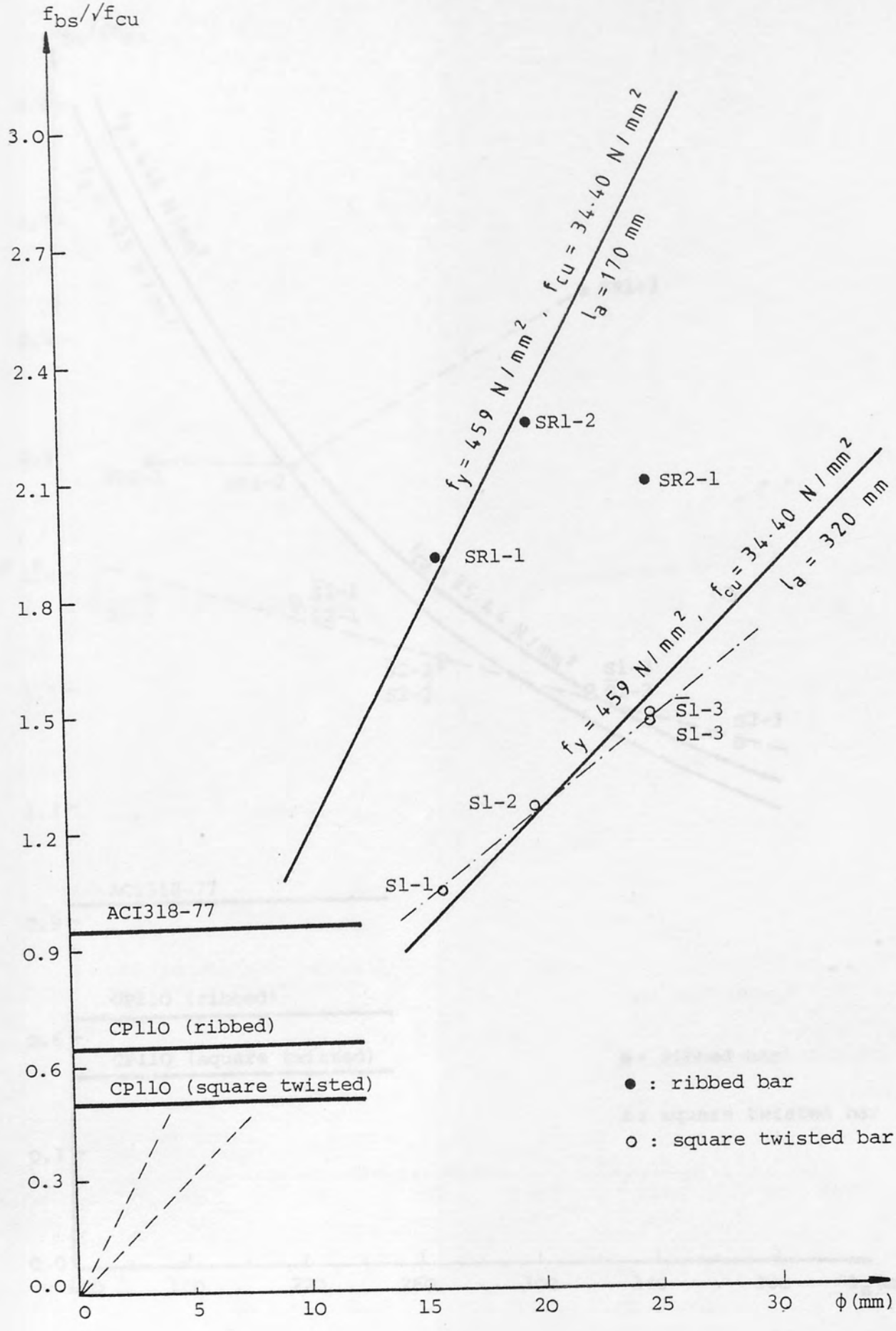

FIGURE 7.3: VARIATION OF THE BOND STRESS WITH BAR SIZE

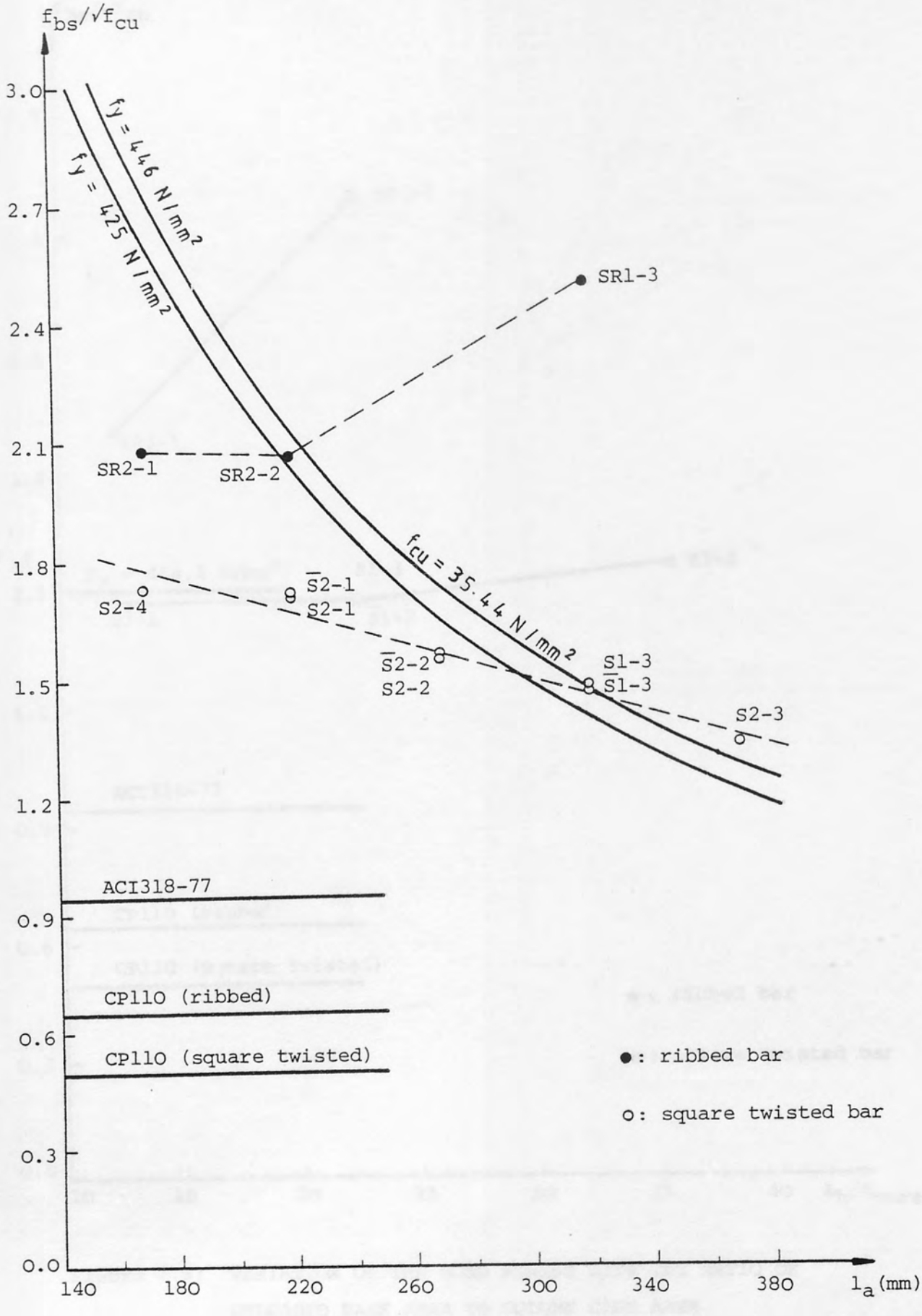

FIGURE 7.4: VARIATION OF THE BOND STRESS WITH ANCHORAGE LENGTH

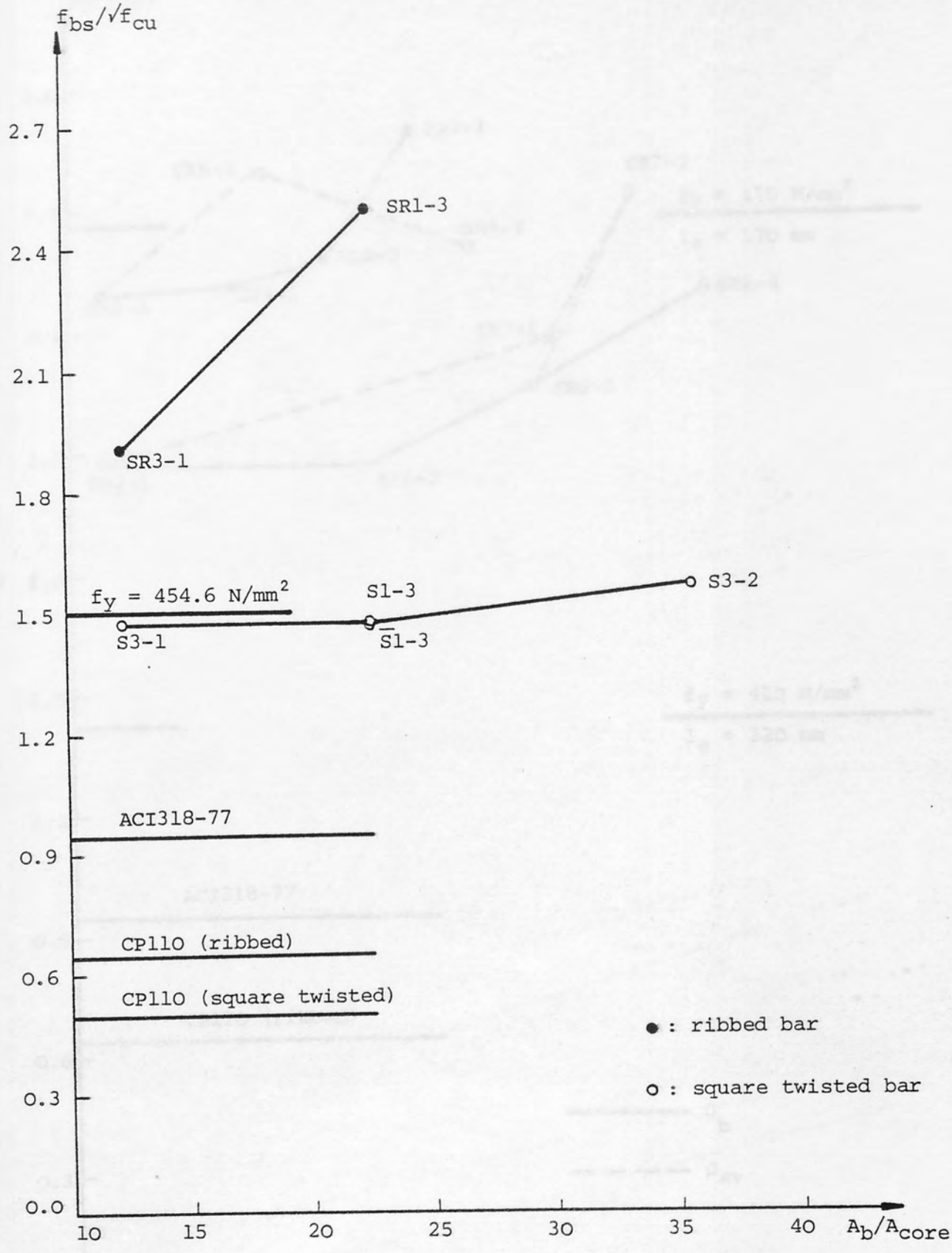

FIGURE 7.5: VARIATION OF THE BOND STRESS WITH THE RATIO OF UNLOADED BASE AREA TO COLUMN CORE AREA

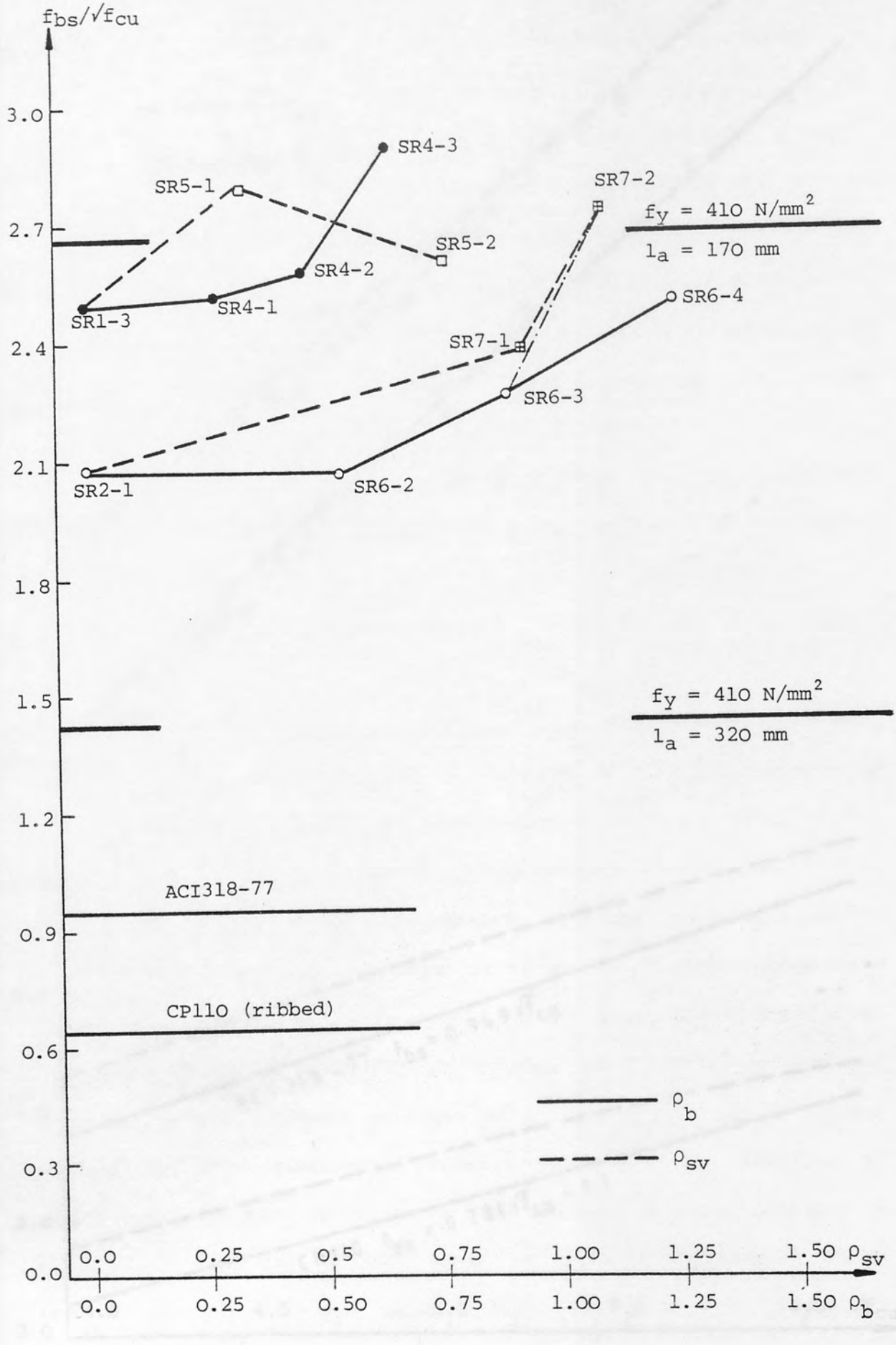

FIGURE 7.6: VARIATION OF THE BOND STRESS WITH TRANSVERSE REINFORCEMENT IN THE BASE

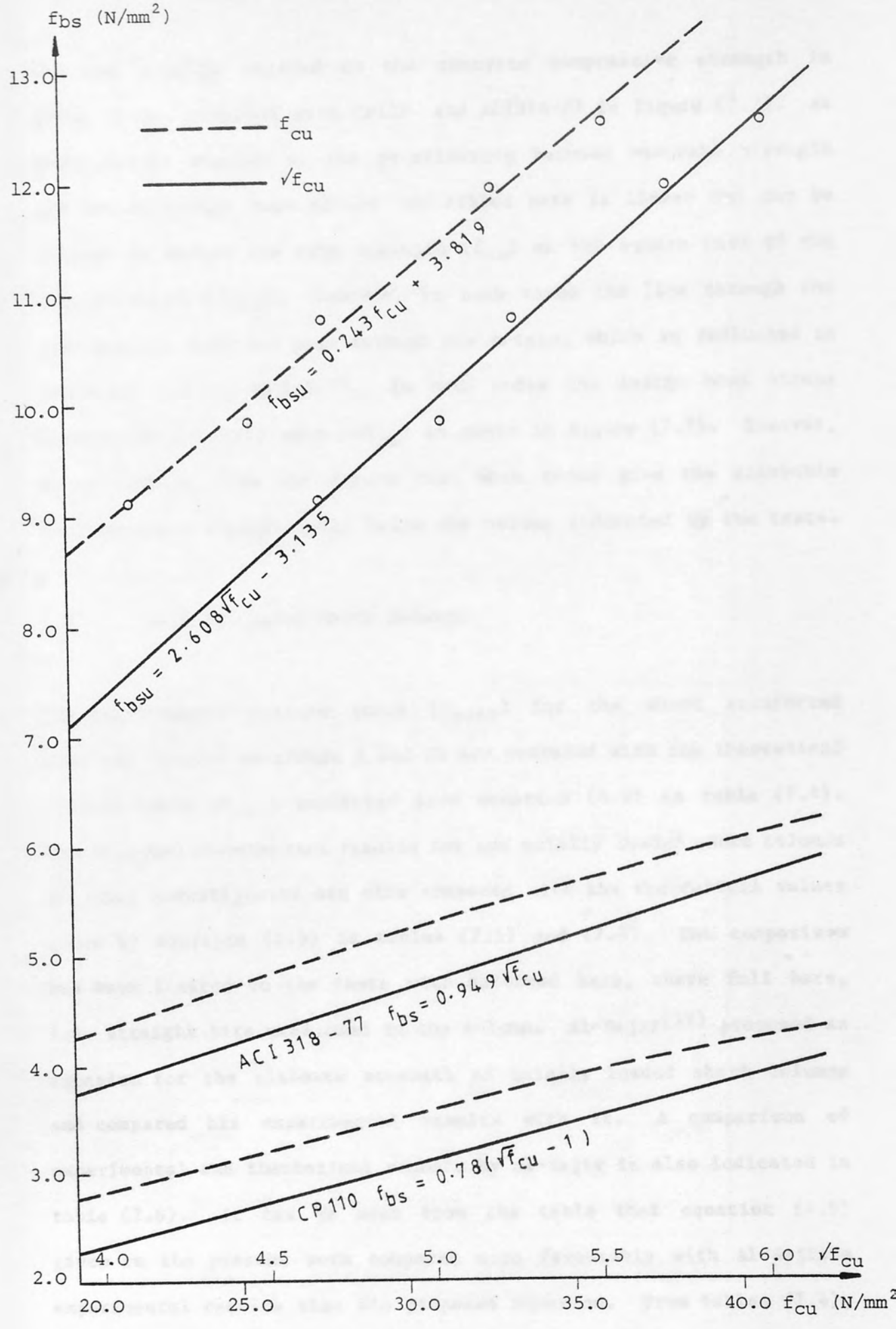

FIGURE 7.7: VARIATION OF THE BOND STRESS WITH CONCRETE COMPRESSIVE STRENGTH (f_{cu}) AND ($\sqrt{f_{cu}}$)

The test results related to the concrete compressive strength in group IX are compared with CP110 and ACI318-77 in figure (7.7). As described in chapter 4, the relationship between concrete strength and the anchorage bond stress for ribbed bars is linear and can be related to either the cube strength (f_{cu}) or the square root of the cube strength ($\sqrt{f_{cu}}$). However, in both cases the line through the test results does not pass through the origin, which is reflected in CP110 but not in ACI318-77. In both codes the design bond stress also varies linearly with ($\sqrt{f_{cu}}$) as shown in figure (7.7). However, it is obvious from the figure that both codes give the allowable bond stresses significantly below the values indicated by the tests.

7.6 Axially Loaded Short Columns

The experimental failure loads (P_{test}) for the short reinforced concrete columns in groups X and XI are compared with the theoretical failure loads (P_{ult}) predicted from equation (4.9) in table (7.4). The relevant experimental results for the axially loaded short columns by other investigators are also compared with the theoretical values given by equation (4.9) in tables (7.5) and (7.6). The comparison has been limited to the tests with deformed bars, where full bars, i.e. straight bars were used in the column. Al-Sajir[59] proposed an equation for the ultimate strength of axially loaded short columns and compared his experimental results with it. A comparison of experimental and theoretical results by Al-Sajir is also indicated in table (7.6). It can be seen from the table that equation (4.9) given in the present work compares more favourably with Al-Sajir's experimental results than his proposed equation. From tables (7.4), (7.5) and (7.6) it can be observed that equation (4.9) is in very good agreement with the experimental results.

Test Specimen	Expt. P_{test} kN	Theo. P_{ult} kN	$\frac{P_{test}}{P_{ult}}$
SR9-1	1775.0	1826.5	0.972
SR9-2	1700.0	1681.5	1.011
SR10-1	1450.0	1442.9	1.005
SR10-2	1325.0	1235.4	1.072
Mean			1.015
Coefficient of variation %			3.55

TABLE 7.4: COMPARISON OF EXPERIMENTAL AND THEORETICAL RESULTS FOR SHORT REINFORCED CONCRETE COLUMNS

Investigator	Test No.	P_{test} kN	P_{ult} kN	$\frac{P_{test}}{P_{ult}}$
Pfister & Mattock[28]	1B	3041.1	3163.7	0.961
	1B1	3246.2	3096.8	1.048
Somerville & Taylor[55]	1	1700.0	1786.4	0.952
Cairns[60]	A300	6310.0	6287.7	1.004
	B300	4350.0	3827.6	1.136
Mean				1.020
Coefficient of variation %				6.59

TABLE 7.5: COMPARISON OF EXPERIMENTAL RESULTS BY OTHER INVESTIGATORS

Test No.	P_{test}	Al-Sajir	present work	Al-Sajir	present work
		P_{ult}	P_{ult}	$\frac{P_{test}}{P_{ult}}$	$\frac{P_{test}}{P_{ult}}$
	kN	kN	kN		
T1-1	1285.0*	1717.8	1521.9	0.748	0.844
T1-2	1544.0	1789.7	1583.0	0.863	0.975
T1-3	1330.0	1511.5	1343.1	0.880	0.990
T1-4	1385.0	1529.3	1363.3	0.906	1.016
T1-5	1395.0	1498.7	1335.6	0.931	1.044
T1-6	1550.0	1551.7	1383.2	0.999	1.120
T2-1	1239.0	1548.4	1380.0	0.800	0.898
T2-2	1312.5	1538.8	1369.6	0.853	0.958
T2-3	1360.0	1577.5	1401.6	0.862	0.970
T2-4	1580.0	1779.8	1575.8	0.888	1.003
T2-5	1281.5	1463.8	1304.7	0.875	0.982
T2-6	1230.0	1349.1	1210.6	0.912	1.016
T3-1	1192.5	1546.8	1380.7	0.771	0.864
T3-2	1160.0	1485.9	1328.5	0.781	0.873
T3-3	1211.3	1495.2	1336.4	0.810	0.906
T3-4	1305.0	1539.8	1374.4	0.848	0.950
T3-5	1451.0	1648.8	1498.0	0.861	0.969
Mean				0.865	0.971
Coefficient of variation %				6.52	6.49

*: punching failure

TABLE 7.6: COMPARISON OF EXPERIMENTAL RESULTS BY AL-SAJIR(59)

CHAPTER 8

CONCLUSIONS AND SUGGESTIONS

8.1 Conclusions

On the basis of the experimental and theoretical investigations presented in this thesis the following conclusions are drawn.

1- The experimental results for ultimate load and bond stress correlate better with the square root of the characteristic concrete cube strength rather than the concrete cube strength.

2- The experimental bond failure load, in the bases without a short reinforced concrete column, increases linearly with increasing the bar size within the range of bars used for both square twisted and ribbed bars.

3- Increases in the anchorage length of the column bars in the foundation produce linear increases in the ultimate load for both square twisted and ribbed bars.

4- An increase in the base plan area, or the ratio of the base unloaded area to the column core area, results in a small increase in the ultimate load for bases with square twisted bars. This effect, although not conclusive, also seems to be significant for the two tests with ribbed bars.

5- The ultimate load increases with the quantity of the bending tensile reinforcement in the foundation, for the tests with ribbed bars.

6- The inclusion of column core confining reinforcement, i.e. links, round the compression bars within the anchorage length, leads to an increase in the bond stress and consequently to an increase in the total loadcarrying capacity of the base with ribbed bars.

7- The ultimate load of the foundation with ribbed bars increases linearly as the characteristic concrete cube strength is increased.

8- The experimental results of the test specimens with a short reinforced concrete column indicate that the total loadcarrying capacity of a short column in axial compression decreases linearly as the size of the column is reduced, the column longitudinal reinforcement being kept constant.

9- Tests in part one and those without a short column in part two show that for an anchorage bond failure of a foundation, failure occurs due to the breakdown of bond between steel and concrete followed by the slip along the anchorage length as the column longitudinal bars shear the concrete. This effect is related to the resistance to the bursting forces provided by the large containment available over the column compression bars in the anchorage length of the base.

10- The resistance to bursting forces in a foundation is dependent on two factors. The first is the size of the foundation relative to the size of column, i.e. the degree of the concrete containment over the column reinforcement. The second is the quantity of reinforcing steel in the foundation, which provides extra confinement to resist the bursting forces.

11- In tests, concreted short columns failed by axial compression in the column. The observed failure mode in the tests indicated that a part of the column length acted as an extra anchorage length, in addition to the embedment length in the base.

12- At comparable loads the slip rate is significantly higher in the bases with square twisted bars than bases with ribbed bars.

13- The distribution of bond stress with loading is nonlinear along the anchorage length of the column bars in the base, for both square twisted and ribbed bars, until first slip takes place.

14- The bond stress is a maximum at the top and a minimum at the bottom region of the anchorage length until first slip, for both square twisted and ribbed bars.

15- Near the column to base interface, before slip occurs, square twisted bars gradually develop high bond stresses in the anchorage length which may exceed the average bond stress at failure. This effect is very pronounced for ribbed bars and the bond stress developed at that location is much greater than the average bond stress at failure.

16- The average bond stress at failure increases with increasing bar size for both square twisted and ribbed bars. This relationship is not linear for ribbed bars but is linear for square twisted bars within the range of sizes used, and may be related to either the diameter or the cross-sectional area of the bar.

17- The ultimate bond stress is significantly influenced by the compressive stress in the reinforcing bar. The anchorage bond stress is higher for a bar stressed at or above the yield, than that for a bar stressed below the yield in compression. The potential bond strength capacity also increases with increasing bar size.

18- The average anchorage bond stress at failure decreases as the embedment length of the column longitudinal bars in the foundation is increased for both square twisted and ribbed bars. This relationship is linear for the square twisted bars but not for ribbed bars.

19- Increasing the plan area of the base, or the ratio of unloaded base area to column core area, leads to a small increase in the ultimate bond stress for square twisted bars. Although not conclusive, this effect appears to be significant as observed in two tests with ribbed bars.

20- Increases in the quantity of tension reinforcement in the base allow significant increases in the ultimate bond stress for ribbed bars.

21- Provision of column core confining steel, i.e. links over the anchorage length of the column bars in the foundation, leads to a significant increase in the ultimate bond stress for ribbed bars.

22- The variation of the anchorage bond stress with the characteristic concrete cube strength is linear and, increases in the concrete strength produce proportional increase in the bond stress for ribbed bars. This relationship may be expressed with respect to either the

cube strength or the square root of the cube strength because there is little to choose between the two relationships. However, it is noted that in both cases the line given by the related equations does not pass through the origin.

23- The tests with concreted columns show that the bond stress developed in the joint zone of the column increases linearly as the plan area of the column is reduced while the column longitudinal reinforcement is kept constant.

24- The tests with concreted columns also show that part of the column length, which acts as an extra anchorage length, is the critical zone, since maximum bond stresses develop in this part of the column rather than the base. This section of the column may be combined with the anchorage length in the foundation to give the true bond length.

25- The theoretical failure loads predicted by equation (4.9) for axially loaded short reinforced concrete columns are in good agreement with the experimental results. The equation may be used to assess the theoretical ultimate load of a short column provided that continuous deformed bars are used.

26- The theoretical analysis shows that the maximum and minimum bond stresses are at the top and bottom parts of the anchorage length, respectively, and vary nonlinearly in between, which confirms the general trend indicated by the experimental results.

27- The theoretical solutions indicate that the distribution of the bond stress along the anchorage length of the column bars in the base is significantly influenced by the bar stiffness factor K, which is the measure of the compressibility of the bar. As K decreases, i.e. the bar becomes more compressible, the magnitude of the bond stress at the top part of the anchorage length increases, which results in local yield in the concrete at smaller loads. As K decreases, the proportion of the load transferred to the concrete by bond by the lower part of the bar in the base, is significantly decreased. The theoretical analysis also shows that the influence of the K on the distribution of the bond stress is more significant for large anchorage lengths.

28- The proposed theoretical method predicts the distribution of bond stress over the anchorage length of column bars in the foundation with reasonable accuracy when compared with the experimental results for both square twisted and ribbed bars.

29- The proposed analytical method determines the vertical displacement with reasonable accuracy for square twisted bars until the first slip of the column longitudinal reinforcement occurs in the base. Beyond this stage, the theoretical analysis yields conservative results when compared with the experimental values.

30- The proposed theory predicts the vertical displacement of ribbed bars with reasonable degree of accuracy by comparison with the experimental results.

31- The theoretical failure loads obtained from the proposed theoretical analysis for the foundations without concreted columns, are in very good agreement with the test results.

32- The test results indicate that the allowable bond stresses specified by the British code CP110[56] are very conservative and should be increased. The test results indicate that the American code ACI318-77[61] also gives conservative results, particularly for ribbed bars, and hence the specified minimum anchorage length could be reduced.

8.2 Suggestions for Further Research

It is evident from the experimental investigation that the end bearing of the column longitudinal bars in the foundation, which could contribute to the strength of the joint, was eliminated in all tests conducted with both square twisted and ribbed bars. It is therefore suggested that further experimental study is required to determine the effect of the end bearing of a bar on the anchorage bond stress and the failure load in the transference of axial load from a column to a base.

In the present study the effect of bending moment was not taken into consideration in the tests because the foundations were supported on an underlying solid steel platen of the testing rigs during loading. However, the bending moment may have a significant influence on the anchorage bond stress of column longitudinal reinforcement for the foundations resting on flexible soils. It is therefore suggested that further experimental work be carried out on foundations sub-

jected to bending due to a supporting bed, which simulates the flexible soil conditions.

The tests, which included ribbed bars and varied base size, were not conclusive and further tests are required. On the other hand, there was an indication from the tests with concreted columns that the part of the column length, which acted as an extra anchorage length, was approximately equal to the column core breadth, i.e. the distance between the column bars. Further investigation with the use of ribbed bars is required in order to determine the specific length of the column section which acts as an extra anchorage length.

In the present investigation, the aggregate size was kept constant in the tests throughout the experimental scheme. It is also suggested that some experimental work with varying size and type of aggregate but constant concrete strength may be informative.

A separate series of theoretical computations with the end bearing of the bar indicated that the distribution of bond stress on the anchorage length of the column bars was not materially different from that of distribution without end bearing. Consequently, a small proportion of the load would be transferred to the concrete by the end bearing. In order to clarify these points further experimental and theoretical studies are required.

It was shown that the proposed theoretical method estimated conservative vertical displacements for square twisted bars beyond the first slip load until failure. Further theoretical work is therefore needed to improve the accuracy of the method for square twisted

bars. Further experimental and theoretical investigations are also required for the load-vertical displacement relationship of both square twisted and ribbed bars when the end bearing of the column longitudinal reinforcement is present in the base.

When the end bearing of the bars was taken into consideration in the theoretical analysis for a number of tests, the results did not show a significant increase in the ultimate load, as described in the previous chapter. Further theoretical investigation with the assessment of more realistic ultimate end bearing strength, is therefore required.

It is suggested that the proposed theoretical method be extended to include other stress situations by introducing the horizontal displacement compatibility into the analysis. Modifying the elastic modulus of steel and concrete at various stress levels may improve the theoretical solutions.

APPENDIX A

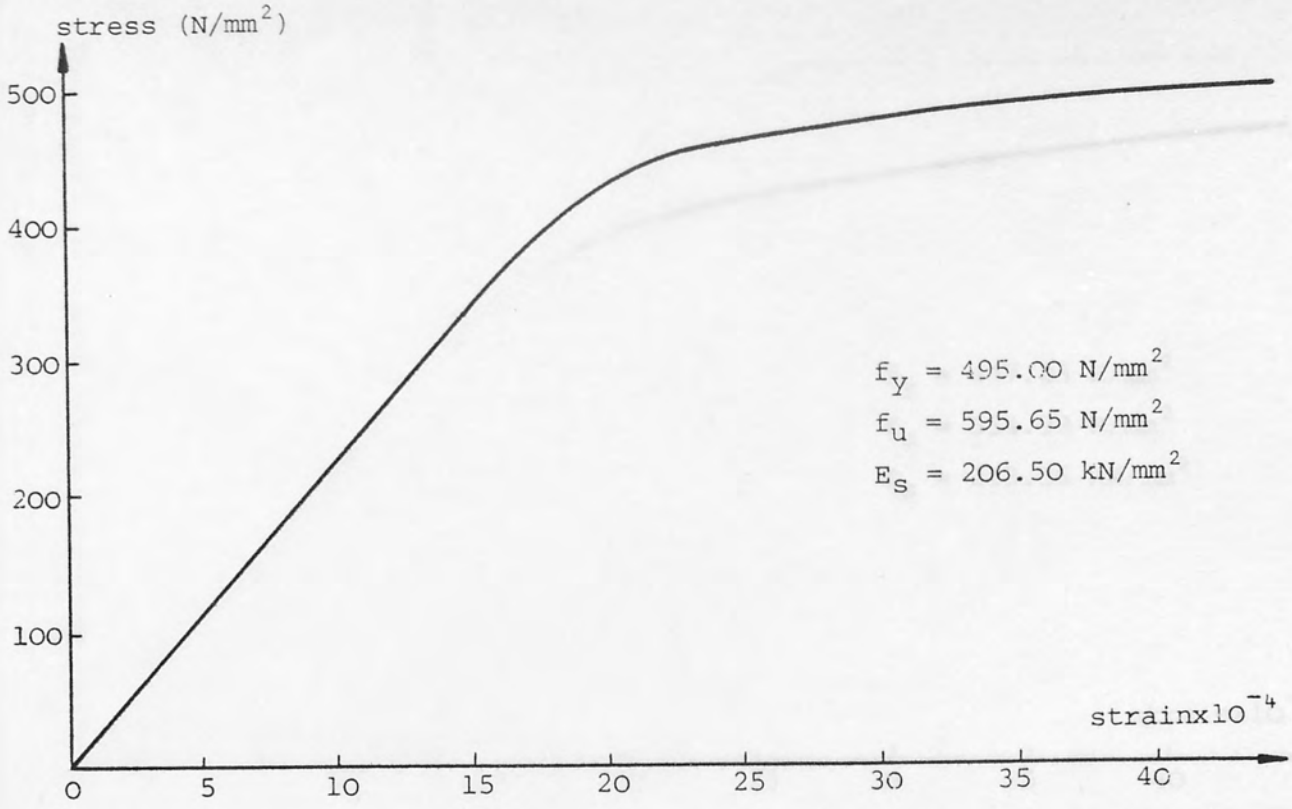

FIGURE A-1: STRESS VERSUS STRAIN CURVE FOR 16mm SQUARE TWISTED BAR

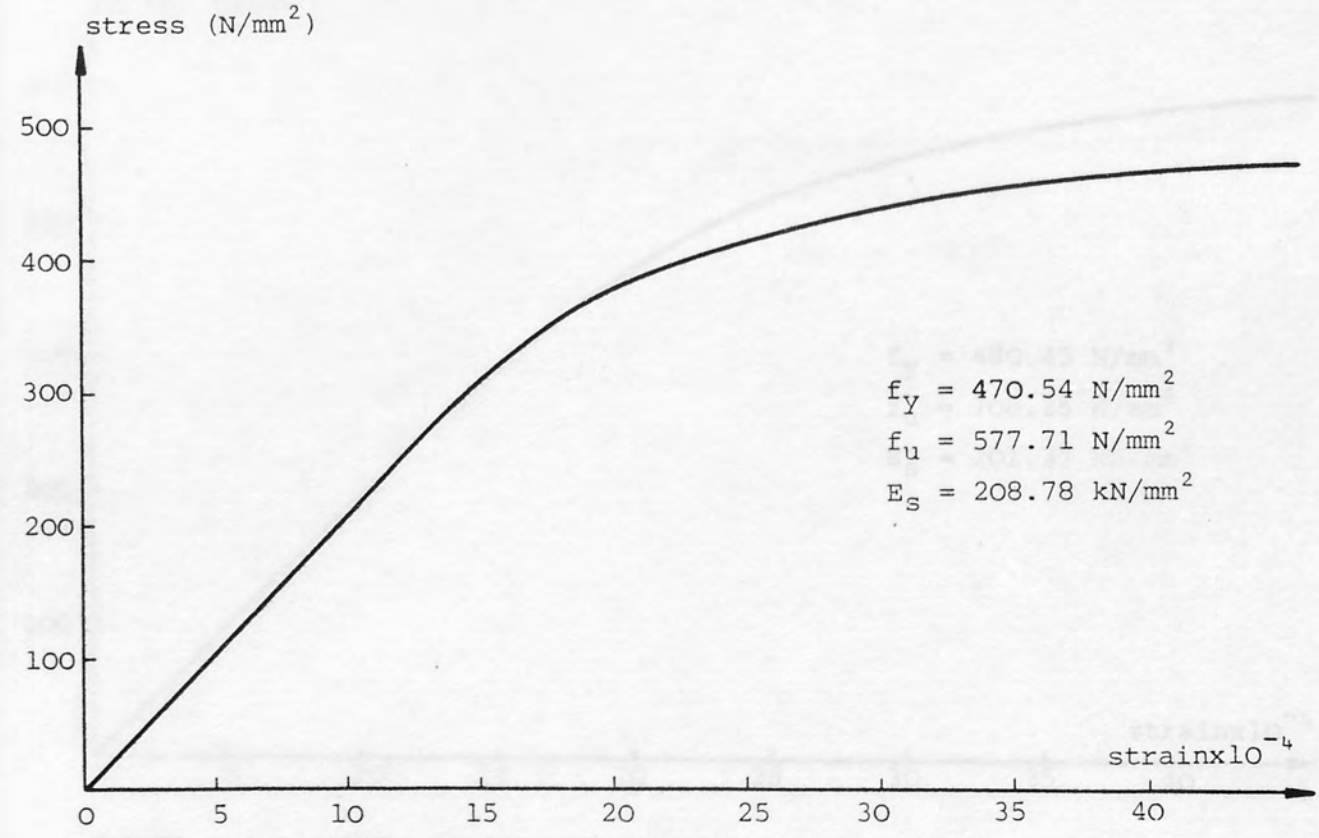

FIGRUE A-2: STRESS VERSUS STRAIN CURVE FOR 20mm SQUARE TWISTED BAR

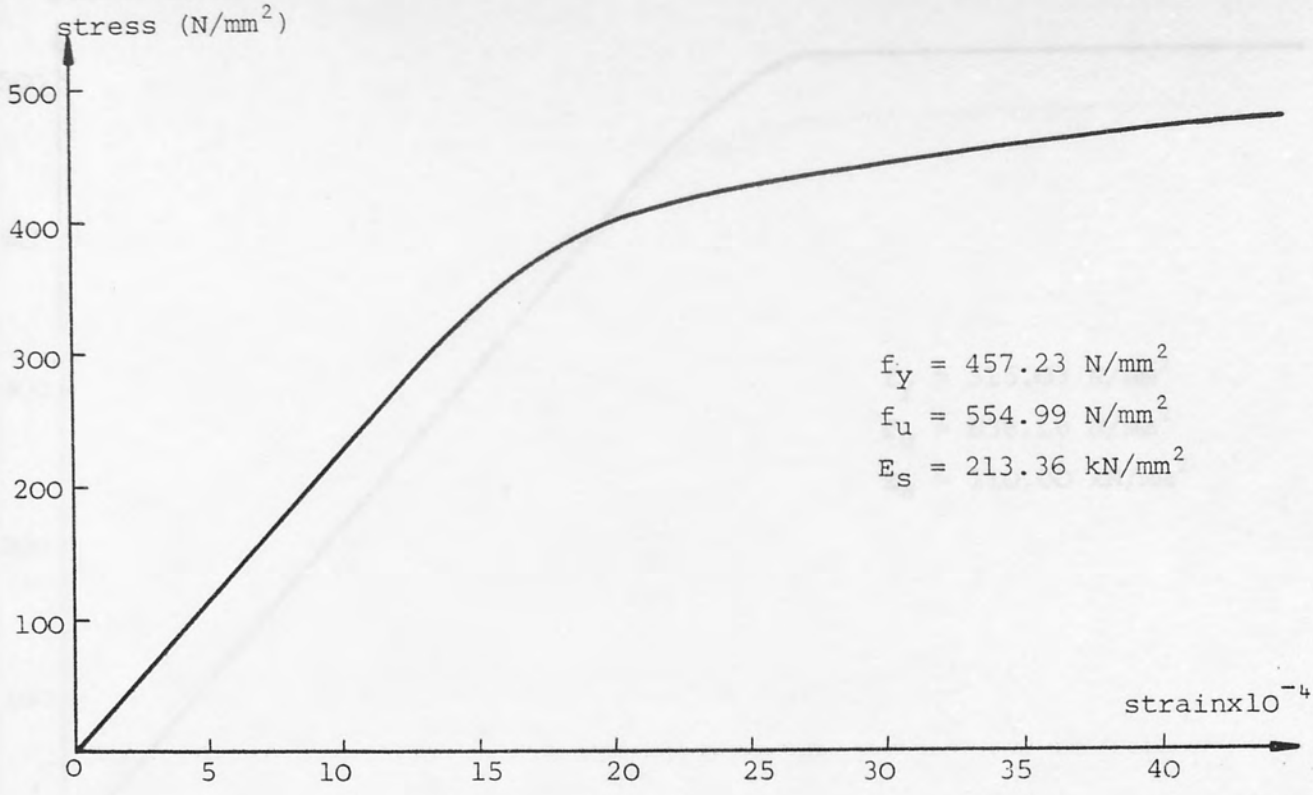

FIGURE A-3: STRESS VERSUS STRAIN CURVE FOR 25mm SQUARE TWISTED BAR

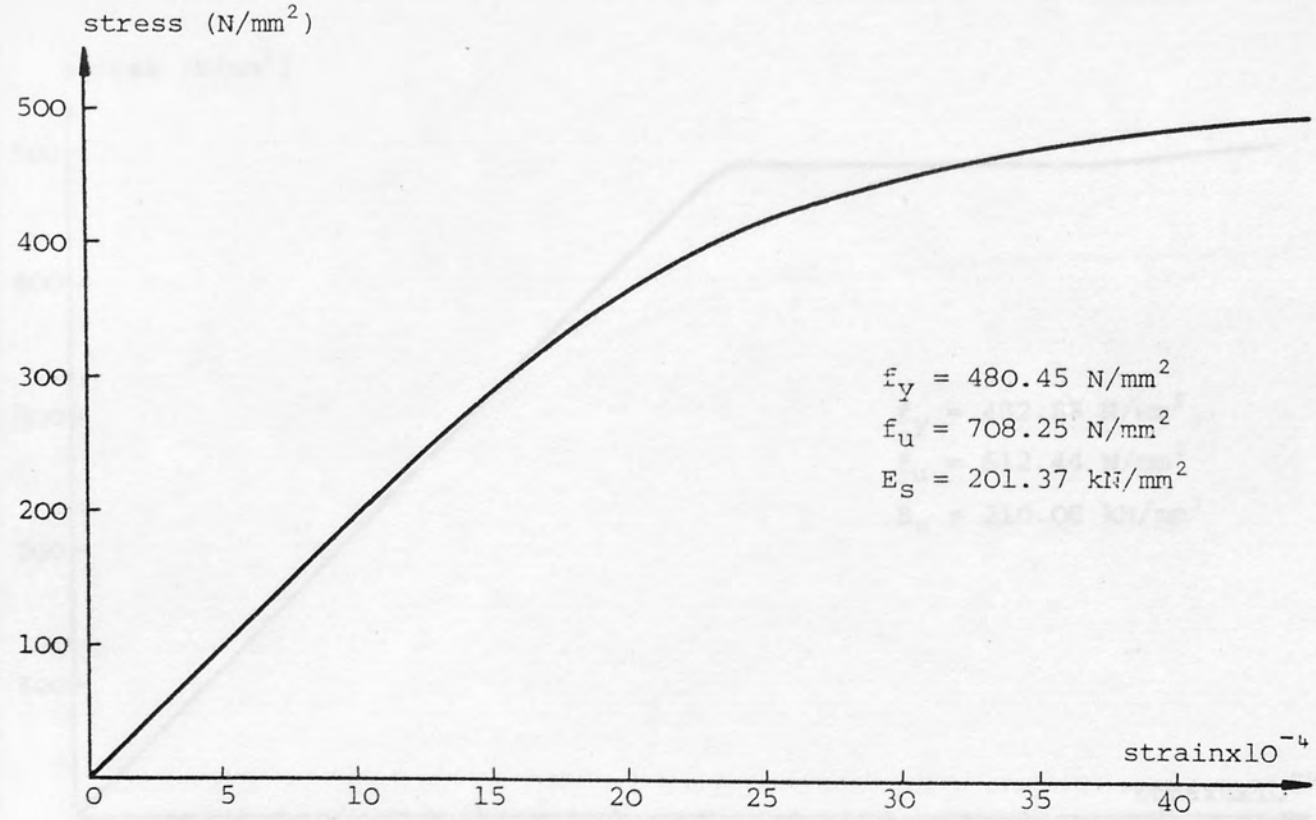

FIGURE A-4: STRESS VERSUS STRAIN CURVE FOR 8mm RIBBED BAR

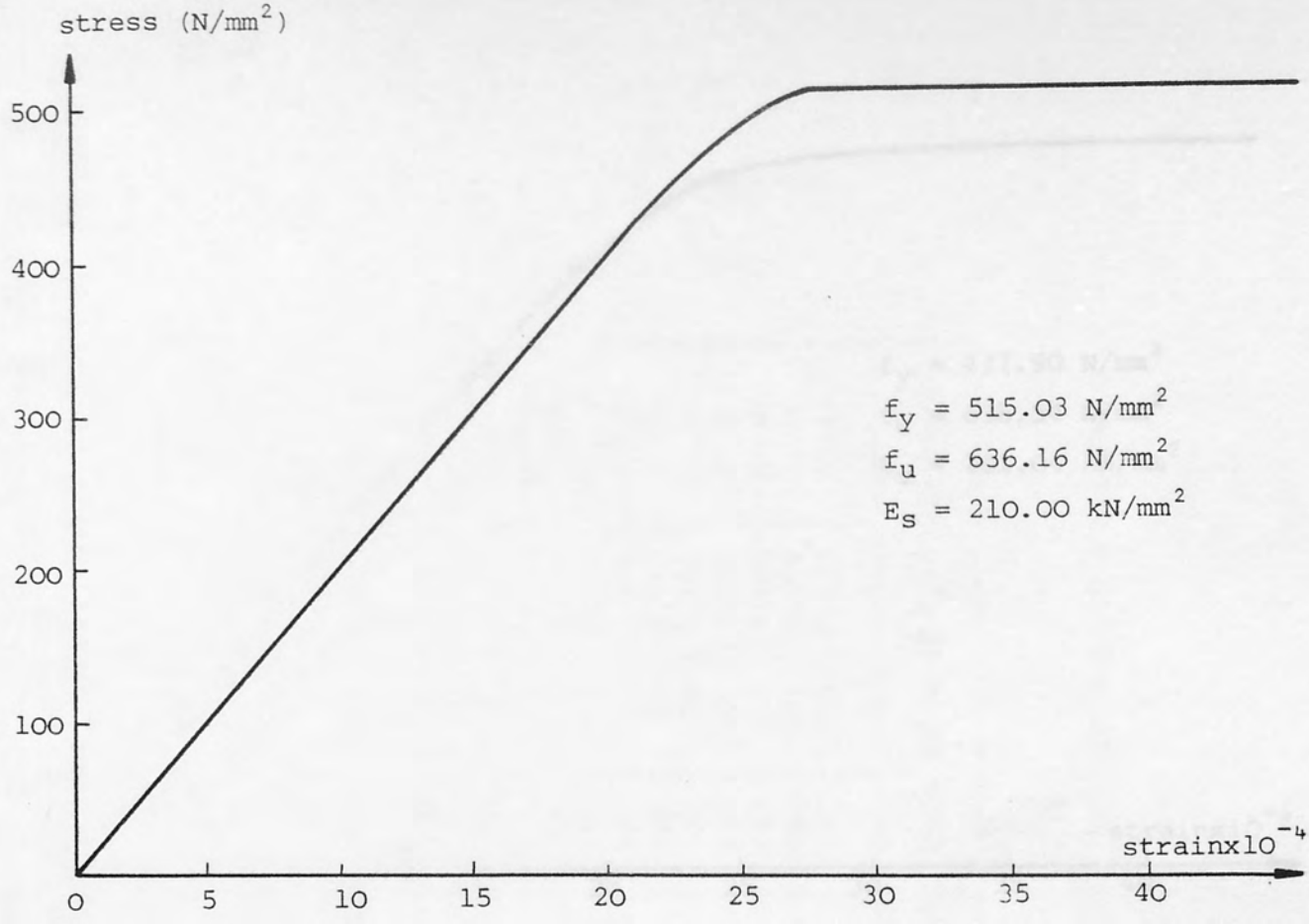

FIGURE A-5: STRESS VERSUS STRAIN CURVE FOR 12mm RIBBED BAR

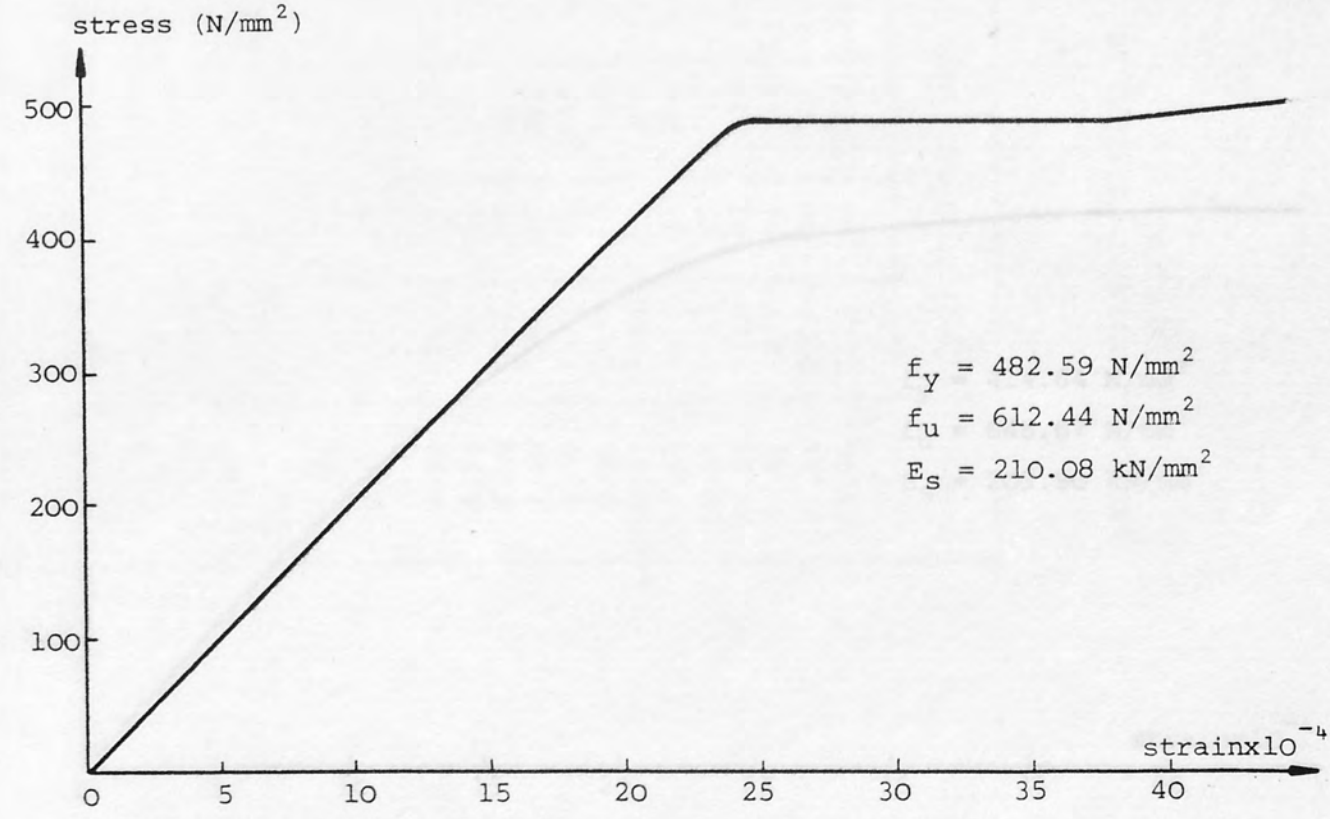

FIGURE A-6: STRESS VERSUS STRAIN CURVE FOR 16mm RIBBED BAR

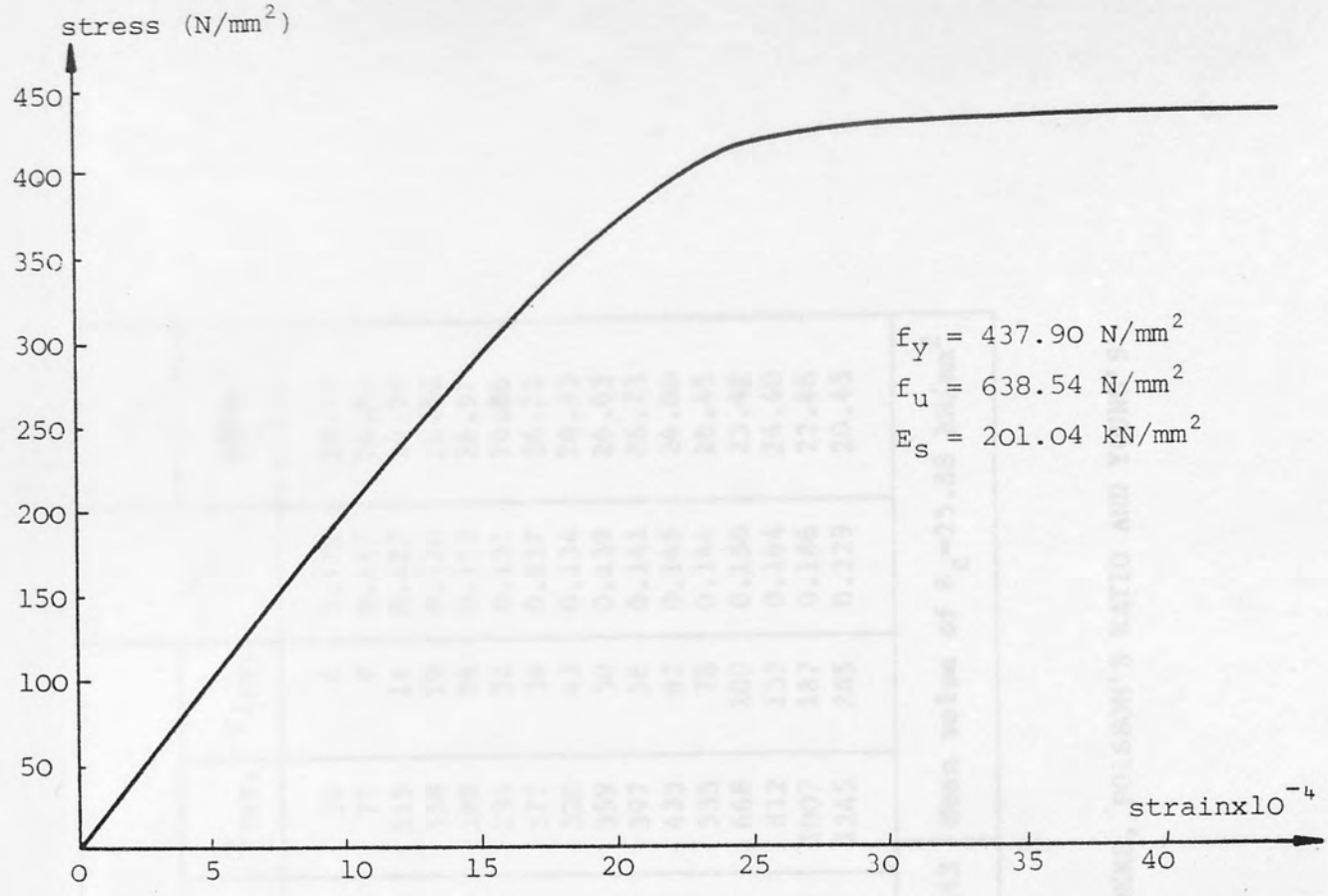

FIGURE A-7: STRESS VERSUS STRAIN CURVE FOR 20mm RIBBED BAR

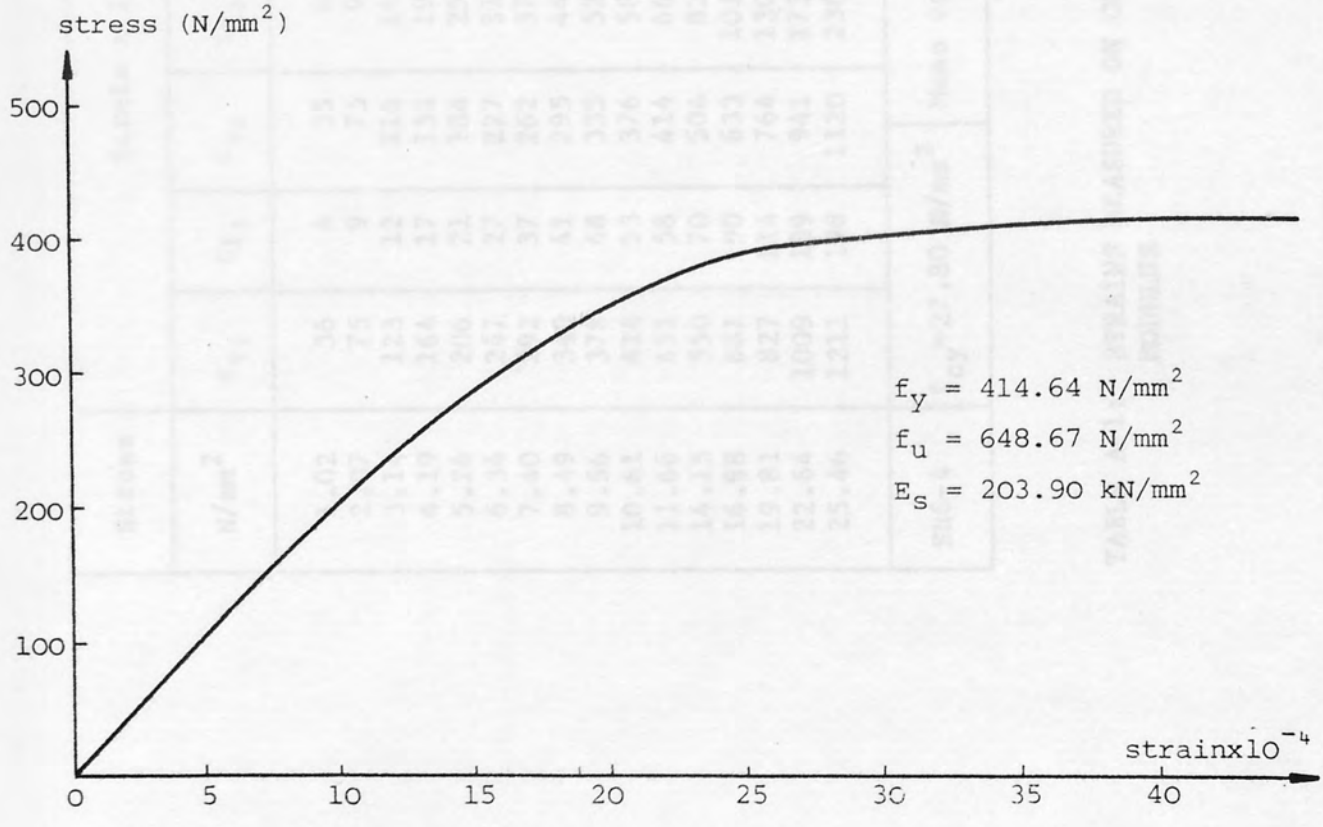

FIGURE A-8: STRESS VERSUS STRAIN CURVE FOR 25mm RIBBED BAR

Stress	Strain x 10^{-6}								ν_c	E_c
N/mm^2	ε_{v1}	ε_{l1}	ε_{v2}	ε_{l2}	ε_{v3}	ε_{l3}	$\varepsilon_{vav.}$	$\varepsilon_{lav.}$		kN/mm^2
1.02	36	4	35	4	37	4	36	4	0.111	28.33
2.07	75	9	75	9	80	8	77	9	0.117	26.88
3.14	123	12	116	14	118	15	119	14	0.117	26.39
4.19	164	17	151	19	158	20	158	19	0.120	26.52
5.26	206	21	184	25	202	27	198	24	0.123	26.57
6.34	247	27	227	31	234	35	236	31	0.131	26.86
7.40	292	37	262	37	277	42	277	38	0.137	26.71
8.49	340	41	295	44	325	44	320	43	0.134	26.53
9.56	378	48	335	52	363	50	359	50	0.139	26.63
10.61	414	53	376	58	401	57	397	56	0.141	26.73
11.66	451	58	414	66	441	64	435	63	0.145	26.80
14.15	550	70	504	82	550	82	535	78	0.146	26.45
16.98	681	90	633	101	689	108	668	100	0.150	25.42
19.81	827	114	764	130	845	155	812	133	0.164	24.40
22.64	1009	139	941	173	1072	250	1007	187	0.186	22.48
25.46	1211	198	1120	236	1405	420	1245	285	0.229	20.45
SR6-4	f_{cy}=27.80 N/mm^2		Mean value of ν_c=0.143				Mean value of E_c=25.88 kN/mm^2			

TABLE A-1: STRAINS MEASURED ON CONCRETE CYLINDERS, POISSON'S RATIO AND YOUNG'S MODULUS

APPENDIX B

The strain and deflection measurements for each individual specimen are tabulated in this appendix. Deflection and strain recordings of the tests and strain recordings in the base reinforcement are presented in tables (B-1) and (B-2), respectively.

In table (B-1) the strain measurement on the column longitudinal bars is given until first slip occurred, while the deflection measurement and the strain recording in the rest of the reinforcement are given until failure for the tests without a short reinforced concrete column. On the other hand, all recorded measurements of strain and deflection in the remainder of the tests, which included a short reinforced concrete column, are given up to failure. The values given for the vertical displacement of the column cage (Δ_v) are the average of four vertically placed dial gauge readings. The horizontal displacements of the column cage (Δ_h) in the x and y directions with respect to the original position of the top steel plate are the two respective horizontally placed dial gauge readings (see figures (2.4) and (2.7) for reference). The sign convention for the values of the horizontal displacement are in accordance with figure (3.9a). In the table, each value for the total shortening of the specimen (Δ_{vt}) is the average of four lower dial gauge readings, while the vertical deflection of the column (Δ_{vc}) and the base (Δ_{vb}) is the average of two corresponding upper dial gauge readings (see figure (2.8) for reference).

In table (B-1), position and spacing of the strain gauges on the column longitudinal bars for the tests conducted with square twisted and ribbed bars are in accordance with figures (2.4), (2.7), (2.8) and table (2.3), respectively. The strain at each gauge location

represents the average of four strain readings on two diagonal legs of the column cage at that particular location. The strain measurement in the links are also given in table (B-1). In the table, each value is the average of four readings at the legs of each link or the average of two readings at the two neighbouring legs of each link as shown in figures (2.7) and (2.8), respectively, and the negative sign indicates tension.

Strain development in the base tension reinforcement mesh up to failure is given in table (B-2). Referencing and spacing of strain gauges are in accordance with figure (2.6), table (2.3) and figure (2.8) for the tests without or with a short reinforced concrete column, respectively. In the table, minus sign indicates tension.

S1-1	Deflection Measurement			Strain Measurement on Column Cage $\varepsilon x10^{-6}$					
		x	y	Gauge postions & referencing					
Load	$\Delta_v.10^{-3}$	$\Delta_h.10^{-3}$	$\Delta_h.10^{-3}$	very top	top				botm.
kN	mm	mm	mm	1	2	3	4	5	6
40	51	0	0	246	209	84	19	5	0
80	286	0	0	488	442	314	238	127	30
110	483	+13	-13	638	565	405	298	178	60
140	825	+13	-13	804	717	552	397	240	85
160	1029	+25	-25	897					
180	1207	+25	-25						
200	1378	+51	-76						
220	1530	+76	-76						
240	1683	+76	-102						
260	2083	+102	-130						
280	2191	+102	-130						
300	2311	+130	-171						
320	2431	+171	-228						
340	2578	+282	-306						
350	2864	+335	-338						
360	2978	+435	-330						
370	3461	+482	-228						
380	4147	+635	-51						
390	4847	+789	+432						

TABLE B-1: DEFLECTION AND STRAIN RECORDINGS

S1-2	Deflection Measurement			Strain Measurement on Column Cage $\varepsilon x10^{-6}$					
		x	y	Gauge postions & referencing					
Load	$\Delta_v.10^{-3}$	$\Delta_h.10^{-3}$	$\Delta_h.10^{-3}$	very top	top				botm.
kN	mm	mm	mm	1	2	3	4	5	6
100	142	-	-	397	365	240	150	70	20
200	353	-	-	733	675	515	362	205	42
250	595	-	-	950	880	582	422	240	67
300	1033	-	-	1120	1030	600	450	265	73
350	1216	-	-	1263					
400	1691	-	-						
430	2051	-	-						
460	2480	-	-						
490	2956	-	-						
510	3195	-	-						
530	3530	-	-						
550	4231	-	-						
570	4865	-	-						
580	5199	-	-						

TABLE B-1: [continued]

S1-3	Deflection Measurement			Strain Measurement on Column Cage $\varepsilon x10^{-6}$					
		x	y	Gauge postions & referencing					
Load	$\Delta_v \cdot 10^{-3}$	$\Delta_h \cdot 10^{-3}$	$\Delta_h \cdot 10^{-3}$	very top	top				botm.
kN	mm	mm	mm	1	2	3	4	5	6
20	0	0	0	50	38	11	5	2	0
40	0	0	0	103	89	32	9	2	0
60	0	0	0	143	123	45	14	4	0
80	13	0	0	196	169	62	15	5	0
100	19	0	0	250	217	84	19	6	0
120	22	0	0	304	268	124	30	15	0
140	25	0	0	351	314	178	41	17	0
160	38	0	0	399	361	209	69	21	0
180	44	0	0	446	405	250	107	27	0
200	57	0	0	498	455	300	159	50	0
220	89	0	0	532	488	332	188	73	4
240	248	-25	+25	568	518	360	208	92	7
260	368	-25	+25	632	568	399	236	118	8
280	476	-25	+25	681	609	416	244	124	10
300	610	-25	+51	734	647	519	-	-	-
320	737	-25	+51	791	-	-	-	-	-
340	870	-25	+51						
360	972	-51	+51						
380	1111	-51	+51						
400	1193	-51	+76						
420	1295	-51	+76						
440	1397	-76	+102						
460	1518	-76	+102						
480	1613	-102	+127						
500	1708	-203	+178						
520	1829	-203	+178						
540	1950	-203	+178						
560	2051	-229	+178						
580	2172	-229	+203						
600	2292	-254	+229						
620	2445	-254	+229						
640	2597	-254	+229						
660	2769	-254	+229						
680	2915	-279	+254						
700	3099	-279	+279						
720	3410	-305	+305						
740	3670	-305	+305						
760	4140	-457	+356						
780	4242	-457	+457						
800	5035	-483	+483						
820	5448	-508	+533						
840	6851	-533	+558						
860	8425	-635	+609						
880	10648	-711	+635						

TABLE B-1: [continued]

$\overline{S1-3}$	Deflection Measurement		
Load	$\Delta_v \cdot 10^{-3}$	$\overset{x}{\Delta_h} \cdot 10^{-3}$	$\overset{y}{\Delta_h} \cdot 10^{-3}$
kN	mm	mm	mm
50	0	0	0
100	13	0	0
150	34	0	0
200	59	-25	+25
250	35	-25	+25
300	425	-51	+51
350	673	-51	+76
400	895	-51	+76
450	1105	-51	+76
500	1492	-51	+76
540	1746	-51	+76
580	2285	-51	+76
620	2565	-76	+102
660	2882	-76	+102
700	3131	-51	+152
730	3763	-25	+152
760	4493	-25	+152
790	5398	-76	+152
810	6554	-102	+203
830	7989	-127	+229
850	9405	-102	+254
870	10659	-127	+279
880	11688	-381	+330
890	12482	-635	+660

TABLE B-1: [continued]

S2-1	Deflection Measurement			Strain Measurement on Column Cage $\varepsilon x10^{-6}$				
		x	y	Gauge Positions & Referencing				
Load	$\Delta_v \cdot 10^{-3}$	$\Delta_h \cdot 10^{-3}$	$\Delta_h \cdot 10^{-3}$	very top	top			botm.
kN	mm	mm	mm	1	2	3	4	5
30	0	0	0	74	54	23	8	0
60	0	0	0	145	118	66	25	5
90	6	0	0	205	175	113	63	7
120	66	0	0	282	247	157	78	8
150	146	-25	+13	355	311	210	106	10
180	235	-25	+13	433	379	243	123	13
210	330	-25	+13	493	435	265	138	18
240	464	-25	+25	564	494	-	-	-
270	584	-25	+25	635	-	-	-	-
300	737	-25	+13					
330	908	-25	+13					
360	1105	-25	+13					
390	1270	-13	0					
420	1442	-13	0					
450	1638	-13	0					
480	1835	-25	0					
510	2089	-51	+25					
540	2400	-76	+51					
560	2489	-76	+51					
580	2597	-76	+51					
600	2769	-103	+58					
620	2953	-103	+76					
640	3150	-127	+89					
660	3556	-152	+114					
680	3816	-158	+140					
700	4369	-152	+178					

TABLE B-1: [continued]

$\overline{S2-1}$	Deflection Measurement		
		x	y
Load	$\Delta_v \cdot 10^{-3}$	$\Delta_h \cdot 10^{-3}$	$\Delta_h \cdot 10^{-3}$
kN	mm	mm	mm
20	0	0	0
40	0	0	0
60	32	0	0
80	51	0	0
100	89	0	0
120	184	0	0
140	229	-25	0
160	260	-51	+25
180	387	-51	+25
200	432	-51	+51
220	552	-51	+51
240	654	-51	+51
260	768	-51	+51
280	870	-51	+51
300	984	-76	+76
320	1079	-76	+76
340	1130	-76	+76
360	1276	-76	+76
380	1378	-102	+76
400	1492	-102	+76
420	1607	-102	+102
440	1746	-102	+102
460	1867	-127	+102
480	2019	-127	+102
500	2127	-127	+102
520	2229	-127	+127
560	2489	-152	+152
580	2642	-178	+152
600	2985	-178	+152
620	3194	-203	+152
640	3448	-203	+178
660	3804	-203	+178
680	4204	-228	+178
700	4661	-228	+178

TABLE B-1: [continued]

S2-2	Deflection Measurement			Strain Measurement on Column Cage $\varepsilon \times 10^{-6}$					
		x	y	Gauge postions & referencing					
Load	$\Delta_v \cdot 10^{-3}$	$\Delta_h \cdot 10^{-3}$	$\Delta_h \cdot 10^{-3}$	very top	top				botm.
kN	mm	mm	mm	1	2	3	4	5	6
40	0	0	0	95	85	33	20	10	0
80	19	0	0	193	182	90	50	25	10
120	92	0	0	300	287	190	140	95	30
160	198	-25	+25	383	365	275	195	125	40
200	318	-38	+38	445	425	335	235	150	60
240	453	-38	+38	565	-	-	-	-	-
280	605	-38	+38						
320	888	-51	+38						
360	1054	-51	+38						
400	1257	-76	+51						
440	1442	-76	+51						
480	1638	-76	+76						
520	1854	-102	+76						
560	2032	-102	+76						
600	2292	-102	+76						
640	2765	-127	+102						
680	3175	-127	+102						
720	3969	-127	+102						
760	6474	-179	+127						
780	10839	-179	+127						

TABLE B-1: [continued]

$\overline{S2}$-2	Deflection Measurement		
		x	y
Load	$\Delta_v \cdot 10^{-3}$	$\Delta_h \cdot 10^{-3}$	$\Delta_h \cdot 10^{-3}$
kN	mm	mm	mm
40	0	0	0
80	25	0	0
120	103	-25	0
160	179	-25	+25
200	356	-25	+25
240	496	-51	+25
280	635	-51	+51
320	903	-76	+51
360	1091	-102	+76
400	1289	-102	+76
440	1486	-102	+76
480	1689	-102	+76
520	1886	-127	+102
560	2026	-127	+102
600	2356	-127	+102
640	2921	-127	+127
680	3289	-102	+177
720	4286	-76	+177
760	7023	-51	+152
780	11620	-127	+177

TABLE B-1: [continued]

S2-3	Deflection Measurement			Strain Measurement on Column Cage $\varepsilon \times 10^{-6}$					
		x	y	Gauge postions & referencing					
Load	$\Delta_v.10^{-3}$	$\Delta_h.10^{-3}$	$\Delta_h.10^{-3}$	very top	top				botm.
kN	mm	mm	mm	1	2	3	4	5	6
40	0	0	0	99	90	41	13	6	0
80	13	0	0	193	181	132	79	38	5
120	184	0	+13	301	290	220	155	85	25
160	375	-13	+25	405	383	289	175	110	33
200	678	-76	+51	500	-	-	-	-	-
240	768	-102	+76						
280	953	-139	+102						
320	1124	-139	+102						
360	1302	-139	+102						
400	1467	-178	+127						
440	1651	-178	+152						
480	1797	-178	+165						
520	1981	-178	+178						
560	2159	-178	+178						
600	2362	-178	+178						
640	2565	-178	+178						
680	2819	-203	+178						
720	3061	-203	+203						
760	3296	-203	+178						
800	4337	-203	+102						
840	5277	-254	+127						
860	7899	-268	+254						
880	8560	-1092	+889						

TABLE B-1: [continued]

S2-4	Deflection Measurement			Strain Measurement on Column Cage $\varepsilon x10^{-6}$			
		x	y	Gauge positions & referencing			
Load	$\Delta_v.10^{-3}$	$\Delta_h.10^{-3}$	$\Delta_h.10^{-3}$	very top	top		botm.
kN	mm	mm	mm	1	2	3	4
30	189	0	0	89	76	29	2
60	298	0	0	141	120	49	3
90	419	0	0	205	173	70	3
120	546	-25	+25	265	217	93	12
150	648	-51	+51	350	274	123	13
180	768	-76	+76	419	330	150	22
210	902	-76	+76	496	389	180	25
240	1041	-76	+76	585	-	-	-
260	1130	-76	+89				
280	1251	-89	+89				
300	1346	-89	+89				
320	1461	-89	+102				
340	1575	-102	+102				
360	1689	-102	+102				
380	1803	-102	+102				
400	1962	-102	+127				
420	2089	-102	+127				
440	2318	-102	+127				
460	2432	-102	+127				
480	2635	-102	+127				
500	2864	-102	+127				
520	3086	-102	+127				
540	3416	-102	+127				
560	4842	-102	+127				

TABLE B-1: [continued]

S3-1	Deflection Measurement			Strain Measurement on Column Cage $\varepsilon x10^{-6}$					
		x	y	Gauge postions & referencing					
Load	$\Delta_v.10^{-3}$	$\Delta_h.10^{-3}$	$\Delta_h.10^{-3}$	very top	top				botm.
kN	mm	mm	mm	1	2	3	4	5	6
20	0	0	0	55	46	19	4	2	0
40	0	0	0	107	95	59	36	14	-3
60	13	0	0	159	147	110	60	19	-1
80	19	0	0	216	200	144	82	30	0
100	25	0	0	272	252	192	129	48	2
120	45	0	0	325	301	244	165	73	4
140	95	0	0	382	355	269	185	96	19
160	191	0	0	436	407	305	214	113	25
180	279	0	0	497	466	360	258	143	35
200	368	-25	+25	547	502	391	278	156	43
220	457	-51	+25	591	544	419	286	166	41
240	559	-51	+25	635	586	432	297	175	34
260	686	-51	+51	674	-	-	-	-	-
280	771	-76	+51						
300	864	-76	+51						
320	1008	-102	+76						
340	1101	-102	+76						
360	1191	-127	+127						
380	1302	-152	+152						
400	1409	-152	+152						
420	1511	-152	+178						
440	1632	-178	+178						
460	1753	-203	+203						
480	1880	-229	+229						
500	1992	-229	+254						
520	2122	-254	+254						
540	2261	-279	+279						
560	2394	-279	+305						
580	2527	-279	+305						
600	2677	-330	+356						
620	2826	-330	+356						
640	2966	-356	+381						
660	3143	-406	+381						
680	3327	-406	+432						
700	3575	-432	+432						
720	3899	-457	+483						
740	4305	-483	+483						
760	4693	-508	+660						
780	5080	-483	+762						
800	9982	-457	+762						
820	10160	-559	+787						
840	10395	-509	+787						
850	10693	-559	+787						
860	10871	-559	+914						

TABLE B-1: [continued]

S3-2	Deflection Measurement			Strain Measurement on Column Cage $\varepsilon \times 10^{-6}$					
		x	y	Gauge postions & referencing					
Load	$\Delta_v \cdot 10^{-3}$	$\Delta_h \cdot 10^{-3}$	$\Delta_h \cdot 10^{-3}$	very top	top				botm.
kN	mm	mm	mm	1	2	3	4	5	6
40	13	0	0	102	89	40	20	5	0
80	64	0	0	205	180	100	44	10	1
120	101	-13	+13	290	255	145	61	21	3
160	203	-25	+25	396	360	225	99	40	5
200	381	-25	+25	496	455	312	178	74	8
240	675	-25	+25	570	-	-	-	-	-
280	872	-25	+25						
320	1064	-51	+51						
360	1258	-51	+76						
400	1429	-76	+76						
440	1651	-101	+89						
480	1892	-114	+102						
520	2095	-114	+102						
560	2413	-127	+102						
600	2756	-139	+127						
640	3054	-165	+139						
680	3454	-178	+178						
720	3880	-203	+203						
760	4464	-216	+228						
800	5378	-254	+279						
840	6928	-330	+368						
880	10128	-457	+457						
900	11665	-660	+640						

TABLE B1: [continued]

SR1-1	Deflection Measurement			Strain Measurement on Column Cage $\varepsilon \times 10^{-6}$			
		x	y	Gauge positions & referencing			
Load	$\Delta_v \cdot 10^{-3}$	$\Delta_h \cdot 10^{-3}$	$\Delta_h \cdot 10^{-3}$	very top	top		botm.
kN	mm	mm	mm	1	2	3	4
50	159	0	0	298	260	140	30
100	222	0	0	591	515	278	48
150	318	0	0	895	793	409	70
200	445	0	0	1134	1050	518	82
250	603	-25	0	1438	1268	613	89
300	902	-25	0	1650	1423	754	76
325	1219	-25	+25				
350	2851	-25	+25				

TABLE B1: [continued]

SR1-2	Deflection Measurement			Strain Measurement on Column Cage $\varepsilon \times 10^{-6}$			
		x	y	Gauge positions & referencing			
Load	$\Delta_v \cdot 10^{-3}$	$\Delta_h \cdot 10^{-3}$	$\Delta_h \cdot 10^{-3}$	very top	top		botm.
kN	mm	mm	mm	1	2	3	4
50	51	0	0	243	225	115	32
100	121	0	0	423	392	217	45
150	191	0	0	614	582	300	57
200	274	-25	0	792	733	378	70
250	330	-25	0	960	879	442	79
300	406	-25	0	1129	1026	473	89
325	438	-25	+25	1207	1091	511	91
350	483	-25	+25	1297	1169	553	97
375	527	-51	+25	1393	1255	588	106
400	572	-51	+25	1477	1330	620	107
425	635	-76	+38	1571	1407	663	105
450	737	-102	+51	1689	1502	699	110
475	857	-102	+64	1812	1593	753	108
500	1181	-102	+127	1944	-	-	-
525	1816	-64	+203				

TABLE B1: [continued]

SR1-3	Deflection Measurement			Strain Measurement on Column Cage $\varepsilon x10^{-6}$					
		x	y	Gauge postions & referencing					
Load	$\Delta_v.10^{-3}$	$\Delta_h.10^{-3}$	$\Delta_h.10^{-3}$	very top	top				botm.
kN	mm	mm	mm	1	2	3	4	5	6
50	19	0	0	157	145	95	70	35	5
100	64	0	0	315	296	205	140	75	12
150	102	0	0	445	418	260	169	92	20
200	146	0	0	540	512	347	207	115	25
250	191	0	0	651	613	407	277	152	33
300	232	0	0	780	740	505	340	185	38
350	254	+25	-25	907	862	597	402	212	45
400	324	+25	-25	1010	957	642	427	225	48
450	368	+25	-25	1188	1130	792	520	267	52
500	426	+25	-38	1357	1285	890	575	292	55
550	476	+25	-38	1450	1364	975	622	315	60
600	539	+38	-38	1655	1558	1070	675	340	63
650	603	+51	-51	1935	1827	1158	718	360	65
700	718	+51	-51	2280*	2018	1237	760	378	68
750	819	+76	-76	2938*	2233*	1303	780	385	70
800	978	+140	-152	3730*	2455*	1358	818	392	71
850	1210	+254	-292						
900	1403	+432	-452						
950	1664	+533	-533						
1000	1968	+635	-584						
1050	2343	+737	-635						
1100	2756	+813	-686						
1150	3258	+889	-737						
1200	3664	+991	-813						
1250	4299	+1092	-838						
1300	4883	+1092	-914						
1350	5810	+1156	-965						
1375	6788	+1270	-1016						

TABLE B1: [continued]

SR2-1	Deflection Measurement			Strain Measurement on Column Cage $\varepsilon x 10^{-6}$			
		x	y	Gauge positions & referencing			
Load	$\Delta_v \cdot 10^{-3}$	$\Delta_h \cdot 10^{-3}$	$\Delta_h \cdot 10^{-3}$	very top	top		botm.
kN	mm	mm	mm	1	2	3	4
20	6	0	0	48	38	2	0
40	13	0	0	95	79	18	0
60	25	0	0	159	131	37	0
80	25	0	0	188	144	39	0
100	25	0	0	235	180	46	0
120	38	0	0	293	235	63	1
140	51	0	0	328	264	92	2
160	70	0	0	379	312	123	3
180	86	0	0	427	356	145	5
200	105	-13	+13	476	401	169	6
220	124	-13	+13	528	448	192	7
240	130	-13	+13	564	480	207	7
260	159	-25	+13	619	530	232	10
280	178	-25	+25	662	568	251	12
300	191	-25	+25	707	608	272	15
320	238	-25	+25	784	676	309	19
340	248	-25	+25	791	681	313	20
360	264	-38	+38	839	723	334	23
380	285	-38	+38	878	757	353	25
400	308	-38	+38	925	796	373	26
420	356	-51	+51	974	837	393	28
440	379	-51	+51	1007	864	407	29
460	426	-51	+63	1035	887	418	27
480	451	-51	+63	1079	923	436	28
500	489	-64	+76	1121	955	455	31
520	540	-64	+76	1171	995	478	37
540	610	-64	+76	1224	1034	501	41
560	660	-76	+76	1266	1067	524	43
580	760	-76	+101	1336	-	-	-
600	940	-76	+101				
620	1168	-76	+101				
630	3955	-101	+127				

TABLE B1: [continued]

S2-2	Deflection Measurement			Strain Measurement on Column Cage $\varepsilon x10^{-6}$				
		x	y	Gauge Positions & Referencing				
Load	$\Delta_v.10^{-3}$	$\Delta_h.10^{-3}$	$\Delta_h.10^{-3}$	very top	top			botm.
kN	mm	mm	mm	1	2	3	4	5
20	3	0	0	51	39	18	5	0
40	13	0	0	109	95	58	24	0
60	10	0	0	160	137	73	30	3
80	19	0	0	212	181	92	37	5
100	35	0	0	241	202	103	38	6
120	48	0	0	299	254	144	60	10
140	70	0	0	353	305	183	80	12
160	73	0	0	407	356	218	98	13
180	89	0	0	461	406	256	116	13
200	101	-25	+25	516	456	288	129	14
220	114	-25	+38	568	504	321	141	16
240	137	-51	+51	621	551	352	154	16
260	146	-51	+51	673	599	382	167	16
280	168	-51	+63	726	647	412	181	18
300	175	-51	+63	780	695	441	194	21
320	197	-51	+76	831	740	469	207	23
340	213	-76	+76	880	785	495	219	26
360	235	-76	+76	928	827	519	231	28
380	254	-76	+76	974	868	544	242	29
400	276	-76	+76	1019	908	566	253	31
420	318	-76	+89	1064	947	590	266	33
440	372	-76	+89	1110	986	612	280	33
460	422	-76	+89	1156	1027	639	292	36
480	483	-89	+102	1202	1065	663	306	37
500	543	-89	+102	1247	1109	688	323	39
520	591	-89	+102	1293	1152	713	334	41
540	626	-102	+102	1340	1198	740	350	44
560	673	-102	+102	1375	-	-	-	-
580	727	-102	+114					
600	781	-114	+114					
620	832	-127	+127					
640	883	-127	+127					
660	941	-127	+127					
680	1003	-127	+139					
700	1064	-127	+139					
720	1135	-139	+152					
740	1224	-152	+152					
760	1347	-152	+165					
780	1746	-165	+179					
800	2318	-179	+179					
820	3516	-152	+203					

TABLE B-1: [continued)

SR3-1	Deflection Measurement		
Load	$\Delta_v \cdot 10^{-3}$	$\Delta_h^x \cdot 10^{-3}$	$\Delta_h^y \cdot 10^{-3}$
kN	mm	mm	mm
25	0	0	0
50	0	0	0
75	19	0	0
100	25	0	0
125	48	+25	-25
150	64	+25	-25
175	67	+25	-25
200	76	+25	-25
225	83	+25	-25
250	95	+25	-25
275	114	+25	-25
300	124	+25	-25
325	140	+25	-25
350	149	+25	-25
375	165	+25	-25
400	187	+25	-25
425	197	+25	-25
450	222	+25	-25
475	245	+25	-25
500	260	+25	-25
525	286	+25	-25
550	311	+25	-25
575	333	+25	-25
600	356	+25	-25
625	381	+25	-25
650	400	+25	-25
675	438	+25	-25
700	457	+25	-25
725	489	+25	-25
750	521	+25	-25
775	546	+25	-25
800	580	+25	-25
825	616	+25	-25
850	641	+25	-25
875	680	+25	-25
900	730	+38	-25
925	791	+38	-25
950	851	+51	-38
975	946	+76	-51
1000	1099	+102	-51
1025	1232	+102	-51
1050	1371	+102	+102
1075	1607	+102	+127
1100	1924	+102	+178

TABLE B-1: [continued]

SR4-1	Deflection Measurement			Strain Measurement $\varepsilon \times 10^{-6}$ on Column Cage					
		x	y	Gauge postions & referencing					
Load	$\Delta_v \cdot 10^{-3}$	$\Delta_h \cdot 10^{-3}$	$\Delta_h \cdot 10^{-3}$	very top	top				botm.
kN	mm	mm	mm	1	2	3	4	5	6
50	19	0	0	127	85	45	25	10	0
100	38	0	0	260	213	137	90	52	15
150	70	0	0	378	313	235	167	95	22
200	102	0	0	491	418	310	225	135	32
250	136	0	0	640	562	408	277	167	37
300	178	0	0	738	652	469	340	212	47
350	238	-25	+25	860	770	545	402	245	57
400	286	-25	+25	965	869	637	480	292	62
450	340	-25	+25	1092	991	741	535	335	65
500	406	-25	+25	1220	1113	772	620	392	67
550	483	-25	+51	1365	1252	872	695	437	65
600	546	-25	+51	1525	1407	980	782	492	70
650	635	-25	+51	1605	1481	1090	865	540	70
700	749	-25	+25	1718	1588	1160	925	545	60
750	895	-51	+51	1835	1693	1310	1020	615	53
800	1060	-51	-102	2485*	2218*	1488	1115	665	55
850	1257	-102	-178	3660*	2805*	1630	1192	710	60
900	1524	-203	-279						
950	1868	-279	-381						
1000	2229	-381	-481						
1050	2730	-432	-533						
1100	3289	-482	-584						
1150	3880	-584	-660						
1200	4591	-660	-685						
1250	5410	-686	-762						
1300	6369	-686	-813						
1350	7582	-712	-1016						

TABLE B-1: [continued]

SR4-2	Deflection Measurement			Strain Measurement on Column Cage $\varepsilon \times 10^{-6}$					
		x	y	Gauge postions & referencing					
Load	$\Delta_v \cdot 10^{-3}$	$\Delta_h \cdot 10^{-3}$	$\Delta_h \cdot 10^{-3}$	very top	top				botm.
kN	mm	mm	mm	1	2	3	4	5	6
50	6	0	0	170	155	102	60	28	0
100	44	0	0	287	261	167	107	60	12
150	70	0	0	432	395	259	175	103	35
200	102	0	0	587	547	386	253	146	41
250	140	0	0	720	675	487	313	172	45
300	168	0	0	870	824	604	391	216	53
350	216	0	0	982	929	709	453	246	65
400	264	0	0	112	1053	760	503	278	70
450	318	-13	+13	1245	1181	852	548	293	70
500	387	-13	+13	1380	1305	950	602	318	72
550	451	-13	+13	1510	1427	1032	647	336	72
600	521	-13	+13	1685	1590	1122	694	353	82
650	596	-13	+13	1827	1722	1227	752	376	81
700	689	-25	+25	2338*	1850	1305	789	388	90
750	794	-64	+64	2983*	2520*	1395	837	403	93
800	965	+154	+178	4270*	3450*	1508	957	405	96
850	1162	+154	+330	5475*	4615*	1583	987	415	97
900	1400	+229	+380						
950	1702	+265	+444						
1000	2165	+305	+483						
1050	2572	+292	+533						
1100	3111	+330	+584						
1150	3759	+368	+609						
1200	4382	+457	+660						
1250	5144	+521	+698						
1300	6229	+609	+762						
1350	6712	+838	+787						
1400	8077	+1016	+889						

TABLE B-1: [continued]

SR4-3	Deflection Measurement			Strain Measurement on Column Cage $\varepsilon x10^{-6}$					
		x	y	Gauge postions & referencing					
Load	$\Delta_v \cdot 10^{-3}$	$\Delta_h \cdot 10^{-3}$	$\Delta_h \cdot 10^{-3}$	very top	top				botm.
kN	mm	mm	mm	1	2	3	4	5	6
50	0	0	0	145	130	60	30	10	0
100	57	0	0	280	262	145	51	25	5
150	69	0	0	405	377	220	90	48	12
200	95	0	0	520	485	318	153	85	12
250	102	0	0	640	597	368	180	98	20
300	118	0	0	785	735	468	250	122	22
350	130	0	0	923	858	545	298	150	25
400	146	0	0	1030	952	610	338	190	28
450	178	-13	+13	1153	1068	698	388	220	30
500	222	-25	+25	1303	1205	780	450	243	33
550	273	-25	+25	1405	1293	845	478	248	35
600	337	-38	+38	1500	1373	880	505	258	40
650	406	-38	+50	1670	1528	948	550	290	50
700	489	+25	+63	1838	1672	1028	590	315	55
750	584	+76	+102	2160*	1852	1090	625	338	65
800	737	+102	+229						
850	914	+178	+330						
900	1156	+229	+381						
950	1461	+305	+432						
1000	1848	+356	+508						
1050	2261	+381	+508						
1100	2743	+355	+533						
1150	3207	+406	+533						
1200	3804	+457	+559						
1250	4553	+483	+588						
1300	5207	+508	+635						
1350	6146	+533	+711						
1400	7125	+559	+787						
1450	8268	+584	+863						
1500	9365	+609	+990						
1550	10109	+635	+1194						

TABLE B-1: [continued]

SR5-1	Deflection Measurement			Strain Measurement on Column Cage $\varepsilon x10^{-6}$					
		x	y	Gauge postions & referencing					
Load	$\Delta_v.10^{-3}$	$\Delta_h.10^{-3}$	$\Delta_h.10^{-3}$	very top	top				botm.
kN	mm	mm	mm	1	2	3	4	5	6
50	0	0	0	155	142	60	30	10	0
100	0	0	0	305	285	165	88	42	5
150	16	0	0	412	384	223	138	70	10
200	51	0	0	562	520	318	215	132	13
250	98	0	0	678	625	383	267	150	18
300	143	0	0	788	725	460	323	200	25
350	178	0	0	900	833	543	383	235	38
400	222	0	0	1010	935	613	433	265	38
450	270	0	0	1200	1119	680	480	285	43
500	311	0	0	1326	1244	760	537	315	48
550	362	0	0	1445	1360	835	583	330	48
600	406	0	0	1585	1495	960	600	355	53
650	457	-25	0	1770	1672	1050	650	375	50
700	527	-25	0	1820	1712	1063	728	385	55
750	591	-33	+25	2200*	1952	1158	800	425	63
800	699	-33	+25						
850	864	0	+51						
900	1099	+76	+127						
950	1384	+127	+228						
1000	1734	+228	+305						
1050	2057	+305	+381						
1100	2496	+432	+431						
1150	2991	+508	+508						
1200	3543	+508	+558						
1250	4046	+508	+635						
1300	4590	+559	+673						
1350	4947	+686	+762						
1400	5709	+762	+833						
1450	6578	+833	+939						
1500	7728	+965	+1176						

TABLE B-1: [continued]

SR5-1	Strain Measurement on Column Cage $\varepsilon x10^{-6}$				
	Gauge positions & referencing				
Load kN	Top Link	Bottom Link	Load kN	Top Link	Bottom Link
50	10	0	750	83	-23
100	14	-5	800	83	-24
150	18	-5	850	83	-24
200	23	-13	900	88	-24
250	29	-12	950	79	-36
300	34	-15	1000	79	-41
350	43	-15	1050	74	-43
400	46	-19	1100	53	-56
450	49	-23	1150	30	-68
500	56	-21	1200	20	-79
550	61	-21	1250	10	-91
600	68	-20	1300	-30	-99
650	68	-31	1350	-65	-115
700	70	-33	1400	-100	-148

TABLE B-1: [continued]

SR5-2	Deflection Measurement			Strain Measurement on Column Cage $\varepsilon x10^{-6}$					
		x	y	Gauge postions & referencing					
Load	$\Delta_v \cdot 10^{-3}$	$\Delta_h \cdot 10^{-3}$	$\Delta_h \cdot 10^{-3}$	very top	top				botm
kN	mm	mm	mm	1	2	3	4	5	6
100	0	0	0	290	272	170	100	52	10
200	48	0	0	520	488	298	160	65	12
300	92	0	0	688	620	357	187	70	15
400	146	+25	-25	855	750	455	208	113	25
500	219	+25	-38	1103	993	620	310	120	25
600	298	+38	-38	1440	1325	855	508	260	28
700	378	+38	-51	1788	1665	1038	620	315	28
800	489	+51	+38	2897*	2212*	1250	742	378	28
900	711	+152	+152	6172*	3322*	1468	867	445	40
1000	1102	+356	+356	10832*	4250*	1690	988	512	60
1100	1632	+432	+457						
1200	2242	+438	+483						
1300	3454	+457	+609						
1400	4547	+483	+762						
1450	5581	+826	+1143						

TABLE B-1: [continued]

SR5-2	Strain Measurement on Column Cage $\varepsilon x10^{-6}$				
	Gauge positions & referencing				
Load kN	Top Link	Upper Middle Link	Middle Link	Lower Middle Link	Bottom Link
	1	2	3	4	5
100	7	15	5	4	-6
200	19	24	10	6	-8
300	55	34	32	-8	-16
400	51	39	39	-9	-16
500	56	41	44	-20	-30
600	35	45	30	-15	-33
700	36	46	32	-13	-29
800	35	41	30	-13	-24
900	19	27	14	-15	-25
1000	-16	-10	-20	-21	-27
1100	-45	-20	-22	-15	-20
1200	-129	-44	-35	-26	-34
1300	-190	-69	-43	-29	-35
1400	-252	-164	-100	-55	-13

TABLE B-1: [continued]

SR6-2	Deflection Measurement			Strain Measurement on Column Cage $\varepsilon x10^{-6}$			
		x	y	Gauge positions & referencing			
Load	$\Delta_v.10^{-3}$	$\Delta_h.10^{-3}$	$\Delta_h.10^{-3}$	very top	top		botm.
kN	mm	mm	mm	1	2	3	4
50	89	0	0	132	115	49	10
100	171	0	0	254	223	107	17
150	251	0	0	375	331	175	28
200	321	0	-13	503	452	246	44
250	394	+25	-25	625	561	296	50
300	476	+25	-25	750	672	350	63
350	562	+25	-25	868	772	395	68
400	654	+25	-38	975	859	428	72
450	756	+25	-51	1099	969	504	73
500	886	+25	-51	1256	1080	566	78
550	1041	+38	-64	1341	1159	621	86
600	1327	+38	-76				
625	1803	+51	-89				

TABLE B-1: [continued]

SR6-3	Deflection Measurement			Strain Measurement on Column Cage $\varepsilon x10^{-6}$			
		x	y	Gauge positions & referencing			
Load	$\Delta_v.10^{-3}$	$\Delta_h.10^{-3}$	$\Delta_h.10^{-3}$	very top	top		botm.
kN	mm	mm	mm	1	2	3	4
50	4	0	0	124	103	42	7
100	70	0	0	249	204	86	14
150	95	0	0	375	305	144	17
200	127	-13	+13	505	397	183	28
250	184	-25	+25	614	476	233	33
300	292	-38	+51	748	580	269	44
350	426	-76	+76	887	692	325	53
400	540	-76	+76	1022	796	367	60
450	641	-114	+102				
500	813	-114	+114				
550	991	-114	+114				
600	1257	-114	+114				
650	1784	-114	+127				

TABLE B-1: [continued]

SR6-4	Deflection Measurement			Strain Measurement on Column Cage $\varepsilon x10^{-6}$			
		x	y	Gauge positions & referencing			
Load	$\Delta_v.10^{-3}$	$\Delta_h.10^{-3}$	$\Delta_h.10^{-3}$	very top	top		botm.
kN	mm	mm	mm	1	2	3	4
50	6	0	0	142	120	54	15
100	32	0	0	312	276	124	28
150	70	0	0	443	395	193	42
200	102	0	0	590	520	256	50
250	124	-13	+13	743	654	314	66
300	152	-13	+13	876	741	352	65
350	191	-25	+13	1028	866	420	84
400	241	-25	+13	1153	941	460	86
450	318	-38	+25	1286	1072	500	88
500	454	-51	+25	1413	1183	559	96
550	609	-76	+25	1523	1278	595	79
600	794	-102	+51				
625	921	-102	+13				
650	1054	-102	+13				
675	1265	-102	+13				
700	1588	-102	+13				
725	2458	-102	+25				

TABLE B-1: [continued]

SR7-1	Deflection Measurement			Strain Measurement on Column Cage $\varepsilon x 10^{-6}$						
		x	y	Gauge postions & referencing						
Load	$\Delta_v \cdot 10^{-3}$	$\Delta_h \cdot 10^{-3}$	$\Delta_h \cdot 10^{-3}$	very top	top		botm.	Top Link	Mid. Link	Botm. Link
kN	mm	mm	mm	1	2	3	4			
50	44	0	0	157	140	78	20	14	3	-8
100	83	0	0	268	238	128	30	26	5	-13
150	121	0	0	393	344	194	36	36	5	-20
200	159	0	0	515	446	233	43	48	7	-25
250	194	0	0	648	539	288	50	59	8	-28
300	235	0	0	757	629	341	58	66	7	-30
350	279	-25	0	876	728	381	67	73	9	-30
400	321	-25	0	991	828	430	74	78	8	-30
450	368	-38	+25	1106	931	498	83	80	4	-30
500	432	-51	+25	1240	1060	560	108	82	-4	-25
550	495	-51	+51	1374	1174	601	110	79	-11	-24
600	594	-51	+51	1498	1286	658	114	67	-24	-28
625	648	-25	+64	1585	1359	685	118	53	-35	-34
650	702	-25	+76	1675	1432	710	120	47	-54	-34
675	772	0	+102	1772	1506	728	116	30	-56	-43
700	857	+13	+127	1888	1616	753	119	9	-76	-51
712.5	1491	+25	+127							

TABLE B-1: [continued]

SR7-2	Deflection Measurement			Strain Measurement on Column Cage $\varepsilon x10^{-6}$				
		x	y	Gauge Positions & Referencing				
Load	$\Delta_v \cdot 10^{-3}$	$\Delta_h \cdot 10^{-3}$	$\Delta_h \cdot 10^{-3}$	very top	top		botm.	Top Link
kN	mm	mm	mm					
50	44	0	0	146	128	56	12	18
100	89	0	0	251	223	107	15	35
150	136	0	0	364	325	156	19	44
200	181	0	0	484	430	213	30	53
250	232	0	0	620	553	278	45	58
300	286	0	0	784	698	341	46	69
350	349	0	0	883	780	378	47	73
400	429	0	0	985	854	422	55	75
450	540	0	0	1090	941	470	64	75
500	648	-25	0	1199	1024	517	72	74
550	768	-25	0	1343	1147	567	79	69
600	918	-52	+25	1475	1252	614	85	58
625	1016	-52	+25	1586	1345	679	96	50
650	1095	-52	+25					46
675	1200	-52	+38					36
700	1324	-52	+51					21
725	1511	-52	+76					-4
750	1905	-25	+76					-76
775	2261	0	+102					-122
800	2563	+25	+102					-177
825	4432	+52	+102					-280

TABLE B-1: [continued]

SR8-1	Deflection Measurement			Strain Measurement on Column Cage $\varepsilon x10^{-6}$			
		x	y	Gauge positions & referencing			
Load	$\Delta_v.10^{-3}$	$\Delta_h.10^{-3}$	$\Delta_h.10^{-3}$	very top	top		botm.
kN	mm	mm	mm	1	2	3	4
50	64	0	0	138	123	78	11
100	127	0	0	247	219	143	30
150	229	0	0	357	318	205	35
200	352	0	0	473	422	263	42
225	403	0	0	525	468	288	50
250	470	-25	0	582	518	314	55
275	540	-25	0	669	605	376	93
300	616	-51	0	730	665	411	105
325	705	-51	0	761	682	404	75
350	878	-51	0	811	721	420	68
375	902	-51	0	864	768	442	71
400	1029	-76	+13	924	822		
425	1156	-101	+25				
450	1353	-101	+25				
475	1601	-127	+51				
500	2121	-127	+76				

TABLE B-1: [continued]

SR8-2	Deflection Measurement			Strain Measurement on Column Cage $\varepsilon x10^{-6}$			
		x	y	Gauge positions & referencing			
Load	$\Delta_v.10^{-3}$	$\Delta_h.10^{-3}$	$\Delta_h.10^{-3}$	very top	top		botm.
kN	mm	mm	mm	1	2	3	4
50	38	0	0	126	108	52	12
100	70	0	0	251	219	107	25
150	108	0	0	356	321	174	43
175	133	0	0	404	360	193	44
200	175	0	0	455	403	218	57
225	229	0	0	530	470	254	58
250	290	0	0	600	530	289	60
275	372	0	0	652	577	311	60
300	470	0	0	705	626	334	63
325	572	0	+13	762	680	362	67
350	692	0	+13	811	724	385	68
375	832	0	+13	868	774	409	72
400	1007	0	+13	920	817	430	75
425	1261	0	+25				
450	1467	-25	+51				
475	2731	-25	+51				

TABLE B-1: [continued]

SR8-3	Deflection Measurement			Strain Measurement on Column Cage $\varepsilon x10^{-6}$			
		x	y	Gauge positions & referencing			
Load	$\Delta_v.10^{-3}$	$\Delta_h.10^{-3}$	$\Delta_h.10^{-3}$	very top	top		botm.
kN	mm	mm	mm	1	2	3	4
50	44	0	0	125	105	46	7
100	76	0	0	239	211	112	23
150	102	0	0	345	301	161	29
200	140	0	0	448	390	209	36
250	165	0	0	556	483	259	42
275	197	0	0	618	546	285	47
300	229	0	0	676	591	313	52
325	271	0	0	733	645	340	56
350	296	0	0	789	689	368	60
375	343	+13	-25	849	741	393	63
400	413	+13	-25	916	789	421	66
425	495	+25	-25	969	840	435	79
450	584	+25	-25	1019	888	463	89
475	711	+25	-25	1087	946	492	92
500	889	+51	-25	1156	997	511	97
525	1245	+51	-25	1210	1043	540	110
550	2689	+51	-25				

TABLE B-1: [continued]

SR8-4	Deflection Measurement			Strain Measurement on Column Cage $\varepsilon x10^{-6}$			
		x	y	Gauge positions & referencing			
Load	$\Delta_v.10^{-3}$	$\Delta_h.10^{-3}$	$\Delta_h.10^{-3}$	very top	top		botm.
kN	mm	mm	mm	1	2	3	4
50	83	0	0	126	109	47	9
100	146	0	0	245	218	83	27
150	216	0	0	364	335	147	40
200	292	0	0	492	452	216	56
250	387	0	0	608	560	279	65
300	483	-25	+25	727	666	336	75
350	597	-25	+25	837	764	387	82
400	737	-25	+25	959	872	443	91
450	889	-25	+25	1058	974	491	92
500	1067	-25	+25	1181	1077	558	99
550	1270	-51	+51	1363	1189	605	100
600	1492	-51	+51	1490	1304	681	105
625	1994	-51	+76				

TABLE B-1: [continued]

SR9-1	Deflection Measurement			Strain Measurement on Column Cage $\varepsilon \times 10^{-6}$						
		x	y	Gauge postions & referencing						
Load	$\Delta_{vc}.10^{-3}$	$\Delta_{vb}.10^{-3}$	$\Delta_{vt}.10^{-3}$	col. top	col. botm.	base top		base botm.	col. upper link	col. lower link
kN	mm	mm	mm	1	2	3	4	5		
100	114	0	114	62	52	40	20	5	37	28
200	229	0	229	147	134	86	45	10	-7	3
300	371	0	371	158	144	116	75	12	-33	-8
400	483	0	483	214	190	149	89	10	-56	-18
500	597	0	597	272	237	185	104	10	-78	-25
600	762	0	762	343	289	226	120	11	-107	-34
700	838	0	838	418	346	273	140	18	-130	-45
800	966	0	972	525	410	325	169	35	-147	-49
900	1080	0	1086	584	453	349	168	24	-206	-72
1000	1207	0	1219	674	505	382	176	23	-255	-89
1100	1356	0	1365	781	562	415	187	22	-312	-106
1200	1524	6	1530	900	620	448	200	24	-384	-124
1300	1701	20	1696	1024	678	480	213	27	-466	-140
1400	1905	45	1899	1197	744	517	227	30	-591	-157
1500	2136	104	2134	1412	812	552	241	33	-774	-176
1600	2489	137	2489	1741	897	586	256	37	-1042	-199
1700	3099	248	3118	2477*	1009	590	252	38	-1616	-231
1750	3531	285	3537	3125*	1206	644	280	41	-2120	-259

TABLE B-1: [continued]

SR9-2	Deflection Measurement			Strain Measurement on column Cage $\varepsilon \times 10^{-6}$						
		x	y	Gauge postions & referencing						
Load	$\Delta_{vc}.10^{-3}$	$\Delta_{vb}.10^{-3}$	$\Delta_{vt}.10^{-3}$	col. top	col . botm.	base top		base botm.	col. upper link	col. lower link
kN	mm	mm	mm	1	2	3	4	5		
100	101	22	98	58	51	34	16	1	-33	-21
200	203	25	203	113	101	70	38	2	-56	-41
300	317	32	311	171	155	109	57	3	-79	-59
400	438	59	440	229	204	146	69	4	-105	-88
500	540	59	542	296	258	181	76	3	-103	-94
600	647	68	652	368	312	217	84	3	-161	-118
700	775	84	770	452	373	253	93	3	-193	-139
800	901	88	901	536	431	286	102	4	-230	-162
900	1042	93	1046	647	495	305	109	6	-277	-194
1000	1143	102	1143	748	558	349	120	8	-332	-222
1100	1348	123	1342	867	626	379	129	8	-405	-256
1200	1600	132	1592	1044	710	408	140	9	-511	-298
1300	1803	139	1795	1210	794	438	154	12	-622	-337
1400	2051	141	2053	1428	907	474	171	13	-781	-386
1500	2296	149	2301	1662	1032	526	195	18	-1000	-436
1550	2413	149	2413	1884	1125	562	209	18	-1181	-474
1600	2692	156	2696	2275*	1233	628	241	24	-1492	-510
1650	3088	178	3099	2898*	1284	663	254	25	-2100	-524

TABLE B-1: [continued]

SR10-1	Deflection Measurement			Strain Measurement on Column Cage $\varepsilon x10^{-6}$						
		x	y	Gauge postions & referencing						
Load	$\Delta_{vc}.10^{-3}$	$\Delta_{vb}.10^{-3}$	$\Delta_{vt}.10^{-3}$	col. top	col. botm.	base top		base botm.	col. upper link	col. lower link
kN	mm	mm	mm	1	2	3	4	5		
100	172	58	178	130	78	57	33	5	-27	-18
200	336	87	349	206	149	113	69	16	-51	-34
300	494	116	508	271	211	162	95	15	-79	-54
400	646	146	660	344	278	210	117	13	-109	-73
500	838	162	832	425	349	265	134	13	-144	-94
600	996	195	1003	521	429	325	151	15	-183	-117
700	1174	205	1181	630	515	387	166	19	-223	-145
800	1292	243	1359	742	601	448	190	26	-268	-174
900	1534	271	1549	867	691	506	210	30	-318	-205
1000	1696	274	1772	1030	787	560	231	36	-387	-242
1100	1988	297	2003	1219	901	613	256	42	-480	-287
1200	2184	325	2205	1450	1019	662	281	50	-619	-350
1250	2478	331	2483	1620	1096	687	295	53	-704	-386
1300	2620	391	2673	1802	1179	715	308	57	-805	-430
1350	2860	458	2864	1974*	1255	739	321	58	-919	-473
1400	3146	480	3156	2376*	1350	765	334	60	-1146	-544
1425	3526	506	3530	3255*	1455	791	346	61	-1824	-650

TABLE B-1: [continued]

SR10-2	Deflection Measurement			Strain Measurement on Column Cage $\varepsilon x10^{-6}$						
		x	y	Gauge postions & referencing						
Load	$\Delta_{vc}.10^{-3}$	$\Delta_{vb}.10^{-3}$	$\Delta_{vt}.10^{-3}$	col. top	col. botm.	base top		base botm.	col. upper link	col. lower link
kN	mm	mm	mm	1	2	3	4	5		
100	317	0	318	103	91	70	26	0	-14	-17
200	529	0	527	197	176	129	52	0	-41	-55
300	691	14	692	302	273	199	88	4	-75	-85
400	884	39	883	405	364	259	104	6	-109	-123
500	1085	81	1080	517	460	315	119	7	-150	-165
600	1292	158	1289	636	560	373	139	12	-197	-212
700	1528	166	1524	774	668	430	165	16	-249	-264
800	1774	172	1772	929	784	488	197	24	-309	-325
900	2132	186	2141	1127	911	548	232	33	-389	-413
950	2263	205	2272	1229	983	583	253	39	-435	-467
1000	2482	222	2491	1366	1063	622	277	47	-492	-536
1050	2660	241	2669	1470	1123	652	292	50	-549	-604
1100	2911	283	2904	1640	1187	676	305	56	-602	-715
1150	3209	343	3207	1837	1250	692	309	52	-732	-900
1200	3472	411	3474	2046*	1341	722	326	57	-838	-1097
1250	3775	447	3777	2301*	1437	752	344	60	-955	-1273
1300	4429	597	4431	3060*	1555	797	353	51	-1386	-1802

TABLE B-1: [continued]

SR4-1	STRAIN MEASUREMENT ON BASE TENSION REINFORCEMENT, $\varepsilon x10^{-6}$											
Load	FIRST LAYER						SECOND LAYER					
kN	1	2	3	4	5	6	1	2	3	4	5	6
50	0	5	0	5	10	0	10	15	0	5	0	10
100	10	5	-10	0	5	5	15	20	-5	0	0	10
150	10	5	-10	-5	5	10	20	20	-10	-5	5	15
200	10	5	-10	-5	5	10	20	10	-15	-5	0	20
250	10	5	-15	-10	0	15	20	15	-15	-15	0	20
300	15	0	-15	-10	0	20	30	15	-15	-15	5	25
350	15	0	-25	-25	0	25	30	15	-25	-20	0	25
400	15	-5	-45	-40	-5	25	35	10	-30	-30	5	30
450	20	-5	-60	-50	-5	30	40	20	-35	-30	10	35
500	20	-5	-75	-65	-5	30	45	25	-40	-35	10	40
550	25	-10	-105	-100	-10	35	40	10	-70	-65	10	40
600	30	-10	-145	-130	-10	40	50	20	-75	-70	10	45
650	30	-15	-150	-145	-15	40	55	15	-95	-90	10	40
700	25	-30	-180	-170	-25	40	40	-10	-130	-130	-15	30
750	25	-35	-200	-195	-35	40	40	-10	-150	-145	-15	25
800	25	-35	-215	-210	-35	45	50	-15	-165	-150	-15	35
850	25	-40	-240	-235	-40	45	40	-20	-180	-175	-25	30
900	30	-40	-255	-250	-40	45	50	-30	-200	-190	-25	40
950	35	-40	-270	-270	-40	55	50	-25	-205	-195	-25	50
1000	30	-50	-295	-290	-50	50	50	-35	-230	-220	-25	45
1050	35	-50	-310	-300	-50	55	55	-30	-240	-235	-30	50
1100	35	-60	-325	-325	-60	55	60	-30	-260	-250	-30	50
1150	35	-75	-350	-345	-65	55	55	-50	-285	-265	-45	50
1200	45	-80	-370	-360	-70	60	65	-55	-290	-280	-50	55
1250	45	-85	-390	-385	-80	65	65	-65	-310	-300	-60	60
1300	45	-95	-420	-410	-105	65	65	-80	-320	-315	-75	65

TABLE B-2: STRAIN RECORDING IN THE BASE

SR4-2	STRAIN MEASUREMENT ON BASE TENSION REINFORCEMENT, $\varepsilon x10^{-6}$											
Load	FIRST LAYER						SECOND LAYER					
kN	1	2	3	4	5	6	1	2	3	4	5	6
50	5	0	-10	-5	0	5	0	5	-10	-10	5	0
100	20	10	-5	-5	5	25	5	0	-10	-10	5	5
150	30	15	-10	-5	10	35	10	5	-10	-10	5	10
200	35	15	-20	-10	5	40	10	5	-15	-20	5	10
250	25	0	-40	-30	5	30	0	5	-20	-25	5	5
300	40	5	-35	-30	5	45	10	0	-25	-30	-5	15
350	45	10	-40	-40	5	55	20	-5	-35	-35	-5	20
400	55	10	-45	-45	0	65	25	0	-35	-40	-5	25
450	50	0	-60	-60	-5	70	20	-10	-50	-60	-15	20
500	50	-5	-75	-75	-10	70	20	-10	-55	-65	-20	20
550	55	-5	-80	-85	-10	75	30	-20	-60	-70	-20	25
600	65	-5	-85	-90	-10	80	35	-20	-65	-70	-20	35
650	65	-5	-105	-115	-15	75	30	-20	-80	-80	-20	30
700	80	-5	-105	-115	-15	85	40	-15	-85	-80	-25	45
750	80	-5	-115	-125	-10	90	50	-25	-85	-90	-35	50
800	95	-10	-130	-135	-10	100	50	-30	-100	-95	-40	45
850	105	-15	-140	-155	-15	105	55	-35	-105	-100	-45	55
900	100	-20	-145	-160	-15	115	60	-40	-115	-110	-50	60
950	105	-30	-165	-175	-25	115	70	-45	-135	-115	-55	65
1000	120	-35	-190	-190	-30	120	70	-55	-155	-130	-65	70
1050	115	-50	-210	-205	-40	115	65	-65	-165	-150	-75	60
1100	115	-65	-235	-220	-50	120	70	-70	-185	-165	-75	65
1150	120	-70	-250	-240	-65	125	70	-75	-200	-185	-80	65
1200	115	-85	-270	-260	-80	125	70	-80	-220	-200	-85	65
1250	115	-105	-285	-270	-100	125	70	-90	-240	-220	-95	70
1300	110	-140	-310	-290	-130	125	70	-100	-270	-240	-105	70
1350	115	-150	-320	-295	-135	125	75	-120	-275	-245	-130	70
1400	115	-170	-335	-305	-185	125	75	-145	-310	-280	-155	70

TABLE B-2: [continued]

SR4-3	STRAIN MEASUREMENT ON BASE TENSION REINFORCEMENT, $\varepsilon x10^{-6}$											
Load	FIRST LAYER						SECOND LAYER					
kN	1	2	3	4	5	6	1	2	3	4	5	6
50	5	0	-10	-15	-5	0	0	-5	-5	-10	-5	0
100	5	0	-20	-20	-10	0	0	-5	-15	-15	-5	0
150	5	-5	-20	-25	-10	0	0	-5	-20	-20	-5	0
200	5	-10	-30	-35	-15	0	0	-10	-25	-30	-10	0
250	5	-10	-35	-40	-15	0	0	-10	-30	-30	-15	0
300	5	-15	-40	-45	-20	0	0	-15	-40	-35	-15	0
350	10	-15	-45	-45	-20	5	5	-15	-40	-40	-15	5
400	10	-20	-50	-55	-25	5	5	-15	-45	-45	-20	5
450	15	-25	-55	-60	-25	10	5	-15	-50	-50	-20	5
500	20	-25	-55	-65	-25	10	10	-15	-55	-60	-20	10
550	25	-25	-65	-75	-25	15	15	-15	-60	-65	-20	15
600	20	-20	-70	-90	-25	15	15	-20	-65	-75	-25	15
650	25	-20	-90	-90	-25	20	20	-20	-75	-90	-25	15
700	25	-25	-100	-110	-25	20	20	-20	-80	-100	-30	15
750	25	-25	-105	-125	-25	25	20	-25	-95	-115	-35	15
800	25	-30	-120	-130	-35	25	20	-30	-100	-130	-40	20
850	30	-30	-145	-155	-35	30	25	-30	-110	-140	-40	20
900	30	-30	-160	-180	-35	30	25	-35	-130	-150	-50	20
950	30	-35	-180	-195	-45	30	25	-45	-140	-160	-55	25
1000	35	-35	-190	-215	-45	35	35	-45	-150	-175	-60	25
1050	40	-40	-205	-225	-50	40	40	-50	-165	-185	-60	30
1100	40	-40	-220	-230	-50	40	40	-55	-180	-195	-65	30
1150	40	-45	-230	-250	-55	40	45	-60	-195	-205	-75	30
1200	40	-60	-245	-275	-60	40	45	-70	-210	-220	-80	30
1250	45	-70	-255	-290	-60	45	45	-80	-220	-240	-90	35
1300	50	-80	-275	-310	-75	50	45	-90	-235	-255	-100	35
1350	50	-100	-295	-330	-75	50	45	-100	-245	-275	-105	35
1400	60	-105	-315	-350	-85	50	50	-105	-260	-295	-110	45
1450	60	-125	-330	-365	-105	55	60	-115	-275	-315	-130	50

TABLE B-2: [continued]

SR6-2	STRAIN MEASUREMENT ON BASE TENSION REINFORCEMENT, $\varepsilon \times 10^{-6}$													
Load	FIRST LAYER							SECOND LAYER						
kN	1	2	3	4	5	6	7	1	2	3	4	5	6	7
50	10	5	-10	-10	-15	0	5	10	5	-5	-5	-10	0	10
100	15	5	-15	-15	-25	0	10	15	5	-15	-10	-15	-5	15
150	15	5	-30	-20	-35	-5	15	20	0	-25	-15	-30	-5	15
200	20	5	-40	-30	-50	-5	20	25	0	-35	-20	-35	-10	20
250	25	5	-55	-40	-70	-10	25	30	-5	-45	-25	-50	-10	25
300	35	5	-85	-50	-100	-10	35	35	-5	-60	-40	-80	-20	30
350	40	-10	-100	-60	-120	-15	40	40	-5	-80	-50	-105	-20	40
400	45	-25	-130	-65	-165	-40	45	40	-20	-115	-65	-135	-30	45
450	50	-35	-175	-70	-190	-50	50	50	-39	-140	-73	-155	-50	50
500	55	-50	-215	-98	-225	-68	55	55	-70	-175	-84	-190	-85	55
550	60	-65	-270	-120	-285	-90	50	65	-95	-200	-90	-220	-105	65
600	70	-90	-305	-130	-320	-130	47	65	-130	-240	-115	-255	-130	75
625	75	-115	-345	-165	-350	-140	40	50	-180	-330	-170	-300	-155	75

TABLE B-2: [continued]

SR6-3	STRAIN MEASUREMENT ON BASE TENSION REINFORCEMENT, $\varepsilon x10^{-6}$													
Load	FIRST LAYER							SECOND LAYER						
kN	1	2	3	4	5	6	7	1	2	3	4	5	6	7
50	7	-11	-24	-14	-16	-	-	4	-5	-20	-11	-12	-	-
100	9	-14	-40	-23	-25	-	-	9	-10	-33	-17	-20	-	-
150	13	-19	-55	-32	-41	-	-	12	-11	-49	-22	-28	-	-
200	19	-24	-74	-43	-54	-	-	17	-16	-69	-31	-38	-	-
250	28	-25	-117	-62	-89	-	-	22	-25	-102	-50	-62	-	-
300	37	-28	-176	-92	-130	-	-	31	-45	-141	-76	-104	-	-
350	48	-38	-210	-124	-187	-	-	37	-90	-174	-105	-157	-	-
400	57	-51	-263	-153	-225	-	-	43	-128	-215	-147	-227	-	-
450	66	-76	-315	-191	-261	-	-	49	-160	-263	-196	-308	-	-
500	72	-117	-358	-228	-313	-	-	54	-200	-313	-256	-385	-	-
550	63	-154	-593	-442	-499	-	-	22	-219	-471	-522	-599	-	-

TABLE B-2: [continued]

SR6-4	STRAIN MEASUREMENT ON BASE TENSION REINFORCEMENT, $\varepsilon \times 10^{-6}$													
Load	FIRST LAYER							SECOND LAYER						
kN	1	2	3	4	5	6	7	1	2	3	4	5	6	7
50	5	0	-25	-15	-25	-10	5	5	-5	-20	-10	-15	-20	10
100	10	-5	-45	-25	-50	-10	10	10	-5	-35	-10	-25	-20	10
150	20	-5	-60	-30	-65	-10	15	15	-5	-45	-20	-35	-20	20
200	25	-5	-75	-40	-85	-10	20	20	-5	-60	-25	-45	-15	25
250	30	-10	-90	-50	-105	-20	20	25	-10	-80	-30	-60	-20	30
300	35	-10	-105	-55	-125	-20	25	30	-15	-85	-40	-70	-15	30
350	40	-10	-120	-65	-145	-20	30	35	-15	-105	-50	-90	-15	35
400	50	-10	-145	-75	-175	-30	35	45	-20	-135	-55	-105	-15	45
450	55	-15	-175	-90	-220	-50	40	50	-30	-165	-70	-140	-10	50
500	60	-35	-205	-110	-270	-55	50	60	-35	-195	-85	-180	-20	60
550	70	-65	-275	-135	-305	-70	50	65	-50	-255	-150	-235	-35	65
600	75	-85	-320	-165	-345	-85	60	65	-75	-305	-190	-280	-55	70
625	80	-95	-340	-185	-375	-95	60	65	-100	-340	-225	-300	-60	70
650	80	-105	-365	-195	-405	-105	65	70	-110	-365	-250	-320	-80	75
675	85	-115	-390	-220	-435	-110	60	70	-125	-405	-280	-350	-85	80
700	90	-135	-435	-255	-465	-140	65	60	-145	-455	-325	-400	-115	80
725	85	-165	-485	-305	-515	-180	55	35	-200	-565	-425	-490	-135	80

TABLE B-2: [continued]

SR7-2	STRAIN MEASUREMENT ON BASE TENSION REINFORCEMENT, $\varepsilon \times 10^{-6}$									
Load	FIRST LAYER					SECOND LAYER				
kN	1	2	3	4	5	1	2	3	4	5
50	2	-15	-24	-17	-10	2	-8	-18	-15	-17
100	11	-13	-31	-19	-14	9	-5	-22	-15	-24
150	13	-17	-47	-30	-34	12	-9	-34	-27	-38
200	16	-21	-77	-45	-57	14	-12	-47	-37	-57
250	18	-24	-119	-67	-83	16	-16	-66	-52	-81
300	28	-22	-157	-87	-104	24	-12	-105	-71	-120
350	37	-17	-187	-125	-146	32	-10	-145	-92	-169
400	42	-18	-237	-168	-176	37	-11	-179	-112	-206
450	50	-24	-271	-200	-217	41	-14	-212	-143	-247
500	56	-36	-308	-224	-255	48	-19	-249	-165	-276
550	61	-72	-344	-249	-295	53	-39	-289	-193	-319
600	67	-96	-396	-278	-363	57	-59	-312	-219	-367
625	67	-113	-407	-300	-386	61	-77	-335	-246	-391
650	68	-119	-437	-313	-398	61	-86	-362	-261	-417
675	65	-133	-460	-326	-417	63	-101	-393	-288	-448
700	61	-145	-484	-340	-430	68	-121	-411	-311	-485
725	46	-180	-512	-370	-484	54	-166	-438	-348	-530
750	38	-227	-657	-483	-549	43	-224	-574	-467	-620
775	29	-259	-713	-561	-655	33	-244	-643	-546	-724
800	18	-290	-834	-604	-718	22	-268	-707	-587	-804
825	14	-327	-974	-644	-787	16	-307	-810	-636	-906

TABLE B-2: [continued]

SR9-1	STRAIN MEASUREMENT ON BASE TENSION REINFORCEMENT, $\varepsilon x10^{-6}$									
Load	FIRST LAYER					SECOND LAYER				
kN	1	2	3	4	5	1	2	3	4	5
100	40	16	1	6	16	43	32	13	20	20
200	24	-8	-35	-23	-11	13	-10	-27	-18	-15
300	17	-26	-56	-46	-45	7	-20	-52	-40	-38
400	20	-35	-82	-56	-59	10	-23	-72	-58	-52
500	23	-40	-101	-70	-76	11	-27	-91	-71	-68
600	42	-44	-115	-77	-84	33	-29	-94	-72	-74
700	36	-51	-154	-105	-123	23	-33	-133	-103	-106
800	50	-53	-163	-109	-127	33	-38	-143	-104	-109
900	48	-56	-215	-142	-185	29	-44	-183	-146	-162
1000	56	-57	-242	-160	-209	35	-49	-214	-167	-184
1100	55	-68	-293	-199	-255	35	-60	-251	-200	-222
1200	58	-85	-334	-231	-296	35	-71	-289	-235	-263
1300	64	-94	-376	-262	-337	39	-84	-338	-268	-312
1400	70	-108	-421	-299	-383	44	-97	-375	-304	-388
1500	79	-125	-467	-340	-438	51	-116	-420	-344	-462
1600	81	-149	-524	-389	-489	54	-136	-494	-390	-524
1700	67	-216	-650	-510	-630	41	-204	-637	-525	-708
1750	62	-245	-688	-577	-697	33	-243	-689	-568	-766

TABLE B-2: [continued]

SR9-2	STRAIN MEASUREMENT ON BASE TENSION REINFORCEMENT, $\varepsilon \times 10^{-6}$									
Load	FIRST LAYER					SECOND LAYER				
kN	1	2	3	4	5	1	2	3	4	5
100	-	-15	-30	-25	-34	1	-10	-22	-17	-23
200	-	-22	-43	-40	-50	4	-15	-36	-27	-36
300	-	-30	-59	-55	-68	7	-21	-53	-39	-50
400	-	-36	-71	-69	-94	10	-25	-68	-48	-63
500	-	-41	-97	-83	-110	14	-29	-84	-57	-77
600	-	-49	-115	-99	-139	19	-29	-97	-65	-94
700	-	-53	-136	-117	-166	24	-32	-114	-77	-113
800	-	-59	-149	-139	-204	27	-38	-133	-92	-132
900	-	-65	-187	-160	-225	28	-43	-155	-112	-151
1000	-	-71	-226	-186	-254	32	-46	-176	-132	-173
1100	-	-79	-256	-214	-290	40	-52	-202	-158	-197
1200	-	-87	-291	-251	-338	42	-57	-230	-187	-228
1300	-	-99	-334	-283	-360	45	-63	-257	-210	-255
1400	-	-109	-357	-315	-404	53	-67	-285	-235	-285
1500	-	-120	-385	-348	-436	55	-74	-314	-259	-314
1550	-	-135	-408	-374	-460	52	-84	-335	-277	-337
1600	-	-147	-425	-400	-478	57	-87	-353	-291	-358
1650	-	-157	-422	-411	-466	61	-92	-360	-298	-369

TABLE B-2: [continued]

SR10-1	STRAIN MEASUREMENT ON BASE TENSION REINFORCEMENT, $\hat{\varepsilon} \times 10^{-6}$									
Load	FIRST LAYER					SECOND LAYER				
kN	1	2	3	4	5	1	2	3	4	5
100	12	-5	-34	-28	-50	5	-7	-40	-24	-32
200	25	-5	-59	-45	-84	11	-5	-70	-41	-57
300	31	-6	-82	-58	-115	13	-9	-103	-61	-89
400	33	-20	-140	-90	-170	16	-12	-145	-86	-135
500	39	-25	-206	-119	-225	19	-14	-197	-121	-194
600	45	-30	-281	-152	-290	26	-16	-257	-162	-260
700	51	-38	-357	-188	-351	31	-18	-329	-203	-340
800	54	-47	-416	-224	-404	33	-23	-386	-241	-400
900	59	-59	-473	-260	-460	40	-26	-443	-280	-460
1000	62	-77	-541	-305	-532	42	-34	-511	-326	-531
1100	63	-101	-611	-354	-608	43	-48	-588	-373	-606
1200	65	-128	-685	-410	-695	45	-72	-674	-427	-692
1250	66	-145	-736	-444	-751	47	-87	-725	-456	-746
1300	66	-164	-794	-485	-813	45	-108	-789	-495	-812
1350	66	-180	-845	-521	-865	46	-123	-843	-526	-868
1400	65	-198	-901	-560	-921	45	-142	-907	-562	-929
1425	65	-215	-956	-596	-973	45	-160	-968	-600	-990

TABLE B-2: [continued]

A P P E N D I X C

This appendix consists of the crack patterns of the concrete on the top and bottom faces of the base and all the faces of the column for the test specimens.

The Legend

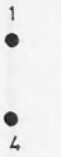

the numbers indicate four column longitudinal bars

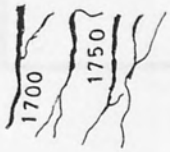

cracks in column and foundation, the numbers refer to the applied load in kN at which part of the crack developed

spalling or missing part of the concrete

F1, F2, F3, F4 column faces 1 to 4, respectively

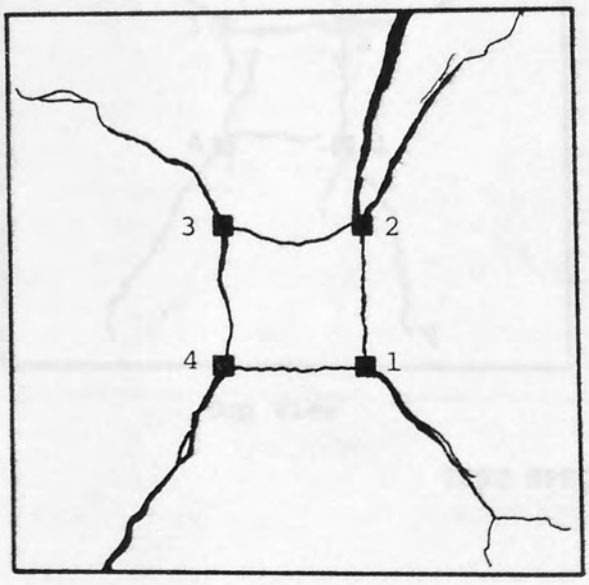

Top View

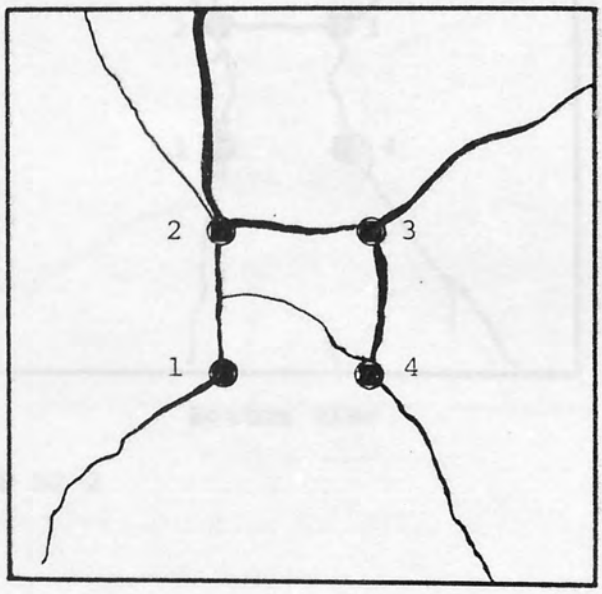

Bottom View

TEST SPECIMEN S2-1

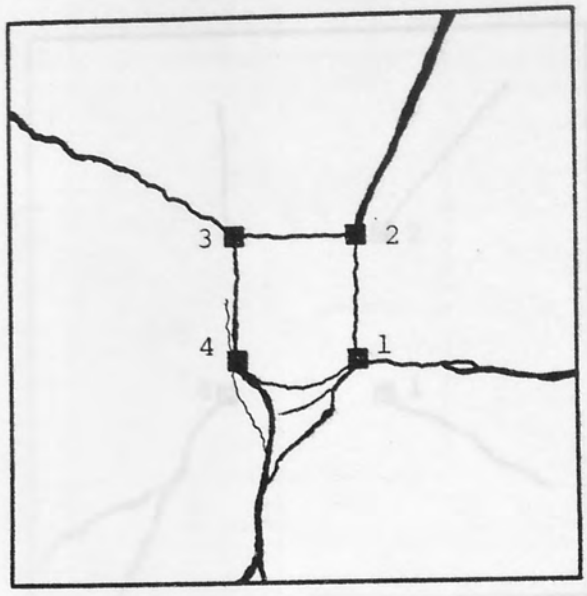

Top View

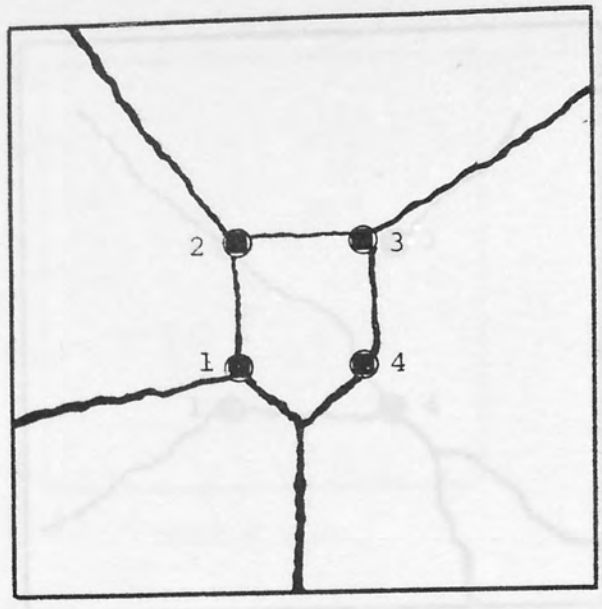

Bottom View

TEST SPECIMEN $\overline{S}2-1$

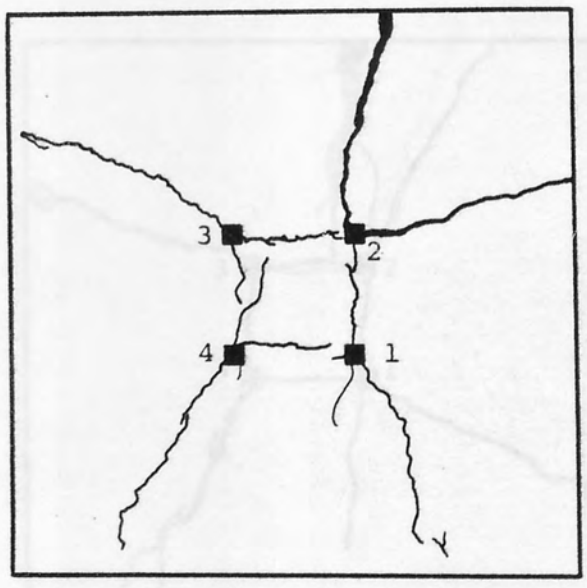

Top View

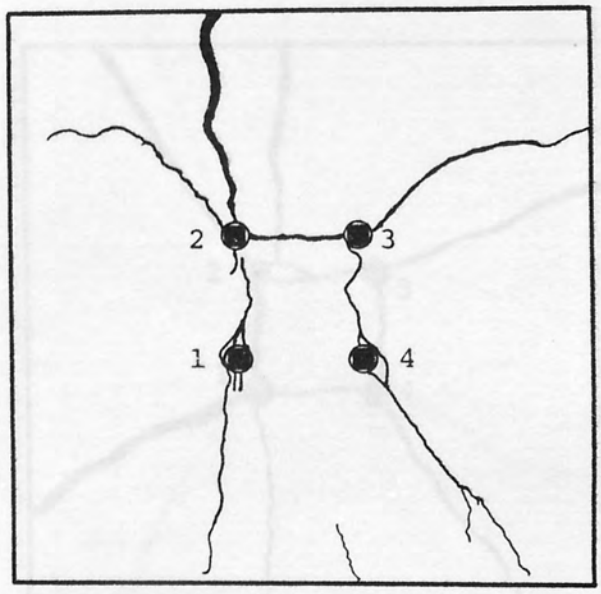

Bottom View

TEST SPECIMEN S2-2

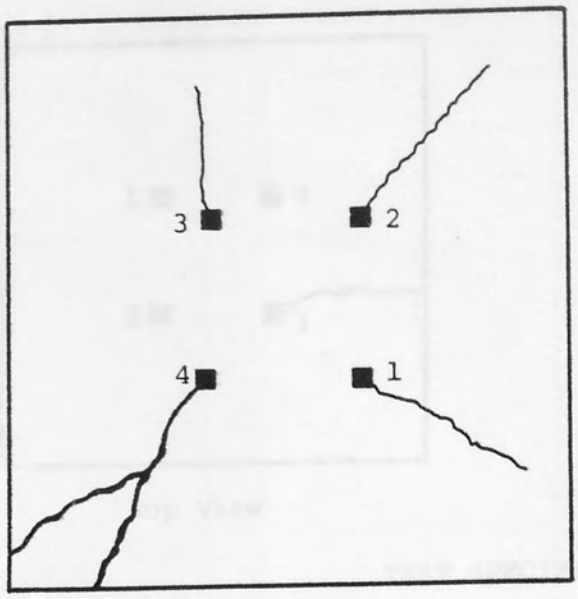

Top View

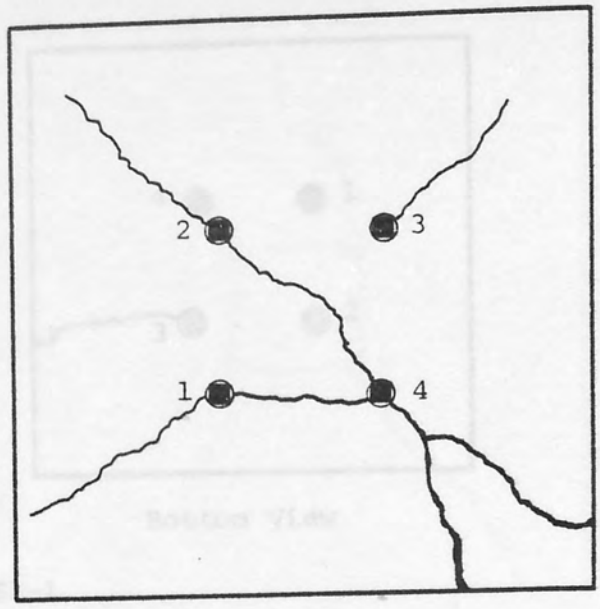

Bottom View

TEST SPECIMEN $\overline{S}2-2$

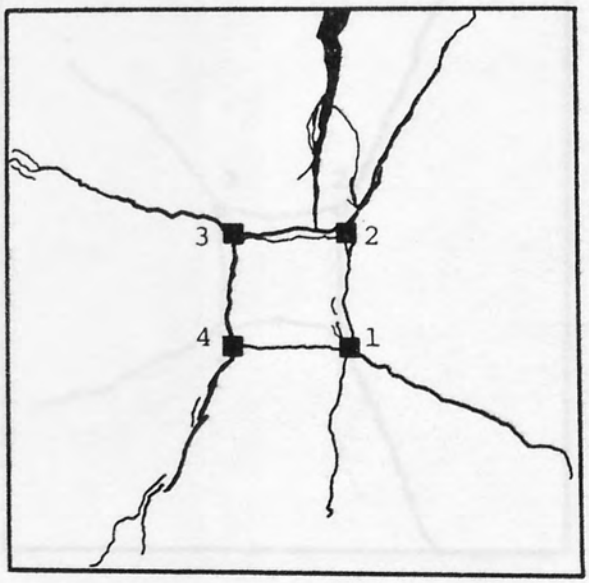

Top View

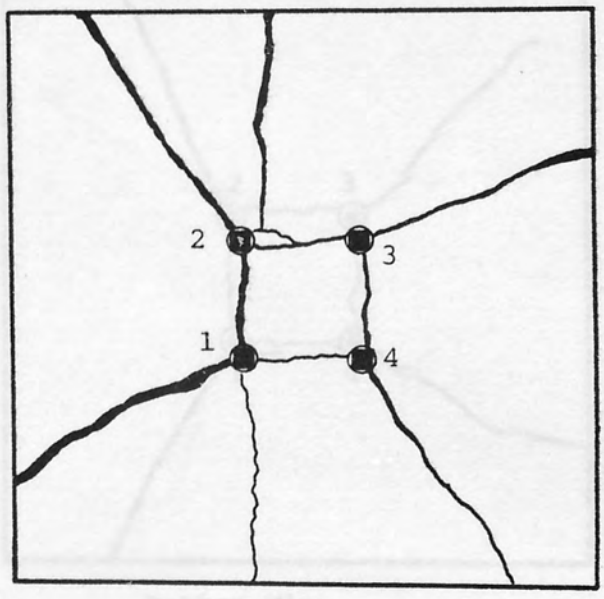

Bottom View

TEST SPECIMEN S2-4

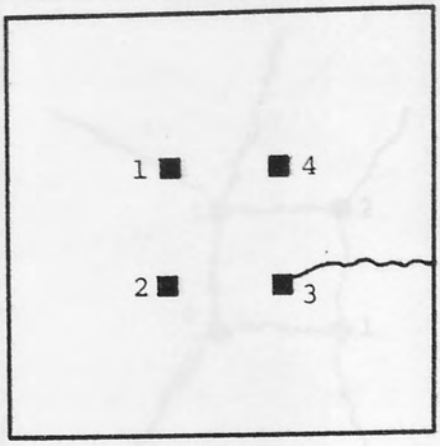

Top View

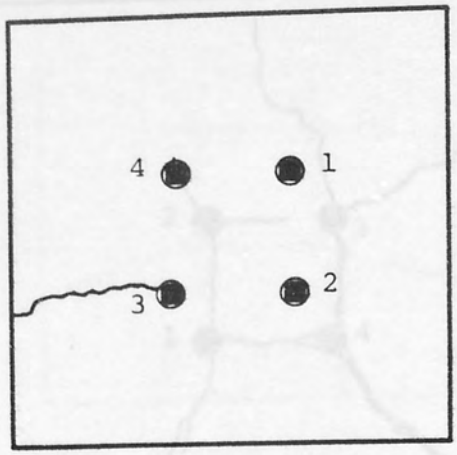

Bottom View

TEST SPECIMEN S3-1

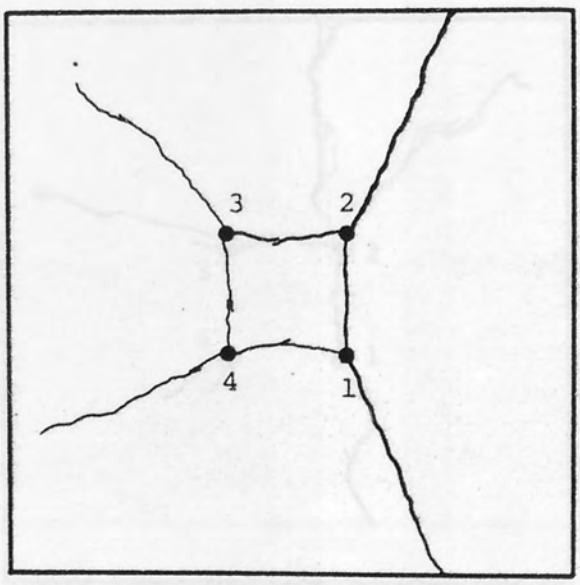

Top View

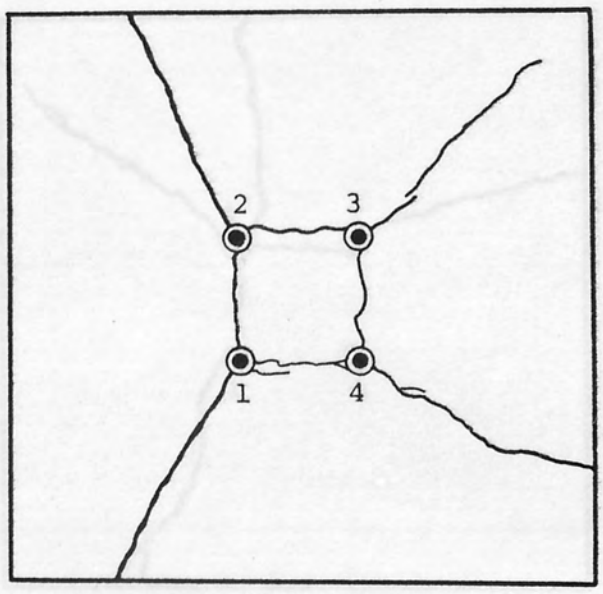

Bottom View

TEST SPECIMEN SR1-2

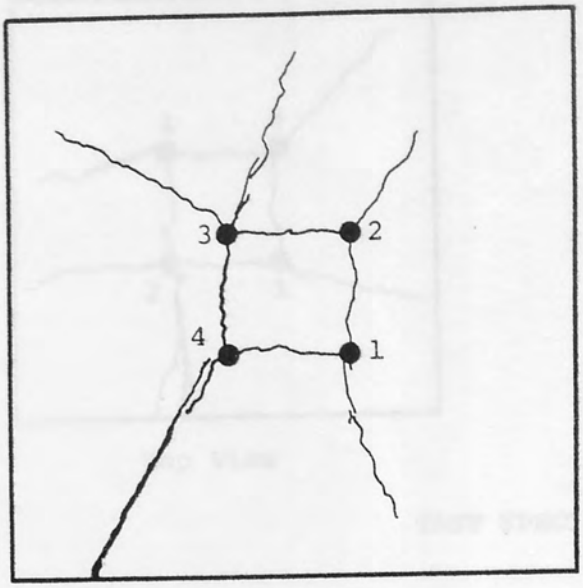

Top View

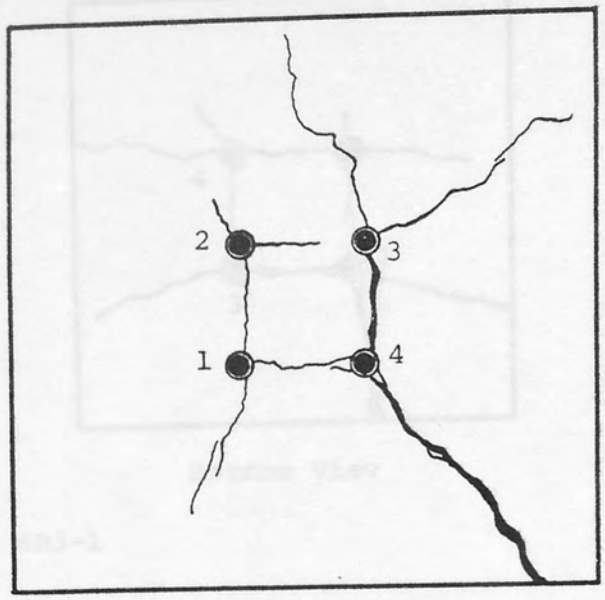

Bottom View

TEST SPECIMEN SR2-1

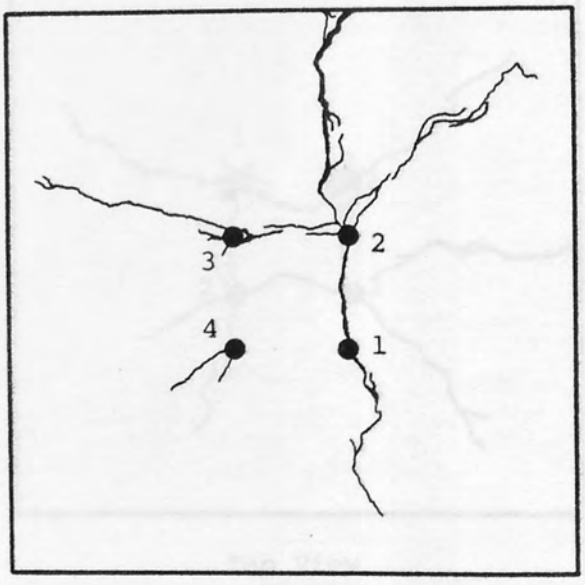

Top View

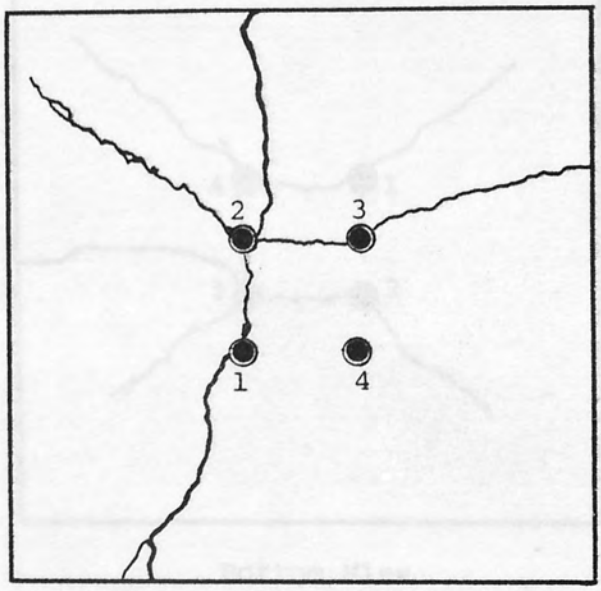

Bottom View

TEST SPECIMEN SR2-2

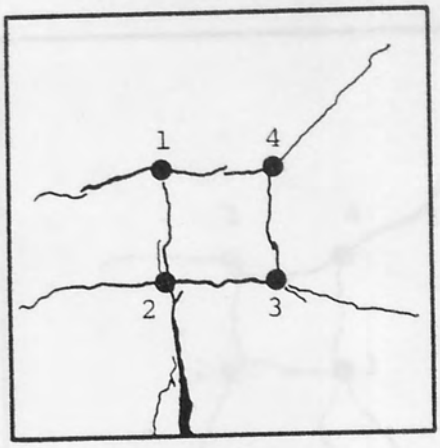

Top View

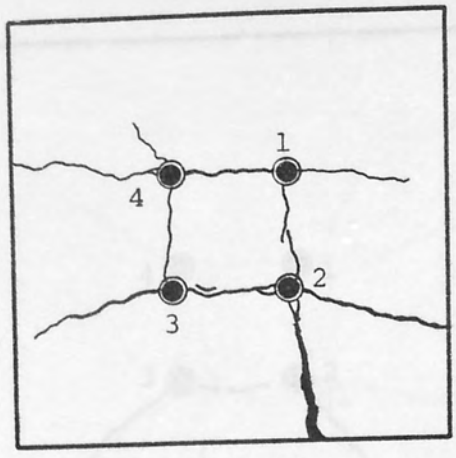

Bottom View

TEST SPECIMEN SR3-1

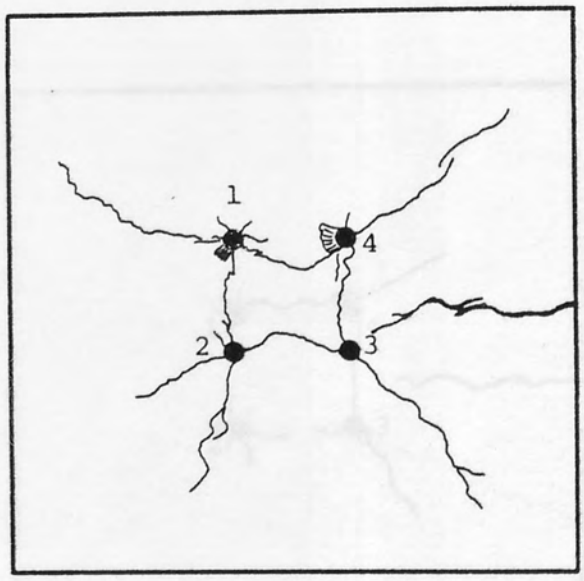

Top View

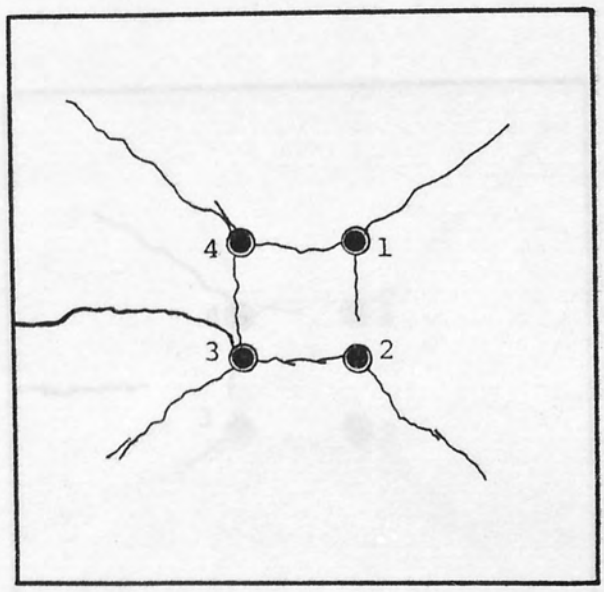

Bottom View

TEST SPECIMEN SR1-3

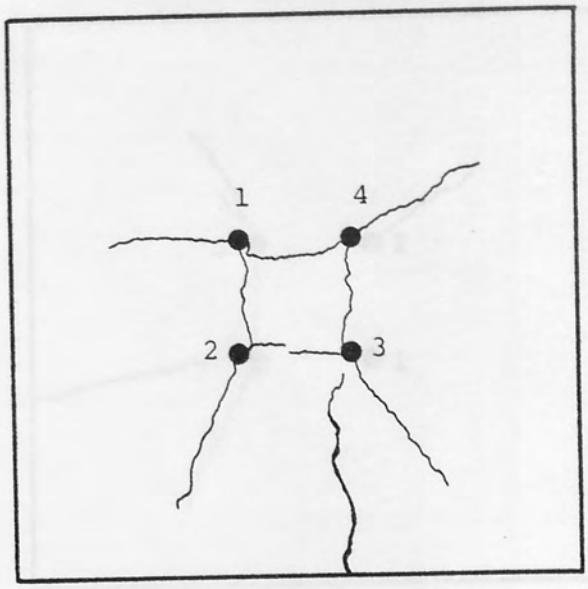

Top View

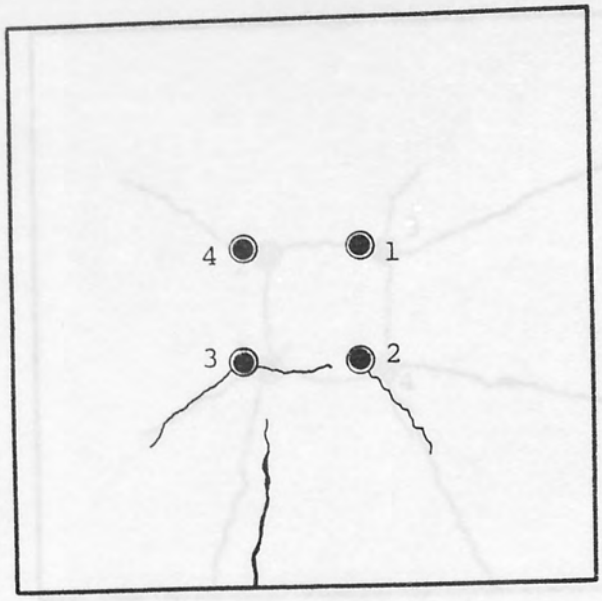

Bottom View

TEST SPECIMEN SR4-1

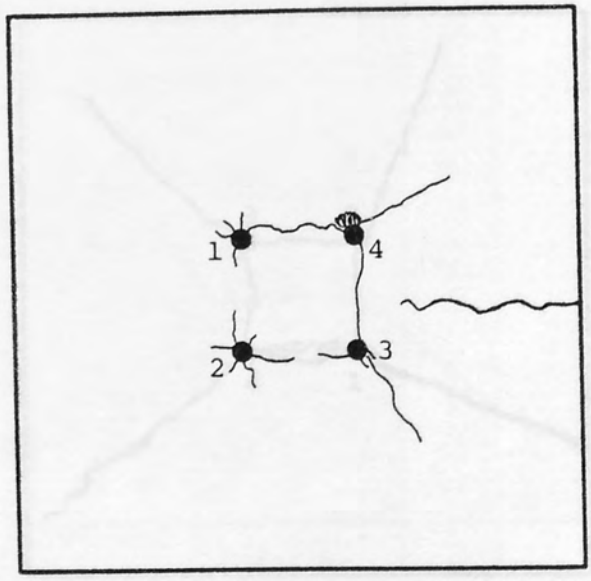

Top View

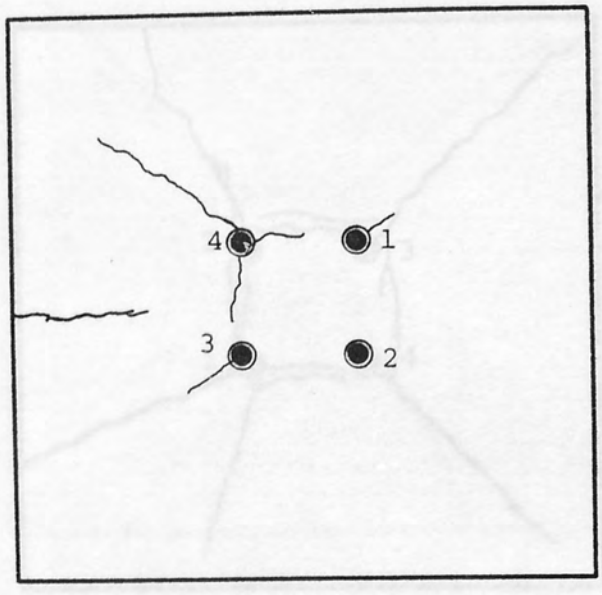

Bottom View

TEST SPECIMEN SR5-1

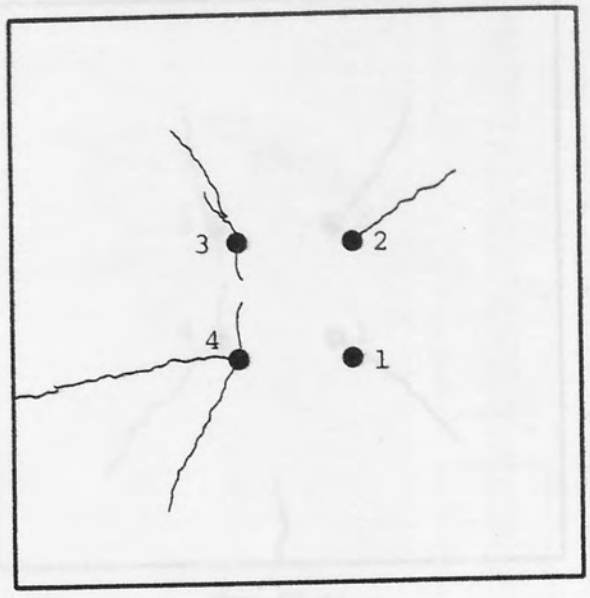

Top View

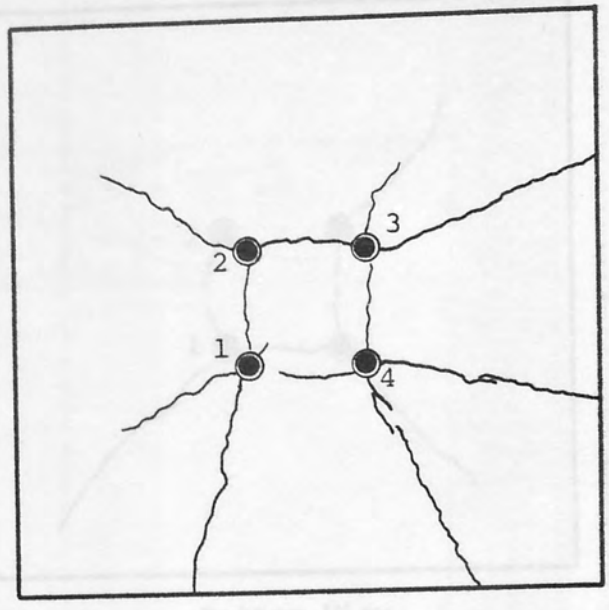

Bottom View

TEST SPECIMEN SR6-2

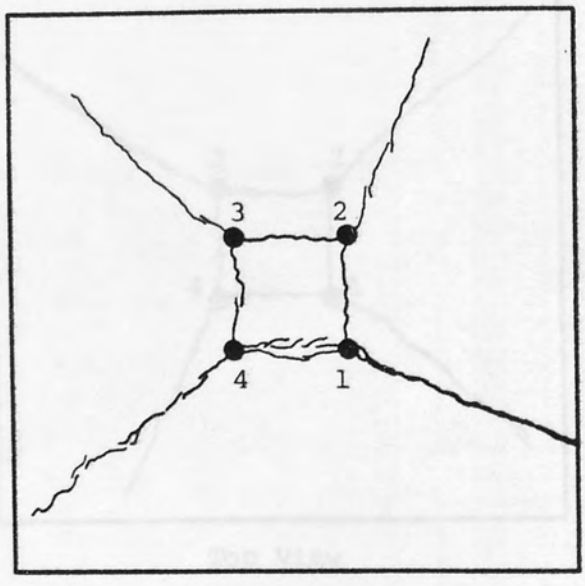

Top View

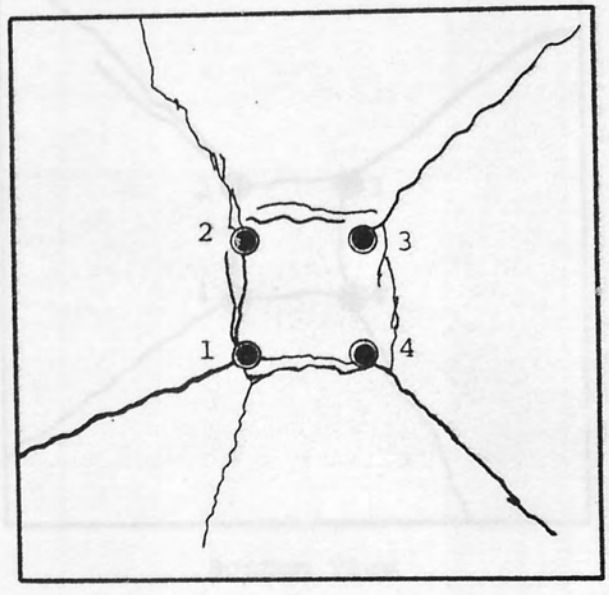

Bottom View

TEST SPECIMEN SR7-1

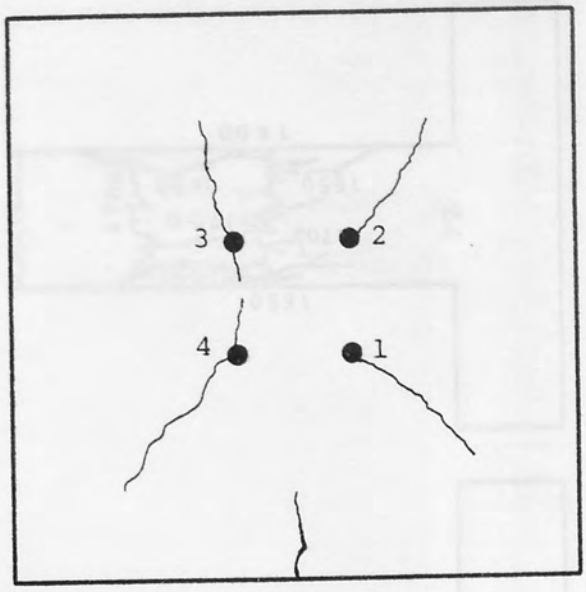

Top View

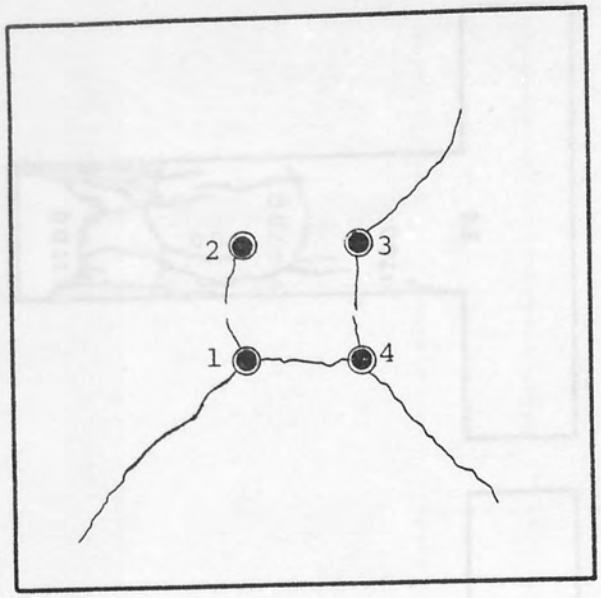

Bottom View

TEST SPECIMEN SR7-2

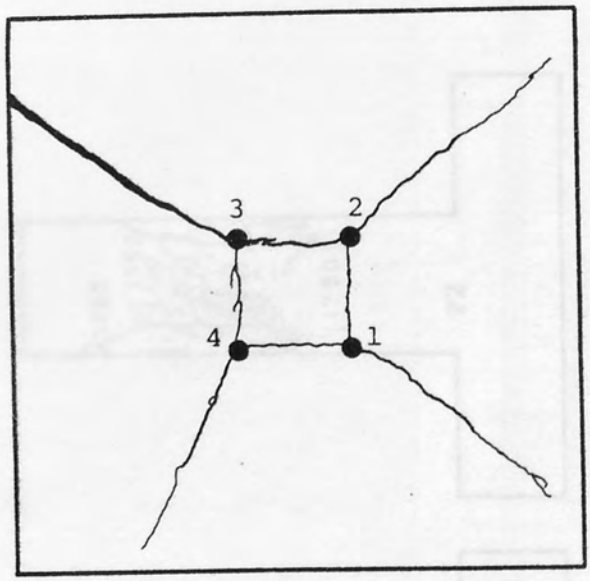

Top View

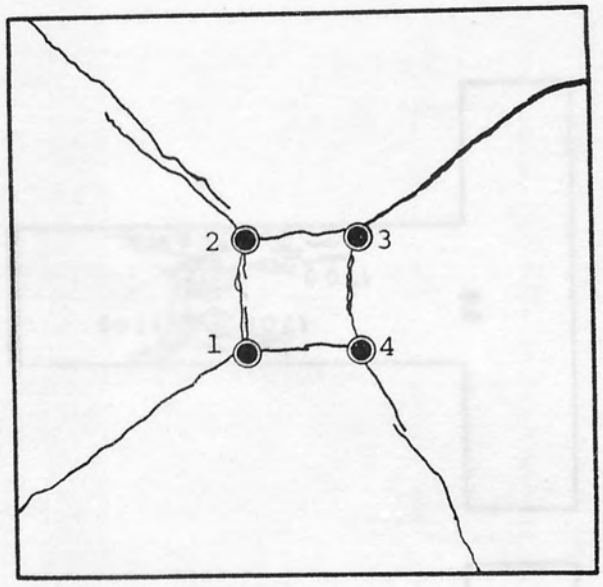

Bottom View

TEST SPECIMEN SR8-4

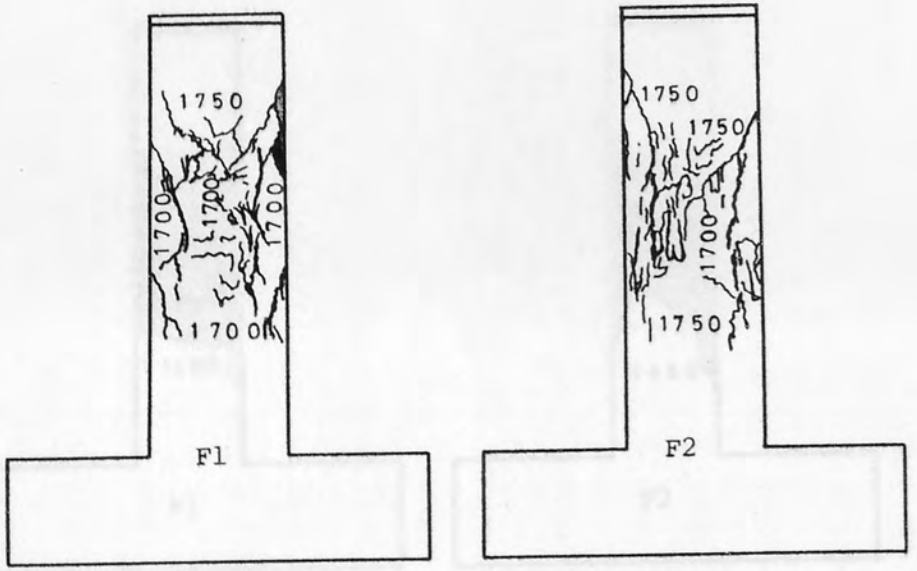

TEST SPECIMEN SR9-1

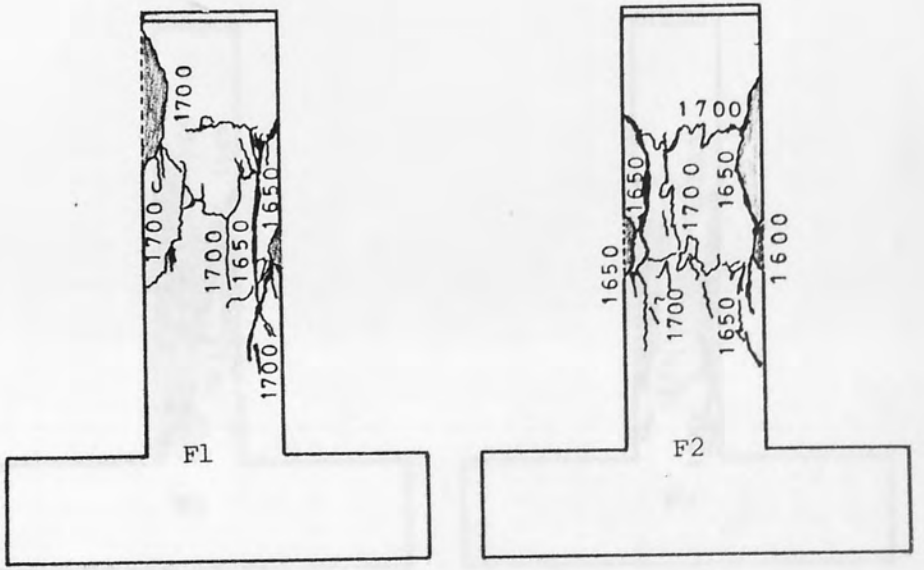

TEST SPECIMEN SR9-2

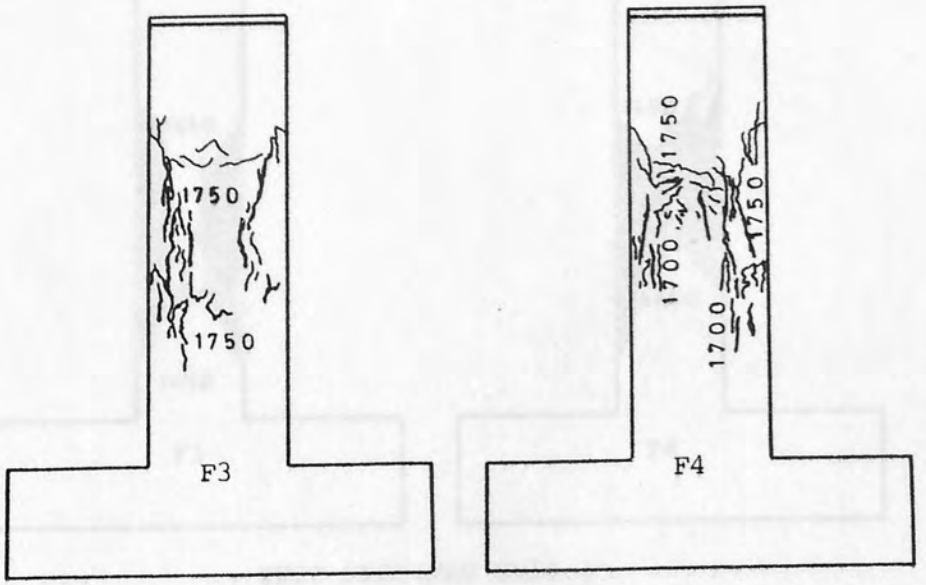

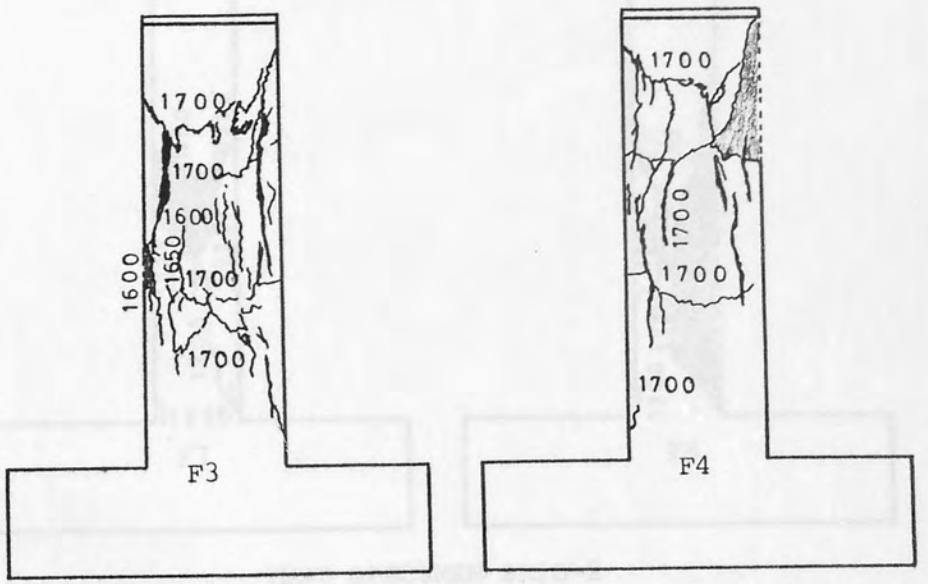

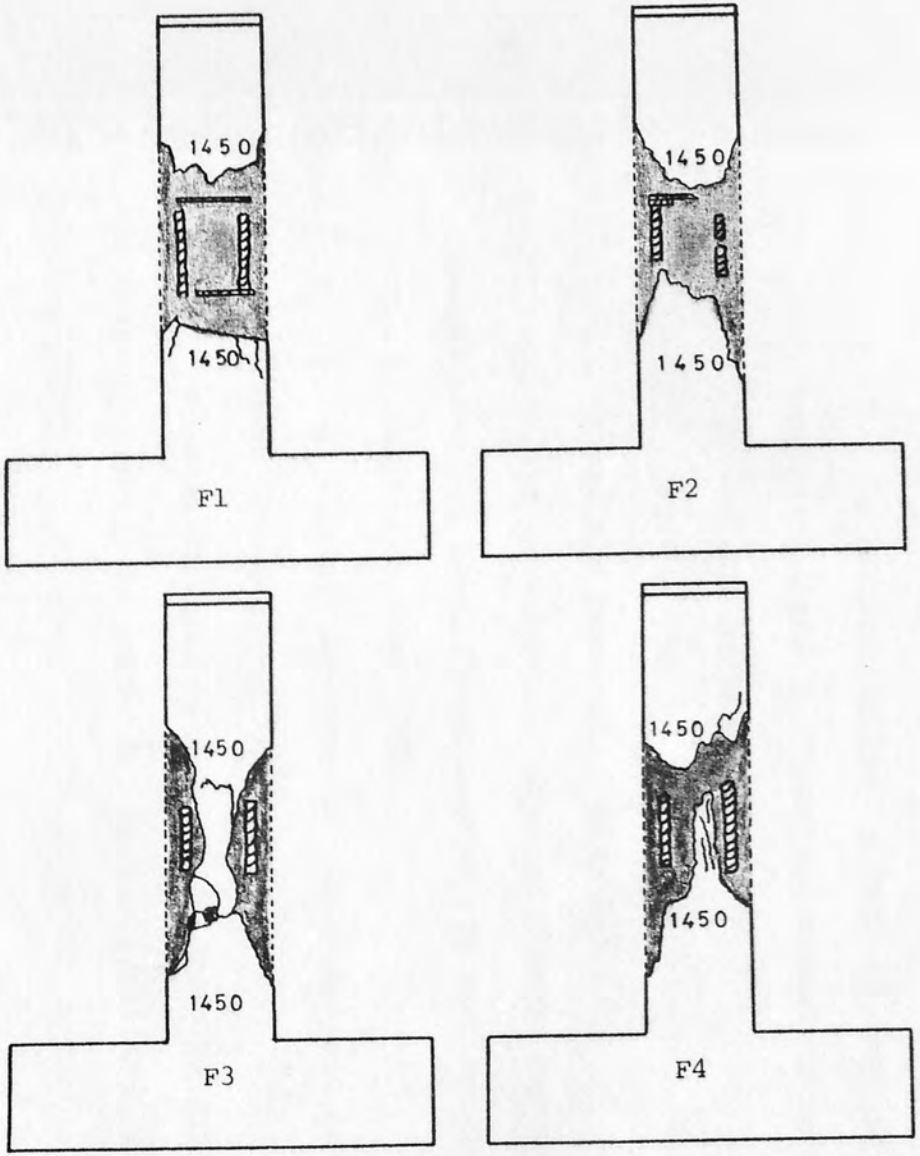

TEST SPECIMEN SR1O-1

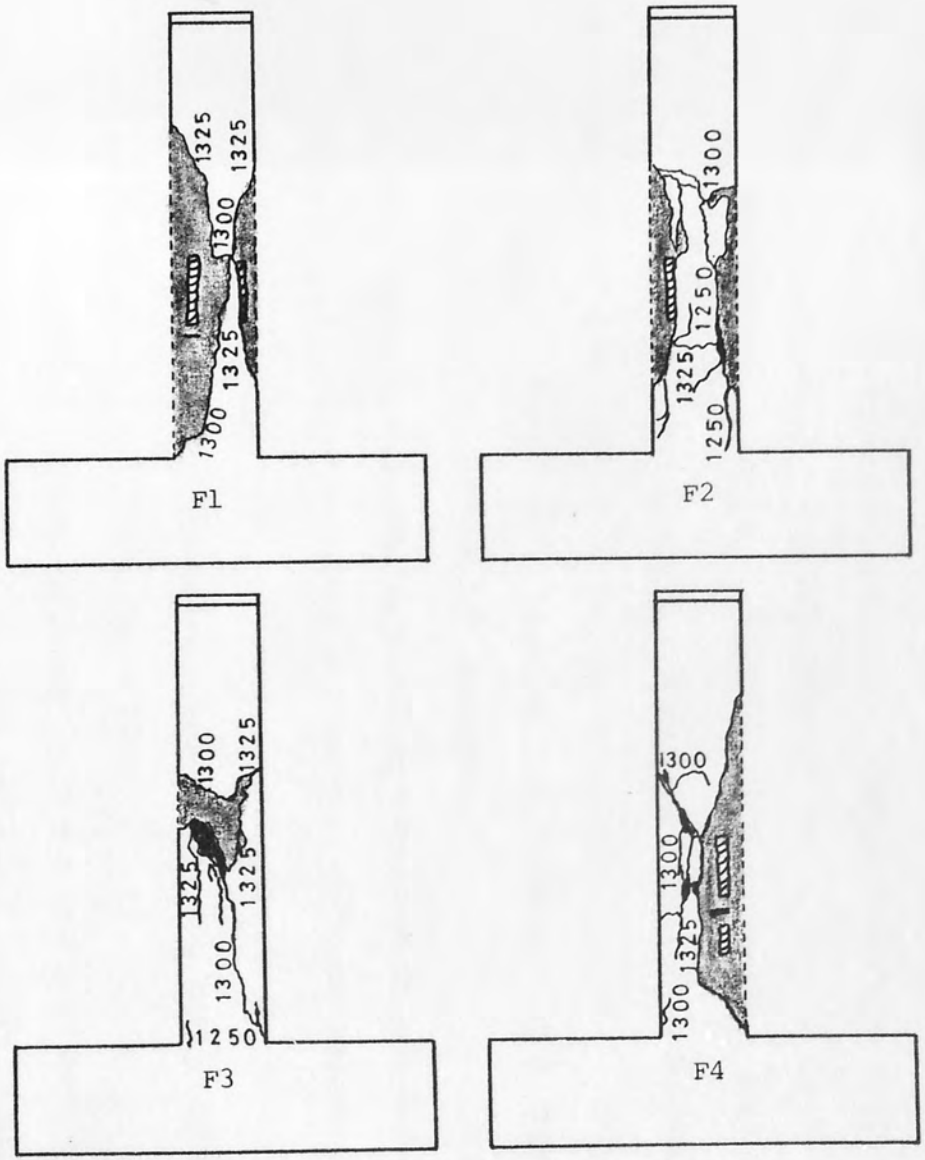

TEST SPECIMEN SR1O-2

REFERENCES

1. TALBOT A.N., Reinforced Concrete Wall Footings and Column Footings, University of Illinois, Engineering Experiment Station, Bulletin No.67, March 1913.

2. ABRAMS D.A., Tests of Bond between Concrete and Steel, University of Illinois, Engineering Experiment Station, Bulletin No.71, December 1913.

3. MINDLIN R.D., Force at a Point in the Interior of a Semi-Infinite Solid, Physics, Vol.7, May 1936.

4. MARSHALL W.T., Experiments on Reinforced Concrete Column Bases, Paper No.5383, Journal of the Institution of Civil Engineers, Vol.22, 1944.

5. MYLREA T.D., Bond and Anchorage, Proceedings of the American Concrete Institute, Vol.44, March 1948.

6. RICHART F.E., Reinforced Concrete Wall and Column Footings, Proceedings of the American Concrete Institute, Vol.45, October and November 1948.

7. KING J.W.H., Some Investigations of the Effects of Core Size and Steel and Concrete Quality in Short Reinforced Concrete Columns, Magazine of Concrete Research, June 1949.

8. WILKINS R.J., Some Experiments on the Load Distribution in Bond Tests, Magazine of Concrete Research, January 1951.

9. MAINS R.M., Measurement of the Distribution of Tensile and Bond Stress along Reinforcing Bars, Proceedings of the American Concrete Institute, Vol.48, November 1951.

10. MEYERHOF G.G., The Bearing Capacity of Concrete and Rock, Magazine of Concrete Research, April 1953.

11. HOGNESTAD E., Shearing Strength of Reinforced Concrete Column Footings, Proceedings of the American Concrete Institute, Vol. 50, November 1953.

12. COWAN H.J., The Strength of Plain, Reinforced and Prestressed Concrete Under the Action of Combined Stresses, with Particular Reference to the Combined Bending and Torsion of Rectangular Sections, Magazine of Concrete Research, December 1953.

13. ELSTNER R.C. and HOGNESTAD E., Shearing Strength of Reinforced Concrete Slabs, Proceedings of the American Concrete Institute, Vol.53, July 1956.

14. LEONHARDT F., On the Need to Consider the Influence of Lateral Stresses on Bond, Symposium on Bond and Crack Formation in Reinforced Concrete, Vol.I, Rilem, Stockholm 1957.

15. HAJNAL-KONYI K., Suggestions for the Comparison of the Bond Resistance of Various Types of Reinforcing Bar, Symposium on Bond and Crack Formation in Reinforced Concrete, Vol.I, Rilem, Stockholm 1957.

16. PARLAND H., Inelasticity of Bond between Steel and Concrete and Distribution of Stress in Steel in Cracked and Uncracked Structural Members, Symposium on Bond and Crack Formation in Reinforced Concrete, Vol.II, Rilem, Stockholm 1957.

17. ODMAN S.T.A., Slip between Reinforcement and Concrete, Symposium on Bond and Crack Formation in Reinforced Concrete, Vol.II, Rilem, Stockholm 1957.

18. REHM G., The Fundamental Law of Bond, Symposium on Bond and Crack Formation in Reinforced Concrete, Vol.II, Rilem, Stockholm 1957.

19. REHM G., Stress Distribution in Reinforcing Bars Embedded in Concrete, Symposium on Bond and Crack Formation in Reinforced Concrete, Vol.II, Rilem, Stockholm 1957.

20. SUBJECT VI., Theories of Bond and Crack Formation, Symposium on Bond and Crack Formation in Reinforced Concrete, Vol.III, Rilem, Stockholm 1957.

21. WHITNEY C.S., Ultimate Shear Strength of Reinforced Concrete Slabs, Footings, Beams and Frame Members Without Shear Reinforcement, Proceedings of the American Concrete Institute, Vol. 54, October 1957.

22. SHELSON W., Bearing Capacity of Concrete, Proceedings of the American Concrete Institute, Vol.54, November 1957.

23. AU T. and BAIRD D.L., Bearing Capacity of Concrete Blocks, Proceedings of the American Concrete Institute, Vol.56, March 1960.

24. ERSOY U. and HAWKINS M., Bearing Capacity of Concrete Blocks, Discussion of a Paper by AU T. and BAIRD D.L., Proceedings of the American Concrete Institute, Vol.56, September 1960.

25. SALVADORI M.G. and BARON M.L., Numerical Methods in Engineering, Second Edition, Prentice-Hall, Inc., Englewood Cliffs, N.J., 1961.

26. FERGUSON P.M. and THOMPSON J.N., Development Length of High Strength Reinforcing Bars in Bond, Proceedings of the American Concrete Institute, Vol.59, July 1962.

27. D'APPOLONIA E. and ROMUALDI J.P., Load Transfer in End-Bearing Steel H-Piles, Journal of the Soil Mechanics and Foundation Division, Proceedings of the American Society of Civil Engineers, SM2, Vol.89, March 1963.

28. PFISTER J.F. and MATTOCK A.H., High Strength Bars as Concrete Reinforcement, Part 5, Lapped Plices in Concentrically Loaded Columns, Journal of the Portland Cement Association, No.2, Vol.5, May 1963.

29. C.U.R. REPORT No.23, An Investigation of the Bond of Deformed Steel Bars with Concrete, Cement and Concrete Association, Translation No.112, London 1964.

30. THURMAN A.G. and D'APPOLONIA E., Computed Movement of Friction and End-Bearing Piles Embedded in Uniform and Stratified Soils, Proceedings, 6th International Conference on Soil Mechanics, Vol.2, Montreal 1965.

31. FERGUSON P.M. and BREEN J.E., Lapped Splices for High Strength Reinforcing Bars, Proceedings of the American Concrete Institute, Vol.62, September 1965.

32. FERGUSON P.M., et al., Bond Stress - The State of the Art, Reported by ACI Committee 408, Proceedings of the American Concrete Institute, Vol.63, October 1966.

33. BRITISH STANDARD BS4190:1967, Specification for Iso Metric Black Hexagon Bolts, Screws and Nuts, Metric Units, British Standards Institution, London 1967.

34. HAWKINS N.M., The Bearing Strength of Concrete Loaded Through Rigid Plates, Magazine of Concrete Research, Vol.20, March 1968.

35. REHM G., The Basic Principles of the Bond between Steel and Concrete, Cement and Concrete Association, Translation No.134, London 1968.

36. ROBERTS N.P., Development Length Bond Stress and Limit-State Design, Concrete, Vol.2, September 1968.

37. POULOS H.G. and DAVIS E.H., The Settlement Behaviour of Single Axially Loaded Incompressible Piles and Piers, Geotechnique, Vol.18, 1968.

38. POULOS H.G., Analysis of the Settlement of Pile Groups, Geotechnique, Vol.18, 1968.

39. MATTES N.S. and POULOS H.G., Settlement of Single Compressible Pile, Journal of the Soil Mechanics and Foundation Divison, Proceedings of the American Society of Civil Engineers, SM1, Vol.95, January 1969.

40. POULOS H.G., The Behaviour of Axially Loaded End-Bearing Piles, Geotechnique, Vol.19, 1969.

41. BRITISH STANDARD BS449:1969, Specification for the Use of Cold Formed Steel Sections in Building, Part 2, British Standards Institution, London 1969.

42. BRITISH STANDARD BS4466:1969, Specification for Bending Dimensions and Scheduling of Reinforcement, British Standards Institution, London 1969.

43. MUKI R. and STERNBERG E., Elastostatic Load-Transfer to a Half-Space from a Partially Embedded Axially Loaded Rod, Int. Journal of Solids and Structures, Vol.6, 1970.

44. RIEVE J.J., Der Haftverbund zwischen Stahl und Beton (Bond between Steel and Concrete), International Association for Bridge and Structural Engineering, Publications (30-1), Swiss Federal Institute of Technology, Zürich 1970.

45. AMERICAN CONCRETE INSTITUTE COMMITTEE 408, Opportunities in Bond Research, Proceedings of the American Concrete Institute, Vol.67, November 1970.

46. LUTZ L.A., Information on the Bond of Deformed Bars From Special Pullout Tests, Proceedings of the American Concrete Institute, Vol.67, November 1970.

47. BRITISH STANDARD BS1881:1970, Part 4, Methods of Testing Concrete for Strength, Metric Units, British Standards Institution, London 1970.

48. GOTO Y., Cracks Formed in Concrete around Deformed Tension Bars, Proceedings of the American Concrete Institute, Vol.68, April 1971.

49. SARGIN M., GHOSH S.K. and HANDA V.K., Effects of Lateral Reinforcement upon the Strength and Deformation Properties of Concrete, Magazine of Concrete Research, Vol.23, June-September 1971.

50. GHOSH S.G., SARGIN M. and HANDA V.K., The Effectiveness of Cover in Reinforced Concrete Compression Members, Proceedings of the Institution of Civil Engineers, Vol.50, November 1971.

51. SOMERVILLE G., Horizontal Compression Joints in Precast Concrete Framed Structures, Ph.D. Thesis, City University, London 1971.

52. POULOS H.G. and MATTES N.S., Settlement and Load Distribution Analysis of Pile Groups, Australian Geomechanics Journal, 1971.

53. POULOS H.G. and MATTES N.S., Displacements in a Soil Mass due to Pile Groups, Australian Geomechanics Journal, 1971.

54. BUTTERFIELD R. and BANERJEE P.K., The Elastic Analyis of Compressible Piles and Pile Groups, Geotechnique Vol.21, 1971.

55. SOMERVILLE G. and TAYLOR H.P.J., The Influence of Reinforcement Detailing on the Strength of Concrete Structures, The Structural Engineer, Vol.50, January 1972.

56. BRITISH STANDARD CODE OF PRACTICE CP110:Part 1:1972, The Structural Use of Concrete, British Standards Institution, London 1972.

57. BRITISH STANDARD BS4360:1972, Specification for Weldable Structural Steel, British Standards Institution, London 1972.

58. ROBERTS N.P. and HO R.C., Behaviour and Design of Tensile Lapped Joints in Reinforced Concrete Beams, Civil Engineering and Public Works Review, January 1973.

59. AL-SAJIR D.K., The Transference of Axial Load from Reinforced Concrete Columns to Bases, M.Phil. Thesis, University of Aston in Birmingham, January 1976.

60. CAIRNS J., The Strength of Lapped Joints in Reinforced Concrete Columns, Ph.D. Thesis, University of Glasgow, October 1976.

61. ACI STANDRAD 318-77, Building Code Requirements for Reinforced Concrete, American Concrete Institute, Detroit, Michigan 1977.

62. ARTHUR P.D. and CAIRNS J.W., Compression Laps of Reinforcement in Concrete Columns, The Structural Engineer, Vol.56B, March 1978.

63. BRITISH STANDARD BS4461:1978, Specification for Cold Worked Steel Bars for the Reinforcement of Concrete, British Standards Institution, London 1978.

64. BRITISH STANDARD BS4449:1978, Specification for Hot Rolled Steel Bars for the Reinforcement of Concrete, British Standards Institution, London 1978.

65. LOSBERG A. and OLSON P.A., Bond Failure of Deformed Reinforcing Bars Based on the Longitudinal Splitting Effect of the Bars, Proceedings of the American Concrete Institute, Vol.76, January 1979.

66. MIRZA S.M. and HOUDE J., Study of Bond Stress-Slip Relationships in Reinforced Concrete, Proceedings of the American Concrete Institute, Vol.76, January 1979.

67. KEMP E.L. and WILHELM W.J., Investigation of the Parameters Influencing Bond Cracking, Proceedings of the American Concrete Institute, Vol.76, January 1979.

68. JIMENEZ R., WHITE R.N. and GERGELY P., Bond and Dowel Capacities of Reinforced Concrete, Proceedings of the American Concrete Institute, Vol.76, January 1979.

69. MORITA S. and KAKU T., Splitting Bond Failure of Large Deformed Reinforcing Bars, Proceedings of the American Concrete Institute, Vol.76, January 1979.

70. SORETZ S. and HÖLZENBEIN H., Influence of Rib Dimensions of Reinforcing Bars on Bond and Bendability, Proceedings of the American Concrete Institute, Vol.76, January 1979.

71. CAIRNS J. and ARTHUR P.D., Strength of Lapped Splices in Reinforced Concrete Columns, Proceedings of the American Concrete Institute, Vol.76, February 1979.

72. REHM G. and ELIGEHAUSEN R., Bond of Ribbed Bars Under High Cycle Repeated Loads, Proceedings of the American Concrete Institute, Vol.76, February 1979.

73. TEPFERS R., Cracking of Concrete Cover along Anchored Deformed Reinforcing Bars, Magazine of Concrete Research, Vol.31, March 1979.

74. JAIRNS J., An Analysis of the Ultimate Strength of Lapped Joints of Compression Reinforcement, Magazine of Concrete Research, Vol.31, March 1979.

75. SKOROBOGATOV S.M. and EDWARDS A.D., The Influence of the Geometry of Deformed Steel bars on their Bond Strength in Concrete, Proceedings Institution of Civil Engineers, Part 2, June 1979.

76. ASTILL A.W. and AL-SAJIR D.K., Compression Bond in Column-to-Base Joints, The Structural Engineer, Vol.58B, March 1980.

77. IVERING J.W., Bond of Tube in Semi-Infinite Elastic Solid, Journal of the Strain Analysis, Vol.15, 1980.

78. TASSIOS T.P. and YANNOPOULOS P.J., Analytical Studies on Reinforced Concrete Members Under Cyclic Loading Based on Bond Stress-Slip Relationships, Proceedings of the American Concrete Institute, Vol.78, May-June 1981.

79. DIEDERICHS U. and SCHNELDER U., Bond Strength at High Temperatures, Magazine of Concrete Research, Vol.33, June 1981.

80. SOMAYAJI S. and SHAH S.P., Bond Stress Versus Slip Relationship and Cracking Response of Tension Members, Proceedings of the American Concrete Institute, Vol.78, May-June 1981.

81. REYNOLDS G.C., Bond Strength of Deformed Bars, Technical Report 548, Cement and Concrete Association, London 1982.

82. BARTOS P., Bond in Concrete - Proceedings of the International Conference on Bond in Concrete held in Paisley, Scotland - Applied Science Publishers, London 1982.

83. TEPFERS R., Tensile Lap Splices with Confining Reinforcement, Bond in Concrete - Proceedings of the International Conference on Bond in Concrete held in Paisley, Scotland - Applied Science Publishers, London 1982.

84. SEFEROVIC E. Experimental Determination of Anchoring Length in the Column-Foundation Joints, Bond in Concrete - Proceedings of the International Conference on Bond in Concrete held in Paisley, Scotland - Applied Science Publishers, London 1982.

85. TANIGAWA Y., BABA K. and YAMADA K., Effect on Bond between Concrete and Deformed Bar on Mechanical Behaviour of Reinforced Concrete Columns, Bond in Concrete - Proceedings of the International Conference on Bond in Concrete held in Paisley, Scotland - Applied Science Publishers, London 1982.

86. REYNOLD G.C. and BEEBY A.W., Bond Strength of Deformed Bars, Bond in Concrete - Proceedings of the International Conference on Bond in Concrete held in Paisley, Scotland - Applied Science Publishers, London 1982.